REPORT DOCUMENTATION PAGE

Form Approved OMB No. 0704-0188

Public reporting burden for this collection of information is estimated to average 1 hour per response, including the time for reviewing instructions, searching existing data sources, gathering and maintaining the data needed, and completing and reviewing the collection of information. Send comments regarding this burden estimate or any other aspect of this collection of information, including suggestions for reducing this burden to Washington Headquarters Services, Directorate for Information Operations and Reports, 1215 Jefferson Davis Highway, Suite 1204, Arlington, VA 22202-4302, and to the Office of Management and Budget, Paperwork Reduction Project (0704-0188), Washington, DC 20503.

1. AGENCY USE ONLY (Leave blank)	2. REPORT DATE	3. REPORT TYPE AND DATES COVERED
	18 June 1997	Conference Proceedings

4. TITLE AND SUBTITLE

Mathematics of Neural Networks - Models, Algorithms and Applications

5. FUNDING NUMBERS

F6170895W0327

6. AUTHOR(S)

Conference Committee

7. PERFORMING ORGANIZATION NAME(S) AND ADDRESS(ES)

Strathclyde University
Energy Systems Division, Mechanical Engineering Dept, James Weir Bldg., 75 Montrose St.
Glasgow G1 1XJ
United Kingdom

8. PERFORMING ORGANIZATION REPORT NUMBER

N/A

9. SPONSORING/MONITORING AGENCY NAME(S) AND ADDRESS(ES)

EOARD
PSC 802 BOX 14
FPO 09499-0200

10. SPONSORING/MONITORING AGENCY REPORT NUMBER

CSP 95-1034

11. SUPPLEMENTARY NOTES

12a. DISTRIBUTION/AVAILABILITY STATEMENT

Approved for public release; distribution is unlimited.

12b. DISTRIBUTION CODE

A

13. ABSTRACT (Maximum 200 words)

The Final Proceedings for Mathematics of Neural Networks and Applications (MANNA 1995), 3 July 1995 - 7 July 1995

The Topics covered include: approximation theory, control theory, genetic algorithms, dynamical systems, numerical analysis, optimization, statistical decision theory, statistical mechanics, computability and information theory.

14. SUBJECT TERMS

15. NUMBER OF PAGES

403

16. PRICE CODE

N/A

17. SECURITY CLASSIFICATION OF REPORT	18. SECURITY CLASSIFICATION OF THIS PAGE	19. SECURITY CLASSIFICATION OF ABSTRACT	20. LIMITATION OF ABSTRACT
UNCLASSIFIED	UNCLASSIFIED	UNCLASSIFIED	UL

MATHEMATICS OF NEURAL NETWORKS

Models, Algorithms and Applications

OPERATIONS RESEARCH/COMPUTER SCIENCE INTERFACES SERIES

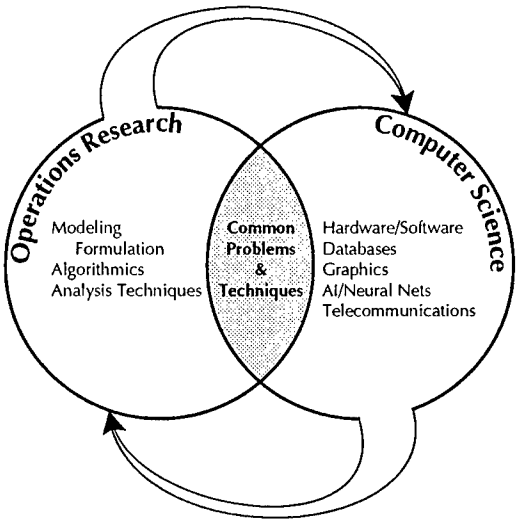

Ramesh Sharda, Series Editor
Conoco/DuPont Chair of Management of Technology
Oklahoma State University
Stillwater, Oklahoma U.S.A.

Other published titles in the series:

Brown, Donald/Scherer, William T.
University of Virginia
Intelligent Scheduling Systems

Nash, Stephen G./Sofer, Ariela
George Mason University
The Impact of Emerging Technologies on Computer Science and Operations Research

Barth, Peter
Max-Planck-Institut fur Informatik, Germany
Logic-Based 0-1 Constraint Programming

Jones, Christopher V.
University of Washington
Visualization and Optimization

Barr, Richard S./ Helgason, Richard V./ Kennington, Jeffery L.
Southern Methodist University
Interfaces in Computer Science and Operations Research: Advances in Metaheuristics, Optimization, and Stochastic Modeling Technologies

MATHEMATICS OF NEURAL NETWORKS

Models, Algorithms and Applications

DISTRIBUTION STATEMENT A
Approved for public release
Distribution Unlimited

EDITED BY

Stephen W ELLACOTT
University of Brighton
United Kingdom

John C MASON
University of Huddersfield
United Kingdom

Iain J ANDERSON
University of Huddersfield
United Kingdom

19970707 089

DTIC QUALITY INSPECTED 3

KLUWER ACADEMIC PUBLISHERS
Boston/London/Dordrecht

Distributors for North America:
Kluwer Academic Publishers
101 Philip Drive
Assinippi Park
Norwell, Massachusetts 02061 USA

Distributors for all other countries:
Kluwer Academic Publishers Group
Distribution Centre
Post Office Box 322
3300 AH Dordrecht, THE NETHERLANDS

Library of Congress Cataloging-in-Publication Data

A C.I.P. Catalogue record for this book is available from the Library of Congress.

Copyright © 1997 by Kluwer Academic Publishers

All rights reserved. No part of this publication may be reproduced, stored in a retrieval system or transmitted in any form or by any means, mechanical, photo-copying, recording, or otherwise, without the prior written permission of the publisher, Kluwer Academic Publishers, 101 Philip Drive, Assinippi Park, Norwell, Massachusetts 02061

Printed on acid-free paper.

Printed in the United States of America

CONTENTS

PREFACE xxi

Part I INVITED PAPERS 1

1 N-TUPLE NEURAL NETWORKS
N. M. Allinson and A. R. Kolcz 3

2 INFORMATION GEOMETRY OF NEURAL NETWORKS —AN OVERVIEW—
Shun-ichi Amari 15

3 Q-LEARNING: A TUTORIAL AND EXTENSIONS
George Cybenko, Robert Gray and Katsuhiro Moizumi 24

4 ARE THERE UNIVERSAL PRINCIPLES OF BRAIN COMPUTATION?
Stephen Grossberg 34

5 ON-LINE TRAINING OF MEMORY-DRIVEN ATTRACTOR NETWORKS
Morris W. Hirsch 41

6 MATHEMATICAL PROBLEMS ARISING FROM CONSTRUCTING AN ARTIFICIAL BRAIN
J. G. Taylor 47

Part II SUBMITTED PAPERS 59

7 THE SUCCESSFUL USE OF PROBABILITY DATA IN CONNECTIONIST MODELS
J. R. Alexander Jr. and J. P. Coughlin 61

8 WEIGHTED MIXTURE OF MODELS FOR ON-LINE LEARNING
P. Edgar An 67

9 LOCAL MODIFICATIONS TO RADIAL BASIS NETWORKS
I. J. Anderson 73

DTIC QUALITY INSPECTED 3

10 A STATISTICAL ANALYSIS OF THE MODIFIED NLMS RULES
E.D. Aved'yan, M. Brown and C.J. Harris 78

11 FINITE SIZE EFFECTS IN ON-LINE LEARNING OF MULTI-LAYER NEURAL NETWORKS.
David Barber, Peter Sollich and David Saad 84

12 CONSTANT FAN-IN DIGITAL NEURAL NETWORKS ARE VLSI-OPTIMAL
V. Beiu 89

13 THE APPLICATION OF BINARY ENCODED 2ND DIFFERENTIAL SPECTROMETRY IN PREPROCESSING OF UV-VIS ABSORPTION SPECTRAL DATA
N Benjathapanun, W J O Boyle and K T V Grattan 95

14 A NON-EQUIDISTANT ELASTIC NET ALGORITHM
Jan van den Berg and Jock H. Geselschap 101

15 UNIMODAL LOADING PROBLEMS
Monica Bianchini, Stefano Fanelli, Marco Gori and Marco Protasi 107

16 ON THE USE OF SIMPLE CLASSIFIERS FOR THE INITIALISATION OF ONE-HIDDEN-LAYER NEURAL NETS
Jan C. Bioch, Robert Carsouw and Rob Potharst 113

17 MODELLING CONDITIONAL PROBABILITY DISTRIBUTIONS FOR PERIODIC VARIABLES
Christopher M Bishop and Ian T Nabney 118

18 INTEGRO-DIFFERENTIAL EQUATIONS IN COMPARTMENTAL MODEL NEURODYNAMICS
Paul C. Bressloff 123

19 NONLINEAR MODELS FOR NEURAL NETWORKS
Susan Brittain and Linda M. Haines 129

20 A NEURAL NETWORK FOR THE TRAVELLING SALESMAN PROBLEM WITH A WELL BEHAVED ENERGY FUNCTION
Marco Budinich and Barbara Rosario 134

21 SEMIPARAMETRIC ARTIFICIAL NEURAL NETWORKS
Enrico Capobianco 140

22 AN EVENT-SPACE FEEDFORWARD NETWORK USING MAXIMUM ENTROPY PARTITIONING WITH APPLICATION TO LOW LEVEL SPEECH DATA
D.K.Y. Chiu, D. Bockus and J. Bradford 146

23 APPROXIMATING THE BAYESIAN DECISION BOUNDARY FOR CHANNEL EQUALISATION USING SUBSET RADIAL BASIS FUNCTION NETWORK
E.S. Chng, B. Mulgrew , S. Chen and G. Gibson 151

24 APPLICATIONS OF GRAPH THEORY TO THE DESIGN OF NEURAL NETWORKS FOR AUTOMATED FINGERPRINT IDENTIFICATION
Carol G. Crawford 156

25 ZERO DYNAMICS AND RELATIVE DEGREE OF DYNAMIC RECURRENT NEURAL NETWORKS
A. Delgado, C. Kambhampati and K. Warwick 161

26 IRREGULAR SAMPLING APPROACH TO NEUROCONTROL: THE BAND-AND SPACE-LIMITED FUNCTIONS QUESTIONS
Andrzej Dzieliński and Rafał Żbikowski 166

27 UNSUPERVISED LEARNING OF TEMPORAL CONSTANCIES BY PYRAMIDAL-TYPE NEURONS.
Michael Eisele 171

28 NUMERICAL ASPECTS OF MACHINE LEARNING IN ARTIFICIAL NEURAL NETWORKS
S.W. Ellacott and A. Easdown 176

29 LEARNING ALGORITHMS FOR RAM-BASED NEURAL NETWORKS
Alistair Ferguson, Laurence C Dixon and Hamid Bolouri 181

30 ANALYSIS OF CORRELATION MATRIX MEMORY AND PARTIAL MATCH–IMPLICATIONS FOR COGNITIVE

PSYCHOLOGY
Richard Filer and James Austin 186

31 REGULARIZATION AND REALIZABILITY IN RADIAL BASIS FUNCTION NETWORKS
Jason A.S. Freeman and David Saad 192

32 A UNIVERSAL APPROXIMATOR NETWORK FOR LEARNING CONDITIONAL PROBABILITY DENSITIES
D. Husmeier, D. Allen and J. G. Taylor 198

33 CONVERGENCE OF A CLASS OF NEURAL NETWORKS
Mark P. Joy 204

34 APPLICATIONS OF THE COMPARTMENTAL MODEL NEURON TO TIME SERIES ANALYSIS
S. Kasderidis and J. G. Taylor 209

35 INFORMATION THEORETIC NEURAL NETWORKS FOR CONTEXTUALLY GUIDED UNSUPERVISED LEARNING
Jim Kay 215

36 CONVERGENCE IN NOISY TRAINING
Petri Koistinen 220

37 NON-LINEAR LEARNING DYNAMICS WITH A DIFFUSING MESSENGER
Bart Krekelberg and John G. Taylor 225

38 A VARIATIONAL APPROACH TO ASSOCIATIVE MEMORY
Abderrahim Labbi 230

39 TRANSFORMATION OF NONLINEAR PROGRAMMING PROBLEMS INTO SEPARABLE ONES USING MULTILAYER NEURAL NETWORKS
Bao-Liang Lu and Koji Ito 235

40 A THEORY OF SELF-ORGANISING NEURAL NETWORKS
S P Luttrell 240

41 NEURAL NETWORK SUPERVISED TRAINING BASED ON A DIMENSION REDUCING METHOD
G.D. Magoulas, M.N. Vrahatis, T.N. Grapsa and G.S. Androulakis 245

42 A TRAINING METHOD FOR DISCRETE MULTILAYER NEURAL NETWORKS
G.D. Magoulas, M.N. Vrahatis, T.N. Grapsa and G.S. Androulakis 250

43 LOCAL MINIMAL REALISATIONS OF TRAINED HOPFIELD NETWORKS
S. Manchanda and G.G.R. Green 255

44 DATA DEPENDENT HYPERPARAMETER ASSIGNMENT
Glenn Marion and David Saad 259

45 TRAINING RADIAL BASIS FUNCTION NETWORKS BY USING SEPARABLE AND ORTHOGONALIZED GAUSSIANS
J. C. Mason, I. J. Anderson, G. Rodriguez and S. Seatzu 265

46 ERROR BOUNDS FOR DENSITY ESTIMATION BY MIXTURES
Ronny Meir and Assaf J. Zeevi 270

47 ON SMOOTH ACTIVATION FUNCTIONS
H. N. Mhaskar 275

48 GENERALISATION AND REGULARISATION BY GAUSSIAN FILTER CONVOLUTION OF RADIAL BASIS FUNCTION NETWORKS
Christophe Molina and Mahesan Niranjan 280

49 DYNAMICAL SYSTEM PREDICTION: A LIE ALGEBRAIC APPROACH FOR A NOVEL NEURAL ARCHITECTURE
Yves Moreau and Joos Vandewalle 285

50 STOCHASTIC NEURODYNAMICS AND THE SYSTEM SIZE EXPANSION
Toru Ohira and Jack D. Cowan 290

51 AN UPPER BOUND ON THE BAYESIAN ERROR BARS FOR GENERALIZED LINEAR REGRESSION
Cazhaow S. Qazaz, Christopher K. I. Williams and Christopher M. Bishop 295

52 CAPACITY BOUNDS FOR STRUCTURED NEURAL NETWORK ARCHITECTURES
Peter Rieper, Sabine Kröner and Reinhard Moratz 300

53 ON-LINE LEARNING IN MULTILAYER NEURAL NETWORKS
David Saad and Sara A. Solla 306

54 SPONTANEOUS DYNAMICS AND ASSOCIATIVE LEARNING IN AN ASSYMETRIC RECURRENT RANDOM NEURAL NETWORK
M. Samuelides, B. Doyon, B. Cessac and M. Quoy 312

55 A STATISTICAL MECHANICS ANALYSIS OF GENETIC ALGORITHMS FOR SEARCH AND LEARNING
Jonathan L. Shapiro, Adam Prügel-Bennett and Magnus Rattray 318

56 VOLUMES OF ATTRACTION BASINS IN RANDOMLY CONNECTED BOOLEAN NETWORKS
Sergey A. Shumsky 323

57 EVIDENTIAL REJECTION STRATEGY FOR NEURAL NETWORK CLASSIFIERS
A. Shustorovich 328

58 DYNAMICS APPROXIMATION AND CHANGE POINT RETRIEVAL FROM A NEURAL NETWORK MODEL
J. Smid and P. Volf 333

59 QUERY LEARNING FOR MAXIMUM INFORMATION GAIN IN A MULTI-LAYER NEURAL NETWORK
Peter Sollich 339

60 SHIFT, ROTATION AND SCALE INVARIANT SIGNATURES FOR TWO-DIMENSIONAL CONTOURS, IN A NEURAL NETWORK ARCHITECTURE
David McG. Squire and Terry M. Caelli 344

61 FUNCTION APPROXIMATION BY THREE-LAYER ARTIFICIAL NEURAL NETWORKS
Shin Suzuki 349

62 NEURAL NETWORK VERSUS STATISTICAL CLUSTERING TECHNIQUES: A PILOT STUDY IN A PHONEME RECOGNITION TASK
G.Tambouratzis, T.Tambouratzis and D.Tambouratzis 355

63 MULTISPECTRAL IMAGE ANALYSIS USING PULSED COUPLED NEURAL NETWORKS
G L Tarr, X Clastres, L Freyss, M Samuelides, C Dehainaut and W Burckel 361

64 REASONING NEURAL NETWORKS
Rua-Huan R. Tsaih 366

65 CAPACITY OF THE UPSTART ALGORITHM
Ansgar H. L. West and David Saad 372

66 REGRESSION WITH GAUSSIAN PROCESSES
Christopher K. I. Williams 378

67 STOCHASTIC FORWARD-PERTURBATION, ERROR SURFACE AND PROGRESSIVE LEARNING IN NEURAL NETWORKS
Li-Qun Xu 383

68 DYNAMICAL STABILITY OF A HIGH-DIMENSIONAL SELF-ORGANIZING MAP
Howard Hua Yang 389

69 MEASUREMENTS OF GENERALISATION BASED ON INFORMATION GEOMETRY
Huaiyu Zhu and Richard Rohwer 394

70 TOWARDS AN ALGEBRAIC THEORY OF NEURAL NETWORKS: SEQUENTIAL COMPOSITION
R. Zimmer 399

CONTRIBUTORS

J. R. Alexander Jr.
Towson State University,
Towson, MD 21032, USA.
Email: e7c1ale@toe.towson.edu

D. Allen
Centre for Neural Networks,
Department of Mathematics,
King's College London,
London WC2R 1LS UK.

N. M. Allinson
Department of Electrical
Engineering and Electronics,
UMIST, Manchester M60 1QD, UK.
Email: allinson@umist.ac.uk

Shun-ichi Amari
University of Tokyo, Tokyo, Japan,
RIKEN Frontier Research Program,
Wako-City, Saitama, Japan.
Email: amari@sat.t.u-tokyo.ac.jp

P. Edgar An
Department of Ocean Engineering,
Florida Atlantic University,
Boca Raton, FL 33431, USA.
Email: ean@oe.fau.edu

I. J. Anderson
School of Computing and Mathematics,
University of Huddersfield, Queensgate,
Huddersfield HD1 3DH, UK.
Email: scomija@zeus.hud.ac.uk

G.S. Androulakis
Department of Mathematics,
University of Patras,
GR-261.10 Patras, Greece.
Email: gsa@math.upatras.gr

James Austin
Advanced Computer Architecture Group,
Department of Computer Science,
University of York,
Heslington, YO1 5DD, UK.

E.D. Aved'yan
Russian Academy of Sciences,
Institute of Control Sciences,
65 Profsoyuznaya str.,
Moscow 117342, Russia.
Email: avedyan@dep07.ics.msk.su

David Barber
Dept. Comp, Sci. and Appl. Maths.,
Aston University, Birmingham B4 7ET, UK.
Web: http://www.ncrg.aston.ac.uk/

V. Beiu
Los Alamos National Laboratory,
Division NIS-1,
Los Alamos, New Mexico 87545, USA.
Email: beiu@lanl.gov

Jan van den Berg
Department of Computer Science,
Erasmus University Rotterdam,
The Netherlands.
Email: jvandenberg@few.eur.nl

N Benjathapanun
Department of Electrical, Electronic and
Information Engineering
City University, Northampton Square,
London EC1V OHB, UK.

Monica Bianchini
Dipartimento di Sistemi e Informatica,
Università degli Studi di Firenze,
Via di Santa Marta, 3,
50139 Firenze, Italy.
Email: monica,marco@mcculloch.ing.unifi.it

Jan C. Bioch
Department of Computer Science,
Erasmus University Rotterdam,
The Netherlands.
Email: bioch@cs.few.eur.nl

Christopher M. Bishop
Neural Computing Research Group,
Dept. of Computer Science and
Applied Mathematics,
Aston University, Birmingham B4 7ET, UK.
Email: c.m.bishop@aston.ac.uk

D. Bockus
Dept. Computing and Information Science,
University of Guelph,
Ontario NIG 2W1, Canada.

Hamid Bolouri
Engineering Research and
Development Centre,
University of Hertfordshire,
College Lane, Hatfield,
Herts, AL10 9AB, UK.

W J O Boyle
Department of Electrical, Electronic and
Information Engineering
City University, Northampton Square,
London EC1V OHB, UK.

J. Bradford
Brock University,
St. Catharines, Ontario, Canada.

Paul C. Bressloff
Department of Mathematical Sciences,
Loughborough University,
Leics. LE11 3TU, UK.
Email : P.C.Bressloff@lut.ac.uk

Susan Brittain
University of Natal,
Pietermaritzburg, South Africa.

M. Brown
ISIS research group,
Dept of Electronics and Computer Science,
Southampton University, Highfield,
Southampton, SO17 1BJ, UK.
Email: mqb@ecs.soton.ac.uk

Marco Budinich
Dipartimento di Fisica & INFN,
Via Valerio 2, 34127, Trieste, Italy.
Email: mbh@trieste.infn.it

William Burckel
Phillips Laboratory,
Kirtland Air Force Base
Albuquerque, New Mexico, USA.

Terry M. Caelli
School of Computing,
Curtin University of Technology,
Perth, Western Australia.
Email: tmc@cs.curtin.edu.au

Enrico Capobianco
Stanford University,
Stanford, CA 94305, USA.
Email: enrico@psych.stanford.edu

Robert Carsouw
Department of Computer Science,
Erasmus University Rotterdam,
The Netherlands.

B. Cessac
University of New-Mexico,
Department of Electrical and
Computer Engineering,
Albuquerque, NM 87131, USA.

S. Chen
Dept. of E.E.E.,
The University of Portsmouth, UK.

Xavier Clastres
Centre d'Etudes et de
Recherches de Toulouse,
2 avenue Edouard Belin, BP 4025,
31055 Toulouse Cedex, France.

D.K.Y. Chiu
Dept. Computing and Information Science,
University of Guelph,
Ontario NIG 2W1, Canada.
Email: dchiu@snowhite.cis.uoguelph.ca

E.S Chng
National University of Singapore,
Institute of System Science,
Heng Mui Keng Terrace,
Kent Ridge, 119597 Singapore.
Email : eschng@iss.nus.sg.

J. P. Coughlin
Towson State University,
Towson, MD 21032, USA.

Jack D. Cowan
Departments of Mathematics and
Neurology, The University of Chicago,
Chicago, IL 60637, USA.
Email: cowan@synapse.uchicago.edu

Carol G. Crawford
U.S. Naval Academy,
Department of Mathematics,
Annapolis MD 21402, USA.
Email: cgc@sma.usna.navy.mil

George Cybenko
Thayer School of Engineering,
8000 Cummings Hall, Dartmouth College,
Hanover, NH 03755 USA.
Email: gvc@dartmouth.edu

Laurence C Dixon
Engineering Research and
Development Centre,
University of Hertfordshire,
College Lane, Hatfield,
Herts, AL10 9AB, UK.

Christopher Dehainaut
Phillips Laboratory,
Kirtland Air Force Base
Albuquerque, New Mexico, USA.

A. Delgado
National University of Columbia,
Elec. Eng. Dept., AA No. 25268, Bogota,
D C, Columbia SA.
Email: adelgado@col1.telecom.com.co

B. Doyon
Unité INSERM 230, Service de Neurologie,
CHU Purpan,
31059 Toulouse Cédex, France.

Andrzej Dzielinski
Department of Mechanical Engineering,
James Watt Building,
University of Glasgow,
Glasgow G12 8QQ, Scotland, UK.
Email: andrzej@mech.gla.ac.uk

A. Easdown
School of Computing and
Mathematical Sciences,
University of Brighton,
Brighton BN1 4GJ, UK.
Email: A.Easdown@brighton.ac.uk

Michael Eisele
The Salk Institute,
Computational Neurobiology Laboratory,
PO Box 85800, San Diego,
CA 92186 - 5800, USA.
Email: eisele@salk.edu

S.W. Ellacott
School of Computing and
Mathematical Sciences,
University of Brighton,
Brighton BN1 4GJ, UK.
Email: S.W.Ellacott@brighton.ac.uk

Stefano Fanelli
Dipartimento di Matematica,
Università di Roma,
"Tor Vergata" Via della Ricerca Scientifica,
00133 Roma, Italy.
Email: fanelli@mat.utovrm.it

Alistair Ferguson
Engineering Research and
Development Centre,
University of Hertfordshire,
College Lane, Hatfield,
Herts, AL10 9AB, UK.
Email: A.Ferguson@herts.ac.uk

Richard Filer
Advanced Computer Architecture Group,
Department of Computer Science,
University of York,
Heslington, YO1 5DD, UK.
Email: rjhf@minster.york.ac.uk

Jason A.S. Freeman
Centre for Neural Systems,
University of Edinburgh,
Edinburgh EH8 9LW, UK.
Email: jason@cns.ed.ac.uk

Laurent Freyss
Centre d'Etudes et de
Recherches de Toulouse,
2 avenue Edouard Belin,BP 4025,
31055 Toulouse Cedex, France.

Jock H. Geselschap
Department of Computer Science,
Erasmus University Rotterdam,
The Netherlands.

G. Gibson
Biomathematics and Statistics,
The University of Edinburgh, UK.

Marco Gori
Dipartimento di Sistemi e Informatica,
Università degli Studi di Firenze,
Via di Santa Marta, 3, 50139 Firenze, Italy.
Email: marco@mcculloch.ing.unifi.it

T.N. Grapsa
Department of Mathematics,
University of Patras,
GR-261.10 Patras, Greece.
Email:grapsa@math.upatras.gr

K T V Grattan
Department of Electrical, Electronic and
Information Engineering
City University, Northampton Square,
London EC1V OHB, UK.

Robert Gray
Thayer School of Engineering,
8000 Cummings Hall, Dartmouth College,
Hanover, NH 03755 USA.

G.G.R. Green
Dept. of Physiological Sciences,
University of Newcastle upon Tyne,
Newcastle upon Tyne, NE1 7RU, UK.
Email: gary.green@ncl.ac.uk

Stephen Grossberg
Boston University, Department of Cognitive
and Neural Systems, and
Center for Adaptive Systems,
677 Beacon Street, Boston, Massachusetts
02215 USA

Linda M. Haines
University of Natal,
Pietermaritzburg, South Africa.
Email: haines@stat.unp.ac.za

C.J. Harris
ISIS research group,
Dept of Electronics and Computer Science,
Southampton University, Highfield,
Southampton, SO17 1BJ, UK.

Morris W. Hirsch
Department of Mathematics,
University of California at Berkeley,
CA 94720-3840 USA.
Email: hirsch@math.berkeley.edu

D. Husmeier
Centre for Neural Networks,
Department of Mathematics,
King's College London,
London WC2R 1LS, UK.
Email: D.Husmeier@bay.cc.kcl.ac.uk

Koji Ito
Interdisciplinary Graduate School of
Science and Engineering, Tokyo Institute of
Technology, 4259, Nagatsuda,
Midori-ku, Yokohama 226, Japan.
Email: ito@ssie.titech.ac.jp

Mark P. Joy
Centre for Research in Information
Engineering, School of Electrical,
Electronic and Information Enineering,
South Bank University, 103, Borough Rd.,
London SE1 OAA, UK.
Email: joympa@vax.sbu.ac.uk

C. Kambhampati
Cybernetics Department,
University of Reading, Whiteknights,
Reading RG6 6AY, UK.

S. Kasderidis
Department of Mathematics,
King's College London,
London WC2R 1LS, UK.

Jim Kay
Dept. of Statistics, University of Glasgow,
Mathematics Building,
Glasgow G12 8QW, UK.
Email: jim@stats.glasgow.ac.uk

Petri Koistinen
Rolf Nevanlinna Institute,
P.O. Box 4, FIN-00014
University of Helsinki, Finland.
Email: petri.koistinen@rni.helsinki.fi

A. R. Kolcz
Department of Electrical
Engineering and Electronics,
UMIST, Manchester M60 1QD, UK.

Bart Krekelberg
Centre for Neural Networks,
King's College London
London WC2R 2LS, UK
Email: bart@mth.kcl.ac.uk

Sabine Kroener
Technische Informatik I,
TU Hamburg-Harburg,
Harburger Schloßstr. 20,
D-21071 Hamburg, Germany.
Email: Kroener@tu-harburg.d400.de

Abderrahim Labbi
Dept. of Computer Science,
University of Geneva,
24 Rue General Dufour, 1121 Geneva 4,
Switzerland.
Email: labbi@cui.unige.ch

Bao-Liang Lu
The Institute of Physical and
Chemical Research (RIKEN),
3-8-31 Rokuban,Atsuta-ku,
Nagoya 456, Japan.
Email: lbl@nagoya.bmc.riken.go.jp

S P Luttrell
Defence Research Agency,
Malvern, Worcs, WR14 3PS, UK.
Email: luttrell@signal.dra.hmg.gb

G.D. Magoulas
Department of Electrical and
Computer Engineering,
University of Patras,
GR-261.10, Patras, Greece.
Email: magoulas@ee-gw.ee.upatras.gr

S. Manchanda
Dept. of Chemical and Process Engineering,
University of Newcastle upon Tyne,
Newcastle upon Tyne, NE1 7RU, UK.
Email: Sunil.Manchanda@ncl.ac.uk

Glenn Marion
Department of Statistics and
Modelling Science, Livingstone Tower,
26 Richmond Street, Glasgow G1 1XH, UK.
Email: glenn@stams.strath.ac.uk

J. C. Mason
School of Computing and Mathematics,
University of Huddersfield, Queensgate,
Huddersfield HD1 3DH, UK.
Email: J.C.Mason@hud.ac.uk

Ronny Meir
Electrical Engineering Department,
Technion, Haifa 32000, Israel.
Email: rmeir@ee.technion.ac.il

H. N. Mhaskar
Department of Mathematics,
California State University,
Los Angeles, California 90032, USA.
Email: hmhaska@calstatela.edu

Katsuhiro Moizumi
Thayer School of Engineering,
8000 Cummings Hall, Dartmouth College,
Hanover, NH 03755 USA.

Christophe Molina
Cambridge University
Engineering Department,
Trumpington Street, Cambridge CB2 1PZ, UK.
Email: cm3@eng.cam.ac.uk

Reinhard Moratz
AG Angewandte Informatik,
Universität Bielefeld, Postfach 100131,
D-33501 Bielefeld, Germany.

Yves Moreau
Katholieke Universiteit Leuven,
Dept. of Electrical Engineering,
ESAT-SISTA Kardinaal Mercierlaan 94,
B-3001 Leuven (Heverlee), Belgium.
Email: moreau@esat.kuleuven.ac.be

B. Mulgrew
Dept. of Electrical Eng.,
The University of Edinburgh, UK.

Ian T Nabney
Neural Computing Research Group,
Aston University, Birmingham, B4 7ET, UK.
Email: nabneyit@aston.ac.uk

Mahesan Niranjan
Cambridge University
Engineering Department,
Trumpington Street, Cambridge CB2 1PZ, UK.
Email: niranjan@eng.cam.ac.uk

Toru Ohira
Sony Computer Science Laboratory
3-14-13 Higashi-gotanda, Shinagawa,
Tokyo 141, Japan.
Email: ohira@csl.sony.co.jp

Rob Potharst
Department of Computer Science,
Erasmus University Rotterdam,
The Netherlands.
Email: robp@cs.few.eur.nl

Marco Protasi
Dipartimento di Matematica,
Università di Roma,"Tor Vergata"
Via della Ricerca Scientifica,
00133 Roma, Italy.
Email: protasi@mat.utovrm.it

Adam Pruegel-Bennett
NORDITA Blegdamsvej 17,
DK-2100 Copenhagen Ø, Denmark.

Cazhaow S. Qazaz
Neural Computing Research Group,
Dept. of Computer Science and
Applied Mathematics,
Aston University, Birmingham B4 7ET, UK.

M. Quoy
Universität Bielefeld,
BiBos, Postfach 100131,
33501 Bielefeld, Germany.

Magnus Rattray
Department of Computer Science,
University of Manchester,
Manchester, M13 9PL, UK.

Peter Rieper
FB Mathematik, Universitaet Hamburg,
Bundesstr. 55, D-20146 Hamburg, Germany.

G. Rodriguez
Department of Mathematics,
University of Cagliari,
viale Merello 92,09123 Cagliari, Italy.

Richard Rohwer
Prediction Co.,
320 Aztec Street, SuiteB,
Santa Fe, NM87501, USA.

Barbara Rosario
Dipartimento di Fisica & INFN,
Via Valerio 2, 34127, Trieste, Italy.
Email: mbh@trieste.infn.it

David Saad
Dept. of Computer Science and
Applied Mathematics, University of Aston,
Birmingham B4 7ET, UK.
Email: D.Saad@aston.ac.uk

M. Samuelides
Centre d'Etudes et de
Recherches de Toulouse,
2 avenue Edouard Belin, BP 4025,
31055 Toulouse Cedex, France.
Email: samuelid@cert.fr.

S. Seatzu
Department of Mathematics,
University of Cagliari,
viale Merello 92, 09123 Cagliari, Italy.

Jonathan L. Shapiro
Department of Computer Science,
University of Manchester,
Manchester, M13 9PL, UK.

Sergey A. Shumsky
P.N.Lebedev Physics Institute,
Leninsky pr.53, Moscow, Russia.
Email: serge@mart7.demos.su

A. Shustorovich
Business Imaging Systems,
Eastman Kodak Company, Rochester, USA.
Email: Sasha@kodak.com

J. Smid
Department of Mathematics,
Morgan State University,
Baltimore, MD 21239 USA.
Email: smid@ltpsun.gsfc.nasa.gov

Sara A. Solla
CONNECT, The Niels Bohr Institute,
Blegdamsvej 17,Copenhagen 2100, Denmark.

Peter Sollich
Department of Physics,
University of Edinburgh,
Edinburgh EH9 3JZ, UK.
Email: P.Sollich@ed.ac.uk

David McG. Squire
School of Computing,
Curtin University of Technology,
Perth, Western Australia.
Email: squizz@cs.curtin.edu.au

Shin Suzuki
Information Science Research Laboratory,
NTT Basic Research Laboratories,
3-1 Morinosato-Wakamiya,
Atsugi-Shi, Kanagawa Pref., 243-01 Japan.
Email: shin@idea.brl.ntt.jp

G.Tambouratzis
Dept. of Mathematics,
Agricultural Univ.of Athens,
Iera Odos 75,
Athens 118 55, Greece.
Email: giorg_t@ilsp.gr

D.Tambouratzis
Dept. of Mathematics,
Agricultural Univ.of Athens,
Iera Odos 75,
Athens 118 55, Greece.

T.Tambouratzis
Institute of Nuclear Technology - Radiation
Protection, NRCPS "Demokritos",
Aghia Paraskevi 153 10, Greece.

Gregory L. Tarr
Phillips Laboratory,
Kirtland Air Force Base
Albuquerque, New Mexico, USA.
Email: Gtarr@euler.plt.af.mil

J. G. Taylor
Department of Mathematics and
Centre for Neural Networks,
King's College, London WC2R 1LS, UK.

Rua-Huan R. Tsaih
Department of Management
Information Systems,
National Chengchi University,
Taipei, Taiwan, ROC.
Email: tsaih@mis.nccu.edu.tw

Joos Vandewalle
Katholieke Universiteit Leuven,
Dept. of Electrical Engineering,
ESAT-SISTA Kardinaal Mercierlaan 94,
B-3001 Leuven (Heverlee), Belgium.

P. Volf
UTIA The Czech Academy of Sciences,
Prague 8, CZ 180 00 Czech Republic.
Email: volf@utia.cas.cz

M.N. Vrahatis
Department of Mathematics,
University of Patras,
GR-261.10 Patras, Greece.
Email: vrahatis@math.upatras.gr

K. Warwick
Cybernetics Department,
University of Reading, Whiteknights,
Reading RG6 6AY, UK.
Email: kw@cyber.reading.ac.uk

Ansgar H. L. West
Neural Computing Research Group,
Aston University,
Aston Triangle, Birmingham B4 7ET, UK.
Email: A.H.L.West@aston.ac.uk

Christopher K. I. Williams
Neural Computing Research Group,
Department of Computer Science and
Applied Mathematics,
Aston University, Birmingham B4 7ET, UK.
Email: c.k.i.williams@aston.ac.uk

Li-Qun Xu
Intelligent Systems Research Group,
BT Research Laboratories
Martlesham Heath,
Ipswich, IP5 7RE, UK.
Email: xulq@info.bt.co.uk

Howard Hua Yang
Lab for Information Representation,
FRP, RIKEN, 2-1 Hirosawa,
Wako-Shi, Saitama 351-01, Japan.
Email: hhy@murasaki.riken.go.jp

Rafal Zbikowski
Department of Mechanical Engineering,
James Watt Building,
University of Glasgow,
Glasgow G12 8QQ, Scotland, UK.

Assaf J. Zeevi
Electrical Engineering Department,
Technion, Haifa 32000, Israel.

Huaiyu Zhu
Santa Fe Institute,
1399 Hyde Park Road,
Santa Fe, NM87501, USA.
Email: zhuh@santafe.edu

R. Zimmer
Computer Science Department,
Brunel University,
Uxbridge, Middx. UB8 3PH, UK.
Email: Robert.Zimmer@brunel.ac.uk

Dedication

This volume is dedicated to Professor Patrick Parks who died in 1995. Patrick was famous both for his work in nonlinear stability and automatic control and for his more recent contributions to neural networks—especially on learning procedures for CMAC systems. Patrick was known to many as a good friend and colleague, and as a gentleman, and he is greatly missed.

PREFACE

This volume of research papers comprises the proceedings of the first International Conference on Mathematics of Neural Networks and Applications (MANNA), which was held at Lady Margaret Hall, Oxford from July 3rd to 7th, 1995 and attended by 116 people. The meeting was strongly supported and, in addition to a stimulating academic programme, it featured a delightful venue, excellent food and accommodation, a full social programme and fine weather - all of which made for a very enjoyable week.

This was the first meeting with this title and it was run under the auspices of the Universities of Huddersfield and Brighton, with sponsorship from the US Air Force (European Office of Aerospace Research and Development) and the London Mathematical Society. This enabled a very interesting and wide-ranging conference programme to be offered. We sincerely thank all these organisations, USAF-EOARD, LMS, and Universities of Huddersfield and Brighton for their invaluable support.

The conference organisers were John Mason (Huddersfield) and Steve Ellacott (Brighton), supported by a programme committee consisting of Nigel Allinson (UMIST), Norman Biggs (London School of Economics), Chris Bishop (Aston), David Lowe (Aston), Patrick Parks (Oxford), John Taylor (King's College, London) and Kevin Warwick (Reading). The local organiser from Huddersfield was Ros Hawkins, who took responsibility for much of the administration with great efficiency and energy. The Lady Margaret Hall organisation was led by their bursar, Jeanette Griffiths, who ensured that the week was very smoothly run.

It was very sad that Professor Patrick Parks died shortly before the conference. He made important contributions to the field and was to have given an invited talk at the meeting.

Leading the academic programme at the meeting were nine invited speakers. Nigel Allinson (UMIST), Shun-ichi Amari (Tokyo), Norman Biggs (LSE), George Cybenko (Dartmouth), Frederico Girosi (MIT), Stephen Grossberg (Boston), Morris Hirsch (Berkeley), Helge Ritter (Bielefeld) and John Taylor (King's College, London). The supporting programme was substantial; out of about 110 who submitted abstracts, 78 delegates were offered and accepted opportunities to contribute papers. An abundance of relevant topics and areas were therefore covered, which was indeed one of the primary objectives.

The main aim of the conference and of this volume was to bring together researchers and their work in the many areas in which mathematics impinges on and contributes to neural networks, including a number of key applications areas, in order to expose current research and stimulate new ideas. We believe that this aim was achieved. In particular the meeting attracted significant contributions in such mathematical aspects as statistics and probability, statistical mechanics, dynamics, mathematical biology and neural sciences, approximation theory and numerical analysis: alge-

bra, geometry and combinatorics, and control theory. It also covered a considerable range of neural network topics in such areas as learning and training, neural network classifiers, memory based networks, self organising maps and unsupervised learning, Hopfield networks, radial basis function networks, and the general area of neural network modelling and theory. Finally, applications of neural networks were considered in such topics as chemistry, speech recognition, automatic control, nonlinear programming, medicine, image processing, finance, time series, and dynamics. The final collection of papers in this volume consists of 6 invited papers and over 60 contributed papers, selected from the papers presented at the conference following a refereeing procedure of both the talks and the final papers. We seriously considered dividing the material into subject areas, but in the end decided that this would be arbitrary and difficult - since so many papers addressed more than one key area or issue.

We cannot conclude without mentioning some social aspects of the conference. The reception in the atmospheric Old Library at LMH was accompanied by music from a fine woodwind duo, Margaret and Richard Thorne, who had first met one of the organisers during a sabbatical visit to Canberra, Australia! The conference dinner was memorable for preliminary drinks in the lovely setting of the Fellows Garden, excellent food, and an inspirational after-dinner speech by Professor John Taylor. Finally the participants found some time to investigate the local area, including a group excursion to Blenheim Palace.

We must finish by giving further broad expressions of thanks to the many staff at Universities of Huddersfield and Brighton, US Air Force (EOARD), London Mathematical Society, and Lady Margaret Hall who helped make the conference possible. We also thank the publishers for their co-operation and support in the publication of the proceedings. Finally we must thank all the authors who contributed papers without whom this volume could not have existed.

PART I

INVITED PAPERS

N-TUPLE NEURAL NETWORKS

N. M. Allinson and A. R. Kolcz

Department of Electrical Engineering and Electronics, UMIST, Manchester, UK.

The N-Tuple Neural Network (NTNN) is a fast, efficient memory-based neural network capable of performing non-linear function approximation and pattern classification. The random nature of the N-tuple sampling of the input vectors makes precise analysis difficult. Here, the NTNN is considered within a unifying framework of the General Memory Neural Network (GMNN) — a family of networks which include such important types as radial basis function networks. By discussing the NTNN within such a framework, a clearer understanding of its operation and efficient application can be gained. The nature of the intrinsic tuple distances, and the resultant kernel, is also discussed, together with techniques for handling non-binary input patterns. An example of a tuple-based network, which is a simple extension of the conventional NTNN, is shown to yield the best estimate of the underlying regression function, $E(Y|\mathbf{X})$, for a finite training set. Finally, the pattern classification capabilities of the NTNN are considered.

1 Introduction

The origins of the N-tuple neural network date from 1959, when Bledsoe and Browning [1] proposed a pattern classification system that employed random sampling of a binary retina by taking N-bit long ordered samples (i.e., N-tuples) from the retina. These samples form the addresses to a number of memory nodes — with each bit in the sample corresponds to an individual address line. The N-tuple sampling is sensitive to correlations occurring between different regions for a given class of input patterns. Certain patterns will yield regions of the retina where the probability of a particular state of a selected N-tuple will be very high for a pattern class (e.g., predominately 'white' or 'black' if we are considering binary images of textual characters). If a set of exemplar patterns is presented to the retina, each of the N-tuple samples can be thought of as estimating the probability of occurrence of its individual states for each class. A cellular neural network interpretation of N-tuple sampling was provided by Aleksander [2]; and as we attempt to demonstrate in this paper its architecture conforms to what we term as the *General Memory Neural Network* (GMNN). Though the N-tuple neural network is more commonly thought of as a supervised pattern classifier, we will consider first the general problem of approximating a function, f, which exists in a D–dimensional real space, $\mathbb{R}^D$. This function is assumed to be smooth and continuous and that we possess a finite number of sample pairs $\{(\mathbf{x}_i, y_i) : i = 1, 2 \ldots, T\}$. We will further assume that this training data is subject to a noise component, that is $y_i = f(\mathbf{x}_i) + \varepsilon$, where ε is a random error term with zero mean. A variant of the NTNN for function approximation was first proposed by Tattersall *et al* [3] and termed the *Single-Layer-Lookup-Perceptron* (SLLUP). The essential elements of the SLLUP are the same as the basic NTNN except that the nodal memories contain numeric weights. A further extension of the basic NTNN, originally developed by Bledsoe and Bisson [4], records the relative frequencies at which the various nodal memories are addressed during training. The network introduced in Section 4 combines aspects of these two networks and follows directly from the consolidated approach presented in Section 2.

We discuss, in Section 3, some details of the NTNN with particular reference to its mapping between sampled patterns on the retina and the N-tuple distance metric,

and the transformation of non-binary element vectors onto the binary retina. The form of the first mapping, which is an approximately exponential function, is the kernel function of the NTNN — though due to the random nature of the sampling, this must be considered in a statistical sense. Finally, a brief note is given on a Bayesian approximation that indicate how these networks can be employed as pattern classifiers.

2 The General Memory Neural Network

Examples of GMNN include *Radial Basis Function* (RBF) [5] networks and the *General Regression Neural Network* (GRNN) [6]. These networks can provide powerful approximation capabilities and have been subject to rigorous analysis. A further class of networks, of which the NTNN is one, have not been treated to such detailed examination. However, these networks (together with others such as the CMAC [7] and the Multi-Resolution Network [8]) are computationally very efficient and better suited to hardware implementation. The essential architectural components of GMNNs are a layer of memory nodes, arranged into a number of blocks, and an addressing element that selects the set of locations participating in the computation of the output response. An extended version of this section is given in [9].

2.1 Canonical Form of the General Memory Neural Network

The GMNN can be defined in terms of the following elements:

- A set of K memory nodes, each possessing a finite number of $|A_k|$ addressable locations.
- An address generator which assigns an address vector
$$A(\mathbf{x}) = [A_1(\mathbf{x}), A_2(\mathbf{x}), \ldots, A_K(\mathbf{x})]$$
to each input point $\mathbf{x}$. The address generated for the kth memory node is denoted by $A_k(\mathbf{x})$.
- The network's output, g, is obtained by combining the contents of selected memory locations, that is
$$[m_1(A_1(\mathbf{x})), m_2(A_2(\mathbf{x})), \ldots, m_k(A_k(\mathbf{x}))] \rightarrow \mathbb{R}, \quad (1)$$
where $m_k(A_k(\mathbf{x}))$ is the content of the memory location selected by the kth memory node by the address generated by $\mathbf{x}$ for that node (this will be identified as simply $m_k(\mathbf{x})$). No specific format is imposed on the nature of the memories other than that the format is uniform for all K nodes.
- A learning procedure exists which permits the network to adjust the nodal memory contents, in response to the training set, so that some error criterion, $\pi(f, g)$, is minimised.

Each node of the network performs a simple vector quantization of the input space into $|A_k|$ cells. For each node, the address generating element can be split into an *index generator* and an *address decoder*. The index generator, I_k, selects a cell for every $\mathbf{x} \in \Omega$ and assigns it a unique index value, $I_k(\mathbf{x}) \in \{1, 2, \ldots, |A_k|\}$; hence the index generator identifies the quantization cell to which the input points belongs. The address decoder uses this generated index value to specify the physical

memory address which then selects the relevant node k. Hence, $A_k(\mathbf{x}) = A_k(I_k(\mathbf{x}))$. Therefore, a cell, R_i^k, can be defined as the set of all input points which result in the selection of an address corresponding to the ith index of the kth node.

$$R_i^k = \{\mathbf{x} \in \Omega : I_k(\mathbf{x}) = i\} \tag{2}$$

Each of the cells is closed and bounded as the input space is compact in $\mathbb{R}^D$. The selection of a cell is given by the following operator or *activation function*

$$S_i^k(\mathbf{x}) = (I_k(\mathbf{x}) = i) = \begin{cases} 1 & \text{if } \mathbf{x} \in R_i^k : i = 1, \ldots, |A_k| \\ 0 & \text{otherwise} \end{cases} \tag{3}$$

The quantization of Ω performed by the individual nodes is combined, through the intersection of the K cells being superimposed, to yield a global quantizer. The number of cells $|A|$ is given by the number of all such distinct intersections.

$$|A| = \sum_{i_1=1}^{|A_1|} \sum_{i_2=1}^{|A_2|} \cdots \sum_{i_k=1}^{|A_k|} \prod_{k=1}^{K} (\{\mathbf{x} \in \Omega : I_k(\mathbf{x}) = i_k\} \neq \emptyset) \tag{4}$$

The upper bound being given by $|A|_{\max} = \prod_{k=1}^{K} |A_k|$. The address generation element of the network is distributed across the nodes, so that the general structure of Figure 1a emerges. Alternatively, the address generation can be considered at the global level (Figure 1b). These two variants are equivalent.

The quantization of the input space by the network produces values that are constant over each cell (We are ignoring, for the present, external kernel functions). The value of f assigned to the ith cell is normally expressed as the average value of f over the cell.

$$f : R_i \rightarrow \frac{\int_{R_i} d_f(\mathbf{u}) f_x(\mathbf{u})\, d\mathbf{u}}{\int_{R_i} f_x(\mathbf{u})\, d\mathbf{u}}, \tag{5}$$

where d_f is given by the squared error function. In most supervised learning schemes, this representation of $f(R_i)$ is estimated inherently through the minimisation of an error function.

For $K = 1$, the GMNN could be simply replaced to a VQ followed by a look-up table. There would need to be at least one input point per quantization cell. The granularity of the quantization needs to be sufficient to meet the degree of approximation performance appropriate for the required task. When there are multiple nodes ($K > 1$), the quantization at the node level can be much coarser which, in turn, increases the probability of input points lying inside a cell. The fine granularity being achieved through the superposition of nodal quantizers. Learning and generalisation are only possible through the use of multiple nodes. Points that are close to each other in the Ω space should share many addresses, and *vice versa.*

2.2 GMNN Distance Metrics

The *address proximity function*, which quantifies the proximity of points in Ω and so the number of generated identical nodal addresses, is given by

$$\kappa : \Omega^2 \rightarrow \{0, 1, \ldots, K\} \quad \kappa(\mathbf{x}, \mathbf{y}) = \sum_{k=1}^{K} (A_k(\mathbf{x}) = A_k(\mathbf{y})) = \sum_{k=1}^{K} (I_k(\mathbf{x}) = I_k(\mathbf{y})) \tag{6}$$

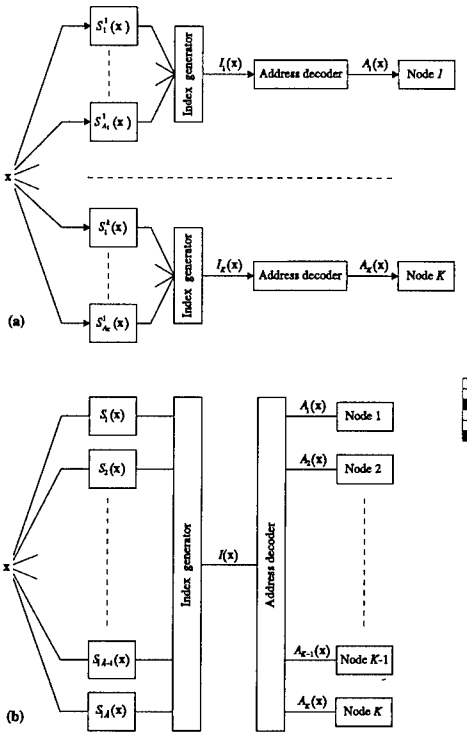

Figure 1 (a) GMNN — address generation considered at the nodal level. (b) GMNN — address generation considered at the global level. These two variants are identical in terms of overall functionality.

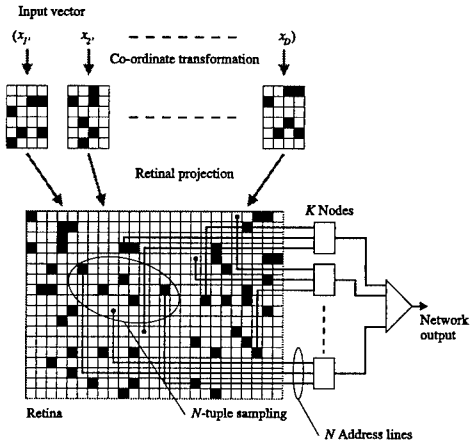

Figure 2 General structure of an NTNN.

The *address distance function*, defined as the number of different generated nodal addresses, is given by

$$\rho : \Omega^2 \rightarrow \{0, 1, \ldots, K\} \quad \rho(\mathbf{x}, \mathbf{y}) = \sum_{k=1}^{K} (A_k(\mathbf{x}) \neq A_k(\mathbf{y})) = \sum_{k=1}^{K} (I_k(\mathbf{x}) \neq I_k(\mathbf{y})) \quad (7)$$

The *binary nodal incidence function*, which returns '1' if two inputs share a common address at a given network node and '0' otherwise, is defined as

$$M_k(\mathbf{x}, \mathbf{y}) = (I_k(\mathbf{x}) = I_k(\mathbf{y})) = \begin{cases} 1 & \Leftrightarrow \quad I_k(\mathbf{x}) = I_k(\mathbf{y}) \\ 0 & \Leftrightarrow \quad I_k(\mathbf{x}) \neq I_k(\mathbf{y}) \end{cases} \quad (8)$$

From these definitions, several properties directly follow.

$$\begin{aligned} \forall(\mathbf{x}, \mathbf{y} \in \Omega) \quad & \rho(\mathbf{x}, \mathbf{x}) = 0 \qquad\qquad \rho(\mathbf{x}, \mathbf{y}) = \rho(\mathbf{y}, \mathbf{x}) \\ & \kappa(\mathbf{x}, \mathbf{x}) = K \qquad\qquad \kappa(\mathbf{x}, \mathbf{y}) = \kappa(\mathbf{y}, \mathbf{x}) \\ & \kappa(\mathbf{x}, \mathbf{y}) = K - \rho(\mathbf{x}, \mathbf{y}) \end{aligned} \quad (9)$$

$$\sum_{k=1}^{K} M_k(\mathbf{x}, \mathbf{y}) = \kappa(\mathbf{x}, \mathbf{y}) \quad (10)$$

2.3 GMNN Error-Based Training

If the address generation elements of the GMNN have been established (based on some *a priori* knowledge about the function to be approximated), then the only element which is modifiable through training is the contents of the nodal memory locations (e.g., the weights). If these locations contain real-valued numbers and the output of the network is formed by summing these numbers, then the response of the GMNN is linear in terms of this weight space. Learning methods based on the minimisation of the square error function are guaranteed to converge under these general circumstances. In the following analysis, we will therefore assume an iterative LMS learning schedule. For a finite training set of T paired samples, the error produced by the network for the jth presentation of the ith training sample is given by

$$y^i - \sum_{k=1}^{K} w_k(\mathbf{x}^i) \tag{11}$$

where $w_k(\mathbf{x}^i)$ is the value of the weight selected by $\mathbf{x}^i$ at the kth node. The participating weights are modified by a value, Δ_j^i, proportional to this error so as to reduce the error.

$$w_k(\mathbf{x}^i) \leftarrow w_k(\mathbf{x}^i) + \Delta_j^i : k = 1, 2, \ldots, K \tag{12}$$

Initially, all weight values are set to zero. As $w_k(\mathbf{x}^i)$ is shared by all points within the neighbourhood $N_k(\mathbf{x}^i)$, this weight updating can affect the network response for points from outside the training set. That is within an input space region given by

$$w_k(\mathbf{x}) \leftarrow w_k(\mathbf{x}) + \Delta_j^i \cdot M_k(\mathbf{x}, \mathbf{x}^i) \tag{13}$$

The output of the network after the training is complete, for an arbitrary $\mathbf{x} \in \Omega$, will depend on all training samples lying within the neighbourhood of $\mathbf{x}$.

$$g(\mathbf{x}) = \sum_{k=1}^{K} w_k(\mathbf{x}) = \sum_{k=1}^{K} \sum_{i=1}^{T} \left(M_k(\mathbf{x}, \mathbf{x}^i) \sum_{j=1}^{T_i} \Delta_j^i \right) \tag{14}$$

Rearranging this expression and using the identity (10), yields

$$g(\mathbf{x}) = \sum_{i=1}^{T} \sum_{j=1}^{T_i} \Delta_j^i \sum_{k=1}^{K} M_k(\mathbf{x}, \mathbf{x}^i) = \sum_{i=1}^{T} \Delta^i \cdot \kappa(\mathbf{x}, \mathbf{x}^i), \text{ where } \sum_{j=1}^{T_i} \Delta_j^i = \Delta^i. \tag{15}$$

We can compare this result with the response of a trained RBF network.

$$g(\mathbf{x}) = \sum_{i=1}^{T} w^i \cdot \kappa(\mathbf{x}, \mathbf{x}^i) \tag{16}$$

For the normalised RBF network, the response is given by

$$g(\mathbf{x}) = \frac{\sum_{i=1}^{T} w^i \cdot \kappa(\mathbf{x}, \mathbf{x}^i)}{\sum_{i=1}^{T} \kappa(\mathbf{x}, \mathbf{x}^i)} \tag{17}$$

and for the GRNN (where the training set response values replace the weight values).

$$g(\mathbf{x}) = \frac{\sum_{i=1}^{T} y^i \cdot \kappa(\mathbf{x}, \mathbf{x}^i)}{\sum_{i=1}^{T} \kappa(\mathbf{x}, \mathbf{x}^i)} \tag{18}$$

Though there are obvious similarities, we can further extend the functionality of the GMNN by incorporating into each nodal memory an integer counter. This nodal counter is incremented whenever the node is addressed, that is $c_k(\mathbf{x}^i) \leftarrow c_k(\mathbf{x}^i) + 1$ (Initially, all counter values are set to zero). Now the response of the GMNN is given by

$$g(\mathbf{x}) = \frac{\sum_{i=1}^{T} \Delta^i \cdot \kappa(\mathbf{x}, \mathbf{x}^i)}{\sum_{i=1}^{T} \kappa(\mathbf{x}, \mathbf{x}^i)} \tag{19}$$

The trained GMNN is equivalent to a set of T units, each centred at one of the training samples, $\mathbf{x}^t$, and possessing height Δ^t and kernel weighting function $\kappa(\cdot, \mathbf{x}^t)$. To complete the equivalence of the GMNN and the GRNN, κ must satisfy the general conditions imposed on kernel functions [10].

2.4 Introduction of External Kernels

The network output is given by the sum of weights corresponding to the selected locations, but the output remains constant over each quantization cell — regardless of the relative position of the input point inside a cell. The network mapping thus becomes discontinuous at the cell boundaries. A solution would be to emphasise weights that correspond to quantization cells that are closer to the current excitation, $\mathbf{x}$, than others. This distance can be defined in terms of the distance between $\mathbf{x}$ and the centroid of R_i^k (where $i = I_k(\mathbf{x})$).

$$d(\mathbf{x}, R_i^k) = d(\mathbf{x}, c_i^k) \tag{20}$$

A smooth, continuous and monotonically decreasing kernel function is then introduced to weight the contributions of the respective nodes to the values of $d(\mathbf{x}, R_i^k(\mathbf{x}))$, where $R_i^k(\mathbf{x})$ is the cell selected by $\mathbf{x}$ for the kth node. The network output now becomes

$$g(\mathbf{x}) = \sum_{k=1}^{K} \sum_{i=1}^{|A_k|} w_i^k \cdot \varphi_i^k(d(\mathbf{x}, R_i^k(\mathbf{x}))) \cdot M_k(c_i^k, \mathbf{x}) \tag{21}$$

A set of $K \cdot |A_k|$ kernel or basis functions can be defined, with centres given by the centroid set $\{c_i^k\}$ and where each kernel has its support truncated to its corresponding quantization region. The network mapping can be expressed as

$$g(\mathbf{x}) = \sum_{k=1}^{K} \sum_{i=1}^{|A_k|} w_i^k \cdot \varphi_i^k(\mathbf{x}) \tag{22}$$

or in its normalised form as

$$g(\mathbf{x}) = \frac{\sum_{k=1}^{K}\sum_{i=1}^{|A_k|} w_i^k \cdot \varphi_i^k(\mathbf{x})}{\sum_{k=1}^{K}\sum_{i=1}^{|A_k|} \varphi_i^k(\mathbf{x})} \tag{23}$$

$\varphi_i^k(\mathbf{x})$ is the kernel function associated with the ith quantization cell of the kth node and truncated to zero at its cell boundaries. Gaussian kernels provide an approximation to this last condition, though B-spline kernels [11] can lead to the total absence of cell discontinuities. The introduction of external weighting kernels is the final step in the GMNN architecture.

3 The N-Tuple Neural Network

The general form of the NTNN was described in the introduction and is shown in Figure 2. The following two sections consider the mapping functions inherent to this network. Namely:

- Conversion of the input vector into the binary format needed for the retina
- Sampling the retina by taking N bit values at a time to the address of one of the K memory nodes.

There is some choice in what form the first of these mappings may take depending on the application, but the retinal N-tuple sampling is common to all NTNNs. Figure 3a indicates how the threshold decision planes of the individual elements of a tuple delineate the input space into discrete regions and why the Hamming distance between tuple values is the obvious choice for a distance metric. Further details of the N-tuple distance metric and input encoding are given in [12, 13].

3.1 Retinal Sampling

The relationship between the number of different addresses generated for two arbitrary inputs, $\mathbf{x}$ and $\mathbf{y}$, and the Hamming distance $H(\mathbf{x},\mathbf{y})$ (i.e., the number of bits for which $\mathbf{x}$ and $\mathbf{y}$ differ) is important as it reveals the nature of the distance metric necessary when a NTNN is used for pattern classification and the form of the kernel for the approximation-NTNN. This relationship can only be expressed in terms of an expectation due the random nature of the sampling. For sampling without repetitions, the expected value of $\rho_{\mathrm{NTNN}}(\mathbf{x},\mathbf{y}) = \rho_{\mathrm{NTNN}}(H)$ is given by

$$E(\rho_{\mathrm{NTNN}}(H)) = K\left(1 - \left(1 - \frac{1}{K}\right)^{H}\right) \tag{24}$$

For small values of H, this can be simplified to

$$E(\rho_{\mathrm{NTNN}}(H)) \approx K\left(1 - \exp\left(-\frac{H}{K}\right)\right) \tag{25}$$

For sampling with repetitions, the expected value is

$$E(\rho_{\mathrm{NTNN}}(H)) = K\left(1 - \exp\left(N \cdot \left(h - \frac{h^2}{2} + \frac{h^3}{3} - \cdots\right)\right)\right) \tag{26}$$

where h is the normalised Hamming distance ($= H/R$). Again, this can be simplified for small values of h, to yield

$$E(\rho_{\mathrm{NTNN}}(H)) \approx K(1 - \exp(-N \cdot h)) \tag{27}$$

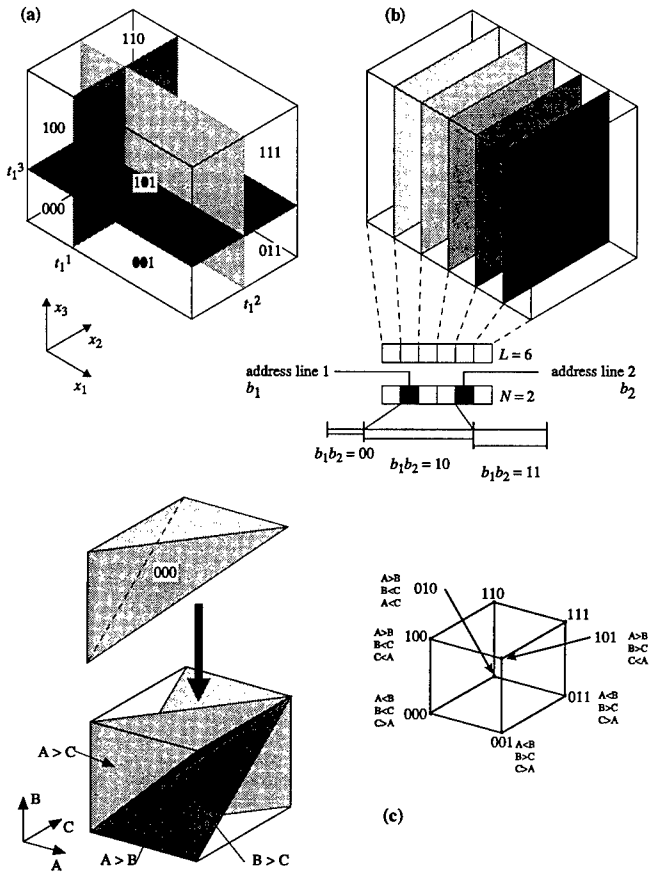

Figure 3 (a) The delineation of input space by the hard decision planes of each tuple element's threshold. Each region is marked by its specific binary state of the 3-tuple, t_1. (b) The thermometer coding inherent in N-tuple sampling. The variable, x_1, is uniformly quantized into six discrete regions ($L = 6$). The indicated 2-tuple partitions this interval into three unequal quantization regions, with the binary state of the 2-tuple indicated. (c) The delineation of the 3-dimensional input space into tetrahedral regions through the use of a ranking code. The binary space representation of the input space is also shown.

There is little difference in the general form of these two sampling methods, though there may be crucial differences in performance for specific tasks. The distance function depends exponentially on the ratio of the Hamming distance, H, between patterns to the retinal size, R. The rate of decrease is proportional to the tuple size.

3.2 Input Encoding

There is a direct and monotonic dependence of ρ_{NTNN} on the Hamming distance in the binary space of the network's retina. For binary patterns, the N-tuple sampling

provides the desired mapping between the input and output addresses. For non-binary input patterns, the situation is not so clear. One obvious solution is to use a thermometer or bar-chart code, where one bit is associated to every level of an input integer. This creates a linear array of 2^n bits for an n-bit long integer. This can produce very large retinas if the input dimensionality and quantization level are large. The use of the natural binary code or Gray code is not feasible. Though these are compact codes, there is no monotonic relationship between input and pattern distances. The concatenation of several Gray codes [3] offers an improvement over a limited region and enhances the dynamic range over the binary and straight Gray code. The exponential dependence of the ρ_{NTNN} on the Hamming distance means that strict proportionality is not required but monotonicity is required within an *active* region of Hamming distances.

The potential of CMAC encoding, and further aspects of input coding methods, are discussed in Kolcz and Allinson [14]. Improvements in the input mapping, which in turn produce a more isotropic kernel, are given in Kolcz and Allinson [15], where rotation and hyper-sphere codings are described. Two further techniques will be briefly introduced here in order to indicate the wide range of possible sampling and coding schemes. Figure 3b shows one input variable, x_1, which is uniformly quantized to six levels and this is sampled by the indicated 2-tuple. The corresponding states of the resultant tuple for the three resulting sub-intervals indicate that thermometer encoding can be inherent in tuple sampling. This concept can be extended to the multivariate case. If the input space, Ω, is a D-dimensional hypercube and each memory node distributes its N address lines among these dimensions, then the space is effectively quantized into $\prod_{d=1}^{D}(N_d+1)$ hyper-rectangular cells. This assumes random sampling, such that there are N_d address lines per input dimensions (where $N_d = N/D$). The placement of tuples can be very flexible (i.e., uniform quantization is not essential) and the sampling process can take into account the density of training points within the input space.

In rank-order coding, the non-binary N-tuple is transformed to a tuple of ranked values (e.g., $\langle 20, 63, 40, 84, 122, 38\rangle$ becomes, in ascending order, the ranked tuple $\langle 0, 3, 2, 4, 5, 1\rangle$). Each possible ordering is assigned a unique consecutive ranking number, which is converted to binary format and then used as the retinal input. Rank-order coding produces an equal significance code. The use of these relationships is equivalent to delineating the input space into hyper-tetrahedrons rather than the usual hyper-rectangles (Figure 3c).

4 N-tuple Regression Network

The framework for GMNN proposed earlier together with the derivation the tuple distance metric are employed here in the development of a modified NTNN which operates as a non-parametric regression estimator. The formal derivation of this network and that the N-tuple kernel is a valid one for estimating the underlying probability function is given in Kolcz and Allinson [16]. The purpose of this section is to show the relative simplicity of this network compared with other implementations.

During the training phase, the network is presented with T data pairs, $(\mathbf{x}^i, y^i)$, where $\mathbf{x}^i$ is the D-dimensional input vector and y^i is the corresponding scalar output of the system under consideration. The input vector is represented by a

unique selection of the K tuple addresses with their associated weight and counter values.

$$\mathbf{x} \rightarrow \begin{cases} \{t_1(\mathbf{x}), t_2(\mathbf{x}), \ldots, t_K(\mathbf{x})\} \\ \{w_1(\mathbf{x}), w_2(\mathbf{x}), \ldots, w_K(\mathbf{x})\} \\ \{a_1(\mathbf{x}), a_2(\mathbf{x}), \ldots, a_K(\mathbf{x})\} \end{cases} \tag{28}$$

During training, each addressed tuple location is updated according to

$$w_k(\mathbf{x}^i) \leftarrow w_k(\mathbf{x}^i) + y^i \text{ and } a_k(\mathbf{x}^i) \leftarrow a_k(\mathbf{x}^i) + 1 \quad \text{for } i = 1, 2, \ldots, T \text{ and } k = 1, 2, \ldots, K \tag{29}$$

Initially all weight and counter values are set to zero. After training, the network output, $\hat{y}(\mathbf{x})$, is obtained from

$$\hat{y}(\mathbf{x}) = \frac{\sum_{k=1}^{K} w_k(\mathbf{x})}{\sum_{k=1}^{K} a_k(\mathbf{x})} \tag{30}$$

An additional condition is where all addressed locations are zero. In this case, the output is set to zero.

$$\sum_{k=1}^{K} a_k(\mathbf{x}) = 0 \rightarrow \hat{y}(\mathbf{x}) = 0 \tag{31}$$

Figure 4 shows the modifications needed to a conventional NTNN to form the N-

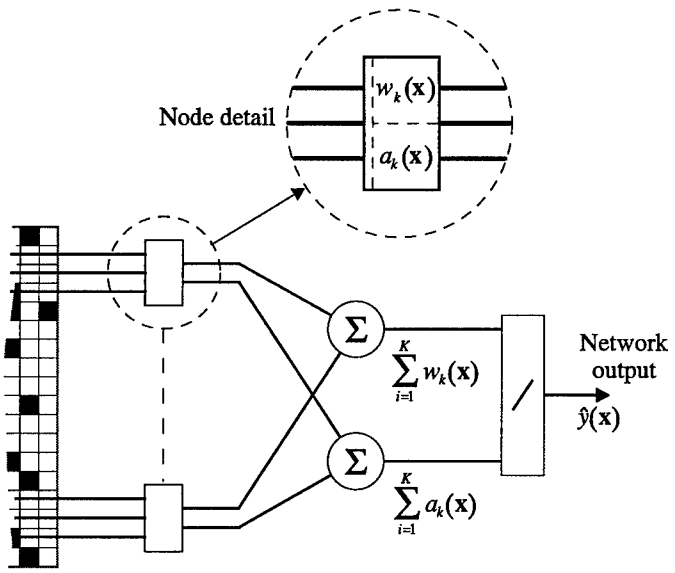

Figure 4 Modifications to the nodes and output elements of the NTNN to yield the N-tuple regression network.

tuple regression network. By considering the tuple distances between inputs, as

defined in terms of the number of different tuple addresses generated, then (30) can be extended to

$$\hat{y}(\mathbf{x}) = \frac{\sum_{k=1}^{K} w_k(\mathbf{x})}{\sum_{k=1}^{K} a_k(\mathbf{x})} = \frac{\sum_{i=1}^{T} y^i \cdot \left(1 - \frac{\rho(\mathbf{x}, \mathbf{x}^i)}{K}\right)}{\sum_{i=1}^{T} \left(1 - \frac{\rho(\mathbf{x}, \mathbf{x}^i)}{K}\right)} \tag{32}$$

This suggests that the network output is an approximate solution of the generalised regression function, $E(Y|\mathbf{x})$, provided that the bracketed term in (32) is a valid kernel function. This function is continuous, symmetrical, non-negative and possesses finite support. These are all necessary conditions. A close approximation (based on the exponential approximation of tuple distances) is also representable as a product of univariate kernel functions. Taken together these provide sufficient conditions for a valid kernel function [17]. A wide ranging set of experiments on chaotic time-series prediction and non-linear system modelling has been conducted [16], which confirm the successful operation of this network. A major advantage of the NTNN implementation over other approaches is its fast, and fixed, speed of operation. Each recall operation involves addressing a fixed number of locations. There is no need for preprocessing large data sets, through data clustering, as is often the case for RBF networks [18].

5 Pattern Classification

So far we have restricted our considerations to the approximation properties of the NTNN, but the other major application — namely, pattern classification — can be discussed within this common framework. The training phase of a supervised network provides estimates of the conditional probabilities of individual pattern classes. The class membership probabilities can be formulated through the Bayes relationship, i.e.,

$$P(\mathbf{x} \in c) = \frac{P(\mathbf{x}|c)P(c)}{P(\mathbf{x})} \tag{33}$$

where c is the class label for a particular class $\{c = 1, 2, \ldots, C\}$. The modified NTNN discussed in Section 4 can be reformulated in terms of this classification. The network through training approximates C indicator functions, which denote membership to an individual class.

$$I_c(\mathbf{x}) = \begin{cases} 1 & \text{if } x \subset c \\ 0 & \text{otherwise} \end{cases} \tag{34}$$

Modifying (32), the indicator functions can be approximated, after training, by

$$I_c(\mathbf{x}) = \frac{\sum_{i=1}^{T} (\mathbf{x}^i \subset c)(1 - \rho(\mathbf{x}, \mathbf{x}^i)/K)}{\sum_{i=1}^{T} (1 - \rho(\mathbf{x}, \mathbf{x}^i)/K)} = \frac{\sum_{k=1}^{K} w_k^c}{\sum_{k=1}^{K} a_k} \equiv P(c) \frac{\sum_{k=1}^{K} P(t_k|c)}{\sum_{k=1}^{K} P(t_k)} \tag{35}$$

This relationship gives the ratio of the cumulative summation of all training points belonging to a class c, which have an N-tuple distance at $0, 1, \ldots, (K-1)$ from $\mathbf{x}$ to a similar cumulative summation for all training points. The decision surfaces

present in the K-dimensional weight space are described by $\sum_{k=1}^{K} w_k = \text{const}$, and the winning class is given by $c_{\text{winner}} = \max_{c=1,2,\ldots,C} \sum_{k=1}^{K} w_k^c$.

6 Conclusions

The unifying approach proposed for a wide class of memory-based neural networks means that practical, but poorly understood, networks (such as the NTNN) can be considered in direct comparison with networks (such as RBF networks) that possess a much firmer theoretical foundation. The random sampling inherent in the N-tuple approach makes detailed analysis difficult so this link is all the more important. The pragmatic advantages of NTNNs has been demonstrated in the regression network described above, where large data-sets can be accommodated with fixed computational overheads. The possible range of input sampling and encoding strategies has been illustrated, but by no means exhaustively. There is still a need to seek other strategies that will provide optimum kernel functions for specified recognition or approximation tasks. The power and flexibility of Bledsoe and Browning's original concept has not, as yet, been fully exploited.

REFERENCES

[1] Bledsoe W W and Browning I, *Pattern recognition and reading by machine*, IRE Joint Computer Conference, 1959, 225–232.

[2] Aleksander I, *Fused adative circuit which learns by example*, Electronics Letters, 1965, 1, 173–174.

[3] Tattersall G D, Foster S and Johnston R D, *Single-layer lookup perceptrons*, IEE Proceedings — F: Radar and Signal Processing, 1991, 138, 46–54.

[4] Bledsoe W W and Bisson C L, *Improved memory matrices for the N-tuple pattern recognition method*, IRE Transactions on Electronic Computers, 1962, 11, 414–415.

[5] Broomhead D S and Lowe D, *Multivariable functional interpolation and adaptive networks*, Complex Systems, 1988, 2, 321–355.

[6] Specht D F, *A general regression neural network*, IEEE Transactions on Neural Networks, 1991, 2, 568–576.

[7] Albus J S, *A new approach to manipulator control: the cerebellar model articulation controller (CMAC)*, Journal of Dynamic Systems, Measurement and Control, 1975, 97, 220–227.

[8] Moody J, *Fast learning in multi-resolution hierarchies*, in Advances in Neural Information Processing 1 (Touretzky D S, ed.), 1989, Morgan Kaufmann: San Mateo, CA, 29–39.

[9] Kolcz A and Allinson N M, *General Memory Neural Network — extending the properties of basis networks to RAM-based architectures*, 1995 IEEE International Conference on Neural Networks, Perth, Western Australia.

[10] Park J and Sandberg, I W, *Universal approximation using radial basis function networks*, Neural Computation, 1991, 3, 246–257.

[11] Kavli T, *ASMOD - an algorithm for adaptive modelling of observational data*, International Journal of Control, 1993, 58, 947–967.

[12] Kolcz A and Allinson N M, *Application of the CMAC-input encoding scheme in the N-tuple approximation network*, IEE Proceedings - E Computers and Digital Techniques, 1994, 141, 177–183.

[13] Kolcz A and Allinson N M, *Enhanced N-tuple approximators*, Proceedings of Weightless Neural Network Workshop 93, 1993, 38–45.

[14] Allinson N M and Kolcz A, *The theory and practice of N-tuple neural networks*, in Neural Networks (Taylor J G, ed.), 1995, Alfred Waller, 53–70.

[15] Kolcz A and Allinson N M, *Euclidean mapping in an N-tuple approximation network*, Sixth IEEE Digital Signal Processing Workshop, 1994, 285–289.

[16] Kolcz A and Allinson N M, *N-tuple regression network*, Neural Networks vol 9 No.5 pp855-870.

[17] Parzen E, *On estimation of a probability density function and mode*, Annals of Mathematical Statistics, 1962, 33, 1065–1076.

[18] Moody J and Darken C J, *Fast learning in networks of locally-tuned processing units*, Neural Computation, 1989, 1, 281–294.

INFORMATION GEOMETRY OF NEURAL NETWORKS —AN OVERVIEW—

Shun-ichi Amari

University of Tokyo, Tokyo, Japan, RIKEN Frontier Research Program, Wako-City, Saitama, Japan. Email: amari@sat.t.u-tokyo.ac.jp

The set of all the neural networks of a fixed architecture forms a geometrical manifold where the modifable connection weights play the role of coordinates. It is important to study all such networks as a whole rather than the behavior of each network in order to understand the capability of information processing of neural networks. What is the natural geometry to be introduced in the manifold of neural networks? Information geometry gives an answer, giving the Riemannian metric and a dual pair of affine connections. An overview is given to information geometry of neural networks.

1 Introduction to Neural Manifolds

Let us consider a neural network of fixed architecture specified by parameters $\boldsymbol{w} = (w_1, \cdots, w_p)$ which represent the connection weights and thresholds of the network. The parameters are usually modifiable by learning. The set N of all such networks is considered a p-dimensional neural manifold, where $\boldsymbol{w}$ is a coordinate system in N. Because it includes all the possible networks belonging to that architecture, the total capabilities of the networks are made clear by studying the manifold N itself. To be specific, let N be the set of multilayer feedforward networks each of which receives an input $\boldsymbol{x}$ and emits an output $\boldsymbol{z}$. The input-output relation is described as

$$\boldsymbol{z} = \boldsymbol{f}(\boldsymbol{x}; \boldsymbol{w})$$

where the total output $\boldsymbol{z}$ depends on $\boldsymbol{w}$ which describes all the connection weights and thresholds of the hidden and output neurons. Let us consider the space S of all the square integrable functions of $\boldsymbol{x}$

$$S = \{\boldsymbol{k}(\boldsymbol{x})\}$$

and assume for the moment that $\boldsymbol{f}(\boldsymbol{x}; \boldsymbol{w})$ is square integrable. The set S is infinite-dimensional L_2 space, and the neural manifold N is a part of it, that is, a p-dimensional subspace embedded in S. This shows that not all the functions are realizable by neural networks.

Given a function $\boldsymbol{k}(\boldsymbol{x})$, we would like to find a neural network whose behavior $\boldsymbol{f}(\boldsymbol{x}; \boldsymbol{w})$ approximates $\boldsymbol{k}(\boldsymbol{x})$ as well as possible. The best approximation is given by projecting $\boldsymbol{k}(\boldsymbol{x})$ to N in the entire space S. The approximation power depends on the shape of N in S. This shows that geometrical considerations are important.

When the behavior of a network is stochastic, it is given by the conditional probability $p(\boldsymbol{z}|\boldsymbol{x}; \boldsymbol{w})$ of $\boldsymbol{z}$ conditioned on input $\boldsymbol{x}$, where $\boldsymbol{w}$ is the network parameters. A typical example is a network composed of binary stochatic neurons: The probability $z = 1$ of such a stochastic neuron is given by

$$\text{Prob}\{z = 1; \boldsymbol{w}\} = \frac{\exp\{\boldsymbol{w} \cdot \boldsymbol{x}\}}{1 + \exp\{\boldsymbol{w} \cdot \boldsymbol{x}\}}, \tag{1}$$

where $z = 0$ or 1. Another typical case is a noise-contaminated network whose output $\boldsymbol{z}$ is written as

$$\boldsymbol{z} = \boldsymbol{f}(\boldsymbol{x}; \boldsymbol{w}) + \boldsymbol{n}, \tag{2}$$

where $\boldsymbol{n}$ is a random noise independent of $\boldsymbol{w}$. If $\boldsymbol{n}$ is subject to the normal distribution with mean 0 and covariance $\sigma^2 I$, I being the identity matrix,

$$\boldsymbol{n} \sim N(0, \sigma^2 I),$$

the conditional probability is given by

$$p(\boldsymbol{z}|\boldsymbol{x}; \boldsymbol{w}) = \text{const} \ \exp\left\{-\frac{[\boldsymbol{z} - \boldsymbol{f}(\boldsymbol{x}, \boldsymbol{w})]^2}{2\sigma^2}\right\}. \tag{3}$$

When input signals $\boldsymbol{x}$ are produced independently from a distribution $q(\boldsymbol{x})$, the joint distribution of $(\boldsymbol{x}, \boldsymbol{z})$ is given by

$$p(\boldsymbol{x}, \boldsymbol{z}; \boldsymbol{w}) = q(\boldsymbol{x}) p(\boldsymbol{z}|\boldsymbol{x}; \boldsymbol{w}). \tag{4}$$

Let S be the set of all the conditional probability distributions (or joint distributions). Let $q(\boldsymbol{z}|\boldsymbol{x})$ be an arbitrary probability distribution in S which is to be approximated by a stochastic neural network of the behavior $p(\boldsymbol{z}|\boldsymbol{x}; \boldsymbol{w})$. The neural manifold N consists of all the conditional probability distributions $p(\boldsymbol{z}|\boldsymbol{x}; \boldsymbol{w})$ (or the joint probability distributions $p(\boldsymbol{x}, \boldsymbol{z}; \boldsymbol{w})$) and is a p-dimensional submanifold of S. A fundamental question arises : What is the natural geometry of S and N? How should the distance between two distributions be measured? What is the geodesic connecting two distributions? It is important to have a definite answer to these problems not only for studying stochastic networks but also for deterministic networks which are not free of random noises and whose stochastic interpretation is sometimes very useful. Information geometry ([3], [17]) answers all of these problems.

2 A Short Review of Information Geometry

Let us consider probability distributions $p(\boldsymbol{y}, \boldsymbol{\xi})$ of random variable $\boldsymbol{y}$, where $\boldsymbol{\xi} = (\xi_1, \cdots, \xi_n)$ is the parameters to specify a distribution. When $\boldsymbol{y}$ is a scalar and normally distributed, we have

$$p(y, \boldsymbol{\xi}) = \frac{1}{\sqrt{2\pi}\sigma} \exp\left\{-\frac{(y-\mu)^2}{2\sigma^2}\right\},$$

where $\boldsymbol{\xi} = (\mu, \sigma)$ is the parameters to specify it. When y is discrete, taking values on $\{0, 1, \cdots, n\}$, we have

$$\text{Prob}\{y, \boldsymbol{\xi}\} = \sum_{i=1}^{n} \xi_i \delta_i(y) + \left(1 - \sum_{i=1}^{n} \xi_i\right) \delta_0(y)$$

where $\delta_i(y) = 1$ when $y = i$ and is equal to 0 otherwise and $\xi_i = \text{Prob}\{y = i\}$.
Let S be the set of such distributions

$$S = \{p(\boldsymbol{y}, \boldsymbol{\xi})\}$$

specified by $\boldsymbol{\xi}$. Then, S can be regarded as an n-dimensional manifold, where $\boldsymbol{\xi}$ is a coordinate system. If we can introduce a distance measure between two nearby points specified by $\boldsymbol{\xi}$ and $\boldsymbol{\xi} + d\boldsymbol{\xi}$ by the quadratic form

$$|d\boldsymbol{\xi}|^2 = \sum_{i,j} g_{ij}(\boldsymbol{\xi}) d\xi_i d\xi_j, \tag{5}$$

the manifold S is said to be Riemannian. The quantity $\{g_{ij}(\boldsymbol{\xi})\}$ is the Riemannian metric tensor. Another important concept is the affine connection by which a geodesic line (an extention of the concept of the straight line in the Euclidean

geometry) is defined. The affine connection is defined by the covariant derivative, and is represented by the three-index parameters $\Gamma_{ijk}(\boldsymbol{\xi})$ formally defined by

$$\Gamma_{ijk} = \langle \nabla_{\boldsymbol{e}_i} \boldsymbol{e}_j, \boldsymbol{e}_k \rangle \tag{6}$$

where $\boldsymbol{e}_i = \partial/\partial\xi_i$ is the natural basis vector field, $\langle \cdot, \cdot \rangle$ is the inner product and ∇ is the covariant derivative. The metric tensor is written as

$$\langle \boldsymbol{e}_i, \boldsymbol{e}_j \rangle = g_{ij}. \tag{7}$$

In the Riemannian geometry, the Levi-Civita connection

$$\Gamma^{(0)}_{ijk} = \frac{1}{2}\left(\frac{\partial}{\partial\xi_i} g_{jk} + \frac{\partial}{\partial\xi_j} g_{ik} - \frac{\partial}{\partial\xi_k} g_{ij}\right) \tag{8}$$

is used usually. This is the only torsion-free metric connection satisfying

$$X\langle Y, Z\rangle = \langle \nabla_X Y, Z\rangle + \langle Y, \nabla_X Z\rangle, \tag{9}$$

for vector fieds, X, Y and Z. More intuitively, a geodesic is the minimum distance curve connecting two points under the Levi-Civita connection.

Information geometry ([3], [17]) defines a new pair of affine connections given, respectively, by

$$\Gamma^{(e)}_{ijk}(\boldsymbol{\xi}) = \Gamma^{(0)}_{ijk} - \frac{1}{2} T_{ijk}, \tag{10}$$

$$\Gamma^{(m)}_{ijk}(\boldsymbol{\xi}) = \Gamma^{(0)}_{ijk} + \frac{1}{2} T_{ijk}, \tag{11}$$

where $T_{ijk}(\boldsymbol{\xi})$ is the tensor defined by

$$T_{ijk} = E\left[\frac{\partial}{\partial\xi_i}\log p \frac{\partial}{\partial\xi_j}\log p \frac{\partial}{\partial\xi_k}\log p\right]. \tag{12}$$

They are called the e- and m-connection, respectively, and are dual in the sense of

$$X\langle Y, Z\rangle = \langle \nabla^{(e)}_X Y, Z\rangle + \langle Y, \nabla^{(m)}_X Z\rangle. \tag{13}$$

The duality of connections is a new concept given rise to by information geometry. When a manifold has a dually flat structure in the sense that the e- and m-Riemann-Christoffel curvature vanish (but the Levi-Civita connection has non-vanishing curvature in general), it has remarkable properties that are dual extensions of Euclidean properties. Exponential families of probability distributions are proved to be dually flat. Intuitively speaking, the set of all the probability distributions $\{p(\boldsymbol{y})\}$ are dually flat, and any parameterized model $S = \{p(\boldsymbol{y}, \boldsymbol{\xi})\}$ is a flat or curved submanifold embedded in it. Hence, it is important to study properties of the dually flat manifold.

When S is dually flat, the divergence function

$$D(\boldsymbol{\xi} : \boldsymbol{\xi}') = \int p(\boldsymbol{y}, \boldsymbol{\xi}) \log \frac{p(\boldsymbol{y}, \boldsymbol{\xi})}{p(\boldsymbol{y}, \boldsymbol{\xi}')} d\boldsymbol{y} \tag{14}$$

is naturally and automatically introduced to S. This is an extension of the square of the Riemannian distance, because it satisfies

$$D(\boldsymbol{\xi} : \boldsymbol{\xi} + d\boldsymbol{\xi}) = \frac{1}{2}\sum g_{ij}(\boldsymbol{\xi}) d\xi_i \xi_j. \tag{15}$$

The divergence satisfies $D(\boldsymbol{\xi}, \boldsymbol{\xi}') \geq 0$ with equality when and only when $\boldsymbol{\xi} = \boldsymbol{\xi}'$. But it is not symmetric in general.

We have the generalized Pythagorus theorem.

Theorem 1 *Let ξ_1, ξ_2 and ξ_3 be three distributions in a dually flat manifold. Then, when the m-geodesic connecting ξ_1 and ξ_2 is orthogonal at ξ_2 to the e-geodesic connecting ξ_2 and ξ_3,*

$$D(\xi_1 : \xi_2) + D(\xi_2 : \xi_3) = D(\xi_1 : \xi_3). \tag{16}$$

The projection theorem is a consequence of this theorem.

Theorem 2 *Let M be a submanifold embedded in a dually flat manifold S. Let P be a point in S, and let $\hat{Q}_P$ is the point in M that minimizes $D(P : Q)$, $Q \in M$, that is, the point in M that gives the best approximation to P. Then, the $\hat{Q}_P$ is the m-geodesic projection of Q to M.*

These properties are applied to various fields of information sciences such as statistics ([3], [11], [16], information theory ([5],[9], control systems theory ([4],[19]), dynamical systems ([14],[18]) etc. It is also useful for neural networks ([6], [10], [7]). We will show how it is applied to neural networks.

3 Manifold of Feedforward Networks and EM Algorithm

In the begining, we show a very simple case of the manifold M of simple stochastic perceptrons or single stochastic neurons. It receives input $\boldsymbol{x}$ and emits a binary output z stochastically, based on the weighted sum $\boldsymbol{w} \cdot \boldsymbol{x}$ of input $\boldsymbol{x}$. The conditional probability of z is written as

$$p(z|\boldsymbol{x}; \boldsymbol{w}) = \frac{e^{z\boldsymbol{w}\cdot\boldsymbol{x}}}{1 + e^{\boldsymbol{w}\cdot\boldsymbol{x}}}. \tag{17}$$

The joint distribution is given by

$$p(\boldsymbol{x}, z; \boldsymbol{w}) = q(\boldsymbol{x})p(z|\boldsymbol{x}; \boldsymbol{w}). \tag{18}$$

Here, we assume that $q(\boldsymbol{x})$ is the normal distribution $N(0, I)$ with mean 0 and covariance metrix I, the identity matrix.

Let M be the set of all the stochastic perceptrons. Since a perceptron is specified by a vector $\boldsymbol{w}$, M is regarded as a manifold homeomorphic to $\boldsymbol{R}^n$ where n is the dimensions of $\boldsymbol{x}$ and $\boldsymbol{w}$. Here, $\boldsymbol{w}$ is a coordinate system of M. We introduce a natural Riemannian geometric structure to M. Then, it is possible to define the distance between two perceptrons, the volume of M itself, and so on. This is done through the Fisher information, since each point (perceptron) in M is regarded as a probability distribution (18). Let $G(\boldsymbol{w}) = \{g_{ij}(\boldsymbol{w})\}$ be a matrix representing the Riemannian metric tensor at point $\boldsymbol{w}$. We define the Riemannian metric by the Fisher information matrix,

$$g_{ij}(\boldsymbol{w}) = E\left[\frac{\partial}{\partial w_i}\log p(z, \boldsymbol{x}; \boldsymbol{w})\frac{\partial}{\partial w_j}\log p(z, \boldsymbol{x}; \boldsymbol{w})\right], \tag{19}$$

where E denotes the expectation over $(z, \boldsymbol{x})$ with respect to the distribution $p(z, \boldsymbol{x}; \boldsymbol{w})$. In order to calculate the metric G explicitly, let $\boldsymbol{e_w}$ be the unit column vector in the direction of $\boldsymbol{w}$ in the Euclidean space $\boldsymbol{R}^n$,

$$\boldsymbol{e_w} = \frac{\boldsymbol{w}}{|\boldsymbol{w}|},$$

where $|\boldsymbol{w}|$ is the Euclidean norm, and $\boldsymbol{e}_{\boldsymbol{w}}^T$ its transpose. We then have the following theorem.

Theorem 3 *The Fisher information metric is given by*

$$g(\boldsymbol{w}) = c_1(w)I + \{c_2(w) - c_1(w)\}\boldsymbol{e}_{\boldsymbol{w}}\boldsymbol{e}_{\boldsymbol{w}}^T, \tag{20}$$

where $w = |\boldsymbol{w}|$ *(Euclidean norm) and* $c_1(w)$ *and* $c_2(w)$ *are given by*

$$c_1(w) = \frac{1}{\sqrt{2\pi}} \int f(w\varepsilon)\{1 - f(w\varepsilon)\} \exp\left\{-\frac{1}{2}\varepsilon^2\right\} d\varepsilon, \tag{21}$$

$$c_2(w) = \frac{1}{\sqrt{2\pi}} \int f(w\varepsilon)\{1 - f(w\varepsilon)\}\varepsilon^2 \exp\left\{-\frac{1}{2}\varepsilon^2\right\} d\varepsilon. \tag{22}$$

The theorem shows that M is a Riemannaian manifold with Riemannian metric $G(\boldsymbol{w})$ which has spherical symmetry. It is remarked that the skewness tensor $T = (t_{ijk})$,

$$t_{ijk} = E\left[\frac{\partial}{\partial w_i}\log p \frac{\partial}{\partial w_j}\log p \frac{\partial}{\partial w_k}\log p\right]$$

vanishes under the distribution $q(\boldsymbol{x}) \sim N(0, I)$. Hence, M is a self-dual Riemannian manifold and no dual affine connections appear in this special case.

We now show some applications of the Riemannian structure.

The volume V_n of the perceptron manifold M is measured by

$$V_n = \int \sqrt{|G(\boldsymbol{w})|}d\boldsymbol{w} \tag{23}$$

where $|G(\boldsymbol{w})|$ is the determinant of $G = (g_{ij})$ which represents the volume density by the Riemanian metric. Let us consider the problem of estimating $\boldsymbol{w}$ from examples. ¿From the Bayesian viewpoint, we consider that $\boldsymbol{w}$ is chosen randomly subject to a prior distribution $p_{\rm pr}(\boldsymbol{w})$. A natural choice of $p_{\rm pr}(\boldsymbol{w})$ is the Jeffrey prior or non-informative prior given by

$$p_{\rm pr}(\boldsymbol{w}) = \frac{1}{V_n}\sqrt{|G(\boldsymbol{w})|}. \tag{24}$$

When one studies learning curve and overtraining ([8]), it is important to take the effect of $p_{\rm pr}(\boldsymbol{w})$ into account. The Jeffrey prior is calculated as follows.

Theorem 4 *The Jeffrey prior and the volume of the manifold are given by*

$$\sqrt{|G(\boldsymbol{w})|} = \frac{1}{V_n}\sqrt{c_2(w)\{c_1(w)\}^{n-1}}, \tag{25}$$

$$V_n = \int \sqrt{c_2(w)\{c_1(w)\}^{n-1}}a_n w^{n-1}dw, \tag{26}$$

respectively, where a_n *is the volume of the unit n-sphere.*

The gradient descent is a well known learning method, which was proposed by Widrow for the analog linear perceptron and extended to non-linear multilayer networks with hidden units ([2],[20] and others). Let $l(\boldsymbol{x}, z; \boldsymbol{w})$ be the loss function when the perceptron with weight $\boldsymbol{w}$ processes an input-output pair $(\boldsymbol{x}, z)$. In many cases, the squared error

$$l(\boldsymbol{x}, z; \boldsymbol{w}) = \frac{1}{2}|z - f(\boldsymbol{w} \cdot \boldsymbol{x})|^2$$

is used. When input-output examples $(\boldsymbol{x}_t, z_t)$, $t = 1, 2, \cdots$, are given, we train the perceptron by the gradient-descent method:

$$\boldsymbol{w}_{t+1} = \boldsymbol{w}_t - c\frac{\partial l(\boldsymbol{x}_t, z_t; \boldsymbol{w}_t)}{\partial \boldsymbol{w}} \tag{27}$$

where $\boldsymbol{w}_t$ is the current value of the weight and it is modified to give $\boldsymbol{w}_{t+1}$ by using the current input-output $(\boldsymbol{x}_t, z_t)$. It was shown that the learning constant c can be replaced by any positive-definite matrix cK ([2]). The natural choice of this matrix is the inverse of the Fisher information metric,

$$\boldsymbol{w}_{t+1} = \boldsymbol{w}_t - cG^{-1}(\boldsymbol{w}_t)\frac{\partial l}{\partial \boldsymbol{w}} \tag{28}$$

from the geometrical point of view, since this is the invariant gradient under general coordinate transformations. However, it is in general not easy to calculate G^{-1} so that this excellent schema is not usually used (see [10]). We can calculate $G^{-1}(\boldsymbol{w})$ explicitly in the perceptron case.

Theorem 5 *The inverse of the Fisher information metric is*

$$G^{-1}(\boldsymbol{w}) = \frac{1}{c_1(w)}I + \left(\frac{1}{c_2(w)} - \frac{1}{c_1(w)}\right)\boldsymbol{e}_{\boldsymbol{w}}\boldsymbol{e}_w^T. \tag{29}$$

This leads to a very simple form of learning

$$\begin{aligned}\boldsymbol{w}_{t+1} &= \boldsymbol{w}_t - c\{z_t - f(\boldsymbol{w}_t.\boldsymbol{x}_t)\}f'(\boldsymbol{w}_t \cdot \boldsymbol{x}_t) \\ &\quad \left[\frac{1}{c_1(w_t)}\boldsymbol{x}_t - \frac{1}{w_t^2}\left(\frac{1}{c_2(w_t)} - \frac{1}{c_1(w_t)}\right)(\boldsymbol{w}_t \cdot \boldsymbol{x}_t)\boldsymbol{w}_t.\right].\end{aligned} \tag{30}$$

This is much more efficient compared to the prevailing simple gradient method. Any acceleration methods can be incorporated with this.

The geometry of the manifold N of multilayer feedforward neural networks can be constructed in principle in the same way. However, it is not so easy to calculate the explicit forms of the metric $g_{ij}(\boldsymbol{w})$ and the connections $\Gamma_{ijk}^{(e)}$ and $\Gamma_{ijk}^{(m)}$. The geometrical structure becomes very complicated because of hidden units.

Neural network researchers sometimes use statistical methods such as the EM algorithm [15]. Information geometry is useful for elucidating such a method [7]. Let $(\boldsymbol{x}, \boldsymbol{y}, \boldsymbol{z})$ be the random variables representing the input, outputs of hidden units and the final output. Let S be the manifold of all the joint probability distributions $q(\boldsymbol{x}, \boldsymbol{y}, \boldsymbol{z})$. The manifold N of the probability distributions $p(\boldsymbol{x}, \boldsymbol{y}, \boldsymbol{z}; \boldsymbol{w})$ realized by the network specified by $\boldsymbol{w}$ forms a submanifold in S.

We want to realize a stochastic input-output relation $q(\boldsymbol{z}|\boldsymbol{x})$ or $q(\boldsymbol{x}, \boldsymbol{z})$ and we do not care about the values $\boldsymbol{y}$ of hidden units so far as the input-output relation is well approximated. All the probability distributions whose marginal distributions are the same, that is, those satisfying

$$\sum_{\boldsymbol{y}} q(\boldsymbol{x}, \boldsymbol{y}, \boldsymbol{z}) = q^*(\boldsymbol{x}, \boldsymbol{z}) \tag{31}$$

form an m-flat submanifold D in S,

$$D_{q^*} = \{q(\boldsymbol{x}, \boldsymbol{y}, \boldsymbol{z}) | \sum_{\boldsymbol{y}} q(\boldsymbol{x}, \boldsymbol{y}, \boldsymbol{z}) = q^*(\boldsymbol{x}, \boldsymbol{z})\}.$$

This is called the data submanifold. The problem of approximation is formulated as follows : Given $q^*(\boldsymbol{x}, \boldsymbol{z})$ obtain the neural network $\boldsymbol{w}^*$ that minimizes $D[q(\boldsymbol{x}, \boldsymbol{y}, \boldsymbol{z}) : p(\boldsymbol{x}, \boldsymbol{y}, \boldsymbol{z}; \boldsymbol{w})]$, that is

$$\min_{q \in D_{q^*},\ p \in N} D[q : p]. \tag{32}$$

Hence, the problem is minimization of the divergence between two submanifolds N and D_{q^*}.

This is iteratively solved as follows:

Step 1 : Given $p_i \in N$, obtain $q_i \in D_{q^*}$ that minimizes $D[q, p_i]$.

Step 2 : Given $q_i \in D_{q^*}$. obtain $p_{i+1} \in N$ that minimizes $D[q_i, p]$.

The step 1 is solved by e-projecting p_i to D_{q^*}. This is equivalent to taking the conditional expectation of hidden variables with respect to p_i. The step 2 is the maximization of the likelihood and is given by m-projecting q_i to N. Hence, the procedure is called the em-algorithm in geometry ([12], [13], [7], [10]) and the EM-algorithm in statistics. The algorithm was shown very effective in the model of mixture of expert nets ([15], and many others). Its geometry was studied by Amari [7]. Xu [21] extended the idea to be applicable to more general neural network learning problems.

4 Manifold of Boltzmann Machines

A Boltzmann machine is a recurrently connected neural network composed of binary stochastic neurons. We show in the beginning a simple Boltzmann machine without hidden units and then study that with hidden units. The behavior of a Boltzmann machine is shown by the following stochastic dynamics : Let $\boldsymbol{x}(t) = (x_1(t), \cdots, x_n(t))$ be the state of the network at time t, where x_i takes on 0 and 1 representing the quiescent and excited states of the ith neuron. At time $t+1$, choose one neuron at random. Let the ith neuron be chosen. Then, the state of the ith neuron changes stochastically by

$$\text{Prob}\{x_i(t+1) = 1\} = \frac{\exp\{u_i\}}{1 + \exp\{u_i\}}, \tag{33}$$

where

$$u_i = \sum_j w_{ij} x_j(t) - w_{i0}, \tag{34}$$

w_{ij} being the connection weights of the ith and jth neurons and w_{i0} being the biasing term of the ith neuron. All the other neurons are unchanged, $x_j(t+1) = x_j(t)$.

The $\boldsymbol{x}(t)$, $t = 1, 2, \cdots$, is a Markov process, and its stationary distribution is explicitly given by

$$p(\boldsymbol{x}, W) = \exp\left\{\frac{1}{2}\sum w_{ij} x_i x_j - \psi(W)\right\} \tag{35}$$

when $w_{ij} = w_{ji}$, $w_{ii} = 0$ hold, where $x_0 = 1$. The set of all the Boltzmann machines forms an $n(n+1)/2$-dimensional manifold B, and $W = \{w_{0i}, w_{ij}, i < j\}$ is a coordinate system of the Boltzmann neural manifold. To each Boltzmann machine W corresponds a probability distribution (35) and vice versa. Therefore, B is identified with the set of all the probability distributions of form (35).

Let S be the set of all the distributions over 2^n states $\boldsymbol{x}$,

$$S = \{q(\boldsymbol{x}) \mid q(\boldsymbol{x}) > 0, \sum_{\boldsymbol{x}} q(\boldsymbol{x}) = 1\}. \tag{36}$$

Then, B is an $n(n+1)/2$-dimensional submanifold embedded in the $(2^n - 1)$-dimensional manifold S. We can show that B is a flat submanifold of S, and that both S and B are dually flat, although they are curved from the Riemannian metric point of view [10].

Given a distribution $q(\boldsymbol{x})$, we train the Boltzmann machine by modifying w_{ij} based on independent examples $\boldsymbol{x}_1, \boldsymbol{x}_2 \cdots$ from the distribution q, for the purpose of obtaining $\hat{W}$ such that $p(\boldsymbol{x}, \hat{W})$ approximates $q(\boldsymbol{x})$ as well as possible. The degree of approximation is measured by the divergence $D[q(\boldsymbol{x}) : p(\boldsymbol{x}, W)]$. The best approximation is given by m-projecting q to B. We have an explicit solution since the manifolds are flat. The stochastic gradient learning was proposed by Ackley, Hinton and Sejnowski [1],

$$W_{t+1} = W_t - \eta \frac{\partial}{\partial W} D[q; p] \tag{37}$$

where the gradient term is not the expectatio form but is evaluated by random example $\boldsymbol{x}_t$. However, from the geometrical poit of view, it is more natural to use

$$W_{t+1} = W_t - \eta G^{-1} \frac{\partial}{\partial W} D[q; p], \tag{38}$$

where G^{-1} is the Fisher information matrix. In this case, the expectation of the trajectory $\hat{W}_t$ of learning is the e-geodesic of B (when the continuous time version is used), see [10]. It is shown that the convergence is much faster in this case, although calculations of G^{-1} are sometimes not easy.

When hidden units exist, we divide $\boldsymbol{x}$ into

$$\boldsymbol{x} = (\boldsymbol{x}^V, \boldsymbol{x}^H), \tag{39}$$

where $\boldsymbol{x}^V$ represents the state of the visible part and $\boldsymbol{x}^H$ represents that of the hidden part. The connection weights are also divided naturally into the three parts $W = (W^V, W^H, W^{VH})$. The probability distribution of the visible part is given by

$$p(\boldsymbol{x}^V; W) = \sum_{\boldsymbol{x}^H} p(\boldsymbol{x}^V, \boldsymbol{x}^H; W). \tag{40}$$

Let S^V and B^V be the manifolds of all the distributions over $\boldsymbol{x}^V$ and those realizable by Boltzmann machines in the form of (40). Then, S^V is flat but B^V is not.

It is easier to treat the extended manifolds of $S^{V,H}$ and $B^{V,H}$ including hidden units. However, only a distribution $q(\boldsymbol{x}^V)$ is specified from the outside in the learning process and its hidden part is not. Let us consider a submanifold

$$D = \{q(\boldsymbol{x}^V, \boldsymbol{x}^H) | \sum_{\boldsymbol{x}^H} q(\boldsymbol{x}^V, \boldsymbol{x}^H) = q(\boldsymbol{x}^V)\}. \tag{41}$$

The submanifold D is m-flat. Because we want to approximate $q(\boldsymbol{x}^V)$ but we do not care about $q(\boldsymbol{x}^H)$ nor the interaction of $\boldsymbol{x}^V$ and $\boldsymbol{x}^H$, the problem reduces to minimizing

$$D[q(\boldsymbol{x}^V, \boldsymbol{x}^H) \ : \ p(\boldsymbol{x}^V, \boldsymbol{x}^H; W)]$$

over all W and $q \in D$, or

$$D[q : p]$$

over all $p \in B^{S,V}$ and $q \in D$. This is the minimization of the divergence between two submanifold D and $B^{S,V}$.

We can use the geometric *em* algorithm which is equivalent to the statistical EM algorithm in this case, too. Since D is m-flat and $B^{S,V}$ is e-flat, the problem is relatively easy to solve (see [7]).

5 Conclusion

We have shown the framework of the information-geometrical method of neural networks. Information geometry has originated from the research on statistical manifolds or families of probability distributions. It proposes a new geometrical notion of the duality of affine connections. It has successfully been applied to statistics, information theory, control systems theory and many others. Neural networks research is one of the promissing fields of applications of information geometry. Its research has just started with expectation that it opens new perspectives to neural networks

REFERENCES

[1] Ackley, D., Hinton, G., and Sejnowski, T., *A learning algorithm for Boltzmann machines*, Cognitive Science, Vol. 9 (1985), pp147–169.

[2] Amari, S., *Theory of adaptive pattern classifiers*, IEEE Trans., Vol. EC-16 (1967), pp299–307.

[3] Amari, S., *Differential-Geometircal Methods in Statistics*, Springer-Verlag, New York (1985).

[4] Amari, S., *Differential geometry of a parametric family of invertible linear systems — Riemannian metric, dual affine connections and divergence*, Mathematical Systems Theory, Vol. 20 (1987), pp53–82.

[5] Amari, S., *Fisher information under restriction of Shannon information in multiterminal situations*, Annals of Institute of Statistical Mathematics, Vol. 41 (1989), pp623–648.

[6] Amari, S., *Dualistic geometry of the manifold of higher-order neurons*, Neural Networks, Vol. 4 (1991), pp443-451.

[7] Amari, S., *Information geometry of EM and em algorithms for neural networks*, Neural Networks, Vol. 8 (1995), No.5.

[8] Amari, S., Murata, N., Müller, K.-R., Finke, M. and Yang, H., *Asymptotic statistical theory of overtraining and cross-validation*, IEEE Trans. NN, submitted (1995).

[9] Amari, S. and Han, T.S., *Statistical inference under multi-terminal rate restrictions — a differential geometrical approach*, IEEE Trans. on Information Theory, Vol. IT-35 (1989), pp217–227.

[10] Amari, S., Kurata, K. and Nagaoka, H., *Information geometry of Boltzmann machines*, IEEE Trans. Neural Networks, Vol. 3 (1992), pp260-277.

[11] Barndorff-Nielsen, O.E., Cox, R.D., and Reid, N., *The role of differential geometry in statistical theory*, International Statistical Review, Vol. 54 (1986), pp83–96.

[12] Csiszár, I., *I-divergence geometry of probability distributions and minimization problems*, Annals of Probability, Vol. 3 (1975), pp146–158.

[13] Csiszár, I. and Tusnády, G., *Information geometry and alternating minimization procedures*, in E.F. Dedewicz, et al. (eds), Statistics and Decisions (Supplementary Issue, No.1 (1984), pp205–237), Munich: Oldenburg Verlag.

[14] Fujiwara, A. and Amari, S., *Dualistic dynamical systems in the framework of information geometry*, Physica D, Vol. 80 (1995), pp317–327.

[15] Jordan, M.I. and Jacobs, R.A., *Higherarchical mixtures of experts and the EM-algorithm*, Neural Computation, Vol. 6 (1994), pp181–214.

[16] Kass, R. E., *The geometry of asymptotic inference (with discussions)*, Statistical Science, Vol. 4 (1989), pp188–234.

[17] Murray, M.K. and Rice, J.W., *Differential Geometry and Statistics*, Chapman & Hall (1993).

[18] Nakamura, Y., *A tau-function for the finite Toda molecule, and information spaces*, Contemporary Mathematics, Vol. 179 (1994), pp205–211.

[19] Ohara, A. and Amari, S., *Differential geometric structures of stable state feedback systems with dual connections*, Kybernetika, Vol. 30 (1994), pp369–386.

[20] Rumelhart, D., Hinton, G.E. and Williams, R.J., *Learning internal representations by error propagation*, in: Parallel Distributed Processing: Explorations in the Microstructure of Cognition, Vol.Vol. 1, Foundations, MIT Press (1986), Cambridge, MA.

[21] Xu, L., *YING-YANG machine: A Bayesian-Kullback scheme for unified learnings and new results on vector quantization*, Proc. ICONIP'95-Beijing (1995).

Q-LEARNING: A TUTORIAL AND EXTENSIONS

George Cybenko, Robert Gray and Katsuhiro Moizumi

Thayer School of Engineering, 8000 Cummings Hall, Dartmouth College, Hanover, NH 03755 USA. Email: gvc@dartmouth.edu

In the past decade, research in neurocomputing has been divided into two relatively well-defined tracks: one track dealing with cognition and the other with behavior. Cognition deals with organizing, classifying and recognizing sensory stimuli. Behavior is more dynamic, involving sequences of actions and changing interactions with an external environment. The mathematical techniques that apply to these areas, at least from the point of neurocomputing, appear to have been quite separate as well. The purpose of this paper is to give an overview of some recent powerful mathematical results in behavioral neurocomputing, specifically the concept of Q-learning due to C. Watkins, and some new extensions. Finally, we propose ways in which the mathematics of cognition and the mathematics of behavior can move closer to build more unified systems of information processing and action.

1 Introduction

The study of artificial neural networks has burgeoned in the past decade. Two distinct lines of research have emerged: the cognitive and the behavioral. Cognitive research deals with the biological phenomenon of recognition, the mathematics of pattern analysis and statistics, and applications in automatic pattern recognition. Behavioral research deals with the biological phenomena of planning and action, the mathematics of time dependent processes, and applications in control and decision-making.

To be mathematically precise, let us discuss simple formulations of each problem type. A cognitive problem typically involves so-called *feature* vectors, $x \in \mathbb{R}^n$. These feature vectors are sensory stimuli or measurements and are presented to us in some random way – that is, we cannot predict with certainty which stimuli will occur next. These observations must be classified and the classification is accomplished by a function $f : \mathbb{R}^n \rightarrow \mathbb{R}^m$. The problem is to build an estimate of the true function, f, based on a sample set of the form $S = \{(x_i, y_i), i = 1, ..., N\}$ which are drawn according to a joint probability distribution on $(x, y) \in \mathbb{R}^{n+m}$, say $\mu(x, y)$. Call the estimate $g(x)$. Typically, $f(x)$ is the conditional expected value of y: $f(x) = \int_y y d\mu(x, y) / \int_y d\mu(x, y)$. A number of distinct situations in cognitive neurocomputing arise depending on the type of information available for estimating f. (See one of the numerous excellent textbooks on neural computing and machine learning for more details.)

- SUPERVISED LEARNING – The sample data, S, is as above so that correct classifications, apart from noise, are part of the data. Moreover, an error criterion is typically provided or constructed on the classifications: $|g(x) - f(x)|$ is some error metric. This situation is closest to traditional statistical regression and uses many classical statistical methods.

- UNSUPERVISED LEARNING – No corrrect or approximate classification values, y, are given. The problem is to organize the data into equivalence classes or clusters and then to label the classes. These labels serve to define f from above and the performance criterion is related to how accurately the equivalence

classes are formed. Unsupervised learning is closely related to clustering and uses techniques from that area.

- REINFORCEMENT LEARNING – As in unsupervised learning, no "correct" response is given but a *reinforcement* is available. A reinforcement can be thought of as an error when $g(x)$ is the estimated response for feature vector x but the correct response f is not available. Reinforcement learning is thus between supervised and unsupervised learning: some performance feedback is provided but not in the form of the correct answer and the deviation of the response from it. The difference between supervised and reinforcement learning has been characterized as the difference between learning from a teacher and learning from a critic. The teacher provides the correct response but the critic only states how bad the system's response was. Reinforcements are often referred to as "rewards" and "punishments" depending on their sizes and the context.

Behavioral neurocomputing derives its problems from planning, decision-making and other applications in which actions over time are of fundamental interest. The mathematical framework, which will be formalized below, involves a system with *states*. Actions are available to move the system into another state, perhaps stochastically. There is an immediate cost associated with taking an action. An action at any given time may be optimal in the short run but may not be the best over the long run when future costs and actions are taken into account. Behavioral applications are therefore most naturally cast as reinforcement learning problems. The goal of behavioral learning is to have a system infer, from empirical data, the state-action pairs which give the smallest average cost.

There are a number of ways that such a behavioral system could be reduced to a cognitive problem. One involves building the following type of training set. Given some initial state, generate a sequence of actions randomly, stopping at some future time. Record the initial state, the action sequence and the ultimate cost of taking that action sequence from that initial state. From this data, build a classifier whose input feature vector is a state and whose output is the action sequence which has minimal cost over all sequences tried. This estimate of the minimal cost to solve the problem from an initial state is an estimate of the *cost-to-go* function.

A related way to solve the problem involves estimating these *cost-to-go* values for each state-action pair. Notice that in a stochastic setting, the action which empirically resulted in the least cost solution may not be the action which leads to the least cost expected value. So averaging is more appropriate than merely keeping track of the minimum cost solution for a given action sequence. The artificial intelligence community has had considerable difficulties with behavioral learning because of difficulties with temporal delays and combinatorial explosions resulting from brute force approaches. Only recently has the mathematics of controlled Markov chains been explored along with solution techniques such as dynamic programming. A major breakthrough in learning optimal actions for such processes has been Watkins' Q-learning [3, 2, 4, 1].

In this paper, we give a quick overview of controlled Markov processes in Section 2. Section 3 presents Watkins' basic results and Section 4 extends those results to describe a system that learns and simultaneously converges to the optimal policy

	Cognitive Learning	Behavioral Learning
Goal	Classifying inputs	Optimizing actions
Related Areas	Statistics Pattern recognition	Control theory Operations research
Relevant Mathematics	Approximation theory Probability	Dynamic programming Stochastic Systems
Status	Sound Theoretical Foundations	Emerging Analytic Theory

Table 1 Cognitive vs. Behavioral Learning.

solution. Section 5 discusses possible areas of intersection between the cognitive and behavioral problems.

2 Markov Decision Processes

The paradigm for *behavioral* neurocomputing can typically be cast as a controlled Markov process which is described below. An environment has a number of states, $X = \{x_i\}$. For each state, there is a set of actions, $A_i = \{a_{ij}\}$, each of which transforms the current state to another state stochastically. This is quantified as a collection of transition probabilities: $p(x_i, a_{ij}, x_k)$ being the probability that applying action a_{ij} in state x_i we land in state x_k at the next time step. These probabilities are independent of time and previous states, hence the stationary Markov character.

Each action engenders a *cost*, $k(x_i, a_{ij})$, which depends only on the state and the action. The goal of a behavioral problem is to minimize this cost over time. Such a temporal cost depends on a *policy* which specifies the actions to be taken at various times in various states. Thus for each time, t, in a policy, we have a vector of actions a_t which tells us which action to apply for any of the possible states the system could be in at time t. Specifically, $a_t(x_i)$ is one of the allowable actions a_{ij} for state x_i. There are a number of ways in which to quantify this temporal cost minimization:

- FREE-TIME MINIMIZATION – A designated state, x_0, terminates the process. We are concerned with the cost of the behavior up to the time this state is reached. Starting in some state x_i and following a policy, $\pi = (a_0, a_1, a_2, ...)$, suppose we follow the trajectory $x_i, x_{i_1}, x_{i_2}, ..., x_{i_{\tau-1}}, x_{0_j}$ the cost will then be

$$\sum_{j=0}^{\tau-1} k(x_{i_j}, a_j(x_{i_j})).$$

  However, since the transitions are stochastic, we must take an expectation over all possible trajectories, starting with x_i and terminating in x_0 with probabilities determined by the policy, π, and the corresponding transitions.

$$V(\pi, i) = E\{\sum_{j=0}^{\tau-1} k(x_{i_j}, a_j(x_{i_j}))\}.$$

- FIXED-TIME MINIMIZATION – As above but the cost is computed up to a fixed time as opposed to when a terminal state is reached.
- AVERAGE-COST MINIMIZATION – The average future cost is minimized (here $0 < \gamma \leq 1$ is the discount factor):

$$V(\pi, i) = \lim_{L \to \infty} \frac{1}{L+1} E\{\sum_{j=0}^{L} \gamma^j k(x_{i_j}, a_j(x_{i_j}))\}.$$

- DISCOUNTED COST MINIMIZATION – Here the cost of future actions are discounted by a constant rate, $0 < \gamma < 1$, so that

$$V(\pi, i) = E[\sum_{j=0}^{\infty} \gamma^j k(x_{i_j}, a_j(x_{i_j}))].$$

We consider only discounted cost minimization problems here. A large body of literature in optimal control theory has been devoted to solving such problems and we review the key elements, leaving out the occasional technical requirements for the results to hold. We focus instead on the general flow of ideas.

First of all, we need only consider policies which are independent of time if we are interested in the optimal policy. The reason is that the process is Markovian and once we reach a state at a point in time, only the future costs can be affected. Since the costs are additive (in a discounted way), an optimal choice of action depends only on the current state. This simplification allows us to consider only policies that are of the form $\pi = (a, a, a, ...)$ where a is a mapping from states to actions.

Secondly, the cost-to-go functions, which we now write as $V(a, i)$ because we are restricting ourselves to stationary policies, satisfy a recurrence relation of the form:

$$V(a, i) = k(x_i, a(x_i)) + \gamma \sum_j p(x_i, a(x_i), x_j) V(a, j).$$

This identity has the following interpretation: using action $a(x_i)$ we go to state x_j with probability $p(x_i, a(x_i), x_j)$; once in state x_j we have the cost-to-go value $V(a, j)$. Weighing these cost-to-go values with the corresponding transition probabilities and adding gives the identity. Stacking these values to form a vector $V(a)$, the above equation becomes a vector-matrix equation of the form:

$$V(a) = k(a) + \gamma P(a) V(a).$$

Thus, every stationary policy satisfies an equation of the above form which can be solved by rewriting it as:

$$(I - \gamma P(a)) V(a) = k(a)$$

where it is assumed that $P(a)$ and $k(a)$ are known for a given policy a. Thus this is a simple linear system of equations which can be solved using standard matrix iterative techniques.

What this shows is that for any policy, there is a computational procedure for computing the cost-to-go function for a fixed action policy. What remains is to find an action policy which will lead to the overall optimal strategy – one that minimizes the cost-to-go function for each state.

Specifically, the optimal policy a^* has the property that

$$V(a^*) = V^* = min_a\{k(a) + \gamma P(a) V^*\}.$$

This policy can be computed using the iteration, starting with V_0 arbitrary,

$$V_{n+1} = min_a\{k(a) + \gamma P(a)V_n\}.$$

Then $V_n \rightarrow V^*$ and the optimal policy is the policy which realizes the minimization above.

3 Watkins' Q-Learning

The behavioral learning problem is to learn the optimal (minimal cost) policy using samples of the following form:

$$s_i = (\eta_i, \zeta_i, \alpha_i, k_i), i = 1, 2, 3, ...$$

These samples are four-tuples with the interpretation that s_i involves a trial use of action α_i on state η_i which resulted in a transition to state ζ_i at a cost of k_i. Given many samples with the same initial state and action, we can estimate the transition probabilities as well as the expected cost of taking that action from that state. With such estimates, a standard solution procedure for computing optimal policies for a Markov decision process can be carried out. This is an off-line, batch approach.

Is there an on-line approach which will learn the optimal strategy adaptively, with guaranteed convergence? The on-line strategy does not compute transition probabilities or costs explicitly. Watkins has given an elegant solution to this problem which he named *Q-learning*. Q-learning uses samples of the above form to update a simple table whose entries converge and whose limit values can easily be used to infer an optimal policy.

Q-learning is motivated by so-called Q-values which are defined as follows:

$$Q^a(x_i, a_{ij}) = K(x_i, a_{ij}) + \gamma P(a)V(a).$$

$Q^a(x_i, a_{ij})$ is the expected cost when starting in state x_i, performing action a_{ij}, and then following policy a thereafter. Let Q^* be the Q-values for the optimal policy a^*, meaning we take some initial action and then follow it with optimal actions thereafter. For these Q-values, we have

$$V(a^*)_i = \min_{a_{ij}}\{Q^*(x_i, a_{ij})\}$$

and the optimal action from state x_i is precisely the action a_{ij} which achieves the minimum.

The beauty of Watkins' Q-learning is that we can adaptively estimate the Q-values for the optimal policy using samples of the above type. The Q-learning algorithm begins with a tableau, $Q_0(x_i, a_{ij})$, initialized arbitrarily. Using samples of the form

$$s_i = (\eta_i, \zeta_i, \alpha_i, k_i), i = 1, 2, 3, ...$$

we perform the following update on the Q-value tableau:

$$Q_i(\eta_i, \alpha_i) = (1 - \beta_i)Q_{i-1}(\eta_i, \alpha_i) + \beta_i(k_i + \gamma V(\zeta_i))$$

where $V(\zeta_i) = \min_\alpha\{Q_{i-1}(\zeta_i, \alpha)\}$. All other elements of Q_i are merely copied from Q_{i-1} without change. The parameters $\beta_i \rightarrow 0$ as $i \rightarrow \infty$.

Theorem 1 *(Watkins [6, 7, 5]) – Let $\{i(x, \alpha)\}$ be the set of indices for which the (x, α) entry of the Q-tableau is updated. If*

$$\sum_{i(x,\alpha)} \beta_{i(x,\alpha)} = \infty \text{ and } \sum_{i(x,\alpha)} \beta^2_{i(x,\alpha)} < \infty$$

then $Q_i(x, \alpha) \rightarrow Q^*(x, \alpha)$ as $i \rightarrow \infty$. Accordingly, $\alpha_i(x) = \text{argmax}_\alpha Q_i(x, \alpha)$ converges to the optimal action for state x.

Proof See [7, 5]. □

This result is remarkable in that it demonstrates that a simple update rule on the Q-tableau results in a learning system which computes the optimal policy. In the next section we show how this method can be embedded into an online system which simultaneously uses the current Q-values to generate policies *and* uses the results to update Q-values in such a way as to satisfy Watkin's theorem. Consequently, the online system learns the optimal policy to which it ultimately converges.

4 Universal On-line Q-Learning

Online optimal learning and asymptotic optimal performance must be a compromise between performing what the learning system estimates to be the optimal actions and persistently exciting all possible state-action possibilities often enough to satisfy the frequencies stipulated in Watkins' Q-learning theorem.

To begin, let us introduce a notion of asymptotically optimal performance. Suppose we have an infinite sequence of state-action pairs that result from an actual realization of the Markov decision process, say $\{(y_i, \alpha_i), i = 0, 1, ...\}$ with (y_i, α_i) meaning that at time i we are in state y_i and execute action α_i, resulting in a transition to state y_{i+1} at the next time. For such a sequence, we have a corresponding sequence of costs v_i which represent the actual costs computed from the realized sequence, v_i being the cost of following the sequence from time i onwards.

We now define *asyptotic average optimality*. Suppose that V_i is the optimal expected cost-to-go for state i. Let $v_i(n_{ij})$ be the observed cost-to-go values for state i when the system is in state i at time n_{ij}. Let $N_M(i)$ be the number of times the process has visited state i up to time M. Then we say that the policy is *asyptotically optimal on average for state* i if

$$\frac{1}{N_M(i)} \sum_{n_{ij} < M} v_i(n_{ij}) \rightarrow V_i$$

as $M \rightarrow \infty$.

In order to establish this result, we need to construct an auxiliary Markov process with states (x_i, a_{ij}) and transition probabilities,

$$p((x_i, a_{ij}), (x_m, a_{mn})) = p(x_i, a_{ij}, x_m)/J_m$$

where J_m is the number of allowable actions in state x_m. This auxiliary process has the following interpretation: the transition probabilities between states are determined by the transition probabilities of the original controlled process with the added ingredient that the actions corresponding to the resulting state are uniformly randomized.

Theorem 2 – *Suppose that there is at least one stationary policy under which the states of the resulting Markov process constitute a single recurrent class (that is, the process is ergodic). Then, with probability 1, there is a mixed nonstationary strategy for controlling the Markov decision process with the following two properties:*
1. The optimal policy is estimated by Q-learning asymptotically;
2. The control is asymptotically optimal on average for all states that have a nonzero stationary occupancy probability under the process' optimal policy.

Proof – The proof consists of three parts. We begin by showing that under the hypothesis that the original process has a stationary policy under which the Markov

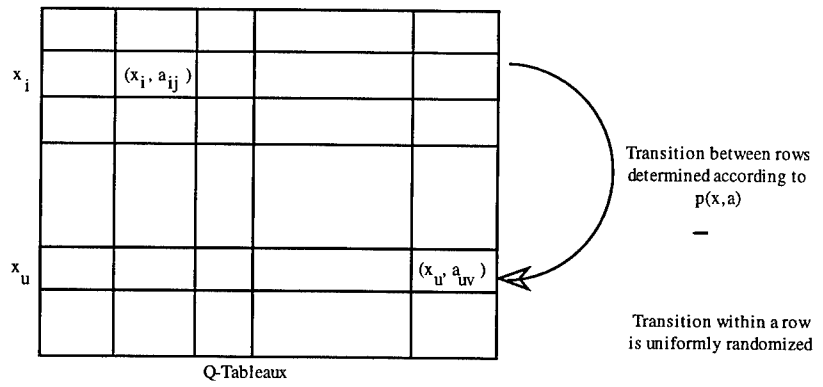

Figure 1 Auxiliary Process Schematic.

process consists of a single recurrent class, the corresponding auxiliary process also has a single recurrent class. Let $a(x)$ be the action for a state x which makes the original process have a single recurrent set. Denote the corresponding transition probabilities by $p_*(x, x') = p(x, a(x), x')$. Let D be the maximal number of actions per state: $D \geq |\{a_{ij}\}|$ for all i. Consider the auxiliary process' canonical partitioning into subclasses of states in which each set of the partition consists of states which are either a) transient or b) recurrent and communicate with each other. Now the $(x, a(x))$ form a subset of the states of the auxiliary process.

Step 1. The auxiliary Process is Recurrent – We will show that any given state of the auxiliary process communicates with every other state. Let (x, a) and (x', a') be any two states of the auxiliary process. We must show that

$$p^{(n)}((x, a), (x', a')) > 0$$

for some n. Pick any state y for which $p(x, a, y) > 0$. By assumption, there is an m for which

$$p_*^{(m)}(y, x') > 0$$

under the special choice of actions, $a(x)$. This means that there is a sequence of states $y_1 = y, y_2, ..., y_m = x'$ for which

$$p(y_i, a(y_i), y_{i+1}) > 0$$

and so

$$p^{(m+1)}((x, a), (x', a')) \geq \frac{p(x, a, y)}{D} \Pi_{i=1}^{m-1} [p(y_i, a(y_i), y_{i+1})/D] > 0.$$

Since all states of the auxiliary process communicate with each other, all states must be recurrent. Thus the auxiliary process consists of a single recurrent set of states. Because the auxiliary process consists of recurrent states, the expected time to visit all states of the auxiliary process is finite and all states will be visited in a finite time with probability 1.

Step 2. A Mixed Policy – We next define a mixed time-dependent strategy for switching between the auxiliary process and a stationary policy based on an esti-

mate of the optimal policy. The mixed strategy begins by choosing actions according to the auxiliary process. At time n_k we switch from the auxiliary process to the process controlled by the policy determined by the Q-table according to

$$a_j(n_k) = \text{argmin}_\alpha Q_{n_k}(x_j, \alpha).$$

At time m_k we switch back to the auxiliary process. For $k = 1, 2, 3, ...$ we have $1 = m_0 < n_k < m_k < n_{k+1} < m_{k+1} ... < \infty$. Let N' the largest expected time to visit all states of the auxiliary process starting from any state and let $N = 2 * N'$. Consider the following experiment which is relevant to the discussion below. Start in any state of the auxiliary process and follow it for N steps at which time we jump to an arbitrary state and run for another N steps, repeating this process indefinitely. Call each such run of N steps a *frame*, numbering them F_i for $i = 1, 2, 3, ...$ We want to concatenate the frames to produce a realization of the auxiliary process. To do this, consider the final state of frame F_i. Since N was chosen to be twice as large as the expected time to visit all states starting from any state, with probability 1 some future frame, say F_{i+j}, includes a visit to the final state of F_i in the first $N/2 = N'$ states of that frame. Concatenate to the end of F_i the history in F_{i+j} following the visit to the final state of F_i. Each step of this concatenation adds at least N' consecutive steps of the auxiliary process so there are an infinite number of visits to all states in the concatenation with probability 1. In the following construction, we implicitly use this property of a concatenation of frames. The definition of n_k is as

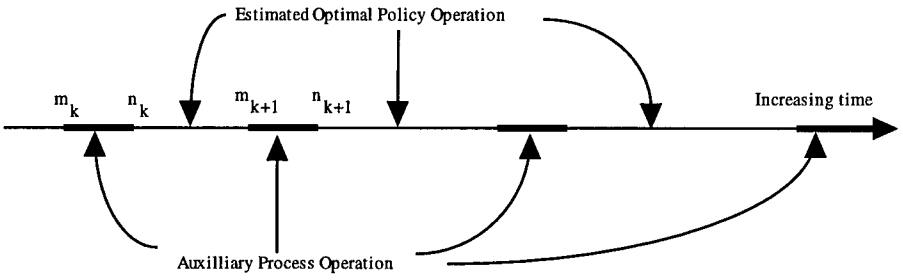

Figure 2 The Mixed Policy Transitions.

follows. At time m_{k-1}, we began following the auxiliary process which is recurrent. We store state transitions of the form

$$(\eta, \zeta, \alpha, \kappa),$$

where η is a state x_i, α is an action taken by the auxiliiary process, ζ is the state of the original process to which the process transitioned and κ is the observed cost of that transition, in a list. Proceed in this manner until either N steps have been taken in this way or until the list contains a sample for each element in the Q-table. If the list to update the Q-table is completed first, we update the Q-table and compute the current optimal actions. In this case, n_k is defined as the time after which the Q-table was updated. Otherwise, define $n_k = m_{k-1} + N$ and continue using the previous estimated optimal actions as a policy. In either case, $m_k = n_k + k * N$ so

we operate the process using the estimated optimal policy for increasingly longer periods of time $k * N$. We then use this list to update the Q-table with the samples in the list.

Assume that the Q-table has M entries. Then for updating the ith element for the jth time in the Q-table from the sample list, use

$$\beta_{j*M+i} = \frac{1}{j * M + i}.$$

According to this scheme, element i is updated for $j = 1, 2, 3, ...$ and the corresponding subset of β's forms an arithmetic subsequence of the harmonic sequence; hence it satifies Watkins' criteria for divergence and squared-convergence.

By the discussion above about frames, this list is filled in a finite amount of time infinitely often with probability 1, but we impose a deterministic limit on the time spent in this mode generating a frame. By construction and Watkins' Theorem, the Q-table values converge to the optimal Q-values and hence the optimal action policy is eventually found.

Step 3. Asymptotic Optimal Convergence – To prove the asymptotic optimal convergence, note that the Q-table updates are performed according to Watkins' criteria so that in the limit the Q-table values determine an optimal stationary policy. Moreover, the time spent operating in the auxiliary mode becomes an asymptotically small fraction of the time spent operating in the estimated optimal policy. Hence, the asymptotic convergence to optimality.

To make this formal, note that asymptotic average optimality depends only on what happens in the limit. Specifically, if we can show that the average of the observed cost-to-go values after some fixed time converges to the optimal value then we are done.

To see this, run the process long enough so that the estimated optimal policy determined by the Q-table is as close as desired to the optimal cost-to-go for the process. This will happen at some finite time with probability 1 although the time is not known a priori. Since we can also wait until k is arbitrarily large, the fraction of time spent in the appoximately optimal mode can be made as close to 1 as we like. Now for a state that has nonzero stationary occupancy probability under the optimal policy, the fraction of time spent operating under the estimated optimal policy approaches 1 and so the empirical cost-to-go also approaches the optimal. For states that have zero occupancy probability under the optimal policy, the empirical cost-to-go will be dominated by the empirical values determined during the auxiliary process operation which will not be optimal in general. Thus the average within the mixed mode of operation is guaranteed to converge to the estimated cost-to-go for the optimal policy but only for states that have nonzero stationary occupancy probabilities under the optimal policy. □

5 Discussion

We have shown that there exists a strategy for operating a Markov Decision Process (under simple conditions) in such a way that the optimal strategy is both learned and the asymptotic operation of the system approaches optimality for states that have nonzero occupancy probabilities under the computed optimal policy. This is only one of many possible strategies for performing both of these simultaneously. The question of which operating procedures are best for fastest convergence to the

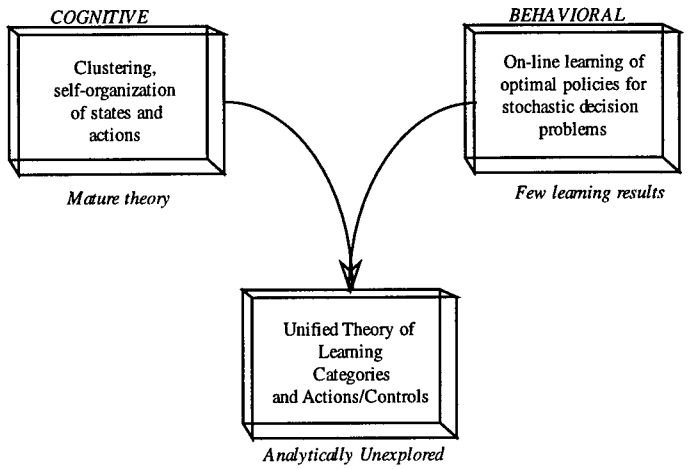

Figure 3 A Unified Learning Theory.

optimal cost-to-go values is beyond the scope of the techniques that we use. It is an important question to pursue in the future.

One of the weaknesses of the Q-Learning framework is that states and actions for the Q-Tableaux must be known a priori. This is restrictive in most dynamic learning situations – it may not be appropriate or possible to select the actual states or actions of a system without significant experimentation first. In general, we would like to simultaneously learn the states, actions and corresponding optimal policies at one time. This subject has been looked into by various researchers but with few analytic results yet. There has been growing interest in dealing with systems that have an infinite (contiuum) of possible states and actions, requiring discretization for Q-Learning. How these states can be clustered or otherwise organized to achieve optimal operation is a challenging question that requires serious future research.

REFERENCES

[1] D. Bertsekas, *Dynamic Programming and Optimal Control.* Athena Scientific, Belmont, MA (1995).

[2] R. Howard, *Dynamic Programming and Markov Processes.* MIT Press, Cambridge, MA (1960).

[3] W.T. Miller III, R.S. Sutton, and P.J. Werbos, *Neural Networks for Control.* MIT Press, Cambridge, MA (1990).

[4] R.S. Sutton, A.G. Barto, and R.J. Williams, *Reinforcement learning is direct adaptive control,* IEEE Control Systems Magazine (April 1992), pp19–22.

[5] J. Tsitsiklis, *Asynchronous stochastic approximation and Q-Learning,* Machine Learning, Vol. 16 (1994), pp185–202.

[6] C.I.C.H. Watkins, *Learning from delayed rewards* Ph.D. Dissertation, University of Cambridge (1989).

[7] C.I.C.H. Watkins and P. Dayan, *Q-Learning,* Machine Learning, Vol.8 (1989), pp279–292.

Acknowledgements

Supported in part by the Air Force Office of Scientific Research research grant F49620-93-1-0266.

ARE THERE UNIVERSAL PRINCIPLES OF BRAIN COMPUTATION?

Stephen Grossberg

Boston University, Department of Cognitive and Neural Systems and Center for Adaptive Systems, 677 Beacon Street, Boston, Massachusetts 02215 USA

1 Introduction

Are there universal computational principles that the brain uses to self-organize its intelligent properties? This lecture suggests that common principles are used in brain systems for early vision, visual object recognition, auditory source identification, variable-rate speech perception, and adaptive sensory-motor control, among others. These are principles of matching and resonance that form part of Adaptive Resonance Theory, or ART. In particular, bottom-up signals in an ART system can automatically activate target cells to levels capable of generating suprathreshold output signals. Top-down expectation signals can only excite, or prime, target cells to subthreshold levels. When both bottom-up and top-down signals are simultaneously active, only the bottom-up signals that receive top-down support can remain active. All other cells, even those receiving large bottom-up inputs, are inhibited. Top-down matching hereby generates a focus of attention that can resonate across processing levels, including those that generate the top-down signals. Such a resonance acts as a trigger that activates learning processes within the system. In the examples described herein, these effects are due to a top-down nonspecific inhibitory gain control signal that is released in parallel with specific excitatory signals.

2 Neural Dynamics of Multi-Source Audition

How does the brain's auditory system construct coherent representations of acoustic objects from the jumble of noise and harmonics that relentlessly bombards our ears throughout life? Bregman [1] has distinguished at least two levels of auditory organization, called primitive streaming and schema-based segregation, at which such representations are formed in order to accomplish auditory scene analysis. The present work models data about both levels of organization, and shows that ART mechanisms of matching and resonance play a key role in achieving the selectivity and coherence that are characteristic of our auditory experience.

In environments with multiple sound sources, the auditory system is capable of teasing apart the impinging jumbled signal into different mental objects, or streams, as in its ability to solve the cocktail party problem. With my colleagues Krishna Govindarajan, Lonce Wyse, and Michael Cohen [5], a neural network model of this primitive streaming process, called the ARTSTREAM model (Figure 1), has been developed that groups different frequency components based on pitch and spatial location cues, and selectively allocates the components to different streams. The grouping is accomplished through a resonance that develops between a given object's pitch, its harmonic spectral components, and (to a lesser extent) its spatial location. Those spectral components that are not reinforced by being matched with the top-down prototype read-out by the selected object's pitch representation are suppressed, thereby allowing another stream to capture these components, as in the

"old-plus-new heuristic" of Bregman [1]. These resonance and matching mechanisms are specialized versions of ART mechanisms.

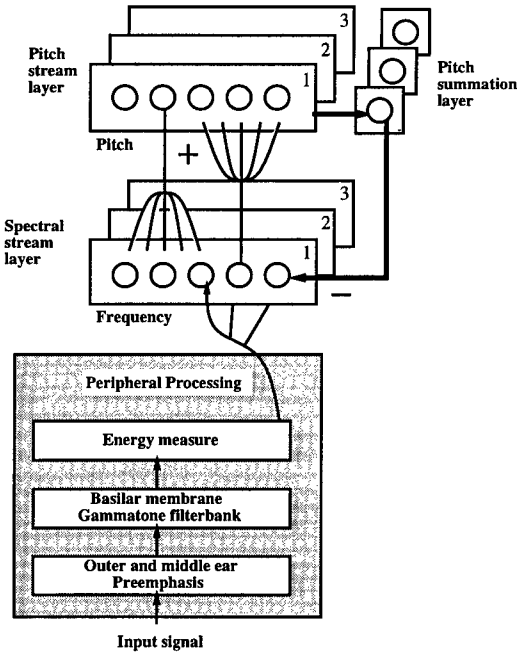

Figure 1 Block diagram of the ARTSTREAM auditory streaming model. Note the nonspecific inhibitory feedback from pitch representations to spectral representations.

The model is used to simulate data from psychophysical grouping experiments, such as how a tone sweeping upwards in frequency creates a bounce percept by grouping with a downward sweeping tone due to proximity in frequency, even if noise replaces the tones at their intersection point. The model also simulates illusory auditory percepts such as the auditory continuity illusion of a tone continuing through a noise burst even if the tone is not present during the noise, and the scale illusion of Deutsch whereby downward and upward scales presented alternately to the two ears are regrouped based on frequency proximity, leading to a bounce percept. The stream resonances provide the coherence that allows one voice or instrument to be tracked through a multiple source environment.

3 Neural Dynamics of Variable-Rate Speech Categorization

What is the neural representation of a speech code as it evolves in real time? With my colleagues Ian Boardman and Michael Cohen [6], a neural model of this schema-based segregation process, called the ARTPHONE model (Figure 2), has been developed to quantitatively simulate data concerning segregation and integration of phonetic percepts, as exemplified by the problem of distinguishing "topic" from "top pick" in natural discourse. Psychoacoustic data concerning categorization of stop consonant pairs indicate that the closure time between syllable final (VC)

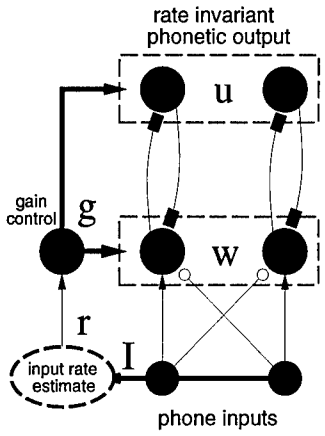

Figure 2 The ARTPHONE model. Working memory nodes (**w**) excite chunks (**u**) through previously learned pathways. List chunks send excitatory feedback down to their item source nodes. Bottom-up and top-down pathways are modulated by habituative transmitter gates (filled squares). Item nodes receive input in an on-center off-surround anatomy. Total input (I) is averaged to control an item rate signal (r) that adjusts the working memory gain (g). Excitatory paths are marked with arrowheads, inhibitory paths with small open circles.

and syllable initial (CV) transitions determines whether consonants are segregated, i.e., perceived as distinct, or integrated, i.e. fused into a single percept. Hearing two stops in a VC–CV pair that are phonetically the same, as in "top pick," requires about 150 msec more closure time than hearing two stops in a VC_1–C_2V pair that are phonetically different, as in "odd ball." As shown by Repp [10], when the distribution of closure intervals over trials is experimentally varied, subjects' decision boundaries between one-stop and two-stop percepts always occurred near the mean closure interval.

The ARTPHONE model traces these properties to dynamical interactions between a working memory for short-term storage of phonetic items and a list categorization network that groups, or chunks, sequences of the phonetic items in working memory. These interactions automatically adjust their processing rate to the speech rate via automatic gain control. The speech code in the model is a resonant wave that emerges after bottom-up signals from the working memory select list chunks which, in turn, read out top-down expectations that amplify consistent working memory items. This resonance may be rapidly reset by inputs, such as C_2, that are inconsistent with a top-down expectation, say of C_1; or by a collapse of resonant activation due to a habituative process that can take a much longer time to occur, as illustrated by the categorical boundary between VCV and VC–CV. The categorization data may thus be understood as emergent properties of a resonant process that adjusts its dynamics to track the speech rate.

4 Neural Dynamics of Boundary and Surface Representation

With my colleagues Alan Gove and Ennio Mingolla [4], a neural network model, called a FACADE theory model (Figure 3), has been developed to explain how

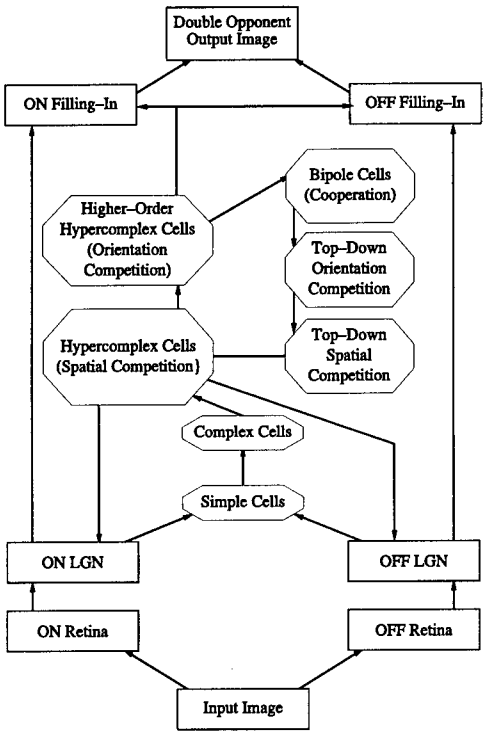

Figure 3 FACADE model macrocircuit. Boundary representation, or BCS, stages are designated by octagonal boxes, surface representation, or FCS, stages by rectangular boxes.

visual thalamocortical interactions give rise to boundary percepts such as illusory contours and surface percepts such as filled-in brightnesses. Top-down feedback interactions are needed in addition to bottom-up feedforward interactions to simulate these data. One feedback loop is modeled between lateral geniculate nucleus (LGN) and cortical area V1, and another within cortical areas V1 and V2. The first feedback loop realizes a resonant matching process, as in ART, which enhances LGN cell activities that are consistent with those of active cortical cells, and suppresses LGN activities that are not. This corticogeniculate feedback, being endstopped and oriented, also enhances LGN ON cell activations at the ends of thin dark lines, thereby leading to enhanced cortical brightness percepts when the lines group into closed illusory contours. The second feedback loop generates boundary representations, including illusory contours, that coherently bind distributed cortical features together. Brightness percepts form within the surface representations through a diffusive filling-in process that is contained by resistive gating signals from the boundary representations. The model is used to simulate illusory contours and surface brightnesses induced by Ehrenstein disks, Kanizsa squares, Glass patterns, and café wall patterns in single contrast, reverse contrast, and mixed contrast con-

figurations. These examples illustrate how boundary and surface mechanisms can generate percepts that are highly context-sensitive, including how illusory contours can be amodally recognized without being seen, how model simple cells in V1 respond preferentially to luminance discontinuities using inputs from both LGN ON and OFF cells, how model bipole cells in V2 with two colinear receptive fields can help to complete curved illusory contours, how short-range simple cell groupings and long-range bipole cell groupings can sometimes generate different outcomes, and how model double-opponent, filling-in and boundary segmentation mechanisms in V4 interact to generate surface brightness percepts in which filling-in of enhanced brightness and darkness can occur before the net brightness distribution is computed by double-opponent interactions. Taken together, these results emphasize the importance of resonant feedback processes in generating conscious percepts in the visual brain.

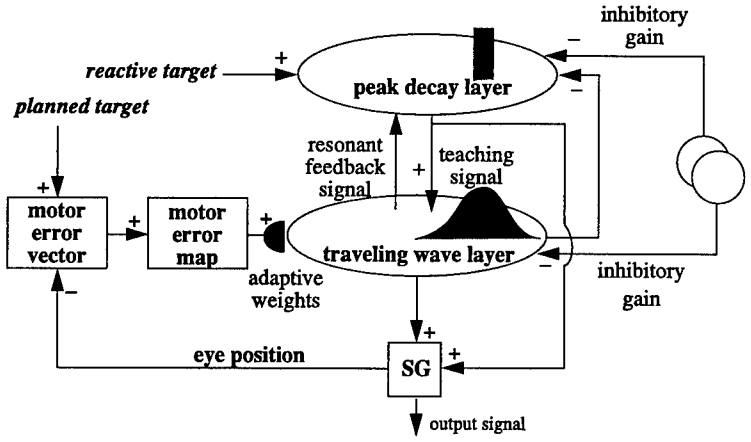

Figure 4 SACCART model for multimodal control of saccadic eye movements by the superior colliculus.

5 Neural Dynamics for Multimodal Control of Saccadic Eye Movements

Saccades are eye movements by which an animal can scan a rapidly changing environment. While the saccadic system plans where to move the eyes, it also retains reflexive responsiveness to fluctuating light sources. These two types of saccades ultimately result in control of the same set of eye muscles. Visually reactive cells encode gaze error in a *retinotopically* activated motor map. Planned targets are coded in *head–centered* coordinates. When two conflicting commands attempt to share control of the saccadic eye movement system, the system must resolve the conflict and coordinate command of one set of eye muscles.

The superior colliculus is a brainstem region that plays a prominent role in both planned and reactive saccades. This region coordinates information to adjust movements of the head and eyes to a stimulus. In order to combine these visual, somatic, and auditory saccade targets in the superior colliculus, the targets in head–centered coordinates are mapped to a gaze motor error in retinotopic coordinates.

How does the saccadic movement system select a target when visual and planned movement commands differ? How do retinal, head–centered, and motor error coordinates interact during the selection process? How are these coordinate systems rendered consistent through learning? Recent data on superior colliculus (SC) reveal a travelling wave of activation whose peak codes the current gaze error [9]. In contrast, Waitzman [12] found that the locus of peak activity in SC remains constant while the activity level at this locus decays as a function of residual gaze error. Why do these distinct cell types exist?

With my colleagues Mario Aguilar, Dan Bullock, and Karen Roberts [8], a neural network model has been developed that answers these questions while providing a functional rationale for both signal patterns (Figure 4). The model assumes that calibration between visual inputs and eye movement commands is learned early in development within a visually reactive saccade system [7]. Visual error signals coded in retinotopic coordinates calibrate adaptive gains to achieve accurate foveation. The accuracy of planned saccades derives from using the gains learned by the reactive system. For this, a transformation between a planned head–centered and a retinotopic target representation needs to be learned. ART matching and resonance control the stability of this learning and the attentive selection of saccadic target locations. Targets in retinotopic and head–centered coordinates are rendered dimensionally consistent so that they can compete for attention to generate a movement command in motor error coordinates. Simulations show how a decaying, stationary activity profile is obtained in the pre–motor layer due to feedback modulation. In addition, a travelling wave activity profile is produced in the motor layer due to modulation from the pre–motor layer and the nature of the local connectivity. The simulations show how this model reproduces physiological data of these two classes of collicular neurons simultaneously during a variety of behavioral tasks (e.g., visual, memory, gap, and overlap conditions), an achievement previously unattained by eye movement models. In addition, the model also clarifies how the SC integrates signals from multiple modalities, and simulates collicular response enhancement and depression produced by multimodal stimuli [11].

6 Concluding Remarks

In addition to these systems are the more familiar ART systems for explaining visual object recognition and its breakdown due to hippocampal lesions that lead to medial temporal amnesia [2]. Taken together, these results provide accumulating evidence that the brain parsimoniously specifies a small set of computational principles to ensure its stability and adaptability in responding to many different types of environmental challenges.

REFERENCES

[1] Bregman, A.S., *Auditory scene analysis.* Cambridge, MA: MIT Press (1990).

[2] Carpenter, G.A. and Grossberg, S., *Normal and amnesic learning, recognition, and memory by a neural model of cortico-hippocampal interactions.* Trends in Neurosciences, Vol. 16 (1993), pp131–137.

[3] Cohen, M.A., Grossberg, S., and Wyse, L.L., *A spectral network model of pitch perception.* Journal of the Acoustical Society of America, Vol. 98 (1995), pp862–879.

[4] Gove, A., Grossberg, S., and Mingolla, E. *Brightness perception, illusory contours, and corticogeniculate feedback.* Visual Neuroscience, Vol. 12 (1995), pp1027–1052.

[5] Govindarajan, K.K., Grossberg, S., Wyse, L.L., and Cohen, M.A., *A neural network model of auditory scene analysis and source segregation.* Technical Report CAS/CNS-TR-94-039,

Boston University (1994).

[6] Grossberg, S., Boardman, I., and Cohen, M.A., *Neural dynamics of variable-rate speech categorization.* Journal of Experimental Psychology: Human Perception and Performance, in press (1994).

[7] Grossberg, S. and Kuperstein, M., *Neural dynamics of adaptive sensory motor control: Expanded edition.* Elmsford, NY: Pergamon Press (1989).

[8] Grossberg, S., Roberts K., Aguilar M. and Bullock, D., *A neural model of multimodal adaptive saccadic eye movement control by superior colliculus.* Tech. Rept. CAS/CNS TR-96-029 (1996).

[9] Munoz, D., Guitton, D., and Pélisson, D., *Control of orienting gaze shifts by the tectoreticulospinal system in the head-free cat, III: Spatiotemporal characteristics of phasic motor discharges.* Journal of Neurophysiology, Vol. 66(5) (1991), pp1642–1666.

[10] Repp, B.H., *A range-frequency effect on perception of silence in speech.* Haskins Laboratories Status Report on Speech Research, SR-61 (1980), pp151–165.

[11] Stein, B.E. and Meredith, M.A., *The merging of the senses.* Cambridge, MA: MIT Press (1993).

[12] Waitzman, D., Ma, T., Optican, L., and Wurtz, R., *Superior colliculus neurons mediate the dynamic characteristics of saccades.* Journal of Neurophysiology, Vol. 66(5) (1991), pp1716–1737.

Acknowledgements

Supported in part by the Air Force Office of Scientific Research (AFOSR F49620-92-J-0225), the Advanced Research Projects Agency (ONR N00014-92-J-4015), and the Office of Naval Research (ONR N00014-91-J-4100 and ONR N00014-92-J-1309). The author wishes to thank Diana Meyers and Cynthia Bradford for their valuable assistance in the preparation of the manuscript.

ON-LINE TRAINING OF MEMORY-DRIVEN ATTRACTOR NETWORKS

Morris W. Hirsch

Department of Mathematics, University of California at Berkeley, USA.

A rigorous mathematical analysis is presented of a class of continuous networks having rather arbitrary activation dynamics, with input patterns classified by attractors by a special training scheme. Memory adapts continually, whether or not a training signal is present. It is shown that consistent input-output pairs can be learned perfectly provided every pattern is repeated sufficiently often, and input patterns are nearly orthogonal.

1 Introduction

Most neural networks used for pattern classification have the following features:

- The training dynamics is separate from the activation dynamics.
- Patterns are classified by fixed points or limit cycles of the activation dynamics.

But biological neural networks— nervous systems— do not conform to these rules. We learn while doing— we learn *by* doing, and if we don't do, we may forget. And chaotic dynamics is the rule in many parts of the cerebral cortex (see the papers by Freeman *et al.*).
Here we look at supervised learning in continuous time nets in which:

- The memory matrix is *always* adapting: the only difference between training and testing is the presence of a training signal. Testing reinforces learning, lack of testing can lead to forgetting, and retraining at any time is possible.
- Patterns are classified by possibly chaotic attractors.
- Training is completed on any single pass through the training set.

The fundamental problem faced by such a system is that presentation of new input patterns affects the memory of old patterns, whether or not a training signal is present; consequently there is a tendency for previously trained memories to degrade. To prevent this from occurring, we constrain the system in two ways:

- Each input pattern is repeated sufficiently frequently, with or without a training signal.
- Input patterns are nearly orthogonal.

When the input patterns are sufficiently orthogonal, depending on the number of patterns, then system parameters can be chosen robustly so that the system learns to give the correct output for each input pattern on which it has consistently trained. The net comprises an input layer of d units which feeds into a recurrently connected activation layer of n units. Inputs and activations can take any real number values. Inputs are drawn from a fixed list of patterns, taken for convenience to be unit vectors. With any input a training signal may be presented for minimum time and then shut off. These training signals need not be consistent, but those patterns

that are trained consistently and tested sufficiently frequently, will respond with the correct output.

Rather than taking outputs to be the usual stable equilibria or limit cycles, we consider outputs to be the attractors (more precisely, their basins) to which the activation dynamics tends. (Compare [2], [4]). Each training signal directs the activation dynamics into the basin of an attractor.

In some biological models it is the attractor as a geometric object, rather than the dynamics in the attractor, that classifies the input. If the components of the activation vector x represent firing rates of cells, then the attractor may corresond to a particular cell assembly, and the useful information is which cell assembly is active, with dynamical details being irrelevant. In this connection compare [8]; [1].

Before giving details of the dynamics, we first describe how the network looks from the outside. From this black box point of view the activation dynamics *appears* to be governed by a differential equation in Euclidean n-space $\mathbb{R}^n$,

$$\frac{dx}{dt} = F(x) + I \tag{1}$$

$$\equiv -x + f(x) + I \tag{2}$$

where $f : \mathbb{R}^n \to \mathbb{R}^n$ is bounded and $I \in \mathbb{R}^n$ is a constant training signal which may be 0. Input patterns are chosen from a finite set of distinct vectors $\xi^a \in \mathbb{R}^d$, $a = 1, \ldots, m$. Training signals are selected from a compact set $S \subset \mathbb{R}^n$ which contains the origin.

At stage k of running the net, an input and a possibly null training signal are presented simultaneously to the net for a certain time interval $[t_{k-1}, t'_k]$ called the k'th *instruction period*, followed by the *computation period* $[t'_k, t_k]$ during which training signal is removed (set to 0) while the same input is present. The activation vector x then settles down to an attractor for the dynamics of the vector field F, that is, for the differential equation

$$\frac{dx}{dt} = -x + f(x), \tag{3}$$

When this process is repeated with a different input and training signal, the activation variable x jumps instantaneously to a new initial position.

To each pattern ξ^a there is associated a special attractor $A^a \subset \mathbb{R}^n$ for (3), and a *target* U^a, which is a positively invariant neighborhood of A^a in $B(A^a)$. It is desired that when ξ^a is input, $x(t)$ goes into U^a and stays there (thus approaching A^a), until the input is changed.

Training consists in using training signals from a special subset $S^a \subset S$ of *proper* training signals asociated with ξ^a. Other nonzero training signals are *improper*.

It turns out that with sufficiently orthogonal input patterns and suitable parameters, any pattern that is trained on a proper training signal at stage k will go to its correct target at a later stage provided that at intervening stages the pattern was presented sufficiently often and no improper training signals were used.

Now we explain how the memory evolves. The time varying *memory matrix* $M \in \mathbb{R}^{n \times d}$ maps static input patterns (column vectors) ξ to dynamic activation vectors x by $x(t) = M(t)\xi$. An auxiliary fast variable $y \in \mathbb{R}^n$ provides a delay between $x(t)$ and $M(t)$: The true dynamics is given by the following *Main System*, where

ξ^T denotes the transpose of ξ:

$$\frac{dM}{dt} = [-x + y + I]\xi^T, \tag{4}$$

$$\lambda\frac{dy}{dt} = f(x) - y, \tag{5}$$

$$x = M\xi. \tag{6}$$

The system's dynamics is thus driven by $M(t)$; there is no independent activation dynamics.

Computing dx/dt and using the fact that $\xi^T\xi = ||\xi||^2 = 1$, we obtain the following system:

$$\frac{dx}{dt} = -x + y + I, \tag{7}$$

$$\lambda\frac{dy}{dt} = f(x) - y. \tag{8}$$

This system is independent of the input ξ; but the interpretation of x depends on ξ, and x (but not y) jumps discontinuously when ξ is changed.

It is interesting to observe that System (7), (8) is equivalent to a single second order equation in x, namely:

$$\lambda\frac{d^2x}{dt^2} + (\lambda + 1)\frac{dx}{dt} + x = f(x) + I, \tag{9}$$

similar to the second order activation dynamics used by W. Freeman *et al.* (see References). The following fact is used:

Proposition 1 *If $x(t)$ obeys Equation (9) and $||f(x)|| \leq \rho$, then $x(t) \to N_\rho(I)$.*

Standard dynamical system techniques (singular perturbations, invariant manifolds) show that the dynamics of System (7), (8) is closely approximated by the that of the simpler system

$$\frac{dx}{dt} = -x + f(x) + I \tag{10}$$

provided λ is small enough.

Example 1 A simple but interesting system of this type has 1-dimensional activation dynamics. For f we take any smooth (Lipschitz also works) sigmoid with high gain $\kappa \gg 1$, having limiting values ± 1. The dynamics of (10) with $I = 0$ has stable equilibria at (approximately) $x = \pm 1$ and an unstable equilibrium at $x = 0$. The 2-dimensional dynamics of System (7), (8) with $I = 0$ has two attracting equilibria near $(1, 1)$ and $(-1, -1)$, and an unstable equilibrium near $(0, 0)$. Every trajectory tends to one of these three equilibria. As training signals we take $I_- = -1$, $I_+ = +1$. When I takes either of these values I^a, (x, y) settles to the global attractor near $(2I^a, 2I^a)$. When I is then set to 0, keeping the same input pattern, then (x, y) relaxes toward (I^a, I^a). This system learns to sort any number of sufficiently orthogonal input patterns into two arbitrary classes after a single pass through the pattern set. A similar system is treated in detail in [9].

Higher dimensional examples can be obtained from this one by taking Cartesian products of n such vector fields, yielding 2^n attracting equilibria. More interesting dynamics can be constructed by changing the vector field in small neighborhoods of the attracting equilibria. In this way attractors with arbitrary dynamics can be constructed.

2 Statement of Results

Notation. $||u|| = \sqrt{u \cdot u}$ denotes the Euclidean norm of vector u. The closed ball of radius ρ about a point z is denoted by $N_\rho(z)$. The closed ρ-neighborhood of a set A is $\bigcup_{z \in A} N_\rho(z)$.
We start with the *data*: f, $\{A^a\}$, $\{U^a\}$, $\{S^a\}$.
We assume given an increasing sequence of times $t_{k-1} < t'_k < t_k$, $k \in \mathbb{N}$. The Main System is run during stage k as described above, taking as initial values at t_{k-1} whatever the terminal values were in the previous stage (if $k > 1$).
We make the following asumptions, in terms of parameters $\epsilon > 0, T > 0, N \geq 1, R > 0, \rho > 0$:

Hypothesis 2

Unit pattern vectors: $||\xi^a|| = 1$.
Separation of patterns: $|\xi^a \cdot \xi^b| < \epsilon$ *for distinct* a, b
Duration of presentation: $t'_k - t_{k-1} > T$ *and* $t_k - t'_k > T$ *for all* k.
Frequency of presentation: *Each pattern* ξ^a *is used as input at least once in every* N *successive stages.*
Initial values: $|y(0)| < 1$, $||M(0)\xi^a|| < R$.
Bound on f**:** $||f(x)|| < \rho$.
Proper training signals: $S^a = \{I \in \S : N_\rho(I) \subset B(A^a)\}$.

The following theorems refer to the main system. They mean that robust parameters can be chosen so that that whenever the pattern from a consistent pair is input after being properly trained once, the output is always correct, whether or not a training signal is input, and regardless of the training signals when other patterns are input; and moreover, all the variables stay within given bounds.
Define time-varying vectors $x^a(t) = M(t)\xi^a \in \mathbb{R}$— the net's *current recall of input* ξ^a.
A pattern ξ^a is *consistently trained* from stages k to l provided that at stage k the input is ξ^a and the training signal is proper, while at each stage r, $k < r \leq l$ at which ξ^a is input,the training signal is either proper or 0 (both may occur at different stages).
ξ^a *tests successfully* during stages k to l provided $x^a(t_j) \in U^a$ whenever $k \leq j \leq l$ and the input for stage j is ξ^a.
Recall that λ is the time constant in Equation (5).

Theorem 3 *There exist positive constants* T_*, τ_*, λ_* *independent of* $N, \epsilon, \{\xi^a\}$ *and computable from the data, with the following property. Assume* $0 < \lambda < \lambda_*$ *and Hypothesis 2 holds with* $T \geq T_*, R \geq R_*$, *and in addition* $\epsilon N \leq \tau_*$. *Then every pattern which is consistently trained from stages* k *to* l, *tests successfully during those stages.*

The quantity

$$\theta = \epsilon N(1+\epsilon)^N$$

plays a key role. Notice that $\theta \to 0$ as $\epsilon N \to 0$.

Theorem 4 *There exist positive constants T_*, R_*, λ_*, independent of $\epsilon, N, \{\xi^a\}$ and computable from the data, with the following property. If $0 < \lambda < \lambda_*$ and Hypothesis 2 holds with $T \geq T_*, R \geq R_*$, then:*

$$||M(t)\xi^a|| < \theta R \tag{11}$$

for all $t \geq 0$, $a = 1, \ldots, m$.

It is clear from (4) that if a vector $\eta \in \mathbb{R}^d$ is orthogonal to all the input patterns, then $M(t)\eta$ is constant. Therefore the Theorem 4 implies that the entries in $M(t)$ are uniformly bounded.

The key to the proofs is the following lemma. Suppose the input is $\xi = \xi^a$ in System (4), (5),(6). Computing dx^b/dt shows $dx^b/dt = (\xi^b \cdot \xi^a)dx^a/dt$, yielding the crucial estimate:

Lemma 5 *If the input is ξ^a and $b \neq a$, then for $t_1 > t_0 \geq 0$ we have:*

$$|x^b(s_1) - x^b(s_0)| \leq \epsilon |x^a(s_1) - x^a(s_0)|. \tag{12}$$

This means that after presentation of ξ^b, subsequent presentation of ξ^a does not alter the net's recall of ξ^b by very much provided ϵ is sufficiently small.

3 Discussion

Theorem 3 means that each consistently trained input pattern yields the correct output attractor regardless of the training of the other patterns, which may be untrained or even inconsistently trained. Moreover the system can be trained or retrained on any patterns without impairing the previous training of the other patterns.

Example 2 An example which illustrates the difficulty in verifying the assumption on proper training signals in Hypothesis 2 is obtained by replacing f in Example 1 by $f_1(x) = f(x) + f(x-1)$. (If f approximates a step function, then f_1 approximates a staircase function.) For high gain the vector field $-x + f_1(x)$ has attracting equilibria very near $-2, 0$ and 2, and unstable equilibria near -1 and 1. The basin of the attraction for the equibrium near 0 is contained in the interval $(-1, 1)$. As we must take $\rho \approx 2$, Hypothesis 2 is violated because $N_2(0) \not\subset (-1, 1)$.

The requirement that input patterns be unit vectors is made only for simplicity. If they are not unit vectors then the assumption on separation of distinct patterns in Hypothesis 2 is changed to

$$\frac{|\xi^a \cdot \xi^b|\,||\xi^b||}{||\xi^a||} < \epsilon,$$

with similar results. The dimension d of the input space is irrelevant to our results. In fact the input patterns could be members of an arbitrary inner product space.

It is not hard to see that some restrictions on the geometry of the patterns is necessary. For example, a set of linearly dependent patterns severely constrains the associated outputs that can be learned.

The training-testing schedule is also crucial. Simple examples show that, as with natural learning systems, if a pattern is not repeated sufficiently often it may be forgotten.

Interesting stochastic questions arise. Suppose, for example, that instead of considering consistently trained patterns, we allow the wrong teaching signal to be given

with small positive probability. Is it true, as seems likely, that under some similar training scheme there is a high probability of correct output?
Some other issues: Is incremental learning possible? Can such nets be usefully coupled? Can more than one layer of memory be trained this way? Is there a good way to approximately orthogonalize inputs by preprocessing?

REFERENCES

[1] Amit, D. J., *The Hebbian paradigm reintegrated: local reverberations as internal representations*, Behavioral and Brain Sciences in press (1995).

[2] Baird, B. & Eeckmann, F. H., *A hierarchical sensory-motor architecture of oscillating cortical area subnetworks*, in: Analysis and Modeling of Neural Systems II, F. H. Eeckman (ed.) Boston: Kluwer (1992), pp96–104.

[3] Baird, B. & Eeckman, F. & Hirsch, M. W., *A neural network associative memory fdor handwritten character recognition using multiple Chua attractors*, IEEE Trans. Circuits & Systems Vol. 40 (1993), pp667–674.

[4] Baird, B. & Hirsch, M. W., *Computing with dynamic attractors*, Biosystems Vol. 34 (1995), pp173–195.

[5] Freeman, W. J., *Simulation of chaotic EEG patterns with a dynamic model of the olfactory system* , Biological Cybernetics Vol. 56 (1987), pp139–143

[6] Freeman, W. J. & Baird, B., *Relation of olfactory EEG to behavior: spatial analysis*, Behavioral Neuroscience Vol. 101 (1987), pp393–408

[7] Freeman, W. J. & Viana di Prisco, G., *EEG spatial pattern differences with discriminated odors manifest chaotic and limit cycle attractors in olfactory bulb of rabbits*, in: Proceedings First Trieste Meeting on Brain Theory, G. Palm & A. Aertsen (eds.) New York: Springer-Verlag (1986).

[8] Hebb, D. O., *The Organization of Behavior*, New York: Wiley (1949).

[9] Hirsch, M. W., *On-line Training of a Continually Adapting Perceptron-Like Network*, Neurocomputing, in press 1996.

Acknowledgements

Partially supported by a grant from the National Science Foundation.

MATHEMATICAL PROBLEMS ARISING FROM CONSTRUCTING AN ARTIFICIAL BRAIN

J. G. Taylor

Department of Mathematics and Centre for Neural Networks, King's College, London, UK.

A beginning is being made on the hard problem of constructing an artificial brain, to try to bridge the gap between neurophysiology and psychology. The approach uses especially the increasing number of results obtained by means of non-invasive instruments (EEG,MEG,PET,fMRI), and the related psychological tasks. The paper describes the program and some of the mathematical problems that it is producing. In particular the class of problems associated with the activities of various coupled modules used in higher order control and attention will be discussed. These include posterior attentional coupled systems, and the anterior motor/action/attention "ACTION" networks, based on biological circuits. The relevance of these modules, and the associated problems, for higher order cognition, are emphasised.

1 Introduction

The Harvard neurologist Gerald Fishbach stated recently "The human brain is the most complicated object on earth". That does indeed seem to be the case, and for a considerable period of time since the beginning of the scientific revolution this fact seems to have led to despair in ever being able to have a reasonable comprehension of it. However there is now a strong sense of optimism in the field of brain sciences that serious progress is being made in the search for comprehension of the mechanisms used by the brain to achieve its amazing powers, even up to the level of consciousness. Part of this optimism stems from the discovery and development of new windows with which to look at the brain, with large groups now being established to exploit the power of the available instruments. There are also new theories of how neurons might combine their activities to produce mind-like behaviour, based on recent developments in the field of artificial neural networks. At the same time there is an ever increasing understanding of the subtleties of the mechanisms used by living neurons. It would thus appear that the mind and brain are being attacked at many levels. The paper attempts to contribute towards this program by starting with a brief survey of the results of non-invasive instruments. Then it turns to consider the inverse problem before discussing the nature of past global brain models. An overview is then given of the manner in which neural modelling may attempt to begin to achieve perception. Problems of neuropsychological modelling are then considered, with the breakdown of tasks into component sub-processes. Mathematical problems associated with constructing neural modules to achieve the required functionality of sub-process are then discussed. Modules to produce possible conscious processing are then considered, and the paper concludes with a summary and discussion of further questions.

2 Non-Invasive Results

There are amazing new windows on the mind. These measure either the magnetic or electric fields caused by neural activity, or the change in blood flow in active regions of the brain to allow oxygen to be brought to support the neural activity. The former techniques are termed magnetoencephalography (MEG) and electroen-

cephalography (EEG), the latter positron emission tomography (PET) and functional magnetic resonance imaging (fMRI) respectively. The techniques of MEG, EEG and fMRI are truly non-invasive since there is no substance penetrating the body, whilst that is not so with PET, in which a subject imbibes a radioactive material which will decay rapidly with emission of positrons (with their ensuing decay to two photons).

The methods have different advantages and disadvantages. Thus EEG is a very accurate measure of the time course of the average electrical current from an aggregate of neurons firing in unison, but is contaminated with conduction currents flowing through the conducting material of the head. Thus although temporal accuracy of a few milliseconds can be obtained spatial accuracy is mainly limited to surface effects, and deep currents are difficult to detect with certainty. MEG does not have the defect of being broadened out spatially by the conduction currents, but has the problem of spatial accuracy, which is slowly becoming resolved (but also has a more difficult one of expense due to the need for special screening and low temperature apparatus for the SQUID devices). fMRI also has considerable expense and low temporal accuracy. Even though the activity from each slice of brain may be assessed in an fMRI machine within about 100 or so milliseconds the blood flow related to the underlying brain activity still requires about 7 seconds to reach its peak. There has been a recent suggestion that hypo-activity from the deoxygenated blood will 'peak' after only about 1 or 2 seconds of input [1], but that is still to be confirmed. Finally PET also has the same problems of slow blood flow possessed by fMRI, but good spatial accuracy. Combining two or more of the above techniques together makes it possible to follow the temporal development of spatially well defined activity [2]. The results stemming from such a combination are already showing clear trends.

The most important result being discovered by these techniques is that

1. activity of the brain for solving a given task is localised mainly in a distinct network of modules,
2. the temporal flow of activity between the modules is itself very specific,
3. the network used for a given task is different, in general, from that used for another task.

It is not proposed to give here a more detailed description of the enormous number of results now being obtained by these techniques, but refer the reader, for example, to the recent book of [2], or the excellent discussion in [3]. However it is important finally to note that the fact there are distinctive signatures that can be picked up by these instruments indicate that aggregates of nerve cells are involved in solving the relevant tasks by the subjects. Thus population activity is involved, and "grandmother" cells are not in evidence. Of course if they were important they would slip through the net. However that there are such characteristic signatures seems to show that the net is sharp enough to detect relevant aggregated activity.

3 Inverse Problems

There has been much work done to decipher the detailed form of the underlying neural activity that gives rise to a particular MEG or EEG pattern, the so-called

"inverse problem". Various approaches have been used to read off the relevant neural processing, mainly in terms of the distribution of the underlying sources of current flow. This latter might be chosen to be extremely discrete, as in the case of the single dipole fits to some of the data. However more complete current flow analyses have been performed recently, as in the case of MFT [4]. This leads to a continuous distribution of current over the brain, in terms of the lead fields describing the effectiveness of a given sensor to detect current at the position of the field in question.

It has been possible to extend this approach to use cross entropy minimisation so as to determine the statistics of the current density distribution in terms of the covariance matrix of the measurements and the sensor mean results [5]. This approach is presently being extended to attempt to incorporate the iteration procedure in the MFT method of [4] so as to make the approach more effective [6].

There are further deep difficulties with the inverse problem. Thus one has to face up to the question of single trials versus averaged values. Averaging has especially been performed on the EEG data so as to remove the noise present. However in the case of successful task performance the subject must have used activity of a set of modules, in a single trial, in a way which avoided the noise. This is an important question that will be taken up in the next section: how is successful performance achieved in an apparently noisy or chaotic dynamical system such as the brain [7]? Averaging only removes the crucial data indicating as to how the solution to this task might be achieved. But single trials appear to be very, very noisy. How do modules share in the processing so as to overcome the variability of neural activity in each of them?

One way to begin to answer this, and the earlier problem about the inverse problem, is to model the neural activity in a direct manner. In other words the actual flow of nerve impulses, and their resultant stimulation of other neural modules, must be attempted. The resulting electric and magnetic fields of this neural activity must then be calculated. This approach will allow more knowledge to be inserted in the model being built than by use of methods like MFT, and so help constrain the solution space better.

4 Neural Modules for Perception

It is possible to develop a program of modelling for the whole brain, so that the spatial and temporal flow patterns that arise from given inputs can be simulated. That also requires the simulation of reasonably accurate input sensors, such as the retina, the nose or the cochlea. There are already simple neural models of such input processors (such as in [8]), so that with care the effects of early processing could already be included.

The order of work then to be performed is that of the development of simple neural modules, say each with about a thousand neurons, and connected up to others in a manner already being determined from known connectivities, such as that of the macaque [9]. An important question of homology has to be solved here, but there is increasing understanding of how to relate the monkey brain to that of the human, so that problem may not be impossible. There is also the difficulty of relating the resulting set of, say, a hundred simplified modules to their correct places on the cortical surface (and to appropriate sub-cortical places) for a particular human

subject. Even assuming the cortical surface is known from an MRI scan, the actual placing of the modules corresponding to different areas might be difficult. However this may be tackled by considering it as a task of minimization of the mismatch between the predictions of the model and the actual values of EEG and MEG signals during a range of input processing, and including sub-cortical structures, such as discussed in [10].

5 Neuropsychological Modelling

There is a big gap between neurons in the brain and the concepts which they support. The job of explaining how the latter arise from the former is formidable. Indeed it is even harder to consider the ultimate of experiences supported, that of consciousness itself. One approach has been to consider the brain as carrying out simple computations. However there has recently been an attack on the notion of the brain as a 'computational' organ, in the sense that "nervous systems represent and they respond on the basis of the representations" [11]. It has been suggested, instead, that brains do not perform such simple computations. Thus "It is shown that simplified silicon nets can be thought of as computing, but biologically realistic nets are non-computational. Rather than structure sensitive rules governed operations on symbolic representations, there is an evolution of self-organising non-linear dynamic systems in a process of 'differing and deferring' " [7].

This claim of non-computationality of the brain is supported by appeals to the discovery of chaos in EEG traces, and also that low-dimensional motion may be involved in the production of percepts in ambiguity removal. However it is well known that neural systems are non-linear, and that such systems can easily have chaotic motions if forced into certain parameter regimes. Thus the dynamics of the whole brain, written as the dynamical system

$$dX/dt = F(X, a)$$

in terms of the high dimensional state vector X, is expected to have chaotic motion for some of the parameter range a, on which the vector field F depends. Thus X could denote the set of compartmental membrane potentials, and F denotes the non-linear Hodgkin-Huxley equations for the production of the nerve impulses. However there are still expected to be "representations" brought about by the changes of the function F by, for example, synaptic modifications caused by learning. If there is no change in the transform function F there seems to be no chance for learning. Hence the claim of [7] seems to be incorrect when the notion of representation is extended to the more general transform function F. This uses the notion of coupled modules in the whole brain, as are observed to be needed by the non-invasive techniques mentioned earlier. Thus the possibility of chaos will not be regarded as problematic to the program being proposed.

It is possible to build neural modules to model some of the important processes observed in psychology. Thus the various sorts of memory and other processes may be modelled as:

- working memory (as a set of neuron buffers)
- semantic memory (as an associative memory)
- episodic memory (as a recurrent net)

- attention (as a lateral inhibitory net)
- action (by means of a population vector encoding)

This is an incomplete list, but can be begun to be made complete. However in order to do that it would appear necessary to consider the manner in which psychological tasks may themselves be broken down. That is done in the next section.

6 Component Sub-Processes

The method to be developed here is to try to decompose complex psychological functions into a set of lower order component sub-processes (CSPs). These latter will attempted to be chosen so as to be independent of each other. That would then make the identification of neural substrates for their performance easier, in the sense that separate neural modules would be expected to support the different CSPs. Lesion deficits would then be expected to show loss of different components of the complex tasks, and hopefully even allow better identification of the CSPs involved. Such a program has already been started for the frontal lobes in [12], where the supposed executive function action of that region has been attempted to be decomposed into a set of CSPs in the case of attention.
The conjecture, then, is that

> Any complex psychological task is decomposable into a set of independent component sub-processes, each of which is distributed across only a few separate brain areas.

Such a conjecture would make the analysis of brain function a problem of mapping the corresponding CSPs onto the appropriate brain areas. There may well be a limit as to how far it is possible to break down a complex psychological task in a manner which still has psychological observability. Thus it might be supposed that some small brain areas may give a contribution to a task which does not have any clearly observable effect on task performance. However the principle of parsimony would lead one to expect that such areas would be rather unlikely, since they do not appear to possess much survival value to the system and so could be dispensed with.
It is possible to group complex tasks under the four main headings:

- Perception
- Movement
- Memory
- Thought

It is further seen that perception itself has at least the two component sub-tasks of construction of codes (in the five separate modalities) and that of representations (such as at feature, object, category, position, body matrix, lexical, phonological and word level). There are numerous sub-divisions of memory (episodic, semantic, implicit, priming, working, active) with considerable overlap with representations (which are the objects of memory). There are functions which are strongly associated with limbic regions, such as goals, values, drives and self representations.

There are also frontally-sited functions, as in attention, social behaviour, planning and actions [13].
The above set of functions is performed by complex brain networks, as demonstrated clearly in [2]. It is a very important but difficult task to attempt to reduce this broad range to a smaller set of underlying elements, the CSPs alluded to above. The following set is proposed as a preliminary version of the required list:

- Analyser (into features, objects or categories)
- Predictor/Actor (as a generator of schema)
- Monitor (for assessing goodness of fit)
- Activator (to promote or inhibit on-going schema or other forms of processing)
- Buffer (for holding activity over a fixed or variable time)
- Clock (for estimating temporal duration)
- Long-term memory stores (both implicit and declarative)
- Goal formation (involving value-memory)
- Drive (arising from internal bodily sources, and being independent of the activator)

There may be other CSPs which must be added to the above list. Moreover the CSPs of a given sort specified above may have different properties amongst each other. Thus there are buffers which hold activity for a fixed time (such as the phonological store [14]) and those which can preserve it over a variable time of up to 30 or so seconds (associated specifically with frontal lobe). Similarly activators can either excite or inhibit, and there may thus be two quite separate sub-classes of modules performing these two disparate functions. However the suggested list of CSPs given above seems to be of enough interest to explore its use in attempting to reduce the complexity of psychological tasks to more manageable proportions. It includes those suggested in [12] for the frontal lobe, where the 'logic CSP' introduced there is assumed to be the schema generator above, and compression of separate inhibitor and excitor modules has been introduced in our list to give a common activator sub-set.
The next step is to develop a neural underpinning for the mental processes at the level of the CSPs listed above. Thus single modules or small coupled nets of them must be constructed which (a) have a close relation to neural modules in the brain from an anatomical and functional point of view (b) appear to cause deficits in processing when there is loss of the relevant module (c) are seen to be active in the performance of a task as determined by some non-invasive measurement.

7 Neural Modules for Component Sub-Processes

There are already a number of modules which may be suggested to solve the above problems (a), (b) and (c). Thus

(i) an *analyser* may be designed from a convolution filter, such as by the use of a Gabor function kernel. Such a filter has similarity to the action of striate visual cortex, and may be directly mapped onto the action of simple cells in area V1, say. There is also a considerable level of understanding of the manner in which such a filter may arise from adaptation to visual input.

(ii) a *predictor* may be constructed as a recurrent net of the form

$$x(t+1) = F(I(t), x(t), x(t-1), ...)$$

where such recurrence leads to the generation of a sequence stored in the nature of the response function F, which may also be modulated by the external input I. Identification of such a system is in terms of well defined recurrence of neural output, as is well known as occurring in hippocampus, for example [15].

(iii) an *activator* may be constructed as a set-point detector, say in the form

$$x(t+1) = Y(-I(t) + s)$$

where Y is the Heaviside step function. Then neuron x is active (to initiate search, say) if the input I (which may be some internal energy level, say) drops below the threshold or set-point s. This can be mapped onto various brain-stem systems.

(iv) *active memory , comparator action, etc*: there are several tasks associated with actions which are not so simple to relate to actual neuranatomical structures, although there is now increasing work on this area of investigation. Some of these are specifically associated with frontal functions. The approach to be adopted here now is to take a specific architecture, that of the ACTION network [16], and determine in which manner it may be able to support the CSPs associated with monitoring, prediction/action (schema generation) and active memory.

The ACTION network comprises the frontal cortex, basal ganglia and associated thalamic nuclei. It is decomposable at least into the four main loops of motor action, frontal eye fields, limbic activity, and cognitive activity [17]. These loops are supposed to have a certain degree of autonomy, so might be expected to play an important role in the support of CSPs.

The architecture of the ACTION net is one of a feedback loop between cortex and thalamus which has threshold modulation by a non-reciprocal disinhibitory feed from cortex down through the basal ganglia to the same area of thalamus as was in contact with the cortex in the first place. The ACTION network is built to capitalise on this structure so as to allow for the development of a flip-flop action between cortex and thalamus. Thus activity arriving at a cortical region from posterior cortex (parietal or temporal areas have important cortico-cortical connections with frontal cortex) may cause the cortico-thalamic loop to be activated, and stay on. Such persistence may crucially require support from the basal ganglia disinhibition, which may be achievable by means of cingulate activation (as 'drive') from some set point detector, or from some goal memory set up there or on another portion of the ACTION network.

Such functionality may thus be seen to support active memory. By the addition of lateral inhibition in the two levels of the basal ganglia it may also be shown to

function as a comparator. Again the successful performance by ACTION to achieve this can be argued for, since if there is an active memory being preserved on cortex and thalamus then a new, but different, one arriving on cortex will produce lateral inhibitory activity in basal ganglia. A competitive action is then fought on the basal ganglia between the earlier activity and that newly arriving. Assuming that there is support for the earlier activity from cingulate, say, as part of drive, then the former activity will win this competition on the basal ganglia. That means that the new activity will not be able to persist on cortex, since its threshold disihibiting mechanism has been lost. Only new activity in agreement with the past activity will be able to continue its activity unchecked, and contribute positively to the previously stored activity on cortex. This latter may then exceed some detection threshold to indicate that a search has been completed successfully, say.

Besides the obvious mathematical questions associated with the development and storage capacity of the proposed cortico-thalamic flip-flop and of the lateral competitive system on the basal ganglia, there is a more fundamental question that needs answering. It is well established experimentally that coding of action in motor or premotor cortex is in terms of a population code. Many cells in motor cortex contribute to the determination of the direction an action will take. Each has its own preferred direction, say α_i, and resulting activity proportional to $[1 + \cos(\theta - \alpha_i)]$, if θ is the direction of the upcoming movement. However it does not seem easy to preserve this activity level by means of a flip-flop memory, since in that case activity is either on or off, and is not graded. Therefore there seems to be a contradiction between the proposed functioning of ACTION as a flip-flop and the presence of a range of preserved activities by population coding.

One way to understand the mode of persistence of the motor cortex population vector is to suppose that the motor cortex has an attractor behaviour arising from its structure as a recurrent net due to the lateral connections it possesses. These connections have been observed as having weights anticorrelated with the preferred direction of movement vector for each cell; the value $w_{ij} = \cos(\alpha_i - \alpha_j)$ would roughly fit the data of [18. In that case the value of the quantity $\sum w_{ij}[1 + \cos(\theta - \alpha_j)]$ may be seen to be proportional to $\cos(\theta - \alpha_i)$ (with constant of proportionality $1/3$). In order to obtain the additional term 1 in the cortical neuron activity it seems necessary to use disinhibition from the basal ganglia side line. This can be achieved by the use of summation of activity from a set of N cortical neurons onto a single basal ganglia neurons (experimentally there is at least a ratio of a hundred cortical neurons to one basal ganglia neuron) and thence to the thalamic cell; the weight of the basal ganglia neurons need only be of order $1/N$ for preservation of the activity.

There now seems to be two possible sources of active memory in frontal cortex. One is that developed in the previous paragraph, which uses a relaxation net of recurrent connections which seems to fit the observed pattern of persistence in motor cortex. The other is that of the previous paragraph, with a set of attractors developed by thalamo-cortical feedback connections (functioning somewhat as a bidirectional associative memory or BAM might). However the former model also needs the activity of appropriately connected, and active, thalamic neurons to feed the threshold disinhibition from thalamus up to the relevant cortical cells. Thus there appears to be some sort of a reconciliation of these two proposed modes of action of the cortico-thalamic- basal ganglia system. It is clear that further analysis,

and much simulation, needs to be performed in order to determine the effectiveness of the ACTION network in this case.

8 Modules for the Mind

There are clearly many modules involved in the creation of consciousness. An important question is if there is a distributed action of the brain to achieve conscious awareness or if there are discrete centres which are to be regarded as the true sites of such experience which is then shared around or broadcast to other such sites so as to give a unified system of response. There is some support for the latter form of neural system for consciousness, since inputs are known to be processed up to a semantic level without reaching awareness. This is associated with the phenomenon of subliminal processing. It is now reasonably well established that awareness and response to a later word or other input may be modified by earlier inputs which have not gained access to the awareness system but which have been processed up to a reasonably high level. The highest level, as noted above, was up to semantic memory, but only for words and not for sentences. It is therefore clear that there are quite high level modules in the brain whose activation does not directly produce consciousness but which are important in the influence their activity may exert on later conscious experiences.

Such a modulating influence has been modelled [19] by means of a coupled set of semantic/ working memory modules. The first of these acts in a feedforward excitatory manner with dedicated nodes (which might arise from some form of topographic map) which feed to similar nodes on a working memory module with longer time constants. This latter net acts as a buffer so as to hold activity for a second or so, in order that earlier context can be properly incorporated in any decision that is taken on the working memory module. This latter has inhibitory connections between incompatible nodes, so that their activity may effect the time to reach a certain threshold of nodes activated by later inputs from the semantic net. It is possible in this manner to model with some accuracy the changes in reaction time in lexical decision tasks brought about by subliminally processed letter strings at an earlier time.

Consciousness seems to reside, therefore, on the working memory modules of the posterior cortex. These are present for a variety of codes, and allow a detailed implementation of the Relational Mind model developed by the author over 20 years ago, and published more recently in a more developed form [20]. However there are various features of consciousness that are missing from this model, in particular the emergence of its uniqueness. Such a feature might be expected to arise from some form of competitive action between the different working memory modules. Such an action might be able to occur in cortex by suitable connection of excitatory outputs from a given working memory module to others. However there is no clear picture of such inhibition, especially between the working memory modules which appear to be at about the same level in the hierarchy of brain modules following cytoarchitectonic and myeloarchitectonic reasoning; these working memory sites may be classified as heteromodal cortex.

In order to resolve this issue of the putative source of long range inhibition in cortex (which is also seen to be absent in the modelling of global EEG patterns) it may be that there are sub-cortical sites of such inhibition which are of importance. It

has been suggested that there are indeed such sites, in particular in the nucleus reticularis thalami (NRT for short) which is a sheet of totally inhibitory neurons which surround the upper and lateral parts of the thalamic nuclei. NRT cells are activated by thalamo-cortical axon collaterals piercing the NRT, as also by cortico-thalamic axon collaterals. A model of this system has been constructed [21] which has been shown to lead to global competition, and even to allow explanation of the relatively long time to reach consciousness determined by the beautiful experiments of Libet and his colleagues [22].

The picture that emerges from these analyses is of a set of coupled semantic (SM)/ working (WM) memories, each for a given code A. There is a competition between the activities of the WMs, the winner being that whose content emerges into consciousness. However this account only deals with posterior sites, so is more correctly denoted C_p, the subscript denoting both posterior and passive. The other important component of consciousness will be denoted as C_a, the subscript now denoting anterior and active. It is that aspect of awareness which the ACTION network, introduced above, can also begin to tackle in terms of the various control operations it can perform. Various aspects of this have been discussed earlier, as part of the consideration of active memory and the comparator action it may support.

9 Conclusions

From what has been outlined briefly above the time seems opportune to mount a program attempting to simulate the brain on a large scale by modelling it as a set of connected modules, each composed of simple neurons connected together by a set of well defined rules. The program can be broken down into separate tasks:

- construct a software simulation with about 100 modules, each with ever more complex neurons,
- include increasingly detailed neuroanatomical analyses so as to include increasing realism,
- develop the simulation so as to allow for a modular analysis of psychological functions and their component sub-processes,
- test the simulation results against non-invasive instrument measurements,
- perform mathematical analyses of the resulting equations using techniques from dynamical systems and statistical mechanics.

The resulting set of models will be able to provide an increasingly detailed basis to explore the manner in which the brain can support the mind.

REFERENCES

[1] Prof H Muller-Gartner, private communication.
[2] MI Posner and ME Raichle *Images of the Mind* Scientific American Library, Freeman (1994).
[3] J Grafman, A Partiot and C Hollnagel, *Fables of the prefrontal cortex* , Behaviour and Brain Sciences, Vol. 18 (1995), pp349–358.
[4] A Ioannides, JPR Bolton and CJS Clarke, *Continuous Probabilistic Solutions to the Biomagnetic Inverse Problem* , Inverse Problems Vol. 6 (1990), pp523–542.
[5] F Alavi, A Ioannides and JG Taylor, *The Biomagnetic Inverse Problem* , in Artificial Neural Networks 2, I Aleksander and JG Taylor (eds), Elsevier Science Publishers (1992).
[6] Ibid, work in progress.

[7] GG Globus, *Towards a Noncomputational Cognitive Neuroscience* J Cognitive Neuroscience Vol. 4, pp299–310.

[8] JG Taylor, *A Silicon Model of Vertbetrate Retinal Processing* , Neural Networks Vol.3 (1990), pp171–178.

[9] DJ Felleman and DC Van Essen, *Distributed Hierarchical Processing in the Primate Cerebral Cortex* , Cerebral Cortex, Vol. 1 (1991), pp1–47.

[10] F Alavi and JG Taylor, *A global competitive network* , Biol Cyb. Vol. 72 (1995), pp233–248.

[11] M Steriade, DA McCormick and TJ Sejnowski, *Thlamocortical Oscillations in the Sleeping and Aroused Brain* , Science Vol. 262 (1993), pp679–685.

[12] DT Stuss, T Shallice, MP Alexander and TW Picton, *A Multidisciplinary Approach to Anterior Attentional Functions* Univ of Toronto preprint, unpublished, (April 1995).

[13] R Bappi, G Bugmann, D Levine and JG Taylor, *Neural Models of Executive Function* , in preparation (1996).

[14] A Baddeley, *Working Memory*, Oxford Univ Press (1986).

[15] M Reiss and JG Taylor, *Does the Hippocampus Store Temporal Patterns?* , Neural Network World Vol. 3 (1992), pp365–384.

[16] JG Taylor, *Modules for the Mind of PSYCHE* , Proc WCNN95, II-967-972 (1995), Lawrence Erlbaum Associates.

[17] GE Alexander, MD Crutcher and MR DeLong, *Basal ganglia thalamocortical circuits: parallel substrates for motor, oculomotor, 'prefrontal' and 'limbic' functions* Prog Brain Res. Vol. 85 (1990), pp119–146.

[18] AP Georgopoulos, M Taira and A Lukashin, *Cognitive Neurophysiology of the Motor Cortex*, Science Vol. 260 (1993), pp47–52.

[19] JG Taylor *Breakthrough to Awareness*, Neural Computation, in press.

[20] JG Taylor *The Relational Mind*, Seminars at Tubingen and London Universities (1973); ibid *Can a Neural Network ever be made to think?*, Neural Network World Vol.1 (1991), pp4–12.

[21] JG Taylor, *Towards a neural network model of the mind* , Neural Network World Vol.2 (1992), pp797–812.

[22] B Libet, WW Alberts, EW Wright Jr, DL Delattre, G Levin and B Feinstein, *Production of Threshold Levels of Conscious Sensation by Electrical Stimulation of Human Somato-Sensory Cortex* , J Neurophysiol Vol.27 (1964), pp546–578.

PART II

SUBMITTED PAPERS

THE SUCCESSFUL USE OF PROBABILITY DATA IN CONNECTIONIST MODELS

J. R. Alexander Jr. and J. P. Coughlin
Towson State University, Towson, USA.

Reggia [10] explored connectionist models which employed "virtual" lateral inhibition, and included the activation of the receiving node in the equations for the flow of activation. Ahuja [1] extended these concepts to include summing the total excitatory and inhibitory flow into a node. He thus introduced the concept that the change of activation of a node depended on the integral of the flow into that node and not just the present activation levels of the nodes to which it is connected. Both Reggia's and Ahuja's models used probability data for the weights. Ahuja's model was further extended by Alexander [2], [3], [4] in the RX model to allow both the weights and the activations of Ahuja's model to be negative, and further, Alexander's model included the prior probabilities of all nodes. Section 1 of this paper contains a complete listing of the RX equations and describes their development. The main result of this paper, the demonstration of the convergence of the system is presented in Section 2. Section 3 briefly describes the experiments testing the RX system and summarizes this article.

1 The RX Equations

The net is two-layered, with the lower level being the J input nodes and upper level the N output nodes. The values of the upper level nodes, $a_i(t)$, are on $[0, 1]$. The prior probability of the existence of the feature associated with the ith node is called $\overline{a}_i$. Values of $a_i(t)$ greater than $\overline{a}_i$ indicate a higher than average chance of occurrence of the feature represented by node i, and those lower, indicate a less than average chance. The activation on the lower level nodes is computed from the range of possible input values to a node. If the smallest observed value is Min_j, the largest Max_j and the average Ave_j. Let $Observ_j$ be the observed value. Then define:

$$m_j = \frac{[Observ_j - Ave_j]}{[Max_j - Ave_j]} \text{ if } Observ_j > Ave_j \quad \text{and}$$

$$m_j = \frac{[Observ_j - Ave_j]}{[Ave_j - Min_j]} \text{ otherwise} \tag{1}$$

Clearly m_j lies on $[-1, 1]$. When m_j assumes the value 1, then the feature represented by m_j is present, with probability one. When m_j is -1 the feature is absent with probability one. A value of zero indicates that no information exists concerning the absence or presence of this feature. Two sets of weights exist. The first is called w_{ij}, and in absolute value indicates the probability of occurrence (if positive, and non-occurrence if negative) of the feature associated with the upper level node (ith), given the existence of activation on the lower level node (jth). The second weight is called v_{ij}, and in absolute value indicates the probability of occurrence (if positive, and non-occurrence if negative) of the feature associated with the lower level node, given the existence of activation on the upper level node.

Two auxiliary functions are to be associated with each $a_i(t)$. The function which conveys the excitatory activation is called $Exc_i(t)$, and the one which conveys the inhibitory is called $Inh_i(t)$. Each is the sum of all the excitatory and inhibitory flow of activation into node i. These functions are defined by their derivatives and,

since the latter are sums of everywhere positive terms, the former are monotone-increasing. Each of the terms used in defining the derivative is a function of all the $a_i(t)$ and is the variable forcing term. There will be one such function for each lower level (j) node, hence a sum need be taken over all the j nodes connected to any given i node. The bounded characteristic is achieved by including in the equation a factor of the form $[N - Exc_i(t)]$. The choice of N as the bound to which $Exc_i(t)$ approaches is somewhat arbitrary.

2 Convergence of the RX Equations

2.1 The RX Equations

$$\dot{a}_i(t) = K_3 * c_u * [1 - a_i(t)] * [Exc_i(t) - Inh_i(t)] \quad (2)$$

$$\dot{a}_i(t) = K_3 * c_l * [a_i(t)] * [Exc_i - Inh_i] \quad (3)$$

According as $a_i(t) \geq \overline{a}_i$ or $a_i(t) \leq \overline{a}_i$ respectively. K_3 is a constant of proportionality, and the values of c_l and c_u are chosen to keep the derivative continuous at $\overline{a}_i$:

$$c_u = 1/(1 - \overline{a}_i), \qquad c_l = 1/\overline{a}_i.$$

$$\dot{Exc}_i(t) = K_1 * \overline{a}_i * [N - Exc_i(t)] * \sum_j [k_{11} * OUTPP_{ij}(t) + k_{12} * outpm_{ij}(t) + k_{13} * outmp_{ij}(t) + k_{14} * OUTMM_{ij}(t)] \quad (4)$$

$$\dot{Inh}_i(t) = K_2 * \overline{a}_i * [N - Inh_i(t)] * \sum_j [k_{21} * outpp_{ij}(t) + k_{22} * OUTPM_{ij}(t) + k_{23} * OUTMP_{ij}(t) + k_{24} * outmm_{ij}(t)] \quad (5)$$

Here $k_{11}, \ldots, k_{24}$ are included for generality.

$$OUTPP_{ij}(t) = \frac{W_{ij} * |a_i(t) - \overline{a}_i|}{\sum_l W_{lj} * |a_l(t) - \overline{a}_l| + \epsilon_d} * m_j \quad (6)$$

with similar expressions for the other $OUTP$ terms and

$$outpp_{ij}(t) = \frac{\sum_{k \neq i} V_{kj} * |a_k(t) - \overline{a}_k|}{\sum V_{lj} * |a_l(t) - \overline{a}_l| + \epsilon_d} * m_j * |a_i(t) - \overline{a}_i| \quad (7)$$

with similar expressions for the other $outp$ terms. The ϵ_d is included so that the denominator never vanishes.

2.2 The Dynamics of the RX Net

The principal result of this section, that the dynamics of the RX system converges, is given in Section 2.3 below. Hirsch [8] defines convergent dynamics by stating that "the trajectory of every initial condition tends to some equilibrium". Prior to stating the theorem, we make some observations about the critical points.
They are labeled as follows:

$$CP_0 = (r_1, r_2, ..r_i, ..r_N, N_1, ..N_N, N_1, ..N_N) \quad (8)$$

and

$$CP_L = (r_1, r_2, ..r_{N-L}, \overline{a}_{N-L+1..N}, N_1, ..N_{N-L}, d_{N-L+1}..d_N, N_1, ..N_{N-L}, d_N..d_N) \quad (9)$$

where r_i (the value of a_i) $\in (0,1)$, and the d_i (the value of Exc_i or Inh_i) $\in [0, N)$. By letting L (the number of the $a_i(t)$ that approach $\overline{a}_i$) range from 0 through N, all critical points may be described simply by stating the value of L, and that of each d_i. Note that the critical points need NOT be isolated. One of the lemmas in [2] has demonstrated that $Exc_i(t)$ and $Inh_i(t)$ are monotone increasing functions. As a result, points of type CP_L may be thought of as "on the way" to CP_0. If $Exc_i(t)$ and $Inh_i(t)$ approach N, then the critical point becomes of type $CP_{(L-1)}$.

The norm adopted in the sequel is the ℓ_1 norm [6] where: $\|X\| = \sum_i |x_i|$. We proved [2] that both $Exc_i(t)$ and $Inh_i(t)$ are bounded monotone increasing functions and that the RX functions are Lipschitzian throughout their domain of definition.

We now discuss the details of the interface of the upper and the lower branches of the equations. Recall, the upper branch is defined for $a_i \in [\overline{a}_i, 1]$, and the lower branch for $a_i \in [0, \overline{a}_i]$, Since each branch is analytic on its domain of definition, and the composite (upper and lower branches considered as one) function is Lipschitzian where the branches meet (at $a_i = \overline{a}_i$), the solutions through any point exist and are unique. To examine stability, it is necessary to look at the derivatives of the RX function and we are confronted with the problem that the derivative, per se, does not exist on the hyper-plane $a_i = \overline{a}_i$. However, the left-hand and right-hand derivatives do exist and for the purpose of calculating stability (in our case convergence) of the solution, we contend that the above conditions are sufficient since convergence is concerned with the behavior of the solutions passing near the critical points.

2.3 Demonstration of the Convergence of the $a_i(t)$:

Theorem 1 *Consider the equations (2) through (9). Given:*

$$0 \leq Exc_i(t_0), Inh_i(t_0) \leq N \text{ and } 0 \leq a_i(t_0) \leq 1, \text{ all } i; -1 \leq m_j \leq 1, \text{ some } m_j \neq 0. \tag{10}$$

Then, under the above initial conditions, all trajectories of the RX system tend to some equilibrium point.

Proof From the definition, $Exc_i(t)$ and $Inh_i(t)$ can be shown to be bounded monotone functions [2], and therefore approach limits, LE_i and LI_i, respectively (see Buck [7], pg 26). The cases that may occur are:

$$\begin{array}{lccl} (1) & LE_i & \neq & LI_i; \\ (2a) & LE_i & = & LI_i = d_i, (d_i < N) \text{ and}; \\ (2b) & LE_i & = & LI_i = N. \end{array}$$

Case (1) By examining separately the cases where $LE_i > LI_i$ and $LI_i > LE_i$, it is easily shown that $a_i(t)$ approaches a limit in either case. (See [2].)

The remaining two cases are, (2a) in which $LE_i = LI_i = d_i < N$, and (2b) in which $LE_i = LI_i = N$. For the space of any triple, a_i, Exc_i, and Inh_i, a plane is formed by $Exc_i = Inh_i$. This is pictured in Figure 1. The line formed by the intersection of the plane with the plane $a_i = \overline{a}_i$ constitutes the ith component of a CP_L type critical point. Thus, this line forms a continuum of critical points.

The flow, in both Cases (2a) and (2b), is considered (1) outside a 2η band (η positive and small) about the plane $a_i = \overline{a}_i$ and (2) inside this band. It is not difficult to analyze what happens outside the band, but pure analysis proofs could not be obtained inside the band. Hence, within the 2η band of the $\overline{a}_i$ plane, the associated linear system was used to analyze the flow of activation.

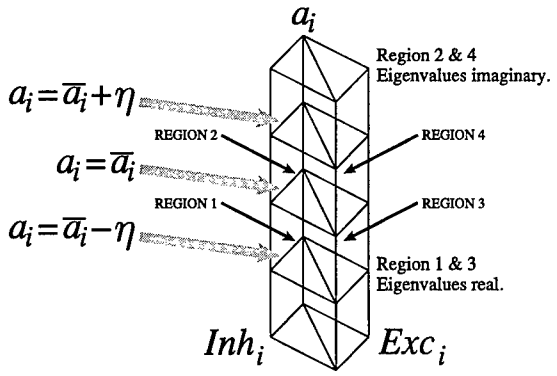

Figure 1 Details of the volume V.

Case (2a) $LE_i = LI_i = d_i$, where $0 < d_i < N$.
(1) Flow outside the 2η band. Equations (8) furnished the result of formally integrating equation (4) and equation (5). The results were:

$$Exc_i(t) = N - [N - Exc_i(t_0)] * e^{-K_1 \overline{a}_i * \int_{t_0}^{t} OUT_i(s)\, ds} \tag{11}$$

$$Inh_i(t) = N - [N - Inh_i(t_0)] * e^{-K_2 \overline{a}_i * \int_{t_0}^{t} out_i(s)\, ds} \tag{12}$$

Assume that after some time T, $a_i(t)$ remains bounded away from the $\overline{a}_i$ plane, by some arbitrarily small amount η. Therefore:

$$I_1 = \int_0^\infty OUT_i(t)\, dt = \int_0^\infty g_1 |a_i - \overline{a}_i|\, dt > \int_0^\infty |g_1|_{\min} \eta\, dt \tag{13}$$

$$I_2 = \int_0^\infty out(t)\, dt = \int_0^\infty g_2 |a_i - \overline{a}_i|\, dt > \int_0^\infty |g_2|_{\min} \eta\, dt. \tag{14}$$

In equation (9), g_1 is $W_{ij}/(\sum_l W_{lj} |a_l - \overline{a}_l| + \epsilon_d)$, and g_2 is

$$(\sum_{k \neq i} V_{kj} |a_l - \overline{a}_l|)/(\sum_l V_{lj} |a_l - \overline{a}_l| + \epsilon_d)$$

Not all the $a_k(t)$ may approach their $\overline{a}_k$. Were this to occur, then I_2 would approach a limit different from I_1. Therefore, LE_i would be greater than LI_i and contrary to the assumption ($LE_i = LI_i = d_i$) would not converge to d_i, contrary to hypothesis.
Under the assumption that $\sum_{k \neq i} V_{kj} |a_k(t) - \overline{a}_k| \neq 0$ we assert that, $g_2 = \mathcal{O}(g_1)$ and $g_1 = \mathcal{O}(g_2)$ ($\mathcal{O}$ stands for "order of"). That is, g_1 and g_2 are of the same order of magnitude (Olmstead [9], p141.) since they are both ratios of fractions whose denominators are not zero. The integrals I_1, and I_2 will therefore diverge and, $Exc_i(t)$ and $Inh_i(t)$ will approach N and not d_i contrary to assumption.
(2) The flow inside the 2η band. Elsewhere [2], the eigenvalues and eigenvectors of the Jacobians on each side of the $a_i(t) = \overline{a}_i$ hyperplane are calculated, and solutions of the associated linear system discussed in detail. It suffices to say that on one side of the hyperplane $a_i(t) = \overline{a}_i$, the eigenvalues are imaginary, and cause elliptical motion about the line, $Exc_i(t) = Inh_i(t)$ (at d_i), which is in the hyperplane

$a_i(t) = \overline{a}_i$. In Figure 1 the imaginary eigenvalues from the linear system characterize the motion above the $\overline{a}_i$ plane, and the real eigenvalues that below this plane. From below the $\overline{a}_i$ plane trajectories in the region where $Exc_i > Inh_i$ (called Region 1 in Figure 1) approach the $\overline{a}_i$ plane from below, and penetrate it. Above the $\overline{a}_i$ plane (Region 2 where $Exc_i > Inh_i$) trajectories travel an elliptic path about the line $Exc_i = Inh_i$ and enter Region 4, (where $Inh_i > Exc_i$). Two situations may occur. First, they may leave the η band and go far enough above it that they may not return. It is known that the integrals diverge in this region and hence $Exc_i(t)$ and $Inh_i(t)$ do not converge to d_i. Second, the trajectories may move back towards the hyperplane $a_i(t) = \overline{a}_i$. They penetrate this plane and pass through to the other side. Once beneath the $\overline{a}_i$ plane they are in Region 3, where $a_i < \overline{a}_i$, and $Inh_i > Exc_i$. The trajectory then moves away from the critical point. Since both Exc_i and Inh_i are monotone non-decreasing, once past d_i, they cannot approach this point again. Therefore, unless trajectories actually encounter a CP_L type critical point, they are driven away from it and into the region where $|a_i - \overline{a}_i| \geq \eta$. The integrals I_1 and I_2 therefore increase, and hence Exc_i and Inh_i, being monotone increasing, will exceed d_i and not approach it as a limit.

Below the $\overline{a}_i$ plane, the eigenvalues are real, but one of them is positive. Bellman, [6] (Theorem 3, p88) has shown that, under conditions which the RX equations obey, (i.e. differentiability Rudin [11], pg 189) critical points possessing positive eigenvalues are unstable. As such, CP_L type critical points are unstable equilibrium points. Instability is not a strong property, and therefore, the possibility of points approaching a CP_L type critical point cannot be dismissed. Elsewhere [2] it is demonstrated that a solution of the linear system does indeed approach $\overline{a}_i$.

We now move on to the last remaining possibility for $Exc_i(t)$ and $Inh_i(t)$: $LE_i = LI_i = N$. {Case (2b)}

(1) Flow outside the 2η band. In this case as in the preceding case it is fairly simple to show that $a_i(t)$ approaches a limit.

(2) Flow inside the 2η band. Flow inside the band is approximated by the linear system, but all trajectories are now those for which $Exc_i(t)$ and $Inh_i(t)$ are within ϵ of N. The approximating linear equations are presented in [2]. As before, the trajectories will eventually reach Region 3, where, although the constants multiplying it are small, the motion is still governed by a positive exponential and $a_i(t)$ will be directed away from $\overline{a}_i$. Thus, it would appear that when $a_i(t)$ leaves the cube of figure 1, it will approach a limit. □

We conclude by proving a lemma.

Lemma 2 *If* $\lim_{t\to\infty} Exc_i(t) = Inh_i(t) = N$, *then* $a_i(t)$ *will not attain* $\overline{a}_i$ *in finite time.*

Proof The proof is by contradiction. Assume for $t > t^*$ that $a_i(t) = \overline{a}_i$. Then, for $t > t^*$, $OUT_i(t) = out_i(t) = 0$. Therefore:

$$\int_0^\infty OUT_i(t)\,dt = \int_0^{t^*} OUT_i(t)\,dt = \alpha \qquad \int_0^\infty out_i(t)\,dt = \int_0^{t^*} out_i(t)\,dt = \beta \tag{15}$$

where α and β are finite numbers. Integrating (4) we have for a solution to $Exc_i(t)$:

$$\lim_{t\to\infty} Exc_i(t) \;=\; N - [N - Exc_i(t_0)]e^{-K_1\overline{a}_i\int_0^\infty OUT_i(t)\,dt}$$

$$= \quad N - [N - Exc_i(t_0)]e^{-K_1 \overline{a}_i \alpha} \neq N.$$

The same can be shown for $Inh_i(t)$. □

It would appear from this lemma, and from the fact that $a_i(t)$ is very near the $\overline{a}_i$ plane, that the trajectories within the volume being considered are moving very slowly. This is to be expected since all terms are small.

We have thus shown in all three cases (1), (2a) and (2b) that all trajectories of the RX system approach limits and hence the demonstration of the convergence of $a_i(t)$ is complete.

3 Summary

The RX equations have been tested both in associative memory and control applications. In associative memory abilities, a back-propagating net's performance only slightly exceeded that of the RX net in a test involving classifying RADAR signals. In control applications a two input, one output node RX net (three neuron controller) performed as well or better than a fuzzy controller in the task of backing a truck to a loading dock. Because of the apparent biological plausibility of the three neuron controller, and the existence of elementary life forms with control circuitry yet no memory circuitry, we offer the speculation that neural memory circuitry has evolved from neural control circuitry [5]. Recall, that the RX net uses probability data as weights and that it involves no learning. In the future, we intend to study more biologically plausible versions of the RX net both in memory and control applications.

REFERENCES

[1] Ahuja S., Soh W., Schwartz A. *A Connectionist Processing Metaphor for Diagnostic Reasoning.* International Journal of Intelligent Systems, (1988).

[2] Alexander, J.R. . *An Analysis of the General Properties and Convergence of a Connectionist Model Employing Probability Data as Weights and Parameters.* PhD Dissertation (1991), University of Maryland Baltimore County, Baltimore MD.

[3] Alexander, J.R. *A Connectionist Model Employing Probability Data as Weights and Parameters.* Intelligent Engineering Systems Through Artificial Neural Networks, Vol 2. (1992), ASME Press, New York NY.

[4] Alexander, J.R. *Calculating the Centroid of a Fuzzy Logic Controller Using an Artificial Neural Net.* Intelligent Engineering Systems Through Artificial Neural Networks, Vol 3. (1993), ASME Press, New York NY.

[5] Alexander, J.R. and Bradley, J. B. *The Three Neuron Controller — History, Theoretical Foundations, and Possible Employment in Adaptive Control.* Intelligent Engineering Systems Through Artificial Neural Networks, Vol 5. (1995), ASME Press, New York NY.

[6] Bellman R. *Stability Theory of Differential Equations*, (1953), New York: McGraw-Hill.

[7] Buck R.C. *Advanced Calculus*, (1956), New York: McGraw-Hill.

[8] Hirsch M. *Convergent Activation Dynamics in Continuous Time Networks.* Neural Networks 2 (1989), pp331–349.

[9] Olmstead J.M.H. *Advanced Calculus.* (1961), New York: Appleton-Century-Crafts, Inc.

[10] Reggia J. *Virtual Lateral Inhibition in Parallel Activation Models of Associative Memory.* Proceedings Ninth International Conference on Artificial Intelligence (1985), pp 244–248.

[11] Rudin W. *Principles of Mathematical Analysis.* (1976), New York: McGraw Hill.

WEIGHTED MIXTURE OF MODELS FOR ON-LINE LEARNING

P. Edgar An

Department of Ocean Engineering,
Florida Atlantic University, Boca Raton, FL 33431, USA.

This paper proposes a weighted mixture of locally generalizing models in an attempt to resolve the trade-off between model mismatch and measurement noise given a sparse set of training samples so that the conditional mean estimation performance of the desired response can be made adequate over the input region of interest. In this architecture, each expert model has its corresponding variance model for estimating the expert's modeling performance. Parameters associated with individual expert models are adapted in the usual least-mean-square sense, weighted by its variance model output. Whereas the variance models are adapted in such a way that expert models of higher-resolution (or greater modeling capability) are discouraged to contribute, except when the local modeling performance becomes inadequate.

1 Background

Artificial neural networks have been widely used in modeling and classification applications because of their flexible nonlinear modeling capabilities over the input region of interest [3]. The merit of individual networks is generally evaluated in terms of cost criterion and learning algorithm by which the free parameters are adapted, and the characteristics of the parametric model. These networks often employ minimum sum-squared error criteria for parameter estimation such that the desired solution is a conditional mean estimator for the given data set, provided that the model is sufficiently flexible [2]. The use of such criterion not only provides a simple iterative procedure for parameter estimation but also the adaptation follows the Maximum Likelihood (ML) principle when the model uncertainty is a realization of independent Gaussian process. Nevertheless in many applications, the generalization performance which utilizes the least-square criterion breaks down when the conditional mean response is estimated using a small set of data samples with an unknown degree of noise uncertainty. This is because the LS criterion maximizes *only* the overall fitting performance defined by the data set, rather than evaluating the model mismatch in any local input region. Thus, a sufficiently flexible model often overfits undesirable noisy components in the data samples whereas a model with restricted degrees of freedom is less likely to converge to the conditional mean of the data response [4]. This paper focuses on an alternative approach in dealing with the bias/variance dilemma, which is based on a variation of the "Mixture-of-Experts" (or ME) [5].

2 Weighted Mixture of Experts (WME)

One alternative solution to the bias/variance dilemma is to incorporate a weighted mixture of expert (or WME) models so that only few experts contribute in any particular input region [5]. The internal structure in each of these experts is fixed, and a separate variance model is used, one for each expert, to evaluate its corresponding expert's performance. If the expert and variance models are chosen to be linear with respect to their adaptable parameters, the resulting learning process can be formulated as a linear optimization problem which enables rapid learning convergence.

The learning process for the WME algorithm is based on the competitive nature among experts in modeling an unknown mapping, and the overall WME output, $\hat{y}(x)$, is simply a linear combination of individual expert model outputs weighted by their variance model outputs, $\alpha_j(x)$, at x

$$\hat{y}(x) = \sum_{j=1}^{m} \frac{\exp(-\alpha_j(x))}{\sum_{k=1}^{m} \exp(-\alpha_k(x))} \hat{y}_j(x) = \sum_{j=1}^{m} p_j(x)\hat{y}_j(x) \tag{1}$$

where $\hat{y}_j(x)$ is the jth expert model output, and α_j is the corresponding variance model output (associated with the jth expert output). $p_j(x)$ can be interpreted as a local fitness measure of the jth expert modeling performance at x, and is bounded $\in [0, 1]$. The error criterion for individual expert models is defined as

$$E_y = \frac{1}{2n} \sum_{i=1}^{n} \left[\sum_{j=1}^{m} p_j(x_i)(y(x_i) - \hat{y}_j(x_i))^2 \right] \tag{2}$$

whereas the cost criterion for adapting the variance models is

$$E_\alpha = \frac{1}{n} \sum_{i=1}^{n} \left[\sum_{j=1}^{m} \lambda_j p_j(x_i) \left(y(x_i) - \hat{y}_j(x_i)\right)^2 \right] \tag{3}$$

where n is the number of data samples, and $y(x_i)$ is the data output for x_i. E_y ensures that each of the experts is allowed to best approximate $y(x_i)$, weighted by $p_j(x_i)$, whereas E_α ensures that all experts are specialized in unique input regions by assigning a smaller $p_j(i)$ for a larger error variance, and vice versa. The term λ_j in (3) regulates the variance estimation among models of varying resolution so that λ_j is larger for higher-resolution experts, and vice versa. If this term was not included, the resulting adaptation would lead to a WME model consisting mainly of high-resolution experts. λ_j can thus be interpreted as a form of regularization which takes in prior knowledge about the set of experts for modeling, and can be set inversely proportional to their degrees of freedom (e.g. total number of free parameters). This criterion is thus different from that proposed in [5] as a result of this regularizing factor λ. In the case where the model structure of any expert is non-uniform across the input region of interest (such as clustering-based radial-basis-functions network), λ_j can be modified in such a way that it varies from one input segment to another.

Like in many artificial neural networks, the iterative procedure can be modified so that the adaptation is carried out sample by sample, and the corresponding cost criterion can be reduced by dropping the first summation term in (2,3). It is generally desirable to maintain equal variance model outputs prior to *on-line* learning to avoid bias toward any particular model structure, unless prior knowledge of the unknown mapping is available (e.g. $\alpha_j(\cdot) = 0$). As training proceeds, the variance models are adapted to form appropriate prior knowledge for combining the experts. These parameterized models can be chosen from a variety of existing locally-generalizing models, such as radial-basis-functions, B-Splines or Cerebellar Model Articulation Controller (or CMAC) networks. These networks are particularly well suited to the WME model implementation because their internal structures are fixed and their parameters are defined over a local region of support, thus enabling rapid learning convergence. Also, the influence of the variance model is restricted to within the

local extent of the training input, and equal contribution will be assigned to regions of unseen data samples. If both variance and expert models generalize globally, the conditional mean estimation performance is likely to deteriorate considerably as a result of temporal instability.

3 Example

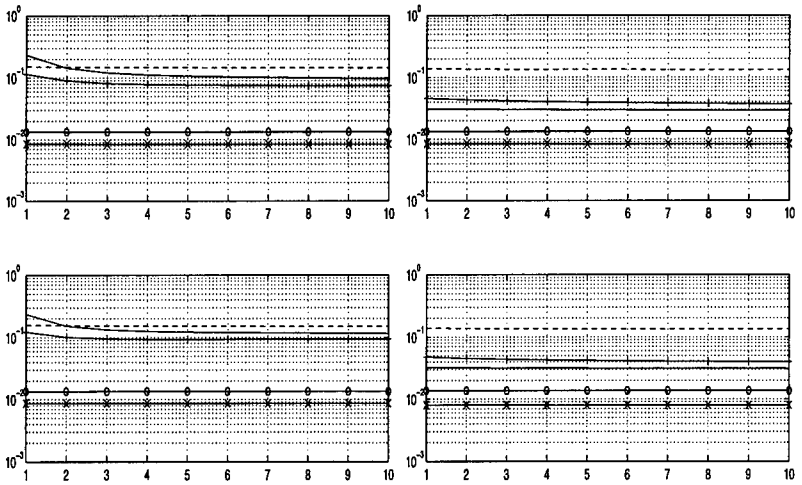

Figure 1 (a) Top: The RMS curves as a function of training cycle number for five different models averaging over 10 independent sets of 500 noiseless (randomly drawn) training samples. '–': single CMAC (C = 2); '- -': single CMAC (C = 7); '+': additive CMACs (C = 2, 7); 'o': WME CMACs (1:1 λ ratio, C = 2, 7); 'x': WME CMACs (1:3 λ ratio, C = 2, 7). (b) bottom: same RMS curves as described in (a) except that the samples are contaminated with zero-mean Gaussian noise of variance 0.1.

Figure 2 (a) Similar configuration to those described in Figure 1 except that each independent training set contains 5000 samples. (b) bottom: same RMS curves as described in (a) except that the samples are contaminated with zero-mean Gaussian noise of variance 0.1.

In this section, the generalization performance and implementation of the WME model are illustrated with an example using a sigmoidal function as desired surface

$$y(x_1, x_2) = 1 + 1/(1 + \exp[-100(x_1 + x_2)]) \tag{4}$$

This surface has a significant gradient along the ridge on the anti-diagonal but zero elsewhere, and thus the WME model is particularly well suited to the surface by fitting high-resolution experts near the anti-diagonal and low-resolution experts to regions with zero gradient. In this example, the WME model is based on two independent expert models, each parameterized as a form of CMAC. As a form of a generalized look-up-table, the CMAC output is a linear combination of a set of

submodel's output weighted by a set of adaptable parameters. Each of the submodels is defined as a union of non-overlapping basis functions of hypercubic support on the input lattice (with the support spanning C number of cells along each input axis), and these submodels are offset relatively along the input diagonal in the standard CMAC where the generalization power is dominant. As the number of submodels is also constrained to be C, which is generally greater than 1, the entire set of basis functions associated with all submodels are thus sparsely distributed on the input lattice. The individual basis function for any input can be either binary or continuous (tapered basis function) so that its response is proportional to some chosen metric norm between the input and the support center. In addition, the layout of the submodels ensures that exactly C parameters are updated at every iteration for a given training sample. One important property of the CMAC network is that a larger C leads to a larger degree of generalization but with fewer adaptable parameters, and vice versa. Thus, the trade-off between the computational cost and modeling capability must be balanced with great care. The CMAC parameters are commonly adapted using the normalized LMS algorithm in order to facilitate fast convergence. Further detail of the CMAC modeling capability and learning convergence can be found in [3].

In the sigmoidal example, the input domains were restricted to $[-1.5, 1.5]^2$ and their submodel offsets were uniform along univariate axes (see [1] for the improved offset scheme). The nonlinear input transformation function associated with each of the parameters was chosen to be linearly tapered along each input axis, and the function output was formed using the standard product operator. The individual expert model output was self-normalized in order to produce a smoother response by minimizing bias toward any particular input region. In both expert models, each input axis was partitioned into 20 intervals, and the learning rate was initially set to 1 (decreased slowly to zero). The generalization parameters, C_1 and C_2, for both expert models (identified as y_1 and y_2) were chosen to be 7 and 2. Thus, the basis support of each cell was seven intervals wide in y_1, but only two in y_2, and there were 186 and 481 adaptable parameters in y_1 and y_2 respectively. λ_1 and λ_2 were chosen to be 1 and 3 respectively because of the approximate ratio of free parameters. The variance models, α_1 and α_2, were parameterized using the same internal structure and learning rule as those of the y_1 and y_2 respectively, but with independent parameter vectors, and the model parameters were adapted using least-mean-squares method. In addition to the WME model ($M1$), four independent models were considered as control comparisons; $M2$: single CMAC (C = 2); $M3$: single CMAC (C = 7); $M4$: additive CMACs (C = 2, 7) where p_1 and p_2 were each set to 0.5, and finally $M5$: WME but with $\lambda_1 = \lambda_2 = 1$. That is, $M2 - M4$ shared identical learning rules and input partitioning with $M1$, except the generalization width, whereas $M1$ and $M5$ were only different in λ_1 and λ_2.

Case 1: RMS Study for Sparse Training Samples

In this case study, 10 independent sets of 500 data samples $\{S1, S2, \cdots, S10\}$ were generated by uniformly randomly interrogating the sigmoidal function within the hypercubic input region $\in [-1, 1]^2$. Each of the five models was independently adapted using individual sample sequentially drawn from $S1$, and the training was carried out over ten sweeps of $S1$. Parameters of these models were then nullified, and the same run was repeated for the rest of the data sets. An expected root-

mean-square (RMS) generalization error curve as a function of training cycle was then generated using 3000 independent testing samples for the five models by averaging the individual RMS performance over the ten data sets. Figure 1a shows the corresponding RMS curves for these models, and Figure 1b shows the similar curves except that the same set of training samples were contaminated with additive Gaussian noise of variance 0.1. It is interesting to observe that $M1$ and $M5$ performed significantly better than the single and additive CMACs (of fixed-$p_{1,2}$), indicating the importance of estimating the variance from the data samples. Also, $M1$ provides a better RMS fit as compared to $M5$, suggesting that the use of λ can be tuned to provide optimal resource sharing. Similar RMS curves for the first 500 training samples averaged over the ten runs also indicated similar profiles as compared to those in Figure 1, suggesting that the WME model consistently performed better than the other four models for on-line learning [1]. More work needs to be investigated on the choice of λ.

Case 2: RMS Study for Abundant Training Samples

In this case study, 10 independent sets of 5000 data samples were instead generated using the identical method described above, and the same procedure was carried out to form the expected RMS curves for the five models. Figure 2a shows the corresponding curves using noiseless samples whereas Figure 2b shows the similar curves using noisy samples. It can be observed that except $M3$ which had almost the same RMS characteristics as those shown in case 1, the modeling performances among the four models were relatively closer, suggesting that for more abundant training samples and sufficient modeling capability, the process for estimating the variance becomes less critical, as expected. Note that for all the RMS curves, noise overfitting problem was not observed because of the diminishing learning rate for adaptation, which can be interpreted as a form of regularization, and is conceptually similar to early-stop training approach [6].

Case 3: Surface Evaluation

To visualize the modeling performance, Figure 3 shows the individual model outputs evaluated at every point of a 50 X 50 grid after 10 training cycles (1 run) using a single set of 500 noisy training samples. The rough surface of $M2$ was due to the smaller local support (less noise averaging) and sparse training samples (insufficient generalization), as opposed to that of $M3$. By estimating the variance over the input region of interest, the surface reconstruction was comparatively better, as compared to that of $M4$. Also, the relative weighting surfaces of p_1 and p_2 of $M1$ were found to follow closely the relative gradient of the sigmoidal surface, as desired.

4 Conclusion

The validity of the WME model is based on the assumption that the conditional mean estimation is the desired learning objective, and the proposed architecture makes use of variance models which estimate the error variance for their expert models, and assign less weighting to those expert models with larger variance. The estimation performance is adapted using a given set of training data, and the set of variance models evolves to form the desired prior in choosing an appropriate set of expert models. It is intuitive that in order for each and every expert to excel in different input regions, their model structures must be unique otherwise the

[1] Results were omitted for space reason.

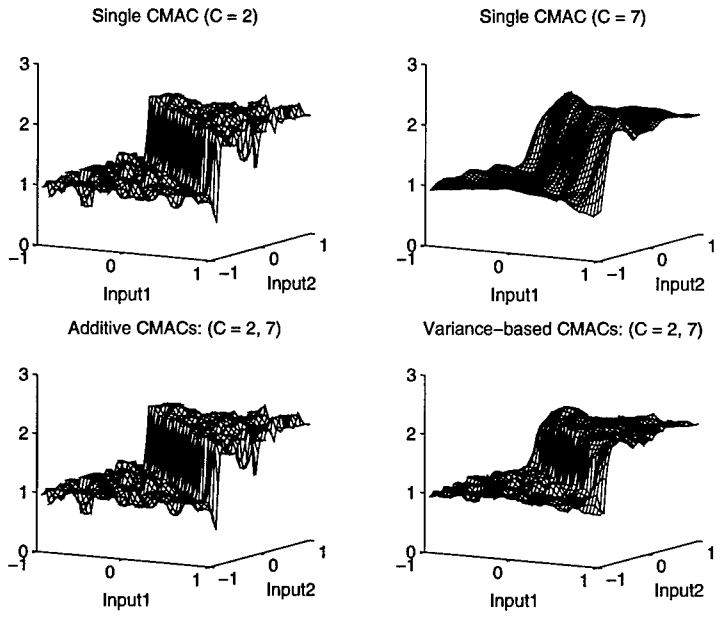

Figure 3 Surface reconstruction after 10 training cycles of iterations using four different models and a single set of 500 noisy training samples. (a) top left: single CMAC (C = 2); (b) top right: single CMAC (C = 7); (c) bottom left: additive CMACs (C = 2, 7); (d) bottom right: WME CMACs (1:3 λ ratio, C = 2, 7).

bias/variance dilemma issue will remain unresolved. Having unique internal expert structures also facilitates implicit model selection problems such that one does not need to search for an *optimal* structure for a single model. It would appear that having a mixture of experts increases the total number of free parameters for optimization, and the resulting network will not be parsimonous. Quite differently, the objective is not to reduce the number of physical parameters, as advocated in many proposed architectures, but rather to reduce the number of effective parameters, governed by the variance models, in such a way that the WME model can be more robust with respect to noise and model mismatch.

REFERENCES

[1] An P.E., Miller W.T., Parks P.C. *Design Improvements in Associative Memories for Cerebellar Model Articulation Controllers (CMAC)*, Proc. Intl. Conf. on Artificial Neural Networks, Helsinki, North Holland, Vol.2 (1991), pp.1207-1210.

[2] Bishop C. *Mixture Density Networks*, Neural Computing Research Group Report NCRG/4288 (1994), Department of Computer Science, Aston University, UK.

[3] Brown M., Harris C.J. NeuroFuzzy Adaptive Modelling and Control (1994), Prentice-Hall.

[4] Geman S., Bienenstock E. *Neural Networks and the Bias/Variance Dilemma*, Neural Computation, Vol. 4 (1992), pp.1-58.

[5] Jacobs R., Jordan M., Nowlan S., Hinton G. *Adaptive Mixtures of Local Experts*, Neural Computation, Vol. 3 (1991), pp.79-87.

[6] Sjoberg J., Ljung L. *Overtraining, Regularization, and Searching for Minimum in Neural Networks*, the 4th IFAC Symposium on Adaptive Systems in Control and Signal Processing, France, (1992) pp.669-674.

LOCAL MODIFICATIONS TO RADIAL BASIS NETWORKS

I. J. Anderson

School of Computing and Mathematics, University of Huddersfield, Queensgate, Huddersfield HD1 3DH, UK.

The form of a radial basis network is a linear combination of translates of a given radial basis function, $\phi(r)$. The radial basis method involves determining the values of the unknown parameters within the network given a set of inputs, $\{\mathbf{x}_k\}$, and their corresponding outputs, $\{f_k\}$. It is usual for some of the parameters of the network to be fixed. If the positions of the centres of the basis functions are known and constant, the radial basis problem reduces to a standard linear system of equations and many techniques are available for calculating the values of the unknown coefficients efficiently. However, if both the positions of the centres and the values of the coefficients are allowed to vary, the problem becomes considerably more difficult. A highly non-linear problem is produced and solved in an iterative manner. An initial guess for the best positions of the centres is made and the coefficients for this particular choice of centres are calculated as before. For each iteration, a small change to the position of the centres is made in order to improve the quality of the network and the values of the coefficients for these new centre positions are determined. The overall algorithm is computationally expensive and here we consider ways of improving the efficiency of the method by exploiting the local stability of the thin plate spline basis function. At each step of the iteration, only a small change is made to the positions of the centres and so we can reasonably expect that there is only a small change to the values of the corresponding coefficients. These small changes are estimated using *local modifications.*

1 Introduction

We consider the thin plate spline basis function

$$\phi(r) = r^2 \log r.$$

This basis function has not been as popular as the Gaussian, $\phi(r) = \exp(-r^2/2\sigma)$, mainly due to its unbounded nature. The thinking behind this is that it is desirable to use a basis function that has near compact support so that the approximating function behaves in a local manner.

A suitable definition of local behaviour for an approximating function of the form given in equation (1) is as follows. The ith coefficient, c_i, of the approximant should be related to the values $\{f_k\}$ for values of k where $\|\mathbf{x}_k - \boldsymbol{\lambda}_i\|$ is small. Thus, the value of the coefficient should be influenced only by the data ordinates whose abscissae values are close to the centre of the corresponding basis function. From this definition one deduces that it is advisable to use basis functions that decay, hence the desire for basis functions with near compact support. However many authors have shown that this deduction is unfounded and it is in fact easier to produce the properties of local behaviour by using unbounded functions [4, 2, 3, 1].

1.1 The Approximation Problem

Given a set of m data points, $(\mathbf{x}_k, f_k)$, for $k = 1, 2, \ldots, m$, it is possible to produce an approximation of the form

$$f(\mathbf{x}) = \sum_{i=1}^{n} c_i \phi(\|\mathbf{x} - \boldsymbol{\lambda}_i\|), \tag{1}$$

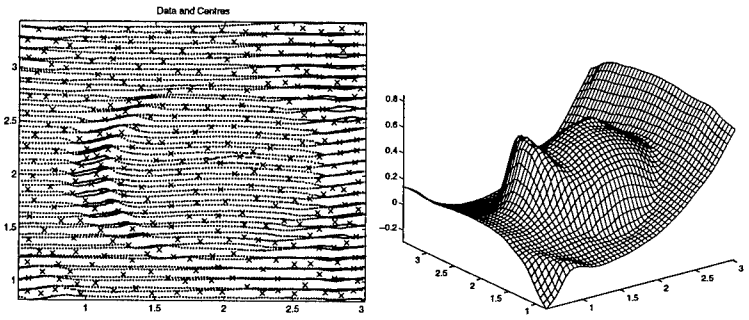

Figure 1 The positions of the data abscissae and the centres of the basis functions, and the surface approximant to the data.

such that

$$f(\mathbf{x}_k) \approx f_k.$$

It is usual for this approximation problem to be solved in the least-squares sense. There are two important categories for such an approximation. The easiest approach is to consider the positions of the centres to be fixed, in which case the approximation problem is linear and is therefore reasonably efficient to solve. The alternative is to allow the positions of the centres to vary or indeed for the number of centres to change. For example, once a preliminary approximation has been completed it is worth examining the results to determine the quality of the approximation. It may be decided that one (or more) regions are unsatisfactory and so extra basis functions or an adjustment of the centres of the current basis functions would be suitable.

Under such circumstances it is usual to recalculate the new coefficients for the approximation problem with respect to the new positions of the centres. Repeating this process too often can be computationally expensive and it is more appropriate to modify the current approximation to take into account the small changes that have been made to the centres.

2 Local Stability of the Thin Plate Spline

This local behaviour of the thin plate spline is demonstrated by the use of an example that consists of approximating $m = 6{,}864$ data points using $n = 320$ basis functions. The centres for these basis functions are produced using a clustering algorithm and the data are fitted in the least-squares sense. Formally, let I be the set of indices for the basis functions, $\{1, 2, \ldots, n\}$. We wish to calculate the values of the coefficients $\{c_i\}$ that minimize the ℓ_2-norm of the residual vector $\mathbf{e}$ which has the components

$$e_k = f_k - \sum_{i \in I} c_i \phi(\|\mathbf{x} - \boldsymbol{\lambda}_i\|),$$

for $k = 1, 2, \ldots, m$. The data, centres and the resulting approximant are shown in Figure 1.

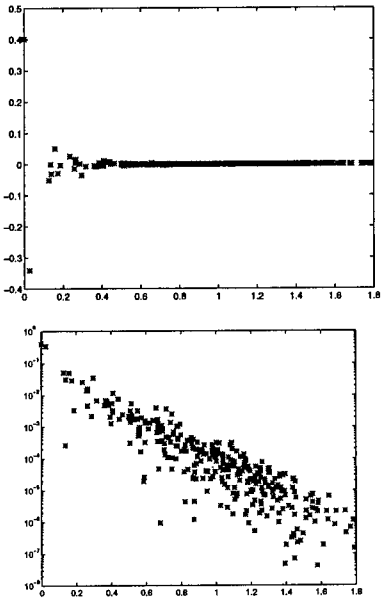

Figure 2 The differences in the coefficients between the two approximants as a function of distance. Standard and logarithmic axes are shown.

Let $j \in I$ be the index for one of the centres. We now perturb this centre by a small amount, $\boldsymbol{\delta}$, such that we produce a new centre;

$$\boldsymbol{\lambda}_j^* = \boldsymbol{\lambda}_j + \boldsymbol{\delta}.$$

All of the other centres are left undisturbed. That is $\boldsymbol{\lambda}_i^* = \boldsymbol{\lambda}_i$ for $i \in I, i \neq j$. Again the data are fitted in the least-squares sense but this time we use the new set of centres, $\{\boldsymbol{\lambda}_i^*\}$. Thus we calculate the values of the coefficients c_i^*, for each $i \in I$, that minimize the ℓ_2-norm of the residual vector $\mathbf{e}^*$ which has the components

$$e_k^* = f_k - \sum_{i \in I} c_i^* \phi(\|\mathbf{x} - \boldsymbol{\lambda}_i^*\|),$$

for $k = 1, 2, \ldots, m$. The two approximants are visually indistinguishable and so we compare the coefficients of the respective fits.

Let d_i be the distance between the centre of the ith basis function and the position of the perturbed centre, $d_i = \|\boldsymbol{\lambda}_i^* - \boldsymbol{\lambda}_j^*\|$. Figure 2 shows the differences between the respective coefficients, $\{(c_i - c_i^*)\}$ of the two fits against the distances $\{d_i\}$. Also shown is the logarithm of the absolute values of the differences between the respective coefficients against the same set of distances.

It can be seen that the differences between the coefficients decay exponentially as the distance between the corresponding centre and the perturbation increases. It is in this sense that we say that the thin plate spline behaves locally.

3 Exploiting the Local Behaviour

Since the effects of perturbing the position of a given centre are only noticeable for the coefficients which correspond to basis functions that are centred in the neigh-

bourhood of the perturbed centre, it seems reasonable that we should be able to retrain the network with these new centre positions by using only the basis functions from this neighbourhood. The coefficients for the other basis functions can be left unchanged on the assumption that they will not be affected by a significant amount. By using only a small number of centres we can expect this local approximation to be significantly faster than the global approach which uses all of the centres.

We adopt an iterative refinement type approach. First we choose to use a given number, q, of basis functions whose centres are nearest to the position of the new perturbed centre. Let $I^* \subset I$ be the set of indices for these q basis functions. Then we calculate the residuals between the original function values and the current estimate for the approximating function. This current estimate is based on the best approximant using the original positions of the centres, but with the basis functions for the new positions of the centres,

$$e_k^* = f_k - \sum_{i \in I} c_i \phi(\|\mathbf{x} - \boldsymbol{\lambda}_i^*\|).$$

We wish to approximate these residuals using the approximating form

$$\sum_{i \in I^*} \delta c_i^* \phi(\|\mathbf{x} - \boldsymbol{\lambda}_i^*\|).$$

This approximation is again done in the least-squares sense. This produces a "correction surface" that we combine with the current estimate for the approximant in order to produce an updated estimate (or combined surface) for the required approximant. The new approximant has the coefficients

$$c_i^{(\text{new})} = \begin{cases} c_i + \delta c_i^* & i \in I^*, \\ c_i & i \notin I^*. \end{cases}$$

The experiment is repeated for various values of q and the results are discussed below.

3.1 Choice of the Data Subset

If we use all of the data and therefore all of the residuals, we find that the resulting correction surface is flat in nature and the local variation around the position of the perturbation has been largely ignored. The reason for this phenomenon is that we are treating each of the data points with equal importance and since there are many more data outside the neighbourhood of interest than the number inside, the former group of data tend to dominate the approximation.

Since we are only using the basis functions that are local to the position of the perturbation, it seems reasonable to use only the data that lie in the neighbourhood of interest. Unfortunately this too has a problem in that we are effectively assigning no importance to the "far-away" data points and so the approximation has a tendency to behave in an uncontrolled manner away from the neighbourhood, in much the same way that the basis functions are uncontrolled.

As a compromise we use a subset of data that consists of all of the data points that are close to the perturbation and a few data points that are sampled randomly from the remainder of the data domain. In the example that we are considering 512 data points were used for the local subset and 512 data points were used to represent the remainder of the domain. By doing this we wish to give more importance to the

local data while still considering the global effect of the correction approximant. An advantage that accrues from this approach is that the local approximation uses fewer data points than the global method and so we can expect the speed of calculating the approximation to be significantly faster.

4 Concluding Remarks

Various values for q were chosen and the local modifications were calculated. The value of the square root of the mean of the squares of the errors (R.M.S.) between all of the original ordinates and the values of the combined surface at the data points produced using the global approach was 7.50×10^{-3} which took about 2,870 seconds to calculate, and the R.M.S. value for the current approximation with the new centres was 15.73×10^{-3}. By applying the local modification, using $q = 7$ an R.M.S. value of 7.52×10^{-3} was obtained in less than three tenths of a second.
Clearly it can be seen that an excellent improvement in the R.M.S. value can be achieved using only a very small number of basis functions. The required fit has been achieved to within an accuracy of one per cent in approximately one ten thousandth of the time needed by the global approach. Visually, there is no difference between the approximations produced by a) the global approach and b) the local modification method.
Future work in this area would concentrate on the following areas.

- Convergence. Since each iteration is so much faster than the global approach we can afford to use the technique many times, using different sets of basis functions. However it would be necessary to confirm that such an approach would continually refine and improve the quality of the approximation.

- No attempt has been made to optimize the size or the positions of the subset of data used for the local modification. It is envisaged that a small but significant improvement in the quality of the approach could be made using such a technique.

- Similarly the size and position of the subset of centres could be optimized. Particular attention could be directed towards the effects of larger perturbations and/or several small perturbations.

REFERENCES

[1] I. J. Anderson. *Local modifications to radial basis networks.* Technical Report RR9505, School of Computing and Mathematics, University of Huddersfield, Huddersfield, UK, (1995).

[2] M. D. Buhmann and C. K. Chui. *A note on the local stability of translates of radial basis functions.* Journal of Approximation Theory, Vol. 74 (1993), pp36–40.

[3] J. Levesley. *Local stability of translates of polyharmonic splines in even space dimension.* Numer. Funct. Anal. and Optimiz., Vol.15 (1994) pp327–333.

[4] M. J. D. Powell. *Radial basis function approximations to polynomials.* In D. F. Griffiths and G. A. Watson, editors, Numerical Analysis, (1987), pp 223–241. Longman Scientific and Technical, 1988.

Acknowledgements

The author wishes to thank C. K. Pink for his comments on earlier drafts of this paper, and also the Department of Conservative Dentistry in the Dental School at the London Hospital Medical College for supplying the data.

A STATISTICAL ANALYSIS OF THE MODIFIED NLMS RULES

E.D. Aved'yan, M. Brown* and C.J. Harris*

Russian Academy of Sciences, Institute of Control Sciences, 65 Profsoyuznaya str., Moscow 117342, Russia. Email: avedyan@dep07.ics.msk.su

**ISIS research group, Dept of Electronics and Computer Science, Southampton University, Highfield, Southampton, SO17 1BJ, UK. Email: mqb@ecs.soton.ac.uk*

This paper analyses the statistical convergence properties of the modified NLMS rules which were formulated in an attempt to produce more robust and faster converging training algorithms. However, the statistical analysis described in this paper leads us to the conjecture that the standard NLMS rule is the only *unconditionally stable* modified NLMS training algorithm, and that the optimal value of the learning rate and region of convergence for the modified NLMS rules is generally less than for the standard NLMS rule.

1 Adaptive Systems and the NLMS Algorithm

Nonlinear networks, such as the Cerebellar Model Articulation Controller (CMAC), Radial Basis Functions (RBF) and B-splines have an "output layer" of linear parameters that can be directly trained using any of the linear learning algorithms that have been developed over the past 40 years. So consider a linear in its parameter vector network of the form:

$$\begin{aligned} y(t) &= \sum_{i=1}^{n} x_i(t)\, w_i(t-1) \\ &= \mathbf{x}^T(t)\, \mathbf{w}(t-1) \end{aligned} \tag{1}$$

where $y(t)$ is the system's output, $\mathbf{w}(t-1) = (w_1(t-1), \ldots, w_n(t-1))$ is the n-dimensional weight vector and $\mathbf{x}(t) = (x_1(t), \ldots, x_n(t))$ is the n-dimensional transformed input vector at time t. This "input" vector $\mathbf{x}$ could possibly be a nonlinear transformation of the network's original input measurements. For a linear system described by equation 1, the Normalised Least Mean Squares (NLMS) learning algorithm for a single training sample $\{\mathbf{x}(t), \widehat{y}(t)\}$ is given by:

$$\Delta\mathbf{w}(t) = \mu \frac{\epsilon_y(t)}{\|\mathbf{x}(t)\|_2^2}\, \mathbf{x}(t) \tag{2}$$

where $\Delta\mathbf{w}(t) = \mathbf{w}(t) - \mathbf{w}(t-1)$ is the weight vector update, $\epsilon_y(t) = (\widehat{y}(t) - y(t))$ is the output error, $\widehat{y}(t)$ is the desired network output at time t and $\mu \in [0, 2]$ is the learning rate. This simple learning rule has a long history, as it was originally derived by Kaczmarz in 1937 [6] and was re-derived numerous times in the adaptive control [7] and neural network literature. When the training data are generated by an equivalent model with an unknown "optimal" parameter vector $\widehat{\mathbf{w}}$ (i.e. there is no modelling error or measurement noise), the NLMS algorithm possesses the property that:

$$\|\epsilon_{\mathrm{w}}(t)\|_2 \leq \|\epsilon_{\mathrm{w}}(t-1)\|_2 \tag{3}$$

where $\epsilon_{\mathrm{w}}(t) = \widehat{\mathbf{w}} - \mathbf{w}(t)$ is the weight error at time t. Hence the estimates of the weight vector approach (monotonically) the true values and this learning rule has many other desirable properties [3].

2 Modified NLMS algorithms

In 1971, a set of Modified NLMS (MNLMS) algorithms was proposed by Aved'yan [1, 2] and they were again rediscovered over 20 years later by Douglas [5]. The MNLMS learning algorithms are derived from the two conditions:

$$\begin{aligned} &\text{Find } \mathbf{w}(t) \text{ such that:} \\ &\qquad \widehat{y}(t) = \mathbf{x}^T(t)\mathbf{w}(t) \\ &\text{and} \quad \|\Delta\mathbf{w}(t)\|_p \text{ is minimised.} \end{aligned} \tag{4}$$

for different values of p where $1 \leq p < \infty$.

These instantaneous learning rules are based on generating a new search direction by minimising an alternative norm in weight space, and three special cases which are worthy of attention are the 1, 2 and ∞-norms. The 2-norm corresponds to the standard NLMS rule which is denoted by **std NLMS**, but the L_1 learning algorithm is:

$$\Delta w_i(t) = \mu \frac{\epsilon_y(t)}{x_k(t)} \delta_{i,k} \tag{5}$$

where $k = \arg\max_i |x_i(t)|$, and this will be referred to as the **max NLMS** rule. The L_∞ training rule is given by:

$$\Delta\mathbf{w}(t) = \mu \frac{\epsilon_y(t)\text{sgn}(\mathbf{x}(t))}{\|\mathbf{x}(t)\|_1} \tag{6}$$

and this will be referred to as the **sgn NLMS** rule [7]. It is fairly simple to show that the *a posteriori* output error is always zero for these learning rules (with $\mu = 1$), so the only difference between them is how they search the weight space. The max NLMS algorithm always updates the weight vector parallel to an axis, and the sgn NLMS rule causes the weight vector update to be at 45° to an axis. This is in contrast to the std NLMS training procedure which always projects the weight vector perpendicularly onto the solution hyperplane generated by the training data [6].

3 A Statistical Analysis

A deterministic analysis of the MNLMS rules has already been completed and it is shown in [4] that certain finite training sets can cause unstable learning in the linear network for the sgn and max NLMS rules, irrespective of the size of the (non-zero) learning rate. The statistical analysis of the MNLMS rules in this paper is based on a model of the input vector where all components are mutually independent random processes with zero mean values, each of which is a sequence of independent identically symmetric distributed random variables. This proivdes the conditions of convergence for the modified algorithms, the optimal value of the learning rate, and the influence of a noise and the mean value of the input process on the convergence conditions.

3.1 Convergence

The process $\mathbf{w}(t)$ converges (in the statistical mean-square sense) to the optimal weight vector, $\widehat{\mathbf{w}}$, if it satisfies the condition $\lim_{t\to\infty} E\left(\epsilon_{\mathbf{w}}^T(t)\epsilon_{\mathbf{w}}(t)\right) = 0$, where $E()$ denotes the statistical expectation operator. The convergence depends greatly on the properties of the input process $\mathbf{x}(t)$, for instance the standard NLMS algorithm does not converge to its optimal values, when the process $\mathbf{x}(t)$ quickly settles to a constant value or when it is varies very slowly: the input signal is not *persistently*

exciting. This situation is even worse for both the max and sgn NLMS algorithms as they search a restricted section of the parameter space and an optimal solution for the training date does not always lie in this region [3].
It is possible to write the Euclidean squared norm of the error in the weight vector $\epsilon_{\mathrm{w}}^T(t)\epsilon_{\mathrm{w}}(t)$ as:

$$\epsilon_{\mathrm{w}}^T(t)\epsilon_{\mathrm{w}}(t) =$$
$$\epsilon_{\mathrm{w}}^T(t-1)\left(\mathbf{I}-\mu\frac{\mathbf{x}(t)\mathbf{s}^T(t)}{\mathbf{x}^T(t)\mathbf{s}(t)}-\mu\frac{\mathbf{s}(t)\mathbf{x}^T(t)}{\mathbf{x}^T(t)\mathbf{s}(t)}+\mu^2\frac{\mathbf{x}(t)\mathbf{s}^T(t)\mathbf{s}(t)\mathbf{x}^T(t)}{\left(\mathbf{x}^T(t)\mathbf{s}(t)\right)^2}\right)\epsilon_{\mathrm{w}}(t-1)x \quad (7)$$

where $\mathbf{s}(t)$ is the current search direction for the different learning rules, when the training data contain no measurment or modelling errors.
Let us denote by $V^2(t) = E\left(\epsilon_{\mathrm{w}}^T(t)\epsilon_{\mathrm{w}}(t)\right)$ the statistical expectation of the Euclidean squared norm of the error in the weight vectors in equation 7. Taking into account the statistical properties of the input vector $\mathbf{x}(t)$ and the fact that the trace of each matrix in these equations is equal to one, it is possible to generate first-order relations:

$$V_*^2(t) = \left(1-2n^{-1}\mu+\beta_*\mu^2\right)V_*^2(t-1) \quad (8)$$

where a $_*$ is used instead of std, sgn and max, and:

$$\beta_{\mathrm{std}} = n^{-1} \quad (9)$$

$$\beta_{\mathrm{sgn}} = E\left(\frac{\mathbf{x}^T(t)\mathbf{x}(t)}{\left(\mathbf{x}^T(t)\mathrm{sgn}(\mathbf{x}(t))\right)^2}\right) \quad (10)$$

$$\beta_{\mathrm{max}} = n^{-1}E\left(\frac{\mathbf{x}^T(t)\mathbf{x}(t)}{x_k^2(t)}\right) \quad (11)$$

For these parameters we have the following inequalities:

$$n^{-1} \leq \beta_{\mathrm{sgn}} \leq 1 \quad (12)$$

$$n^{-1} \leq \beta_{\mathrm{max}} \leq 1 \quad (13)$$

The value of the parameters β_{sgn} and β_{max} depends on the probability distribution function of the vector $\mathbf{x}(t)$ and can be calculated analytically in the special cases shown below.
From equation 8, it follows that not only are the convergence conditions for the std, sgn and max NLMS algorithms, respectively:

$$0 < q_* = \left(1-2n^{-1}\mu+\beta_*\mu^2\right) < 1 \quad (14)$$

but also the optimal value of the learning rate $\widehat{\mu}$ by which values of $q_{\mathrm{std}}, q_{\mathrm{sgn}}$ and q_{max} are minimal:

$$\widehat{\mu}_* = (n\beta_*)^{-1} \quad (15)$$

and consequently:

$$\widehat{q}_* = \left(1-\beta_* n^{-1}\right) \quad (16)$$

These values determine the convergence time of the respective algorithms, and:

$$\mu_{\mathrm{sgn}}^* \leq \mu_{\mathrm{std}}^* = 1 \quad (17)$$

$$\mu_{\mathrm{max}}^* \leq \mu_{\mathrm{std}}^* = 1 \quad (18)$$

$$q_{\mathrm{sgn}}^* \geq q_{\mathrm{std}}^* = \left(1-n^{-1}\right) \quad (19)$$

$$q_{\mathrm{max}}^* \geq q_{\mathrm{std}}^* = \left(1-n^{-1}\right) \quad (20)$$

Hence it follows that optimal value of the learning rate and the region of convergence for the sgn and max NLMS rules are less than for the std NLMS rule, and that the convergence time for the std NLMS rule is less than for the other sgn and max NLMS rules. However, it is possible to get the analytical expression for β in equations 10 and 11 in certain special cases.

When $x_i(t)$ has a *Laplace* distribution: $p(x_i) = \alpha^{-1} \exp(-|x_i|/\alpha)$, then $\beta_{\text{sgn}} = 2/(n+1)$ and $\widehat{\mu}_{\text{sgn}} = (n+1)/2n$ for the sgn NLMS rule. The corresponding region of convergence is equal to $0 < \mu_{\max} < (n+1)$ in contrast with the std NLMS rule where $0 < \mu_{\text{std}} < 2$. Hence, for large n, the convergence rate of the sgn NLMS rule is approximately twice as large as the std NLMS rule.

When $x_i(t)$ has a *uniform* distribution $p(x_i) = 1/2\alpha$, $|x_i| < \alpha$, then $\beta_{\max} = (n+2)/3n$, and $\widehat{\mu}_{\max} = 3/(n+2)$. The corresponding region of convergence is $0 < \mu_{\max} < 6/(n+2)$ and it follows that for large n, the time of convergence of the std NLMS rule is equal to cn where c is a constant whereas for the max NLMS rule this time is equal to $cn(n+2)/3$.

These examples shows that the std NLMS rule has a larger convergence rate when compared with the sgn and the max NLMS algorithm for these *specific* input distributions. The MNLMS rules therefore represent a tradeoff between computational simplicity and stability/convergence rate.

3.2 The Influence of Noise

Assuming that the output data are corrupted with an additive, statistically independent, white noise sequence $\xi(k)$, with variance σ_ξ^2, and that the input vector has the same statistical properties as were mentioned above, then:

$$V_*^2(t) = (1 - 2n\mu + \beta_*\mu^2)V_*^2(t-1) + \mu^2\sigma_\xi^2 d_* \tag{21}$$

where the disturbance terms d_* are given by:

$$d_{\text{std}} = E\left(\left(\mathbf{x}^T(t)\mathbf{x}(t)\right)^{-1}\right) \tag{22}$$

$$d_{\text{sgn}} = nE\left(\left(\mathbf{x}^T(t)\text{sgn}(\mathbf{x}(t))\right)^{-1}\right) \tag{23}$$

$$d_{\max} = E\left(\left|x_k^{-1}(t)\right|\right) \tag{24}$$

Comparing equations 8 and 21, it follows that if the convergence conditions for the std, sgn and max NLMS algorithms (see inequality 14) remain constant, then after a transient period, the variance equals:

$$V_{\text{std}}^2 = n\sigma_\xi^2 \frac{\mu}{2-\mu} \tag{25}$$

$$V_{\text{sgn}}^2 = n\sigma_\xi^2 d_{\text{sgn}} \frac{\mu}{2-\beta_{\text{sgn}}\mu n} \tag{26}$$

$$V_{\max}^2 = n\sigma_\xi^2 d_{\max} \frac{\mu}{2-\beta_{\max}\mu n} \tag{27}$$

After the initial "transient" convergence, the mean value of the process $\mathbf{w}(t)$ will be equal to $\widehat{\mathbf{w}}$ and the weight vector will "jitter" around the mean value with a variance given in equations 25-27. This region of convergence was termed a *minimal capture zone* by Parks and Militzer [8]. For a specific input distribution, the size of the minimal capture zone can be made arbitrary small by choosing a small learning rate, μ, but this would also decrease the rate of convergence.

3.3 The Influence of Mean Value of the Input Process

The presence of the mean value in the input vector decreases the rate of convergence for all these algorithms. For the std NLMS algorithm, the presence of non zero mean value, m_x, in the input vector increases the time of convergence approximately $(1 + m_x^2/\sigma_x)$ times in comparison with the case when the mean value is zero. Hence, it is desirable to both centralise the input vector and also transform it such that all components of the vector have the same variances.

3.4 Simulation and Discussion

The simulation, shown in Figure 1, illustrates the dynamical evolution of the Euclidean norm of the error in the weight vector for these algorithms. In this figure, the learning rates are set to their near-optimal values derived above. The adaptive system has 5 inputs, the optimal weight vector is $\widehat{\mathbf{w}} = (0.22, 0.32, 0.42, 0.53, 0.63)$ and the random, Gaussian input vector has the statistical properties described above and these results support the theoretical conclusions.

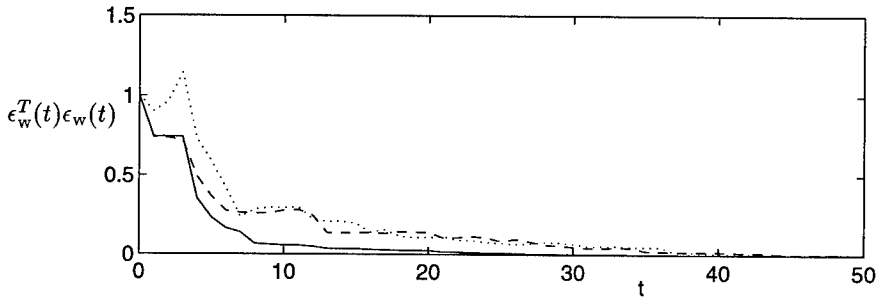

Figure 1 The evolution of the magnitude of the error in the weight vector when it is trained using the std NLMS rule (solid line), sgn NLMS rule (dashed line) and the max NLMS rule (dotted line), with $\mu_{\text{std}} = 1$ and $\mu_{\text{sgn}} = \mu_{\text{max}} = 0.5$.

The MNLMS rules were originally proposed as a computationally efficient method for increasing the rate of convergence of the NLMS algorithm as they search weight space in orthogonal directions. However, this has serious implications for the stability and rate of convergence of these instantaneous algorithms as has been pointed out in this paper. For any network with 3 or more coefficients, the MNLMS procedures could potentially be unstable and their persistently exciting conditions are more severe than the standard NLMS rule.

REFERENCES

[1] E.D. Aved'yan, *Bestimmung der Parameter linearer Modelle stationärer und instationärer Strecken*, Messen, Steuern, Regeln, Vol.14:9 (1971) 348–350.

[2] E.D. Aved'yan, *Learning Systems*, Springer Verlag, London, UK, (1995).

[3] M. Brown and C. Harris, *Neurofuzzy Adaptive Modelling and Control*, Prentice Hall, Hemel-Hempstead, UK, (1994).

[4] M. Brown and P.E. An and C.J. Harris, *A Stability Analysis of the Modified NLMS Rules*, submitted to IEEE Trans. Signal Processing, (1995).

[5] S.C. Douglas, *A Family of Normalised LMS Algorithms*, IEEE Signal Processing Letters, Vol.1:3 (1994) pp49–51.

[6] S. Kaczmarz, *Angenäherte Auflösung von Systemen Linearer Gleichungen*, Bull. Int. Acad. Pol. Sci. Lett and Cl. Sci. Math. Nat. Ser. A., (1937) pp355–357.

[7] J.I. Nagumo and A. Noda, *A Learning Method for System Identification*, IEEE Trans. Automatic Control, Vol.12:3 (1967) pp282–287.

[8] P.C. Parks and J. Militzer, *Convergence Properties of Associative Memory Storage for Learning Control Systems*, Automation and Remote Control, Vol. 50:2 (1989) 254–286.

Acknowledgements

The authors gratefully acknowledge the financial support of Lucas aerospace during the preparation of this manuscript and Dr Aved'yan also acknowledges the financial support of the Fundamental Research Foundation of Russia, grant 93-012-448. He also wishes to thank the Royal Society of London for their support through a joint project on "Overall Behaviour of Adaptive Control Systems Using Neural Networks for Identification or Learning", (1993-1996), Ref. No. 638072.P622.

This paper is dedicated to the memory of Patrick Parks.

FINITE SIZE EFFECTS IN ON-LINE LEARNING OF MULTI-LAYER NEURAL NETWORKS.

David Barber, Peter Sollich* and David Saad

Dept. Comp, Sci. and Appl. Maths., Aston University, Birmingham B4 7ET, UK. Web: http://www.ncrg.aston.ac.uk/

** Department of Physics, University of Edinburgh, Mayfield Road, Edinburgh EH9 3JZ, UK.*

We extend the recent progress in thermodynamic limit analyses of mean on-line gradient descent learning dynamics in multi-layer networks by calculating the fluctuations possessed by finite dimensional systems. Fluctuations from the mean dynamics are largest at the onset of specialisation as student hidden unit weight vectors begin to imitate specific teacher vectors, and increase with the degree of symmetry of the initial conditions. Including a term to stimulate asymmetry in the learning process typically significantly decreases finite size effects and training time.

Recent advances in the theory of on-line learning have yielded insights into the training dynamics of multi-layer neural networks. In *on-line learning*, the *weights* parametrizing the *student* network are updated according to the error on a single example from a stream of examples, $\{\boldsymbol{\xi}^\mu, \tau(\boldsymbol{\xi}^\mu)\}$, generated by a *teacher* network $\tau(\cdot)$[1]. The analysis of the resulting weight dynamics has previously been treated by assuming an infinite input dimension (*thermodynamic limit*) such that a mean dynamics analysis is exact[2]. We present a more realistic treatment by calculating corrections to the mean dynamics induced by finite dimensional inputs[3].
We assume that the *teacher* network the student attempts to learn is a *soft committee machine*[1] of N inputs, and M hidden units, this being a one hidden layer network with weights connecting each hidden to output unit set to $+1$, and with each hidden unit n connected to all input units by $\mathbf{B}_n (n = 1..M)$. Explicitly, for the N dimensional training input vector $\boldsymbol{\xi}^\mu$, the output of the teacher is given by,

$$\zeta^\mu = \sum_{n=1}^{M} g(\mathbf{B}_n \cdot \boldsymbol{\xi}^\mu), \tag{1}$$

where $g(x)$ is the activation function of the hidden units, and we take $g(x) = \mathrm{erf}(x/\sqrt{2})$. The teacher generates a stream of training examples $(\boldsymbol{\xi}^\mu, \zeta^\mu)$, with input components drawn from a normal distribution of zero mean, unit variance. The *student* network that attempts to learn the teacher, by fitting the training examples, is also a soft committee machine, but with K hidden units. For input $\boldsymbol{\xi}^\mu$, the student output is,

$$\sigma(\mathbf{J}, \boldsymbol{\xi}^\mu) = \sum_{i=1}^{K} g(\mathbf{J}_i \cdot \boldsymbol{\xi}^\mu), \tag{2}$$

where the student weights $\mathbf{J} = \{\mathbf{J}_i\} (i = 1..K)$ are sequentially modified to reduce the *error* that the student makes on an input $\boldsymbol{\xi}^\mu$,

$$\epsilon(\mathbf{J}, \boldsymbol{\xi}^\mu) = \frac{1}{2} (\sigma(\mathbf{J}, \boldsymbol{\xi}^\mu) - \zeta^\mu)^2 = \frac{1}{2} \left(\sum_{i=1}^{K} g(x_i^\mu) - \sum_{n=1}^{M} g(y_n^\mu) \right)^2, \tag{3}$$

with the *activations* defined $x_i^\mu = \mathbf{J}_i \cdot \boldsymbol{\xi}^\mu$, and $y_n^\mu = \mathbf{B}_n \cdot \boldsymbol{\xi}^\mu$. Gradient descent on the error (3) results in an update of the student weight vectors,

$$\mathbf{J}^{\mu+1} = \mathbf{J}^\mu - \frac{\eta}{N}\delta_i^\mu \boldsymbol{\xi}^\mu, \tag{4}$$

where,

$$\delta_i^\mu = g'(x_i^\mu)\left[\sum_{n=1}^{M} g(y_n^\mu) - \sum_{j=1}^{K} g(x_j^\mu)\right], \tag{5}$$

and g' is the derivative of the activation function g. The typical performance of the student on a randomly selected input example is given by the generalisation error,

$$\epsilon_g = \langle \epsilon(\mathbf{J}, \boldsymbol{\xi}) \rangle, \tag{6}$$

where $\langle .. \rangle$ represents an average over the gaussian input distribution. One finds that ϵ_g depends only on the *overlap parameters*, $R_{in} = \mathbf{J}_i \cdot \mathbf{B}_n$, $Q_{ij} = \mathbf{J}_i \cdot \mathbf{J}_j$, and $T_{nm} = \mathbf{B}_n \cdot \mathbf{B}_m (i,j = 1..K; n,m = 1..M)$[2], for which, using (4), we derive (stochastic) *update equations*,

$$R_{in}^{\mu+1} - R_{in}^\mu = \frac{\eta}{N}\delta_i^\mu y_n^\mu, \tag{7}$$

$$Q_{ik}^{\mu+1} - Q_{ik}^\mu = \frac{\eta}{N}\left(\delta_i^\mu x_j^\mu + \delta_k^\mu x_i^\mu\right) + \frac{\eta^2}{N^2}\delta_i \delta_k \boldsymbol{\xi}^\mu \cdot \boldsymbol{\xi}^\mu. \tag{8}$$

We average over the input distribution to obtain deterministic equations for the mean values of the overlap parameters, which are self-averaging in the thermodynamic limit. In this limit we treat $\mu/N = \alpha$ as a continuous variable and form differential equations for the *thermodynamic overlaps*, R_{in}^0, Q_{ik}^0,

$$\frac{dR_{in}^0}{d\alpha} = \eta \langle \delta_i y_n \rangle, \tag{9}$$

$$\frac{dQ_{ik}^0}{d\alpha} = \eta \langle \delta_i x_k + \delta_k x_i \rangle + \eta^2 \langle \delta_i \delta_k \rangle. \tag{10}$$

For given initial overlap conditions, (9,10) are integrated to find the mean dynamical behaviour of a student learning a teacher with an arbitrary numbers of hidden units[2] (see fig.(1a)). Typically, ϵ_g decays rapidly to a *symmetric phase* in which there is near perfect symmetry between the hidden units. Such phases exist in learnable scenarios until sufficient examples have been presented to determine which student hidden unit will mimic which teacher hidden unit. For perfectly symmetric initial conditions, such *specialisation* is impossible in a mean dynamics analysis. The more symmetric the initial conditions are, the longer the trapping in the symmetric phase (see fig.(2a)). Large deviations from the mean dynamics can exist in this symmetric phase, as a small perturbation from symmetry can determine which student hidden unit will specialise on which teacher hidden unit[1].
We rewrite (7,8) in the general form

$$a^{\mu+1} - a^\mu = \frac{\eta}{N}\left(F_a + \eta G_a\right), \tag{11}$$

where $F_a + \eta G_a$ is the *update rule* for a general overlap parameter a. In order to investigate finite size effects, we make the following ansaetze for the deviations of

the update rules F_a (the same form is made for G_a) and overlap parameters a from their thermodynamic values,[1]

$$F_a = F_a^0 + \triangle F_a + \frac{1}{N} F_a^1, \qquad a = a^0 + \sqrt{\frac{\eta}{N}} \triangle a + \frac{\eta}{N} a^1, \tag{12}$$

where $\langle \triangle F_a \rangle = \langle \triangle a \rangle = 0$. The update rule *ansatz* is motivated by observing that the activations have variance $\mathcal{O}(1)$ which, iterated through (11) yield overlap variances of $\mathcal{O}\left(N^{-1}\right)$. Terms of the form, $\triangle a$ represent *dynamic* corrections that arise due to the random examples, and a^1 represent *static* corrections such that the mean of the overlap parameter a is given by $a^0 + \eta a^1/N$ - the thermodynamic average plus a correction. In order to simplify the analysis, we assume a small learning rate, η, so that the thermodynamic overlaps are governed by,

$$\frac{da^0}{d\tilde{\alpha}} = F_a^0, \tag{13}$$

where F_a^0 is the update rule F_a averaged over the input distribution, and the rescaled learning rate is given by

$$\tilde{\alpha} = \eta \alpha. \tag{14}$$

Substituting (12) in (11) and averaging over the input distribution, we derive a set of coupled differential equations [2] for the (scaled) covariances $\langle \triangle a \triangle b \rangle$, and static corrections a^1,

$$\frac{d\langle \triangle a \triangle b \rangle}{d\tilde{\alpha}} = \sum_c \langle \triangle a \triangle c \rangle \frac{\partial F_b^0}{\partial c^0} + \sum_c \langle \triangle b \triangle c \rangle \frac{\partial F_a^0}{\partial c^0} + \langle \triangle F_a \triangle F_b \rangle \tag{15}$$

$$\frac{1}{2}\frac{d^2 a^0}{d\tilde{\alpha}^2} + \frac{da^1}{d\tilde{\alpha}} = \sum_b b^1 \frac{\partial F_a^0}{\partial b^0} + \frac{1}{2}\sum_{bc} \langle \triangle b \triangle c \rangle \frac{\partial^2 F_a^0}{\partial b^0 \partial c^0} + G_a^1. \tag{16}$$

Summations are over all overlap parameters, $\{Q_{ij}, R_{in} | i,j = 1..K, n = 1..M\}$. The elements $\langle \triangle F_a \triangle F_b \rangle$ are found explicitly by calculating the covariance of the update rules F_a, and F_b. Initially, the fluctuations $\langle \triangle F_a \triangle F_b \rangle$ are set to zero, and equations (13,15) are then integrated to find the evolution of the covariances, $\mathrm{cov}(a,b) = (\eta/N)\langle \triangle a \triangle b \rangle$, and the corrections to the thermodynamic average values, $(\eta/N)a^1$. The average finite size correction to the generalisation error is given by

$$\epsilon_g = \epsilon_g^0 + \frac{\eta}{N}\epsilon_g^1, \tag{17}$$

where,

$$\epsilon_g^1 = \sum_a a^1 \frac{\partial e_g^0}{\partial a} + \frac{1}{2}\sum_{ab} \langle \triangle a \triangle b \rangle \frac{\partial^2 \epsilon_g^0}{\partial a^0 \partial b^0}. \tag{18}$$

These results enable the calculation of finite size effects for an arbitrary learning scenario. For demonstration, we calculate the finite size effects for a student with two hidden units learning a teacher with one hidden unit. In this over-realisable case, one of the student hidden units eventually specialises on the single teacher hidden unit, while the other student hidden unit decays to zero. In fig.(1), we plot the thermodynamic limit generalisation error alongside the $\mathcal{O}\left(N^{-1}\right)$ correction. In fig.(1a) there is no significant symmetric phase, and the finite size corrections (fig.(1b))

[1] If the order parameter represented by c is Q_{11}, then $c^0 = Q_{11}^0$, and $\triangle c = \triangle Q_{11}$.

[2] The small-fluctuations *ansatz* necessarily yields equations of the same form as presented in [4] for the weight component dynamics. Here they are for the order parameter of the system.

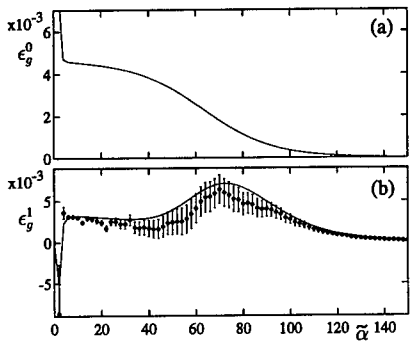

Figure 1 Two student hidden units, one teacher hidden unit. Non zero initial parameters: $Q_{11} = 0.2, Q_{22} = R_{11} = 0.1$. (a) Thermodynamic generalisation error, ϵ_g^0. (b) $\mathcal{O}\left(N^{-1}\right)$ correction to the generalisation error , ϵ_g^1. Simulation results for $N = 10, \eta = 0.1$ and (half standard deviation) error bars are drawn.

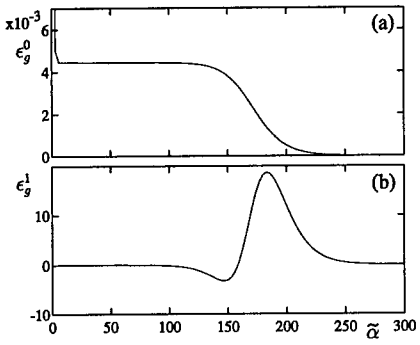

Figure 2 Two student hidden units, one teacher hidden unit. Initially, $Q_{11} = 0.1$, with all other parameters set to zero. (a) Thermodynamic generalisation error ϵ_g^0. (b) $\mathcal{O}\left(N^{-1}\right)$ correction to the generalisation error, ϵ_g^1.

are small. For a finite size correction of less than 10%, we would require an input dimension of around $N > 25\eta$. For the more symmetric initial conditions (fig.(2a)) there is a very definite symmetric phase, for which a finite size correction of less than 10% (fig.(2b)) would require an input dimension of around $N > 50,000\eta$. As the initial conditions approach perfect symmetry, the finite size effects diverge, and the mean dynamical theory becomes inexact. Using the covariances, we can analyse

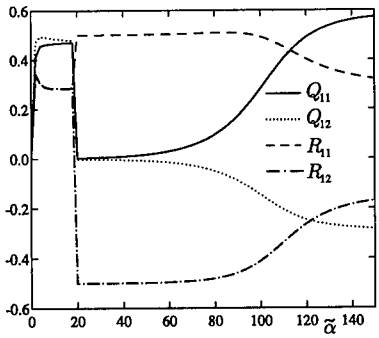

Figure 3 (a) The normalised components of the principal eigenvector for the isotropic teacher. $M = K = 2$, ($Q_{22} = Q_{11}, R_{22} = R_{11}$). Non zero initial parameters $Q_{11} = 0.2$, $Q_{22} = 0.1$, $R_{11} = 0.001, R_{22} = 0.001$.

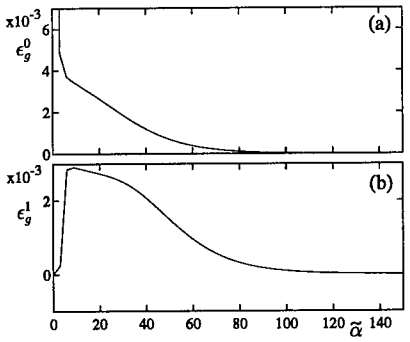

Figure 4 Two student hidden units, one teacher hidden unit. The initial conditions are as in fig.(2).(a) Thermodynamic generalisation error, ϵ_g^0. (b) $\mathcal{O}\left(N^{-1}\right)$ correction to the generalisation error, ϵ_g^1.

the way in which the student breaks out of the symmetric phase by specialising its hidden units. For the isotropic teacher scenario $T_{nm} = \delta_{nm}$, and $M = K = 2$, learn-

ing proceeds such that one can approximate, $Q_{22} = Q_{11}, R_{22} = R_{11}$. By analysing the eigenvalues of the covariance matrix $\langle \triangle a \triangle b \rangle$, we found that there is a sharply defined principal direction, the components of which we show in fig.(3). Initially, all components of the principal direction are similarly correlated, which corresponds to the symmetric region. Then, around $\tilde{\alpha} = 20$, as the symmetry breaks, R_{11} and R_{21} become maximally anti-correlated, whilst there is minimal correlation between the Q_{11} and Q_{12} components. This corresponds well with predictions from perturbation analysis[2]. The symmetry breaking is characterised by a specialisation process in which each student vector increases its overlap with one particular teacher weight, whilst decreasing its overlap with other teacher weights. After the specialisation has occured, there is a growth in the anti-correlation between the student length and its overlap with other students. The asymptotic values of these correlations are in agreement with the convergence fixed point, $R^2 = Q = 1$.

In light of possible prolonged symmetric phases, we break the symmetry of the student hidden units by imposing an ordering on the student lengths, $Q_{11} \geq Q_{22} \geq \ldots \geq Q_{KK}$, which is enforced in a 'soft' manner by including an extra term to (3),

$$\epsilon^{\dagger} = \frac{1}{2} \sum_{j=1}^{K-1} h \left(Q_{j+1j+1} - Q_{jj} \right), \tag{19}$$

where $h(x)$ approximates the step function,

$$h(x) = \frac{1}{2} \left(1 + \mathrm{erf} \left(\frac{\beta}{\sqrt{2}} x \right) \right). \tag{20}$$

This straightforward modification involves the addition of a gaussian term in the student weight lengths to the weight update rule (4). In fig.(4), we show the overlap parameters and their fluctuations for β=10, $K = 2, M = 1$. This graph is to be compared to fig.(2) for which the initial conditions are the same. There is now no collapse to an initial symmetric phase from which the student will eventually specialize. Also, the initial convergence to the optimal values is much faster. As there is no symmetric phase, the finite size corrections are much reduced and are largest around the initial value of $\tilde{\alpha}$ where the overlap parameters are most symmetric, decreasing rapidly due to the driving force away from this near-symmetric region. For the case in which the teacher weights are equal, the constraint (19) prevents the student from converging optimally. A naive scheme to prevent this is to adapt the steepness, β, such that it is inversely proportional to the average of the gradients Q_{ii}, which decreases as the dynamics converge asymptotically.

We conjecture that such symmetry breaking is potentially of great benefit in the practical field of neural network training.

REFERENCES

[1] M. Biehl and H. Schwarze, *Learning by online gradient descent*, Journal of Physics A Vol.28 (1995), pp643–656.

[2] D. Saad and S .Solla, *Exact solution for online learning in multilayer neural networks.* Physical Review Letters, Vol. 74(21) (1995). pp4337-4340.

[3] P. Sollich, *Finite size effects in learning and generalization in linear perceptrons*, Journal of Physics A Vol.27 (1994), pp7771–7784.

[4] T. Heskes, Journal of Physics A Vol.27 (1994), pp5145–5160.

Acknowledgements

This work was partially supported by the EU grant ERB CHRX-CT92-0063.

CONSTANT FAN-IN DIGITAL NEURAL NETWORKS ARE VLSI-OPTIMAL

V. Beiu

Los Alamos National Laboratory, Division NIS-1, Los Alamos, New Mexico 87545, USA. Email: beiu@lanl.gov

The paper presents a theoretical proof revealing an intrinsic limitation of digital VLSI technology: its inability to cope with highly connected structures (e.g. neural networks). We are in fact able to prove that efficient digital VLSI implementations (known as *VLSI-optimal* when minimising the AT^2 complexity measure — A being the *area* of the chip, and T the *delay* for propagating the inputs to the outputs) of neural networks are achieved for small-constant *fan-in* gates. This result builds on quite recent ones dealing with a very close estimate of the *area* of neural networks when implemented by threshold gates, but it is also valid for classical Boolean gates. Limitations and open questions are presented in the conclusions.

Keywords: neural networks, VLSI, fan-in, Boolean circuits, threshold circuits, $\mathbf{F}_{n,m}$ functions.

1 Introduction

In this paper a *network* will be considered an acyclic graph having several input nodes (*inputs*) and some (at least one) output nodes (*outputs*). The nodes are characterised by *fan-in* (the number of incoming edges — denoted by Δ) and *fan-out* (the number of outgoing edges), while the network has a certain *size* (the number of nodes) and *depth* (the number of edges on the longest input to output path). If with each edge a synaptic *weight* is associated and each node computes the weighted sum of its inputs to which a non-linear activation function is then applied (*artificial neuron*), the network is a *neural network* (NN):

$$\mathbb{Z}_k = (z_0, ..., z_{n-1}) \in \mathbb{R}^n, k = 1, ..., m, \text{ and } f(\mathbb{Z}_k) = \sigma\left(\sum_{i=0}^{n-1} w_i z_i + \theta\right), \quad (1)$$

with $w_i \in \mathbb{R}$ the synaptic *weights*, $\theta \in \mathbb{R}$ known as the *threshold*, and *sigma* a non-linear activation function. If the non-linear activation function is the threshold (logistic) function, the neurons are *threshold gates* (TGs) and the network is just a *threshold gate circuit* (TGC) computing a *Boolean function* (BF). The cost functions associated to a NN are *depth* and *size*. These are linked to $T \approx$ *depth* and $A \approx$ *size* of a VLSI chip. Unfortunately, NNs do not closely follow these proportionalities as:

- the *area* of the connections counts [2, 3, 9];
- the *area* of one neuron is related to its associated *weights*.

That is why the *size* and *depth* complexity measures are not the best criteria for ranking different solutions when going to silicon [11]. Several authors have taken into account the *fan-in* [1, 9, 10, 12], the total number of connections, the *total number of bits needed to represent the weights* [8, 15] or even more precise approximations like the *sum of all the weights and thresholds* [2–7]:

$$area \propto \sum_{all\ neurons} \left(\sum_{i=0}^{n-1} |w_i| + |\theta|\right). \quad (2)$$

An equivalent definition of 'complexity' for a NN is $\sum_{i=0}^{n-1} w_i^2$ [16]. It is worth mentioning that there are also several sharp limitations for VLSI implementations like: (i) the maximal value of the *fan-in* cannot grow over a certain limit; (ii) the

maximal ratio between the largest and the smallest *weight*. For simplification, in the following we shall consider only NNs having n binary inputs and k binary outputs. If real inputs and outputs are needed, it is always possible to quantize them up to a certain number of bits such as to achieve a desired precision. The *fan-in* of a gate will be denoted by Δ and all the logarithms are taken to base 2 except mentioned otherwise. Section 2 will present previous results for which proofs have already been given [2–7]. In section 3 we shall prove our main claim while also showing several simulation results.

2 Background

A novel synthesis algorithm evolving from the decomposition of *COMPARISON* has recently been proposed. We have been able to prove that [2, 3]:

Proposition 1 The computation of *COMPARISON* of two n-bit numbers can be realised by a Δ-ary tree of *size* $\mathcal{O}(n/\Delta)$ and *depth* $\mathcal{O}(\log n/\log\Delta)$ for any integer *fan-in* $2 \leq \Delta \leq n$.

A class of Boolean functions $\mathbb{F}_\Delta$ having the property that $\forall f_\Delta \in \mathbb{F}_\Delta$ is linearly separable has afterwards been introduced as: *"the class of functions f_Δ of Δ input variables, with Δ even, $f_\Delta = f_\Delta(g_{\Delta/2-1}, e_{\Delta/2-1}, ..., g_0, e_0)$, and computing $f_\Delta \stackrel{def}{=} \bigvee_{j=0}^{\Delta/2-1}\left[g_j \wedge \left(\bigwedge_{k=j+1}^{\Delta/2-1} e_k\right)\right]$"*. By convention, we consider $\bigwedge_{i=\alpha}^{\alpha-1} e_i \stackrel{def}{=} 1$. One restriction is that the input variables are pair-dependent, meaning that we can group the Δ input variables in $\Delta/2$ pairs of two input variables each: $(g_{\Delta/2-1}, e_{\Delta/2-1}), ..., (g_0, e_0)$, and that in each such group one variable is 'dominant' (i.e. when a dominant variable is 1, the other variable forming the pair will also be 1):

$$\mathbb{F}_\Delta \stackrel{def}{=} \left\{ f_\Delta | f_\Delta : \{(0,0),(0,1),(1,1)\}^{\Delta/2} \rightarrow \{0,1\}, \Delta/2 \in \mathbb{N}^*, \right.$$
$$\left. f_\Delta = \bigvee_{j=0}^{\Delta/2-1}\left[g_j \wedge \left(\bigwedge_{k=j+1}^{\Delta/2-1} e_k\right)\right], g_i \Rightarrow e_i, i = 0, 1, ..., \Delta/2-1 \right\}.$$

Each f_Δ can be built starting from the previous one $f_{\Delta-2}$ (having a lower *fan-in*) by copying its synaptic *weights*; the constructive proof has led to [5]:

Proposition 2 The *COMPARISON* of two n-bit numbers can be computed by a Δ-ary tree neural network with polynomially bounded integer *weights* and *thresholds* ($\leq n^k$) having *size* $\mathcal{O}(n/\Delta)$ and *depth* $\mathcal{O}(\log n/\log\Delta)$ for any integer *fan-in* $3 \leq \Delta \leq \log^k n$.

For a closer estimate of the *area* we have used equation (2) and proved [5]:

Proposition 3 The neural network with polynomially bounded integer *weights* (and *thresholds*) computing the *COMPARISON* of two n-bit numbers occupies an *area* of $\mathcal{O}(n \cdot 2^{\Delta/2}/\Delta)$ for all the values of the *fan-in* (Δ) in the range 3 to $\mathcal{O}(\log n)$. The result presented there is:

$$AT^2(n,\Delta) \cong \frac{2^{\Delta/2}}{\Delta} \cdot \frac{8n\Delta - 6n - 5\Delta}{\Delta - 2} \cdot \frac{\log^2 n}{\log^2 \Delta} = \mathcal{O}\left(\frac{n \log^2 n \cdot 2^{\Delta/2}}{\Delta \log^2 \Delta}\right) \qquad (3)$$

and for $\Delta = \log n$ this is the best (i.e. smallest) one reported in the literature. Further, the synthesis of a class of Boolean functions $\mathbf{F}_{n,m}$ — functions of n input variables having m groups of ones in their truth table [13] — has been detailed [4]:

Proposition 4 Any function $f \in \mathbf{F}_{n,m}$ can be computed by a neural network with polynomially bounded integer *weights* (and *thresholds*) of *size* $\mathcal{O}(mn/\Delta)$ and

depth $\mathcal{O}(\log(mn)/\log\Delta)$ and occupying an *area* of $\mathcal{O}(mn\cdot 2^{\Delta}/\Delta)$ if $2m \leq 2^{\Delta}$ for all the values of the *fan-in* (Δ) in the range 3 to $\mathcal{O}(\log n)$.
More precisely we have:

$$T(n,m,\Delta) = \left\lceil \frac{\log n - 1}{\log\Delta - 1} \right\rceil + \left\lceil \frac{\log m + 1}{\log\Delta} \right\rceil = \mathcal{O}\left(\frac{\log(mn)}{\log\Delta}\right) \qquad \text{and}$$

$$A(n,m,\Delta) < 2m\cdot\left(\frac{4n\cdot 2^{\Delta}}{\Delta} + \frac{5(n-\Delta)\cdot 2^{\Delta/2}}{\Delta(\Delta-2)}\right) + \Delta\cdot\left\lceil\frac{2m-1}{\Delta-1}\right\rceil = \mathcal{O}\left(\frac{mn\cdot 2^{\Delta}}{\Delta}\right)$$

which leads to:

$$AT^2(n,m,\Delta) = \mathcal{O}\left(\frac{mn\cdot\log^2(mn)\cdot 2^{\Delta}}{\Delta\cdot\log^2\Delta}\right). \tag{4}$$

For $2m > 2^{\Delta}$ the equations are much more intricate, while the complexity values for *area* and for AT^2 are only reduced by a factor (equal to the *fan-in* [6, 7]). If we now suppose that a feed-forward NN of n inputs and k outputs is described by m examples, it can be directly constructed as simultaneously implementing k different functions from $\mathbf{F}_{n,m}$ [4, 6, 7]:

Proposition 5 Any set of k functions $f\in\mathbf{F}_{n,i}$, $i = 1, 2, ..., m$, $i \leq m \leq 2^{\Delta-1}$ can be computed by a neural network with polynomially bounded integer *weights* (and *thresholds*) having *size* $\mathcal{O}(m(2n+k)/\Delta)$, *depth* $\mathcal{O}(\log(mn)/\log\Delta)$ and occupying an *area* of $\mathcal{O}(mn\cdot 2^{\Delta}/\Delta + mk)$ if $2m \leq 2^{\Delta}$, for all the values of the *fan-in* (Δ) in the range 3 to $\mathcal{O}(\log n)$.

The architecture has a first layer of COMPARISONs which can either be implemented using classical Boolean gates (BGs) or — as it has been shown previously — by TGs. The desired function can be synthesised either by one more layer of TGs, or by a classical two layers AND-OR structure (a second hidden layer of AND gates — one for each hypercube), and a third layer of k OR gates represents the outputs. For minimising the *area* some COMPARISONs could be replaced by AND gates (like in a classical disjunctive normal form implementation).

3 Which is the VLSI-Optimal Fan-In?

Not wanting to complicate the proofs, we shall determine the VLSI-optimal *fan-in* when implementing *COMPARISON* (in fact: $\mathbf{F}_{n,1}$ functions) for which the solution was detailed in *Propositions 1* to *3*. The same result is valid for $\mathbf{F}_{n,m}$ functions as can be intuitively expected either by comparing equations (3) and (4), or because:

- the *delay* is determined by the first layer of COMPARISONs; while
- the *area* is determined by the same first layer of COMPARISONs (the additional *area* for implementing the symmetric 'alternate addition' [4] can be neglected).

For a better understanding we have plotted equation (3) in Figure 1.

Proposition 6 The VLSI-*optimal* (which minimises the AT^2) neural network which computes the *COMPARISON* of two n-bit numbers has small-constant *fan-in* 'neurons' with small-constant bounded *weights* and *thresholds*.

Proof: Starting from the first part of equation (3) we can compute its derivative:

$$\frac{d(AT^2)}{d\Delta} = \frac{2^{\Delta/2}\log^2 n}{\Delta^2(\Delta-2)^2\log^3\Delta}\times\left(8n\Delta^3\log\Delta - 22n\Delta^2\log\Delta + 12n\Delta\log\Delta\right.$$

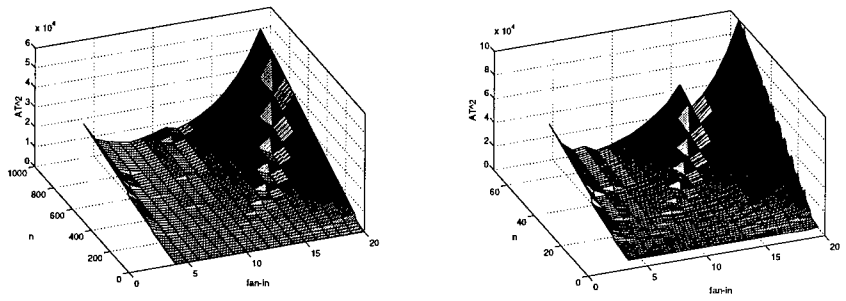

Figure 1 The AT^2 values of COMPARISON — plotted as a 3D surface — versus the number of inputs n and the *fan-in* Δ for: (a) many inputs $n \leq 1024$ ($4 \leq \Delta \leq 20$); and (b) few inputs $n \leq 64$ ($4 \leq \Delta \leq 20$). It can be very clearly seen that a 'valley' is formed and that the 'deepest' points constantly lie somewhere between $\Delta_{minim} = 5$ and $\Delta_{maxim} = 10$.

$$
\begin{aligned}
&- 5\Delta^3 \log \Delta + 10\Delta^2 \log \Delta - \frac{16}{\ln 2} n\Delta^2 \log \Delta + \frac{24}{\ln 2} n\Delta \log \Delta \\
&- \frac{24}{\ln 2} n \log \Delta + \frac{10}{\ln 2} \Delta^2 \log \Delta - \frac{32}{\ln 2} n\Delta^2 + \frac{88}{\ln 2} n\Delta - \frac{48}{\ln 2} n \\
&+ \frac{20}{\ln 2} \Delta^2 - \frac{40}{\ln 2} \Delta \Big)
\end{aligned}
$$

which — unfortunately — involves transcendental functions of the variables in an essentially non-algebraic way. If we consider the simplified 'complexity' version of equation (3) we have:

$$\frac{d(AT^2)}{d\Delta} \cong \frac{d}{d\Delta} \left(\frac{n \log^2 n \cdot 2^{\Delta/2}}{\Delta \log^2 \Delta} \right) = \frac{2^{\Delta/2}}{\Delta \log^2 \Delta} \cdot \left(\frac{\ln 2}{2} - \frac{1}{\Delta} - \frac{2}{\Delta \ln \Delta} \right)$$

which when equated to zero leads to $\ln \Delta(\Delta \ln 2 - 2) = 4$ (also a transcendental equation). This has $\Delta = 6$ as 'solution' and as the *weights* and the *thresholds* are bounded by $2^{\Delta/2}$ (*Proposition 4*) the proof is concluded. □

The proof has been obtained using several successive approximations: neglecting the ceilings and using a 'simplified' complexity estimate. That is why we present in Figure 2 exact plots of the AT^2 measure which support our previous claim. It can be seen that the optimal *fan-in* 'constantly' lies between 6 and 9 (as $\Delta_{optim} = 6...9$, one can minimise the *area* by using COMPARISONs only if the group of ones has a length of $\alpha \geq 64$ — see [4–7]). Some plots in Figure 2 are also including a TG-optimal solution denoted by SRK [14] and the logarithmic *fan-in* solution ($\Delta = \log n$) denoted B_lg [5].

4 Conclusions

This paper has presented a theoretical proof for one of the intrinsic limitations of digital VLSI technology: *there are no 'optimal' solutions able to cope with highly connected structures.* For doing that we have proven the contrary, namely that constant *fan-in* NNs are VLSI-*optimal* for digital architectures (either Boolean or using TGs). Open questions remain concerning *'if'* and *'how'* such a result could be extended to purely analog or mixed analog/digital VLSI circuits.

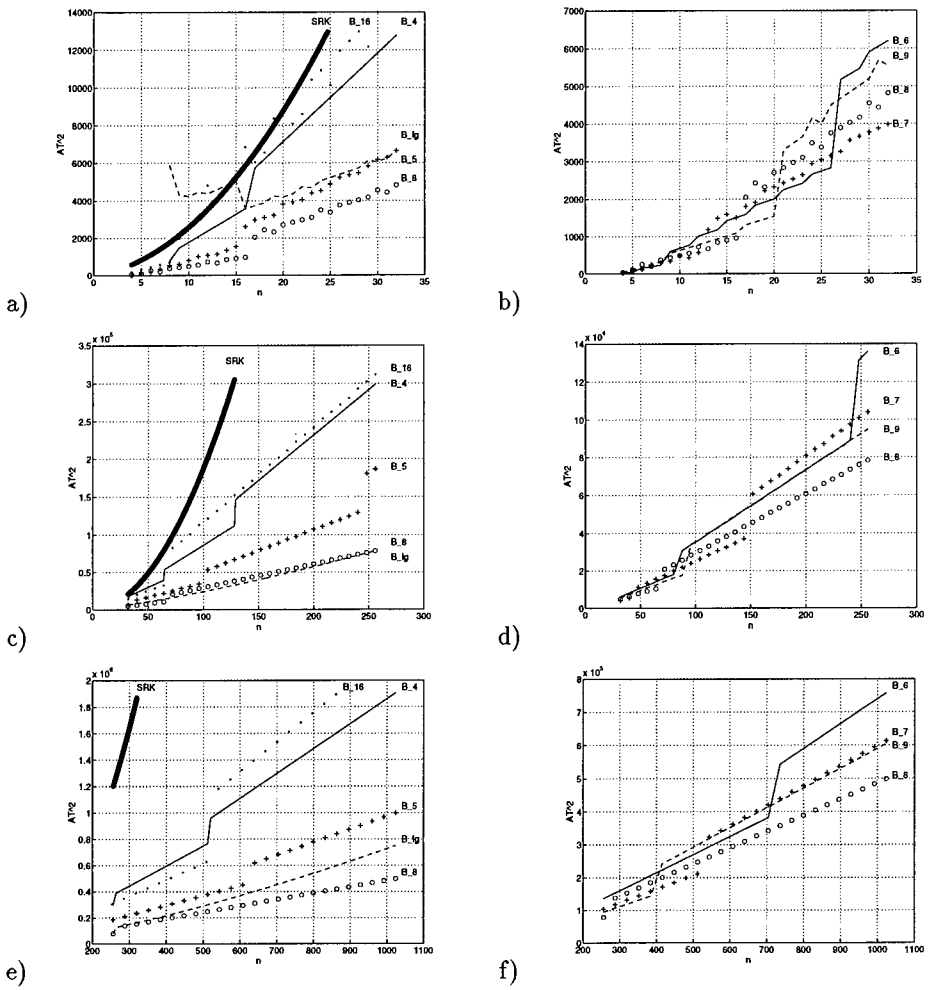

Figure 2 The AT^2 values of COMPARISON for different number of inputs n and *fan-in* Δ (B_Δ): (a) for $4 \leq n \leq 32$ including the SRK [14] solution; (b) detail showing the optimum *fan-in* for the same interval ($4 \leq n \leq 32$); (c) for $32 \leq n \leq 256$ including the SRK [14] solution; (d) detail showing the optimum *fan-in* for the same interval ($32 \leq n \leq 256$); (e) for $256 \leq n \leq 1024$ including the SRK [14] solution; (f) detail showing the optimum *fan-in* for the same interval ($256 \leq n \leq 1024$).

REFERENCES

[1] Y.S. Abu-Mostafa, *Connectivity Versus Entropy*, in: Neural Information Processing Systems (Proc. NIPS*87, Denver, Colorado), ed. D.Z. Anderson, American Institute of Physics, New York, (1988) pp1–8.

[2] V. Beiu, J.A. Peperstraete, J. Vandewalle and R. Lauwereins, *Efficient Decomposition of COMPARISON and Its Applications*, in: ESANN'93 (Proc. European Symposium on Artificial Neural Networks '93, Brussels, Belgium), ed. M. Verleysen, Dfacto, Brussels, (1993) pp45–50.

[3] V. Beiu, J.A. Peperstraete, J. Vandewalle and R. Lauwereins, *COMPARISON and Threshold Gate Decomposition*, in: MicroNeuro '93 (Proc. International Conference on Microelectronics for Neural Networks '93, Edinburgh, UK), eds. D.J. Myers and A.F. Murray, UnivEd Tech. Ltd., Edinburgh, (1993) pp83–90.

[4] V. Beiu, J.A. Peperstraete, J. Vandewalle and R. Lauwereins, *Learning from Examples and VLSI Implementation of Neural Networks*, in: Cybernetics and System Research '94 (Proc. European Meeting on Cybernetics and System Research '94, Vienna, Austria), ed. R. Trappl, World Scientific Publishing, Singapore, (1994) pp1767–1774.

[5] V. Beiu, J.A. Peperstraete, J. Vandewalle and R. Lauwereins, *Area-Time Performances of Some Neural Computations*, in: SPRANN '94 (Proc. International Symposium on Signal Processing, Robotics and Neural Networks '94, Lille, France), eds. P. Borne, T. Fukuda and S.G. Tzafestas, GERF EC, Lille, (1994) pp664–668.

[6] V. Beiu and J.G. Taylor, *VLSI Optimal Neural Network Learning Algorithm*, in: Artificial Neural Nets and Genetic Algorithms (Proc. Int. Conf., Ales, France), eds. D.W. Pearson, N.C. Steele and R.F. Albrecht, Springer-Verlag, Vienna, (1995) pp61–64.

[7] V. Beiu and J.G. Taylor, *Area-Efficient Constructive Learning Algorithms*, in Proc. CSCS-10 (10th International Conference on Control System and Computer Science, Bucharest, România), ed. I. Dumitrache, PUBucharest, Bucharest, (1995), pp293–310.

[8] J. Bruck and J. Goodman, *On the Power of Neural Networks for Solving Hard Problems*, in: Neural Information Processing Systems (Proc. NIPS*87, Denver, Colorado), ed. D.Z. Anderson, American Institute of Physics, New York, (1988) pp137–143.

[9] D. Hammerstrom, *The Connectivity Analysis of Simple Associations -or- How Many Connections Do You Need*, in: Neural Information Processing Systems (Proc. NIPS*87, November, Denver, Colorado), ed. D.Z. Anderson, American Institute of Physics, New York, (1988) pp338–347.

[10] H. Klaggers and M. Soegtrop, *Limited Fan-In Random Wired Cascade-Correlation*, in: MicroNeuro'93 (Proc. International Conference on Microelectronics for Neural Networks, Edinburgh '93, UK), eds. D.J. Myers and A.F. Murray, UnivEd Tech. Ltd., Edinburgh, (1993) pp79–82.

[11] A.V. Krishnamoorthy, R. Paturi, M. Blume, G.D. Linden, L.H. Linden and S.C. Esener, *Hardware Tradeoffs for Boolean Concept Learning*, in WCNN'94 (Proc. World Conference on Neural Networks '94, San Diego, USA), Lawrence Erlbaum and INNS Press, Hillsdale, (1994) Vol. 1, pp551–559.

[12] D.S. Phatak and I. Koren, *Connectivity and Performance Tredeoffs in the Cascade-Correlation Learning Architecture*, IEEE Trans. on Neural Networks Vol. 5(6) (1994), pp930–935.

[13] N.P. Red'kin, *Synthesis of Threshold Circuits for certain Classes of Boolean Functions*, Kibernetica Vol. 5 (1970), pp6–9. Translated in Cybernetics Vol. 6(5) (1973), pp540–544.

[14] K.-Y. Siu, V. Roychowdhury and T. Kailath, *Depth-Size Tradeoffs for Neural Computations*, IEEE Trans. on Computers Vol. 40(12) (1991), pp1402–1412.

[15] R.C. Williamson, *ϵ-Entropy and the Complexity of Feedforward Neural Networks*, in: Neural Information Processing Systems (Proc. NIPS*90, Denver, Colorado), eds. R.P. Lippmann, J.E. Moody and D.S. Touretzky, Morgan Kaufmann, San Mateo, (1991), pp946–952.

[16] B.-T. Zhang and H. Mühlenbein, *Genetic Programming of Minimal Neural Networks Using Occam's Razor*, Technical Report: Arbeitspapiere der GMD 734, Schloß Birlinghoven, Sankt Augustin, Germany (1993).

Acknowledgements

This research work has been started while Dr. Beiu was with the Katholieke Universiteit Leuven, Belgium, and has been supported by a grant from the Concerted Research Action of the Flemish Community entitled: "Applicable Neural Networks". The research has been continued under the Human Capital and Mobility programme of the European Community as an Individual Research Training Fellowship ERB4001GT941815: "Programmable Neural Arrays", under contract ERBCHBICT941741. The scientific responsibility is assumed by the author, who is on leave of absence from the "Politechnica" University of Bucharest, Romania.

THE APPLICATION OF BINARY ENCODED 2ND DIFFERENTIAL SPECTROMETRY IN PREPROCESSING OF UV-VIS ABSORPTION SPECTRAL DATA

N Benjathapanun, W J O Boyle and K T V Grattan
Department of Electrical, Electronic and Information Engineering
City University, Northampton Square, London EC1V OHB, UK.

This paper describes classification of UV-Vis optical absorption spectra by binary encoding segments of the second derivative of the absorption spectra according to their shape. This allows successful classification of spectra using the Back Propagation Neural Network analysis (BPNN) algorithm where other preprocessing schemes have failed. It is also shown that once classified, estimation of chemical species concentration using a further stage of BPNN is possible. Data for the study are derived from laboratory-based measurements of UV-Vis optical absorption spectra from mixtures of common chemical pollutants.

1 Introduction

This study has the goal of developing artificial intelligence methods, to analyse UV-Vis spectra and hence determine actual chemical species and their concentrations in real-time in-line monitor systems. Prior to the study, a wide range of NN methods (BP, Radial Base, Kohonen, etc.), topologies and iteration conditions were evaluated for their ability to classify and/or estimate components in the data. All these methods were unsuccessful and pointed to the need for a more knowledge-based approach. In the present work two approaches to preprocessing the data before classification by BPNN are evaluated. The first method, 2nd derivative spectrometry, relies only on the spectral data and if successful would give self-classifying, self learning solutions. The second method, a modification of 2nd derivative spectrometry [1], depends on knowledge of the absorption spectra of expected constituent species.

2 Experimental

Data for the study were obtained from laboratory-based UV-Vis optical absorption spectra measurements taken from mixtures of three common chemical pollutants in water prepared at three different concentrations. Stock solutions were prepared from addition of *Sodium Nitrate, Ammonia* solution and *Sodium Hypochlorite* to distilled water and these were mixed in all possible combinations to provide a set of training data with 64 members. 64 samples were also mixed for a test set at concentrations approximately 30% greater than those for the training set. Species and concentrations are summarised in Table 1. The apparatus used in the experiments consisted of a Hewlett-Packard 8452A diode array spectrometer equipped with a 1 cm quartz cell operated remotely using proprietary software. All spectroscopic data were transferred to computer via a serial interface for analysis using Microsoft Windows based software including the Neural Desk v2.1 Neural Network software package[2]. UV intensity spectra of the solution were recorded from 190 to 820 nm with 2 nm interval. Absorption spectra were calculated from the intensity spectra using equation (1) with spectra from distilled water as a reference. For data

	TRAINING SET							
NH_3-A	=	105.83 mg/l	Cl_2-A	=	49.23 mg/l	NO_3-A	=	7.75 mg/l
NH_3-B	=	32.55 mg/l	Cl_2-B	=	24.62 mg/l	NO_3-B	=	3.88 mg/l
NH_3-C	=	11.18 mg/l	Cl_2-C	=	6.15 mg/l	NO_3-C	=	1.94 mg/l
	TESTING SET							
NH_3-D	=	137.7 mg/l	Cl_2-D	=	60.48 mg/l	NO_3-D	=	9.75 mg/l
NH_3-E	=	45.9 mg/l	Cl_2-E	=	30.24 mg/l	NO_3-E	=	4.88 mg/l
NH_3-F	=	15.3 mg/l	Cl_2-F	=	5.04 mg/l	NO_3-F	=	1.95 mg/l

Table 1 Chemical species and concentrations used to obtain the data sets.

analysis, data points 4nm apart were used, giving data arrays of 43 points.

$$A = \log_{10}\left(\frac{I_{blank} - \text{darkcurrent}}{I_{sample} - \text{darkcurrent}}\right) \quad (1)$$

Figure 1 shows absorption spectra obtained for the three individual species and the spectra when these are mixed together. These spectra are typical of those obtained for this study and they exemplify two important features of UV-Vis spectrometry. Firstly, UV-Vis spectral peaks from water are in general broad and overlapping, typically 30nm wide - this makes them difficult to discern. Secondly, the dynamic range in absorption for the contaminant species is high. Consequently when two or more species are mixed at high concentrations very little light is left for measurement, and the signal to noise level is reduced. The experimental data set is also subject to some systematic error due to base line shifts representative of drift in the experimental apparatus over long time periods (days) and also because of undetermined chemistry due to reactions between components in the mixture. However these factors should not limit the ability to classify the spectra, only the ability to quantify, as each constituent in a sample should result in its own distinctive adsorption peak, even if the relationship between peak height and concentration contains some error and/or is non-linear.

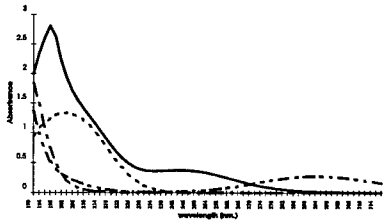

Figure 1 The absorbance spectra of NO_3 7.75 mg/l, NH_3 105.83 mg/l and Cl_2 49.23mg/l and a mixture of these (solid line).

3 Simulating Data Patterns by Adding Systematic Noise

To obtain sufficient training and testing sample sets [3], a systematic noise characteristic of stray light in the optical system was added to the raw data in the range

0-5% in intervals of 0.5%, using formula (2), in a similar manner to the work of Gemperline et al [4]. This generated 704 training patterns and 704 test patterns

$$A_{i\lambda}(generate) = A_{i\lambda} + \log\left(1 + \frac{E}{10^{A_{i\lambda}}}\right) \quad (2)$$

where $A_{i\lambda}$ is the absorption of the ith component at the wavelength λ, and E is the fraction of stray light added.

4 Results

A summary of conditions for the BPNN classifiers used after the preprocessing steps is given in Table 2. Figure 2 shows a diagram of the root mean square training error against iteration epoch and Figure 3 is a diagram of the percentage error in the testing set after intervals of 200 epochs. A minimum in the error in Figure 3 indicates the best compromise between under training and over training.

Stochastic back-propagation: learning rate = 0.1, alpha = 0.9	Network Topology		
Pre-processing	inputs	hidden	outputs
2nd derivative values	21	5	3
Encode the shape of 2nd derivative spectra	22	5	3

Table 2 Summary of conditions for the BPNN classifiers used after the preprocessing steps.

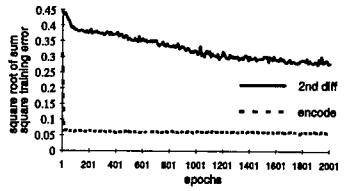

Figure 2 Training error as a function of epoch for preprocessing with PCA, 2nd Derivative spectra, and Binary Encoded 2nd Derivative Spectra.

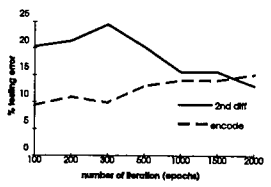

Figure 3 Testing error after every 200 training epochs as a function of epoch for preprocessing with PCA, 2nd Derivative spectra, and Binary Encoded 2nd Derivative Spectra.

5 2nd Derivative Preprocessing with BPNN classification

Following the procedure of Antonov and Stoyanov [5] whereby the spectra are transformed into differential absorption spectra which increase the likelihood of discerning spectral features related to the presence of a species, in this trial, a data set of 704 spectra of 21 values of the second derivative with respect to wavelength ($d^2A/d\lambda^2$) were prepared. As shown in Figure 2 and Figure 3 this scheme is not successful at classifying the data.

6 Binary Encoded 2nd Derivative Preprocessing

The idea behind binary encoding the 2nd derivative spectra is to obtain a code that represents the shape of the spectral data that is as independent as possible of

the intensity of the data. The procedure consists of binary encoding segments of the second derivative of the absorption spectra according to the state of the slope, i.e. of the third derivative. Only relevant data are used, that is data from around the absorption speaks of expected species. In detail the binary encoding scheme consists of: firstly, segmenting the 2nd derivative spectra between 190 - 350 nm into 10 segments as shown in Figure 3, with the segment between 206 and 224 divided into two segments to ensure that the minimum in this region is included; secondly, encoding the slope in each segment with a 2 bit binary code of 01 for decreasing, 10 for increasing, 11 for convex, and 00 for unchanged; and thirdly, using the resulting 22 bit code as input to a classifying BPNN network. The topology of this network is 22 input nodes, 5 hidden nodes, and 3 output nodes. The three outputs determine whether Nitrate, Chlorine, or Ammonia are present. As can be seen in Figures 2 and 3, the classification was much more accurate than in the previous attempt and the training error converged to a small value very quickly. This results in a 93.75% prediction confidence overall for classification. However an error of 6.25% is obtained for the case of a mixture of Ammonia and Nitrate which is mis-predicted as a mixture of Ammonia, Nitrate and Chlorine. However as will be shown in the next section when this classification was followed up by the third stage of estimation the mis-identified chlorine is predicted as occurring at a low, insignificant level. Thus overall the two stages tend to cancel out the error.

7 Estimation of Concentration

Following on from the binary encoded second derivative preprocessing, the scheme for estimation of concentration also uses a knowledge of components expected in the spectra. Here one of seven possible networks which predict concentration is chosen depending on the output of the classification network. The seven networks cover all the possibilities of the 1. Chlorine, 2. Nitrate, 3. Chlorine and Nitrate, 4. Ammonia, 5. Chlorine and Ammonia, 6. Nitrate and Ammonia and 7. Chlorine, Nitrate and Ammonia. These are described in the next section. In this scheme absorption peak shape data for the various components; Nitrate at 210 nm, Hypochlorite at 290 nm and Monochloramine at 245 nm are used to determine the input variables for the seven BPNNs used for estimating concentration. The inputs used are the 7 values of absorbance centred around the peak region of each species as depicted in Table 4. Training and Testing data for these BPNN was generated, using extinction coefficient data for each of the expected components and varying the concentration of each species over the ranges shown in Table 3. The extinction coefficients data sets required for this were obtained by partial least squares fitting the absorption spectra using the combined original raw training and testing data sets. Data from this new training set was used with one of the following network topologies, depending on the output of the classification network. The various networks were: 3 hidden nodes for 7 inputs for the cases with 1 outputs node, 4 hidden nodes for 14 inputs for the cases with 2 outputs, and 5 hidden nodes for 21 inputs for the cases with 3 outputs. The algorithm used was Stochastic BP with 0.1 learning rate and 0.9 momentum. It is worth noting that these estimation networks are linear since they were trained using data from a linear model of absorbance. Testing data for the estimating networks were generated by selecting the values of absorption half way between the values of absorption used for the training set and adding 5% stray light; i.e. $E = 0.05$ in (2).

The training and testing error for the Ammonia and Chlorine network was typical of the result obtained for all the estimation networks. For this the network error converged very quickly from an error of 0.1889 at 1st epoch to less than 0.0025 after only 100 epochs. The testing error also reduced to a minimum of 0.015 after 500 training epochs. The overall accuracy of the estimating networks is shown in Table 4. This figure tabulates the number of training patterns and the resulting error for the networks described in the text.

Concentration Varying (mg/l)				
Net	Chlorine	Nitrate	Ammonia	INPUTS Absorption units at
1.	4.5 – 40.0	—	—	279–303 nm
2.	—	1.2 – 8.0	—	203–227 nm
3.	4.0 – 40.0	1.2 – 8.0	—	279–303 & 203–227 nm
4.	—	—	4.5 – 40.0	191–219 nm
5.	4.0 – 40.0	—	4.0 – 38.0	191–219 & 231–255 & 279–303 nm
6.	—	1.2 – 8.0	4.0 – 40.0	191–227 nm
7.	5.0 – 40.0	1.0 – 8.0	5.0 – 40.0	191–227 & 231–255 & 279–303 nm

Table 3 Concentration range of each species used in generating training patterns. 1.Chlorine (7 inputs) 2. Nitrate (7 inputs) 3. Chlorine and Nitrate (14 inputs) 4. Ammonia (7 inputs) 5.Chlorine and Ammonia (21 inputs) 6. Nitrate and Ammonia (9 inputs) 7. Chlorine, Nitrate and Ammonia (23 inputs).

ALGORITHM	Stochastic BP with 0.1 learning rate and 0.9 momentum	
Network	patterns	Result Error
1. Chlorine	356	0.03%
2. Nitrate	137	0.05%
3. Chlorine and Nitrate	350	0.18% & 0.20%
4. Ammonia	356	0.04%
5. Chlorine and Ammonia	350	0.72% & 0.17%
6. Nitrate and Ammonia	350	0.68% & 0.56%
7. Chlorine, Nitrate and Ammonia	512	0.13% & 1.72% & 1.03%

Table 4 Network's Topology and Performance.

8 Conclusions

In laboratory-based trials, 2nd-derivative analysis is found to be an ineffective pre-processing method in BPNN classification of UV-Vis absorption from water samples. This follows on from earlier work in which various NN algorithms including BPNN were evaluated for classification and estimation and also found ineffective. Subsequently a more knowledge-based approach has been formulated which restricts itself to determining the presence and concentration of a range of expected species. The scheme involves a three stage process. In the first stage shape information is derived by binary encoding segments of the second derivative of the absorp-

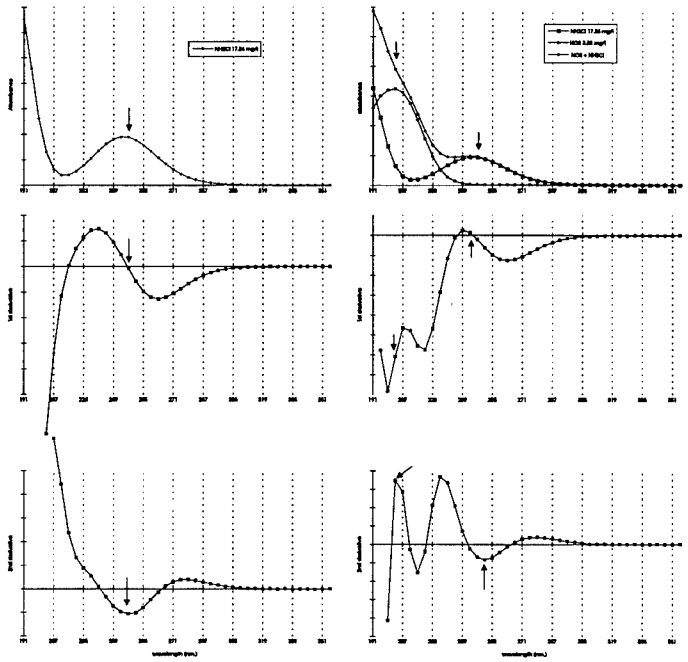

Figure 4 Absorption spectra and 1st and 2nd derivative spectra for monochloroamine and monochloroamine plus nitrate.

tion spectra according to their shape. The rationale of this stage is to reduce the spectral information to shape sensitive factors. This is found significantly to ease classification of the spectra by a second stage of BPNN analysis. For estimation of concentration of species absorption data for the expected species is used to train a second stage of BPNN, segmentation of the spectra and selection of relevant inputs for the second stage BPNN is determined from the absorption data for the expected species, to give the best segmentation pattern and minimum number of network inputs. The two-step approach taken to classification and then estimation is better than a one step approach. The first-step network specifies which species are likely to occur and the second-step network can then focus on a few inputs that strongly correlate with the presence of the expected species. Also the second-step provides a filter that compensates for classification of species at low concentration levels or incorrect identification of species due to low level signals with noise.

REFERENCES

[1] Sommer, L., *Analytical absorption spectrophotometry in the visible and ultraviolet: the principles*, (1989) Elsevir.

[2] *Neural Desk: User's Guide*, Neural Computer Sciences, (1992).

[3] Hammerstrom, D. M., *Working with neural networks*, IEEE Spectrum, July (1993), pp46–53.

[4] Gemperline, P. J., Long, J. R. and Gregoriou, V. J., *Nonlinear Multivarate Calibration Using Principal Components Regression and Artificial Neural Networks*, Anal. Chem., Vol. 63 (1991), pp2313–2323.

[5] Antonov, L. and Stoyanov, S., *Analysis of the Overlapping Bands in UV-Vis Absorption spectroscopy*, Applied Spectroscopy, Vol. 47 (1993), no. 7, pp1030–1035.

A NON-EQUIDISTANT ELASTIC NET ALGORITHM

Jan van den Berg and Jock H. Geselschap
Department of Computer Science,
Erasmus University Rotterdam, The Netherlands.
Email: jvandenberg@few.eur.nl

The statistical mechanical derivation by Simic of the Elastic Net Algorithm (ENA) from a stochastic Hopfield neural network is criticized. In our view, the ENA should be considered a *dynamic penalty method*. Using a linear distance measure, a *Non-equidistant* Elastic Net Algorithm (NENA) is presented. Finally, a *Hybrid* Elastic Net Algorithm (HENA) is discussed.

1 Stochastic Hopfield and Elastic Neural Networks

Hopfield introduced the idea of an energy function into neural network theory [5]. Like Simic [8], we use Hopfield's energy expression multiplied by -1, i.e.

$$E(\mathbf{S}) = \tfrac{1}{2}\sum_{ij} w_{ij} S_i S_j + \sum_i I_i S_i, \tag{1}$$

where $\mathbf{S} \in \{0,1\}^n$ and all $w_{ij} \geq 0$. Making the units stochastic, the network can be analyzed applying statistical mechanics. We concentrate on the free energy [6, 6]

$$F = \langle E(\mathbf{S}) \rangle - T\mathcal{S}, \tag{2}$$

where $T = 1/\beta$ is the temperature, where $\langle E(\mathbf{S}) \rangle$ represents the average energy, and where $\mathcal{S}$ equals the so-called entropy. A minimum of F corresponds to a thermal equilibrium state [6]. We shall apply the next theorem [10, 11]:

Theorem 1 *In mean field approximation, the free energy F_c of constrained stochastic binary Hopfield networks, submitted to the constraint $\sum_i S_i = 1$ equals*

$$F_c(\mathbf{V}) = -\tfrac{1}{2}\sum_{ij} w_{ij} V_i V_j - \tfrac{1}{\beta}\ln[\sum_i \exp(-\beta(\sum_j w_{ij} V_j + I_i))]. \tag{3}$$

The stationary points of F_c are found at state space points where

$$V_i = \mathrm{P}(S_i = 1 \ \wedge \ \forall j \neq i : S_j = 0) = \frac{\exp(-\beta(\sum_j w_{ij} V_j + I_i))}{\sum_l \exp(-\beta(\sum_j w_{lj} V_j + I_l))}. \tag{4}$$

Let S_p^i denote whether the salesman at time i occupies space-point p or not ($S_p^i = 1$ or 0). Then the corresponding Hamiltonian may be stated as [8]

$$E(\mathbf{S}) = \tfrac{1}{4}\sum_i \sum_{pq} d_{pq}^2 S_p^i (S_q^{i+1} + S_q^{i-1}) + \tfrac{\alpha}{4}\sum_i \sum_{pq} d_{pq}^2 S_p^i S_q^i. \tag{5}$$

The first term represents the sum of distance-squares, the second term penalizes the simultaneous presence of the salesman at more than one position. The other constraints, which should guarantee that every city is visited once, can be built-in 'strongly' using $\forall i : \sum_j S_{ij} = 1$. Eventually, one finds [8, 12] the free energy

$$\begin{aligned} F_{\mathrm{tsp}}(\mathbf{V}) \ = \ & -\tfrac{1}{4}\sum_i \sum_{pq} d_{pq}^2 V_p^i (V_q^{i+1} + V_q^{i-1}) - \tfrac{\alpha}{4}\sum_i \sum_{pq} d_{pq}^2 V_p^i V_q^i - \\ & \tfrac{1}{\beta}\sum_p \ln\big[\sum_i \exp(-\tfrac{\beta}{2}\sum_q d_{pq}^2 (\alpha V_q^i + V_q^{i+1} + V_q^{i-1}))\big]. \end{aligned} \tag{6}$$

On the other hand, the 'elastic net' algorithm [2] has the energy function

$$E_{\text{en}}(\mathbf{x}) = \tfrac{\alpha_2}{2}\sum_i \mid \mathbf{x}^{i+1} - \mathbf{x}^i \mid^2 - \tfrac{\alpha_1}{\beta}\sum_p \ln \sum_j \exp(\tfrac{-\beta^2}{2} \mid \mathbf{x}_p - \mathbf{x}^j \mid^2). \qquad (7)$$

Here, $\mathbf{x}^i$ represents the i-th elastic net point and $\mathbf{x}_p$ represents the location of city p. Application of gradient descent on (7) yields the updating rule:

$$\Delta\mathbf{x}^i = \tfrac{\alpha_2}{\beta}(\mathbf{x}^{i+1} - 2\mathbf{x}^i + \mathbf{x}^{i-1}) + \alpha_1 \sum_p \Lambda^p(i)(\mathbf{x}_p - \mathbf{x}^i), \qquad (8)$$

where $\Lambda^p(i) = \exp(-\frac{\beta^2}{2} \mid \mathbf{x}_p - \mathbf{x}^i \mid^2)/\sum_l \exp(-\frac{\beta^2}{2} \mid \mathbf{x}_p - \mathbf{x}^l \mid^2)$ and where the time-step $\Delta t = 1/\beta$ equals the current temperature T.

2 Why the ENA is a Dynamic Penalty Method

Three objections against Simic's derivation of (7) (with $\alpha_1 = \alpha_2 = 1$) from (6) are given. To derive a free energy expression in the standard form (2), Simic applies a Taylor series expansion on the last term of (6). We try to do the same. Taking

$$f(\mathbf{x}) = \sum_p \ln\big[\sum_i \exp(x_p^i)\big], \qquad (9)$$

$$a_p^i = -\beta\tfrac{\alpha}{2}\sum_q d_{pq}^2 V_q^i, \quad \text{and} \quad h_p^i = -\beta\tfrac{1}{2}\sum_q d_{pq}^2(V_q^{i+1} + V_q^{i-1}), \qquad (10)$$

and using (4) (adapted to the TSP, with $\alpha \gg 1$), we obtain [12]

$$\begin{aligned} f(\mathbf{a}+\mathbf{h}) &= \sum_p \ln\big[\sum_i \exp(a_p^i)\big] + \sum_{ip} h_p^i \frac{\partial f}{\partial x_p^i}(a_p^i) + \mathcal{O}(\mathbf{h}^2) \qquad (11)\\ &\approx \sum_p \ln \sum_i \exp\big(-\beta\tfrac{\alpha}{2}\sum_q d_{pq}^2 V_q^{i)} - \tfrac{\beta}{2}\sum_i\sum_{pq} d_{pq}^2 V_p^i (V_q^{i+1} + V_q^{i-1}). \end{aligned}$$

Substitution of this result in (6) yields:

$$\begin{aligned} F_{\text{app}}(\mathbf{V}) = {} & \tfrac{1}{4}\sum_i\sum_{pq} d_{pq}^2 V_p^i (V_q^{i+1} + V_q^{i-1}) - \tfrac{\alpha}{4}\sum_i\sum_{pq} d_{pq}^2 V_p^i V_q^i - \\ & \tfrac{1}{\beta}\sum_p \ln \sum_i \exp\big(-\beta\tfrac{\alpha}{2}\sum_q d_{pq}^2 V_q^{i)}. \qquad (12) \end{aligned}$$

Objection 1. Since h_p^i is proportional to β, the Taylor-approximation (11) does not hold for high values of β. This is a fundamental objection because during the execution of the ENA, β is increased step by step. □

Next, Simic performs a 'decomposition of the particle (salesman) trajectory':

$$\mathbf{x}^i = \langle \mathbf{x}(i) \rangle = \sum_p \mathbf{x}_p \langle S_p^i \rangle = \sum_p \mathbf{x}_p V_p^i. \qquad (13)$$

$\mathbf{x}(i)$ is the stochastic and $\mathbf{x}^i$ the average position of the salesman at time i. Using the decomposition, Simic writes $\sum_q d_{pq}^2 V_q^i = \mid \mathbf{x}_p - \mathbf{x}^i \mid^2$. By this, he makes a crucial transformation from a linear function in V_p^i into a quadratic one in $\mathbf{x}^i$. Substitution of the result in (12) (with $\alpha = \beta$), neglect of the second term, and application of the decomposition (13) on the first term of (12) finally yield (7).

Objection 2. Careful analysis [12] shows that in general

$$\sum_q d_{pq}^2 V_q^i = \sum_q (\mathbf{x}_p - \mathbf{x}_q)^2 V_q^i \neq \mid \mathbf{x}_p - \mathbf{x}^i \mid^2 . \qquad \square$$

Energy (6) is a special case of a generalized free energy of type (3), whose stationary points are solutions of $V_p^i = \exp(-\beta \sum_{jq} w_{pq}^{ij} V_q^j) / \sum_l \exp(-\beta \sum_{jq} w_{pq}^{lj} V_q^j)$. Whatever is the temperature, these stationary points are found at states where on average, *all* strongly submitted *constraints are fulfilled*. Moreover, stationary points of a free energy of type (3) are often maxima [11, 12].

Objection 3. An analysis of the free energy of the ENA (section 3) yields a very different view: both terms of (7) create a set of minima. A *competition* takes place between feasibility and optimality, where the current temperature determines the overall effect. This corresponds to the classical penalty method. A difference from that approach is that here – like in the Hopfield-Lagrange model [9] – the penalty weights change dynamically. Consequently, we consider the ENA a *dynamic penalty method*. □

The last observation corresponds to the theory of so-called deformable templates [7, 13], where the corresponding Hamiltonian equals

$$E_{\mathrm{dt}}(\mathbf{S}, \mathbf{x}) = \frac{\alpha_2}{2} \sum_i \mid \mathbf{x}^{i+1} - \mathbf{x}^i \mid^2 + \sum_{pj} S_p^j \mid \mathbf{x}_p - \mathbf{x}^j \mid^2 . \qquad (14)$$

A statistical analysis [7, 13] of E_{dt} yields the free energy (7). A comparison between (7) and (14) clarifies that the first energy expression is derived from the second one by adding noise exclusively to the penalty terms.

3 An Analysis of the ENA

We can analyze the ENA by inspection of the energy landscape [3, 12]. The general behavior of the algorithm leads to large-scale, global adjustments early on. Later on, smaller, more local refinements occur. *Equidistance* is enforced by the first, 'elastic ring term' of (7), which corresponds to parabolic pits in the energy landscape. *Feasibility* is enforced by the second, 'mapping term' corresponding to pits whose width and depth depend on T. Initially, the energy landscape appears to shelve slightly and is lowest in regions with high city density. On lowering the temperature a little, the mapping term becomes more important: it creates steeper pits around cities. By this, the elastic net starts to stretch out. We next consider two potential, nearly final states of a problem instance with 5 *permanently* fixed cities and 5 variable elastic net points, of which 4 are *temporarily* fixed. The energy landscape of the remaining elastic net point is displayed. Figure 1 shows the case where 4 of the 5 cities have already caught an elastic net point.

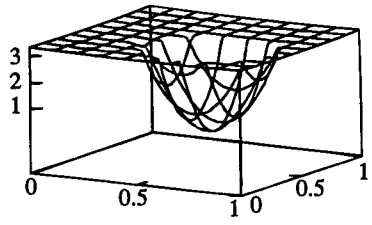

Figure 1 The energy landscape, a non-feasible state.

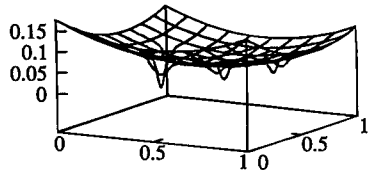

Figure 2 The energy landscape, an almost feasible state.

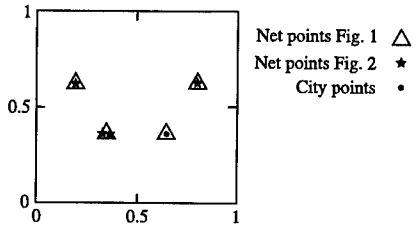

Figure 3 Net points and city point positions.

The landscape of the 5-th ring point exhibits a large pit situated above the only non-visited city. If the point is not too far away from the non-visited city, it can still be caught by it. It demonstrates, that a too rapid lowering of the temperature may lead to a non-valid solution. In figure 2, an almost feasible final solution is shown, where 3 net points coincide with 3 cities. A 4-th elastic net point is precisely in the middle between the two close cities. Now, the mapping term only produces some small pits. The elastic net term has become perceptible too. Hence, the remaining elastic net point is most probably forced to the middle of its neighbors making the final state more or less equidistant, but not feasible! Thus, it is possible to end up in a non-feasible solution if (a) the parameter T is lowered too rapidly[1] or if (b) two close cities have caught the same net point.

4 Alternative Elastic Net Algorithms

In order to use a correct distance measure and at the same time, to get rid of the equidistance property, we adopt a *linear* distance measure in (7):

$$F_{\text{lin}}(\mathbf{x}) = \alpha_2 \sum_i \mid \mathbf{x}^{i+1} - \mathbf{x}^i \mid - \frac{\alpha_1}{\beta} \sum_p \ln \sum_j \exp(\frac{-\beta^2}{2} \mid \mathbf{x}_p - \mathbf{x}^j \mid^2). \qquad (15)$$

Applying gradient descent, the corresponding motion equations are found [3]. A self-evident analysis shows that, like in the original ENA, the elastic net forces try to push elastic net points onto a straight line. There is, however, an important difference: once a net point is situated in *any* point on the straight line between its neighboring net points, it no longer feels an elastic net force. Equidistance is not pursued anymore and the net points have more freedom to move towards cities. We therefore conjecture that the NENA will find feasible solutions more easily. Since the elastic net forces are normalized by the new algorithm, a tuning problem arises. To solve this problem, all elastic net forces are multiplied by a same factor. The final updating rule becomes:

$$\Delta \mathbf{x}^i = \frac{\alpha_2}{\beta} \frac{1}{m} \sum_1^m \mid \mathbf{x}^{i+1} - \mathbf{x}^i \mid \left(\frac{\mathbf{x}^{i+1} - \mathbf{x}^i}{\mid \mathbf{x}^{i+1} - \mathbf{x}^i \mid} + \frac{\mathbf{x}^{i-1} - \mathbf{x}^i}{\mid \mathbf{x}^{i-1} - \mathbf{x}^i \mid} \right) + \alpha_1 \sum_p \Lambda^p(i)(\mathbf{x}_p - \mathbf{x}^i).$$

Finally, we merged the ENA and the NENA into a hybrid one (HENA): the algorithm starts using ENA (to get a balanced stretching out) and, after a certain number of steps, switches to NENA (to try to guarantee feasibility).

[1] In optimal annealing[1], the temperature is decreased carefully to *escape* from local minima. Instead, here this is done to *end up* in a local (i.e., a constrained) minimum.

5 Experiments

We started using the 5-city configuration of section 3. Using 5 up to 12 elastic net points, the ENA produced only non-feasible solutions. Using 15 elastic net points, the optimal feasible solution is always found. Using 5 elastic net points, the NENA occasionally produced the optimal solution. A gradual increase of the number of elastic net points results into a rise of the percentage of optimal solutions found. Using only 10 elastic net points, we obtained a 100% score. Testing a 15-city-problem, we had the similar experiences. However, the picture started to change having 30-city problem instances. As a rule, both algorithms are equally disposed to find a valid solution, but the quality of the solutions of the original ENA is generally better. Trying even larger problem instances, the NENA more frequently found a non-valid solution: inspection shows a strong *lumping* effect of net points around cities and sometimes a certain city is completely left out. At this point, the hybrid approach of HENA comes to mind. Up to 100 cities, we were unable to find parameters which yield better solutions than the original ENA.

6 Conclusions and Outlook

Elastic neural networks are *dynamic penalty methods*, therefore always having a *tuning* problem. Contrary to simulated annealing, the network should *end up* in a local, constrained minimum. Trying the ENA, it may come up with a non-valid solution if two cities are close to each other. To guarantee feasibility more easily, we implemented a new algorithm, having a *linear* distance measure. The success of it is limited to small problem instances, showing that the *quadratic distance measure* is an *essential* ingredient of the original ENA. Trying a hybrid algorithm, we did not find parameters which yield a better performance. In future research, an alternative for HENA can be considered by realizing a *gradual* switch from the ENA to the NENA. Likewise, other formulations of penalty terms can be tested.

REFERENCES

[1] E. Aarts and J. Korst, *Simulated Annealing and Boltzmann Machines, A Stochastic Approach to Combinatorial Optimization and Neural Computing*, John Wiley & Sons (1989).

[2] R. Durbin and D. Willshaw, *An Analogue Approach of the Travelling Salesman Problem Using an Elastic Net Method*, Nature, Vol. 326 (1987), pp689–691.

[3] J.H. Geselschap, *Een Verbeterd 'Elastic Net' Algoritme (An Improved Elastic Net Algorithm)*, Master's thesis, Erasmus University Rotterdam, Comp. Sc. Dept., (1994).

[4] J. Hertz, A. Krogh, and R.G. Palmer, *Introduction to the Theory of Neural Computation*, Addison-Wesley (1991).

[5] J.J. Hopfield, *Neural Networks and Physical Systems with Emergent Collective Computational Abilities*, Proceedings of the National Academy of Sciences, USA Vol. 79 (1982), pp2554–2558.

[6] G. Parisi, *Statistical Field Theory*, Addison-Wesley (1988).

[7] C. Peterson and B. Söderberg, *Artificial Neural Networks and Combinatorial Optimization Problems*, to appear in: Local Search in Combinatorial Optimization, E.H.L. Aarts and J.K. Lenstra eds., John Wiley & Sons.

[8] P.D. Simic, *Statistical Mechanics as the Underlying Theory of 'Elastic' and 'Neural' Optimisations*, Network, Vol. 1 (1990), pp88–103.

[9] J. van den Berg and J.C. Bioch, *Constrained Optimization with the Hopfield-Lagrange Model*, in: Proceedings of the 14th IMACS World Congress (1994), pp470–473.

[10] J. van den Berg and J. C. Bioch, *On the (Free) Energy of Stochastic and Continuous Hopfield Neural Networks*, in: Neural Networks: The Statistical Mechanics Perspective, J.-H. Oh, C. Kwon, S. Cho eds., World Scientific (1995), pp233–244.

[11] J. van den Berg and J.C. Bioch, *Some Theorems Concerning the Free Energy of (Un)Constrained Stochastic Hopfield Neural Networks*, in: Lecture Notes in Artificial Intelligence 904,

EuroCOLT'95 (1995), pp298–312.
[12] J. van den Berg and J.H. Geselschap, *An analysis of various elastic net algorithms*, Technical Report EUR-CS-95-06, Erasmus University Rotterdam, Comp. Sc. Dept. (1995).
[13] A.L. Yuille, *Generalized Deformable Models, Statistical Physics, and Matching Problems*, Neural Computation, Vol. 2 (1990), pp1–24.

UNIMODAL LOADING PROBLEMS

Monica Bianchini, Stefano Fanelli*,
Marco Gori and Marco Protasi*

Dipartimento di Sistemi e Informatica, Università degli Studi di Firenze,
Via di Santa Marta, 3, 50139 Firenze, Italy.
Email: monica,marco@mcculloch.ing.unifi.it
** Dipartimento di Matematica, Università di Roma,*
"Tor Vergata" Via della Ricerca Scientifica, 00133 Roma, Italy.
Email: fanelli,protasi@mat.utovrm.it

This paper deals with optimal learning and provides a unified viewpoint of most significant results in the field. The focus is on the problem of local minima in the cost function that is likely to affect more or less any learning algorithm. We give some intriguing links between optimal learning and the computational complexity of loading problems. We exhibit a computational model such that the solution of all loading problems giving rise to unimodal error functions require the same time, thus suggesting that they belong to the same computational class.
Keywords: Backpropagation, computational complexity, optimal learning, premature saturation, spurious and structural local minima, terminal attractor.

1 Learning as Optimisation

Supervised learning in multilayered networks (MLNs) can be accomplished thanks to Backpropagation (BP), which is used to minimise pattern misclassifications by means of gradient descent for a particular nonlinear least squares fitting problem. Unfortunately, BP is likely to be trapped in local minima and indeed many examples of local extremes have been reported in the literature.

The presence of local minima derives essentially from two different reasons. First, they may arise because of an *unsuitable* joint choice of the functions which defines the network dynamics and the error function. Second, local minima may be inherently related to the structure of the problem at hand. In [5], these two cases have been referred to as *spurious* and *structural* local minima, respectively. Problems of sub-optimal solutions may also arise when learning with *high* initial weights, as a sort of *premature neuron saturation* arises, which is strictly related to the neuron fan-in. An interesting way of facing this problem is to use the "*relative cross-entropy metric*" [10], for which the erroneous saturation of the output neurons does not lead to plateaux, but to very high values of the cost. When using the cross-entropy metric, the repulsion from such configurations is much more effective, and underflow errors are likely to be avoided.

There have also been attempts to provide theoretical conditions aimed at guaranteeing local minima free error surfaces. So far, however, only some sufficient conditions have been identified that give rise to unimodal error surfaces. Examples are the the case of *pyramidal networks* [8], commonly used in pattern recognition, *radial basis function networks* [2], and *non-linear autoassociators* [3]. The identification of similar conditions ensures global optimisation just by using simple gradient descent. Instead of looking for local algorithms like gradient descent, techniques that guarantee global optimisation may be explored. Of course, one of the main problems to face is that most interesting tasks give rise to the optimisation of functions with even several thousand variables. This makes it very unlikely that most classic approaches [11] can be directly and successfully applied. Instead, the proposal of

successful algorithms has to face effectively the *curse of dimensionality* typical of most interesting practical problems.

Statistical training methods have been previously proposed in order to alleviate the local convergence problem. These methods introduce noise to connection weights during training, but suffer from extremely slow convergence due to their probabilistic nature.

Several numerical algorithms for global optimisation have also been presented, in which BP is revisited from the viewpoint of dynamical system theory. Barhen *et al.* [1] have proposed the *TRUST* algorithm (for *Terminal Repeller Unconstrained Subenergy Tunneling*) that formulates global optimisation as the solution of a system of deterministic differential equations, where $E(W)$ is the function to be optimised, while the connection weights are the states of the system. The dynamics used is achieved upon application of the gradient descent to a modified cost which transforms each encountered local minimum into a maximum, so that the gradient descent can escape from it to a lower valley. A related algorithm, called *Magic Hair-Brushing*, has been proposed in [6]. The system dynamics is now modified through a deformation of the gradient field for eliminating the local minima, while preserving the global structure of the function. All these algorithms exhibit a good performance in many practical cases but, unfortunately, their optimal convergence is not formally guaranteed, unless starting from a "*good*" initial point.

2 The Class of Unimodal Loading Problems

Most experiments with multilayer perceptrons and BP are performed in a sort of *magic* atmosphere where data are properly supplied to the network which begins learning without knowing whether or not the experiment will be successful either in terms of optimal convergence and generalisation. A *trial and error* scheme is usually employed, aimed at adjusting the architecture in subsequent experiments so as to meet the desired requirements. To some extent, this way of performing experiments is inherently plagued by the suspect that the used numerical optimisation algorithm might fail. Moreover, though optimal learning may be attained with networks having a growing number of hidden neurons [14], the generalisation to new examples is not guaranteed. The intuitive feeling that, in order to obtain a good convergence behaviour, generalisation must be sacrificed, may be effectively formalised in a sort of "*uncertainty principle of learning*" in which the variable representing optimal convergence and generalisation are like conjugate variable in Quantum Mechanics [7]. These potential sources of failure of learning algorithms give rise to a sort of *suspiciousness* that turns out to be the unpleasant companion of every experiment. This seems to be interwound with the ambitious task of learning too general functions.

Let us focus on the complexity issues related to the loading of the weights independently of the consequent generalisation to new examples. This makes sense once a consistent formulation of the learning problem in terms of both the chosen examples and the neural architecture was provided. We address the problem of establishing the computational requirements of special cases in which the loading of the weights can be expressed in terms of optimisation of unimodal error functions.

2.1 Canonical Form of Gradient Descent Learning

Let us consider the following learning equation:

$$\frac{dW}{dt} = -\gamma \nabla_W E = f(t, W), \tag{1}$$

where $E(W)$ is the cost function and $W \in \mathbb{R}^m$ is the weight vector. Let us choose $\gamma \doteq \frac{\Psi(E)}{\|\nabla_W E\|^2}$, being Ψ a non-negative continuous function of E. Based on this choice of the learning rate, the dynamics of the error function becomes

$$\frac{dE}{dt} = (\nabla_W E)^T \frac{dW}{dt} = (\nabla_W E)^T \left(-\frac{\Psi(E)}{\| \nabla_W E \|^2} \nabla_W E \right) = -\Psi(E), \tag{2}$$

which makes the cost function continuously decreasing to zero. Those configurations for which $\nabla_W E = 0$ are singular points that attract the learning trajectory [4]. Special cases of this reduction to a canonical structure, where the learning is forced by function Ψ and is independent of the problem at hand, have been explored in the literature. White [13] has suggested to introduce a varying learning rate so that the error dynamics evolves following the equation $\frac{dE}{dt} = -\Psi(E) \doteq -aE$, $a > 0$, whose solution is a decaying exponential such that reaching the $E = 0$ *attractor* will theoretically take infinite time. In practice, this may not necessarily be a problem, as the attractor may be approached sufficiently close in a reasonable amount of time, even if, for ill-conditioned systems, it can still be prohibitive to reach a satisfactory solution. Unfortunately, feedforward neural networks do often result in dynamical systems that are ill-conditioned or mathematically *stiff* and thus the convergence is generally very slow.

In [12] the canonical reduction of equation (2) is based on choosing $\Psi(E) \doteq E^k$, $0 < k < 1$, which leads to an error dynamics based on the differential equation $\frac{dE}{dt} = -E^k$, having a singularity at $E = 0$ violating the Lipschitz condition. If $E_0 \geq 0$ is the initial value of the cost, then the closed form solution is $E(t) = (E_0^{1-k} - (1-k)t)^{\frac{1}{1-k}}$, $t \leq t_e$, where $t_e = \frac{E_0^{1-k}}{1-k}$ (Fig. 1a). In the finite time t_e the transient beginning from $E(0) = E_0$ reaches the equilibrium point $E = 0$, which is a "*terminal attractor.*"

In this paper, we are interested in finding terminal attractors and, particularly, in minimising the time t_e required to approach the optimal solution. The choice $\Psi(E) \doteq \eta$ fulfills our needs. Consequently $t_e = E_0/\eta$ and, in particular, when selecting $\eta = E_0/\sigma$, the terminal attractor is approached for $t_e = \sigma$ (Fig. 1b), independently of the problem at hand, while the corresponding weight updating equation becomes

$$\frac{dW}{dt} = -\frac{E_0}{\sigma} \frac{\nabla E}{||\nabla E||^2}. \tag{3}$$

This way of forcing the dynamics leads to establish intriguing links between the concept of unimodal problems and their computational complexity. In fact, learning attractors in finite time is not only useful from a numerical point of view but, in the light of the considerations on the canonical equations (2), is interesting for the relationships that can be established between different problems giving rise to local minima free cost functions.

2.2 Computational analyses

Let us introduce the following classes of loading problems [9].

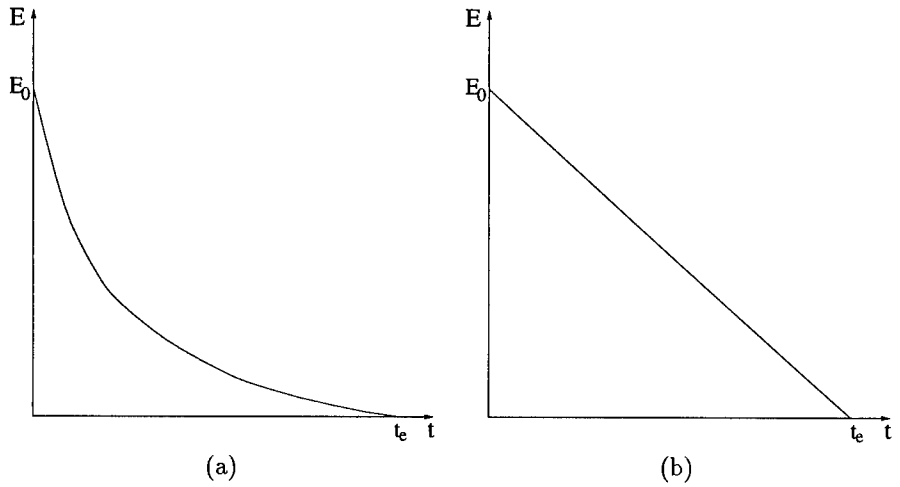

Figure 1 Terminal attraction using (a) $\Psi(E) \doteq E^k, 0 < k < 1$, and (b) $\Psi(E) \doteq \eta$.

Definition 1 *A loading problem P is unimodal, $P \in \mathcal{UP}$, provided that there exists an associated unimodal error function $E(P, W)$ whose optimisation represents the solution of P.*

Note that a given loading problem can be approached in the framework of optimisation using different error functions. For example, the loading of the weights in a multilayer perceptron using linearly-separable patterns may led to sub-optimal solution when choosing error functions where the targets are different from the asymptotical values of the squashing functions. Nevertheless, it is always possible to get rid of these spurious local minima and provide a formulation based on a local minima free error function.
In order to evaluate the computational cost for learning problems belonging to $\mathcal{UP}$ it is convenient to refer to the parallel computational model offered by differential equation (1). We assume that there exists a continuous system implementing this differential equation and then consider the following computational class.

Definition 2 *Let us consider the class of loading problems P for which there exists a formulation according to the differential equation (1) such that $\forall \tau > 0$ the loading of the weights ends in a finite time $t_e : t_e \leq \tau$. This class is referred to as the class of finite time loading problems and is denoted by $\mathcal{FT}$.*

Because of the previous analysis on gradient descent the following result holds.

Theorem 3 $\mathcal{UP} \subset \mathcal{FT}$.

Proof If $P \in \mathcal{UP}$ then one can always formulate the loading according to differential equation (3) and the gradient descent is guaranteed not to get stuck in local minima. Because of equation (2) the learning process ends for $t_e = \sigma$. Hence, $\forall \tau > 0$, if we choose $\sigma \leq \tau$ we conclude that $P \in \mathcal{FT}$. □
This theoretical result should not be overvalued since it is based on a computational

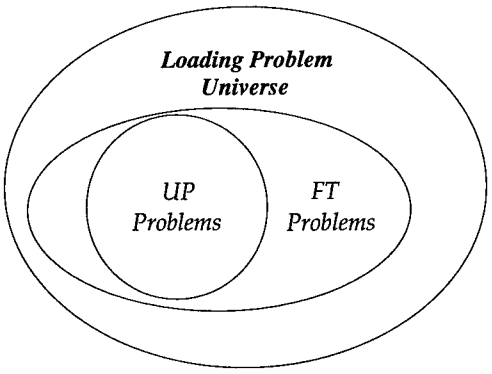

Figure 2 The class of unimodal learning problem can be learned in constant time.

model that does not care of problems due to limited energy. When choosing τ arbitrarily small, the slope of the energy in Fig. 1b goes in fact to infinite.
One may wonder whether problems can be found in $\mathcal{FT}$ that are not in $\mathcal{UP}$ (see Fig. 2). This does not seem easy to establish and is an open problem that we think deserves further attention.

3 Conclusions

The presence of local minima does not necessarily imply that a learning algorithm will fail to discover an optimal solution, but we can think of their presence as a boundary beyond which troubles for any learning technique are likely to begin.
In this paper we have proposed a brief review of results dealing with optimal learning, and we have discussed of problems of sub-optimal learning. Most importantly, when referring to a continuous computational model, we have shown that there are some intriguing links between computational complexity and the absence of local minima. Basically all loading problems that can be formulated as the optimisation of unimodal functions are proven to belong to a unique computational class. Note that this class is defined on the basis of computational requirements and, therefore, seems to be of interest independently of the neural network context in which it has been formulated.
We are confident that these theoretical results open the doors for more thoroughly analyses involving discrete computations, that could shed light on the computational complexity based on ordinary models of Computer Science.

REFERENCES

[1] J. Barhen, J. W. Burdick, and B. C. Cetin, *Terminal Repeller Unconstrained Subenergy Tunneling (TRUST) for fast global optimization*, Journal of Optimization Theory and Applications, Vol.77 (1993), pp97–126.

[2] M. Bianchini, P. Frasconi, and M. Gori, *Learning without local minima in radial basis function networks*, IEEE Transactions on Neural Networks, Vol. 6, (1995), pp749–756.

[3] M. Bianchini, P. Frasconi, and M. Gori, *Learning in multilayered networks used as autoassociators*, IEEE Transactions on Neural Networks, Vol. 6, (1995), pp512–515.

[4] M. Bianchini, M. Gori, and M. Maggini, *Does terminal attractor backpropagation guarantee global optimization?*, in International Conference on Artificial Neural Networks, Springer-Verlag, (1994), pp377–380.

[5] M. Bianchini and M. Gori, *Optimal learning in artificial neural networks: A review of theoretical results*, Neurocomputing, Vol.13 (October 1996), No.5, pp313–346.

[6] J. Chao, W. Ratanasuwan, and S. Tsujii, *How to find global minima in finite times of search for multilayer perceptrons training*, in International Joint Conference on Neural Networks, IEEE Press, Singapore, (1991), pp1079–1083.

[7] P. Frasconi and M. Gori, *Multilayered networks and the C-G uncertainty principle*, in SPIE International Conference, Science of Artificial Neural Networks, Orlando, Florida, 1993, pp396–401.

[8] M. Gori and A. Tesi, *On the problem of local minima in backpropagation*, Transactions on Pattern Analysis and Machine Intelligence, Vol. 14 (1992), pp76–86.

[9] J. S. Judd, *Neural Network Design and the Complexity of Learning.* Cambridge (1990), London: The MIT Press.

[10] T. Samad, *Backpropagation improvements based on heuristic arguments*, in International Joint Conference on Neural Networks, IEEE Press, Washington DC, (1990), pp565–568.

[11] Torn and Zilinkas, *Global Optimization*, Lecture Notes in Computer Sciences, (1987).

[12] S. Wang and C. H. Hsu, *Terminal attractor learning algorithms for backpropagation neural networks*, in International Joint Conference on Neural Networks, IEEE Press, Singapore, 1991, pp183–189.

[13] H. White, *The learning rate in backpropagation systems: an application of Newton's method*, in International Joint Conference on Neural Networks, IEEE Press, Singapore, 1991, pp679–684.

[14] X. Yu, *Can backpropagation error surface not have local minima?*, IEEE Transactions on Neural Networks, Vol. 3 (1992), pp1019–1020.

Acknowledgements

We thank P. Frasconi, M. Maggini, F. Scarselli, and F. Schoen for fruitful discussions and suggestions.

ON THE USE OF SIMPLE CLASSIFIERS FOR THE INITIALISATION OF ONE-HIDDEN-LAYER NEURAL NETS

Jan C. Bioch, Robert Carsouw and Rob Potharst
Department of Computer Science, Erasmus University Rotterdam, The Netherlands. Email: bioch,robp@cs.few.eur.nl

Linear decision tree classifiers and LVQ-networks divide the input space into convex regions that can be represented by membership functions. These functions are then used to determine the weights of the first layer of a feedforward network.
Subject classification: AMS(MOS) 68T05, 92B20
Keywords: decision tree, feedforward neural network, LVQ-network, classification, initialisation

1 Introduction

In this paper we mainly discuss the mapping of a linear tree classifier (LTC) onto a feedforward neural net classifier (NNC) with one hidden layer. According to Park [9] such a mapping results in a faster convergence of the neural net and in avoiding local minima in network training. In general these mappings are also interesting because they determine an appropriate architecture of the neural net. The LTC used here is a hierarchical classifier that employs linear functions at each node in the tree. For the construction of decision trees we refer to [10, 5, 12]. Several authors [11, 4, 9] discuss the mapping of an LTC onto a feedforward net with one or two hidden layers, see also [3, 2]. A discussion of a mapping onto a net with two hidden layers can be found in Sethi [11] and Ivanova&Kubat [4]. A mapping onto a net with *one* hidden layer is discussed in Park [9]. In his approach the mapping is based on representing the convex regions induced by an LTC by linear membership functions. However, in Park [9] no explicit expression for the coefficients of the membership functions is given. These coefficients depend on a parameter ρ that in his paper has to be supplied by the user. In section 2 we show that in general it is not possible to find linear membership functions that represent the convex regions induced by an LTC. It is however possible to find subregions that can be represented by linear membership functions. We derive explicit expressions for the aforementioned parameter ρ, in section 3. This makes it possible to control the approximation of the convex regions by membership functions and therefore of the initialisation of the neural net. In section 4 we also briefly discuss the use of LVQ-networks [6, 7] for such an initialisation.

2 Non-existence of Linear Membership Functions

Suppose we are given a multivariate decision tree $(\mathcal{N}, \mathcal{L}, \mathcal{D})$. In this notation, $\mathcal{N}$ is the set of nodes of the tree, $\mathcal{L}$ is the set of leaves of the tree and $\mathcal{D}$ is the set of linear functions $d_k : \mathbb{R}^n \to \mathbb{R}, k \in \mathcal{N}$. In any node k of the tree, the linear function d_k is used to decide which branch to take. Specifically, we go left if $d_k(x) > 0$, right if $d_k(x) \leq 0$, see figure 1. A decision tree induces a partitioning of $\mathbb{R}^n$: each leaf ℓ corresponds with a convex region R_ℓ, which consists of all points $x \in \mathbb{R}^n$, that get assigned to leaf ℓ by the decision tree. For example, region R_5 consists of all $x \in \mathbb{R}^n$ with $d_1(x) \leq 0$ and $d_3(x) \leq 0$.

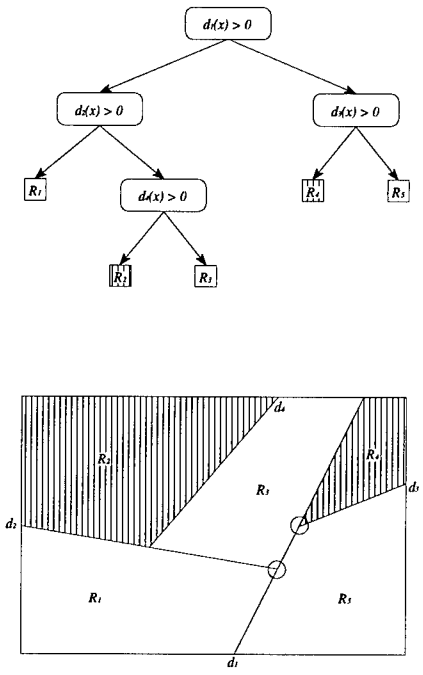

Figure 1 The convex regions induced by a classification tree.

We will now discuss the idea of linear membership functions to represent the convex regions induced by an LTC, and we show that these functions are in general not possible.
In [9] the following 'theorem' is given without proof, though supplied with heuristic reasoning for its plausibility, see also equation 2 in the next section:

Conjecture (Park[9]) *For every decision tree* $(\mathcal{N}, \mathcal{L}, \mathcal{D})$ *there exists a set of linear membership functions* $M = \{m_\ell, \ell \in \mathcal{L}\}$, *such that for any* $\ell, \ell' \in \mathcal{L}$, *with* $\ell \neq \ell'$:

$$m_\ell(x) > m_{\ell'}(x), \forall x \in R_\ell. \tag{1}$$

According to [9] the coefficients of a linear membership function can be used to initialise the weights of the connections of a hidden unit with the input layer. For example, the decision tree in figure 1 can be mapped onto a one-hidden-layer network with 3 inputs, 5 hidden units and 2 outputs. The weights in the input-to-hidden layer are chosen according to the membership functions.
In [2] we have presented a minimal counterexample to Park's conjecture, and we also argued that a mapping is only possible if the decision boundaries are parallel. In

the next theorem we show that neither linear nor quadratic membership functions that represent the convex regions induced by an LTC can exist.

Theorem 1 *Let $(\mathcal{N}, \mathcal{L}, \mathcal{D})$ be a decision tree, with at least two non-parallel decision boundaries. Then the convex regions induced by this tree cannot be represented by a set of quadratic polynomials.*

Proof Let R_1, R_2 and R_3 be regions induced by a decision tree such that the regions R_1 and $R_2 \cup R_3$ are separated by the hyperplane $d_1(x) = 0, x \in \mathbb{R}^n$. We assume that $d_1(x) > 0$ on R_1 and $d_1(x) < 0$ on $R_2 \cup R_3$. Similarly, R_2 and R_3 are separated by $d_2(x) = 0$, such that $d_2(x) > 0$ on R_2 and $d_2(x) < 0$ on R_3. Note that such regions will always be induced by a subtree of a decision tree, unless all decision boundaries are parallel. Let m_1, m_2 and m_3 respectively denote the membership functions of R_1, R_2 and R_3. By definition $m_1 = 0$ on the hyperplane $d_1(x) = 0$. Similarly, $m_2 = 0$ on $d_2(x) = 0$. (Note, that we actually know only that m_2 is zero on half of the hyperplane $d_2(x) = 0$. However, using a simple result from algebraic geometry it follows that m_2 must be zero on the whole hyperplane $d_2(x) = 0$.)
Now, let $D_{12} = m_1 - m_2$. Then D_{12} is zero on $d_1(x) = 0$, because $D_{12} > 0$ on R_1 and $D_{12} < 0$ on $R_2 \cup R_3$. As a consequence of Hilbert's Nullstellensatz d_1 is a factor of D_{12}. Therefore, there exists a polynomial function e such that $D_{12} = d_1 e$. Since D_{12} is at most quadratic by assumption, we conclude that e is a constant or a linear function. However, since both $d_1 e$ and d_1 are positive on R_1 and negative on R_2, the function e is positive on $R_1 \cup R_2$. Since the degree of e is ≤ 1, e must be a positive constant. Similarly, we have $D_{13} = d_1 f$, where f is a positive constant. Therefore $D_{23} = d_1(f - e)$. This contradicts the fact that D_{23} is zero on $d_2(x) = 0$.
□

Remark In [2] it is shown that under the conditions of Theorem 1, the membership functions m_i can be represented by multivariate polynomials, albeit of degree ≥ 5.

3 An Approximated Mapping of a Decision Tree onto a One-hidden-layer Neural Network

We will show in this section that the difficulties encountered in the preceding section may be circumvented by requiring that the points we consider are not too close to the hyperplanes associated with the decision tree.
Let $(\mathcal{N}, \mathcal{L}, \mathcal{D})$ be a decision tree. We will restrict the regions R_ℓ by assuming that $\forall k \in \mathcal{N} : 0 < e \leq |d_k(x)| \leq E$, where e and E are positive constants. The set of points in R_ℓ satisfying this condition will be denoted by S_ℓ. Hence, S_ℓ is a convex subregion of R_ℓ. Note also that R_ℓ can be approximated by S_ℓ with arbitrary precision, by varying the constants e and E.
In [9] Park considers the following set of linear membership functions:

$$m_\ell(x) = \sum_{k \in P_\ell} s_{\ell k} c_k d_k(x), \tag{2}$$

where P_ℓ is the set of nodes on the path from the root to the leaf ℓ. The constants $s_{\ell k}$ are defined such that:

$$s_{\ell k} d_k(x) > 0. \tag{3}$$

The constants $c_k > 0$ are determined experimentally in [9]. Here we will derive an explicit expression for these constants. Since as we have shown above that in general these constants cannot exist if $x \in R_\ell, \ell \in \mathcal{L}$, we will now assume that $x \in S_\ell$.

Theorem 2 *Let $(\mathcal{N}, \mathcal{L}, \mathcal{D})$ be a decision tree. Then there exists a set of linear functions $M = \{m_\ell, \ell \in \mathcal{L}\}$, such that for any $\ell, \ell' \in \mathcal{L}$, with $\ell \neq \ell'$:*

$$\forall x \in S_\ell : m_\ell(x) > m_{\ell'}(x). \tag{4}$$

Proof Let $\mathcal{T}$ be the set of terminal nodes of the tree. An internal node t is called terminal if both children of t are leaves. Further, if n_1 and n_2 are two nodes, then we write $n_1 < n_2$ if n_1 is an ancestor of n_2. Suppose that $n_a \notin \mathcal{T}$, and ℓ, ℓ' are two leaves such that n_a is the *last common ancestor* of ℓ and ℓ'.
We decompose the function $m_{\ell'}$ as follows: $m_{\ell'}(x) = \sum_{n_i < n_a} s_{\ell i} c_i d_i(x) + \sum_{n_j \geq n_a} s_{\ell' j} c_i d_j(x)$, where $n_i \in P_\ell$ and $n_j \in P_{\ell'}$. By applying (3) to the node n_a, it can be seen that $s_{\ell a} = -s_{\ell' a}$. From this we conclude $m_\ell(x) - m_{\ell'}(x) = 2s_{\ell a} c_a d_a(x) + \Sigma_1 - \Sigma_2$, where $\Sigma_1 = \sum_{n_i > n_a} s_{\ell i} c_i d_i(x)$, with $n_i \in P_\ell$ and $\Sigma_2 = \sum_{n_j > n_a} s_{\ell' j} c_j d_j(x)$, with $n_j \in P_{\ell'}$. To assure that (4) holds, we require that $(\Sigma_2 - \Sigma_1)/(2s_{\ell a} d_a(x)) < c_a$. Since Σ_1 is positive we can satisfy the last condition by taking $\Sigma_2/(2s_{\ell a} d_a(x)) < c_a$, or $\frac{E}{2e} \sum_{n_j > n_a} c_j \leq c_a$. This yields the following sufficient condition for the constants c_j:

$$\frac{E}{2e} \max_{\ell \in \mathcal{L}_a} \left\{ \sum_{n_j > n_a} c_j \right\} \leq c_a, \tag{5}$$

where $n_j \in P_\ell$ and $\mathcal{L}_a$ is the set of leaves of the subtree with root n_a. Condition (5) implies: $c_a \geq \frac{E}{2e} \sum_{n_j > n_a} c_j$, where $n_j \in \mathcal{P}$ and $\mathcal{P}$ is the *longest* possible path from node n_a to some leaf. From condition (5) it also follows that the constants c_a are determined up to a constant factor. It is easy to see that the constants can be determined recursively by choosing positive values c_t for the set of terminal nodes $t \in \mathcal{T}$. □

Theorem 3 *Let $\rho = 1/(1 + \frac{E}{2e})$. Then $m_\ell(x) = \sum_k s_{k\ell} \rho^{\delta(r) - \delta(k)} d_k(x)$ are linear functions for which (4) holds. Here $\delta(k)$ denotes the length of the longest possible path from node n_k to a terminal node.*

Proof Using the formula for the partial sum of a geometric series this result can be obtained straightforwardly, see [2]. □
Another expression for the constants c_a can be obtained by using the fact that a decision tree $(\mathcal{N}, \mathcal{L}, \mathcal{D})$ in practical situations is derived from a finite set of examples $V \subset \mathbb{R}^n$. See [2].

4 Another Initialisation Method

In this section we consider another well-known classifier: Learning Vector Quantisation (LVQ) networks [6, 7]. This method can be used to solve a classification problem with m classes and data-vectors $x \in \mathbb{R}^n$. It is known that the LVQ-network induces a so-called Voronoi tesselation of the input space, see [6] chapter 9. Training

of an LVQ-network yields prototype vectors $w_j \in \mathbb{R}^n, j = 1, \ldots, m$ such that an input vector x belongs to class j iff the distance to w_j is smallest:

$$\forall i \neq j : ||w_j - x|| \leq ||w_i - x|| \Rightarrow x \in R_j.$$

It is easy to see that this is equivalent with

$$w_j^T x - \frac{1}{2} w_j^T w_j \geq w_i^T x - \frac{1}{2} w_i^T w_i.$$

Now define the linear membership function m_i as:

$$m_i(x) = w_i^T x - \frac{1}{2} w_i^T w_i.$$

Then

$$x \in R_i \iff m_i(x) > m_j(x), \forall j \neq i.$$

Since an LVQ-network is good classifier and can be trained relatively fast, it is a good alternative for the initialisation of a neural net using linear membership functions. In [2] we show that an LVQ-network cannot induce the convex regions induced by an LTC.

Discussion: We have proven that linear (or quadratic) membership functions representing the convex regions of a linear decision tree in general do not exist. However, we give explicit formulae for the approximation of such functions. This allows us to control the degree of approximation. Currently, we are investigating how to determine an appropriate approximation in a given application. Furthermore, we discussed the use of another simple classifier, namely an LVQ-network for initialising neural nets, see also [2].

REFERENCES

[1] J.C. Bioch, M. van Dijk and W. Verbeke, *Neural Networks: New Tools for Data Analysis?*, in: M. Taylor and P. Lisboa (eds.) Proceedings of Neural Networks Applications and Tools, IEEE Computer Society Press, pp28–38 (1994).

[2] J.C. Bioch, R. Carsouw and R. Potharst, *On the Use of Simple Classifiers for the Initialisation of One-Hidden-Layer Neural Nets*, Technical Report eur-cs-95-08, Dept. of Computer Science, Erasmus University Rotterdam (1995).

[3] R. Carsouw, *Learning to Classify: Classification by neural nets based on decision trees*, Masterthesis (in Dutch), Dept. of Computer Science, Erasmus University Rotterdam, February (1995).

[4] I. Ivanova, M. Kubat and G. Pfurtscheller, *The System TBNN for Learning of 'Difficult' Concepts*, in: J.C. Bioch and S.H. Nienhuys-Cheng (eds), Proceedings of Benelearn94, Tech. Rep. eur-09-94, Dept. of Computer Science, Erasmus University Rotterdam, pp230–241 (1994).

[5] U.M. Fayad and K.B. Irani, *On the Handling of Continuous-Valued Attributes in Decision Tree Generation*, Machine Learning, Vol. 8 (1992), pp88–102.

[6] J. Hertz, A. Krogh, R.G. Palmer, *Introduction to the theory of neural computation*, Addison-Wesley (1991).

[7] T. Kohonen, *Self-Organization and Associative Memory*, Berlin: Springer Verlag, 3rd edition (1989).

[8] M.L. Minsky, S.A. Papert, *Perceptrons*, 2nd edition, MIT Press (1988).

[9] Y. Park, *A Mapping From Linear Tree Classifiers to Neural Net Classifiers*, Proceedings of IEEE ICNN, Vol. I (1994), pp94–100, Orlando, Florida,.

[10] Y. Park and J. Sklansky, *Automated Design of Linear Tree Classifiers*, Pattern Recognition, Vol. 23, No. 12 (1990), pp1393-1412.

[11] A.K. Sethi, *Entropy Nets: From Decision Trees to Neural Networks*, Proceedings of the IEEE, Vol. 78, No. 10 (1990), pp1606–1613.

[12] J.R. Quinlan; *C4.5 Programs for Machine Learning*, Morgan Kaufmann (1993).

MODELLING CONDITIONAL PROBABILITY DISTRIBUTIONS FOR PERIODIC VARIABLES

Christopher M Bishop and Ian T Nabney
Neural Computing Research Group, Aston University, Birmingham, B4 7ET, UK. Email: c.m.bishop@aston.ac.uk

Most conventional techniques for estimating conditional probability densities are inappropriate for applications involving periodic variables. In this paper we introduce three related techniques for tackling such problems, and test them using synthetic data. We then apply them to the problem of extracting the distribution of wind vector directions from radar scatterometer data.

1 Introduction

Many applications of neural networks can be formulated in terms of a multi-variate non-linear mapping from an input vector x to a target vector t: a conventional network approximates the regression (i.e. average) of t given x. But for mappings which are multi-valued, the average of two solutions is not necessarily a valid solution. This problem can be resolved by estimating the conditional probability $p(t|x)$. In this paper, we consider techniques for modelling the conditional distribution of a periodic variable.

2 Density Estimation for Periodic Variables

A commonly used technique for *unconditional* density estimation is based on mixture models of the form

$$p(t) = \sum_{i=1}^{m} \alpha_i \phi_i(t) \tag{1}$$

where α_i are called mixing coefficients, and the component functions, or kernels, $\phi_i(t)$ are typically chosen to be Gaussians [7, 9]. In order to turn this into a model for conditional density estimation, we simply make the coefficients and adaptive parameters into functions of the input vector x using a neural network which takes x as input [4, 1, 5]. We propose three methods for modelling the conditional density.

2.1 Mixtures of Wrapped Normal Densities

The first technique transforms $\chi \in \mathbb{R}$ to the periodic variable $\theta \in [0, 2\pi)$ by $\theta = \chi \bmod 2\pi$. The transformation maps density functions p with domain $\mathbb{R}$ into density functions $\tilde{p}$ with domain $[0, 2\pi)$ as follows:

$$\tilde{p}(\theta|x) = \sum_{N=-\infty}^{\infty} p(\theta + N2\pi|x) \tag{2}$$

This periodic function is normalized on the interval $[0, 2\pi)$, since

$$\int_0^{2\pi} \tilde{p}(\theta|x)d\theta = \int_{-\infty}^{\infty} p(\chi|x)d\chi = 1 \tag{3}$$

Here we shall restrict attention to Gaussian ϕ:

$$\phi(t|x) = \frac{1}{(2\pi)^{c/2}\sigma_i(x)^c} \exp\left\{-\frac{\|t - \mu_i(x)\|^2}{2\sigma_i(x)^2}\right\} \tag{4}$$

where $t \in \mathbb{R}^c$.

A mixture model with kernels as in equation (4) can approximate any density function to arbitrary accuracy with suitable choice of parameters [7, 9]. We use a

standard multi-layer perceptron with a single hidden layer of sigmoidal units and an output layer of linear units. It is necessary that the mixing coefficients $\alpha_i(x)$ satisfy the constraints

$$\sum_{i=1}^{m} \alpha_i(x) = 1, \quad 0 \leq \alpha_i(x) \leq 1. \tag{5}$$

This can be achieved by choosing the $\alpha_i(x)$ to be related to the corresponding network outputs by a normalized exponential, or *softmax* function [4]. The centres μ_i of the kernel functions are represented directly by the network outputs; this was motivated by the corresponding choice of an uninformative Bayesian prior [4]. The standard deviations $\sigma_i(x)$ of the kernel functions represent *scale* parameters and so it is convenient to represent them in terms of the exponentials of the corresponding network outputs. This ensures that $\sigma_i(x) > 0$ and discourages $\sigma_i(x)$ from tending to 0. Again, it corresponds to an uninformative prior. To obtain the parameters of the model we minimize an error function E given by the negative logarithm of the likelihood function, using conjugate gradients. (The maximum likelihood approach underestimates the variance of a distribution in regions of low data density [1]. For our application, this effect will be small since the number of data points is large.) In practice, we must restrict the value of N. We have taken the summation over 7 complete periods of 2π. Since the component Gaussians have exponentially decaying tails, this introduces negligible error provided the network is intialized so that the kernels have their centres close to 0.

2.2 Mixtures of Circular Normal Densities

The second approach is to make the kernels themselves periodic. Consider a velocity vector v in two-dimensional Euclidean space for which the probability distribution $p(v)$ is a symmetric Gaussian. By using the transformation $v_x = \|v\| \cos\theta$, $v_y = \|v\| \sin\theta$, we can show that the conditional distribution of the direction θ, given the vector magnitude $\|v\|$, is given by

$$\phi(\theta) = \frac{1}{2\pi I_0(m)} \exp\{m \cos(\theta - \psi)\} \tag{6}$$

which is known as a *circular normal* or *von Mises* distribution [6]. The normalization coefficient is expressed in terms of the modified Bessel function, $I_0(m)$, and the parameter m (which depends on $\|v\|$) is analogous to the inverse variance parameter in a conventional normal distribution. The parameter ψ gives the peak of the density function. Because of the $I_0(m)$ term, care must be taken in the implementation of the error function to avoid overflow.

2.3 Expansion in Fixed Kernels

The third technique uses a model consisting of a fixed set of periodic kernels, again given by circular normal functions as in equation (6). In this case the mixing proportions alone are determined by the outputs of a neural network (through a softmax activation function) and the centres ψ_i and width parameters m_i are fixed. We selected a uniform distribution of centres, and $m_i = m$ for each kernel, where the value for m was chosen to give moderate overlap between the component functions.

3 Application to Synthetic Data

We first consider some synthetic test data. It is generated from a mixture of two triangular distributions where the centres and widths are taken to be linear functions

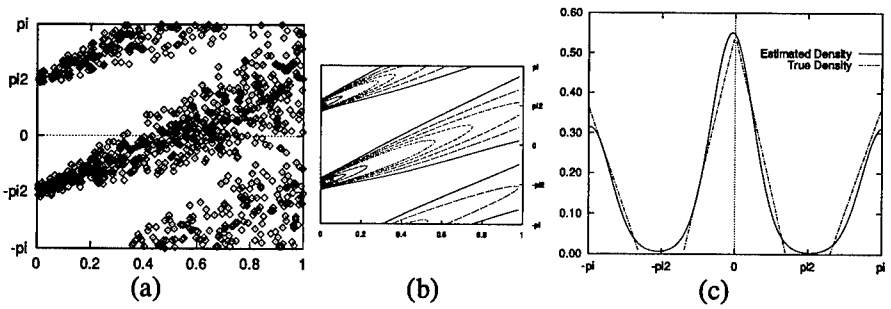

Figure 1 (a) Scatter plot of the synthetic training data. (b) Contours of the conditional density $p(\theta|x)$ obtained from a mixture of adaptive circular normal functions as described in Section 2.2. (c) The distribution $p(\theta|x)$ for $x = 0.5$ (solid curve) from the adaptive circular normal model, compared with the true distribution (dashed curve) from which the data was generated.

of a single input variable x. The mixing coefficients are fixed at 0.6 and 0.4. Any values of θ which fall outside $(-\pi, \pi)$ are mapped back into this range by shifting in multiples of 2π. An example data set generated in this way is shown in Figure 1. Three independent datasets (for training, validation and testing) were generated, each containing 1000 data points. Training runs were carried out in which the number of hidden units and the number of kernels were varied to determine good values on the validation set. Table 1 gives a summary of the best results obtained, as determined from the test set. The mixture of adaptive circular normal functions performed best. Plots of the distribution from the adaptive circular normal model are shown in Figure 1.

Method	Centres	Hidden Units	Validation Error	Test Error
Wrapped normal	6	7	1177.1	1184.4
Adaptive circular normal	6	8	1109.5	1133.9
Fixed kernel	36	7	1184.6	1223.5

Table 1 Results obtained using synthetic data.

4 Application to Radar Scatterometer Data

The European Remote Sensing satellite ERS-1 [8, 3] has three C-band radar antennae which measure the total backscattered power σ_0 along three directions. When the satellite passes over the ocean, the strengths of the backscattered signals are related to the surface ripples of the water which in turn are determined by the low-level winds. Extraction of the wind vector from the radar signals represents an inverse problem which is typically multi-valued. Although determining the wind speed is relatively straightforward, the data gives rise to *aliases* for the direction. For example, a wind direction of θ will sometimes give rise to similar radar sig-

nals to a wind direction of $\theta + \pi$, and there may be further aliases at other angles. Modelling the conditional distribution of wind direction provides the most complete information for further processing to 'de-alias' the wind directions.

A large set of ERS-1 measurements has been assembled by the European Space Agency in collaboration with the UK Meteorological Office. Labelling of the dataset was performed using wind vectors from the Meteorological Office Numerical Weather Prediction model. These values were interpolated from the inherently coarse-grained model to regions coincident with the scatterometer cells. To provide a challenging task, the data was selected from low pressure (cyclonic) and high pressure (anti-cyclonic) circulations. Ten wind fields from each of the two categories were used: each wind field contains $19 \times 19 = 361$ cells each of which represents an area of approximately 26km $\times$ 26km. Training, validation and test sets each contained 1963 patterns.

The inputs used were the three values of σ_0 for the aft-beam, mid-beam and fore-beam, and the sine of the incidence angle of the mid-beam (which strongly influences the signal received). The σ_0 inputs were scaled to have zero mean and unit variance. The target value was expressed as an angle (in radians) clockwise from the satellite's forward path. Table 2 gives a summary of the preliminary results obtained. This is a more complex domain than the synthetic problem so there were more difficulties with local optima. This problem was considerably reduced (to about 25% of the runs) by starting training with the centres of the kernel functions approximately uniformly spaced in $[0, 2\pi)$. Of the adaptive-centre models, the one with six centres

Method	Centres	Hidden Units	Validation Error	Test Error
Wrapped normal	4	20	2474.6	2446.2
Adaptive circular normal	6	20	2308.0	2337.9
Fixed kernel	36	24	2028.9	1908.9

Table 2 Results on satellite data.

has the lowest error on the validation data: however fewer centres are actually required to model the conditional density function reasonably well.

5 Discussion

All three methods give reasonable results, with the adaptive-kernel approaches beating the fixed-kernel technique on synthetic data, and the reverse on the scatterometer data. The two fully adaptive methods give similar results.

Note that there are two structural parameters to select: the number of hidden units in the network and the number of components in the mixture model. The use of a larger, fixed network structure, together with regularization to control the effective model complexity, would probably simplify the process of model order selection.

REFERENCES

[1] C M Bishop, *Mixture density networks.* Technical Report NCRG/4288, Neural Computing Research Group, Aston University, U.K. (1994).

[2] C. M. Bishop, *Neural Networks for Pattern Recognition.* Oxford University Press (1995).

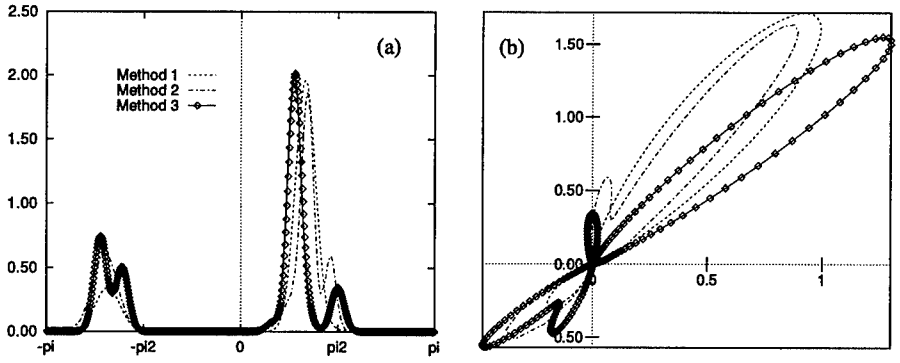

Figure 2 Plots of the conditional distribution $p(\theta|\mathbf{x})$ obtained using all three methods. (a) and (b) show linear and polar plots of the distributions for a given input vector from the test set. The dominant alias at π is evident. In both plots, the solid curve represents method 1, the dashed curve represents method 2, and the curve with circles represents method 3.

[3] C. M. Bishop and C. Legleye, *Estimating conditional probability distributions for periodic variables*, in: D. S. Touretzky, G. Tesauro, and T. K. Leen, editors, Advances in Neural Information Processing Systems, Vol. 7 (1995), pp641–648, Cambridge MA, MIT Press.

[4] R A Jacobs, M I Jordan, S J Nowlan, and G E Hinton, *Adaptive mixtures of local experts*, Neural Computation, Vol. 3 (1991), pp79–87.

[5] Y Liu, *Robust neural network parameter estimation and model selection for regression*, in: Advances in Neural Information Processing Systems, Vol.6 (1994), pp192–199, Morgan Kaufmann.

[6] K V Mardia, *Statistics of Directional Data*. Academic Press, London (1972).

[7] G J McLachlan and K E Basford, *Mixture models: Inference and Applications to Clustering*. Marcel Dekker, New York (1988).

[8] S Thiria, C Mejia, F Badran, and M Crepon, *A neural network approach for modeling nonlinear transfer functions: Application for wind retrieval from spaceborne scatterometer data*, Journal of Geophysical Research, Vol. 98(C12) (1993), pp22827–22841.

[9] D M Titterington, A F M Smith, and U E Makov, *Statistical Analysis of Finite Mixture Distributions*, John Wiley, Chichester (1985).

Acknowledgements

We are grateful to the European Space Agency and the UK Meteorological Office for making available the ERS-1 data. The contributions of Claire Legleye in the early stages of this project are also gratefully acknowledged. We would also like to thank Iain Strachan and Ian Kirk of AEA Technology for a number of useful discussions relating to the interpretation of this data.

INTEGRO-DIFFERENTIAL EQUATIONS IN COMPARTMENTAL MODEL NEURODYNAMICS

Paul C. Bressloff

Department of Mathematical Sciences, Loughborough University, Leics. LE11 3TU, UK.

Most neural network models take a neuron to be a point processor by neglecting the extensive spatial structure of the dendritic tree system. When such structure is included, the dynamics of a neural network can be formulated in terms of a set of coupled nonlinear integro-differential equations. The kernel of these equations contains all information concerning the effects of the dendritic tree, and can be calculated explicitly. We describe recent results on the analysis of these integro-differential equations.

The local diffusive spread of electrical activity along a cylindrical region of a neuron's dendrites can be described by the *cable equation*

$$\frac{\partial V}{\partial t} = -\epsilon V + D\frac{\partial^2 V}{\partial \xi^2} + I(x,t) \tag{1}$$

where x is the spatial location along the cable, $V(x,t)$ is the local membrane potential at time t, ϵ is the decay rate, D is the diffusion coefficient and $I(x,t)$ is any external input. Note that equation (1) is valid provided that conductance changes induced by synaptic inputs are small; in the dendritic spines the full Nernst-Planck equations must be considered [1]. A *compartmental model* replaces the cable equation by a system of coupled ordinary differential equations according to a space-discretization scheme [2]. The complex topology of the dendrites is represented by a simply-connected graph or tree Γ. Each node of the tree $\alpha \in \Gamma$ corresponds to a small region of dendrite (compartment) over which the spatial variation of physical properties is negligible. Each compartment α can be represented by an equivalent circuit consisting of a resistor R_α and capacitor C_α in parallel, which is joined to its nearest neighbours $< \beta, \alpha >$ by junctional resistors $R_{\alpha\beta}$. We shall assume for simplicity that the tree Γ is coupled to a single somatic compartment via a junctional resistor $\hat{R}$ from node $\alpha_0 \in \Gamma$. (Figure 1). The boundary conditions at the terminal nodes of the tree can either be open (membrane potential is clamped at zero) or closed (no current can flow beyond the terminal node).
An application of Kirchoff's law yields the result

$$C_\alpha \frac{dV_\alpha}{dt} = -\frac{V_\alpha}{R_\alpha} + \sum_{<\beta,\alpha>} \frac{V_\beta - V_\alpha}{R_{\alpha\beta}} + \frac{U - V_{\alpha_0}}{\hat{R}}\delta_{\alpha,\alpha_0} + I_\alpha(t), \quad \alpha \in \Gamma \tag{2}$$

$$C\frac{dU}{dt} = -\frac{U}{R} + \frac{V_{\alpha_0} - U}{\hat{R}} \tag{3}$$

where $V_\alpha(t)$ is the membrane potential of compartment $\alpha \in \Gamma$ and $U(t)$ is the membrane potential of the soma. It can be shown that there exists a choice of parameterisation (where all branches are uniform) for which equation (2) reduces to the matrix form [3]

$$\frac{d\mathbf{V}}{dt} = 2\sigma \mathbf{Q}\mathbf{V}(t) - (\epsilon + 2\sigma)\mathbf{V}(t) + U(t)\mathbf{a} + \mathbf{I}(t) \tag{4}$$

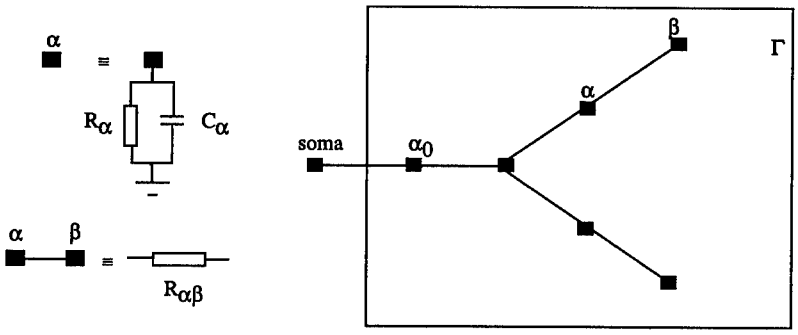

Figure 1 Compartmental model of a neuron.

where $a_\alpha = \delta_{\alpha,\alpha_0}$ and σ, ϵ are global longitudinal and transverse decay rates respectively. The matrix $\mathbf{Q}$ generates an unbiased random walk on the tree Γ. That is, $\mathbf{Q} = \mathbf{D}^{-1}\mathbf{A}$ where $\mathbf{A}$ is the adjacency matrix of Γ, $A_{\alpha\beta} = 1$ if the nodes α and β are adjacent and $A_{\alpha\beta} = 0$ otherwise, and $\mathbf{D} = \mathrm{diag}(d_\alpha)$ where d_α is the coordination number of node α. Our choice of parameterisation is particularly useful since it allows one to study the effects of dendritic structure using algebraic graph theory (see below). More general choices of parameterisation where each branch is nonuniform, say, can be handled using perturbation theory.

Since the output of the neuron is determined by the somatic potential $U(t)$, we can view the dendritic potentials as auxiliary variables. In particular, using an integrating factor we can solve equation (4) for $\mathbf{V}(t)$ in terms of $U(t)$ and $\mathbf{I}(t)$. Substitution into equation (3) then yields the integro-differential equation (assuming without loss of generality that $\mathbf{V}(0) = 0$ and $\hat{R}C = 1$)

$$\frac{dU}{dt} = -\rho U(t) + \int_0^t \sum_{\alpha\in\Gamma} G_{\alpha_0\alpha}(t-t')\,[U(t')\delta_{\alpha,\alpha_0} + I_\alpha(t')]\,dt' \tag{5}$$

where $\rho = 1/RC + 1/\hat{R}C$ and

$$G_{\alpha\beta}(t) = \mathrm{e}^{-(\epsilon+2\sigma)t}\left[\mathrm{e}^{2\sigma t\mathbf{Q}}\right]_{\alpha\beta} \tag{6}$$

is the dendritic membrane potential response of compartment α at time t due to a unit impulse stimulation of node β at time $t = 0$ in the absence of the term $U(t)\mathbf{a}$ on the right-hand side of equation (4). All details concerning the passive effects of dendritic structure are contained within $\mathbf{G}(t)$. Note that in deriving equation (5) we have assumed that the inputs $I_\alpha(t)$ are voltage-independent. Thus we are ignoring the effects of shunting and voltage-dependent ionic gates.

One way to calculate $G_{\alpha\beta}(t)$, equation (6), would be to diagonalize the matrix $\mathbf{Q}$ to obtain (for a finite tree)

$$G_{\alpha\beta}(t) = \mathrm{e}^{-(\epsilon+2\sigma)t}\sum_r u_{r\alpha}u_{r\beta}\mathrm{e}^{2\sigma\lambda_r t} \tag{7}$$

where $\{\lambda_r\}$ forms the discrete spectrum of $\mathbf{Q}$ and $\mathbf{u}_r$ are the associated eigenvectors. It can be shown that the spectral radius $\rho(\mathbf{Q}) = 1$ and an application of the *Perron-Frobenius Theorem* establishes that (a) $\lambda = 1$ is a nondegenerate eigenvalue and (b) eigenvalues appear in real pairs $\pm\lambda_r$. However, such a diagonalization procedure is

rather cumbersome for large trees and does not explicitly yield the dependence on tree topology. An alternative approach is to exploit the fact that $\mathbf{Q}$ generates a random walk on Γ. That is, expand equation (6) to obtain

$$G_{\alpha\beta}(t) = \mathrm{e}^{-(\epsilon+2\sigma)t} \sum_{r=0}^{\infty} \frac{(2\sigma t)^r}{r!} [\mathbf{Q}^r]_{\alpha\beta} \tag{8}$$

where $[\mathbf{Q}^r]_{\alpha\beta}$ is equal to the probability of an unbiased random walk on Γ reaching α from β in r steps. Using various reflection arguments, which is equivalent to a *generalized method of images*, one can express $G_{\alpha\beta}(t)$ as a series involving the response function of an infinite, uniform chain of dendritic compartments [3,4],

$$G_{\alpha\beta}(t) = \mathrm{e}^{-(\epsilon+2\sigma)t} \sum_{\mu}^{(\alpha\beta)} b_\mu I_{M_\mu}(2\sigma t) \tag{9}$$

where I_n is the modified Bessel function of integer order n. In equation (9), the summation is over trips μ starting at node β and ending at node α, and a trip is a restricted kind of walk in which changes of direction can only take place at branching nodes or terminal nodes of the tree. The length of a trip (number of steps) is given by M_μ. The constant coefficients b_μ are determined by various factors picked up along a trip according to the following "Feynman Rules". (i) A factor of $+1$ on reflection from a closed terminal node and a factor of -1 on reflection from an open terminal node. (ii) A factor of $2/d_\alpha$ when a trip passes through a branching node with coordination number $d_\alpha > 2$. (iii) A factor of $2/d_\alpha - 1$ when a trip reflects at a branching node of coordination number d_α. (iv) A factor of $2/d_\alpha$ when a trip terminates at a branching node ($d_\alpha > 2$) or a closed terminal node ($d_\alpha = 1$).

The series (9) will typically involve an infinite number of terms. However, for any fixed t, trips with length $M_\mu >> \sqrt{\sigma t}$ can be neglected so that the sum over μ can be truncated to include only a finite number of terms. Thus, using an efficient algorithm for generating trips should provide an efficient method for calculating $\mathbf{G}(t)$ at small and intermediate times. Moreover, one can also extract information concerning the long-time behaviour by Laplace-transforming (9)

$$\begin{aligned} \tilde{G}_{\alpha\beta}(z) &= \frac{1}{2\sigma[\lambda_+(z) - \lambda_-(z)]} \sum_{\mu}^{(\alpha\beta)} b_\mu \lambda_-(z)^{M_\mu}, \\ \lambda_\pm(z) &= \frac{z+\hat{\epsilon}}{2\sigma} \pm \sqrt{\left(\frac{z+\hat{\epsilon}}{2\sigma}\right)^2 - 1} \end{aligned} \tag{10}$$

where $\hat{\epsilon} = \epsilon + 2\sigma$. The resulting summation over trips can be performed explicitly to yield a closed expression for $\tilde{\mathbf{G}}(z)$ [5]. In the remainder of this paper we consider some examples illustrating the effects of dendritic structure on neurodynamics. We shall find that the Laplace transform $\tilde{\mathbf{G}}(z)$ plays a crucial role in determining the stability of these systems.

A major issue at the single neuron level is the effect of the coupling between soma and dendrites on the input-output response of a neuron satisfying equation (5), which may be rewritten in the form

$$\frac{dU}{dt} = -\rho U(t) + \int_0^t H(t-t')U(t')dt' + \hat{I}(t),$$

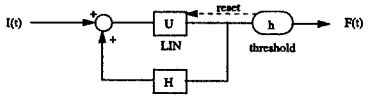

Figure 2 Schematic diagram of a compartmental model leaky integrator neuron (LIN) indicating the feedback arising from the electrical coupling between the soma and dendrites.

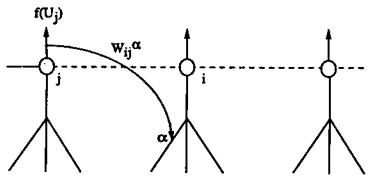

Figure 3 A network of compartmental model neurons indicating the axo-dendritic connection from neuron j to compartment α of neuron i.

$$\hat{I}(t) = \int_0^t \sum_{\alpha\in\Gamma} G_{\alpha_0\alpha}(t-t')I_\alpha(t')dt' \tag{11}$$

This describes a leaky-integrator neuron with external input $\hat{I}(t)$ and an additional feedback term mediated by the kernel $H(t) = G_{\alpha_0\alpha_0}(t)$, which takes into account the underlying coupling between $U(t)$ and the dendritic potentials. The model is represented schematically in figure 2. Since both $H(t)$ and $\hat{I}(t)$ are continuous on $[0,\infty)$ we can apply a variation of parameters formula to obtain

$$U(t) = Z(t)U(0) + \int_0^t Z(t-t')\hat{I}(t')dt', \quad Z(t) = \mathcal{L}^{-1}\left[\frac{1}{z+\rho-\tilde{H}(z)}\right](t) \tag{12}$$

where $\mathcal{L}^{-1}$ indicates the inverse Laplace transform. An interesting application of the model is to the case of *reset* where the neuron's somatic potential is reset to a zero resting level whenever it reaches a threshold h and fires. Let T_n denote the nth firing-time of the neuron. Then $U(t)$ evolves according to equation (11) for $T_n < t < T_{n+1}$ and $U(T_N) = h$ so that $U(T_n^+) = 0$. It can be shown that the firing-times evolve according to a *second-order* difference equation rather than a first-order one typical of standard *integrate-and-fire* models. (For more details see Ref. [6]). Thus the coupling between soma and dendrites can have non-trivial consequences for dynamical behaviour.

Now consider a network of N neurons labelled $i = 1,...,N$ each with identical dendritic structure. Let W_{ij}^α denote the synaptic weight of the connection from neuron j impinging on compartment $\alpha \in \Gamma$ of neuron i. The associated output is taken to be of the form $W_{ij}^\alpha f(U_j)$ where f is a sigmoidal output function, (see figure 3). Equation (5) then leads to a set of coupled integro-differential equations

$$\frac{dU_i}{dt} = -\rho U_i(t) + \int_0^t \left[\sum_{j\neq i}\sum_{\beta\in\Gamma} W_{ij}^\beta G_{\alpha_0\beta}(t-t')f(U_j(t'))\right]dt' \tag{13}$$

Note that for simplicity we are neglecting the feedback arising from the coupling between the soma and dendrites of the same neuron. Further, let the output function f satisfy $f(x) = \tanh(\kappa x)$. Then $f(0) = 0$ so that $\mathbf{U} = 0$ is a fixed point solution of (13). Linearization about the zero solution with $f'(0) = \kappa$ gives

$$\frac{dU_i}{dt} = -\rho U_i(t) + \int_0^t \sum_{j\neq i} H_{ij}(t-t')U_j(t')dt' \tag{14}$$

$$H_{ij}(t) = \kappa \sum_{\beta} W_{ij}^{\beta} G_{\alpha_0 \beta}(t) \tag{15}$$

Assume that the weights satisfy the condition $\sum_{\beta \in \Gamma} |W_{ij}^{\beta}| < \infty$ for all $i, j = 1, ..., N$ so that the convolution kernel $\mathbf{H}(t)$ is a continuous $N \times N$ matrix whose elements lie in $L^1[0, \infty)$. That is, $\int_0^{\infty} |H_{ij}(t)| dt < \infty$ for all $i, j = 1, ..., N$ It can then be proven [7] that the zero solution of equation (14) is asymptotically stable if and only if

$$\Delta(z) \equiv \det \left[(\rho + z)\mathbf{I} - \tilde{\mathbf{H}}(z) \right] \neq 0 \quad \text{when} \quad \text{Re} z \geq 0 \tag{16}$$

where $\tilde{\mathbf{H}}(z)$ is the Laplace transform of the kernel $\mathbf{H}$ and $\mathbf{I}$ is the $N \times N$ unit matrix, which can be calculated explicitly from equations (15) and (10). Condition (16) requires that no roots of the so called *characteristic function* should lie in the right-half complex plane.

It can also be established that if the stability condition (16) is met for the linear system (14), then the zero solution of the full nonlinear system (13) is locally asymptotically stable [7]. On the other hand, if $\Delta(z)$ has at least one root in the right-half complex plane then the linear system (14) is unstable. The corresponding instability of the full nonlinear system is harder to analyse; in such cases one has to bring in techniques such as bifurcation theory to investigate the effects of the nonlinearities on the behaviour of the system at the point of marginal stability where one or more eigenvalues cross the imaginary axis [8].

It is clear from equation (15) that the stability of a recurrent network depends on the particular distribution of axo-dendritic connections across the network. We end this paper by presenting some recent results concerning such stability. Detailed proofs are presented elsewhere [8,9]. First, suppose that the weights decompose into the product form $W_{ij}^{\alpha} = J_{ij} P_{\alpha}$, $P_{\alpha} \geq 0$, and $\sum_{\alpha} P_{\alpha} = 1$. Thus the distribution of axon collaterals across the dendritic tree of a neuron is *uncorrelated* with the location of the presynaptic and postsynaptic neurons in the network. Assuming that the weight matrix $\mathbf{J}$ can be diagonalized with eigenvalues w_r, $r = 1, ..., N$ then equation (16) reduces to

$$(z + \rho) - \kappa w_r \sum_{\beta \in \Gamma} P_{\beta} \tilde{G}_{\alpha_0 \beta}(z) = 0 \tag{17}$$

Two particular results follow from equation (17).

I. The zero solution is (locally) asymptotically stable if

$$\kappa |w_r| < \rho \left[\sum_{\beta \in \Gamma} P_{\beta} \tilde{G}_{\alpha_0 \beta}(0) \right]^{-1}$$

for all $r = 1, ..., N$. Taking $P_{\beta} = \delta_{\beta, \bar{\beta}}$, for example, shows that the passive membrane properties of the dendritic tree can stabilize an equilibrium. This follows from the property that for compartments sufficiently far from the soma, $\tilde{G}_{\alpha_0 \bar{\beta}}(0) < \tilde{G}_{\alpha_0 \alpha_0}(0)$.

II. The passive membrane properties of the dendrites can induce oscillations via a supercritical Hopf bifurcation [8]. At the point of marginal stability there exists a pair of pure imaginary roots $z = \pm i\omega$ satisfying equation (17) for a nondegenerate eigenvalues $w^* = \min_r \{w_r\}$ such that $w^* < 0$ and all roots of equation (17) for $w_r > w^*$ have negative definite real part.

When one considers the synaptic organisation of the brain, it becomes apparent that the decoupling of network and dendritic coordinates is an oversimplification. One example of this concerns the recurrent collaterals of pyramidal cells in the olfactory cortex [10]. These collateralls feed back excitation onto the basal dendrites of nearby pyramidal cells and onto the apical dendrites of distant pyramidal cells. This suggests that in our model the distance of a synapse from the soma should increase with the separation $|i-j|$; this leads to a reduction in the effectiveness of the connection (ignoring active processes). On the other hand, there is growing experimental evidence that the reduction in the effectiveness of distal synapses may be compensated by a number of mechanisms including increases in the density of synapses at distal locations and voltage-dependent gates on dendritic spines [10]. We can incorporate the former possibility by taking W_{ij}^{α} to be an increasing function of the degree of separation of compartment α from the soma at α_0. If this is combined with the previous feature then we have a third result.

III. The passive membrane properties of the dendritic tree can induce spatial pattern formation (arising from a Turing-like instability) in a purely excitatory or inhibitory network when the dependence of the weight distribution on dendritic and network coordinates is correlated. Thus one does not require a competition between excitatory and inhibitory connections (Mexican hat function) to induce the formation of coherent spatial structures.

Finally, note that all the results presented in this paper have a well-defined continuum limit. In particular, introduce a length-scale l corresponding to the length of an individual compartment. One then finds that in the limit $l \to 0$ such that $\sigma/l^2 \to D$, equation (4) reduces to the cable equation (1) on each branch of the tree such that current $\partial V/\partial x$ is conserved at each branching node and V is continuous at a branching node. Equation (10) with $\alpha l = \xi, \beta l = \xi', L_\mu = M_\mu l$ becomes

$$\lim_{l\to 0} \frac{\tilde{G}_{\alpha\beta}(z)}{l} = \tilde{G}(\xi,\xi';z) = \frac{1}{2}\sqrt{\frac{1}{D(z+\epsilon)}} \sum_{\mu}^{(\xi,\xi')} b_\mu \exp\left(-\sqrt{\frac{z+\epsilon}{D}} L_\mu\right)$$

REFERENCES

[1] Sejnowski TJ and Qian N. In *Single neuron computation* (ed. T. Mckenna, J. Davis and S. F. Zornetzer), San Diego: Academic Press (1992) pp117–139.

[2] Rall W. In: *Neural Theory and Modeling* (R. F. Reiss ed.), Stanford University Press, Stanford (1964), pp73–97.

[3] Bressloff PC and Taylor JG, *Biol. Cybern.* Vol.70, pp199–207.

[4] Abbott LF, Farhi E and Gutmann S, *Biol. Cybern.* Vol.66 (1991), pp49–60.

[5] Bressloff PC, Dwyer VM and Kearney MJ, *J. Phys. A*, Vol.29 (1996), pp1881–1896.

[6] Bressloff PC, *Physica D* Vol.80 (1995), p399.

[7] Burton TA , *Volterra Integral and Differential Equations* Academic Press, London (1983).

[8] Bressloff PC , *Phys. Rev. E* Vol.50 (1994), pp2308-2319.

[9] Bressloff PC, *Biol. Cybern.*, Vol.73 (1995), pp281–290.

[10] Shepherd GM ed., *The Synaptic Organization of the Brain* Oxford University Press, Oxford (1990).

NONLINEAR MODELS FOR NEURAL NETWORKS

Susan Brittain and Linda M. Haines

University of Natal, Pietermaritzburg, South Africa. Email: haines@stat.unp.ac.za

The statistical principles underpinning hidden-layer feed-forward neural networks for fitting smooth curves to regression data are explained and used as a basis for developing likelihood- and bootstrap-based methods for obtaining confidence intervals for predicted outputs.

Keywords: Hidden–layer feed–forward neural networks; nonlinear regression; nonparametric regression; confidence limits; predicted values.

1 Introduction

Hidden-layer feed–forward neural networks are used extensively to fit curves to regression data and to provide surfaces from which classification rules can be deduced. The focus of this article is on curve-fitting applications and two crucial statistical insights into the workings of neural networks in this context are presented in Section 2. Approaches to developing confidence limits for predicted outputs are explored in Section 3 and some conclusions given in Section 4.

2 Statistical Insights

Consider the following single hidden-layer feed–forward neural network used to model regression data of the form, $(x_i, y_i), i = 1, \ldots, n$. The input layer comprises a neuron which inputs the x-variable and a second neuron which inputs a constant or bias term into the network. The hidden–layer comprises two neurons with logistic activation functions and an additional neuron which inputs a bias term and the output layer provides the predicted y-value through a neuron with a linear activation function. The connection weights, $\theta = (\theta_1, \ldots, \theta_7)$, are defined in such a way that the output, o, from the network corresponding to an input, x, can be written explicitly as

$$o = \theta_5 + \frac{\theta_6}{1 + e^{-(\theta_1 + \theta_2 x)}} + \frac{\theta_7}{1 + e^{-(\theta_3 + \theta_4 x)}}. \quad (1)$$

If in addition the network is trained to minimize the error sum-of-squares, $\sum_{i=1}^{n}(y_i - o_i)^2$, then it is clear that implementing this neural network is *equivalent* to using the method of least squares to fit the nonlinear regression model, $y_i = o_i + \epsilon_i, i = 1, \ldots, n$, where the error terms, ϵ_i, are independently and identically distributed with zero mean and constant variance, to the data. The weights of the network correspond to parameters in the regression model, training corresponds to iteration in an appropriate optimization algorithm, and generalization to prediction. In fact the nonlinear regression model just described is not in any way *meaningful* in relation to the data and the broad modelling procedure should rather be viewed as one of smoothing. In the present example, two logistic functions are scaled and located so that their sum, together with a constant term, approximates an appropriate smooth curve. Overall therefore it is clear that the underlying mechanism of a hidden-layer feed–forward neural network is that of nonlinear regression and that the broad principle underpinning such a network is that of nonparametric regression.

3 Confidence Limits for the True Predicted Values

Consider a hidden-layer feed–forward neural network represented formally as the nonlinear regression model,

$$y_i = \eta(x_i, \theta) + \epsilon_i, \quad i = 1, \ldots, n, \quad (2)$$

where y_i is the observed value at x_i, $\theta = (\theta_1, \ldots, \theta_p)$ is a $p \times 1$ vector of unknown parameters, $\eta(\cdot)$ is a nonlinear function describing the network, and the error terms, ϵ_i, are uncorrelated with mean, 0, and constant variance, σ^2. Then the least squares estimator of θ, denoted $\hat{\theta}$, is that value of θ which minimizes the error sum-of-squares, $S(\theta) = \sum_{i=1}^{n}[y_i - \eta(x_i, \theta)]^2$, and the estimator of σ^2, denoted s^2, is given by $S(\hat{\theta})/(n-p)$. The mean predicted value at x_g for model (2), and hence for the underlying neural network, is given by $\eta(x_g, \hat{\theta})$ and confidence intervals for the corresponding true value, $\eta(x_g, \theta)$, can be derived from likelihood theory or by resampling methods.

3.1 Likelihood Theory

Linearization method : Suppose that the errors in model (2) are normally distributed and suppose further that this model can be satisfactorily approximated by a linear one, and that $V(\hat{\theta})$, the estimated asymptotic variance of the least squares estimator, $\hat{\theta}$, is taken to be $s^2 \left[\sum_{i=1}^{n} g(x_i, \theta) g(x_i, \theta)^T\right]^{-1}_{\hat{\theta}}$, where $g(x_i, \theta) = \partial\eta(x_i, \theta)/\partial\theta, i = 1, \ldots, n$, and the subscript $\hat{\theta}$ denotes evaluation at that point. Then the standard error of the mean predicted value at x_g is given by $SE[\eta(x_g, \hat{\theta})] = s\sqrt{g(x_g, \theta)^T_{\hat{\theta}}\ V(\hat{\theta})\ g(x_g, \theta)_{\hat{\theta}}}$, where $g(x_g, \theta) = \partial\eta(x_g, \theta)/\partial\theta$, and an approximate $100(1-\alpha)\%$ confidence interval for $\eta(x_g, \theta)$ can be expressed quite simply as

$$\eta(x_g, \hat{\theta}) \pm t^{\star} SE[\eta(x_g, \hat{\theta})], \tag{3}$$

where $t^{\star}$ denotes the appropriate critical t-value with $n-p$ degrees of freedom.

Example 1 : Data were generated from model (2) with deterministic component (1) corresponding to the neural network described in Section 2 and with normally distributed error terms. The parameter values were taken to be

$$\theta = (0.5, 0.5, 1, -1, 0.1, 1, 1.5)$$

and $\sigma = 0.01$, 25 x-values, equally spaced between -12 and 12, were selected, and simulated y-values, corresponding to these x-values, were obtained. The approximate 95% confidence limits to $\eta(x_g, \theta)$ for $x_g \in [-12, 12]$, were calculated using formula (3) and are summarized in the plots of $\pm t^{\star} SE[\eta(x_g, \hat{\theta})]$ against x_g shown in Figure 1. The interesting, systematic pattern exhibited by these limits depends on the design points, $x_i, i = 1, \ldots, n$.

Profile likelihood method : Suppose again that the errors in model (2) are normally distributed and let $S(\hat{\theta}|\eta_g^c)$ denote the minimum error sum-of-squares for a fixed value, η_g^c, of the true predicted value, $\eta(x_g, \theta)$. Then the profile log-likelihood for $\eta(x_g, \theta)$ is described, up to an additive constant, by the curve with generic point, $(\eta_g^c, S(\hat{\theta}|\eta_g^c))$, and a likelihood-based $100(1-\alpha)\%$ confidence interval for $\eta(x_g, \theta)$ comprises those values of η_g^c for which

$$S(\hat{\theta}|\eta_g^c) - S(\hat{\theta}) \leq t^{\star 2} s^2. \tag{4}$$

For Example 1 the requisite values of the conditional sum-of-squares, $S(\hat{\theta}|\eta_g^c)$, for a particular x-value, x_g, were obtained by reformulating the deterministic component of the model as $\eta(x, \theta) = \eta_g + \eta_1(x, \theta) - \eta_1(x_g, \theta)$ with $\eta_1(x, \theta) = \frac{\theta_6}{1+e^{-(\theta_1+\theta_2 x)}} + \frac{\theta_7}{1+e^{-(\theta_3+\theta_4 x)}}$, and by minimizing the resultant error sum-of-squares for appropriate fixed values of the parameter, $\eta_g = \eta(x_g, \theta)$. For each value of $x_g \in [-12, 12]$

so considered, the profile log-likelihood for the true predicted value, $\eta(x_g, \theta)$, was approximately quadratic and the attendant 95% confidence limits were calculated as the two values of η_g^c satisfying the equality condition in expression (4) by using the bisection method. A plot of these 95% confidence limits, centered at the maximum likelihood estimator, $\eta(x_g, \hat{\theta})$, against x_g, are shown, together with those found by the linearization method, in Figure 1. It is clear from this figure that the confidence

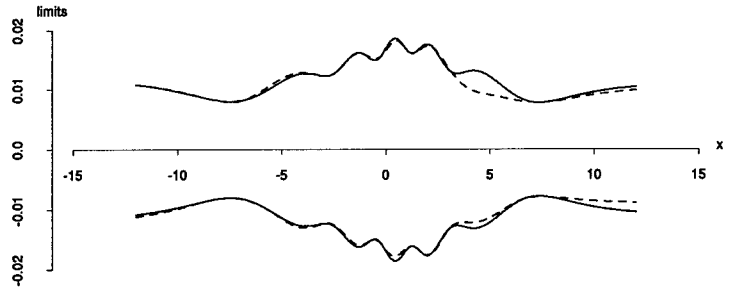

Figure 1 Linearization (solid line) and profile likelihood (dashed line) methods.

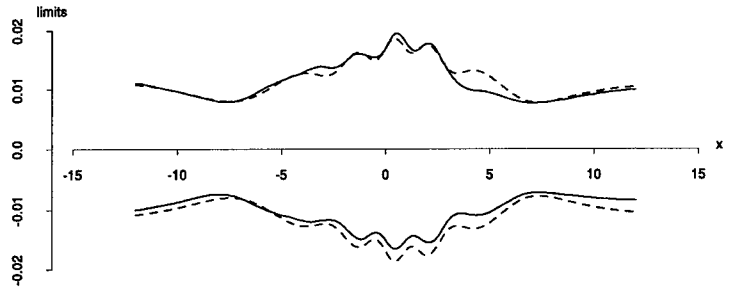

Figure 2 Bootstrap residuals (solid line) and linearization (dashed line) methods.

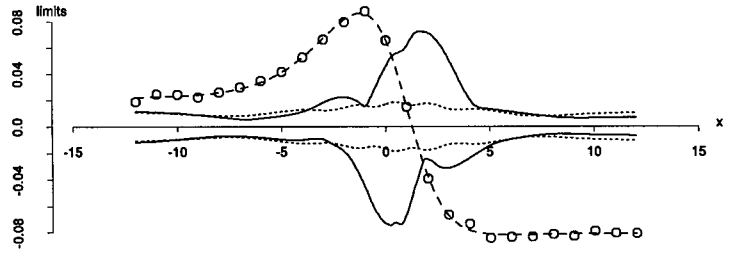

Figure 3 Bootstrap pairs (solid line) and linearization (dotted line) methods; fitted curve (dashed line) and data points (circles).

limits for $\eta(x_g, \theta)$ obtained from these two methods are very similar.

3.2 Bootstrap Methods

Bootstrapping residuals : Suppose that the least squares estimate, $\hat{\theta}$, of the parameters in model (2) is available. Then confidence intervals for true predicted values, $\eta(x_g, \theta)$, can be obtained by bootstrapping the standardized residuals, $e_i = [y_i - \eta(x_i, \hat{\theta})]\sqrt{\frac{n}{n-p}}$ for $i = 1, \ldots, n$, following the procedure for regression models outlined in [1]. For example 1, the resultant 95% bootstrap confidence limits for predicted values, $\eta(x_g, \theta)$, with $x \in [-12, 12]$ were centered at the corresponding bootstrap means, and a plot of these limits against x is shown in Figure 2, together with the the corresponding limits obtained from the linearization method. It is clear from this figure that the broad pattern exhibited by the two sets of confidence limits is the same but that the limits are systematically displaced. An attempt to correct the bootstrap percentiles for bias by implementing the BC_a method of [1] produced limits which were very different from the uncorrected ones.

Bootstrapping pairs : An alternative to bootstrapping the residuals is to bootstrap the data pairs, $(x_i, y_i), i = 1, \ldots, n$, directly, following the procedure given in [1]. Approximate 95% confidence intervals for the true predicted values of Example 1 were obtained in this way and the results, in the form of plots of the confidence limits centered about the bootstrap mean against x, are shown in Figure 3, together with a plot of the corresponding centered limits obtained from the linearization method. Clearly the confidence limits obtained by bootstrapping the data pairs are *wildly* different from those found by the other methods investigated in this study. The reason for this is clear from the suitably scaled plots of the data points and the fitted curve which are superimposed on the plots of the confidence limits in Figure 3 so that the x-values coincide. In particular, only 4 of the 25 observations are taken at x-values corresponding to the steep slope of the fitted curve between $x = -1$ and $x = 2.5$ and the probability that at least one of these points is *excluded* from the bootstrap sample is high, *viz.* 0.8463. As a consequence the bootstrap least squares fitted curve is expected to be, and indeed is, extremely unstable in the region of this slope.

3.3 Comparison of Methods

It is clearly important to generalize the results found thus far. To this end, 400 data sets were simulated from the model setting of Example 1 and, from these, coverage probabilities with a nominal level of 95% for a representative set of true predicted values were evaluated using the likelihood-based and the bootstrap methods of the previous two subsections. The results are summarized in Table 1 and clearly reinforce those obtained for Example 1. In particular, the coverage probabilities provided by the linearization and the profile likelihood-based methods are close to nominal, while those obtained by bootstrapping the residuals are consistently low over the range of x-values considered and those obtained by bootstrapping the data pairs are very erratic.

4 Conclusions

The aim of this present study has been to critically compare selected methods for setting confidence limits to the predicted outputs from a neural network. Both of the likelihood-based methods investigated produced surprisingly good results. In particular, the linearization method proved quick and easy to use, while the profile

Method	x-values for true predicted outputs						
	-10	-5	-2.5	0	2.5	5	10
Linearization	95	95.75	95.75	94.75	92.25	92.5	94.75
Profile likelihood	95.5	94.5	93.5	96	95.25	95	93.25
Bootstrap residuals	91.75	93.5	94	91.5	90	91.75	94.5
Bootstrap pairs	89.75	90.75	96.5	97.25	98.5	92.5	91

Table 1 Coverage probabilities for a nominal level of 95% and 400 simulations.

likelihood approach, which is more rigorous, was a little more difficult to implement. In contrast, the bootstrap methods for finding the required confidence limits were, necessarily, highly computer-intensive, and the results disappointing. On balance, it would seem that, to quote Wu [2], "The linearization method is a winner".

REFERENCES

[1] Efron, B. and Tibshirani, R.J., *An Introduction to the Bootstrap.* Chapman & Hall (1994), New York.

[2] Wu, C.F.J., *Jackknife, bootstrap and other resampling methods in regression analysis*, Annals of Statistics, Vol. 14 (1986), pp1261–1295.

Acknowledgements

The authors wish to thank the University of Natal and the Foundation for Research Development, South Africa, for funding this work.

A NEURAL NETWORK FOR THE TRAVELLING SALESMAN PROBLEM WITH A WELL BEHAVED ENERGY FUNCTION

Marco Budinich and Barbara Rosario
Dipartimento di Fisica & INFN, Via Valerio 2, 34127, Trieste, Italy.
Email: mbh@trieste.infn.it

We present and analyze a Self Organizing Feature Map (SOFM) for the NP-complete problem of the travelling salesman (TSP): finding the shortest closed path joining N cities. Since the SOFM has discrete input patterns (the cities of the TSP) one can examine its dynamics analytically. We show that, with a particular choice of the distance function for the net, the energy associated to the SOFM has its absolute minimum at the shortest TSP path. Numerical simulations confirm that this distance augments performances. It is curious that the distance function having this property combines the distances of the neuron and of the weight spaces.

1 Introduction

Solving difficult problems is a natural arena for a would-be new calculus paradigm like that of neural networks. One can delineate a sharper image of their potential with respect to the blurred image obtained in simpler problems.

Here we tackle the Travelling Salesman Problem (TSP, see [Lawler 1985], [Johnson 1990]) with a Self Organizing Feature Map (SOFM). This approach, proposed by [Angéniol 1988] and [Favata 1991], started to produce respectable performances with the elimination of the non- injective outputs produced by the SOFM [Budinich 1995]. In this paper we further improve its performances by choosing a suitable distance function for the SOFM.

An interesting feature is that this net is open to analytical inspection down to a level that is not usually reachable [Ritter 1992]. This happens because the input patterns of the SOFM, namely the cities of the TSP, are discrete. As a consequence we can show that the energy function, associated with SOFM learning, has its absolute minimum in correspondence to the shortest TSP path.

In what follows we start with a brief presentation of the working principles of this net and of its basic theoretical analysis (section 2). In section 3 we propose a new distance function for the network and show its theoretical advantages while section 4 contains numerical results. The appendix contains the detailed description of parameters needed to reproduce these results.

2 Solving the TSP with self-organizing maps

The basic idea comes from the observation that in one dimension the exact solution to the TSP is trivial: always travel to the nearest unvisited city. Consequently, let us suppose we have a smart map of the TSP cities onto a set of cities distributed on a circle, we will easily find the shortest tour for these "image cities" that will give also a path for the original cities. It is reasonable to conjecture that the better the distance relations are preserved, the better will be the approximate solution found. In this way, the original TSP is reduced to a search of a good neighborhood-preserving map: here we build it via unsupervised learning of a SOFM.

The TSP we consider is constituted of N cities randomly distributed in the plane (actually in the (0,1) square). The net is formed by N neurons logically organized

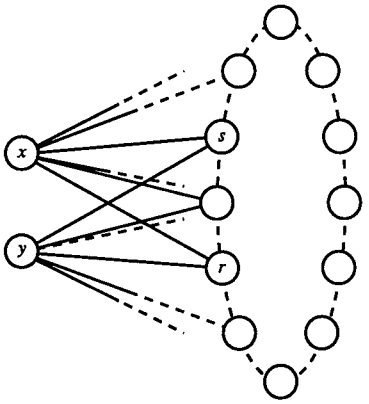

Figure 1 Schematic net: not all connections from input neurons are drawn.

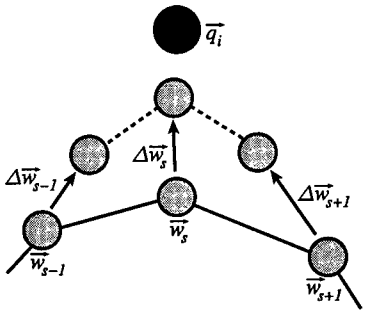

Figure 2 Weights modification in a learning step: neurons (small gray circles) are moved towards the pattern $\vec{q}$ (black circle) by an amount given by (1). The solid line represents the neuron ring. The shape of the deformation of the ring is given by the relative magnitude of the $\Delta\vec{w}$ that is in turn given by the distance function h_{rs}.

in a ring. The cities are the input patterns of the network and the (0,1) square its input space.

Each neuron receives the $(x, y) = \vec{q}$ coordinates of the cities and has thus two weights: $(w_x, w_y) = \vec{w}$. In this view both patterns and neurons can be thought as points in two dimensional space. In response to input $\vec{q}$, the r-th neuron produces output $o_r = \vec{q} \cdot \vec{w}_r$. Figure 1 gives a schematic view of the net while figure 2 represents both patterns and neurons as points in the plane.

Learning follows the standard algorithm [Kohonen 1984]: a city $\vec{q}_i$ is selected at random and proposed to the net; let S be the most responding neuron (ie the neuron nearest to $\vec{q}_i$) then all neuron weights are updated with the rule:

$$\Delta\vec{w}_r = \epsilon h_{rs} (\vec{q}_i - \vec{w}_r) \tag{1}$$

where $0 < \epsilon < 1$ is the learning constant and h_{rs} is the distance function.

This function determines the local deformations along the chain and controls the number of neurons affected by the adaptation step (1); thus it is crucial for the evolution of the network and for the whole learning process (see figure 2).

Step (1) is repeated several times while ϵ and the width of the distance function are being reduced at the same time. A common choice for h_{rs} is a Gaussian-like function like $h_{rs} = e^{-\left(\frac{d_{rs}}{\sigma}\right)^2}$ where d_{rs} is the distance between neurons r and s (the number of steps r and s) and σ is a parameter which determines the number of neurons r such that $\Delta\vec{w}_r \neq 0$; during learning $\epsilon, \sigma \to 0$ so that $\Delta\vec{w}_r \to 0$ and $h_{rs} \to \delta_{rs}$.

After learning, the network maps the two dimensional input space onto the one dimensional space given by the ring of neurons and neighboring cities are mapped

onto neighboring neurons. For each city its image is given by the nearest neuron. From the tour on the neuron ring one obtains the path for the original TSP[1]
The standard theoretical approach to these nets considers the expectation value $E[\Delta\vec{w}_r|\vec{w}_r]$ [Ritter 1992]. In general $E[\Delta\vec{w}_r|\vec{w}_r]$ cannot be treated analytically except when the input patterns have a discrete probability distribution as it happens for the TSP. In this case, $E[\Delta\vec{w}_r|\vec{w}_r]$ can be expressed as the gradient of an energy function, i.e. $E[\Delta\vec{w}_r|\vec{w}_r] = -\epsilon\Delta_{\vec{w}_r}V(W)$, with

$$V(W) = \frac{1}{2N}\sum_{rs} h_{rs} \sum_{q_i \in F_s} (\vec{q}_i - \vec{w}_r)^2 \tag{2}$$

where $W = \{\vec{w}_r\}$ and the second sum is over the set of all the cities $\vec{q}_i$ having $\vec{w}_s$ as nearest neuron, i.e. the cities contained in F_s , the Voronoi cell of neuron having $\vec{w}_s$. On average, $V(W)$ decreases during learning since . $E[\Delta V|W] = -\epsilon\sum_r \|\nabla_{\vec{w}_r}V\|^2$. Substantially, in this case, there exists an energy function which describes the dynamics of the SOFM and which is minimized during learning; formally, the learning process is the descent along the gradient of $V(W)$. Unfortunately $V(W)$ escapes analytical treatment until the end of the learning process when some simplifications are applicable. Since at the end of learning $h_{rs} \to \delta_{rs}$, we can suppose h_{rs} is significantly different from zero only for $r = s, s \pm 1$; in this case (2) becomes

$$V(W) \cong \frac{1}{2N}\sum_s \sum_{q_i \in F_s} \left[h_{s-1,s}(\vec{q}_i - \vec{w}_{s-1})^2 + h_{ss}(\vec{q}_i - \vec{w}_s)^2 + h_{s+1,s}(\vec{q}_i - \vec{w}_{s+1})^2\right] \tag{3}$$

In addition, simulations support that, at the end of learning, most neurons are selected by just one city to which they get nearer and nearer. This means that F_s, contains just one city, let's call it $\vec{q}_{i(s)}$, and that $\vec{w}_s \to \vec{q}_{i(s)}$, consequently

$$V(W) \cong \frac{1}{2N}\sum_s \left[h_{s-1,s}(\vec{q}_{i(s)} - \vec{q}_{i(s-1)})^2 + h_{s+1,s}(\vec{q}_{i(s)} - \vec{q}_{i(s+1)})^2\right] \tag{4}$$

and assuming h_{rs} symmetric i.e. $h_{s-1,s} = h_{s+1,s} = h$, we get

$$\begin{aligned} V(W) &= \frac{h}{2N}\sum_s \left[(\vec{q}_{i(s)} - \vec{q}_{i(s-1)})^2 + (\vec{q}_{i(s)} - \vec{q}_{i(s+1)})^2\right] \\ &= \frac{h}{N} L_{TSP^2} \end{aligned}$$

where L_{TSP^2} is the length of the tour of TSP considering the squares of the distances between cities. Thus the Kohonen algorithm for TSP minimizes an energy function which, at the end of the leaning process, is proportional to the sum of the squares of the distances. Numerical simulations confirm this result.

3 A New Distance Function

Our hypothesis is that we can obtain better results for the TSP using a distance function h_{rs} such that, at the end of the process, $V(W)$ is proportional to the simple length of the tour L_{TSP}, namely $V(W) \propto \sum_s(\vec{q}_{i(s)} - \vec{q}_{i(s-1)}) = L_{TSP}$ since, in general, minimizing L_{TSP^2} is not equivalent to minimizing L_{TSP}. We thus consider

[1]The main weakness of this algorithm is that, in about half of the cases, the map produced is not injective. The definition of a continuous coordinate along the neuron ring solves this problem yielding a competitive algorithm [Budinich 1995].

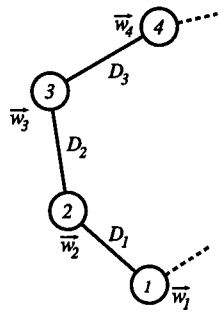

Figure 3 Distances between neurons $s = 4$ and $r = 1$: $D_{1,4} = D_1 + D_2 + D_3$ and $d_{1,4} = 3$.

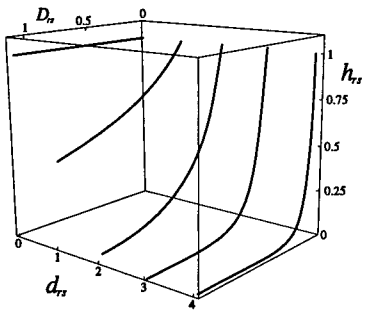

Figure 4 Set of h_{is} given by (5) for $0 < D_{is} < 1$ and $d_{is} = 0, 1, \ldots, 4$.

a function h_{rs} depending both on the distance d_{rs} and on another distance D_{rs} defined in weight space:

$$D_{rs} = \sum_{j=r+1}^{3} |\vec{w}_j - \vec{w}_{j-1}|$$

If we define

$$h_{rs} = \left(1 + \frac{D_{rs}}{\sigma}\right)^{-d_{rs}^2} \tag{5}$$

when $\sigma \to 0$, we get for $h_{s\pm1,s}$

$$h_{s\pm1,s} = \left(1 + \frac{D_{s\pm1,s}}{\sigma}\right)^{-1} \cong \frac{\sigma}{D_{s\pm1,s}} = \frac{\sigma}{|\vec{w}_s - \vec{w}_{s\pm1}|} \cong \frac{\sigma}{|\vec{q}_{i(s)} - \vec{q}_{i(s\pm1)}|}$$

and substituting this expression in (4) we obtain $V(W)$

$$\begin{aligned} &\cong \frac{1}{2N} \sum_s \left[\frac{\sigma}{|\vec{q}_{i(s)} - \vec{q}_{i(s-1)}|} (\vec{q}_{i(s)} - \vec{q}_{i(s-1)})^2 + \frac{\sigma}{|\vec{q}_{i(s)} - \vec{q}_{i(s+1)}|} (\vec{q}_{i(s)} - \vec{q}_{i(s+1)})^2 \right] \\ &= \frac{\sigma}{N} \sum_s |\vec{q}_{i(s)} - \vec{q}_{i(s+1)}| \\ &= \frac{\sigma}{N} L_{TSP} \end{aligned}$$

With this choice of h_{rs} the minimization of the energy $V(W)$ is equivalent to the minimization of the TSP path. We remark that the introduction of the distance D_{rs} between weights is a slightly unusual hypothesis for this kind of nets that usually keep well separated neuron and weight spaces in the sense that the distance function h_{rs} depends only on the distance d_{rs}.

4 Numerical Results

Since the performances of this kind of TSP algorithms are good for problems with more than 500 cities and more critical in smaller problems [Budinich 1995], we began testing the performances produced by the new distance function (5) in problems with 50 cities.

City set	Min. length	[Durbin 1987]	[Budinich 1995]	This algorithm
1	5.8358	2.47%	1.65%	0.96%
2	5.9945	0.59%	1.66%	0.31%
3	5.5749	2.24%	1.06%	1.05%
4	5.6978	2.85%	1.37%	0.70%
5	6.1673	5.23%	5.25%	0.43%
Average		2.68%	2.20%	0.69%

Table 1 Comparison of the best TSP solution obtained in 10 runs of the various algorithms. Rows refer to the 5 different problems each of 50 cities randomly distributed in the (0,1) square. Column 2 reports the length of the best known solution for the given problem. Columns 3 to 5 contain the best lengths obtained by the three algorithms under study expressed as percentual increments from the minimal length; the number of runs of the algorithms is respectively: unknown, 5 and 10. Last row gives the increment averaged over the 5 city sets.

We compared the quality of TSP solutions obtained with this net to those of two other algorithms both deriving from the idea of a topology preserving map and that both actually minimizes L_{TSP^2} : the elastic net of Durbin and Willshaw [Durbin 1987] and this same algorithm with a standard distance choice.
As a test set, we considered the very same 5 sets of 50 randomly distributed cities used for the elastic net.
Table 1 contains a comparison of the best TSP path obtained in several runs of the different algorithms expressed as percentual increments over the best known solution for the given problem. Another measure of the quality of the solution is the mean length obtained in the 10 runs. The percentual increment of these mean lengths, averaged over the 5 sets, was for this algorithm 2.49%, showing that even the averages found with the new distance function are better than the minima found with the elastic net.
These results clearly show that distance choice (5) gives better solutions in this SOFM application, thus supporting the guess that an energy $V(W)$ directly proportional to the length of the tour L_{TSP}, is better tuned to this problem.
One could wonder if adding weight space information to the distance function could give interesting results also in other SOFM applications.

Appendix

Here we describe the network setting that produces the quoted numerical results. Apart from the distance definition (5) we apply a standard Kohonen algorithm and exponentially decrease parameters ϵ and σ with learning epoch n_e (a learning epoch corresponds to N weights update with rule (1))

$$\epsilon = \epsilon_0 \alpha^{n_e} \qquad \sigma = \sigma_0 \beta^{n_e}$$

and learning stops when ϵ reaches $5 \cdot 10^{-3}$. Numerical simulations clearly indicate that best results are obtained when the final value of σ is very small ($\approx 5 \cdot 10^{-3}$) and when ϵ and σ decrease together reaching their final value at the same time. Consequently given values for α and σ_0 one easily finds β. In other words there are just three free parameters to play with to optimize results, namely ϵ_0 and σ_0 and α.

After some investigation we obtained the following values that produce the quoted results: $\epsilon_0 = 0.8$, $\sigma_0 = 14$ and $\alpha = 0.9996$.

REFERENCES

[1] B Angeniol, de G. La Croix Vaubois and J.-Y. Le Texier, *Self Organising Feature Maps and the Travelling Salesman Problem*, Neural Networks Vol.1 (1988), pp289–293.

[2] M Budinich, *A Self-Organising Neural Network for the Travelling Salesman Problem that is Competitive with Simulated Annealing*, to appear in: Neural Computation.

[3] R. Durbin and D. Willshaw, *An Analogue Approach to the Travelling Salesman Problem using an Elastic Net Method*, Nature Vol.336 (1987), pp689–691.

[4] F Favata amd R Walker. *A Study of the Application of Kohonen-type Neural Networks to the Travelling Salesman Problem*, Biological Cybernetics Vol. 64 (1991), pp463–468.

[5] D. S. Johnson, *Local Optimization and the Traveling Salesman Problem*, in: Proceedings of the 17th Colloquium on Automata, Languages and Programming, Springer-Verlag (1990) New York, pp446–461.

[6] T. Kohonen, *Self-Organisation and Associative Memory*, Springer-Verlag (1984, 3rd Ed. 1989), Berlin Heidelberg.

[7] E. L. Lawler, J. K. Lenstra , A. G. Rinnoy Kan and D. B. Shmoys (editors), *The Traveling Salesman Problem — A Guided Tour of Combinatorial Optimization*, John Wiley & Sons, New York (1990), IV Reprint, p474.

[8] H. Ritter, T. Martinez and K. Schultern, *Neural Computation and Self Organising Maps*, Addison-Wesley Publishing Company (1992), Reading Massachusetts , p306.

SEMIPARAMETRIC ARTIFICIAL NEURAL NETWORKS

Enrico Capobianco
Stanford University, Stanford, CA 94305, USA.
Email: enrico@psych.stanford.edu

In this paper Artificial Neural Networks are considered as an example of the semiparametric class of models which has become very popular among statisticians and econometricians in recent years. Modelling and learning aspects are discussed. Some statistical procedures are described in order to learn with infinite-dimensional nuisance parameters, and adaptive estimators are presented.

Keywords: Semiparametric Artificial Neural Networks; Profile Likelihood; Efficiency Bounds; Asymptotic Adaptive Estimators

1 Introduction

We look at the interface between statistics and artificial neural networks (ANN) and study stochastic multilayer neural networks with unspecified functional components. We call them **Semiparametric Neural Networks** (SNN). The fact that no absolute requirements come from biological considerations represents an important motivation for SNN. Many technical issues arise from the statistical inference perspective; we (**A**) stress the importance of computing likelihood-based criterion functions in order to exploit the large sample statistical properties pertaining to the related estimators and (**B**) measure the asymptotic efficiency of the estimators from given network architectures.

2 ANN and Likelihood Theory

A stochastic machine with a vector of synaptic weights w, the input(output) vectors $x(y)$ (given a conditional density function $f(y/x)$) and the data set dimension T, is used to compute w through a learning algorithm based on the minimization of some fitting criterion function of estimated residuals or prediction errors. Consider a likelihood function $L(Y,\theta)$, where $Y = (y_1,\ldots,y_T)'$ is the sample observation vector and $\theta = (\theta_1,\ldots,\theta_p)'$ is a vector of parameters. These three elements can fully characterize a taxonomy of models, differentiated by the sample size and the dimension of the parameter space where the optimization of the chosen criterion function must be done. For instance, in a network where all the activation functions are specified and the dimension of θ is $p < \infty$, i.e., in a fully parametric situation, the solution to the optimization problem is to maximize $l = \sum_{i=1}^{T} lnL(y_i,\theta)$ over the weight space Θ. On the other hand, the activation functions can be reasonably left unspecified, apart from some smoothness conditions. This choice permits a shift from a parametric to a more nonparametric setting, where the likelihood function now admits a modified form $L(Y,\lambda)$, with $\lambda = (w,g,h)$ and w,g,h that indicate respectively the weight vector, the unknown output and hidden layer activation functions. A more restricted context, but still semiparametric in nature, occurs when g or h are in fact specified; networks here closely resemble the semiparametric and nonparametric extensions of the Generalized Linear Models [7] described in [6]. As a result, the likelihood function is now more constrained, with $L(Y,\delta)$ and $\delta = (w,g,\bar{h})$ or $\delta = (w,\bar{g},h)$. If a stochastic one-hidden layer feedforward neural

network is represented by:

$$y = G(x, w) = F[\gamma_0 + \sum_{j=1}^{q} \alpha_j f(\gamma_j + \sum_{i=1}^{s} v_{ij} x_i)] \quad (1)$$

where $w = (\alpha', v', \gamma')'$ is the vector of weights and F/f are the specified output/hidden layer activation functions, then a likelihood-based criterion function, under a gaussian distribution of p(y/x,w), is directly related to the sum-of-squared errors scaled by the output variance. For $F(z) = z$, we have that:

$$max \ \sum_t lnp(y_t/x_t, w) \equiv \ min \ \frac{1}{2} \sum_t \frac{1}{\sigma_t^2} (y_t - G(x_t, w))^2 \quad (2)$$

Whenever Gaussianity is assumed but not verified, a **quasi-maximum likelihood** criterion is given. Conditionally gaussian time series models are specified in terms of a gaussian distribution for y_t, conditioned on the information available at time t-1; here too a likelihood function can be computed and thus (2) holds[1]. When the likelihood function relies on unknown components we deal with an ill-posed optimization problem and some form of regularization is required. If the entire parameter vector can be decomposed in "interest" w and "nuisance" η components, such that $\hat{\theta} = (\hat{w}, \hat{\eta})$ represents the ML estimator of θ, $\tilde{\theta}(w) = (w, \tilde{\eta}_{\bar{w}})$ is a constrained initial estimator for θ, i.e., an estimator computed from an initially fixed value of the parameters of interest, not necessarily a ML value. Inference for w can be based on the so-called **profile** or **concentrated** log-likelihood function $PL(w) = L(\tilde{\theta}(w))$. We seek the value w^* which maximizes PL(w); it is $w^* = \hat{w}$, at least for the case of a finite dimensional nuisance parameter space. In other words, a ML estimate is computed in two sequential stages: (1) an estimate is obtained for η, given an initial consistent value of w; (2) the MLE for w conditional to $\tilde{\eta}_{\bar{w}}$ is calculated by maximizing a likelihood-based criterion function where the previous estimate of η has been plugged-in. Hence the name profile log-likelihood.

3 The Semiparametric Approach to ANN

The bias/variance dilemma [4] is crucial in ANN as it is in nonparametric statistical inference. If the relation between the input and the output variables is unknown, as for the function $E(y_t/\mathcal{F}_t)$ in nonlinear regression or $E(y_t/\mathcal{Y}_{t-1})$ in time series prediction problems [2] ANN will try to exploit their "universal approximation" properties. But whereas parametric and potentially incorrect models lead to high bias, nonparametric models lead to high variance, given the presence of parameters of infinite dimension; therefore, the loss of efficiency is a likely price to pay. We usually observe noisy input data, according to some underlying probability distribution; thus, for some aspects, the advantage is that data could be replicated under certain conditions that offer a solution for the data-size constraint and thus soften

[1] The normalized mean squared error [12] cost function $E = \frac{1}{T\hat{\sigma}_T^2} \sum_t (y_t - \hat{y}_t)^2$ can also be used. Otherwise, the likelihood can be formed in terms of the prediction errors $v_t = y_t - E(y_t/y_{t-1}, \ldots, y_1)$, given that $var(v_t) = var(y_t/y_{t-1}, \ldots, y_1)$. Moreover, the $\hat{w}$ value that minimizes $\frac{1}{T} \sum_t (y_t - G(x_t, w))^2$ is equivalent to the NLS estimator [13] and this converges to the network optimal weights w^* as $n \to \infty$.

[2] $\mathcal{F}_t$ or $\mathcal{Y}_{t-1}$ represent information up to the time t or t-1 (lags only included for $\mathcal{Y}_{t-1}$).

the "curse of dimensionality"[3].

An important aspect in SNN is related to the functional form of the I/O relation. The approximation ability of the network depends on the characteristics of the underlying functional relation; usually sigmoidal-type or RBF-type ANN work well, but when the activation functions are left unspecified, projection pursuit regression [3] and other highly parameterized techniques represent possible solutions. We consider pure minimization and iterative estimation strategies; the former are based on the decomposition of the parameter vector, $\theta = (w, \eta)$, where w represents the weights and the bias terms considered together and η represents the infinite-dimensional nuisance parameter[4], and the latter are **Newton-Raphson** (NR)-type procedures. We address the optimization problem in the Profile ML setting introduced before. But another challenging issue is the weight estimation accuracy, at least asymptotically. By working with an initially unrestricted likelihood-based performance measure we would like to obtain, in statistical terms, a lower bound [8, 9, 10] for the asymptotic variance (AV) of the parametric component of the semiparametric model such that we are able to generalize the usual parametric bound given by the inverse of the **Fisher Information Matrix** (FIM). We equivalently calculate the **Semiparametric Efficiency Bounds** (SEB) for the parameters of interest, which quantify the efficiency loss resulting from a semiparametric model compared to a parametric one[5].

4 Parametric and Nonparametric Estimation Theory

The discussion here draws mainly on [8], [10] and [11], where the concept of marginal Fisher's bound for asymptotic variances in parametric models is generalized. If it is true that *a nonparametric problem is at least as difficult as any of the parametric problems obtained by assuming we have enough knowledge of the unknown state of nature to restrict it to a finite dimensional set*, it is important to look for a method that obtains a lower bound for the AV of the parametric component of the initially unrestricted model[6]. Since a one-dimensional sub-problem asymptotically as difficult as the original multidimensional problem often exists, *we could express the parameter space as a union* of these one-dimensional sub-problems (paths or directions along w, like $F_w : F_w \in \mathcal{F}$) and estimate the parameter of interest *to select one of the sub-problems proceeding as if the true parameter would lay on this curve.* The question is: which sub-problem should be selected? First, we should verify the existence of an estimator for a " curve " defined in the infinite-dimensional nuisance parameter space, corresponding to one of the possible one-dimensional

[3]These distributional assumptions make a substantial difference in terms of the **global or local statistical efficiency** that an estimator can achieve. While for global efficiency we mean that an estimator is accurate regardless of the true underlying distributions, for local efficiency the same holds only for some specific distributions related to the nonparametric component of the model.

[4]η can stand for the unknown hidden layer activation functions, the noise density which randomly perturbs the input/output pattern data, the weights or even the same activation functions.

[5]In the ANN context we could make comparisons between SNN and sigmoidal-type or other networks on the grounds of the statistical efficiency of the related learning algorithms.

[6]If a sequence of estimators (θ_n) satisfies $\sqrt{n}(\theta_n - \theta) \rightarrow_d N(0, V)$, then V is the asymptotic variance of (θ_n) and for the ML estimator, under regular conditions, equals I_θ^{-1}, where I_θ is the FIM.

sub-problems. Given $\theta = (w, \eta)$, consider the smooth curve $\theta(t) : \ a < t < b$ designed in the space $W \times \Upsilon$ by the map $t \rightarrow \theta(t) = (w(t), \eta(t))$. According to a possible parameterization inducted by $w(t) = t$, the map becomes $w \rightarrow (w, \eta_w)$ with $\eta_{w_0} = \eta_0$ and for each curve η_w we can compute the associated score functions U_w,U_η such that, $\frac{d}{dw} l(w, \eta_w) \ |_{w=w_0} = \frac{\partial l}{\partial w}(w_0, \eta_0) + \frac{\partial l}{\partial \eta}(w_0, \eta_0)(\frac{d}{dw}\eta_w \ |_{w=w_0})$ (or simply $U_w + U_\eta$) and the information matrix $E_0(\frac{d}{dw} l(w, \eta_w) \ |_{w=w_0})^2 = E(U_w + U)^2$, where $U \in span(U_\eta)$. Repeating the procedure for all the possible η_w we can find the minimum FIM, which is given by $inf(E_0(U_w + U)^2 = E_0(U_w + U^*) = i_w$, where U^* is the projection of U_w onto $span(U_\eta)$. In particular, we define the curve η_w^* for which this minimum is achieved as the **Least Favorable Curve** (LFC). With a semiparametric model, in order for η_w^* to be LFC, the following relation must be satisfied:

$$E([\frac{\partial l(w, \eta_w^*)}{\partial w}] \ |_{w=w_0})^2 \leq E([\frac{\partial l(w, \eta_w)}{\partial w}] \ |_{w=w_0})^2 \tag{3}$$

for each curve $w \rightarrow \eta_w$ in the nuisance functional space Υ[7]. Following the parametric case, the marginal FIM for w in a semiparametric model is given by:

$$i_w = inf_\eta E([\frac{\partial l(w, \eta_w)}{\partial w}] \ |_{w=w_0})^2 \tag{4}$$

or alternatively $i_w = E_0(U_w + U_\eta^*)$, with $U_\eta^* = \frac{\partial}{\partial \eta} \dot{l}(w_0, \eta_0)(t^*))^2$, where $t^* \in \Upsilon$ represents the tangent vector to the curve η_w at w_0 and $\frac{\partial \dot{l}}{\partial \eta}$ is a Frechet derivative[8]. Now, $i_w^{-1} = V$ is the lower bound for the AV of a regular[9] estimator of w in the semiparametric model. In summary, every semiparametric estimator has an AV comparable to the Cramer-Rao bound of a semiparametric model; therefore, the bound is not less than the bound of every parametric sub-model, i.e. the *sup* V of all these bounds. This is the semiparametric AV bound or SEB, whose attainment reflects the ability to estimate adaptively.

5 Adaptive Estimation

In practice, accurate estimation and unrestricted model specification can be contrasting aspects of a problem. Adaptive estimation is a solution since it suggests that full efficiency can still be attained even under an initially unrestricted model[10]. A pure minimization method for adaptively estimating semiparametric models is the one described in Section 2 and adopted in [10], the **Generalized Profile Likelihood** (GPL)[11]. For a regular estimator the **convolution theorem** [2] applies,

[7] In practice [10] for a nonparametric regression or density estimation problem $\hat{\eta}_w$ often converges to the LFC; otherwise, we could verify that its limit is such that a least favorable direction is found.

[8] We say that T is *Frechet differentiable* at x if there exists a function $\dot{T}_x : X \rightarrow Y$ which is linear and continuous such that $lim_{|h| \rightarrow 0} \frac{||T(x+h) - T(x) - \dot{T}_x(h)||}{||h||} = 0$ (see [2]).

[9] Given a local DGP, i.e. a stochastic process where for every sample size n the data are distributed according to θ_n, with $\sqrt{n}(\theta_n - \theta_0)$ bounded, an estimator $W \subset \Theta$ is called **regular in a parametric sub-model** if, for each true value θ_0 of the parameter vector, $\sqrt{n}(\hat{w} - w(\theta_n))$ has a limit distribution not dependent on the local DGP and **regular** if the property holds for every parametric sub-model.

[10] An adaptive estimator can be found to exist or not. In any case, the model is required to satisfy conditions related more to the underlying structure or functional relations than to the possible adaptive estimation procedures [9].

[11] Generalized because the first step estimator for the nuisance parameter vector is not required to be an ML estimator.

thus giving an asymptotic distribution for $\sqrt{n}(\hat{w}-w_0)$ equal to that of Z+U, where $Z \sim N(0,V)$ and U an independent noise; V is the SEB, as shown when U is gaussian and thus $Var(\hat{w}) = V + E(UU') >> V$. If η_w is a curve in Υ, we require that the estimator $\hat{w}$ obtained by maximizing $l(w, \tilde{\eta}_{\bar{w}})$ has an asymptotic distribution as the one of the estimator obtained by $l(w, \eta_w)$, or equivalently we require that the two functions have the same local behavior; then, the SEB should be attained. If $\hat{w}$ is the maximizer of $l(w, \tilde{\eta}_{\bar{w}})$, then $\sqrt{n}(\hat{w} - w_0) \rightarrow_D N(0, i_w^{-1})$ is expected, because when η_w is LFC the bias disappears asymptotically, due to the orthogonality of the score functions. Thus, under some regularity conditions, an estimator for w can be obtained by maximizing the GPL criterion function and the estimator is asymptotically efficient. The value of the SEB is given by the inverse of:

$$\hat{i}_w = -\frac{1}{n}[\frac{\partial^2 l(w, \tilde{\eta}_{\bar{w}})}{\partial w' \partial w}] \mid_{w=\hat{w}} \tag{5}$$

5.1 The Algorithm Applied to ANN; an Example

Consider the example in [1]: suppose we have a stochastic machine with an input vector $x \subset R^s$, a p-dimensional weight vector w and the binary output is $y = \pm 1$ according to p(y/x,w), where $p(y = 1/x, w) = k[f(x, w)]$ and $p(y = -1/x, w) = 1 - k[f(x, w)]$, $k(f) = \frac{1}{1+e^{-\beta f}}$, β is the inverse of the so-called temperature parameter and f represents a smooth hidden layer activation function (therefore our nuisance parameters). The general form of the conditional log-likelihood function $l(y/x, w) = lnp(y/x, w)$ is $\mathcal{L} = \sum_i [y_i \ln D(w)] + (1 - y_i) \ln[(1 - D(w))]$, where $D(w) = k[f(x_i, w)]$. According to the GPL procedure, we *(1) estimate initially w via BP with a network of fixed structure (i.e. f represented with one of the usually specified forms) (2) obtain a nonparametric estimate $\hat{f}$ conditionally on the estimated w, thus finding $\hat{D}$ (3) plug in $\hat{f}_{\bar{w}}$ and maximize the GPL criterion function w.r.t. w (where $\hat{D}$ in fact replaces D^* which represents an estimable and locally approximating version of the unknown function D) (Δ) calculate $\hat{w}$ and repeat steps 2-3-4 till we go as close as possible to the SEB*[12]. Thus the stochastic machine specifies the probabilities $p(y = \pm 1/x, w)$.

5.2 Relationships between GPL and Learning Consolidation

When fully iterative algorithms are considered, **consolidation of network learning** proposed in [13] becomes important, since BP is only one of the possible **recursive m-estimators** that locally solve optimization problems and is asymptotically inefficient relative to a NR-type estimator, regardless of the local minimizer. Thus, BP can be improved with regard to the accuracy of the estimate through just one NR step. In [8] one-step *semiparametric m-estimators* are considered[13]; they are based on the zero mean and finite variance *influence function* (IF) $\psi(z)$ of a single observation on the estimator, such that $\sqrt{n}(\hat{\phi} - \phi) = \sum_i \frac{\psi_i}{\sqrt{n}} + o_p(1)$, and they

[12]Note that (A) $\hat{w}(\hat{D})$ that maximizes $L(\hat{D}(w))$ should behave like $\hat{w}(D)$, where $\hat{w}(D) = argsup_w L(D(w))$ (a consistent estimator is required, given that $L(\hat{D}(w) \rightarrow_{pr} L(D(w))$ uniformly in w) (B) given $AV = \frac{1}{G}$, where according to [1] $G = (g_{ij})$ is the FIM and $g_{ij} = \beta^2 \int \sum_y k(1-k) \frac{\partial f}{\partial w_i} \frac{\partial f}{\partial w_j} p(x) dx$ is the generic component of G, we must compare AV with the inverse of (5).

[13]These estimators are asymptotically efficient after one iteration from a consistent initial estimate of the parameter of interest and with the functions of the likelihood consistently estimated.

solve moment equations of the form $\frac{\sum_i m(z_i,\phi,\hat{\eta})}{n} = 0$, given a general interest parameter ϕ. The m(.) function, similar to the *estimating functions* adopted in [5], can represent the *First Order Conditions* for the *maximum* of a criterion function Q, and η maximizes the expected value of the same function. This method is equivalent to GPL when f is the density from a given distribution function F, Q is the log-likelihood function, m(.) the score function and $\eta(\phi, F)$ is the limit, for the nonparametric component, that maximizes the expected value of $lnf(z/\phi,\eta)$. With $\hat{\phi} = argmax_\phi \sum_i lnf(z_i/\phi, \tilde{\eta}_{\tilde{\phi}})$ as the GP(Max)L estimator, where the estimation of η does not affect the AV, and given $M = \frac{\partial E(m(z,\phi,\eta_0))}{\partial \phi} \mid_{\phi=\phi_0}$ nonsingular, we have $\psi(z) = M^{-1}m(z,\phi,\eta_0)$ and $\dot{\phi} = \hat{\phi} + \frac{\sum_i \hat{\psi}(z_i,\hat{\phi})}{n}$, which is the one-step version of GP(Max)L estimator.

6 Conclusions

We analyzed semiparametric neural networks, described a general model set-up and discussed the related asymptotic estimation issues. The degree of success in solving the bias/variance dilemma is often a case-dependent problem requiring a reparameterization of the model in the hope of finding adaptive estimators. SEB tell us about the asymptotic statistical efficiency of the chosen estimator.

REFERENCES

[1] S.Amari and N.Murata, Statistical *Theory of Learning Curves under Entropic Loss Criterion*, Neural Comput., Vol.5 (1993), pp140–153.

[2] P.Bickel, C.A.J.Klaassen, Y.Ritov and J.A.Wellner, *Efficient and Adaptive Estimation of Semiparametric Models*. The John Hopkins University Press (1993).

[3] J.H.Friedman and W.Stuetzle, *Projection Pursuit Regression*, JASA, Vol. 76 (1981), pp817–823.

[4] S.Geman, E.Bienenstock and R.Doursat, *Neural Networks and the bias/variance dilemma*, Neural Comput., Vol. 4 (1992), pp1–58.

[5] M.Kawanabe and S.Amari, *Estimation of networks parameters in semiparametric stochastic perceptron*, Neural Comput., Vol. 6 (1994), pp1244–1261.

[6] P.A.Jokinen, *A nonlinear network model for continuous learning*, Neurocomp., Vol. 3 (1991), pp157–176.

[7] R.McCullagh and J.A.Nelder, *Generalized Linear Models*, Chapman and Hall (1989).

[8] W.K.Newey, *Semiparametric efficiency bounds*, J. Appl. Ec.trics, Vol. 5 (1990), pp99–135.

[9] W.K.Newey, *The asymptotic variance of semiparametric estimators*, Econometrica, Vol.62 (1994), pp1349–1382.

[10] T. Severini and W.H. Wong, *Profile likelihood and conditionally parametric models*, An. Stat., Vol. 20 (1992), pp1768–1802.

[11] C. Stein, *Efficient nonparametric testing and estimation*, in: Proceedings Third Berkeley Symposium in Mathematics, Statistics and Probability, University of California Press, Berkeley, (1956) Vol. 1, pp187–196.

[12] A.S.Weigend and N.A.Gershenfeld, *Time series prediction: forecasting the future and understanding the past*, Santa Fe, Proc. Vol. XV (1994), Addison-Wesley.

[13] H. White, *Artificial Neural Networks. Approximation and learning theory*, Blackwell, (1992).

Acknowledgements

The author thanks two anonymous referees for their suggestions.

AN EVENT-SPACE FEEDFORWARD NETWORK USING MAXIMUM ENTROPY PARTITIONING WITH APPLICATION TO LOW LEVEL SPEECH DATA

D.K.Y. Chiu, D. Bockus and J. Bradford*

University of Guelph, Ontario, Canada.

** Brock University, St. Catharines, Ontario, Canada.*

This paper describes an event-space feedforward network based on partitioning of the input space using maximum entropy criterion. It shows how primitives defined as partitioned hypercells (event space) can be selected for the purpose of class discrimination. Class discrimination of a hypercell is evaluated statistically. Observed primitives corresponding to observed characteristics in selected hypercells are used as inputs to a feedforward network in classification. Preliminary experimental results using simulated data and as it pertains to speaker discrimination using low-level speech data have shown very good classification rates.

1 Introduction

This paper proposes a feedforward network whose input layer is reconfigured during the training phase depending on the generation and selection of newly defined primitives. As the primitives are identified through partitioning of the input outcome space, so would the construction of the input nodes which corresponds to defining the primitive set. The primitives are defined through the selection of partitioned hypercells corresponding to certain feature values of the data selected for classification. Thus, an observed primitive in a datum would correspond to an observed selected characteristic (or range of values) which eventually determine the datum's classification. Since the input layer in the network is reconfigured depending on the selected hypercells identified, we call it a self-configurable neural network [2]. The two processes of primitive generation and classification are integrated and "closely coupled".

2 Maximum Entropy Partitioning

When discretizing the outcome space based on partitioning of the data, the discretization process becomes a partitioning process. The Maximum Entropy Partitioning (MEP) process generates a set of hypercells through partitioning of the outcome space of n continuous valued variables (or features) [1,3,4,7]. This method bypasses the problem of non-uniform scaling for different variables in multivariate datum compared to the commonly used equal-width partitioning algorithm, and minimizes the information loss after partitioning [3].

Given n variables in n-dimensional space, the MEP process partitions a data set into k^n hypercells based on the estimated probabilities of the data. The value k represents the number of intervals that a dimension is divided into. Let P be the probability distribution where the process produces a quantization of P into:

$$P(R_i), i = 1, 2, \ldots, k^n, \tag{1}$$

where R_i denotes a hypercell. To maximize the information represented by R_i, the partitioning scheme which maximizes Shannon's entropy function defined below is

used:

$$H(R) = -\sum_{i=1}^{k^n} P(R_i) \log P(R_i). \tag{2}$$

The function $H(R)$ now becomes the objective function where information can be maximized according to the maximization of $H(R)$. With one variable, maximization occurs when the expected probability $P(R_i)$ is approximately $1/k$ of the training data with repeated observations. This creates a narrower interval where the probability density is higher [3]. In the proposed method, the partitioning process is done based on the marginal probability distribution on each variable to avoid combinatorial complexity.

In our data representation (such as low-level speech data), the jth datum is represented by a set of $I(j)$ points which are denoted by $Z_j = \{x_i = (x_{1i}, x_{2i}, ..., x_{ni}) | i = 1, ..., I(j)\}$. That is, Z_j composes of sets of n-vectors. A set of partition boundaries are determined by combining all the data into a single set that we call the "data universe" denoted by U. Hence, U is defined as the union of all the training data:

$$U = \{Z_j | j = 1, \ldots, J\} = Z_1 \cup Z_2 \cup \cdots \cup Z_J \tag{3}$$

Each data is assumed to have an assigned class label C_m in L_c classes, $1 \leq m \leq L_c$. In n-dimensional space, the set of hypercells generated after partitioning is then defined as $R = \{R_i | i = 1, 2, ..., k^n\}$, where each R_i is bounded by intervals that partition the data universe. The intervals that bound R_i are composed of the boundary points which will be determined by an algorithm [3].

3 Selection of the Partitioned Hypercells

Representation of individual datum Z_j is based on the same partitioning scheme generated from partitioning the data universe. Each generated hypercells from the partitioning cordons off a set of points in Z_j. Since our partitioning is based on the marginal probability distributions, a hypercell R_i on datum Z_j that has significantly more points than expected can be evaluated using the following statistic also known as the standard residual [5]:

$$D(R_i, Z_j) = \frac{\text{obs}(R_i, Z_j) - \exp(R_i, Z_j)}{\sqrt{\exp(R_i, Z_j)}} \tag{4}$$

where $\exp(R_i, Z_j)$ is defined as the average number of points observed in a hypercell R_i, calculated as $M(Z_j)/k^n$, and $\text{obs}(R_i, Z_j)$ is the number of points in Z_j observed in the same hypercell, given that $M(Z_j)$ is the total number of points in Z_j. Since the statistic follows a normal distribution, it is therefore possible to evaluate a hypercell which has significant characteristic in the data, based on the normal distribution according to a confidence level. If the expected value calculated using the null hypothesis so that each hypercell has equal probability of occurrence, then this equation has the properties of an approximate normal distribution with a mean of 0 and a variance of 1. In cases where the asymptotic variance differs from 1, then an adjustment to the standard residual is required in order to yield better approximations [5]. The significance of a hypercell is determined by comparing $D(R_i, Z_j)$ to the tabulated z-values of a predefined confidence level using the standard normal distribution. That is, the hypercell R_i is selected as significant based on:

$$\delta(R_i, Z_j) = \begin{cases} 1 & D(R_i, Z_j) \geq z \\ 0 & \text{otherwise} \end{cases} \tag{5}$$

where z is the tabulated z-value of a certain degree of confidence level.
As each datum is partitioned using the same scheme generated from partitioning the data universe, the number of data Z_j with significant $D(R_i, Z_j)$ (or $\delta(R_i, Z_j) = 1$) and class label C_m is denoted as $\eta(R_i, C_m)$, (or $\eta(R_i, C_m) = \sum_{Z_j} \delta(R_i, Z_j)$ for $Z_j \in C_m$). Let $e(R_i)$ be the average number of data per class whose hypercell R_i is significant, or:

$$e(R_i) = \frac{\sum_{m=1}^{L_c} \eta(R_i, C_m)}{L_c}, \quad \forall Z_j \in U \tag{6}$$

and let

$$\theta(R_i) = \sum_{m=1}^{L_c} \frac{[\eta(R_i, C_m) - e(R_i)]^2}{e(R_i)}, \quad \forall Z_j \in U \tag{7}$$

reflects the extent of class discrimination for a hypercell R_i in the data universe. Since $\theta(R_i)$ has an asymptotic Chi-square distribution, the relevance of a hypercell can be evaluated by applying the Chi-square test. After $\theta(R_i)$ is calculated, it is compared to a tabulated χ^2 value with $L_c - 1$ degrees of freedom based on a presumed confidence level. The function described in equation (3.5) indicates the hypercell's statistical relevance for class discrimination:

$$\beta(R_i) = \begin{cases} 1 & \text{if } \theta(R_i) \geq \chi^2_{L_c - 1} \\ 0 & \text{otherwise} \end{cases} \tag{8}$$

Hypercells that are not identified as statistically relevant are partitioned further, using the same criterion of maximum entropy, until there exists an insufficient number of points, or a predefined depth has been reached. We call this method hierarchical maximum entropy partitioning [1,3]. The rationale of using partitioning iteratively is to identify useful characteristics at a more restricted interval when relevant characteristic is not found at a larger interval. The hypercells that surpass the threshold value are marked as having an acceptable degree of class discrimination with $\beta(R_i) = 1$, and these selected hypercells can be relabeled as $\{R_s^*\}$ indicated by the superscript. The set $\{R_S^*\}$ corresponds to the set of input nodes in the feedforward network. When labeled, as $(R_1^*, R_2^*, \ldots, R_S^*)$, they correspond to a set of data value characteristics that are selected to have acceptable class discrimination information.

4 Self Configurable Event-Space Feedforward Network

The number of inputs to the feedforward network depends on the number of iterations and selected hypercells. As more iterations of the partitioning process are performed, then more hypercells are generated and identified as statistically relevant. This is analogous to the use of more refined characteristics of the data for class discrimination if sampling reliability is not a concern.
Given a datum Z_j and the generated hypercell R_S^*. Let $\text{obs}(R_S^*, Z_j)$ be the number of points Z_j has in R_S^*, $\exp(R_S^*, Z_j) = M(Z_j)/k^n$ be the expected average number of points, where $M(Z_j)$ is the total number of points in Z_j. Substituting $\text{obs}(R_S^*, Z_j)$ and $\exp(R_S^*, Z_j)$ into equation (4), we calculate the statistic for Z_j, denoted as $D(R_S^*, Z_j)$. Define a binary decision function for all the selected hypercells $\{R_S^*\}$ for Z_j as:

$$\alpha(R_s^*, Z_j) = \begin{cases} 1 & \text{if } D(R_s^*, Z_j) \geq z \\ 0 & \text{otherwise} \end{cases} \tag{9}$$

where z is a tabulated z-value for a given confidence level. Then Z_j is represented by a vector as:

$$W_j = (\alpha(R_1^*, Z_j)\theta(R_1^*), \alpha(R_2^*, Z_j)\theta(R_2^*), \ldots \alpha(R_s^*, Z_j)\theta(R_s^*),) \quad (10)$$

where $\alpha(R_s^*, Z_j)$ indicates whether a selected characteristic is observed in Z_j , that is, a selected primitive is observed, and $\theta(R_s^*)$ is the estimated relevance of R_s^* based on the analysis from the data universe.

A binary vector V_j can be used as an approximation to W_j, for each data where simplicity of inputs is desired. It is defined as:

$$V_j = (\alpha(R_1^*, Z_j)\beta(R_1^*), \alpha(R_2^*, Z_j)\beta(R_2^*), \ldots \alpha(R_s^*, Z_j)\beta(R_s^*),) \quad (11)$$

Each component $\alpha(R_i^*, Z_j)\beta(R_s^*)$ is the product of $\alpha(R_i^*, Z_j)$ which identifies significant characteristics in the data Z_j, and $\beta(R_s^*)$, which identifies the hypercells (or primitives) based on the data universe. In other words, a component is 1 only if the primitive is statistically significant in Z_j, and statistically discriminating in U.

This approximation does not provide the detailed information contribution to the class discrimination as does the W_j vector. However, V_j usually provides faster training times with additional analysis information. $\beta(R_i^*)$ is defined as a binary element in the vector V_j and is always equal to 1 for the selected hypercells. The $\beta(R_i^*)$ value replaces $\theta(R_i^*)$ in equation (10) so that it is now represented by a 1, thus V_j is rewritten as:

$$V_j = (\alpha(R_1^*, Z_j), \alpha(R_2^*, Z_j), \ldots \alpha(R_S^*, Z_j),) \quad (12)$$

5 Training and Classification of the Network

A network can be trained using the standard back-propagation algorithm with the supervised class label for each datum where the vector W_j or V_j is the input. In the testing phase, a new datum Z_j with an unknown class label is assumed to belong to one of the given classes, hence it is expected that the partitioning scheme generated from the training session can be applied as well. Z_j is partitioned to the predefined levels according to the same scheme identified in training on the data universe. Then Z_j is converted to the corresponding vectors W_j or V_j using equation (10) or (12).

These vectors are applied to the feedforward network. The output node with the highest activation which surpasses a threshold value, identifies the class of the unknown input datum. If there is no output node with an activation surpassing the threshold, then the datum remains as unclassified (or rejected).

6 Experimentation with Speech Data

To show how the algorithm performs on low level speech data, we performed an experiment on its ability to identify relevant speech characteristics as well as its ability to distinguish the speaker identity. The data used for these experiments involved 3 speakers, on 3 words pronounced as "quit", "printer" and "end". Three classes of data were defined, one corresponding to each speaker. Each of the three words was spoken 10 times by each speaker, resulting in 30 speech sample data per speaker, and a total of 90 samples. Each speech sample is represented by a set of points composed of three variables as a 3-vector (time, frequency, amplitude). A single utterance generated slightly over 12,000 data points.

The experiment used the "hold-out test" to evaluate the algorithm for speaker identification. Each run consisted of selecting 5 samples on a word randomly from

each speaker class for training. The remaining 5 samples were used for testing. With 3 speakers, each run consists of 15 test data and 15 training data. With 3 words, and performing 10 runs on each word, a total of 30 runs was done for a total of 450 test samples. The results from the experiments showed that the system performed reasonably well. A total of 369 out of 450 were classified correctly. Of those that were not classified, about half were rejected. Total success rate was about 82%.

7 Experimentation with Classifying Data Forming Interlocking Spirals

These experiments illustrate the algorithm on classifying overlapping interlocking spirals of points [6]. In this set of experiments, the data are generated using different parameters to define two classes of data so that each data consists of a number of points forming spirals. Here, the points in a spiral were artificially generated so that the points in a spiral could overlap with points in another data even though they may belong to different class. Thus classification of each data has to depend on a large number of points jointly. Each data sample was composed of 96 points. To create a problem with probabilistic uncertainty, but more difficult, a degree of randomness was introduced so that each spiral as well as each point in it had the radius shifted by a random quantity.

In total, 60 data samples were generated for use in all the experiments. The experiment consisted of 10 runs where each run was composed of 30 training data, 15 per class. The test set then used the remaining 30 unchosen samples, once again 15 per class. In 89 runs, using different confidence levels and number of intervals. The results based on a total of 2670 test samples were: correctly recognized 92.9%, rejected 5.0% and incorrectly classified 2.1%.

REFERENCES

[1] Bie C., Shen H. and Chiu D.K.Y., *Hierarchical maximum entropy partitioning in texture image analysis*, Pattern Recognition Letter, Vol. 14 (1993), pp421–429.

[2] Chiu, D.K.Y. *Towards an event-space self-configurable neural network*, Proc. 1993 IEEE Intern. Conference on Neural Networks (1993), pp956–961.

[3] Chiu D.K.Y. *Information discovery through hierarchical maximum entropy discretization and synthesis*, Knowledge Discovery in Databases, G. Piatetsky, Shapiro and W.J. Frwley, MIT/AAAI press (1991), pp125–140.

[4] Shen, H.C., Bie C. and Chiu D.K.Y., *A texture-based distance measure for classification*, Pattern Recognition, Vol. 26 (1993), No. 9, pp1429–1437.

[5] Haberman, S.J. *The analysis of residuals in cross- classified tables*, Biometrics 29 (1973), pp205–209.

[6] Lang, K.J. and Witbrock, M.J *Learning to tell two spirals apart*, Proc 1988 Connectionist Models Summer School, Carnegie Mellon University, Morgan Kaufman Publishers (1988), pp52–59.

[7] Wong, A.K.C. and Chiu, D.K.Y., *Synthesizing statistical knowledge from incomplete mixed-mode data*, IEEE Trans. PAMI, Vol. PAMI-9 (1987), No.6, pp796–805.

APPROXIMATING THE BAYESIAN DECISION BOUNDARY FOR CHANNEL EQUALISATION USING SUBSET RADIAL BASIS FUNCTION NETWORK

E.S. Chng, B. Mulgrew* , S. Chen and G. Gibson*****

National University of Singapore, Institute of System Science, Heng Mui Keng Terrace, Kent Ridge, 119597 Singapore. Email : eschng@iss.nus.sg.

** Dept. of Electrical Eng., The University of Edinburgh, UK.*

*** Dept. of E.E.E., The University of Portsmouth, UK.*

**** Biomathematics and Statistics, The University of Edinburgh, UK.*

The aim of this paper is to examine the application of radial basis function (RBF) network to realise the decision function of a symbol-decision equaliser for digital communication system. The paper first study the Bayesian equaliser's decision function to show that the decision function is nonlinear and has a structure identical to the RBF model. To implement the full Bayesian equaliser using RBF network however requires very large complexity which is not feasible for practical applications. To reduce the implementation complexity, we propose a model selection technique to choose the important centres of the RBF equaliser. Our results indicate that reduced-sized RBF equaliser can be found with no significant degradation in performance if the subset models are selected appropriately.

Keywords: RBF network, Bayesian equaliser, neural networks.

1 Introduction

The transmission of digital signals across a communication channel is subjected to noise and intersymbol interference (ISI). At the receiver, these effects must be compensated to achieve reliable data communications[1, 2]. The channel, consisting of the transmission filter, transmission medium and receiver filter, is modelled as a finite impulse response (FIR) filter with a transfer function $H(z) = \sum_{i=0}^{n_a-1} a(i)z^{-i}$. The effects on the randomly transmitted signal $s(k) = s = \{\pm 1\}$ through the channel is described by

$$r(k) = \hat{r}(k) + n(k) = \sum_{i=0}^{n_a-1} s(k-i)a(i) + n(k) \tag{1}$$

where $r(k)$ is the corrupted signal of $s(k)$ received by the equaliser at sampled instant time k, $\hat{r}(k)$ is the noise-free observed signal, $n(k)$ is the additive Gaussian white noise, $a(i)$ are the channel impulse response coefficients, and n_a is the channel's memory length[1, 2]. Using a vector of the noisy received signal $\mathbf{r}(k) = [r(k), \cdots, r(k-m+1)]^T$, the equaliser's task is to reconstruct the transmitted symbol $s(k-d)$ with the minimum probability of mis-classification, P_E. The integers m and d are known as the feedforward and delay order respectively. The measure of an equaliser's performance P_E, or more commonly expressed as the bit error rate (BER), BER $= \log_{10} P_E$, in communication literature [1], is expressed with respect to the signal to noise ratio (SNR) where the SNR is defined by

$$\text{SNR} = \frac{E[\hat{\mathbf{r}}(k)]}{E[n^2(k)]} = \frac{\sigma_s^2(\sum_{i=0}^{i=n_a-1} a(i)^2)}{\sigma_e^2} = \frac{\sum_{i=0}^{i=n_a-1} a(i)^2}{\sigma_e^2} \tag{2}$$

where $\sigma_s^2 = 1$ is the transmit symbol variance and σ_e^2 is the noise variance.

The transmitted symbols that affect the input vector $\mathbf{r}(k)$ is the transmit sequence $\mathbf{s}(k) = [s(k), \cdots, s(k-m-n_a+2]^T$. There are $N_s = 2^{m+n_a-1}$ possible combinations

of these input sequences, i.e. $\{\mathbf{s}_j\}, 1 \leq j \leq N_s$[2]. In the absence of noise, there are N_s corresponding received sequences $\hat{\mathbf{r}}_j(k), 1 \leq j \leq N_s$, which are referred to as channel states. The values of the channel states are defined by,

$$\mathbf{c}_j = \hat{\mathbf{r}}_j(k) = F[\mathbf{s}_j], \qquad 1 \leq j \leq N_s, \tag{3}$$

where the matrix $F \in R^{m \times (m+n_a-1)}$ is

$$\begin{bmatrix} a(0) & a(1) & \dots & a(n_a-1) & 0 & \dots & \dots & \dots & \dots & 0 \\ 0 & a(0) & a(1) & \dots & a(n_a-1) & 0 & \dots & \dots & \dots & 0 \\ \vdots & \vdots & \vdots & \dots & \dots & \dots & \dots & \dots & \dots & 0 \\ 0 & \dots & \dots & \dots & \dots & \dots & a(0) & a(1) & \dots & a(n_a-1) \end{bmatrix} \tag{4}$$

Due to the additive noise, the observed sequence $\mathbf{r}(k)$ conditioned on the channel state $\hat{\mathbf{r}}(k) = \mathbf{c}_j$ is a multi-variable Gaussian distribution with mean at $\mathbf{c}_j$,

$$p(\mathbf{r}(k)|\mathbf{c}_j) = (2\pi\sigma_e^2)^{-m/2} \exp(-\|\mathbf{r}(k) - \mathbf{c}_j\|^2/(2\sigma_e^2)). \tag{5}$$

The set of channel states $C_d = \{\mathbf{c}_j\}_{j=1}^{N_s}$ can be divided into two subsets according to the value of $s(k-d)$, i.e.

$$C_d^{(+)} = \{\hat{\mathbf{r}}(k)|s(k-d) = +1)\}, \tag{6}$$

$$C_d^{(-)} = \{\hat{\mathbf{r}}(k)|s(k-d) = -1)\}, \tag{7}$$

where the subscript d in C_d denotes the equaliser's delay order applied.
To minimise the probability of wrong decision, the optimum decision function is based on determining the maximum *a posteriori* probability $P(s(k-d) = s|\mathbf{r}(k))$ [2] given observed vector $\mathbf{r}(k)$, i.e.,

$$\hat{s}(k-d) = \text{sgn}(\ P(s(k-d) = +1|\mathbf{r}(k)) - P(s(k-d) = -1|\mathbf{r}(k))\ ) \tag{8}$$

where $\hat{s}(k-d)$ is the estimated value of $s(k-d)$. It has been shown in [2] that the Bayesian decision function can be reduced to the following form,
$f_b(\mathbf{r}(k)) =$

$$\sum_{\mathbf{c}_j \in C_d^{(+)}} \exp(-\|\mathbf{r}(k) - \mathbf{c}_j\|^2/(2\sigma_e^2)) - \sum_{\mathbf{c}_k \in C_d^{(-)}} \exp(-\|\mathbf{r}(k) - \mathbf{c}_k\|^2/(2\sigma_e^2)) \tag{9}$$

It is therefore obvious that $f_b(.)$ has the same functional form as the RBF model [2, 3] $f_{\text{rbf}}(\mathbf{r})$,

$$f_{\text{rbf}}(\mathbf{r}) = \sum_{i=1}^{N} w_i \phi(\|\mathbf{r} - \mathbf{c}_i\|^2/\alpha) \tag{10}$$

where N is the number of centres, w_i are the feedforward weights, $\phi(.)$ are the nonlinearity, $\mathbf{c}_i$ are the centres of the RBF model, and α is a constant. The RBF network is therefore ideal to model the optimal Bayesian equaliser [2].
Example of decision boundary: As an example, the Bayesian decision boundaries realised by a RBF equaliser with feedforward order $m = 2$ for channel $H(z) = 0.5 + 1.0z^{-1}$ is considered. Fig 1a lists all the 8 possible combinations of the transmitted signal sequence $\mathbf{s}(k)$ and the corresponding channel states $\mathbf{c}_i$. Fig. 1b depicts the corresponding decision boundaries for the different delay orders. Note that the decision boundary is dependent on the channel state positions and delay order parameter.

S/No	Transmitted symbols			Channel State	
i	$\mathbf{s}(k)$			$\mathbf{c}_i$	
	$[\,s(k)$	$s(k\text{-}1)$	$s(k\text{-}2)\,]$	$[\,\hat{r}(k)$	$\hat{r}(k\text{-}1)\,]$
1	1	1	1	1.5	1.5
2	1	1	-1	1.5	-0.5
3	1	-1	1	-0.5	0.5
4	1	-1	-1	-0.5	-1.5
5	-1	1	1	0.5	1.5
6	-1	1	-1	0.5	-0.5
7	-1	-1	1	-1.5	0.5
8	-1	-1	-1	-1.5	-1.5

Fig (a) : State Table

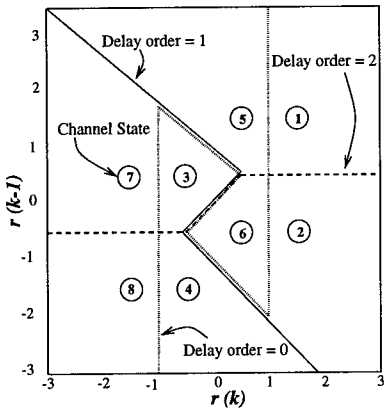

Fig (b) : Decision boundaries

Figure 1 (a) Transmit sequences and channel states for channel $H(z)$, (b) Corresponding Bayesian decision boundaries for various delay orders.

2 Selecting Subset RBF Model

The implementation of the full RBF Bayesian equaliser requires the use of all N_s channel states. Such implementation however may be impractical if N_s is large. In some cases, the complexity may be reduced by using a subset of the N_s channel states to generate the RBF decision function. For example, it is obvious that the decision boundary using delay $d = 1$ for $H(z)$ (Fig. 1b) can be realised approximately by a RBF network using $\{\mathbf{c}_3, \mathbf{c}_4, \mathbf{c}_5, \mathbf{c}_6\}$ as centres. If the realised decision boundary using the subset RBF equaliser is very similar to the full Bayesian equaliser, the classification performance of the two equalisers would also be very similar. That is, the implementation complexity of the RBF equaliser is reduced by using only the important channel states that define the decision boundary.

To understand how centres affect decision boundary, we analyse the effects of centre positions on boundary position when $\sigma_e \rightarrow 0$. Let $\mathbf{r}_0$ be the set of all boundary points. I.e., $f_b(\mathbf{r}_0)$ equals to 0. Therefore, if $\mathbf{r}(k) \in \mathbf{r}_0$, Eq. 9 becomes

$$\sum_{\mathbf{c}_j \in C_d^{(+)}} \exp(-\|\mathbf{r}_0 - \mathbf{c}_j\|^2/(2\sigma_e^2)) = \sum_{\mathbf{c}_k \in C_d^{(-)}} \exp(-\|\mathbf{r}_0 - \mathbf{c}_k\|^2/(2\sigma_e^2)). \qquad (11)$$

When $\sigma_e \rightarrow 0$, the sum on the l.h.s. of Eq. 11 becomes dominated by the closest centres to $\mathbf{r}_0$, i.e.

$$\{U_d^+\} \;=\; \min_{\mathbf{c}_j \in C_d^{(+)}} \{\|\mathbf{r}_0 - \mathbf{c}_j\|\}. \qquad (12)$$

This is because the contribution from the terms $\exp(-\|\mathbf{r}_0 - \mathbf{c}_j\|^2/(2\sigma_e^2))$ for centres $\mathbf{c}_j \notin U_d^+$ converges much more quickly to zero when $\sigma_e \rightarrow 0$ than terms for centres belonging to U_d^+. Similarly, the sum on the r.h.s of Eq. 11 becomes dominated by the closest terms for centres belonging to U_d^-, where $U_d^- = \min_{\mathbf{c}_k \in C_d^{(-)}} \{\|\mathbf{r}_0 - \mathbf{c}_k\|\}$.

At very high SNR, the asymptotic decision boundaries are hyper-planes between pairs of channel states belonging to $\{U_d^+\}$ and $\{U_d^-\}$ [4].
However, not all channel states of $\{U_d^+, U_d^-\}$ are required to define the decision boundary. This can be observed from the example illustrated in Fig. 1b for decision boundary realised using delay order $d = 2$. By visual insepection (Fig. 1b), it is obvious that $\{\mathbf{c}_3, \mathbf{c}_7\} \in U_d^+$ and $\{\mathbf{c}_4, \mathbf{c}_8\} \in U_d^-$. The decision boundary formed using centres $\{\mathbf{c}_3, \mathbf{c}_4\}$ and $\{\mathbf{c}_7, \mathbf{c}_8\}$ are however the same. Therefore, in this case, only 1 pair of channel states, either $\{\mathbf{c}_3, \mathbf{c}_4\}$ or $\{\mathbf{c}_7, \mathbf{c}_8\}$, is sufficient to approximate that region of decision boundary.
To find the set of important centres $\{U_{ds}^+, U_{ds}^-\}$ for the subset RBF equaliser, we propose the following algorithm,

Algorithm 1 : Finding U_{ds}^+, U_{ds}^-

For $\mathbf{c}_j \in C_d^{(+)}$
  For $\mathbf{c}_k \in C_d^{(-)}$
    $\mathbf{r}_{j,k}^* = \mathbf{c}_j + (\frac{\mathbf{c}_k - \mathbf{c}_j}{2})$
    if $\left[\begin{array}{l} f_b(\mathbf{r}_{j,k}^*) = 0 \text{ and} \\ \mathbf{c}_j = \min_{\mathbf{c}_i \in C_d^{(+)}} \{\|\mathbf{r}_0 - \mathbf{c}_i\|\} \text{ and} \\ f_s(\mathbf{r}_{j,k}^*) \neq 0 \end{array}\right]$
      $\mathbf{c}_j \rightarrow U_{ds}^+$, $\mathbf{c}_k \rightarrow U_{ds}^-$
  next $\mathbf{c}_k$,
next $\mathbf{c}_j$.

where $f_s(.)$ = RBF model formed using the current selected channel states from $\{U_{ds}^+, U_{ds}^-\}$ as centres and $f_b(.)$ is the full RBF Bayesian equaliser's decision function.

2.1 Subset Model Selection : Some Simulation Results

Simulations were conducted to select subset RBF equalisers from the full model. The following channels which have the same magnitude but different phase response were used,

$$H1(z) = 0.8745 + 0.4372z^{-1} - 0.2098z^{-2} \quad (13)$$

$$H2(z) = 0.2620 - 0.6647z^{-1} - 0.6995z^{-2} \quad (14)$$

The feedforward order used was $m = 4$, resulting in a full model with $N_s = 2^{m+n_a-1} = 64$ centres. Using SNR condition at 16dB, simulations were conducted to compare the performance of the subset RBF and full RBF equalisers for the two channels. The results are tabulated in Table 1a and 1b respectively; The first column of each table indicates the delay order parameter, the second column indicates the number of channel states selected to form the subset model while the third and fourth columns list the BER performance of the two equalisers and the last column indicates if the channel states belonging to the different transmit symbol, i.e. $C_d^{(+)}$ and $C_d^{(-)}$, are linearly or not-linearly separable. Our results show that reduced size RBF equaliser with performance very similar to the full model's performance can usually be found for equalisation problem that is linearly separable.

Delay	Subset Size	Subset log(Pe)	Full-model log(Pe)	Decision Boundary
0	56	-4.09	-4.09	Linear Sep.
1	57	-4.14	-4.14	Linear Sep.
2	32	-4.11	-4.12	Linear Sep.
3	32	-4.11	-4.12	Linear Sep.
4	48	-1.91	-1.91	Not-Linear Sep.
5	64	-0.97	-0.97	Not-Linear Sep.

Table a : Channel H1(z)

Delay	Subset Size	Subset log(Pe)	Full-model log(Pe)	Decision Boundary
0	56	-0.80	-1.30	Not-Linear Sep.
1	46	-2.99	-2.99	Linear Sep.
2	38	-3.38	-3.38	Linear Sep.
3	56	-3.43	-3.43	Linear Sep.
4	55	-3.32	-3.32	Not-Linear Sep.
5	64	-3.41	-3.41	Not-Linear Sep.

Table b : Channel H2(z)

Table 1 Comparing the performance of the full-size (64 centres) RBF equaliser, subset RBF equaliser for Channel $H1(z)$ (Table 1a) and Channel $H2(z)$ (Table 1b) at SNR=16db.

3 Conclusions

This paper examined the application of RBF network for channel equalisation. It was shown that the optimum symbol-decision equaliser can be realised by a RBF model if channel statistic is known. The computational complexity required to implement the full Bayesian function using the RBF network is however considerable. To reduce implementation complexity, a method of model selection to reduce the number of centres in the RBF model is proposed. Our results indicate that the model size, and hence implementation complexity, can be reduced without significantly compromising classification performance in some cases.

REFERENCES

[1] S.U.H.Qureshi, *Adaptive equalization*, Proc. IEEE, Vol. 73 (1985), No. 9, pp1349–1387.

[2] S.Chen, B.Mulgrew and P.M.Grant, *A clustering technique for digital communications channel equalization using radial basis function networks*, IEEE Trans. Neural Networks, Vol. 4 (1993), No. 4, pp570–579.

[3] M.J.D.Powell, *Radial basis functions for multivariable interpolation: a review*, Algorithms for Approximation, J.C.Mason and M.G.Cox (Eds), Oxford (1987) pp143–167.

[4] R.A.Iltis, *A randomized bias technique for the importance sampling simulation of Bayesian equalisers*, IEEE Trans. Communications, Vol. 43 (1995), pp1107–1115.

APPLICATIONS OF GRAPH THEORY TO THE DESIGN OF NEURAL NETWORKS FOR AUTOMATED FINGERPRINT IDENTIFICATION

Carol G. Crawford

U.S. Naval Academy, Department of Mathematics, Annapolis, USA.

This paper presents applications of graph theory to the design of graph matching neural networks for automated fingerprint identification. Given a sparse set of minutiae from a fingerprint image, complete with locations in the plane and (optionally) other labels such as ridge angles, ridge counts to nearby minutiae and so on, this approach to matching begins by constructing a graph-like representation of the minutiae map, utilizing proximity graphs, such as the sphere-of-influence graphs. These graph representations are more robust to noise such as translations, rotations and deformations. This paper presents the role of these graph representations in the design of graph matching neural networks for the matching and classification of fingerprint images.

1 Introduction

Matching the representations of two images has been the focus of extensive research in computer vision and artificial intelligence. In particular, the problem of matching fingerprint, images has received wide attention and varying approaches to its solution. In this paper we present results of an ongoing collaborative research program which combines techniques and methods from graph theory and neural science to design algorithms for graph matching neural networks.

This collaborative approach with Eric Mjolsness, University of Southern California, San Diego, and Anand Rangarajan, Center for Theoretical and Applied Neural Science at Yale, is an outgrowth of an initial investigation for the Federal Bureau of Investigation to their existing Integrated Automated Fingerprint Identification System, IAFIS.

In this research program, algorithms and techniques from discrete mathematics, graph theory and computer science are combined to develop methods and algorithms for representing and matching fingerprints in a very large database, such as the one at the FBI. The Federal Bureau of Investigation and National Institute of Standards and Technology provided a small database of fingerprints. This database, together with the software environment at the Center for Theoretical and Applied Neural Science at Yale University have provided a test bed for these algorithms. The following presents the background of the fingerprint problem and this research together with a special emphasis on the role of proximity graphs in the design of the graph matching neural networks.

2 Fingerprint Images, Minutiae and Graph Representations

2.1 Minutiae Maps

Fingerprint matching and identification dates back to 1901 when it was introduced by Sir Edward Henry for Scotland Yard. After sorting the fingerprints into classes such as whorls, loops and arches, matches are made according to comparisons of minutiae. Minutiae include such indications as ridge endings, islands and bifurcations, with fingerprints averaging 100 or more per print. Today fingerprints are initially stored on computer as a raw minutiae map in the form of a list of minutiae positions and ridge angles in a raster-scan order. In American courts a positive

matching of a dozen minutiae usually suffices for identification. However, for an average computer to make these dozen matches the process would entail locating every minutiae in both prints and then comparing all ten-thousand-plus possible pairings of these minutiae. In addition, the minutiae map itself is very non-robust to likely noise such as translations, rotations, and deformations, which can change every minutiae positions. A subtler form of noise is the gradual increase in ridge width or image scale typically encountered in moving from the top of the image to the bottom. Thus, it is desirable to determine graph- like representations which are more robust to noise and less susceptible to problems with missing minutiae.

2.2 Graph Representations of Minutiae Maps

Given a sparse set of minutiae from one fingerprint image, complete with their locations in the plane and (optionally) other labels such as ridge angles, ridge counts to nearby minutiae and so on, we construct a graph- like representation of the minutiae map. By considering relationships between pairs of minutiae such as their geometric distance in the plane, or the number of intervening ridges between them, we can begin to construct features which are robust against translations and rotations at least. However, there still exists the very serious problem of reorderings of the minutiae forced by rotation and missing or extra minutiae. This "problem" must be addresses by defining a reordering- independent match metric between two such graphs.

Complete Graphs and Planar Distances

The simplest example of a labelled graph representation would be the complete graph where every pair of minutiae are linked by an "edge" in the graph. Edges would be labelled by the 2-d Euclidean distance between the minutiae. Note that this graph would require a special definition of the match metric to handle missing, extra and reordered minutiae. Furthermore, most of the edges would connect distant minutiae whose relationships, such as planar distance or ridge count, are subject to noise and provide less real information than nearby edges. So for reasons of robustness and computational cost, it makes sense to consider instead various kinds of "proximity graphs", which keep only the edges between minutiae that are "neighbors" according to some criterion.

Sphere-of-influence Graphs and Other Proximity Graph Representations

Sphere-of-Influence graphs comprise the first set of proximity graphs which we considered in our goal of determining a better class of minutiae map representations. First introduced by Toussaint [9], sphere- of-influence graphs provide a potentially robust representation for minutiae maps. These graphs are capable of capturing low-level perceptual structures of visual scenes consisting of dot patterns. . A very active group of researchers have developed a series of significant results dealing with this class of graphs. We refer the reader to the work of M. Lipman, [4,5,6]; F. Harary, [5,6]; M. Jacobson, [5,6]; T. S. Michael,[7,8]; and T. Quint, [7,8].

The following definition is referred to by Toussaint, [9]. Let $V = (P_1, \ldots, P_n)$ be a finite set of points in the plane. For each point p in V, let r_p be the closest distance to any other set of points in the set, and let C_p be the circle of radius r_p centered at p. The *sphere- of-influence graph, or SIG*, is a graph on V with an edge between points p, q if and only if the circles C_p, C_q intersect in at least two

places. For various illustrations of sphere-of-influence graphs we refer the reader to the excellent presentation by Toussaint in [9].

One can note from the prior example that perceptually salient groups of dots become even more distinct in the corresponding sphere-of-influence graph. However, SIGs represent only one group of an even richer class of graphs we refer to as proximity graphs. These graphs also offer various benefits in their potential for providing robust representations of minutiae maps. Proximity graphs all share the property that they only contain edges corresponding between minutiae that are "neighbors" according to some given criterion. The graphs which have turned out to be most promising representations include *relative neighborhood graphs, delauney triangulations, voronoi diagrams, minutiae distance graphs and generalized sphere-of-influence graphs.* We refer the reader to an excellent survey article by Toussaint for more details on proximity graphs. [9]

Generalized Sphere-of-Influence Graph Representations

K-sphere-of-influence graphs (k-SIGs) are generalizations of SIGs, in which a vertex is connected to k nearby. vertices depending only on their relative distances, not absolute distances.(Guibas, Pach, and Sharir [10]). Given a set V of n points in R^d, the *kth sphere-of- influence* of a point x in V is the smallest closed ball centered at x and containing more than k points of V (including x). The case for $k = 1$ yields the standard sphere-of-influence graph. The it kth sphere-of-influence graph, $G_k(V)$ *of* V is a graph whose vertices are the points of V, and two points are connected by an edge if their k-th spheres -of - influence intersect.

K-SIGs are especially suitable for minutiae map representations because of the fact that connections depend on relative distances. This property provides a form of scale invariance. Each edge can be labelled with the integer k, recording whether it connects nearby ($k = 1$) or farther minutiae pairs. Unfortunately, this scale robustness is bought at the price of increased susceptibility to missing minutiae. When a minutiae goes missing, not only is there an unavoidable effect on the graph by the deletion of the node, but there is a gratuitous "splash" effect of the edges between nearby pairs of the remaining minutiae: their k-numbers change despite the fact that their planar distance do not. This effect is mitigated by the match metric, which changes only gradually with k, but it is still undesirable.

Finally, we define yet another graph which is a hybrid between planar distance graphs and k-SIGs. We begin by creating a k-SIG with an overly large value of k. However, we label the edges with the planar distance d. Next we find the local image scale factor by finding the best constant of proportionality between d and k in each image region. Divide all d's by this coefficient to turn them into less noisy, noninteger versions of k, and then let this scaled version of d be the importance rating for an edge. Then proceed to a graph and a match metric as in the planar distance example. For this hybrid representation minutiae deletion only affects d via the local scaling factor, which is determined by many different value of k and is therefore fairly robust, preserving scale invariance.

3 Graph-Matching Neural Network Implementation

Graph representations of minutiae maps provide only the first step in developing a matching scheme for fingerprints. This second part of this research effort is devoted to the design of graph matching algorithms and their implementation as neural

networks. As outlined in prior sections these algorithms are based on proximity graphs which only contain edges for nearby minutiae. These edges are then labelled with features and with and "edge importance rating" that directly affects the weight given to that edge in the match metric. In this scenario one can construct a nested series of graphs including more and more edges of less and less importance or greater and greater distance, until either some cut off limit is reached or all possible edges between minutiae in the map are included in the largest graph. In this class of algorithms the match metric between two such graphs is insensitive to arbitrary reorderings of the minutiae in either graph, and is implementable as an analog neural network. Finally, the match metric will contain adjustable weighting parameters which determine the relative weights of matching edges as a function of their importance rating, and the relative weights of any other labelling information attached to the vertices or edges of the graphs. These parameters are then determined statistically by a steepest-descent training algorithm applied to a data base of minutiae maps, followed by testing-set validations, exactly as is done in the conventional neural network paradigm.

3.1 Relaxation Networks for Graph Matching — Deterministic Annealing and Lagrangian Decomposition

The neural network implementation of this research effort has been conducted at Yale University's Center for Theoretical and Applied Neural Science in cooperative efforts with E. Mjolsness and A. Rangarajan. This implementation has concentrated on the use of relaxation neural networks for matching the labelled graphs corresponding to minutiae maps. It should be noted that neural network approaches to graph matching share the feature of other recent approaches to graph matching in that they are not restricted to looking for isomorphisms, but seek to minimize the distance between two graphs. Graph isomorphism occurs when the distance is zero. The approach at Yale utilizes deterministic annealing to generalize to inexact, weighted graph matching.

In [11] Mjolsness and Rangarajan formulate the problems as follows: given graphs G and g, find a permutation matrix m that brings the two sets of vertices into correspondence. A permutation matrix is a zero one matrix whose rows and columns sum to one. Within the framework of *deterministic annealing* one can easily formulate the permutation matrix constraints. In this setting the row or column constraints are *winner-take-alls* and either set (but not both sets) of constraints separately can be exactly imposed used deterministic annealing methods.

This deterministic annealing approach is similar to a *Lagrangian decomposition* approach in that the row and column constraints are satisfied separately. Lagrange multipliers are then used to equate the two solutions. Other methods do exist to satisfy both the row and column constraints and this method (for obtaining a permutation matrix) is equivalent w.r.t. fixpoints to the one presented in [12]. A fixpoint preserving transformation [13] is applied to the graph matching distance resulting in the ability to express the combination of the graph matching distance constraint and the permutation matrix constraint using terms that are linear in the permutation matrix M.

Due to the existence of unavoidable symmetries in graph matching and the resulting global minima, a symmetry- breaking term is added in order to always obtain

a permutation matrix. The symmetry-breaking term is similar to the hysteretic annealing performed in [14,15] and is suitable for the deterministic approach being used. The symmetry-breaking term is reversed via another fixpoint preserving transformation. The network then performs minimization with respect to the Lagrange parameters and maximization with respect to the permutation matrix. In 11] simulation results are shown for the isomorphism problem with 100 node random, undirected graphs and for the weighted graph matching problem with 100 node random graphs with uniform noise added to the connections.

REFERENCES

[1] Chen Gould, M S Jacobson Schelp and D West, *A characterization of influence graphs of prescribed graph*, Vishwa Internat. J. Graph Theory, Vol.1 (1992), pp77–81.

[2] C. Crawford and E Mjolsness, *Graph Matching and Image Processing Neural Networks for Fingerprint Identification*, Technical Report for The Federal Bureau of Investigation, (September 1992), pp1–14.

[3] C. Crawford and E Mjolsness, *Automated Fingerprint Identification: An Independent Study, Research Report* YALE/DCS/RR-920, (October 1991), pp1–30, also published as Technical Report for The Federal Bureau of Investigation.

[4] M J.Lipman, *Integer realizations of sphere-of-influence graphs*, Congress Numerantium, Vol. 91 (1991), pp63–70.

[5] Harary, M S Jacobson, M J Lipman, and F R McMorris, *Abstract sphere-of-influence graphs*, Math. Comput. Modelling, Vol. 17 (1993), pp77–83.

[6] T. S. Michael and T Quint, *Sphere-of-influence graphs defined on a prescribed graph.* (submitted).

[7] T S. Michael and T Quint, *On Sphere-of-influence graphs in the plane*, (submitted)

[8] T S Michael and T Quint, *Sphere-of-influence graphs: small clique and star factors*, (submitted)

[9] G T Toussaint, *A graph-theoretic primal sketch*, Computational Morphology, Elsevier North Holland, Arnsterdarn (1988), pp229–260.

[10] Guibas, Pach and Sharir, *Generalized sphere-of-influence graphs in higher dimensions*, manuscript, Tel-Aviv University, (1992).

[11] A Rangarajan and E Mjolsness, *A Lagrangian Relaxation Network for Graph Matching*, (submitted).

[12] A L Yuille and J J Kosowsky, *Statistical physics algorithms that converge*, Technical Report 92–7 (1992), Harvard Robotics Laboratory.

[13] A H Gee and R W Prager, *Polyhedral combinatorics and neural networks*, Neural Computation, Vol.6 (1994), pp161–180.

[14] S. V. B Aiyer, M Niranjan, and F Fallside, *A Theoretical investigation into the performance of the Hopfield model*, IEEE, Trans. Neural Networks. Vol.1 (1990), pp204–215.

Acknowledgements

Research supported by The Office of Naval Research contract N0001494WR23025. This work is an outgrowth of a cooperative program with Eric Mjolsness of The University of Southern California and Anand Rangarajan of The Center for Theoretical and Applied Neural Science at Yale University This program was originally funded by The Federal Bureau of Investigation.

ZERO DYNAMICS AND RELATIVE DEGREE OF DYNAMIC RECURRENT NEURAL NETWORKS

A. Delgado, C. Kambhampati* and K. Warwick*

National University of Columbia, Elec. Eng. Dept., AA No. 25268, Bogota, D C, Columbia SA. Email: adelgado@col1.telecom.com.co

**Cybernetics Department, University of Reading, UK.*

In this paper the differential geometric control theory is used to define the key concepts of relative degree and zero dynamics for a Dynamic Recurrent Neural Network (DRNN). It is shown that the relative degree is the lower bound for the number of neurons and the zero dynamics are responsible for the approximating capabilities of the network.

1 Introduction

Most of the current applications of neural networks to control nonlinear systems rely on the classical NARMA approach [1,2]. This procedure, powerful in itself, has some drawbacks [3]. On the other hand, a DRNN is described by a set of nonlinear differential equations and can be analysed using differential geometric techniques [4].

In this work, the important concepts of zero dynamics and relative degree from the differential geometric control theory are formulated for a control affine DRNN.

2 Mathematical Preliminaries

Consider the nonlinear control affine system

$$\begin{aligned}
\dot{x}_1 &= x_2 \\
\dot{x}_2 &= x_3 \\
&\vdots \\
\dot{x}_{r-1} &= x_r \\
\dot{x}_r &= f_r(x_1, \ldots, x_r, x_{r+1}, \ldots, x_n) + g_r \cdot u \\
\dot{x}_{r+1} &= f_{r+1}(x_1, \ldots, x_r, x_{r+1}, \ldots, x_n) + g_{r+1} \cdot u \\
&\vdots \\
\dot{x}_n &= f_n(x_1, \ldots, x_r, x_{r+1}, \ldots, x_n) + g_n \cdot u \\
y &= x_1
\end{aligned} \tag{1}$$

these equations can be written in compact form

$$\begin{aligned}
\dot{x} &= f(x) + g \cdot u \\
y &= h(x)
\end{aligned} \tag{2}$$

where $x \in \mathbb{R}^n$, $u \in \mathbb{R}$, $y \in \mathbb{R}$, $f(x)$ and g are vector fields, $h(x)$ is a scalar field. For the system (1) there are two key concepts in the differential geometric framework, that is the zero dynamics and the relative degree.

2.1 Zero Dynamics

The zero dynamics of the system (1) describe its behaviour when the output $y(t)$ is forced to be zero [4]. With the output zero, the initial state of the system must be set to a value such that $(x_1(0), \ldots, x_r(0))$ are zero, whereas $(x_{r+1}(0), \ldots, x_n(0))$ can be chosen arbitrarily. In addition, the input $u(t)$ must be the solution of the

equation

$$0 = f_r(0,\ldots,0,x_{r+1}(t),\ldots,x_n(t)) + g_r \cdot u \tag{3}$$

Solving for $u(t)$ in (3) and replacing in the remaining equations, the zero dynamics are given by the set of differential equations

$$\begin{aligned} \dot{x}_{r+1} &= f_{r+1}(0,\ldots,0,x_{r+1},\ldots,x_n) - \frac{g_{r+1}}{g_r} f_r(0,\ldots,0,x_{r+1},\ldots,x_n) \\ &\vdots \\ \dot{x}_n &= f_n(0,\ldots,0,x_{r+1},\ldots,x_n) - \frac{g_n}{g_r} f_r(0,\ldots,0,x_{r+1},\ldots,x_n) \end{aligned} \tag{4}$$

The zero dynamics play a role similar to that of the zeros of the transfer function in a linear system. If the zero dynamics are stable then the system (1) is said to be minimum phase.

2.2 Relative Degree

The relative degree of a dynamical system is defined as the number of times that the output $y(t)$ must be differentiated with respect to time in order to have the input $u(t)$ appearing explicitly or is the number of state equations that the input $u(t)$ must go through in order to reach the output $y(t)$.

The nonlinear system (2) is said to have relative degree r [3,4] if

$$\begin{aligned} L_g L_f^i h(x) &= 0, \qquad i = 0,\ldots,r-2 \\ L_g L_f^{r-1} h(x) &\neq 0 \end{aligned}$$

3 DRNN

A DRNN is described by the set of nonlinear differential equations

$$\begin{aligned} \dot{\chi}_i &= -\chi_i + \sum_{j=1}^{N} w_{ij} \cdot \sigma(\chi_j) + \gamma_i \cdot u \\ y &= \chi_1, \qquad i = 1,\ldots,N \end{aligned} \tag{5}$$

or in matrix form

$$\begin{aligned} \dot{\chi} &= -\chi + W \cdot \Sigma(\chi) + \Gamma \cdot u \\ y &= \chi_1 \end{aligned} \tag{6}$$

where $\chi \in \mathbb{R}^N$, $W \in \mathbb{R}^{N\times N}$, $\Gamma \in \mathbb{R}^{N\times 1}$, and $\Sigma(\chi) = (\sigma(\chi_1),\ldots,\sigma(\chi_N))^{\mathrm{T}}$.

For control purposes it was demonstrated [3] that the network (6) can approximate nonlinear systems of the class (2), the resulting model can be analysed using the differential geometric framework. The aim of this paper is to propose a canonical structure for the network (6) in order to get any desired relative degree with a zero dynamics similar to (4).

Theorem 1 *The DRNN (6) with the following matrices W and Γ can have any relative degree $r \in [2, N]$*

$$W = \begin{bmatrix} \omega_{11} & \omega_{12} & 0 & \cdot & \cdot & \cdot & \cdot & \cdot & \cdot & 0 \\ \omega_{21} & \omega_{22} & \omega_{23} & 0 & \cdot & \cdot & \cdot & \cdot & \cdot & 0 \\ \cdot & \cdot & \cdot & \cdot & \cdot & \cdot & \cdot & \cdot & \cdot & \cdot \\ \cdot & \cdot & \cdot & \cdot & \cdot & \cdot & \cdot & \cdot & \cdot & \cdot \\ \omega_{r-11} & \omega_{r-12} & \cdot & \cdot & \cdot & \omega_{r-1r} & 0 & \cdot & \cdot & 0 \\ \omega_{r1} & \omega_{r2} & \cdot & \cdot & \cdot & \omega_{rr} & \cdot & \cdot & \cdot & \omega_{rN} \\ \omega_{r+11} & \omega_{r+12} & \cdot & \cdot & \cdot & \omega_{r+1r} & \cdot & \cdot & \cdot & \omega_{r+1N} \\ \cdot & \cdot & \cdot & \cdot & \cdot & \cdot & \cdot & \cdot & \cdot & \cdot \\ \cdot & \cdot & \cdot & \cdot & \cdot & \cdot & \cdot & \cdot & \cdot & \cdot \\ \omega_{N1} & \omega_{N2} & \cdot & \cdot & \cdot & \omega_{Nr} & \cdot & \cdot & \cdot & \omega_{NN} \end{bmatrix}$$

$$\Gamma = \begin{bmatrix} 0 & 0 & \cdot & \cdot & 0 & \gamma_r & \gamma_r & \cdot & \cdot & \gamma_N \end{bmatrix}^{\mathrm{T}}$$

in other terms

$$\omega_{ij} = 0; \gamma_i = 0, \quad i = 1, \ldots, r-1, \quad j = i+2, \ldots, N$$

This particular structure is called the **staircase** structure. Note that the minimum number of neurons is the relative degree r. For a desired relative degree $r = 1$, the coefficient γ_1 must be nonzero.

Proof Applying the definition of relative degree

$$\begin{aligned} y &= \chi_1 \\ \dot{y} &= \dot{\chi}_1 = \omega_{11} \cdot \sigma(\chi_1) + \omega_{12} \cdot \sigma(\chi_2) \end{aligned}$$

after the first derivative, every new derivative of $y(t)$ introduces a new state equation (staircase structure). Then after r derivatives of the output $y(t)$, the input $u(t)$ appears explicitly. □

Theorem 2 *The network of the* **Theorem 1** *with a sigmoid function $\sigma(0) = 0$ has a zero dynamics described by the set of differential equations*

$$\dot{\chi}_i = -\chi_i + \sum_{j=r+i}^{N} (\omega_{ij} - \frac{\gamma_i}{\gamma_r} \omega_{rj}) \cdot \sigma(\chi_j), \qquad i = r+1, \ldots, N$$

Proof The zero dynamics are defined as the resulting dynamics when the output $y(t)$ is constrained to be zero. In the structure proposed $y(t) = 0$ means that the first r state variables are zero $\chi_1(t) = \cdots = \chi_r(t) = 0$ and $\sigma(\chi_1(t)) = \sigma(\cdots) = \sigma(\chi_r(t)) = 0$ The equation for $\dot{\chi}_r(t)$ becomes

$$0 = \sum_{j=r+i}^{N} \omega_{rj} \cdot \sigma(\chi_j) + \gamma_r \cdot u$$

solving for u

$$u = -\frac{1}{\gamma_r} \sum_{j=r+i}^{N} \omega_{rj} \cdot \sigma(\chi_j)$$

replacing the control u in the last $N - r$ equations

$$\dot{\chi}_i = -\chi_i + \sum_{j=r+1}^{N} \omega_{ij} \cdot \sigma(\chi_j) - \frac{\gamma_i}{\gamma_r} \sum_{j=r+1}^{N} \omega_{rj} \cdot \sigma(\chi_j) \qquad i = r+1, \ldots, N$$

Finally

$$\dot{\chi}_i = -\chi_i + \sum_{j=r+1}^{N} (\omega_{ij} - \frac{\gamma_i}{\gamma_r}\omega_{rj}) \cdot \sigma(\chi_j) \qquad i = r+1, \ldots, N$$

□

Example: Consider the following staircase DRNN

$$\begin{aligned}
\dot{\chi}_1 &= -\chi_1 + \omega_{11} \cdot \sigma(\chi_1) + \omega_{12} \cdot \sigma(\chi_2) \\
\dot{\chi}_2 &= -\chi_2 + \omega_{21} \cdot \sigma(\chi_1) + \omega_{22} \cdot \sigma(\chi_2) + \omega_{23} \cdot \sigma(\chi_3) + \gamma_2 \cdot u \\
\dot{\chi}_3 &= -\chi_3 + \omega_{31} \cdot \sigma(\chi_1) + \omega_{32} \cdot \sigma(\chi_2) + \omega_{33} \cdot \sigma(\chi_3) + \gamma_3 \cdot u \\
y &= \chi_1 \\
\sigma(0) &= 0
\end{aligned}$$

Relative Degree: The first derivative of the output is

$$\dot{y} = \dot{\chi}_1 = -\chi_1 + \omega_{11} \cdot \sigma(\chi_1) + \omega_{12} \cdot \sigma(\chi_2)$$

the input u does not appear so the relative degree is greater than one. The second derivative of the output is

$$\ddot{y} = -\dot{\chi}_1 + \omega_{11} \cdot \sigma'(\chi_1) \cdot \dot{\chi}_1 + \omega_{12} \cdot \sigma'(\chi_2) \cdot \dot{\chi}_2$$

where

$$\sigma'(\chi_i) = \frac{d\sigma(\chi_i)}{d\chi_i}.$$

Replacing $\dot{\chi}_1$ and $\dot{\chi}_2$

$$\begin{aligned}
\ddot{y} &= (-1 + \omega_{11} \cdot \sigma'(\chi_1))(-\chi_1 + \omega_{11} \cdot \sigma(\chi_1) + \omega_{12} \cdot \sigma(\chi_2)) \\
&\quad + \omega_{12} \cdot \sigma'(\chi_2) \cdot (-\chi_2 + \omega_{21} \cdot \sigma(\chi_1) + \omega_{22} \cdot \sigma(\chi_2) + \omega_{23} \cdot \sigma(\chi_3) + \gamma_2 \cdot u)
\end{aligned}$$

notice that the input appears explicitly so the relative degree is $r = 2$.

Zero Dynamics: The proposed network has three states and relative degree two, so the zero dynamics has one state.

Following the definition of zero dynamics [4], $y = \chi_1 = 0$. The first state equation is reduced to

$$0 = -0 + \omega_{11} \cdot \sigma(0) + \omega_{12} \cdot \sigma(\chi_2)$$

this yields $\chi_2 = 00$. The second state equation is

$$0 = -0 + \omega_{21} \cdot \sigma(0) + \omega_{22} \cdot \sigma(0) + \omega_{23} \cdot \sigma(\chi_3) + \gamma_2 \cdot u$$

solving for the input

$$u = -\frac{\omega_{23}}{\gamma_2} \cdot \sigma(\chi_3)$$

replacing u in the remaining state equation, the zero dynamics is

$$\dot{\chi}_3 = -\chi_3 + (\omega_{33} - \frac{\gamma_3}{\gamma_2}\omega_{23}) \cdot \sigma(\chi_3)$$

In the simulations [5, 6] a single link manipulator of relative degree 2 and without zero dynamics was identified with a DRNN, the resulting model has the same relative degree but **it needs** the zero dynamics in order to improve the plant approximation.

4 Conclusions

A DRNN, is described naturally by a set of nonlinear differential equations and can be analysed within the framework of the differential geometric control theory. There are two key concepts in this framework : the zero dynamics and the relative degree.

Two theorems were formulated and proved, as a result a particular structure is proposed for a DRNN in order to get any desired relative degree $r \in [1, N]$ and the canonical zero dynamics (4). The **relative degree** is a **lower bound** for the **number of neurons** and the **zero dynamics** are responsible for the **approximating capabilities** of the neural network. That is, for multilayer networks the approximating capabilities reside in the hidden layers and for recurrent networks the approximating capabilities reside in the zero dynamics.

REFERENCES

[1] Chen, S. and Billings, S. A., *Neural networks for nonlinear dynamic system modelling and identification*, Int. J. Control, Vol. 56 (1992). pp319–346.

[2] Narendra, K.S. and Parthasarathy, K., *Identification and control of dynamical systems using neural networks*, IEEE Transactions on Neural Networks, Vol.1 (1990), pp4–26.

[3] Delgado, A., Kambhampati, C. and Warwick, K., *Dynamic recurrent neural network for system identification and control*, IEE Proceedings, Part D, Vol. 142 (1995), pp307–314.

[4] Isidori, A., *Nonlinear Control Systems*, Springer-Verlag (1989).

[5] Delgado, A., Kambhampati, C. and Warwick, K., *Identification of nonlinear systems with a dynamic recurrent neural network*, Proceedings of the IEE — IV international conference on ANNs. Cambridge (1995), pp318–322.

[6] Delgado, *Input/output linearization of control affine systems using neural networks* PhD Thesis, Dept. Cybernetics, Reading University (1996).

Acknowledgements

The author A. Delgado would like to thank to the Colombian Institute for the Development of Science and Technology (COLCIENCIAS) and to the National University of Colombia for supporting his PhD studies at the Cybernetics Department of the University of Reading.

IRREGULAR SAMPLING APPROACH TO NEUROCONTROL: THE BAND-AND SPACE-LIMITED FUNCTIONS QUESTIONS

Andrzej Dzieliński and Rafał Żbikowski

Department of Mechanical Engineering, James Watt Building, University of Glasgow, Glasgow G12 8QQ, Scotland, UK. Email: andrzej@mech.gla.ac.uk

The use of feedforward neural networks (FNNs) for non-linear control based on the input-output discrete-time description of systems is presented. The discussion focusses on coupling of reconstruction techniques for n-D irregularly sampled space- and/or band-limited functions with feedforward neural networks. The essence of the approach is to use the multi-dimensional irregular sampling theory to obtain the neural network representation of interpolating filter as well as bounds for accuracy of the interpolation from the finite set. Key questions from the relations between band- and space-limited functions are addressed and their consequence on neurocontrol are underlined.
Subject classification: AMS(MOS) 62D05, 93C10, 92B20, 93C35

Keywords: sampling theory, nonlinear control systems, neural networks, multi-dimensional systems

1 Introduction

This paper focusses on the discrete-time input-output model of a deterministic non-linear single-input single-output (SISO) system

$$y(k+1) = f(y(k), \ldots, y(k-n+1), u(k), \ldots, u(k-m+1)) \qquad (1)$$

with output $y \in [a,b] \subset \mathbb{R}$, and input $u \in [c,d] \subset \mathbb{R}$ and $f: D \to [a,b]$ with the domain of definition $D = [a,b]^n \times [c,d]^m \subset \mathbb{R}^{n+m}$. This model is referred to as NARMA (Non-linear Auto-Regressive Moving Average) model (see [1]) and is usually obtained by discretisation of a deterministic non-linear (Lipschitz) continuous-time SISO system described by controlled ordinary differential equations. NARMA models are valid only locally and with this caveat it may be a starting point for the considerations of non-linear dynamic systems modelling in the context of neurocontrol (see [6])

2 Generation of Irregular Samples by a Dynamic System

In practice f in (1) is often unknown, and modelling has to be based on the given pairs of multi-dimensional samples $((y_k, \ldots, y_{k-n+1}, u_k, \ldots, u_{k-m+1}), y_{k+1})$, where we put $y_k = y(k)$ etc. for brevity. Given the samples

$$\xi_k = (y_k, \ldots, y_{k-n+1}, u_k, \ldots, u_{k-m+1})$$

and $f(\xi_k)$, the issue is to reconstruct the multi-variable function f, a problem from multi-dimensional signal processing (note that it is completely separate from the question of band-limiting of y). The approach was introduced by Sanner & Slotine [3], but they assumed that the multi-dimensional samples are uniform, i.e., regularly distributed in the domain D of f. This seems to be a simplification, as the dynamics of (1) manifest themselves through irregular samples. For example, if f is linear, i.e., $y_{k+1} = a_0 y_k + \ldots + a_{n-1} y_{k-n+1} + b_0 u_k + \ldots + b_{m-1} u_{k-m+1}$, then even for constant input the output will not take values in constant increments, but according to the slope of the hyperplane determined by f. Thus even uniformity of u cannot, in general, ensure regular distribution of values of y, because the irregularity of the distribution represents f.

We now examine in detail the nature of this process in low dimensions (as this can be illustrated graphically). We look at the way nonuniform samples, i.e., ξ_k in the

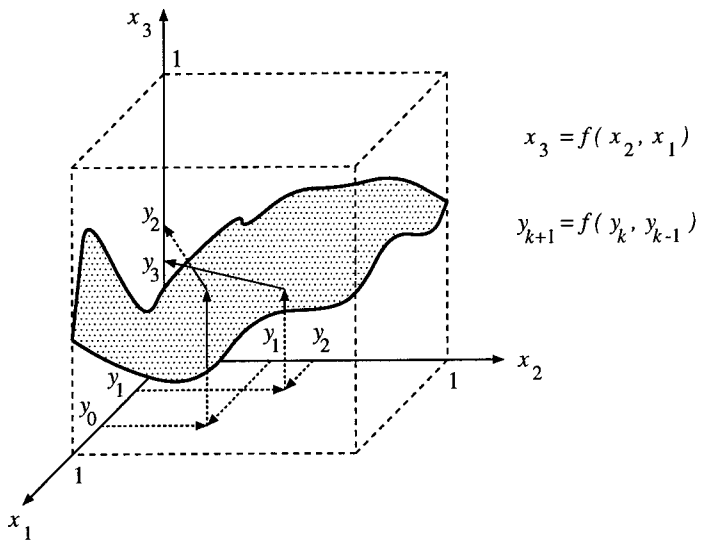

Figure 1 Iterative map $f: [0,1] \times [0,1] \to [0,1]$ defined by $y_{k+1} = f(y_k, y_{k-1})$.

pairs $(\xi_k, f(\xi_k))$, are generated when f is the right-hand side (RHS) of a dynamic system. For simplicity, instead of dealing with a controlled system of type (1), we concentrate on the low-order autonomous case

$$y_{k+1} = f(y_k, y_{k-1}), \tag{2}$$

with $y \in [0,1]$. Thus $\xi_k = (y_k, y_{k-1})$. We also assume that f is continuous; its domain, $D = [0,1]^2$ for (2), is compact (and connected).

The essential observation is that y_k, i.e., ξ_k of the pairs $(\xi_k, f(\xi_k))$ occur in the x_1x_2 plane in a nonuniform (irregular) way. They will be, in general, unevenly spaced and their pattern of appearance will depend on the dynamics of (2), or the shape of $f: [0,1] \times [0,1] \to [0,1]$.

The sample points $\xi_k = (y_k, y_{k-1})$ appear in the x_1x_2 plane, according to the iterative process (2); see Fig. 1. If we start with $\xi_1 = (y_1, y_0)$, where $y_1 \in Ox_2$ and $y_0 \in Ox_1$, then we can read out y_2 from the surface representing f. Then y_2 is reflected through $x_3 = x_2$ on the x_2x_3 plane, becoming a point on the Ox_2 axis. In the same time y_1 is reflected through $x_2 = x_1$ on the x_1x_2 plane, becoming a point on the Ox_1 axis. This results in the point (y_1, y_2) in the x_1x_2 plane, corresponding to the sample $\xi_2 = (y_2, y_1)$. We can now read out y_3 from the surface representing f and repeat the process for $k = 3$. Now y_3 'migrates' from Ox_3 to Ox_2 and y_2 from Ox_2 to Ox_1 generating the point (y_2, y_3) on the x_1x_2 plane corresponding to the sample $\xi_3 = (y_3, y_2)$ etc.

Thus, we have to address the issue of nonuniform sampling and to provide at least the existence conditions for function recovery with any degree of accuracy from a sufficiently large *finite* number of irregular samples making this way the application of neural networks plausible.

3 Band-limited and Space-limited Functions

The crucial question we are dealing with is whether the non-linear functions describing dynamical systems as NARMA models (1) are strictly band-limited or space-limited in the sense usually used in Signal Processing. Also important are the consequences of these properties for the reconstruction of such functions. The related question is how their extensions to the whole domain $\mathbb{R}^{n+m}$ functions are constructed. This is important, because we are going to use the harmonic analysis tools and especially Fourier Transform or Fourier Series. Thus we extend f to be equal to 0 outside its natural domain $D = [a,b]^n \times [c,d]^m$. For simplicity, the subsequent considerations concern mainly the 1-D case.

We shall say that a function $f(x)$ is *band-limited* if its Fourier transform (multi-dimensional) is zero outside a finite region, and its energy is finite, i.e.,

$$F(\omega) = 0 \quad \text{for} \quad |\omega| > \Omega \quad \text{and} \quad \mathrm{E} = \frac{1}{2\pi}\int_{-\Omega}^{\Omega} |\mathrm{F}(\omega)|^2 \mathrm{d}\omega < \infty.$$

ω and Ω being vectors, in general. Analogously we shall say that a function is *space-limited* in multi-dimensional case if

$$f(x) = 0 \quad \text{for} \quad |\mathrm{x}| > \mathrm{X} \quad \text{and} \quad \mathrm{E} < \infty.$$

The problem is: are the 'usual' functions encountered in dynamic systems description really band-limited or space-limited? From the theory of complex functions we know that any function that is band-limited is analytic in its domain, i.e., is an entire function. On the other hand, an entire function cannot vanish on an interval, except for the case $f(x) \equiv 0$; thus it is not space-limited. So f cannot be band-limited and space-limited at the same time. This is a manifestation of the *uncertainty principle* of harmonic analysis. For if we want to localise a function $f(x)$ in its (spatial) domain, it must be composed of very many $\sin \omega x$ and thus $\Delta\omega$ must be large and vice-versa. Generally, the uncertainty principle of harmonic analysis says: *It is impossible for a non-zero function and its Fourier transform to be simultaneously very small.*

4 Concentration Problem and Prolate Spheroidal Wave Functions

Knowing that a non-trivial band-limited function cannot be space-limited we naturally come to the question: what kind of *approximately* space-limited function corresponds to a given band-limited function. In practical terms we are looking for a function whose 'energy' outside the given spatial region is small enough to be indistinguishable from the energy of (strictly) space-limited function. Therefore, we may define a meaningful measure of concentration of a function as

$$\alpha^2(X) = \frac{\int_{-X/2}^{X/2} |f(x)|^2 dx}{\int_{-\infty}^{\infty} |f(x)|^2 dx}.$$

We want to determine how large $\alpha^2(X)$ can be for a given band-limited f; dually one may define an appropriate measure of concentration of the amplitude spectrum of $f(x)$, say $\beta^2(\Omega)$. Note that if $f(x)$ were indeed space-limited to $(-X/2, X/2)$, then $\alpha^2(X)$ would have its largest value, namely unity. To solve the problem of maximising $\alpha^2(X)$ we have to express $f(x)$ in terms of its amplitude spectrum $F(\omega)$ and find the $F(\omega)$ for which $\alpha^2(X)$ achieves maximal value. This is a classical

problem of mathematical physics (see [2]) and we know that the maximising $F(\omega)$ must satisfy the integral homogeneous Fredholm equation of the second kind

$$\int_{-\Omega}^{\Omega} \frac{\sin \pi T(\omega' - \omega'')}{\pi(\omega' - \omega'')} F(\omega'')d\omega'' = \alpha^2(X)F(\omega'), \qquad |\omega'| \leq \Omega. \tag{3}$$

The solutions to equation (3) are known as *prolate spheroidal wave functions (pswf)* and they provide a useful set of band-limited functions (see [5] for more details).

5 The $2X\Omega$ Theorem

Our principal question was how well the band-limited and space-limited functions (with above mentioned restrictions) are suited to model real-world dynamic automatic control systems. To shed more light on it let us recall the so-called $2X\Omega$ Theorem [4]. Its practical engineering formulation says that if $X\Omega$ is large enough, then the space of functions of space range X and 'bandwidth' Ω has dimension $\lceil 2X\Omega \rceil$. To formulate it in a more rigorous manner we have to introduce the notion of space-limited and band-limited functions in a way avoiding their dependence on the detailed behaviour of functions or their Fourier transforms at infinity.

So, we say that a function $f(x)$ is space-limited in multi-dimensional case to the interval $(X/2, X/2)$ at level ε if

$$\int_{|x|>X/2} |f(x)|^2 dx < \varepsilon,$$

i.e., if the energy outside this space region is less than it is, in some sense, essential for us. The same way we say that a function is band-limited with bandwidth Ω at level ε if

$$\int_{|\omega|>\Omega/2} |F(\omega)|^2 d\omega < \varepsilon,$$

i.e., the energy outside the frequency range is less than the value we are interested in. Using these newly defined functions we may state that every function is both space-limited and band-limited at level ε (for some X and Ω) as opposed to only one function ($f(x) \equiv 0$) which is both space-limited and band-limited in the strict sense.

To complete the reformulation of the $2X\Omega$ Theorem we need one more definition. We say that a set of functions $\mathcal{F}$ has an approximate dimension N at level ε on the interval $(-X/2, X/2)$ if there exists a set of $N = N(X, \varepsilon)$ functions $\phi_1, \phi_2, \ldots, \phi_N$ such that for each $f(x) \in \mathcal{F}$ there exist $a_1, a_2, \ldots, a_N$ such that

$$\int_{-X/2}^{X/2} \Big[f(x) - \sum_{j=1}^{N} a_j \phi_j(x) \Big]^2 dx < \varepsilon \tag{4}$$

and there is no set of $N-1$ functions that will approximate every $f(x) \in \mathcal{F}$ this way. This definition says, in other words, that every function in $\mathcal{F}$ can be approximated in $-X/2 < x < X/2$ by a function in the linear span of $\phi_1, \phi_2, \ldots, \phi_N$, so that the difference between the function and its approximation is less than ε.

Restated version of the theorem has now the following form:

Theorem 1 *Let $\mathcal{F}_\varepsilon$ be the set of functions space-limited to $(-X/2, X/2)$ at level ε and band-limited to $(-\Omega, \Omega)$ at level ε. Let $N(\Omega, X, \varepsilon, \varepsilon')$ be the approximate dimension of $\mathcal{F}_\varepsilon$ at level ε'. Then for every $\varepsilon' > \varepsilon$*

$$\lim_{X\to\infty} \frac{N(\Omega, X, \varepsilon, \varepsilon')}{X} = 2\Omega, \qquad \lim_{\Omega\to\infty} \frac{N(\Omega, X, \varepsilon, \varepsilon')}{\Omega} = 2X.$$

In fact these limits do not depend on ε and the set of functions which in real world we must consider to be limited both in space and frequency will be always asymptotically $2X\Omega$-dimensional.

6 Conclusions

In this paper we have shown how the irregular samples are generated by a dynamic system. We argue that in general this is an intrinsic feature of the NARMA model and our attempts to reconstruct the function f should be set in the irregular sampling context. The most important question in this setting is the one of space- and band-limitedness of the function under consideration. The result of paramount importance from the point of view of function approximation by *finite, linear* combinations of functions is given in the form of the $2X\Omega$ theorem. Equation (4) stipulates the existence of a *finite* approximation of a given nonlinear function by a *linear* combination of functions. It also gives the lower bound for the number of these functions. This allows the application of neural network with known (finite) number of neurons.

On the other hand, the $2X\Omega$ theorem is also interesting from the point of view of function reconstruction from its irregularly spaced samples. In this case we have to assume that our function to be reconstructed is band-limited. From practical considerations it has to be space-limited as well. This problem is normally solved in the context of the theory of complex functions analytic in the entire domain (entire functions and their special types). Let us notice that applying the $2X\Omega$ Theorem, instead of using entire functions of exponential type (as is usually the case in irregular sampling), which is quite restrictive, we deal with functions which are square-integrable—a condition that is easily fulfilled in most practical cases.

REFERENCES

[1] S. Chen and S. A. Billings. *Representation of non-linear systems: the NARMAX model.* International Journal of Control, Vol. 49 (1989), pp1013–1032.

[2] R. Courant and D. Hilbert. *Methods of Mathematical Physics*, Vol. 1. Interscience Publishers (1955), New York.

[3] R. M. Sanner and J.-J. E. Slotine. *Gaussian networks for direct adaptive control.* IEEE Transactions on Neural Networks, Vol. 3 (1992), pp837–863.

[4] D. Slepian. *Some comments on Fourier analysis, uncertainty and modelling.* SIAM Review, Vol. 25(3) (July 1983), pp379–393.

[5] D. Slepian and H. O. Pollak. *Prolate spheroidal wave functions, Fourier analysis and uncertainty, I.* The Bell System Technical Journal, Vol. 40(1) (January 1961), pp43–64.

[6] R. Żbikowski, K. J. Hunt, A. Dzieliński, R. Murray-Smith, and P. J. Gawthrop. *A review of advances in neural adaptive control systems.* Technical Report of the ESPRIT NACT Project TP-1, Glasgow University and Daimler-Benz Research, (1994). (Available from FTP server ftp.mech.gla.ac.uk as PostScript file /nact/nact_tp1.ps).

Acknowledgements

Work supported by ESPRIT III Basic Research Project No. 8039 *Neural Adaptive Control Technology*

UNSUPERVISED LEARNING OF TEMPORAL CONSTANCIES BY PYRAMIDAL-TYPE NEURONS.

Michael Eisele

The Salk Institute, Computational Neurobiology Laboratory, PO Box 85800, San Diego, CA 92186 - 5800, USA. Email: eisele@salk.edu

An unsupervised learning principle is proposed for individual neurons with complex synaptic structure and dynamical input. The learning goal is a neuronal response to temporal constancies: If some input patterns often occur in close temporal succession, then the neuron should respond either to all of them or to none. It is shown that linear threshold neurons can achieve this learning goal, if each synapse stores not only a weight, but also a short-term memory trace. The online learning process requires no biologically implausible interactions. The sequence of temporal associations can be interpreted as a random walk on the state transition graph of the input dynamics. In numerical simulations the learning process turned out to be robust against parameter changes.

1 Introduction

Many neocortical neurons show responses that are invariant to changes in position, size, illumination, or other properties of their preferred stimuli (see review [5]). These temporal "constancies" or "invariants" do not have to be inborn: In numerical simulations [2, 3, 6] neurons could learn such responses by associating stimuli that occur in close temporal succession. Similar temporal associations have also been observed experimentally [4].

In most numerical simulations [2, 6] temporal associations were formed with the help of "memory traces" which are running averages of the neuron's recent activity: If the stimulus S_i is often followed by the stimulus S_j, a strong response of the neuron to S_i causes a large memory trace at the time of stimulus S_j, which teaches the neuron to respont to S_j, too. By presenting the stimuli in reverse temporal order $S_j \rightarrow S_i$, the response to stimuli S_i is likewise strengthened by the response to stimulus S_i.

This simple learning scheme does no longer work, if the input dynamics is irreversible, that is if only the transition $S_i \rightarrow S_j$ occurs. In the following a more complex learning scheme will be presented, which can form associations in both temporal directions of an irreversible input dynamics. For this purpose an additional memory trace will have to be stored in each synapse. Numerical results are presented for neuronal input generated by a Markov process which is simpler than naturally occuring input, but irreversible and highly stochastic. A temporal constancy in such a dynamics consists of a set of states which are closely connected to each other by temporal transitions. The learned synaptic excitation can be derived from the neuronal firing pattern by interpreting the sequence of temporal associations as a random walk between Markov states.

2 Neuron Model

The model neuron was chosen to have the simple activation dynamics of a linear threshold unit, but a complicated learning dynamics. The input signal is generated by a temporally discrete, autonomous, stochastic dynamics with a finite number N of states S_i. Each state is connected with a sensory afferent. At any time t the afferent of the present state $R(t) \in \{S_0, \ldots S_N\}$ is set active ($x_j(t) = 1$ for

$R(t) = S_j$), while all the other afferents are set passive ($x_i(t) = 0$ for $R(t) \neq S_i$). Each afferent forms one synapse with the model neuron. The sum of weighted inputs is called the neuron's activity $a(R(t)) = \sum_i w_i x_i(t)$. If the activity exceeds a threshold θ, the neurons output $y(R(t))$ is 1, otherwise it is 0.

The memory trace $<p>_r$ of any quantity p is defined as its exponentially weighted past average at time t. The subscript r indicates over which time scale $1/\eta_r$ the average is done (with $0 < \eta_r < 1$).

$$<p>_r(t) := \eta_r \sum_{\tau=1}^{\infty} p(t-\tau) \cdot (1-\eta_r)^{(\tau-1)} \quad (1)$$

$$\Rightarrow <p>_r(t+1) - <p>_r(t) = \eta_r \cdot (p(t) - <p>_r(t)) \quad (2)$$

The neuron model includes a variable threshold $\theta(t)$ and a variable synaptic decay term $\rho(t)$, which serve to keep the neuron's average output y and activity a near the preset values $\overline{y}, \overline{a} > 0$.

$$\theta(t) := <\theta>_\theta(t) \cdot (1 + \eta_y \cdot (<y>_\theta(t) - \overline{y})) \quad (3)$$

$$\rho(t) := <\rho>_\rho(t) + \frac{1}{\eta_w <a>_\rho(t)} \cdot \left(<\sum_i \triangle w_i>_\rho(t) + \eta_\rho \cdot (<a>_\rho(t) - \overline{a}) \right) \quad (4)$$

(Remember that the memory traces $<\theta>_\theta(t)$ and $<\rho>_\rho(t)$ at time t do not depend on $\theta(t)$ or $\rho(t)$.) If the total synaptic change $\sum_i \triangle w_i$ is positive and if the activity a exceeds its target $\overline{a}$, ρ will decrease on a time scale $1/\eta_\rho$, causing a subsequent decrease of synaptic weights in eq. (6). The time scales $1/\eta_\theta$ and $1/\eta_\rho$ of the averages are set large compared to the recurrence time of sensory input patterns. The rate $\eta_y \approx 1/3$ determines how much the threshold θ is increased, if the average output $<y>_\theta$ exceeds its target $\overline{y}$.

Synaptic learning processes determine the synaptic weights w_i and the synaptic short-term memory traces q_i, which measure the contribution that a synapse has recently made to the neuronal activity a.

$$q_i(t) := \left\langle \frac{w_i \cdot x_i}{a} \right\rangle_f (t) \quad (5)$$

$$\triangle w_i(t) := \eta_w w_i(t) x_i(t) \left(\alpha_p \frac{<z>_p(t)}{a(t)} - \rho(t) \right) + \eta_w \alpha_f z(t) q_i(t) \quad (6)$$

The decay term $\rho(t)$ was defined above. The past and future prefactors α_f and α_p will be discussed below. The quantity $z(t)$ models the postsynaptic depolarization that effects the learning process. It is defined as a sum $z(t) := a(t) + \gamma y(t)$ of the depolarization a caused by other synaptic inputs and the depolarization caused by the firing y of the postsynaptic neuron, weighted by a factor $\gamma > 0$.

This synaptic learning rule can be rewritten into a more comprehensible form by defining modified synaptic changes $\widetilde{\triangle w_i}$:

$$\widetilde{\triangle w_i}(t) := \eta_w w_i(t) x_i(t) \left(\frac{\alpha_p}{a(t)} \eta_p \sum_{\tau=1}^{\infty} z(t-\tau) \cdot (1-\eta_p)^{(\tau-1)} + \frac{\alpha_f}{a(t)} \eta_f \sum_{\tau=1}^{\infty} z(t+\tau) \cdot (1-\eta_f)^{(\tau-1)} - \rho(t) \right) \quad (7)$$

By inserting definitions (1) and (5) into eq. (6) one can easily show that the modified synaptic changes cause approximately the same total changes in the long run:

$\sum_{t=1}^{T} \Delta w_i(t) \approx \sum_{t=1}^{T} \widetilde{\Delta w_i}(t)$ for large T. The approximation is good, if the learning period T is much larger than the duration $1/\eta_f$ of the synaptic memory trace q_i. It is exact, if the depolarization $z(t)$ is zero for $t < 1$ and $t > T$.

The definition (7) of $\widetilde{\Delta w_i}$ resembles resembles an unsupervised Widrow-Hoff-rule, in which the desired activity of the neuron depends on an exponentially weighted average of past and future postsynaptic depolarizations $z(t \pm \tau)$. Because the future depolarizations $z(t+\tau)$ are not yet known at time t, the memory traces q_i had to be introduced in order to construct the online learning rule (6) of $\Delta w_i(t)$.

3 Interpretation of Temporal Associations as a Random Walk

After a sufficiently long time t_0, any successful learning process should reach a quasistationary state, in which synaptic changes cancel each other in the long run. In the following we will derive the neural activities $a(S_i)$ in the quasistationary state from the neural outputs $y(S_j)$ and the transition rules of the input dynamics. Even in the quasistationarity state, the quantities w_i, θ, and ρ will fluctuate irregularily, if the input is generated by a stochastic dynamics. We assume that the learning rates η_w, η_θ and η_ρ are so small that these fluctuations can be neglected. Then the activity a, the output y, and the depolarization $z = a + \gamma y$ depend on time t only through the state $R(t)$ of the input dynamics. Under the assumption that the input dynamics is ergodic, the temporal average $\sum_{t=1}^{T} \widetilde{\Delta w_i}(t+t_0)/T$ can be replaced by an average over all possible trajectories $\ldots \to R(-1) \to R(0) \to R(1) \to \ldots$ of the input dynamics. By definition, quasistationarity has been reached, if these average weight changes vanish for all synapses. Using definition (7) of $\widetilde{\Delta w_i}$, the condition of quasistationarity now reads:

$$a(R(0)) \stackrel{!}{=} \frac{\alpha_f}{\rho} \cdot \sum_{R(1),R(2),\ldots} \left(P_f(R(0)\to R(1)\to R(2)\ldots)\eta_f \sum_{\tau=1}^{\infty} z(R(\tau))(1-\eta_f)^{(\tau-1)} \right)$$
$$+ \frac{\alpha_p}{\rho} \cdot \sum_{\ldots,R(-2),R(-1)} \left(P_p(\ldots R(-2)\to R(-1)\to R(0))\eta_p \sum_{\tau=1}^{\infty} z(R(-\tau))(1-\eta_p)^{(\tau-1)} \right) \quad (8)$$

for any state $R(0)$. Here $P_f(R(0) \to R(1) \to \ldots)$ denotes the probability measure that a trajectory starting at $R(0)$ will subsequently pass through $R(1)$, $R(2)$, ... Analogously, $P_p(\ldots \to R(-1) \to R(0))$ denotes the relative probabilities of trajectories ending at $R(0)$.

The right hand side of eq. (8) can be interpreted as an average over random jumps between states of the input dynamics. Every jump starts at state $R(0)$. It jumps with probability α_f/ρ into the future and with probability α_p/ρ into the past. The jump length τ is exponentially distributed, with a mean of $1/\eta_f$ (or $1/\eta_p$) time steps being transversed. If the dynamics is stochastic, several end states may be reached after $\pm\tau$ time steps. The end state $R(\pm\tau)$ is then chosen according to the transition probabilities P_f or P_p, which were defined above. The effective depolarization $z = a + \gamma y$ of the end state is averaged over all possible jumps. According to eq. (8), this average should equal the activity $a(R(0))$ at the start state $R(0)$.

The activity $a(R(0))$ at the start state still depends on the unknown activity $a(R(\pm\tau))$ at the end state. The latter can again be interpreted as an average over random jumps, which start from state $R(\pm\tau)$. By repeating this concatenation of

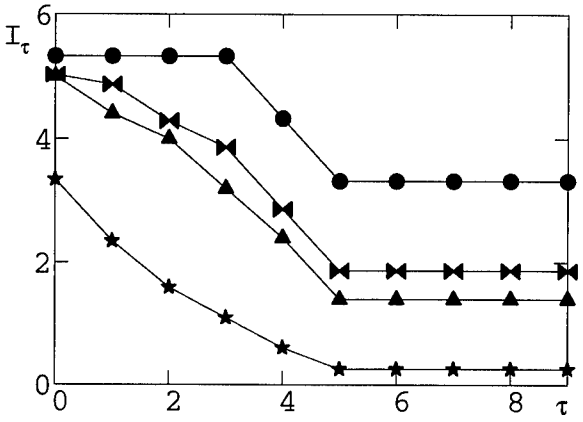

Figure 1 I_τ is the information which a first spike at time t transmits about the state of the input dynamics at time $t+\tau$. A neuron responding to a randomly chosen set of 32 states would convey very little information (stars). A neuron with suitable learning parameters (see text) can improve its response: Circle: response to an optimal set of 32 states at $t \approx 10^6$. Triangle: response to 33 states at $t \approx 2 \cdot 10^6$, if the "drift" is slightly positive ($\alpha_f = 0.55$; $\alpha_p = 0.45$; $\eta_f = \eta_p = 0.8$). Bowtie: response to 31 states at $t \approx 2.5 \cdot 10^6$, if a maximal drift ($\alpha_f^a = \alpha_p^b = 0$) is compensated by interactions of two different dendrites.

jumps, one forms a random walk (which should not be confused with a trajectory of the input dynamics). By averaging eq. (8) over all start states $R(0)$ one can easily show that the total jump probability $\alpha_f/\rho + \alpha_p/\rho \approx 1/(1+\gamma\overline{y}/\overline{a}) < 1$, so that the random walk is of finite mean length $\overline{a}/(\gamma\overline{y})$. Thus one can sum γy over the end states of all jumps in a random walk and average this sum over all the random walks starting at S_j. According to construction, this average shold equal the activity $a(S_j)$, once that the learning process has reached quasistationarity.

4 Numerical Results

The learning algorithm was tested with input generated by a special Markov process, whose high internal symmetry permits an accurate assessment of the learning process. Each of its $10 \cdot 2^5 = 320$ equally probable states is denoted by a digit sequence $C\ B_1B_2B_3B_4B_5$, with $C \in \{0,1,\ldots 9\}$ and $B_i \in \{0,1\}$. Each state $C\ B_1B_2B_3B_4B_5$ forms two equally probable transitions to the states $C'\ B_2B_3B_4B_50$ and $C'\ B_2B_3B_4B_51$, with $C' \equiv C+1 \bmod 10$.

With suitable learning parameters ($\overline{y} = 0.1$, $\gamma = 0.1$, $\alpha_f = \alpha_p = 0.5$, and $1/\eta_f = 1/\eta_p = 1.25$, $\eta_w \approx 0.04$) and random initial synaptic weights the neuron needed 1 million time steps of online learning to develop a quasistationary response. It responded to 32 states of the Markov process, namely the 8 states $0\ B_1B_2B_301$ (with $B_1B_2B_3 \in \{000,001,\ldots 111\}$), the 8 states $1\ B_1B_201B_5$, the 8 states $2\ B_101B_4B_5$, and the 8 states $3\ 01B_3B_4B_5$. According to the rules of the input dynamics, these four groups of states are always passed in the given order. Thus the neuron always responds for 4 consequetive time steps. By its first spike ($y(t) = 1$ after $y(t-1) = 0$) it transmits an information $I_\tau = \log_2(320/8) \approx 5.3$ about the state $R(t=\tau)$ of the input dynamics at the present moment $\tau = 0$ and the next three time steps

$\tau = 1, 2$ or 3 (see fig. 1). One can prove that this is one of the "most constant" responses to the input dynamics, in the sense that no neuron with mean firing rate $\overline{y} = 0.1$ can transmit more information I_τ by its first spike or show more than 4 consequetive responses at some times without showing less than 4 consequetive responses at other times.

A deeper analysis of the properties of the random walk showed that the learning process is robust against almost all parameter changes (as long as $\eta_f, \eta_p, \eta_w, \eta_\theta, \eta_\rho$, and γ remain small enough). The one critical learning parameter is $\alpha_f/\eta_f - \alpha_p/\eta_p$, the mean drift of the random walk into the future direction per jump. In the extreme case $\alpha_p = 0$ the learning goal (8) would require the neuron's strongest activity to preceed its output $y = 1$ in time, which is inconsistent with the output being caused by the neuron's strongest activity. Only if the drift was rather small, did the learning process converge to quasistationarity (triangles in fig. 1).

There is a way to turn the learning process robust against changes in α_f and α_p. One constructs a neuron with two different dendrites, differing in the values ρ, $<\rho>_\rho$, $<\sum_i \triangle w_i>_\rho$, and $<a>_\rho$ and the synaptic learning parameters $\alpha_f, \alpha_p, \eta_f, \eta_p$: In dendrite a the drift $\alpha_f^a/\eta_f^a - \alpha_p^a/\eta_p^a$ is chosen negative, in dendrite b the drift $\alpha_f^b/\eta_f^b - \alpha_p^b/\eta_p^b$ is chosen positive. This learning process always reached quasistationarity in numerical simulation. The early part of neuronal responses was caused by dendrite b, the late part by dendrite a. The worst choice of learning parameters (maximal drift $\alpha_f^a = \alpha_p^b = 0$) still produced a rather good neuronal response (bowties in fig. 1). The known anatomical connections in the neocortex suggest that dendritic type a might correspond to apical dendrites and dendritic type b to basal dendrites[1]. This speculative hypothesis might be tested by simulating networks of such neurons.

REFERENCES

[1] Eisele, M., *Vereinfachung generierender Partitionen von chaotischen Attraktoren,* (German) PhD-thesis, Appendix D, ISSN 0944-2952 Jül-report 3021, KFA-Jülich, Jülich (1995).

[2] Földiak, P., *Learning invariance from transformation sequences,* Neural Computation, Vol.3 (1991), pp194–200.

[3] Mitchison, G. J., *Removing time variation with the anti-hebbian differential synapse,* Neural Computation, Vol.3 (1991), pp312–320.

[4] Miyashita, Y. & Chang, H.-S., *Neuronal correlate of pictorial short-term memory in the primate temporal cortex,* Nature, Vol. 331 (1988), pp68–70.

[5] Oram, M. W. & Perret, D. I., *Modeling visual recognition from neurobiological constraints,* Neural Networks, Vol.7 (1994), pp945–972.

[6] Wallis, G., Rolls, E. T., & Foldiak, P., *Learning invariant responses to the natural transformations of objects,* Int. Joint Conf. on Neural Net., Vol.2 (1993), pp1087–1090.

Acknowledgements

The author thanks F. Pasemann for many useful discussions and E. Pöppel and G. Eilenberger for general support. This work was done at the KFA Jülich, Germany.

NUMERICAL ASPECTS OF MACHINE LEARNING IN ARTIFICIAL NEURAL NETWORKS

S.W. Ellacott and A. Easdown

School of Computing and Mathematical Sciences, University of Brighton, Brighton BN1 4GJ, UK. Email: S.W.Ellacott@brighton.ac.uk

In previous papers e.g. [5] the effect on the learning properties of filtering or other preprocessing of input data to networks was considered. A strategy for adaptive filtering based directly on this analysis will be presented. We focus in Section 2 on linear networks and the delta rule since this simple case permits the approach to be easily tested. Numerical experiments on some simple problems show that the method does indeed enhance the performance of the epoch or off line method considerably. In Section 3, we discuss briefly the extension to non-linear networks and in particuar to backpropagation. The algorithm in its simple form is, however, less successful and current research focuses on a practicable extension to non-linear networks.

1 Introduction

In previous papers e.g. [5] the effect on the learning properties of filtering or other preprocessing of input data to networks was considered. Such filters are usually constructed either on the basis of knowledge of the problem domain or on statistical or other properties of the input space. However in the paper cited it was briefly pointed out that it would be possible to construct filters designed to optimise the learning properties directly by inferring spectral properties of the iteration matrix during the learning process, permitting the process to be conditioned dynamically. The resulting technique is naturally parallel and easily carried out alongside the learning rule itself, incurring only a small computational overhead. Here we explore this idea.

2 Linear Theory

Although not the original perceptron algorithm, the following method known as the *delta rule* is generally accepted as the best way to train a simple perceptron. Since there is no coupling between the rows we may consider the single output perceptron. Denote the required output for an input pattern $\mathbf{x}$ by y, and the weights by the vector $\mathbf{w}^T$. Then,

$$\delta \mathbf{w} = \eta(y - \mathbf{w}^T\mathbf{x})\mathbf{x}$$

where η is a parameter to be chosen called the *learning rate* [7],p.322 . Thus given a current iterate weight vector $\mathbf{w_k}$,

$$\mathbf{w_{k+1}} = \mathbf{w_k} + \eta(y - \mathbf{w_k}^T\mathbf{x})\mathbf{x} = (I - \eta\mathbf{x}\mathbf{x}^T)\mathbf{w_k} + \eta y\mathbf{x} \qquad (1)$$

since the quantity in the brackets is scalar. The bold subscript $\mathbf{k}$ here, denotes the *kth* iterate, not the *kth* element. We will consider a fixed and finite set of input patterns $\mathbf{x_p}$, $p = 1 \ldots t$, with corresponding output y_p. If we assume that the patterns are presented in repeated cyclic order, the presented $\mathbf{x}$ and corresponding y of (1) repeat every t iterations, and given a sufficiently small η, the corresponding weights go into a limit t-cycle: see [3] or [5]. Of course this is not the only or necessarily best possible presentation scheme [2], but other methods require *a priori* analysis of the data or dynamic reordering. Since we are assuming that we have a fixed and finite set of patterns $\mathbf{x_p}$, $p = 1 \ldots t$, an alternative strategy is not to update the weight vector until the whole epoch of t patterns has been presented.

This idea is attractive since it actually generates the steepest descent direction for the least sum of squares error over all the patterns. We will call this the *epoch method* to distinguish it from the usual delta rule. (Other authors use the term *off line learning.*) This leads to the iteration

$$\mathbf{w_{k+1}} = \Omega \mathbf{w_{k+1}} + \eta \sum_{p=1}^{t} (y_p \mathbf{x_p}) \tag{2}$$

where $\Omega = (I - \eta X X^T) = (I - \eta L)$. Here X is the $n \times t$ matrix whose columns are the $\mathbf{x_p}$'s. The k in (2) is, of course, not equivalent to that in (1), since it corresponds to a complete epoch of patterns. There is no question of limit cycling, and, indeed a fixed point will be a true least squares minimum $\mathbf{w}^*$. To see this, put $\mathbf{w_{k+1}} = \mathbf{w_k} = \mathbf{w}^*$ and observe that (2) reduces to the normal equations for the least squares problem. Moreover the iteration (2) is simply steepest descent for the least squares problem, applied with a fixed step length. Clearly $L = XX^T$ is symmetric and positive semi definite. In fact, provided the $\mathbf{x_p}$ span, it is (as is well known) strictly positive definite. The eigenvalues of Ω are $1 - \eta$(*the corresponding eigenvalues of* L), and hence for η sufficiently small $\varrho(\Omega) = \|\Omega\|_2 < 1$. Unfortunately, however, (2) generally requires a smaller value of η than (1) to retain numerical stability [3], [5]. How can we improve stability of (2) or indeed (1)? Since these are linear iterations it is only necessary to remove the leading eigenvalue of the iteration matrix. Specifically we seek a matrix T such that if each input vector $\mathbf{x_p}$ is replaced by $T\mathbf{x_p}$, more rapid convergence will result. We see from (2) that the crucial issue is the relationship between the unfiltered update matrix $\Omega = (I - \eta X X^T)$ and its filtered equivalent $(I - \eta T X X^T T^T) = \Omega'$ say. In general these operations may be defined on spaces of different dimension: see e.g. [5], but here we assume T is $n \times n$. To choose T we compute the largest eigenvalue and corresponding eigenvevtor of XX^T. This may be carried out by the power method [6], p.147 at the same time as the ordinary delta rule or epoch iteration: the computation can be performed by running through patterns one at a time, just as for the learning rule itself. We get a normalised eigenvector $\mathbf{p_1}$ of XX^T corresponding to the largest eigenvalue λ_1 of XX^T. Set

$$T = I + (\lambda_1^{-1/2} - 1)\mathbf{p_1}\mathbf{p_1}^T. \tag{3}$$

A routine calculation shows that TXX^TT^T has the same eigenvectors as XX^T, and the same eigenvalues but with λ_1 replaced by 1. Each pattern $\mathbf{x_p}$ should then be multiplied by T, and, since we are now iterating with different data, the current weight estimate $\mathbf{w}$ should be multiplied by

$$T^{-1} = I + (\lambda_1^{1/2} - 1)\mathbf{p_1}\mathbf{p_1}^T. \tag{4}$$

We may then repeat the process to remove further eigenvalues. Basically the same idea can be used for the iteration with the weights updated after each pattern as in (1), but it is less convenient: for simplicity, our numerical experiments refer only to the application to (2). Two small examples are discussed: in each case four eigenvalues are removed though in fact for the first example, only the first eigenvalue is significant.

The first example is a 'toy' problem taken from [5],p113. There are four patterns and $n = 3 : \mathbf{x_1} = (1,0,0)^T, \mathbf{x_2} = (1,1,0)^T, \mathbf{x_3} = (1,1,1)^T$ and $\mathbf{x_4} = (1,0,1)^T$. The corresponding outputs are $y_1 = 0, y_2 = y_3 = y_4 = 1$. Figure 1 shows the number of

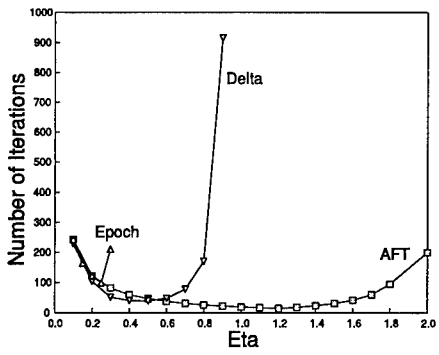

Figure 1

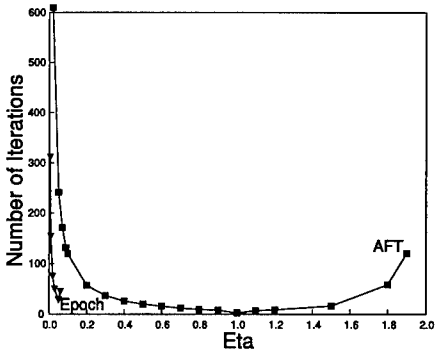

Figure 2

epochs required to obtain agreement in the weights (at the end of the epoch for the delta rule) to an error or 1E-8, for various values of η and for the three methods: the delta rule (1), the epoch or off line method (2) and the Adaptive Filtering Method (AFT) using (3).

As a slightly more realistic example we also considered the Balloon Database B from the UCI Repository of Machine learning and domain theories [1]. This is a set of sixteen 4-vectors which are linearly separable. Figure 2 compares the perfomance of the epoch and AFT methods: on this very well behaved database the epoch method actually performs better in terms of iterations than the delta rule even though it requires a larger value of η. With $\eta = 1$, AFT requires only three epochs and good performance is obtained over a wide range, whereas the best obtainable with the epoch method is 28 with $\eta = 0.05$ and this is a very sharp minimum: $\eta = 0.03$ requires 49 iterations, and $\eta = 0.06$ requires 45.

3 Non-linear Networks

The usefulness of linear neural systems is limited, since many pattern recognition problems are not linearly separable. We will define a general nonlinear delta rule. The *backpropagation rule* [7], pp.322-328 used in many neural net applications is a special case of this. For the linear network the dimension of the input space and the number of weights are the same: n in our previous notation. Now we will let M denote the *total number* of weights and n the input dimension. So the input patterns $\mathbf{x}$ to our network are in $\mathbb{R}^n$, and we have a vector $\mathbf{w}$ of parameters in $\mathbb{R}^M$ describing the particular instance of our network: i.e. the vector of synaptic weights. For a single layer perceptron with m outputs, the vector $\mathbf{w}$ is the the $m \times n$ weight matrix, and thus $M = mn$. For a multilayer perceptron, $\mathbf{w}$ is the cartesian product of the weight matrices in each layer. For brevity we consider just a single output. The network computes a function $g : \mathbb{R}^M \times \mathbb{R}^n \rightarrow \mathbb{R}$. In [4] or [5] it is shown that the generalised delta rule becomes

$$\delta \mathbf{w} = \eta(y - g(\mathbf{w}, \mathbf{x}) \nabla g(\mathbf{w}, \mathbf{x}) \tag{5}$$

∇g takes the place of $\mathbf{x}$ in (1). Observe that a change of weights in any given layer will cause a (linear) change in the *input* vector to the succesive hidden layer. Thus the required gradient is obtained by i) differentiating the current layer with respect

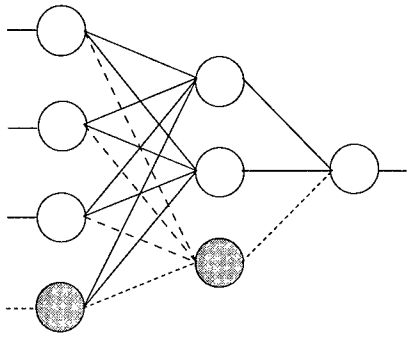

Figure 3

to the weights in the layer and ii) multiplying this by the matrix representation of the Fréchet derivative *with respect to the inputs* in the succeeding layers. Thus, let the *kth* weight layer, $k = 1, 2, \ldots K$, say, have weight matrix W_k : each row of these matrices forms part of the parameter vector $\mathbf{w}$. On top of each weight layer is a (possibly) non-linear layer. At each of the m (say) hidden units we have an activation function: h_j for the jth unit. The function $\mathbf{h}$ whose jth co-ordinate function is h_j is a mapping $\mathbb{R}^m \to \mathbb{R}^m$. However for a multilayer perceptron it is rather special in that h_j only depends on the jth element of its argument: in terms of derivatives this means that the Jacobian H of $\mathbf{h}$ is diagonal. Let the H and $\mathbf{h}$ for the units layer *after* the kth weight layer also be subscripted k. (Input units to the bottom layer just have identity activation, as is conventional.) Finally suppose that the input to the kth weight layer (i.e. the output from the units of the previous layer) are denoted $\mathbf{v_k}$, with $\mathbf{v_1} = \mathbf{x}$. A small change δW_k in the kth weight matrix causes the input to the corresponding unit layer to change by $\delta W_k \mathbf{v_k}$. The Fréchet derivative of a weight layer $W_r \mathbf{v_r}$ with respect to its input $\mathbf{v_r}$ is of course just W_r. Thus the output is changed by $H_K W_K H_{K-1} W_{K-1} \ldots H_k \delta W_k \mathbf{v_k}$. Since this expression is linear in δW_k it yields for each individual element that component of the gradient of g corresponding to the weights in the kth layer. To see this, recall that the gradient is actually just a Fréchet derivative, i.e. a linear map approximating the change in output. In fact we might as well split up W_k by rows and consider a change $(\delta \mathbf{w_{i,k}})^T$ in the ith row (only). This corresponds to $\delta W_k = \mathbf{e_i}(\delta \mathbf{w_{i,k}})$, so $\delta W_k \mathbf{v_k} = \mathbf{e_i}(\delta \mathbf{w_{i,k}})\mathbf{v_k} = \mathbf{e_i}\mathbf{v_k}^T(\delta \mathbf{w_{i,k}})^T = V_{i,k}(\delta \mathbf{w_{i,k}})^T$, say, where $V_{i,k}$ is the matrix with ith row $\mathbf{v_k}$, and zeros elsewhere. Thus, that section of ∇g in (5) which corresponds to changes in the ith row of the kth weight matrix is $H_K W_K H_{K-1} W_{K-1} \ldots H_k V_{i,k}$. The calculation is illustrated in the following example. Figure 3 shows the architecture. The shaded neurons represent bias neurons with activation functions the identity, and the input to the bias neuron in the input layer is fixed at 1. The smaller dashed connections have weights fixed at 1, and the larger dashed ones have weights fixed at 0. (This approach to bias has been adopted to keep the matrix dimensions consistent.) All other neurons have the standard activation function $a = 1/(1 + e^x)$. Other than the bias input, the data is the same as the first example in Section 2. Let the initial weights be

0.01	0.03	0.05	0
0.02	0.04	0.06	0
0	0	0	1

between the inputs and hidden layers numbering from the top in 3. Thus no bias is applied (but weights in rows 1 and 2 in the last column are trainable), and the bottom row of weights is fixed. Weights are

0.01	0.02	0.02

between hidden and output layer, so a bias of 0.03 is applied to the output neuron and this is trainable. With input $\mathbf{x_1} = (1, 0, 0, 0)^T$ and $y_1 = 1$, we find that (working to 4dp) the output from the non-bias hidden units are 0.5025 and 0.5050. The bias output is of course 1. The output from the output unit is 0.5113. Using the fact that the derivative of the standard activation function is $a(1-a)$, the diagonal elements of the 3×3 matrix H_1 are 0.2500, 0.2500 and 1 from the bias unit. The off diagonal elements are, of course, 0. H_2 is a 1×1 matrix (i.e. a scalar) with value 0.2499. Ignoring terms corresponding to fixed weights we have 11 trainable weights: 8 below the hidden layer and 3 above. ∇g is a thus an 11-vector with the first three elements (say) corresponding to the hidden-to-output weights. (This is the convenient ordering for backpropagation, as the output gradient terms must be computed first.) So the first three elements of ∇g are given by $H_2 V_{1,2} = 0.2499 V_{1,2} = 0.2499 \mathbf{v}_2^T$ (since $\mathbf{e_1}$ is here a 1-vector with element 1) = (0.1256, 0.1262, 0.2499). Proceeding to the sub-hidden layer weights, the first four elements are given by $H_2 W_2 H_1 V_{1,1}$. The product $H_2 W_2 H_1$ evaluates to (0.0006, 0.0012, 0.0075). $V_{1,1} = \mathbf{e_1 v_1^T}$, which has (1,0,0,1) as first row and zeros elsewhere. Hence elements 4 to 7 of ∇g are (0.0006, 0, 0, 0.0006). Similarly elements 8 to 11 of ∇g are (0.0012, 0, 0, 0.0012).

Experiments with the adaptive filtering algorithm have as yet been less successful than in the linear case, due to problems of underdetermination and non-stationarity. These difficulties, which do not appear to be insurmountable, are the focus of current research.

REFERENCES

[1] *The uci repository of machine learning and domain theories*, ftp from ics.uci.edu: /pub/machine-learning-database.

[2] C. Cachin, *Pedagogical pattern selection strategies*, Neural Networks Vol.7 No.1 (1994), pp175–181.

[3] S.W. Ellacott, *An analyis of the delta rule*, in Proceedings of the International Neural Net Conference, Kluwer Academic Publishers (1990), pp956–959.

[4] S.W. Ellacott, *Techniques for the mathematical analysis of neural networks*, J. Computational and Applied Mathematics, Vol.50 (1993), pp283–297.

[5] S.W. Ellacott, *Aspects of the numerical analysis of neural networks* Acta Numerica, Cambridge University Press (1994).

[6] E Isaacson and H.B. Keller, *Analysis of numerical methods*, Wiley (1966).

[7] D.E. Rumelhart and J.L. McClelland. *Parallel and distributed processing: explorations in the microstructure of cognition*, Vols.1 and 2, MIT (1986).

LEARNING ALGORITHMS FOR RAM-BASED NEURAL NETWORKS

Alistair Ferguson, Laurence C Dixon and Hamid Bolouri

Engineering Research and Development Centre,
University of Hertfordshire College Lane, Hatfield, Herts, AL10 9AB, UK.

RAM-based neural networks are designed to be hardware amenable, which affects the choice of learning algorithms. Reverse differentiation enables derivatives to be obtained efficiently on any architecture. The performance of four learning methods on three progressively more difficult problems are compared using a simulated RAM network. The learning algorithms are: reward-penalty, batched gradient descent, steepest descent and conjugate gradient. The applications are: the 838 encoder, character recognition, and particle classification. The results indicate that reward-penalty can solve only the simplest problem. All the gradient-based methods solve the particle task, but the simpler ones require more CPU time.

1 Introduction

The driving force behind RAM-based neural networks is their ease of hardware realisation. The desire to retain this property influences the design of learning algorithms. Traditionally, this has led to the use of the reward-penalty algorithm, since only a single scalar value needs to be communicated to every node [7]. The mathematical tool of *reverse differentiation* enables derivatives of an arbitrary function to be obtained efficiently at an operational cost of less than three times the original function. Using three progressively more complex problems, the performance of three gradient-based algorithms and reward-penalty are compared.

2 HyperNet Architecture

HyperNet is the term used to denote the hardware model of a RAM-based neural architecture proposed by Gurney [5], which is similar to the pRAM of Gorse and Taylor [4]. A neuron is termed a multi-cube unit (MCU), and consists of a number of subunits, each with an arbitrary number of inputs. j and k reference nodes in the hidden and output layers respectively, with $i = 1, \ldots, I$ indexing the subunits. μ denotes the site addresses, and is the set of bit strings $\mu_1 \ldots, \mu_n$ where n denotes the number of inputs to the subunit. z_c refers to the c^{th} real-valued input, with $z_c \in [0, 1]$ and $\hat{z}_c \equiv (1 - z_c)$. For each of the 2^n site store locations, two sets are defined: $c \in M^{ij}_{\mu 0}$ if $\mu_c = 0$; $c \in M^{ij}_{\mu 1}$ if $\mu_c = 1$. The access probability $P(\mu^{ij})$ for location μ in subunit i of hidden layer node j is therefore $P(\mu^{ij}) = \prod_{c \in M^{ij}_{\mu 0}} \hat{z}_c \prod_{c \in M^{ij}_{\mu 1}} z_c$. The subunit response ($s$) is then gained by summing the proportional site values, which are in turn accumulated to form the multi-cube activation (a). The node's output (y) is given by passing the MCU activation through a sigmoid transfer function ($y = \sigma(a) = 1/(1 + e^{-\frac{a}{\rho}})$). The complete forward pass of a two layer network of HyperNet nodes is given in Table 1. in the form of a computational graph.

Gradient-based algorithms require the extraction of error gradient terms. Reverse differentiation [10] enables derivatives to be obtained efficiently on any architecture. Functions are usually composed of simple operations, and this is the basis on which reverse accumulation works. A computational graph with vertices 1 to N connected by arcs is constructed. The first n vertices are the independent variables, with the results of subsequent basic operations $f_u(.)$ stored in intermediate variables

Computational Graph	Reverse Accumulation

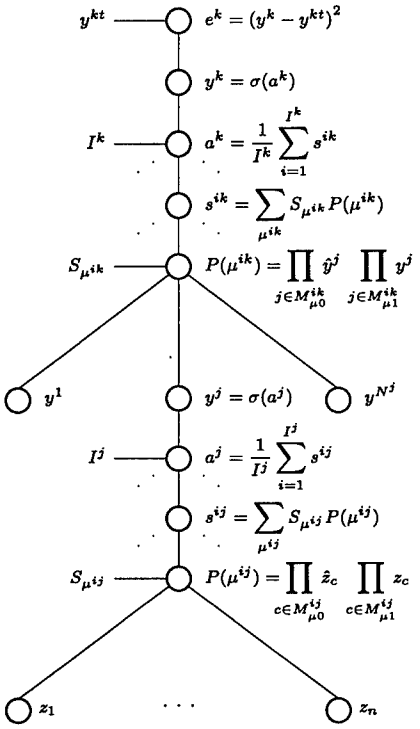

$$\bar{e}^k = 1$$

$$\bar{y}^k = 2(y^k - y^{kt})\bar{e}^k$$

$$\bar{a}^k = \sigma\prime(a^k)\bar{y}^k$$

$$\bar{s}^{ik} = \frac{1}{I^k}\bar{a}^k$$

$$\bar{S}_{\mu^{ik}} = P(\mu^{ik})\bar{s}^{ik}$$

$$\bar{P}(\mu^{ik}) = S_{\mu^{ik}}\bar{s}^{ik}$$

$$\bar{y}^j = \sum_{\substack{k \text{ where} \\ j \in M^{ik}_{\mu 1}}} \left(\prod_{\substack{c \in M^{ik}_{\mu 1} \\ c \neq j}} y^c \prod_{c \in M^{ik}_{\mu 0}} \hat{y}^c \right) \bar{P}(\mu^{ik})$$

$$- \sum_{\substack{k \text{ where} \\ j \in M^{ik}_{\mu 0}}} \left(\prod_{c \in M^{ik}_{\mu 1}} y^c \prod_{\substack{c \in M^{ik}_{\mu 0} \\ c \neq j}} \hat{y}^c \right) \bar{P}(\mu^{ik})$$

$$\bar{a}^j = \sigma\prime(a^j)\bar{y}^j$$

$$\bar{s}^{ij} = \frac{1}{I^j}\bar{a}^j$$

$$\bar{S}_{\mu^{ik}} = P(\mu^{ij})\bar{s}^{ij}$$

Table 1 Forward and reverse accumulation of a two layer network of real-valued HyperNet nodes.

$x_u = f_u(.), u = n+1, \ldots, N$ with $F(x) = x_N$. The gradient vector $g(x) = \partial F(x)/\partial x$ can then be obtained by defining $\bar{x} = \partial x_v/\partial x_u, u = 1, \ldots, v$ for vertex u, and applying the chain rule. The process thus starts at vertex N, where $\bar{x}_N = 1$, and percolates down. The reverse accumulation of a two layer HyperNet network is also given in Table 1.

3 Learning Algorithms

The reward-penalty algorithm used is an adaptation of the P-model associative algorithm devised by Barto [2] and modified for HyperNet nodes by Gurney [5]. A single scalar reinforcement signal, calculated from a performance measure, is globally broadcast. The internal parameters are updated using this signal, and local information. The performance metric used is the mean-squared error on the output layer ($e = 1/N^k \sum_{k=1}^{N^k} [\sigma(a^k) - y^{kt}]^2$ where y^{kt} is the target output for node k, and N^k is the number of output layer nodes). The binary reward signal is then probabilistically generated: $r = 1$ with the probability $(1 - e)$; $r = 0$

otherwise. Given a reward signal ($r = 1$) the node's internal parameters are modified so that the current output is more likely to occur from the same stimulus. A penalising step ($r = 0$) should have the opposite effect. The update is therefore $\Delta S_\mu = \alpha\,[r(\check{y} - y) + \hat{r}\lambda(1 - \check{y} - y)]$ where α is the learning rate, λ is the degree of penalising, and $\check{y} \equiv y^{kt}$ for output layer nodes and is the closest extreme for hidden layer nodes: $\check{y} = 1$ if $y > 0.5$; $\check{y} = 0$ if $y < 0.5$; or $\check{y} = 1$ with probability 0.5 if $y = 0.5$.

Gradient descent is the simplest gradient technique, with the update $\Delta S = -\alpha\bar{S}$, where α is the step size and $\bar{S}$ is the gradient term. In the trials reported here, *batched* updating was used, where the gradients are accumulated over the training set (an epoch) before being applied. Gradient descent has also been applied to RAM-based nodes by Gurney [5], and Gorse and Taylor [4].

Steepest Descent represents one of the simplest learning rate adaption techniques. A line search is employed to determine the minimum error along the search direction. The line search used was proposed by Armijo [1], and selects the largest power of two learning rate that reduces the network error.

Successive steps in steepest descent are inherently perpendicular [6], thus leading to a zig-zag path to the minimum. A better search direction can be obtained by incorporating some of the previous search direction. Momentum is a crude example. Conjugate gradient utilises the previous direction with the update rule $\Delta S = \alpha\,\delta S = \alpha(-\bar{S} + \beta\,\delta S^{-})$ where δS^{-} refers to the change on the previous iteration. β is calculated to ensure that successive steps are conjugate, and was calculated using the Polak-Ribiere rule [9].

4 Benchmark Applications

The 838 encoder is an auto-associative problem which has been widely used to demonstrate the ability of learning algorithms [6]. Both the input and output layers contain $n = 8$ nodes, with $\log_2 n = 3$ hidden layer nodes. Presentation of n distinct patterns requires a unique encoding for each to be formulated at the hidden layer. Of the n^n possible encodings, $n!$ are unique. Thus for the 838 encoder, only 40,320 unique encodings exist in the 16,777,216 possible, or 0.24%. The network is fully connected, with every MCU containing only one subunit. The training vectors consist of a single set bit, which is progressively shifted right.

The character set database is a subset of that utilised by Williams [11], and consists of twenty-four examples of each letter of the alphabet, excluding 'I' and 'O'. Each are sixteen by twenty-four binary pixels in size, and were generated from UK postcodes. Nineteen examples of each letter form the training set. A randomly generated configuration was utilised, with each pixel mapped only once. Eight inputs per subunit, and seven subunits per MCU resulted in seven neurons in the hidden layer. The output layer contains twelve nodes, each with a single subunit fully connected to the hidden layer.

The particle scattering images were generated by a pollution monitoring instrument previously described by Kaye [8]. Data was collected on eight particle types, namely: long and short caffeine fibres; 12μm and 3μm silicon dioxide fibres; copper flakes; 3μm and 4.3μm polystyrene spheres; and salt crystals. The training set comprised fifty randomly selected images of each type, quantised to 16^2 5-bit images to reduce computational load. A fully connected network was used, with sixteen

hidden, and six output layer MCUs. Every MCU consisted of two subunits, each with eight randomly generated connections. A more complete description of the airborne particle application can be found in [3].

5 Experimental Results

The site store locations were randomly initialised for all but reward-penalty, where they simply set to zero. The convergence criteria was 100% classification for the 838 encoder, and 95% for the other applications. Parameter settings were gleaned experimentally for the reward-penalty and gradient descent algorithms. The gradient descent setting of ρ was also used for steepest descent and conjugate gradient. The results are averaged over ten networks for the simpler problems, and five for the particle task. Table 2 summarises the parameter settings, and results for the four algorithms on the three applications. "Maximum", "mean", "deviation", and "coefficient" are in epochs, with the latter two being the standard deviation and coefficient of variation ($V = \frac{s}{\bar{x}} \cdot 100$) respectively. * denotes unconverged networks, and hence the maximum cycle limit. "CPU / cycle" is based on actual CPU time (secs) required on a Sun SPARCstation 10 model 40. "Total time" is given by "mean" $\times$ "CPU / cycle".

For the 838 encoder, conjugate gradient was the fastest, requiring marginally less time than reward-penalty and almost six and a half times fewer cycles. The character recognition task highlights the difference in learning ability. Reward-penalty was unable to converge, being more than three orders of magnitude away from the desired error. Batched gradient descent again demonstrated consistent learning, but was still the slowest of the gradient-based algorithms. The results for the particle task exemplify the problem of steepest descent: every network became trapped and required a relatively large number of cycles to be freed. The power of conjugate gradient also becomes clear, needing five times fewer cycles then gradient or steepest descent. Reward-penalty was not tried due to its failure on the simpler character problem.

6 Conclusions

The performance of various learning algorithms applied to a RAM-based artificial neural network have been investigated. Traditionally, reward-penalty has been applied to these nodes due to its inherent hardware amenability. The experiments reported here suggest that reinforcement learning is bested suited to simple problems. With respect to the gradient-based algorithms, gradient descent was consistently the slowest algorithm. While steepest descent was the fastest on the character recognition task, it had a tendency to become trapped. Conjugate gradient was by far the best algorithm, being fastest on two of the three applications.

REFERENCES

[1] L. Armijo, *Minimisation of functions having lipschitz continuous first partial derivatives.* Pacific Journal on Mathematics, Vol. 16 (1966), pp1–3.

[2] A. G. Barto and M. I. Jordan, *Gradient following without back-propagation in layered networks*, in: Proc. Int. Conf. Neural Networks (ICNN '87), IEEE, Vol. II (1987), pp629–636.

[3] A. Ferguson, T. Sabisch, P.H. Kaye, L.C.W. Dixon and H. Bolouri, *High-speed airborne particle monitoring using artificial neural networks*, Advances in Neural Information Processing Systems 8 (1996),.MIT Press, pp980–986.

[4] D. Gorse and J.G. Taylor, *Training strategies for probabilistic RAMs*, Parallel Processing in Neural Systems and Computers, Elsevier Science Publishers (1990), pp31–42.

Task	Parameters	Reward-Penalty	Gradient Descent	Steepest Descent	Conjugate Gradient
838 Encoder	ρ	0.35	0.21	0.21	0.21
	λ	0.7	NA	NA	NA
	α	32	4	NA	NA
	Maximum	449	578	107	75
	Mean ($\bar{x}$)	239	499	55	37
	Deviation (s)	181	74	32	23
	Coefficient (V)	76	15	58	62
	CPU / cycle (secs)	0.004	0.006	0.020	0.024
	Total time (secs)	0.980	2.944	1.089	0.881
Alphabetic Character Recognition	ρ	1.75	0.21	0.21	0.21
	λ	0.8	NA	NA	NA
	α	4	2	NA	NA
	Maximum	10000*	259	60	63
	Mean ($\bar{x}$)	-	244	50	41
	Deviation (s)	-	19	8	14
	Coefficient (V)	-	8	16	34
	CPU / cycle (secs)	2.90	6.47	13.85	32.45
	Total time (secs)	-	1579	692	1331
Airborne Particle Classification	ρ	-	0.9	0.9	0.9
	α	-	1	NA	NA
	Maximum	-	1014	1190	197
	Mean ($\bar{x}$)	-	828	890	156
	Deviation (s)	-	111	250	49
	Coefficient (V)	-	13	28	31
	CPU / cycle (secs)	-	56.44	133.93	190.55
	Total time (secs)	-	46733	119199	29726

Table 2 Summary of the performance of the training algorithms applied to the benchmark tests.

[5] K. N. Gurney, *Training nets of hardware realisable sigma-pi units*, Neural Networks, Vol. 5 (1992), pp289–303.

[6] J. Hertz, A. Krogh and R.G. Palmer, *Introduction to the Theory of Neural Computation*, Addison-Wesley (1991).

[7] T. K. L. Hui, P. Morgan, K.N. Gurney and H. Bolouri, *A cascadable 2048-neuron VLSI artificial neural network with on-board learning*, in: Artificial Neural Networks 2, North-Holland (1992), pp647–651.

[8] P. H. Kaye, E. Hirst, J.M. Clark and M. Francesca, *Airborne particle shape and size classification from spatial light scattering profiles*, Journal of Aerosol Science, Vol. 23 (1992), pp597–611.

[9] E. Polak, *Computational Methods in Optimisation*, Academic Press (1971).

[10] L. B. Rall, *Automatic Differentiation*, Springer-Verlag (1981).

[11] P. M. Williams, *Some experiments using n-tuple techniques for alphanumeric pattern classification*, report 575, The Post Office Research Centre, Ipswich, (1977).

ANALYSIS OF CORRELATION MATRIX MEMORY AND PARTIAL MATCH–IMPLICATIONS FOR COGNITIVE PSYCHOLOGY

Richard Filer and James Austin

Advanced Computer Architecture Group, Department of Computer Science, University of York, Heslington, YO1 5DD, UK. Email: rjhf@minster.york.ac.uk

This paper describes new work on partial match using Correlation Matrix Memory (CMM), a type of binary associative neural network. It has been proposed that CMM can be used as an inference engine for expert systems, and we suggest that a partial match ability is essential to enable a system to deal with real world problems. Now, an emergent property of CMM is an ability to perform partial match, which may make CMM a better choice of inference engine than other methods that do not have partial match. Given this, the partial match characteristics of CMM have been investigated both analytically and experimentally, and these characteristics are shown to be very desirable. CMM partial match performance is also compared with a standard database indexing method that supports partial match (Multilevel Superimposed Coding), which shows CMM to compare well under certain cirumstances, even with this heavily optimised method. Parallels are drawn with cognitive psychology and human memory.

Keywords: Correlation Matrix Memory, Neural Network, Partial Match, Human Memory.

1 Introduction

Correlation Matrix Memory (CMM) [4] has been suggested as an inference engine, possibly for use in an expert system [1]. Touretsky and Hinton [7] were the first to implement successfully a reasoning system in a connectionist architecture, and there have been several neural network based systems suggested since. However, only the systems [1, 7] can be said to use a truly distributed knowledge representation (the issue of localist versus distributed knowledge representation will not be discussed here), for instance SHRUTI [6] is an elaborate system using temporal synchrony. The SHRUTI model was developed with a localist representation and, although a way of extending the model to incorporate a semi-distributed representation is given, this is not a natural extension of the model; moreover, it is difficult to see how learning could occur with either form of knowledge representation. Many of the properties that have become synonymous with neural networks actually rely on the use of a distributed knowledge representation. These are: (a) a graceful degradation of performance with input data corruption; (b) the ability to interpolate between input data and give a sensible output, and (c) a robustness to system damage. Partial match ability is very much connected with (a) and (b), which give neural network systems their characteristic flexibility. Here we suggest that a certain flexibility in reasoning is invaluable in an inference engine because, in real world problems, the input data is unlikely to be a perfect match for much of the time. The CMM-based inference engine suggested by Austin [1] uses a distributed knowledge representation, and therefore this system can, in principle, offer the desired flexibility. The focus of this paper is a full analysis of the partial match ability of CMM, including a comparison with a conventional database indexing method that offers partial match. This conventional database indexing method is Multilevel Superimposed Coding [3]. Section 2 contains a more detailed description of CMM and partial match, including an analysis of the theoretical partial match performance of CMM. Section 3 compares CMM partial match with Multilevel

Superimposed Coding, and Section 4 considers how these results may be relevant to cognitive psychology and the study of human memory.

2 CMM and Partial Match

CMM is a type of binary associative memory, which can be thought of as a matrix of binary weights. The fundamental process which occurs in CMM is the association by Hebbian learning of binary vectors representing items of information, which subsequently allows an item of information to be retrieved given the appropriate input. CMM allows very fast retrieval and, particularly, *retrieval in a time which is independent of the total amount of information stored in the memory for given CMM size.* In [1], a symbolic rule such as X⇒Y can be encoded by associating a binary vector code for X, the rule antecedent, with a binary vector code for Y, the rule consequent. The rule can be recalled subsequently by applying the code for X to the memory and retrieving the code for Y. Multiple antecedent items can be represented by superimposing (bitwise OR) the binary vector codes for each item prior to learning. A fixed weight, sparse encoding is used to generate codes with a coding rate that optimizes storage wrt. number of error bits set in the output, which are bits set *in error* due to interactions between the binary representations stored in the CMM [11]. CMM learning is given by:

$$\boldsymbol{M}^{i+1} = \boldsymbol{M}^{i} \oplus I\ \overline{O} \tag{1}$$

where $\boldsymbol{M}^i$ is the $m \times m$ CMM at iteration i, I and O are m-bit binary vector codes to be associated, and $\oplus$ means OR each corresponding element. Hence to obtain CMM at iteration $i+1$, I and O are multiplied and the result ORed with $\boldsymbol{M}^i$. Note that learning is accomplished in a single iteration. CMM retrieval is given by:

$$\overline{\Gamma} = \overline{I}\ \boldsymbol{M} \tag{2}$$

$$O = \text{L–max}(\Gamma, l) \tag{3}$$

where I would be one of a pair of vectors previously associated in $\boldsymbol{M}$, and the function L–max(Γ, l) [2] selects the l highest integers in the integer vector, Γ, to be the l set bits in the output, O. Storage wrt. error is maximised when [11]:

$$n = \log_2 m \tag{4}$$

where n is the number of set bits in each m-bit binary vector; usually, we choose $l = n$. In a symbolic rule matching context, partial match would allow a rule that has multiple items in the antecedent to fire when only a subset of the items are present. In terms of the binary vector code representation being considered here and if the input to the CMM contains z set bits, a full match input is characterised by the greatest possible number of set bits ($z = n$), while a partial match has less set bits than this ($\frac{n}{k} \leq z < n$, where k is the number of antecedent items). Because of the way in which multiple input data are superimposed, CMM partial match is em insensitive to the order in which items are presented as input. For example, consider the following symbolic rule:

$$\text{engine_stalled} \wedge \text{ignition_ok} \wedge \text{fuelgauge_low} \Longrightarrow \text{refuel}$$

Normally, to check if a subset {engine_stalled , ignition_ok} is a partial match, it would be necessary at least to look at all the possible orderings of the subset, but with CMM this is not necessary. We term this emergent property **Combinatorial**

Partial Match. CMM could equally be used in frame based reasoning, where partial match would allow an entire frame to be recalled given a subset of the frame.

Partial Match Performance

If each input learned by the CMM, I, is obtained by hashing and superimposing the attributes that identify each record, then the CMM can be used subsequently to locate the record in memory, using I (or a partial match for I), by associating I with an output code, O, that represents the location of the record. Hence CMM can be used as a database indexing method. However, if multiple matches occur and multiple locations are represented in the CMM output, then output codes may be so overlapped that it is impossible to identify individual codes. Therefore, a method is needed to decode the CMM output but giving the minimum number of false positives (records that appear to be a match in the CMM but are not true matches) and no false negatives (records that appear not to be a match in the CMM but are true matches). We suggest here a novel method of identifying which output codes may be present in the CMM output, whereby output codes are subdivided and stored in buckets in memory, according to where the middle set bit (MB) appears in each code (Fig. 1). This approach allows us simply to identify all set bits in the output that could be MBs, then if all the buckets corresponding to these bits are searched, we are guaranteed no false negative matches.

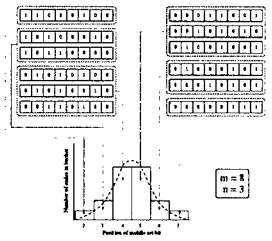

Figure 1 How output codes are divided up into buckets in secondary storage according to the position of the middle set bit (MB); in general, $m-(n-1)$ buckets are needed.

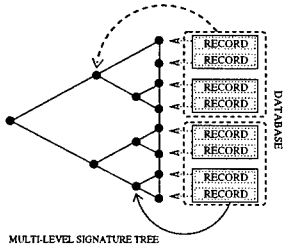

Figure 2 Multilevel Superimposed Coding (from [3]).

The partial match performance of CMM is considered in terms of the fraction, γ, of the index memory (which may be held in a slow secondary storage device) that must be searched in order to answer a given partial match query; the smaller this fraction is, the better. Other measures of performance are: computation reduction (the proportion of the total number of bits in the index that must be searched — not considered here), and the physical size of the index (in the comparison, we allow both methods the same index size). We show that this fraction, γ, depends only on: m, the dimension of the $m \times m$ CMM; z, the number of set bits in I, and t, the expected number of matches that will be found. If we first consider the absolute amount of memory that must be searched, this amount is due to two components: ω_1, the amount of memory that must be searched in order to obtain the CMM output, and ω_2, the amount of memory representing output codes that must be searched in order to decode the CMM output. For ω_1, only z rows of the $m \times m$

CMM are needed to obtain the CMM output, hence:

$$\omega_1 = zm \text{ bits} \tag{5}$$

To derive an expression for ω_2, we first look at the expected number of matches with items stored in the CMM that will be found, t, which gives us the expected number of set bits in the CMM output due only to true matches:

$$\kappa_1 = (1 - \left(\frac{m-n}{m}\right)^t)m \text{ bits} \tag{6}$$

But we must also take account of erroneously set bits, which occur due to interactions between the binary representations stored in the CMM (see [11] for an eloquent explanation of why this occurs):

$$\kappa_2 = (m-n)q^z \text{ bits} \tag{7}$$

where q is the proportion of all m^2 bits in the CMM that are set, which at maximum storage is 50%. $\kappa_1 + \kappa_2$ is now the total expected number of set bits in O; however, for our purposes, we can ignore $n-1$ of these bits because these $n-1$ bits represent bits that cannot possibly be MBs[1], giving:

$$\kappa_3 = \kappa_1 + \kappa_2 - (n-1) \text{ bits} \tag{8}$$

κ_3 is the number of set bits in O that could be MBs, or equivalently *the number of output code buckets that must be searched.* Now, each output code bucket contains on average $\frac{p}{m-(n-1)}$ output codes, where p is the number of records in the CMM, and each output code can be encoded in n^2 bits, hence:

$$\omega_2 = \frac{pn^2}{m-(n-1)}\kappa_3 \approx \frac{pn^2}{m}\kappa_3 \text{ bits} \tag{9}$$

Note that, for a given p, if m is chosen such that $q = 50\%$, then $p \approx \frac{m^2}{3(\ln m)^2}$ [5] (i.e. p may be expressed in terms of m). We can now write:

$$\gamma = \frac{\omega_1 + \omega_2}{m^2 + pn^2} \tag{10}$$

This result has been verified experimentally (up to $m = 1000$, however a lack of space unfortunately does not permit the discussion of these experimental results here).

3 A Comparison with Multilevel Superimposed Coding

Multilevel Superimposed Coding (MSC) [3] has been chosen as the conventional database indexing method that supports partial match because of the similarities of this method with our method, also MSC is used by several companies (e.g. Daylight CIS Inc.) for indexing their large databases. In MSC (Fig. 2), records are identified by hashing and superimposing attribute values into a binary code using multiple hash functions to gain access at multiple levels to a binary tree. Note that the resultant codes are of a different length, which is why multiple hash functions are needed. As before, the idea is to search as little of the index as possible, and the ideal state of affairs when locating a single record would be if at each node only one branch were taken. However, if the index is poorly conditioned then all branches may need to be searched, which would then be equivalent to performing a linear search on the entire index.

[1] Consider O comprising just one output code: O has n set bits, only one of which can be a middle set bit (MB); therefore $n-1$ of the set bits are not MBs (this generalises to the general case of O comprising multiple output codes).

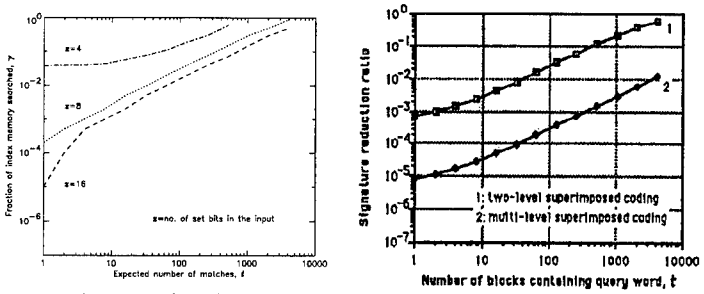

Figure 3 A comparison in terms of partial match performance between CMM (left) and MSC (right, (2); from [3]), for varying expected number of matches. Overall index size = 1.5 GB (both methods).

Kim and Lee [3] consider an example case of an index for a database of 2^{24} records, for which MSC requires a 24 level tree with *24 hash functions.* The analysis for MSC relies on specifying t, the expected number of matches, and both methods are allowed the same amount of storage (1.5 GB). The results are shown in Fig. 3, and concern the fraction of each index that must be searched versus the expected number of matches. Remembering that a full match input is characterised by the greatest possible number of set bits ($z = n$), while a partial match has less set bits than this ($\frac{n}{k} \leq z < n$), we observe from Fig. 3 that CMM approaches the performance achieved by MSC provided (1) that the input is well specified, and (2) that few true matches exist in the database. Even with a less well specified input and with several matches, CMM still performs reasonably well (especially considering the relative simplicity of the CMM method in comparison with the heavily optimised and much less straightforward MSC method).

4 Implications for Cognitive Psychology

In presenting this work to colleagues from differing backgrounds — some in psychology — it has become clear that this work may have relevance to cognitive psychology and the study of human memory. The **Encoding Specificity Principle** due to Endel Tulving [10] states: *"Only that can be retrieved that has been stored, and how it can be retrieved depends on how it was stored."* And in [8] Tulving states: *"On the unassailable assumption that cue A has more information in common with the trace of the A-T [T for target word] pair of studied items than with the trace of the B-T pair, we can say that the probability of successful retrieval of the target item is a monotonically increasing function of the information overlap between the information present at retrieval and the information stored in memory."* The Encoding Specificity Principle is by no means the only theory to explain this aspect of human memory function, and a number of experiments have been performed by protagonists of this or other theories. The work presented in this paper could be taken in support of the Encoding Specificity Principle, but this is not the intention of the authors. However, CMM could provide a model of the low level workings of human memory and, as such, the results of those experiments performed in relation to the Encoding Specificity Principle are most interesting. For instance, in [9], 674 subjects learned a list of 24 target words, (1) with one of two sets of cue words, or (2) without cue words; the cue words were chosen to each have an association of 1%

with the corresponding target word. In retrieval, subjects were asked to remember the list (a) with cues; (b) without cues, or (c) with wrong cues (a cue word taken from the alternative list). The experimental results are given in terms of the mean number of words remembered and are as follows, given in descending order of the mean number of words remembered: (1a) 14.93; (2b) 10.62; (1b) 8.72; (2a) 8.52; (1c) 7.45. What is interesting for CMM as a model of memory, is the difference between the results of experiments (1a) and (1b). If one postulates that the target word and the cue word are somehow stored together, like the input to a CMM, and that the output would be the equivalent of a pointer to the target word then the results of this paper can be interpreted in the light of the results in [9]. To do so, it is necessary to envisage some indexing mechanism in the human brain for retrieving information from memory that works best when there is little index memory to be searched, which is perfectly plausible. Then (1a) would correspond to a full match input, which would be expected to give best retrieval performance, as was found to be the case in the experiments; similarly, (1b) would correspond to a partial match input, which would be expected to give a rather worse retrieval performance, again as was found to be the case.

5 Conclusions

We have analysed the partial match performance of CMM, in line with the proposed use of CMM as an inference engine for an expert system that must solve real world problems. The analysis has enabled a comparison with a conventional database indexing technique that supports partial match, the results of which suggest CMM is good at performing partial match when the input is well specified and few matches exist. Interestingly, a similar behaviour is observed in human memory experiments and, although we would not go so far as to suggest that human memory is so simple as CMM, we observe that there are similarities that would support the use of CMM, or CMM partial match, as a model of some of the low level workings of human memory in further experiments in cognitive psychology.

REFERENCES

[1] J. Austin, *Correlation Matrix Memories for Knowledge Manipulation*, in: International Conference on Neural Networks, Fuzzy Logic, and Soft Computing, Japan (1994), Iizuka.

[2] D. Casasent and B. Telfer, *High Capacity Pattern Recognition and Associative Processors*, Neural Networks, Vol. 4(5) (1994), pp687–98.

[3] Y.M. Kim and D.L. Lee, *An Optimal Multilevel Signature File for Large Databases*, In Fourth International Conference on Computing and Information, IEEE (1992).

[4] T. Kohonen and M. Ruohonen, *Representation Of Associated Data By Matrix Operators*, IEEE Transactions on Computers, (July 1973).

[5] J-P. Nadal and G. Toulouse, *Information Storage in Sparsely Coded Memory Networks*, Network, Vol. 1 (1990), pp61–74.

[6] L. Shastri and V. Ajjanagadde, *From Simple Associations to Systematic Reasoning*, Behavioural & Brain Sciences, Vol. 16(3) (1993), pp417–93.

[7] D.S. Touretsky and G.E. Hinton, *A Distributed Connectionist Production System*, Cognitive Science, Vol. 12 (1988), pp423–66.

[8] E. Tulving, *Relation Between Encoding Specificity and Levels of Processing*, in: Levels of Processing in Human Memory. John Wiley & Sons (1979), London.

[9] E. Tulving and S. Osler, *Effectiveness of Retrieval Cues in Memory for Words*, Journal of Experimental Psychology, Vol. 77(4) (1968), pp593–601.

[10] E. Tulving and D.M. Thomson, *Encoding Specificity and Retrieval Processes in Episodic Memory*, Psychological Review, Vol. 80 (1973), pp352–73.

[11] D.J. Willshaw, O.P. Buneman, and H.C. Longuet-Higgins, *Non-Holographic Associative Memory*, Nature, Vol. 222 (1969), pp960–62.

REGULARIZATION AND REALIZABILITY IN RADIAL BASIS FUNCTION NETWORKS

Jason A.S. Freeman and David Saad*

Centre for Neural Systems, University of Edinburgh, Edinburgh EH8 9LW, UK. Email: jason@cns.ed.ac.uk

** Department of Computer Science & Applied Mathematics, University of Aston, Birmingham B4 7ET, UK. Email: D.Saad@aston.ac.uk*

Learning and generalization in a two-layer Radial Basis Function network (RBF) is examined within a stochastic training paradigm. Employing a Bayesian approach, expressions for generalization error are derived under the assumption that the generating mechanism (teacher) for the training data is also an RBF, but one for which the basis function centres and widths need not correspond to those of the student network. The effects of regularization, via a weight decay term, are examined. The cases in which the student has greater representational power than the teacher (over-realizable), and in which the teacher has greater power than the student (unrealizable) are studied. Finally, simulations are performed which validate the analytic results.

1 Introduction

When considering supervised learning in neural networks, a quantity of particular interest is the *generalization error*, a measure of the average deviation between desired and actual network output across the space of possible inputs. Generalization error consists of two components: approximation error and estimation error. Given a particular architecture, approximation error is the error made by the optimal student of that architecture, and is caused by the architecture having insufficient representational power to exactly emulate the teacher; it is an asymptotic quantity as it cannot be overcome even in the limit of an infinite amount of training data. If the approximation error is zero, the problem is termed realizable; if not, it is termed unrealizable. Estimation error is the error due to not having selected an optimal student of the chosen architecture; it is a dynamic quantity as it changes during training and is caused by having insufficient data, noisy data or a learning algorithm which is not guaranteed to reach an optimal solution in the limit of an infinite amount of data. There is a trade-off between representational power and the amount of data required to achieve a particular error value (the sample complexity) in that the more powerful the student, the greater the ability to eliminate the approximation error but the larger the amount of data required to find a good student.

This paper employs a Bayesian scheme in which a probability distribution is derived for the weights of the student; similar approaches can be found in [6, 1, 2] and [3]. In [7], a bound is derived for generalization error in RBFs under the assumption that the training algorithm finds a global minimum in the error surface; regularization is not considered. For the exactly realizable case, Freeman *et al.* calculate generalization error for RBFs using a similar framework to that employed here [2].

2 The RBF Network and Generalization Error

The RBF architecture consists of a two-layer fully-connected network, and is a universal approximator for continuous functions given a sufficient number of hidden units [4]. The hidden units will be considered to be Gaussian basis functions, param-

eterised by a vector representing the position of the basis function centre in input space and a scalar representing the width of the basis function. These parameters are assumed to be fixed by a suitable process, such as a clustering algorithm. The output layer computes a linear combination of the activations of the basis functions, parameterised by the adaptive weights $\mathbf{w}$ between hidden and output layers.

Training examples consist of input-output pairs $(\boldsymbol{\xi}, \zeta)$. The components of $\boldsymbol{\xi}$ are uncorrelated Gaussian random variables of mean 0, variance σ_ξ^2, while ζ is generated by applying $\boldsymbol{\xi}$ to a teacher RBF and corrupting the output with zero-mean additive Gaussian noise, variance σ_η^2. The number, position and widths of the teacher hidden units need not correspond to those of the student, allowing investigation of over-realizable and unrealizable cases. The mapping implemented by the teacher is denoted f_T, and that of the student f_S. Note it is impossible to examine generalization error without some *a priori* belief in the teacher mechanism [9]. The training algorithm for the adaptive weights is considered stochastic in nature; the selected noise process leads to the following form for the likelihood:

$$\mathcal{P}(D|\mathbf{w}, \beta) \propto \exp(-\beta E_D) \tag{1}$$

where E_D is the training error. This form resembles a Gibbs distribution; it also corresponds to the constraint that minimizing the training error is equivalent to maximizing the likelihood [5]. This distribution can be realised by employing the Langevin algorithm, which is simply gradient descent with an appropriate noise term added to the weights at each update [8]. To prevent over-dependence of the distribution of student weight vectors on the noise, it is necessary to introduce a regularizing factor, which can be viewed as a Bayesian *prior*:

$$\mathcal{P}(\mathbf{w}|\gamma) \propto \exp(-\gamma E_W) \tag{2}$$

where E_W is a penalty term based here on the magnitude of the student weight vector. Employing Bayes' theorem, one can derive an expression for the probability of a student weight vector given the training data and training parameters:

$$\mathcal{P}(\mathbf{w}|D, \gamma, \beta) \propto \exp\left(-\beta E_D - \gamma E_W\right) \tag{3}$$

The common definition of generalization error is the average squared difference between the target function and the estimating function:

$$E(\boldsymbol{w}) = \langle (f_S(\boldsymbol{\xi}, \boldsymbol{w}) - f_T(\boldsymbol{\xi}))^2 \rangle \tag{4}$$

where $\langle \cdots \rangle$ denotes an average w.r.t. the input distribution. In practice, one only has access to the test error, $\frac{1}{P_{TEST}} \sum_{p=1}^{P_{TEST}} (\zeta_p - f_S(\boldsymbol{\xi}_p, \mathbf{w}))^2$. This quantity is an approximation to the expected risk, defined as the expectation of $(\zeta - f_S(\boldsymbol{\xi}, \mathbf{w}))^2$ w.r.t. the joint distribution $\mathcal{P}(\boldsymbol{\xi}, \zeta)$. With an additive noise model, the expected risk decomposes to $E + \sigma_\eta^2$, where σ_η^2 is the variance of the noise.

When employing stochastic training, two possibilities for average generalization error arise. If one weight vector is selected from the ensemble, as in usually the case in practice, equation (4) becomes:

$$E_G(\gamma, \beta) = \left\langle \int d\mathbf{w}\, \mathcal{P}(\mathbf{w}|D, \gamma, \beta)\, (f_S(\boldsymbol{\xi}, \boldsymbol{w}) - f_T(\boldsymbol{\xi}))^2 \right\rangle \tag{5}$$

Alternatively, one can take a Bayes-optimal approach which, for squared error, requires taking the mean estimate of the network. It is computationally impractical

to find this, but it is interesting as it represents the result of the best guess, in an average sense. In this case generalization error takes the form :

$$E_B(\gamma,\beta) = \left\langle \left(\int d\mathbf{w}\, \mathcal{P}(\mathbf{w}|D,\gamma,\beta)\, f_S(\boldsymbol{\xi},\mathbf{w}) - f_T(\boldsymbol{\xi}) \right)^2 \right\rangle \tag{6}$$

In order to examine generic architecture performance independently of the particular data employed, an average over datasets is performed, taking into account both the position of the data in input space and the noise.

Defining E_D as the sum of squared errors over the training set and defining the regularization term $E_W = \|w\|^2$, E_G and E_B can be found from equations (3), (5) and (6). The calculation is straightforward until the average over the dataset; the complications and their resolution are discussed in [3]. Schematically:

$$E_G = \text{Student Output Variance} + \text{Noise Error} + \text{Student-Teacher Mismatch} \tag{7}$$

$$E_B = \text{Noise Error} + \text{Student-Teacher Mismatch} \tag{8}$$

The student output variance and noise error are estimation error only; the student-teacher mismatch is both estimation and approximation error.

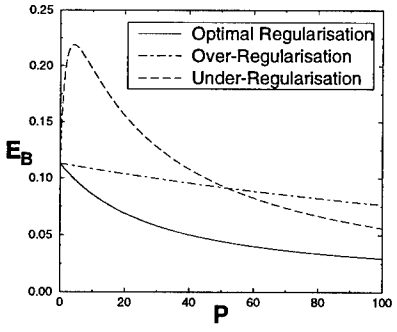

Figure 1 The effects of regularization: the solid curve represents optimal regularization($\gamma = 2.7, \beta = 1.6$), the dot-dash curve illustrates the over-regularised case ($\gamma = 2.7, \beta = 0.16$), and the dashed curve shows the highly under-regularised case ($\gamma = 2.7, \beta = 16$). The student and teacher were matched, each consisting of 3 centres at $(1,0), (-0.5, \sqrt{3}/2)$ and $(-0.5, -\sqrt{3}/2)$. Noise of variance 1 was employed.

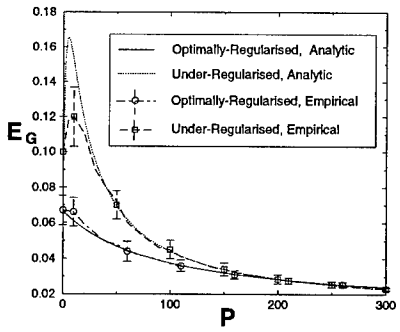

Figure 2 Simulation results. The curves are for a realizable case with three centres at $(1,0)$, $(-0.5, \sqrt{3}/2)$ and $(-0.5, -\sqrt{3}/2)$, with centre width $\sqrt{2}/2$ and noise of variance $2/\beta$. The empirical curves were generated by exhaustive training at each value of P, and represent averages over 100 trials. The error bars are at 1 standard deviation of the empirical distribution.

3 Analysis of Generalization Error

3.1 The Effects of Regularization

While the effects of regularization are similar for E_G and E_B, the optimal parameter settings, found by minimizing equations (7) and (8) w.r.t. γ and β, are quite

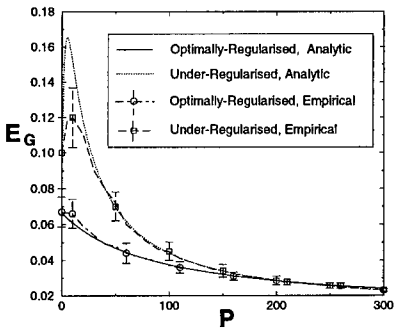

Figure 3 The Over-realizable Case: the dashed curve shows the over-realizable case with training optimised as if the student matches the teacher ($\gamma = 3.59, \beta = 2.56$), the solid curve illustrates the over-realizable case with training optimised with respect to the true teacher ($\gamma = 3.59, \beta = 1.44$), while the dot-dash curve is for the student matching the teacher ($\gamma = 6.52, \beta = 4.39$). All the curves were generated with one teacher centre at $(1,0)$; the over-realizable curves had two student centres at $(1,0)$ and $(-1,0)$. Noise with variance 1 was employed.

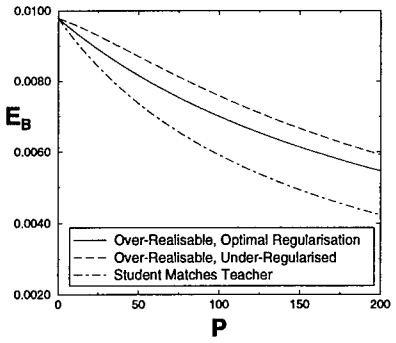

Figure 4 The unrealizable case: the solid curve denotes the case where the student is optimised as if the teacher is identical to it ($\gamma = 2.22, \beta = 1.55$); the dashed curve demonstrates the student optimised with knowledge of the true teacher ($\gamma = 2.22, \beta = 3.05$), while, for comparison, the dot-dash curve shows a student which matches the teacher ($\gamma = 2.22, \beta = 1.05$). The curves were generated with two teacher centres at $(1,0)$ and $(-1,0)$; the unrealizable curves employed a single student at $(1,0)$; noise of variance 1 was utilised.

different. As discussed in [2], for E_G it is necessary to optimise γ and β jointly, while for E_B, only the *ratio* of γ to β need be considered; this optimal ratio is independent of P. This dissimilarity is due to the variance term in E_G, which is minimised by taking $\beta \to \infty$. These findings hold for both realizable and unrealizable cases. To demonstrate the effects of regularization in a realizable scenario, consider figure 1 where E_B is plotted versus P for three cases. The solid curve illustrates optimal regularization and shows the lowest value of generalization error that can be achieved on average; the dot-dash curve represents the over-regularised case, in which the prior dominates the likelihood, showing how reduction in generalization error is substantially slowed. The dashed curve is for the highly under-regularised case, which in the $\gamma/\beta \to 0$ case gives a divergence in both E_G and E_B. Although under-regularization is initially more damaging than over-regularization, its effects are recovered from more rapidly. As training proceeds, the likelihood comes to dominate the prior, making the incorrect setting of the prior irrelevant; this proceeds more rapidly when the prior is weak with respect to the likelihood.

3.2 The Over-Realizable and Unrealizable Scenarios

Operationally, selecting a form for the student implies that one is prepared to believe that the teacher has an identical form. Therefore optimization of training parameters must be performed on this basis. When the student is overly powerful

this leads to under-regularization, as the magnitude of the teacher weight vector is believed to be larger than the true case. This is shown in figure 3; the dashed curve represents generalization error for the under-regularised case where the training parameters have been optimised as if the teacher matches the student, while the solid curve represents the same student, but with training optimised with respect to the true teacher. Employing an overly-powerful student rather than the optimally-matched student can drastically slow the reduction of generalization error. Even with training optimised with respect to the true teacher, the matching student greatly out-performs the overly-powerful version due to the necessity to suppress the redundant parameters. The effect is shown in figure 3; generalization error for the matching student is given by the dot-dash curve, while that of the overly-powerful but correctly optimised student is given by the solid curve. In the unrealizable scenario, where the teacher is more powerful than the student, optimization of training parameters under the belief that the teacher has the same form as the student leads to over-regularization, as the assumed magnitude of the teacher weight vector is greater than the true magnitude. This effect is shown in figure 4, in which the solid curve denotes generalization error for the over-regularised case based on the belief that the teacher matches the student, while the dashed curve shows the error for an identical student when the parameters of the true teacher are known; this knowledge permits optimal regularization. The most significant effect of the teacher being more powerful than the student is the fact that the approximation error is no longer zero, as the teacher can never be exactly emulated by the student. This is also illustrated in figure 4, where the dot-dash curve represents the learning curve when the student matches the teacher (with zero asymptote), while the two upper curves show an under-powerful student, and have non-zero asymptotes.

3.3 Simulations

To validate the analytic results, simulations were performed for optimally-regularised and under-regularised realizable cases. The simulations involved exhaustive training of RBF networks using Langevin updating. The empirical results were generated by averaging over 100 runs, approximating generalization error using a large, noiseless test set. The results are shown in figure 2; an excellent fit between analytic and simulated results is found for $P > 50$. In the region where P is small in the under-regularised case, the analytic mean is larger than the simulation result. In the small P region, this case is particularly vulnerable to the approximation employed in the dataset average (see [3]). The errorbars are also large in this region, as the distribution of student weights is relatively unconstrained.

4 Conclusion

Under-regularization initially causes very poor generalization, which can be overcome rapidly with the addition of more training data. Over-regularization is initially less damaging, but requires a large quantity of training data in order to overcome the effect. In the over-realizable case, there is a tendency to under-regularise due to over-estimating the complexity of the teacher. There is also an increase in sample complexity. In the unrealizable case, under-estimating the complexity of the teacher leads to over-regularization.

REFERENCES

[1] A. Bruce and D. Saad, *Statistical mechanics of hypothesis evaluation*, J. Phys. A: Math. Gen., Vol. 27 (1994), pp3355 – 3363.

[2] J. Freeman and D. Saad, *Learning and generalization in radial basis function networks*, Neural Computation, Vol. 7 (1995), pp1000–1020.

[3] J. Freeman and D. Saad, To appear in *Neural Networks*, (1995),

[4] E. Hartman, J. Keeler, and J. Kowalski, *Layered neural networks with gaussian hidden units as universal approximators*, Neural Computation, Vol. 2 (1990), pp210–215.

[5] E. Levin, N. Tishby, and S. Solla, *A statistical approach to learning and generalization in layered neural networks*, In Colt (1989), pp245–260.

[6] D. MacKay, *Bayesian interpolation*, Neural Computation, Vol. 4 (1992), pp415–447.

[7] P. Niyogi and F. Girosi, *On the relationship between generalization error, hypothesis complexity and sample complexity for radial basis functions*, Technical report, AI Laboratory, MIT (1994).

[8] T. Rögnvaldsson, *On langevin updating in multilayer perceptrons*, Neural Computation, Vol. 6 (1994), pp916–926.

[9] D. Wolpert, *On the connection between in-sample testing and generalization error*, Complex Systems, Vol. 6 (1992), pp47–94.

Acknowledgements

This work was supported by EU grant ERB CHRX-CT92-0063.

A UNIVERSAL APPROXIMATOR NETWORK FOR LEARNING CONDITIONAL PROBABILITY DENSITIES

D. Husmeier, D. Allen and J. G. Taylor
Centre for Neural Networks, Department of Mathematics, King's College London, UK.

A general approach is developed to learn the conditional probability density for a noisy time series. A universal architecture is proposed, which avoids difficulties with the singular low-noise limit. A suitable error function is presented enabling the probability density to be learnt. The method is compared with other recently developed approaches, and its effectiveness demonstrated on a time series generated from a non-trivial stochastic dynamical system.

1 Introduction

Neural networks are used extensively to learn time series, but most of the approaches, especially those associated with the mean square error function whose minimisation implies approximating the predictor $x(t) \rightarrow x(t+1)$, will only give information on a mean estimate of such a prediction. It is becoming increasingly important to learn more about a time series, especially when it involves a considerable amount of noise, as in the case of financial time series. This note is on more recent attempts to learn the conditional probability distribution of the time series, so the quantity

$$P(x(t+1)|\mathbf{x}(t)) \tag{1}$$

where $\mathbf{x}(t)$ denotes the time-delayed vector with components $(x(t), x(t-1), \ldots, x(t-m))$, for some suitable integer m.

An important question is as to the nature of a neural network architecture that can learn such a distribution when both very noisy and nearly deterministic time series have to be considered. A variety of approaches have independently been recently proposed (Weigend and Nix, 1994; Srivastava and Weigend, 1994; Neuneier et al, 1994), and this plethora of methods may lead to a degree of uncertainty as to their relative effectiveness. We here want to extend the discussion of an earlier paper (Allen and Taylor, 1994) and will derive the minimal structure of a universal approximator for learning conditional probability distributions. We will then point out the relation of this structure to the concepts mentioned above, and will finally apply the method to a time series generated from a stochastic dynamical system.

2 The General ANN Approach

2.1 Minimal Required Network Structure

Let us formulate the problem in terms of the cumulative probability distribution

$$F(y|\mathbf{x}(t)) = p(x(t+1) \leq y|\mathbf{x}(t)) = \int_{-\infty}^{y} p(y'|\mathbf{x}(t))\, dy' \tag{2}$$

first, as this function does not become singular in the noise-free limit of a deterministic process, but reduces to

$$F(y|\mathbf{x}(t)) = \theta(y - f(\mathbf{x}(t))) \tag{3}$$

(where $\theta(.)$ is the threshold or Heaviside function, $\theta(x) = 1$ if $x \geq 0$, 0 otherwise). We want to derive the structure of a network that, firstly, is a universal approx-

imator for $F(.)$ and, secondly, obtains the noise-free limit of (3). It is clear that a difficulty would arise if the universal approximation theorem of neural networks were applied directly to the function $F(y, \mathbf{x}(t))$ so as to expand it in terms of the output of a single hidden layer net,

$$F(y|\mathbf{x}(t)) = \sum_i a_i S\left(\sum_{j=0}^{m} w_{ij} x_j + b_i y - \vartheta_i\right), \tag{4}$$

where $x_j := x(t-j+1)$, $S(x) = 1/(1+e^{-x})$, and a_i, w_{ij}, b_i, ϑ_i are constants with obvious interpretation in neural network terms (a_i output weights, ϑ_i thresholds, w_{ij}, b_i weights between input and hidden layer). Trying to obtain the deterministic case (3), the best one can get from (4) in the limit when $a_i \to \delta_{i,i_0}$ (Kronecker delta) and the weights of the hidden nodes become very large (so that each sigmoid function $S(.)$ entering in (4) becomes a threshold function $\theta(.)$), is the expression

$$F(y|\mathbf{x}(t)) \to \theta\left(y - \sum_j c_j x_j - s\right), \tag{5}$$

with constants c_j, s. Thus at best it is only possible to approximate the deterministic limit of a linear process, with $f(\mathbf{x})$ a linear function of its variable.

To be able to handle the split between the single predicted variable y and the input variable $\mathbf{x}$, we proceed by developing a universal one-layer representation for y first, and then do the same for the remaining variable $\mathbf{x}$ successively. Thus at the first step results

$$F(y|\mathbf{x}(t)) = \sum_i a_i S(\beta_i(y - \mu_i)), \tag{6}$$

where β_i is the steepness of the sigmoid function, and μ_i a given threshold. We then expand each μ_i by means of the universal approximation theorem in terms of a further hidden layer network, resulting in

$$\mu_i(\mathbf{x}) = \sum_j b_{ij} S\left(\sum_k c_{ijk} x_k - \vartheta_{ij}\right). \tag{7}$$

In order that the right hand side of (6) be a cumulative probabilty distribution, i.e. $F(-\infty|\mathbf{x}) = 0$, $F(\infty|\mathbf{x}) = 1$ and $F(y|\mathbf{x})$ monotone increasing in the variable y, the following conditions are imposed on the coefficients entering eq.(6):

$$\beta_i > 0, \quad a_i \geq 0, \quad \sum_i a_i = 1 \tag{8}$$

This can be realized by taking β_i and a_i as functions of new variables ξ_i and ς_i, e.g. $\beta_i = (\xi_i)^2$, and $a_i = (\varsigma_i)^2 / \sum_k (\varsigma_k)^2$ or $a_i = \exp(\varsigma_i) / \sum_k \exp(\varsigma_k)$.

It is now possible to see that the deterministic limit (3) arises smoothly from the universal two-hidden-layer architecture of equations (6) and (7) when $a_i \to \delta_{i,j}$ and $\beta_j \to \infty$, i.e., for one output weight one and all the others zero, and a large steepness parameter for the unit connected to the non-vanishing weight.

2.2 Moments

One of the attractive properties of the use of sigmoid response functions is that it is possible to give (after some algebra) a closed form for the moment generating

function (Allen, Taylor, 1994),

$$M(t) := \int_{-\infty}^{\infty} \exp(ty)p(y|\mathbf{x})\,dy = \sum_i \frac{a_i(\pi t/\beta_i)\exp(\mu_i t)}{\sin(\pi t/\beta_i)}, \tag{9}$$

from which all the moments arising from the conditional probability density (1) can be calculated, e.g.

$$E(Y) = \lim_{t\to 0}\frac{dM(t)}{dt} = \sum_i a_i\mu_i \tag{10}$$

$$E(Y^2) = \lim_{t\to 0}\frac{d^2M(t)}{dt^2} = \sum_i a_i\left[\mu_i^2 + \frac{1}{3}\left(\frac{\pi}{\beta_i}\right)^2\right] \tag{11}$$

For $a_i \to \delta_{ij}$, $\beta_j \to \infty$ the deterministic limit ensues, with $E(Y^m) = [E(Y)]^m$.

2.3 The Error Function

It is now necessary to suggest a suitable error function in order to make the universal expression given by (6) and (7) the true conditional cumulative distribution function given by the available data. As the true value for $x(t+1)$ is not known, one cannot use standard mean square error. Let us assume that the process is stationary. Then the negative expectation value of the logarithm of the likelihood,

$$E = -\langle\log(p(x(t+1)|\mathbf{x}(t)))\rangle \approx -\frac{1}{N}p(x(t+1)|\mathbf{x}(t)), \tag{12}$$

is the appropriate choice, based on Kullback's Lemma (see, e.g., Papoulis, 1984), according to which (12) in terms of the true (unknown) probability density, p_{true}, is always smaller than (12) in terms of the probability density predicted by the network, p. Hence by minimising (12) one can hope to always "get closer" to p_{true}.

2.4 Regaining the Conditional Probability Density

In order to get back to the conditional probability density, we have to take the derivative of the output of (6) with respect to the target, y, yielding

$$p(y|\mathbf{x}) = \frac{\partial F(y|\mathbf{x})}{\partial y} = \frac{\partial S(\beta(y-\mu(\mathbf{x})))}{\partial y} = \beta S(\beta(y-\mu(\mathbf{x})))(1-S(\beta(y-\mu(\mathbf{x})))) \tag{13}$$

This function is Gaussian-shaped, so our resulting network structure can be summarized as follows: The output node, which predicts the conditional probability density $p(x(t+1) = y|\mathbf{x}(t))$, is connected to a layer of RBF-like nodes. The output of the ith "RBF"-unit is determined by its input, $x(t+1)$ (the same for all nodes), and its centre, μ_i, the latter being an $\mathbf{x}$-dependent function implemented in a seperate one-hidden- layer network with the usual sigmoidal hidden nodes. The parameters a_i and β_i have obvious interpretations as a priori probability and inverse kernel width, respectively. (Note that from (10) and (11) one gets $\sigma_i = \pi/(\sqrt{3}\beta_i)$ for the standard deviation of the ith kernel, i.e. its "width"). The same structure can basically be found in the other approaches mentioned above too, with the following differences and simplifications.

3 Comparison with Other Approaches

The CDEN (Conditional Density Estimation Network) of Neuneier et al. (1994) uses only one hidden layer for computing all of the $\mu_i(\mathbf{x})$, which corresponds to simplifying (7) by making c_{ijk} and ϑ_{ij} independent of the subscript i. This simplification is certainly justified when the $\mu_i(\mathbf{x})$ are of a similar functional form, with

Network	"RBF" kernel function	μ_i **x**-dependent	σ_i **x**-dependent	a_i **x**-dependent
As proposed here	$S'(.)$	yes, seperate hidden layers	no	no
CDEN	Gaussian	yes, 1 shared hidden layer	yes	yes
Soft histograms	triangular	no, from preprocessing	no, from preprocessing	yes
Weigend, Nix	1 Gaussian	yes	yes	unity

Table 1 Comparison between the different network architectures mentioned in the text.

similar a priori probabilities, but may cause difficulties when this assumption is strictly violated. On the other hand, the CDEN includes a further generalisation of the architecture proposed here by making the kernel widths, σ_i, and the output weights, a_i, **x**-dependent, computing them as outputs of seperate one- hidden-layer networks. This is not necessary in order for the architecture to be a universal approximator, but may lead to a considerable reduction of the "RBF"-layer size, the latter, though, at the expense of additional complexity in other parts of the network. It thus depends on the specific problem under consideration if this further generalisation is an advantage.

The *soft histogram* approach proposed by Srivastava and Weigend (1994) is identical to a mixture of triangular-shaped "RBF"-nodes, $P(y|\mathbf{x}) = \sum_i a_i(\mathbf{x})R_i(y)$, with $R_i(y) = h_i(y-\mu_{i-1})/(\mu_i-\mu_{i-1})$ if $\mu_{i-1} \leq y \leq \mu_i$, $R_i(y) = h_i(\mu_{i+1}-y)/(\mu_{i+1}-\mu_i)$ if $\mu_i \leq y \leq \mu_{i+1}$, and $R_i(y) = 0$ otherwise. The "heights" h_i are related to the kernel widths $\sigma_i =: \mu_{i+1} - \mu_{i-1}$ by $h_i = 2/\sigma_i$ in order to ensure that the the normalisation condition $\int_{-\infty}^{\infty} P(y|\mathbf{x})\,dy = 1$ is satisfied. The kernel centres result from a preprocessing "binning" procedure (described in [Srivastava, Weigend 1994]). The output of the network is thus similar to the CDEN and the model proposed in this paper, with the difference that now only the output weights $a_i(\mathbf{x})$ are **x**-dependent, whereas the kernel centres, μ_i, are held constant.

Finally the architecture introduced by Weigend and Nix (1994) reduces the size of the "RBF" layer to only one node, assuming a Gaussian probability distribution, which is completely specified by μ and σ, both of which are given as the (**x**-dependent) output of a seperate network branch. Obviously, this parametric approximation reduces the network complexity, but leads to a biased prediction.

4 Simulation

We tested the performance of our method on an artificial time series generated from a stochastic coupling of two stochastic dynamical systems,

$$x(t+1) = \Theta(\xi - \vartheta)\alpha x(t)[1-x(t)] + (1-\Theta(\xi-\vartheta))\,[1-x^{\kappa}(t)]\,, \qquad (14)$$

where $\Theta(.)$ symbolizes the Heaviside function, as before, and the parameters α, κ and ξ are random variables drawn from a uniform distribution, $\xi \in [0,1]$, $\alpha \in [3,4]$, $\kappa \in [0.5, 1.25]$. The prior probabilities of the two processes are determined by the

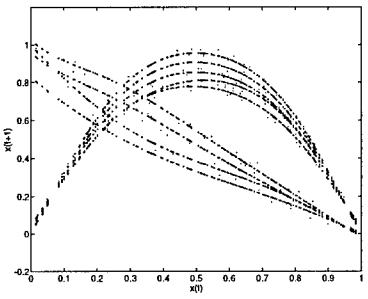

Figure 1 Centres of the "RBF"-kernels, $\mu_i(x(t))$, after training (black lines). The grey dots show a state-space plot of the time series.

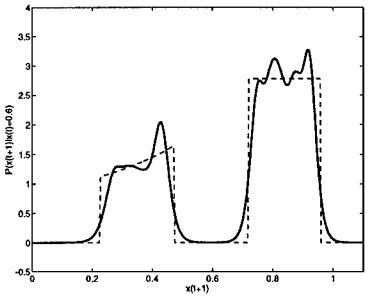

Figure 2 Cross section of the true (narrow graph) and predicted (bold graph) conditional probability density, $P(x(t+1) = y|x(t) = 0.6)$.

treshold constant ϑ, which was chosen such that we got a ratio of 2:1 in favour of the left process (i.e., $\vartheta = 1/3$). We applied a network with ten "RBF"-nodes to learn the conditional probability density of this time series. Figure 1 shows a state space plot of the time series (dots) and the centre positions of the "RBF"-kernels, $\mu_i(x(t))$ (black lines). Figure 2 shows a cross-section of the conditional probability density for $x(t) = 0.6$, $P(x(t+1) = y|x(t) = 0.6)$, and compares the correct function (narrow grey line) with the one predicted by the network (bold black line). Apparently the network has captured the relevant features of the stochastic process and correctly predicts the existence of two clusters. Note that a conventional network for time series prediction, which only predicts the conditional mean of the process, would be completely inappropriate in this case as it would predict a value between the two clusters, which actually never occurs. The same holds for the network proposed by Weigend and Nix, which would predict a value for $x(t+1)$ between the two clusters, too, and a much too large error bar resulting from the assumption of a Gaussian distribution.

5 Conclusions

A general approach to the learning of conditional probability densities for stationary stochastic time series has been presented, which overcomes the limitation of restricted reduction to the noise-free case. The minimal architecture required for the network to be a universal approximator *and* to contain the non-restricted noise-free case was found to be of a two-hidden-layer structure. We have shown that the other recently developed approaches to the same problem are of a very similar form, differing basically only with respect to the $\mathbf{x}$-dependence of the parameters and the functional form of the "RBF"-kernels. Which architecture one should finally adopt depends on the specific problem under consideration. While the structure proposed by Weigend and Nix is suitable for a computationally cheap, but biased approximation of $p(x(t+1)|\mathbf{x}(t))$ (approximation by a single Gaussian), the CDEN, the method of soft histograms and the network proposed here offer a more accurate, but also computationally more expensive determination of the whole conditional

probability density. It is an important subject of further research to assess the relative merits and drawbacks of the latter three models by carrying out comparative simulations on a set of benchmark problems.

REFERENCES

[1] Allen DW and Taylor JG , *Learning Time Series by Neural Networks*, Proc ICANN (1994), ed Marinaro M and Morasso P, Springer, pp529–532.

[2] Neuneier R, Hergert F, Finnoff W and Ormoneit D, *Estimation of Conditional Densities: A Comparison of Neural Network Approaches*, Proc ICANN (1994), ed Marinaro M and Morasso P, Springer, pp689–692.

[3] Papoulis, A., *Probability, Random Variables and Stochastic Processes*, McGraw-Hill (1984).

[4] Srivastava AN and Weigend AS, *Computing the Probability Density in Connectionist Regression*, Proc ICANN (1994), ed Marinaro M and Morasso P, Springer, pp685–688.

[5] Weigend AS and Nix DA, *Predictions with Confidence Intervals (Local Error Bars)*, Proc ICONIP (1994), ed Kim M-W and Lee S-Y,Korea Advanced Institute of Technology, pp847–852.

CONVERGENCE OF A CLASS OF NEURAL NETWORKS

Mark P. Joy

Centre for Research in Information Engineering,
School of Electrical, Electronic and Information Enineering,
South Bank University, 103, Borough Rd., London SE1 OAA, UK.
Email: joympa@vax.sbu.ac.uk

The additive neural network model is a nonlinear dynamical system and it is well-known that if either the weight matrices are symmetric or the dynamical system is cooperative and irreducible (with isolated equilibria) then the net exhibits convergent activation dynamics. In this paper we present a convegence thoerem for additive neural nets with ramp sigmoid activation functions having a row-dominant weight matrix. Of course, such nets are not, in general, cooperative or possess symmetic weight matices. We also indicate the application of this theorem to a new class of neural networks – the Cellular Neural Networks – and consider its usefulness as a practical result in image processing applications.

1 Introduction

In the last few years the definition of the neural network dynamical system has expanded rapidly. This paper concerns neural networks associated with the set of ODEs:

$$\dot{x}_i = -x_i + \sum_{j=1}^{n} b_{ij} f(x_j) + I, \tag{1}$$

where $x \in \mathbb{R}^n$, describes the activity levels of n 'neurons', b_{ij} is a real constant representing the connection strength from neuron j to neuron i, f is a sigmoid function and I represents a clamped input. In order to facilitate the analysis of (1) we define f as a *ramp* sigmoid:

$$f(x) = \frac{1}{2}(\mid x+1 \mid - \mid x-1 \mid). \tag{2}$$

We wish to investigate the activation dynamics of these nets operating as CAMs. Upon presentation of an input the net should 'flow', eventually settling at a stationary point of the dynamical system which represents output in the form of n reals. With this dynamic in mind we wish to prevent, by judicious design, any of the more exotic dynamical behaviour exhibited by nonlinear systems. What we seek to prove is that the union of the basins of attraction of equilibria comprises the whole phase space. It is natural then to make the following definition:

Definition 1 *A dynamical system is said to be convergent if for every trajectory* $\phi_t(x)$ *we have:*

$$\lim_{t\to\infty} \phi_t(x) = \eta,$$

where η *is an equilibrium point.*

It is possible to relax this definition in different ways and still have workable definitions of the behaviour we require. For more details, see the excellent paper by Hirsch, [1].

It is easy enough to show that solutions, $x(t, x_0)$ to (1), have bounded forward closure if $\|x_0\| \leq K$, $K > 0$, in the sup norm. We will assume boundedness of

inital conditions throughout, so that the phase space Ω is a compact subset of $\mathbb{R}^n$. By standard theory, all trajectories can be extended to have domain of definitions equal to the whole of $\mathbb{R}$.

Since f is linear in the three segments defined by: $\mid x \mid \leq 1, x > 1$ and $x < -1$, the CNN vector field is piecewise linear. The regions of Ω on which the vector field is constant will be called *partial* or *total saturation* regions depending on whether some cells are in their linear region or not. It is clear (by piecewise linearity) that if any total saturation region contains a stable equilibrium it is a trapping region; whilst the absence of an equilibrium means that all trajectories will leave such a region. Finally, Jacobians are constant on the various partial saturation regions.

The analysis of large-scale interconnected systems often proceeds by investigating the behaviour of the system thought of as a collection of subunits. When we can describe the dynamical behaviour of the subunits successfully we may make progress towards the description of the behaviour of the system as a whole by supposing that the connections between units are so weak that the dynamical behaviour of the isolated units dominate. In [2] an analysis of a type of additive neural net was presented which presumed a *strict row-diagonally dominant* condition on the feedback matrix $B = (b_{ij})$; namely:

$$b_{ii} - 1 > \sum_{i \neq j} \mid b_{ij} \mid . \tag{3}$$

Roughly speaking (3) says that in terms of the dynamics, the self-feedback of each CNN cell dominates over the summed influences from its neighbours and may therefore be viewed as an example of the above large-scale system analysis. In section III of [2], the authors conjectured that (3) is sufficient to ensure convergence of the associated net; furthermore they outlined a method of proof. In this note we show that this conjecture is true by giving a rigorous argument built on their ideas.

2 Convergence of the Dynamical System.

Of prime importance to our result is the fact that if $B - I$ satisfies (3), then each total saturation region contains a (unique) equilibrium point; this is the substance of:

Lemma 2 *If B is strictly row-diagonally dominant, then every total saturation region contains an equilibrium.*

Proof We borrow some notation from [3]; let $S \subset \{1, \ldots, n\}$ be of cardinality m and define the following sets:

$$\Lambda_m = \{\varepsilon = (\varepsilon_1, \ldots, \varepsilon_n) \mid \varepsilon_i = 0, i \in S \text{ and } \varepsilon \in \{-1, 1\}, \text{ for } i \notin S\},$$

where:

$$\Lambda = \{(\varepsilon_1, \ldots, \varepsilon_n) \mid \varepsilon_i \in \{-1, 1\}\}.$$

Then for each $\varepsilon \in \Lambda$ define:

$C(\varepsilon) = \{(x_1, \ldots x_n) \in \Omega \mid\mid x_i \mid < 1, \text{ if } \varepsilon_i = 0, x_i \geq 1, \text{ if } \varepsilon_i = 1, x_i \leq -1, \text{otherwise}\}.$

Firstly we consider the total saturation region $C(\varepsilon_s)$, for some $\varepsilon_s \in \Lambda_0$. Suppose that an equilibrium $\bar{x}$ for the linear system of equations restricted to $C(\varepsilon_s)$, satisfies $f(\bar{x}_i) = 1$; then:

$$\bar{x}_i = b_{ii} + \sum_{j \neq i} b_{ij} f(\bar{x}_j) \geq b_{ii} - \sum_{j \neq i} \mid b_{ij} \mid \geq 1,$$

provided that (3) is satisfied. Similarly, if $f(\bar{x}_i) = -1$, $\bar{x}_i \leq -1$. Thus each total saturation region contains a (unique) equilibrium. □

Much more than lemma (2) is true, in fact it is possible to show that there exists an equilibrium in each partial and total saturation region, if and only if $B - I$ satisfies (3). In this case it is possible, by a linearly invertible change of variables (Grossberg's $S\Sigma$-exchange), to consider the dynamical system operating on a closed hypercube, a so-called BSB system ("Brain-State-In-A-Box"), then the existence equilibria at each corner of the hypercube is shown in [4].

Our main theorem is:

Theorem 3 *If $B-I$ is strictly row-diagonally dominant then the dynamical system (1) with N cells defined by:*

$$\dot{x} = -x + Bf(x),$$

is convergent.

Proof By Gerschgorin's Circle theorem (see [5]), if (3) is satisfied all the Gerschgorin discs lie in the right half-plane. Thus any unsaturated variable, corresponding to a cell operating in its linear region, has an associated eigenvalue with positive real part. It follows that trajectories decay from partial saturation regions and the linear region since at least one eigenvalue of the Jacobian has positive real part there (unless, of course a trajectory lies in the stable manifold of an unstable equilibrium point, in which case it converges to an equilibrium anyway).

Once a hyperplane $x_i = \pm 1$ has been crossed by a trajectory $\phi(t)$, say at at time t_0, then at no future time $t > t_0$, will this trajectory satisfy $\mid \phi_i(t) \mid < 1$. To see this consider the vector field along the hyperplane H_i^+, defined by $x_i = 1$. We have:

$$\dot{x}_i = b_{ii} - 1 + \sum_{j \neq i} b_{ij} f(x_j), \tag{4}$$

and it follows that $\dot{x}_i > 0$ along H_i^+ since the maximum value that the summation term in (4) attains equals:

$$\sum_{j \neq i} \mid b_{ij} \mid,$$

because $\mid f(x) \mid \leq 1$ for all x. (An identical argument along $x_i = -1$ holds). Thus the vector field points 'outwards', i.e in the direction of increasing $\mid x_i \mid$, along the hyperplanes forming the boundary of the individual linear regions and therefore no trajectory can decay across any $H_i^{\pm}$ with $\mid \phi_i \mid$ decreasing.

If we define:

$$\rho(\phi(t,x)) = \#\ (\text{saturated components of } \phi(t,x)),$$

then the argument in the previous paragraph shows that $\rho(t)$ is a non-decreasing function (defined on $\{x\} \times [0, \infty)$), which is bounded above by N. Thus $\lim_{t \to \infty} \rho(t)$ exists and actually must equal N (if not, given some $T > 0$, there is at least one unsaturated cell, i.e there exists i_k, say, such that $\mid \phi_{i_k}(x,t) \mid < 1$, for all $t \geq T$ and $1 \leq k \leq N$. However, since the real parts of the corresponding eigenvalues are positive, there exists a $t_0 > T$ such that $\mid \phi_{i_k}(x,t_0) \mid > 1$, which is a contradiction). Since all total saturation regions contain a stable equilibrium point by Lemma 2, and the basin of attraction of such an equilibrium contains the total saturation region, all trajectories converge. □

By an identical argument we are able to prove the more general result:

Theorem 4 *If an additive neural network described by (1) satisfies the condition:*

$$b_{ii} - 1 > \sum_{j \neq i}^{n} | b_{ij} | + | I_i | \tag{5}$$

then it is convergent.

3 Applications to CNNs and Final Remarks

Recently a new class of neural networks called *Cellular Neural Networks (CNNs)*, has been introduced, (see [6]); such nets are recurrent, continuous time networks described by (1), with a particular structure on B, called the *feedback* matrix, (that arises from the architecture of the net), together with a ramp sigmoid activation function. Therefore our results (3) and (4) from the previous section apply to such nets.

The concept of a CNN is rooted in 2D nonlinear Filter Theory, and Cellular Automata. The neurons are arrayed on a two-dimensional grid and any fixed neuron can be thought of as a centre neuron which is connected, through a neighbourhood of size $r \geq 1$, to its nearest neighbours; i. e. any cell which can be arrived at in a kings walk of length $\leq r$ on a chessboard. Neighbourhood sizes can increase in size up to a fully interconnected net, but usually we insist on $r = 1$ so that only the 'nearest' neighbours are connected. The intention of this architecture is to facilitate the fabrication of such a device onto a chip, for reducing connections increases the chances of a successful implementation.

CNNs have found a variety of interesting and useful applications and most cases share the common idea that solutions to processing tasks are represented as constant attracting trajectories of the associated dynamical system. Upon presentation of an input image, coded as an array of grey-scale pixels, the CNN should operate as a CAM, 'flowing' to an output image.

The strict row-diagonal dominance of the feedback matrix is a severe restriction on the parameters because in practical terms such a CNN would not process bipolar images. A trajectory with a 'bipolar' initial condition would of course lie in a total saturation region. If (3) holds all such regions are contained in the basin of attraction of a stable equilibrium point $\bar{x}$. The output of the CNN, $f(\bar{x})$, would then be identical to the input image and we would observe no transformation of such an image. As proved in [2], (3) is a necessary and sufficient condition for the existence of a stable equilibrium in each total saturation region. Conditions weaker than (3) would therefore allow bipolar images to undergo change because any trajectory with initial conditions in a total saturation region which contains no equilibrium must leave this region and hence undergo a nonlinear transformation. In practice therefore we seek weaker conditions which ensure complete stability.

As a final remark, let us return to the more general case considered in the first sections of this paper. We have a compact phase space, partitioned by the PWL vector field. If the matrix B has eigenvalues with positive real parts one would like to be able to say that trajectories are 'expanding' and thus reach total saturation regions. However, there are examples of CNNs with such eigenvalues possessing closed orbits – all that one can say is that no trajectory can remain in a partial

saturation region if such an eigenvalue exists. The diagonal dominance condition ensures that recrossing of a partial saturation boundary cannot occur and as we have seen this has a profound effect on the global behaviour of trajectories.

REFERENCES

[1] M. W. Hirsch, *Activation dynamics in continous time nets*, Neural Networks, Vol. 2 (1989), pp331–349.

[2] F. A. Savaci and J. Vandewalle, *On the stability analysis of cellular neural networks*, IEEE Trans. Circuits Syst., Vol. 40 (1993), pp213 – 215.

[3] J. H. Li, A. N. Michel, and W. Porod, *Analysis and synthesis of a class of neural networks: Linear systems operating on a closed hypercube*, IEEE Trans. Circuits Syst., Vol. 36 (1989), pp1405–1422.

[4] S. Hui and S. H. Zak, *Dynamical analysis of the brain-state-in-a-box (BSB) neural models*, IEEE Trans. Neural Networks, Vol. 3 (1992), pp86–94.

[5] R. A. Horn and C. R. Johnson, *Matrix Analysis*, Cambridge University Press (1990), Cambridge UK.

[6] L.O. Chua and L. Yang, *Cellular neural networks: Theory*, IEEE Trans. Circuits Syst., Vol. 35, (1988), pp1257 – 1272.

APPLICATIONS OF THE COMPARTMENTAL MODEL NEURON TO TIME SERIES ANALYSIS

S. Kasderidis and J. G. Taylor

Department of Mathematics, King's College London, UK.

In this paper we discuss an extended model neuron in ANN. It is the compartmental model which has already been developed to model living neurons. This type of neuron belongs to the class of temporal processing neurons. Learning of these neurons can be achieved by extending the model of Temporal Backpropagation. The basic assumption behind the model is that the single neuron is considered as possessing finite spatial dimension and not being a point processor (integrate and fire). Simulations and numerical results are presented and discussed for three applications to time series problems.

1 Introduction

Most models of a neuron used in ANN neglect the spatial structure of a neuron's extensive dendritic tree system. However, from a computational viewpoint there are a number of reasons for taking into account such a structure. (i) The passive membrane properties of a neuron's dendritic tree leads to a spread of activity through the tree from the point of stimulation at a synapse. Hence spatial structure influences the temporal processing of synaptic inputs. (ii) The spatial relationship of synapses relative to each other and the soma is important. (iii) The geometry of the dendritic tree ensures that different branches can function almost independently of one another. Moreover, there is growing evidence that quite complex computations are being performed within the dendrites prior to subsequent processing at the soma.

The (linear) cable theory models try to explain the creation of the action potential [1]. These models belong to the class of Hodgkin-Huxley derived models. The one-dimensional cable theory describes current flow in a continuous passive dendritic tree using P.D.E.s. These equations have straightforward solutions for an idealised class of dendritic trees that are equivalent to unbranched cylinders. For cases of passive dendritic trees with a general branching structure the solutions are more complicated. When the membrane properties are voltage dependant then the analytical approach using linear cable theory is no longer valid. One way to account for the geometry of complex neurons has been explored by Abbott et al. [2]. Using path-integral techniques, they construct the membrane potential response function (Green's function) of a dendritic tree described by a linear cable equation. The response function determines the membrane potential arising from the instantaneous injection of a unit current impulse at a given point on the tree.

A complementary approach to modelling a neuron's dendritic tree is to use a compartmental model in which the dendritic system is divided into sufficiently small regions or compartments such that spatial variations of the electrical properties within a region are negligible. The P.D.E.s of cable theory then simplify to a system of first order O.D.E.s. From these equations we can then calculate the response function, i.e. the law with which the action potential is created, see [3], [4], [5]. Using the previous ideas, we construct an artificial neuron through appropriate simplifications in the structure of the neurobiological compartmental model and its response function.

2 The Compartmental Model Neuron

2.1 The Transfer Function

The artificial neuron is composed of a set of compartments, in which connections from other neurons of the network are arriving. The transfer function for neuron i in the layer l in time instance t has the form:

$$y_{li}(t) = s(V_{li}^0(t)) = s\left(\sum_{n=0}^{T}\sum_{\beta=0}^{m} f_{|\beta|}(n)u^{\beta}(n)\right) \tag{1}$$

$$u_{\beta}(n) = \sum_{j=1}^{M_{li}^{\beta}} w_{lij}^{\beta}(n)y_{(l-1)j}(t-n) \tag{2}$$

where s is any suitable nonlinear function, usually the sigmoid, $V_{li}^0(t)$ is the net potential at "soma" (compartment 0) at time t, T is the number of time steps used to keep a history of the neuron, m is the number of compartments in the neuron, M_{li}^{β} is the number of incoming weights to compartment β (note that this number is compartment related), $u^{\beta}(n)$ is the net potential at compartment β at time instance n and $f_{|\beta|}(n)$ is a kernel function corresponding to the response function of the respective neurobiological model and has the following general form:

$$f_{|\alpha-\beta|}(t) = G(\alpha,t;\beta,0) = e^{\frac{-t}{\tau}} I_{|\alpha-\beta|}\left[\frac{2t}{\gamma}\right] \tag{3}$$

The parameters γ and τ determine effectively the delay rate in the propagation of the signal from compartment β at time 0 (a stimulus is coming there) to compartment α at time t. The function $I_n(t)$ is the modified Bessel function of integer order n.

For the purpose of the artificial neuron the parameters can either remain constant or adapt during the simulation. The connections that exist between neurons are assumed to be like the ones of the Temporal Backpropagation case, i.e. having tapped delays up to a desirable order N, see [6]. In this way the neuron produces a signal that depends also on the previous values of its input.

2.2 The Learning Law

In applying the compartmental model to problems of supervised learning we devise a learning law that is based on Temporal Backpropagation, but is modified appropriately to account for the existence of distinct compartments. Assuming an MSE error function and a sigmoid transfer function of the type:

$$f(x) = \frac{1}{1+e^{-x}} \tag{4}$$

then the learning law (stochastic case) has the following form:

$$w_{lij}^{x(new)}(s) = w_{lij}^{x(old)}(s) + \Delta w_{lij}^{x(new)}(s) \tag{5}$$

$$\Delta w_{lij}^{x(new)}(s) = (-\eta)f_{|x|}(s)y_{(l-1)j}(t-s)\delta_{li}(t) + \alpha\Delta w_{lij}^{x(old)}(s) \tag{6}$$

$$\delta_{li}(t) = s'(t)(-2)e_{li}(t) \quad \text{for} l = L \tag{7}$$

$$\delta_{li}(t) = s'_{li}(t)\sum_{p=1}^{M'_{li}}\sum_{t'=t}^{t+T_{(l+1)p}} \delta_{(l+1)p}(t')f_{|d|}(t'-t)w_{(l+1)pi}^{d}(t'-t) \tag{8}$$

In the above equations, η and α are the learning rate and momentum coefficients, $s = 0...T_{li}$ is a temporal index, T_{li} is the temporal dimension of neuron i at layer l. In equation (6) t is referring to current time and s is then the time delay from current time. L is the output layer, $e_{li}(t)$ is the error in the output layer, s' is the derivative of the transfer function, M'_{li} is the number of outgoing connections from neuron i. W_{lij} are the weights connecting neuron j at layer $(l-1)$ to neuron i at layer l. In the notation we take into account that the weights are associated with different compartments. The index x in the weights denotes that compartment in which an incoming connection is terminated and the index d is the compartment (of neuron p at layer $(l+1)$) to which an outgoing connection of i is connected. Finally the δ_{li} are defined as follows:

$$\delta_{li}(t) \equiv \frac{\partial E}{\partial V_{li}(t)} \tag{9}$$

where E is the error function and $V_{li}(t)$ is the activation of the neuron before the transfer function.

3 Simulation Results

We tested the model using three time series: the logistic map series near its chaotic region, an astronomical series which describes the interaction of a gravitational wave with a distribution of particles in the interstellar media [7], and a solid state physics series which describes the chaotic voltage oscillations in the NDR region of the I-U characteristics registered in $V_2\ O_5$ single crystals [8]. In all cases the parameters γ and τ were kept constant.

3.1 Logistic Map

In Fig. 1 we see the performance of the model in comparison with a Temporal Backpropagation network of same degrees of freedom. The network for the compartmental model employed was a 1-15-1 architecture with 3 tapped delay lines for the case of hidden neurons and 1 line for the output unit. In both networks we used 400 points for training, 200 points for validation and 250 points for testing the mapping that was achieved. In the testing set after the first 200 points we used multi-step iterative prediction for the remaining 50 points. The parameters γ and τ had values 1.0 and 2.0 respectively. The incoming connections from the hidden neurons to the output neuron were connected to compartment number zero ("soma").

The parameters for the logistic map were $\lambda = 3.8$ and the initial condition was $x_0 = 0.1$ In Fig. 1 we see the region of multi-step prediction, ranging from number 900 up to number 932 for both methods. The solid line is the logistic map series, the sparse dashed line is the Compartmental model prediction and the dense dashed line is the Temporal Backpropagation model.

We see initially that after two points with correct match the Compartmental model does not predict correctly the following twelve points. The same behaviour is observed for the Temporal Backpropagation model. But afterwards, strangely enough, the model closely follows the underlying mapping for the remaining points. This behaviour extends further in the series.

3.2 Astronomical Series

In Fig. 2 we see a series that is describing the interaction of a gravitational wave with the interstellar plasma. The interaction that is shown is chaotic.

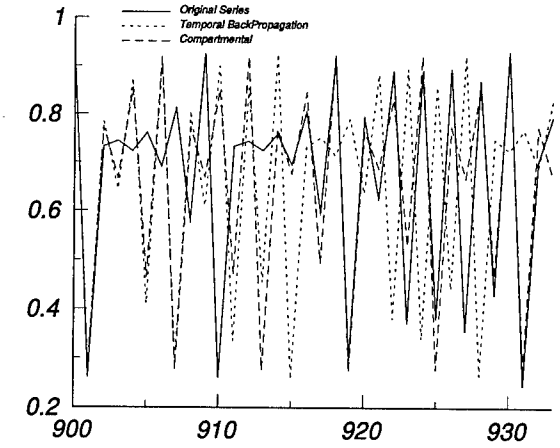

Figure 1 Logistic Time Series. Logistic map, I=3.8. T=1, G=2. Network 1-15-1. TDimH = 3, TDimO = 1. Multistep Prediction region 900-932.

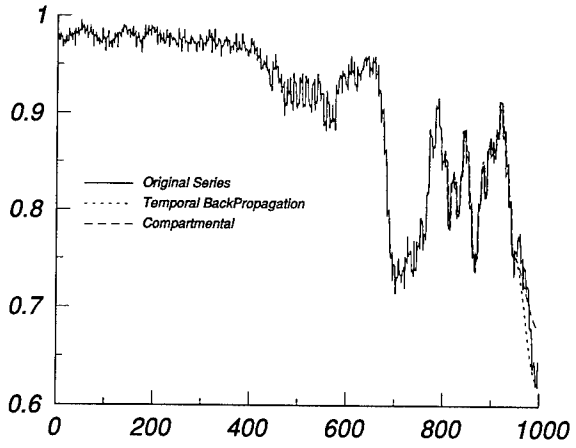

Figure 2 Astrophysical Time Series. T = 1, G = 1. Network 1-5-1. TDimH = 3, TDimO = 1. Connections to "soma".

Again the Compartmental and Temporal Backpropagation models were used for comparison. The architecture that was employed was a 1-5-1 network with 3 tapped delays for the hidden neurons and 1 delay line for the output neuron. The τ and γ parameters were 1.0 and 1.0 respectively. The incoming connections to output neuron were connected to the "soma" . Again 400 points were used, here though from the range 400–800, because we wanted to avoid the initial transient period. The prediction that was sought was in the range of 800–1000, and 150 points were used for single step prediction and the remaining 50 points were generated by a multi-step prediction scheme.

The solid line corresponds to the original series, the sparse and dense dashed lines represent the Compartmental and Temporal Backpropagation model predictions respectively.
Fig. 2 shows that a good approximation of the underlying map was achieved by both models even though a fairly simple architecture was employed and the training set was not the most representative.

3.3 Solid State Series

In Fig. 3 we see a series that is describing the chaotic voltage oscillations in the NDR region of the crystal.

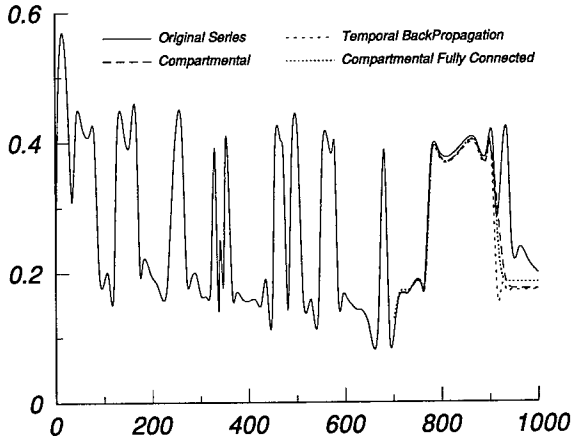

Figure 3 Solid State Physics Time Series. T=1, G=2. Network 1-5-1. TDimH = 8, TDimO = 2. Connections to "soma". Network 1-5-1. TDimH = TDimO = 1.5 comps/neuron. Fully connected.

Again the Compartmental and Temporal Backpropagation models were used for comparison. The architecture that was employed was a 1-5-1 network with 8 tapped delays for the hidden neurons and 2 delay line for the output neuron. The τ and γ parameters were 1.0 and 2.0 respectively. The incoming connections to output neuron were connected to the "soma". For training, 450 points were used, from the range 1–450, 200 points were used for validation in the range 500–700. The prediction that was sought was in the range of 700–1000, and 200 points were used for single step prediction and the remaining 100 points were generated by a multi-step prediction scheme.
Here we try to tackle also the problem of how the incoming weights to a neuron should be distributed among its compartments. Here instead of connecting just to one compartment, we tested the idea of connecting to all the compartments. For this purpose we used a 1-5-1 network structure, with 1 tapped delay line per hidden and output neuron. But instead the neurons consist of 5 compartments each, where we are connecting the incoming signal from every other neuron. The key to note here is that the value of the incoming signal is the same for all the five compartments, but different weights exist for every connection to a specific compartment.

In Fig. 3 the solid line corresponds to the original series, the flat sparse and exponentially decaying dense dashed lines represent the Compartmental and Temporal Backpropagation model predictions respectively. The dense dashed line is the Compartmental model with full connectivity to all compartments.
Fig. 3 shows that a good approximation of the underlying map was achieved by both models even though a fairly simple architecture was employed. We were surprised by the fact that the best approximation to the underlying map was achieved by the fully connected model.
Finally we have to mention here, that for comparison the parameters of the nets were chosen to produce exactly the same number of free parameters (weights) namely fifty for all three models.

4 Conclusion

From these initial simulations we see that in general the Compartmental model is at least as successful as the Temporal Backpropagation model for the time series involved. Even though fairly simple architectures were used, the underlying mapping was approximated reasonably well as the single step predictions are showing. For the multi-step predictions further simulations are needed, in order to specify a more appropriate architecture and parameter range that leads to better performance.
Further research is now being carried out to investigate the complex couplings of the parameters that control the behaviour of the model. Also a major issue of the model is the scheme with which we choose to assign the incoming connections of each neuron to its compartments [11].

REFERENCES

[1] Koch and Segev, editors, *Methods in Neural Modeling*, MIT Press (1989).
[2] Abbott, L. F., Farhi, E., Gutmann, S., *The path integral for dendritic trees*, Biological Cybernetics, Vol. 66 (1991), pp61–70.
[3] Bressloff, P. C., *Dynamics of a compartmental model integrate-and-fire neuron with somatic potential reset*, Physica D, submitted.
[4] Bressloff, P. C., Taylor, J. G., *Compartmental response function for dendritic trees*, Biological Cybernetics, Vol. 70 (1993), pp199–207.
[5] Bressloff, P. C., Taylor, J. G., *Spatio-temporal pattern processing a compartmental model neuron*, Physica Review E, Vol. 47 (1993), pp2899–2912.
[6] Wan, E., *Finite Impulse Response Neural Networks for Autoregressive Time Series Prediction*, in: Predicting the Future and Understanding the Past, eds. by A. Weigend and N. Gershenfeld, SFI Studies in the Sciences of Complexity, Proc. Vol. XVII (1993), Addison-Wesley.
[7] Kleidis, K., Varvoglis, H., Papadopoulos, D., *Interaction of charged particles with gravitational waves of various polarizations and directions of propagation*, Astronomy and Astrophysics, Vol. 275 (1993), pp309–317.
[8] Karakotsou, C., Anagnostopoulos, A., Kambas, K., Spyridelis, J., *Chaotic voltage oscillations in the negative-differential-resistance region of the I-U curves of V_2O_5 crystals*, Physical Review B, Vol. 46 (1992), No. 24, p16144.
[9] Kasderidis, S., Taylor, J. G., *The compartmental model neuron and its application to time series analysis*, in proceedings of IEEE Workshop on Nonlinear Signal and Image Processing, Neos Marmaras, Greece, (June 20–22 1995), p58.
[10] Kasderidis, S., Taylor, J. G., *The compartmental model neuron*, proceedings of WCNN (July 17–21 1995), Washington D.C., USA.
[11] Kasderidis, S., Taylor, J. G., King's College preprint (to appear).

Acknowledgements

During this work the first author was supported by a grant of the Greek State Scholarship Foundation.

INFORMATION THEORETIC NEURAL NETWORKS FOR CONTEXTUALLY GUIDED UNSUPERVISED LEARNING

Jim Kay

Dept. of Statistics, University of Glasgow, Mathematics Building, Glasgow G12 8QW, UK. Email: jim@stats.glasgow.ac.uk

The purpose of this article is to describe some new applications of information-theoretic concepts in unsupervised learning with particular emphasis on the implementation of contextual guidance during learning and processing.

1 Introduction

Building on earlier work by Linsker, and Becker and Hinton [8, 2] , Kay and Phillips [7] used the concept of three-way mutual information in order to define a new class of objective functions designed to maximise the transfer of the information shared between a set of inputs (the receptive field) and outputs that is predictably related to the context(the contextual field) in which the learning occurs and termed one of this new class of objective functions **Coherent Infomax**. In addition they introduced a new activation function which combines information flowing from the receptive and contextual fields in a novel way within local processors. Two illustrations of the role of contextual guidance are given in [7] and further demonstrations are provided in [9]. This work, however, considered only the case where the local processors have binary output units. In this article the methodology proposed in [7] is extended to the case of general multivariate Gibbs distributions but will be described, for simplicity, in the particular case of multivariate binary outputs. The article proceeds as follows. In section 2 notation will be described and probabilistic modelling of the multivariate outputs considered. The definition of suitable objective functions will be discussed in section 3 and various local objective functions introduced. The learning rules will be presented in section 4 and finally in section 5 computational issues will be briefly considered.

2 Probabilistic Modelling

We consider a local processor having multiple outputs. This processor receives input from two distinct sources, namely, its receptive field inputs,$\mathbf{R} = \{R_1, R_2, ..., R_m\}$ and its contextual field inputs,$\mathbf{C} = \{C_1, C_2, ..., C_n\}$ and produces its outputs,$\mathbf{X} = \{X_1, X_2, ..., X_p\}$, where $\mathbf{R}$, $\mathbf{C}$ and $\mathbf{X}$ are taken to be random vectors and we adopt the usual device of denoting a random variable by a capital letter and its observed value by the corresponding lower-case letter. In order to allow explicitly for the possibility of incomplete connectivity we define connection neighbourhoods for the ith ouput unit X_i. Let $\partial i(r)$, $\partial i(c)$ and $\partial i(x)$ denote, respectively, the set of indices of the RF input units, the set of indices of the CF inputs and the set of indices of the outputs that are connected to the ith output unit X_i. The corresponding random variables are denoted by $\mathbf{R}_{\partial i}, \mathbf{C}_{\partial i}, \mathbf{X}_{\partial i}$ respectively and the set of all components of $\mathbf{X}$ excluding the ith component is $\mathbf{X}_{-i}$. The weights on the connections into the ith output unit are given by w_{ij}, v_{ij} and u_{ij} for the jth RF input, jth CF input and the jth output unit respectively and we assume that the weights connecting

the output units to each other are symmetric. We now define the integrated fields in relation to the ith output unit.
$S_i(r) = \sum_{j \in \partial i(r)} w_{ij} R_j - w_{i0}$ is the RF integrated field.
$S_i(c) = \sum_{j \in \partial i(c)} v_{ij} C_j - v_{i0}$ is the CF integrated field.
$S_i(x) = \sum_{j \in \partial i(x)} u_{ij} X_j$ is the output integrated field.
The weights w_{i0} and v_{i0} are biases.
The activation function at the ith output unit is now a function of three integrated fields and we shall take it to have the following form

$$A_i = A(s_i(r), s_i(c)) + s_i(x) \equiv a_i + s_i(x). \tag{1}$$

although we shall derive the learning rules in the general case. This particular way of incorporating the integrated output has been chosen so that this local activation function at the ith output unit is consistent with the definition of a multivariate model for $\mathbf{X}$. The activation function A which binds the activity of the RF and CF integrated fields is that proposed in [7] defined by

$$A(s_1, s_2) = \frac{1}{2} s_1 (1 + \exp(2 s_1 s_2)) \tag{2}$$

We assume that the output vector $\mathbf{X}$ follows a binary markov random field model [3] conditional on the RF and CF inputs, with probability mass function

$$Pr(\mathbf{X} = \mathbf{x} | \mathbf{R} = \mathbf{r}, \mathbf{C} = \mathbf{c}) = \frac{\exp(\sum_{i=1}^{p} a_i x_i + \frac{1}{2} \sum_{i=1}^{p} \sum_{j \in \partial i(x)} u_{ij} x_i x_j)}{Z(\mathbf{a}, \mathbf{u})} \tag{3}$$

where $Z(\mathbf{a}, \mathbf{u})$ is the normalisation constant (i.e. not a function of $\mathbf{x}$) required to ensure that the probabilities sum to unity. This model is a regression model in two distinct senses. Firstly, via the terms $\{a_i\}$ which are general nonlinear functions of the RF and CF inputs, it is a nonlinear regression of the outputs with respect to all of the inputs. Secondly, when written in conditional form in equation (3), it expresses an auto-regression for each output unit in terms of the other output units in its neighbourhood. The formulation developed in the above model has the advantage of interfacing a feed-forward network between layers with a recurrent network structure within the output layer within a single coherent probabilistic framework. Not only that but it is also possible to connect the multiple output local processors themselves in a multi-layered network structure in a probabilistically coherent manner.
From this model the local conditional distributions may be derived. As we shall see using these distributions provides a local structure to the learning rules and, under the restrictions on the output connection weights, the Hammersley-Clifford theorem [3] ensures that working locally with the conditional models is equivalent to assuming a coherent global model for the outputs. However in the case were the output units are fully, mutually connected the equations presented here hold without any necessity to invoke this theorem to ensure probabilistic coherence and are derived using the basic rules of probability.
The local conditional distribution for the ith output is

$$\theta_i \equiv Pr(X_i = 1 | \mathbf{R}_{\partial i} = \mathbf{r}_{\partial i}, \mathbf{C}_{\partial i} = \mathbf{c}_{\partial i}, \mathbf{X}_{\partial i} = \mathbf{x}_{\partial i}) = 1/(1 + \exp(-A_i)). \tag{4}$$

Here $A_i = a_i + s_i(x)$, where a_i is any general differentiable function of the integrated RF and CF fields.

3 Global and Local Objective Functions

We now consider a global objective function based on the joint distribution of all outputs, RF inputs and CF inputs. In the case of multivariate outputs, we consider the general version of the objective function introduced in [7] which is

$$F = I(\mathbf{X};\mathbf{R};\mathbf{C}) + \phi_1 I(\mathbf{X};\mathbf{R}|\mathbf{C}) + \phi_2 I(\mathbf{X};\mathbf{C}|\mathbf{R}) + \phi_3 H(\mathbf{X}|\mathbf{R},\mathbf{C}). \quad (5)$$

Here the term I(**X**;**R**;**C**) is the three-way mutual information between the random vectors **X**,**R** and **C** given by

$$I(\mathbf{X};\mathbf{R};\mathbf{C}) = I(\mathbf{X};\mathbf{R}) - I(\mathbf{X};\mathbf{R}|\mathbf{C}) \quad (6)$$

and

$$I(\mathbf{X};\mathbf{R}) = H(\mathbf{X}) - H(\mathbf{X}|\mathbf{R}) \quad (7)$$

is the mutual information shared between the random vectors **X** and **R** and the symbol H denotes Shannon's entropy. For further details see [4]. The objective function in equation (5) is based on the three-way mutual information and the three possible conditional measures of (two-way) mutual information.
For the purposes of modelling this is expressed as

$$F = H(\mathbf{X}) - \psi_1 H(\mathbf{X}|\mathbf{R}) - \psi_2 H(\mathbf{X}|\mathbf{C}) - \psi_3 H(\mathbf{X}|\mathbf{R},\mathbf{C}). \quad (8)$$

In terms of the output, and indeed the input, units this is a **global** objective function and general learning rules have been derived in the general case of Gibbs distributions. However these lead to learning rules that are global and also computationally challenging in their exact form and so we now describe a particular local approximation to the global objective function F; other definitions of locality are possible [5]. In this multiple output case, it is natural to think of the processing locally in terms of each output unit using the information available to it from its RF, CF and output neighbourhoods. This suggests that one might focus in turn on the joint distribution of, say, the ith output and its RF and CF inputs **given** the neighbouring output units. From this perspective it then seems natural to introduce the concept of the **conditional** three-way mutual information shared by the ith output and its RF and CF inputs given the neighbouring outputs denoted by

$$I(X_i;\mathbf{R}_{\partial i};\mathbf{C}_{\partial i}|\mathbf{X}_{\partial i}) = I(X_i;\mathbf{R}_{\partial i}|\mathbf{X}_{\partial i}) - I(X_i;\mathbf{R}_{\partial i}|\mathbf{C}_{\partial i},\mathbf{X}_{\partial i}) \quad (9)$$

It is possible to decompose the global three-way mutual information as follows.

$$I(\mathbf{X};\mathbf{R};\mathbf{C}) = I(X_i;\mathbf{R}_{\partial i};\mathbf{C}_{\partial i}|\mathbf{X}_{\partial i}) + I(\mathbf{X}_{-i};\mathbf{R};\mathbf{C}) \quad (10)$$

This decomposition may be repeated recursively and is of particular relevance when the output units represent some one-dimensional structure such as a time series ; then the well-known general factorisation of joint probability into a product of a marginal and conditional distributions allows the general three-way mutual information to be written as a sum of local conditional three-way mutual information terms. However such simplicity is not possible here, although this first-step decomposition shows that the conditional three-way information is a part of the global three-way information in a well-defined sense. The same conditioning idea may be applied to the other components of information within the objective function F and this leads to the specification of a local objective function for the ith output unit defined as follows

$$\begin{aligned} F_i \;=\; & I(X_i;\mathbf{R}_{\partial i};\mathbf{C}_{\partial i}|\mathbf{X}_{\partial i}) + \phi_1 I(X_i;\mathbf{R}_{\partial i}|\mathbf{C}_{\partial i},\mathbf{X}_{\partial i}) \\ & + \phi_2 I(X_i;\mathbf{C}_{\partial i}|\mathbf{R}_{\partial i},\mathbf{X}_{\partial i}) + \phi_3 H(X_i|\mathbf{R}_{\partial i},\mathbf{C}_{\partial i},\mathbf{X}_{\partial i}), \end{aligned} \quad (11)$$

and we express $\{F_i\}$ in the more useful form

$$F_i = H(X_i|\mathbf{X}_{\partial i}) - \psi_1 H(X_i|\mathbf{R}_{\partial i}, \mathbf{X}_{\partial i}) - \psi_2 H(X_i|\mathbf{C}_{\partial i}, \mathbf{X}_{\partial i}) - \psi_3 H(X_i|\mathbf{R}_{\partial i}, \mathbf{C}_{\partial i}, \mathbf{X}_{\partial i}) \tag{12}$$

This means that we envisage each output unit working to maximise F_i and because of the the fact that mutually distinct sets of weights connect into each of the outputs this is equivalent to maximising the sum of the $F_i s$. We view this sum as a locally-based approximation to the global objective function F. In the extreme case where the outputs are conditionally independent this sum is equivalent to F. Obviously the approximation will be better the smaller are the sizes of the output neighbourhood sets relative to the number of outputs. We now provide formulae for the local entropic terms and the components of local information for the ith output unit.

$$H(X_i|\mathbf{R}_{\partial i}, \mathbf{C}_{\partial i}, \mathbf{X}_{\partial i}) = \langle \theta_i \log \theta_i + (1-\theta_i)\log(1-\theta_i) \rangle_{\mathbf{R}_{\partial i}, \mathbf{C}_{\partial i}, \mathbf{X}_{\partial i}} \tag{13}$$

$$H(X_i|\mathbf{R}_{\partial i}, \mathbf{X}_{\partial i}) = \langle E^{(i)}_{\mathbf{R}_{\partial i}, \mathbf{X}_{\partial i}} \log E^{(i)}_{\mathbf{R}_{\partial i}, \mathbf{X}_{\partial i}} + (1 - E^{(i)}_{\mathbf{R}_{\partial i}, \mathbf{X}_{\partial i}}) \log(1 - E^{(i)}_{\mathbf{R}_{\partial i}, \mathbf{X}_{\partial i}}) \rangle_{\mathbf{R}_{\partial i}, \mathbf{X}_{\partial i}} \tag{14}$$

$$H(X_i|\mathbf{C}_{\partial i}, \mathbf{X}_{\partial i}) = \langle E^{(i)}_{\mathbf{C}_{\partial i}, \mathbf{X}_{\partial i}} \log E^{(i)}_{\mathbf{C}_{\partial i}, \mathbf{X}_{\partial i}} + (1 - E^{(i)}_{\mathbf{C}_{\partial i}, \mathbf{X}_{\partial i}}) \log(1 - E^{(i)}_{\mathbf{C}_{\partial i}, \mathbf{X}_{\partial i}}) \rangle_{\mathbf{C}_{\partial i}, \mathbf{X}_{\partial i}} \tag{15}$$

$$H(X_i|\mathbf{X}_{\partial i}) = \langle E^{(i)}_{\mathbf{X}_{\partial i}} \log E^{(i)}_{\mathbf{X}_{\partial i}} + (1 - E^{(i)}_{\mathbf{X}_{\partial i}}) \log(1 - E^{(i)}_{\mathbf{X}_{\partial i}}) \rangle_{\mathbf{X}_{\partial i}} \tag{16}$$

It follows that the components of local information at the ith output unit are as follows.

$$I(X_i; \mathbf{R}_{\partial i}; \mathbf{C}_{\partial i}|\mathbf{X}_{\partial i}) = (16) - (15) - (14) + (13),$$

$$I(X_i; \mathbf{R}_{\partial i}|\mathbf{C}_{\partial i}, \mathbf{X}_{\partial i}) = (15) - (13),$$

$$I(X_i; \mathbf{C}_{\partial i}|\mathbf{R}_{\partial i}, \mathbf{X}_{\partial i}) = (14) - (13),$$

$$H(X_i|\mathbf{R}_{\partial i}, \mathbf{C}_{\partial i}, \mathbf{X}_{\partial i}) = (13)$$

The $\{E\}$ terms are averages of the output probabilities at the ith unit and are defined at the end of section 4.

4 The Learning Rules

Using the locally-based objective functions developed in section 2 and the formulation so far, it turns out that the learning rules for all weights have the same general structure as those introduced in [7].

We describe the gradient ascent learning rules in relation to the ith output unit.

$$\frac{\partial F_i}{w_{is}} = \langle (\psi_3 A_i - \bar{O}_i)\theta_i(1-\theta_i)\frac{\partial A_i}{\partial s_i(r)} R_s \rangle_{\mathbf{R}_{\partial i}, \mathbf{C}_{\partial i}, \mathbf{X}_{\partial i}}, \tag{17}$$

for each RF input s which connects into the ith output unit.

$$\frac{\partial F_i}{v_{is}} = \langle (\psi_3 A_i - \bar{O}_i)\theta_i(1-\theta_i)\frac{\partial A_i}{\partial s_i(c)} C_s \rangle_{\mathbf{R}_{\partial i}, \mathbf{C}_{\partial i}, \mathbf{X}_{\partial i}}, \tag{18}$$

for each CF input s which connects into the ith output.

$$\frac{\partial F_i}{\partial u_{is}} = \langle (\psi_3 A_i - \bar{O}_i)\theta_i(1-\theta_i)\frac{\partial A_i}{\partial s_i(x)} X_s \rangle_{\mathbf{R}_{\partial i}, \mathbf{C}_{\partial i}, \mathbf{C}_{\partial i}}, \tag{19}$$

for each output unit s which connects into the ith output. Note that these learning rules are **local** and this results from the decision to separately maximise the local

objective functions $\{F_i\}$(or equivalently to maximise the sum of the $\{F_i\}$). The dynamic average for the ith output unit is

$$\bar{O}_i = \log \frac{E^{(i)}_{\mathbf{X}_{\partial i}}}{(1 - E^{(i)}_{\mathbf{X}_{\partial i}})} - \psi_1 \log \frac{E^{(i)}_{\mathbf{R}_{\partial i},\mathbf{X}_{\partial i}}}{(1 - E^{(i)}_{\mathbf{R}_{\partial i},\mathbf{X}_{\partial i}})} - \psi_2 \log \frac{E^{(i)}_{\mathbf{C}_{\partial i},\mathbf{X}_{\partial i}}}{(1 - E^{(i)}_{\mathbf{C}_{\partial i},\mathbf{X}_{\partial i}})}. \quad (20)$$

Here the dynamic averages are more complicated than in the single output case and their calculation involves storing the average probability at the ith output unit for each pattern of the other outputs that connect into the ith output unit, for the combination of each of the neighbouring output and RF input patterns and for the combination of each of the neighbouring output and CF input patterns. However various approximations are possible [5] The various averages of the probability at the ith output unit are defined as follows. $E^{(i)}_{\mathbf{X}_{\partial i}} = \langle \theta_i \rangle_{\mathbf{R}_{\partial i},\mathbf{C}_{\partial i}|\mathbf{X}_{\partial i}}$, $E^{(i)}_{\mathbf{R}_{\partial i},\mathbf{X}_{\partial i}} = \langle \theta_i \rangle_{\mathbf{C}_{\partial i}|\mathbf{R}_{\partial i},\mathbf{X}_{\partial i}}$, $E^{(i)}_{\mathbf{C}_{\partial i},\mathbf{X}_{\partial i}} = \langle \theta_i \rangle_{\mathbf{R}_{\partial i}|\mathbf{C}_{\partial i},\mathbf{X}_{\partial i}}$, and the required partial derivatives may be easily calculated.

5 Some Computational Details

The computation may be performed using on-line learning as was the case in [7] or, alternatively, using batch learning. In the case of on-line learning the weight change rules are applied with the averaging brackets removed and the required conditional averages of output probabilities may be updated dynamically during learning after the presentation of each pattern via recursive computation. In particular recursive computation may be used to avoid the need to explicitly calculate the statistics of the input data and then employ a two-stage approach to the learning. The methodology has been applied in a number of computational experiments described in [6] which demonstrate the feasibility of the approach. It is shown there that the differences between the Infomax and Coherent Infomax computational goals described by [7] hold in this more general set up and that the multiple output unit is capable of representing its inputs by means of population codes. Further experimentation is currently in progress and this will address the computational feasibility of scaling up to large multiple output units and evaluate various approximations for the conditional dynamic averages.

REFERENCES

[1] M. W. Hirsch, *Activation dynamics in continous time nets*, Neural Networks, Vol.2 (1989), pp331–349.

[2] Becker S and Hinton G E, *Self-organizing neural network that discovers surfaces in random-dot stereograms.* Nature Vol. 355 (1992), pp161-3

[3] Besag J E, *Spatial analysis and the statistical analysis of lattice systems (with discussion)*, J. R. Statist. Soc. Ser. B Vol. 36 (1974), pp192-236.

[4] Hamming R W, *Coding and Information Theory* Englewood Cliffs, NJ: Prentice-Hall (1980).

[5] Kay J W, *Information-theoretic neural networks for the contextual guidance of learning and processing: mathematical and statistical considerations*, Technical Report, Biomathematics and Statistics Scotland (1994). (See http://www.stats.gla.ac.uk/~jim/)

[6] Kay J W, Floreano D and Phillips W A, *Contextually guided unsupervised learning using multivariate binary local processors*, submitted to Neural Networks, (1996).

[7] Kay J W and Phillips W A, *Activation functions, computational goals and learning rules for local processors with contextual guidance*, Neural Computation, in press (1997).

[8] Linsker R, *Self-organization in a perceptual network*, IEEE Computer, March (1988), pp105-17.

[9] Phillips W A Kay J W and Smyth D, *The discovery of structure by multi-stream networks of local processors with contextual guidance*, Network Vol. 6 (1995), pp225-246.

CONVERGENCE IN NOISY TRAINING

Petri Koistinen

Rolf Nevanlinna Institute, P.O. Box 4, FIN-00014 University of Helsinki, Finland. Email: petri.koistinen@rni.helsinki.fi

A minimization estimator minimizes the empirical risk associated with a given sample. Sometimes one calculates such an estimator based not on the original sample but on a pseudo sample obtained by adding noise to the original sample points. This may improve the generalization performance of the estimator. We consider the convergence properties (consistency and asymptotic distribution) of such an estimation procedure. Subject classification: AMS(MOS)62F12

1 Introduction

In backpropagation training one usually tries to minimize the empirical risk

$$r_n(t) := \frac{1}{n}\sum_{i=1}^{n} \|Y_i - g(X_i, t)\|^2 = \min!,$$

where $x \mapsto g(x,t)$ denotes the input/output mapping of a multilayer perceptron whose weights comprise the vector t. When the training sequence $\{Z_i\}$, $Z_i = (X_i, Y_i)$, consists of i.i.d. (independent and identically distributed) random vectors, it is known that under general conditions the parameter τ_n minimizing the empirical risk is strongly consistent for the minimizer set of the population risk $r(t) = E\|Y_1 - g(X_1, t)\|^2$. Further, if the sequence $\{\tau_n\}$ converges towards an isolated minimizer t^* of r, then under reasonable conditions, $\sqrt{n}(\tau_n - t^*)$ converges in distribution to a normal distribution with mean zero, see White [8].

Here we consider what happens in the above procedure when instead of the original data one uses data generated by adding noise to the original sample points. Such a practice has been suggested by several authors, see [4] for references. The relationship of this procedure to regularization has been investigated in many recent papers, see [6, 3, 1, 7]. In the present paper we outline both consistency and asymptotic distribution results for noisy training. The results are based on the doctoral thesis of the author [5], where the interested reader can find rigorous proofs and results which are more general than what can be covered here. The consistency results obtained in the thesis are much stronger than the previous results of Holmström and Koistinen [4]. Asymptotic distribution results in our setting have not been available previously.

2 The Statistical Setting

The original sample is part of a sequence $Z_1, Z_2, \ldots$ of random vectors taking values in IR^k. The noisy sample is generated by replacing each original sample point $Z_1, \ldots, Z_n$ with $s \geq 1$ pseudo sample points

$$Z_{nij}^{\#} = Z_i + h_n N_{ij}, \quad i = 1, \ldots, n, j = 1, \ldots, s. \tag{1}$$

Here the h_n's are positive random variables called the smoothing parameters. We assume that the noise vectors N_{ij}'s are i.i.d. and independent of the Z_i's and the h_n's. The smoothing parameters are allowed to depend on the $\{Z_i\}$-sequence. We need to let h_n converge to zero to ensure consistency, and therefore the pseudo sample points are not i.i.d. This prevents us from using standard convergence results for minimization estimators to analyze the convergence properties of noisy training.

We next define empirical measures associated with the original and the pseudo observations. Let δ_x denote the probability measure with mass one at $x \in \mathbb{R}^k$, and define the probability measure

$$\mu_n := n^{-1} \sum_{i=1}^{n} \delta_{Z_i},$$

i.e., μ_n places mass $1/n$ at each of the observations $Z_1, \ldots, Z_n$. We call μ_n the empirical measure of the first n observations. Similarly, we define the empirical measure $\mu_{ns}^{\#}$ of the pseudo observations $Z_{nij}^{\#}, i = 1, \ldots, n, j = 1, \ldots, s$ as the probability measure which places mass $1/(ns)$ at each of these ns points. The measures μ_n and $\mu_{ns}^{\#}$ are examples of what are called random probability measures; the randomness arises from the fact that the measures depend on the observed values of random vectors.

For the consistency results, we need to assume that the empirical measures μ_n converge weakly, almost surely, towards some probability measure μ in $\mathbb{R}^k$; in symbols, $\mu_n \overset{\text{a.s.}}{\Rightarrow} \mu$. The definition of this mode of convergence for any sequence $\{\lambda_n\}$ of random probability measures in $\mathbb{R}^k$ is as follows,

$$\lambda_n \overset{\text{a.s.}}{\Rightarrow} \mu \quad \text{if and only if} \quad \left(\forall f \in C_b : \int f \, d\lambda_n \to \int f \, d\mu \right), \quad \text{almost surely,}$$

where C_b is the set of bounded continuous functions $\mathbb{R}^k \to \mathbb{R}$. An argument due to Varadarajan [2, Th 11.4.1] then implies that for measures in $\mathbb{R}^k$,

$$\lambda_n \overset{\text{a.s.}}{\Rightarrow} \mu \quad \text{if and only if} \quad \int f \, d\lambda_n \overset{\text{a.s.}}{\to} \int f \, d\mu, \quad \forall f \in C_b. \tag{2}$$

Unlike the condition of the actual definition, condition (2) is often easy to verify. E.g., if $Z_1, Z_2, \ldots$ are i.i.d., then the strong law of large numbers implies that the empirical measures $\mu_n \overset{\text{a.s.}}{\Rightarrow} \mu$, where μ denotes the common law of the Z_i's on $\mathbb{R}^k$. The same conclusion holds by the ergodic theorem, if the sequence $\{Z_i\}$ is stationary and ergodic.

Suppose that the empirical measures $\mu_n \overset{\text{a.s.}}{\Rightarrow} \mu$, where μ is some (nonrandom) probability measure in $\mathbb{R}^k$. Let $T \subset \mathbb{R}^m$ be our parameter set and let there be defined a loss function ℓ on $\mathbb{R}^k \times \mathbb{R}^m$. The aim is to select the parameter $t \in T$ such that the risk

$$r(t) := \int \ell(z,t) \, \mu(dz), \quad t \in T \tag{3}$$

is minimal. Here the measure μ is supposed to be unknown, so we cannot solve the problem directly. Instead we may try to minimize either the empirical risk associated with the original observations

$$r_n(t) := \frac{1}{n} \sum_{i=1}^{n} \ell(Z_i, t) = \int \ell(z,t) \, \mu_n(dz) \tag{4}$$

or the empirical risk associated with the noisy observations

$$r_{ns}^{\#}(t) := \frac{1}{ns} \sum_{i=1}^{n} \sum_{j=1}^{s} \ell(Z_{nij}^{\#}, t) = \int \ell(z,t) \, \mu_{ns}^{\#}(dz). \tag{5}$$

3 Consistency

If $A \subset T$, define the distance of $t \in T$ from A by $d(t, A) := \inf\{\|t-y\| : y \in A\}$, with the convention that $d(t, \emptyset) = \infty$. We write $\operatorname{argmin}_T r$ for the (possibly empty) set of points that minimize r on T. We seek conditions guaranteeing for our estimators θ_n that

$$d(\theta_n, \operatorname*{argmin}_T r) \overset{\text{a.s.}}{\to} 0.$$

If this holds, we say that θ_n is strongly consistent for the set $\operatorname{argmin}_T r$.
The following result is proved in [5].

Theorem 1 *Let $s \geq 1$. If $h_n \overset{\text{a.s.}}{\to} 0$, and for some probability measure μ, $\mu_n \overset{\text{a.s.}}{\Rightarrow} \mu$, then also $\mu_{ns}^{\#} \overset{\text{a.s.}}{\Rightarrow} \mu$, as $n \to \infty$.*

This motivates the following approach. Let $\{\lambda_n\}$ be a sequence of random probability measures and μ a nonrandom probability measure such that $\lambda_n \overset{\text{a.s.}}{\Rightarrow} \mu$ and let

$$R_n(t) := \int \ell(z, t)\, \lambda_n(dz). \tag{6}$$

Suppose that θ_n is a random vector with values in T such that

$$R_n(\theta_n) = \inf_T R_n + o(1), \quad \text{(a.s.)}. \tag{7}$$

Under certain conditions, θ_n is then strongly consistent for the set $\operatorname{argmin}_T r$, as is formulated in the following theorem. Hence we obtain a consistency theorem for any estimator τ_n coming close enough to minimizing r_n. Provided $h_n \overset{\text{a.s.}}{\to} 0$, we also obtain a consistency theorem for any estimator $\tau_{ns}^{\#}$ coming close enough to minimizing $r_{ns}^{\#}$.

Theorem 2 *Let the parameter set T be compact and let $\lambda_n \overset{\text{a.s.}}{\Rightarrow} \mu$. Suppose ℓ is continuous on $\mathbb{R}^k \times T$ and dominated by a continuous, μ-integrable function, i.e.,*

$$|\ell(z, t)| \leq L(z), \quad z \in \mathbb{R}^k, t \in T,$$

where $L \geq 0$ is continuous and $\int L\, d\mu < \infty$. If in addition, $\int L\, d\lambda_n \overset{\text{a.s.}}{\to} \int L\, d\mu$, then any random vector satisfying (7) is strongly consistent for the set $\operatorname{argmin}_T r$.

In practice, the most useful dominating functions are the scalar multiples of the powers $|z|^p, p \geq 1$. If $\int |z|^p\, \mu_n(dz) \overset{\text{a.s.}}{\to} \int |z|^p\, \mu(dz) < \infty$ and $E|N|^p < \infty$, then it can be shown that also $\int |z|^p\, \mu_{ns}^{\#}(dz) \overset{\text{a.s.}}{\to} \int |z|^p\, \mu(dz)$. This facilitates checking the conditions of the previous theorem.

4 Asymptotic Distribution

A consistency result does not tell how quickly the estimator converges. One way to characterize this rate is by giving an asymptotic distribution for the estimator. Our asymptotic distribution results are of the form $\sqrt{n}(\theta_n - t^*) \overset{\text{d}}{\to} N(0, C)$, i.e., they state that $\sqrt{n}(\theta_n - t^*)$ converges in distribution to a normal law with mean zero and a covariance matrix C. Here t^* denotes a minimizer of r. Such a result says that the law of θ_n collapses towards a point mass at t^* at a very specific rate, e.g., in the sense that for any $\epsilon > 0$, $n^{1/2-\epsilon}|\theta_n - t^*|$ converges to zero in probability and $n^{1/2+\epsilon}|\theta_n - t^*|$ converges to infinity in probability.
Henceforth we assume that the original observations $Z_1, Z_2, \ldots$ are i.i.d. and that the noise vectors have mean zero. The effect of noisy training in linear regression is

relatively straightforward to analyze. This is the case where z is the pair (x, y), $x \in \mathbb{R}^{k-1}$, $y \in \mathbb{R}$ and $\ell(z,t) = (x^T t - y)^2$. Denote the minimizer of r_n by τ_n and the minimizer of $r_{ns}^{\#}$ by $\tau_{ns}^{\#}$. If $h_n = o_p(n^{-1/4})$, i.e., if $n^{1/4}h_n$ converges in probability to zero, then it turns out that $\tau_{ns}^{\#}$ and τ_n have the same asymptotic distribution. If h_n converges to zero at some slower rate, then the situation is more complicated; when it can be obtained, the asymptotic distribution of $\tau_{ns}^{\#}$ then typically depends on the sequence $\{h_n\}$.

The same kind of results hold also more generally. Let now $t^* \in T$ satisfy $\nabla r(t^*) = 0$, i.e., t^* is a stationary point of the risk r. We assume that t^* is an isolated stationary point in the interior of T. Further, we assume that ℓ is a C^3-function on $\mathbb{R}^k \times \mathbb{R}^m$, and that Z_1 has a compactly supported law. Then the matrices

$$A := E[\nabla_{tt}^2 \ell(Z_1, t^*)], \quad B := \mathrm{Cov}[\nabla_t \ell(Z_1, t^*)]$$

are well defined. Here ∇_t and ∇_{tt}^2 denote the gradient and Hessian operators with respect to t, respectively. We assume that A is invertible and that B is nonzero. Further, we assume that the noise vectors have a compactly supported law and that the smoothing parameters satisfy $0 \le h_n \le M$ for some constant M.

Under these assumptions, let $h_n = o_p(n^{-1/4})$. Let $\{\tau_n\}$ be a sequence of T-valued random vectors such that

$$\tau_n \xrightarrow{\mathrm{p}} t^*, \quad \text{and} \int \nabla_t \ell(z, \tau_n)\, \mu_n(dz) = o_p(n^{-1/2}),$$

and let $\{\tau_{ns}^{\#}\}$ be a sequence of T-valued random vectors such that

$$\tau_{ns}^{\#} \xrightarrow{\mathrm{p}} t^*, \quad \text{and} \int \nabla_t \ell(z, \tau_{ns}^{\#})\, \mu_{ns}^{\#}(dz) = o_p(n^{-1/2}).$$

Here τ_n and $\tau_{ns}^{\#}$ renders the respective empirical risk stationary in an asymptotic sense. It is shown in [5] that then

$$\sqrt{n}(\tau_n - t^*) \xrightarrow{\mathrm{d}} N(0, A^{-1}BA^{-1}) \quad \text{and} \quad \sqrt{n}(\tau_{ns}^{\#} - t^*) \xrightarrow{\mathrm{d}} N(0, A^{-1}BA^{-1}). \tag{8}$$

That is, the asymptotic distributions of τ_n and $\tau_{ns}^{\#}$ coincide. The asymptotic distribution for τ_n is naturally the same as in [8, Th. 2]; the result for $\tau_{ns}^{\#}$ is new.

This asymptotic distribution can be used, e.g., to construct an asymptotic confidence interval for t^* or for $r(t^*)$, the risk at t^*. Instead of this, we now use this result to characterize the generalization performance of our estimators. Let the sequence $\{\theta_n\}$ stand either for $\{\tau_n\}$ or for $\{\tau_{ns}^{\#}\}$. The generalization performance of θ_n can be characterized by the law of $r(\theta_n)$, the risk evaluated at the estimator. It can be shown that its asymptotic distribution is now given by

$$n[r(\theta_n) - r(t^*)] \xrightarrow{\mathrm{d}} \frac{1}{2} U^T A U, \quad \text{where} \quad U \sim N(0, A^{-1}BA^{-1}). \tag{9}$$

5 Conclusions

We have outlined new results for the convergence properties of minimization estimators in noisy training. The main conditions in the consistency result are that the empirical measures associated with the original sample converge weakly, almost surely, towards some measure μ and that the smoothing parameters $h_n \to 0$, almost surely.

The main conditions for the asymptotic distribution result are the following: the original sample points are i.i.d., the noise vectors have zero mean and $h_n = o_p(n^{-1/4})$.

Under certain additional conditions we then have that the asymptotic distributions of τ_n and $\tau_{ns}^{\#}$ are identical, where τ_n denotes the minimizer of the empirical risk associated with original sample and $\tau_{ns}^{\#}$ the minimizer of the empirical risk associated with the noisy sample. This implies that the asymptotic distributions of $r(\tau_n)$ and $r(\tau_{ns}^{\#})$ coincide and hence additive noise can have only a higher-order effect on the performance of a minimization estimator as the sample size goes to infinity. However, numerical evidence indicates that additive noise sometimes does improve the generalization performance of a minimization estimator, at least with small sample sizes. It remains to be seen whether this effect can be quantified by analyzing the distribution of $r(\tau_{ns}^{\#})$ using more refined asymptotic methods.

REFERENCES

[1] C.M. Bishop, *Training with noise is equivalent to Tikhonov regularization*, Neural Computation, Vol. 7 (1995), pp108–116.

[2] R.M. Dudley, *Real Analysis and Probability*, Wadsworth & Brooks/Cole, Pacific Grove, CA, (1989).

[3] Y. Grandvalet and S. Canu, *Comments on "noise injection into inputs in back propagation learning"*, IEEE Trans. Systems, Man, and Cybernetics, Vol. 25 (1995), pp678–681.

[4] L. Holmström and P. Koistinen, *Using additive noise in back-propagation training*, IEEE Trans. Neural Networks, Vol. 3 (1992), pp24–38.

[5] P. Koistinen, *Convergence of minimization estimators trained under additive noise*, Research reports A 12, Rolf Nevanlinna Institute, Helsinki University of Technology (1995), (Doctoral thesis).

[6] K. Matsuoka, *Noise injection into inputs in back-propagation learning*, IEEE Trans. Systems, Man, and Cybernetics, Vol. 22 (1992), pp436–440.

[7] R. Reed, R.J. Marks II, and S. Oh, *Similarities of error regularization, sigmoid gain scaling, target smoothing, and training with jitter*, IEEE Trans. Neural Networks, Vol. 6 (1995), pp529–538.

[8] H. White, *Learning in artificial neural networks: A statistical perspective*, Neural Computation, Vol. 1 (1989), pp425–464.

NON-LINEAR LEARNING DYNAMICS WITH A DIFFUSING MESSENGER

Bart Krekelberg and John G. Taylor
Centre for Neural Networks, King's College London, London WC2R 2LS, UK. Email: bart@mth.kcl.ac.uk

The diffusing messenger Nitric Oxide plays an important role in the learning processes in the brain. This diffusive learning mechanism adds a non-linear and non-local effect to the standard Hebbian learning rule. A diffusive learning rule can lead to topographic map formation but also has a strong tendency to homogenise the synaptic strengths. We derive a non-linear integral equation that describes the fixed point and show which parameter regimes lead to non-trivial solutions.

Keywords: Nitric Oxide, self-organization, topographic maps

Introduction

Most learning rules used in neurobiological modelling are based on Hebb's postulate that a synaptic connection is strengthened if and only if there is both a post-synaptic and pre-synaptic depolarization at that particular synapse. Recent physiological research, however, shows that this assumption is not always warranted. Experiments in areas varying from rat hippocampus to cats' visual cortex show that there is a non-local effect in learning.

This non-local learning is often thought to be mediated by *retrograde messengers*. Nitric Oxide (NO) is a candidate for such a messenger which is produced post-synaptically (both in the dendrites and the soma [1]), then diffuses through the intracellular space and is taken up pre-synaptically. The chemical properties of NO allow it to diffuse over relatively long distances in the cortex; with a diffusion constant of $3.3 \times 10^{-5} cm^2/s$ and a half-life in the intracellular fluid of $4 \sim 6$ seconds, it has an effective range of at least $150 \mu m$. If NO were an ordinary neurotransmitter it would be hard to understand how the specificity of neuronal connections in the brain on a scale smaller than this could be achieved. An explanation has been found in experimental setups with locally modifiable concentration of NO: physiologists have been able to demonstrate that low levels of NO lead to *depression* of synaptic strengths (LTD) and high levels lead to Long Term Potentiation (LTP) (For recent reviews see [3, 8]). This non-linearity in the dependence of the synaptic change on the NO concentration is crucial to attain specificity in a network with a diffusing messenger.

Detailed simulations of such a a non-linear and non-local learning rule have been performed in [2, 7]. In these simulations pattern formation in the weights was seen to occur but, as the input patterns and the initial (partly topographic) weight distributions were already organized, it is difficult to tell how general these results are. In [5] we analysed networks with a diffusing messenger in a linearised reaction-diffusion framework and found that homogeneous weights were the dominant solutions of the dynamics. Following up a suggestion in [4] that Nitric Oxide could underlie a mechanism similar to the neighbourhood function in the SOFM. we showed in [6] that a diffusing messenger can indeed support the development of topographic maps without the need for a Mexican Hat lateral interaction.

Here we extend our previous analysis to arrive at a fuller account of the non-linear effects. We derive a general fixed point equation for the weights and determine which parameter regimes admit non-zero homogeneous solutions.

1 The Model

We consider a neural field consisting of leaky integrator neurons with activity u, all *sampling* their input with a synaptic density function r from a field of synapses with strengths s. Note that this implies that synapses do not "belong" to a neuron, a neuron just takes its input from the synapses within its reach (determined by the function r). Inputs $a(x, x_0)$ are Gaussian shaped with the maximum at x_0 and spread σ. The inputs are presented with equal probability at each position x_0. Nitric Oxide is produced *in the dendrites* at a rate proportional to the local depolarization, decays at a rate -1 and has diffusion constant κ. Learning is non-linearly dependent on the local NO level through the function f which captures the qualitative effects described above (see also 2). Given an input centred at x_0, the dynamical equations can be written as:

$$\begin{aligned} \dot{u}(x, x_0) &= -u(x) + \int dx' r(x, x') s(x') a(x', x_0), \\ \dot{n}(x, x_0) &= -n(x) + s(x) a(x, x_0) + \kappa \nabla^2 n(x, x_0), \\ \dot{s}(x) &= -s(x) + f[n(x, x_0)] a(x, x_0). \end{aligned}$$

We assume (as in [7]) that *all* learning is dependent on the local NO level and there is no *direct* dependence on the post-synaptic depolarization (see Discussion). The local NO level that determines the change in synaptic strength depends on the details of the post-synaptic production of NO and the pre-synaptic *measurement* process. As the details of this process are as yet unknown, we use a Gaussian Green's function ($G(x, x')$) to model the spatial distribution of NO. This approximation is exact if the NO is produced in a short burst and measured some fixed period of time later. The real process of production and measurement will presumably be more complicated, but we expect that at least the qualitative features are well described by a Gaussian kernel. With these approximations and averaging over all patterns, the fixed point equation for the learning dynamics can be written in the form of the following non-linear Fredholm integral equation.

$$s(x) = \int dx_0 \, a(x, x_0) f \left[\int dx' \, G(x, x') s(x') a(x', x_0) \right]. \tag{1}$$

In section 2 we substitute the simplest non-linear function that still captures the qualitative features observed in experiments:

$$f(n) = -n(n - D)(n - P) \tag{2}$$

with D and P two parameters that can be determined directly from experiments. The unphysical values of f for negative NO concentration merely stabilise the trivial fixed point, and the decrease of f after its positive maximum can either be interpreted as toxicity of a high concentration of NO or an easy way of modelling a saturation of the NO production. The important features of the function are the negative values for small NO concentration (LTD) and positive values (LTP) for high NO concentration.

2 Analysis

In appendix 4 we use the assumptions about the non-linearity, the spread of NO (ρ) and the width (σ) of the Gaussian inputs in equation 1 to derive the following

expression in Fourier space for the fixed point of the dynamics.

$$\begin{aligned} s(k) &= -DPN_1 s(k) e^{-\beta_1 k^2} \\ &+ (D+P)N_2 \int dk' \, s(k') s(k'-k) e^{-(k'^2-k'k)/2(\rho+\sigma)} e^{-k^2\beta_2} \\ &- N_3 \iint dk'dk'' \, s(k') s(k'') s(k'+k''-k) e^{-\frac{(k'^2-(k'-k'')k+k''^2)}{2(\rho+\sigma)}} e^{-\beta_3 k^2} \end{aligned} \tag{3}$$

where the parameters are defined by:

$$\begin{aligned} N_n &= \left(\frac{a_0^{n+1} \pi^{(n+1)/2}}{\sqrt{(\rho+\sigma)^{(n-1)}(\sigma^2+(n+1)\rho\sigma)}} \right) \\ \beta_n &= \frac{1}{4} \left(\frac{1}{\rho+\sigma} + \frac{\sigma^2}{(\rho+\sigma)^n(\rho^2+(n+1)\rho\sigma)} \right) \end{aligned}$$

To derive the conditions under which the dynamics admit homogeneous solutions for the weights, we substitute the solution $s(k) = s_h \delta(k)$ in equation 3 and derive the following third order polynomial in s_h:

$$s_h = -DPN_1 s_h + (D+P)N_2 s_h^2 - N_3 s_h^3. \tag{4}$$

Clearly, the zero-weight solution is a fixed point, and non-trivial homogeneous solutions can be determined by finding the two remaining roots of this equation. Non-trivial homogeneous solutions exist if s_h has at least one positive real solution. This is the case if the width σ of the stimuli satisfies the following constraint:

$$\frac{\rho}{\sigma(\sigma+3\rho)^2} \leq 1 - \frac{4DP}{(D+P)^2}, \tag{5}$$

and in the limiting case, the homogeneous solution is given by

$$s_h = \frac{D+P}{\sqrt{4\pi} a_0} \sqrt{(\rho+\sigma)\left(\frac{\sigma^2+4\rho\sigma}{\sigma^2+3\rho\sigma}\right)}$$

For widths larger than this limiting case there will be *two* fixed points of which only the largest is a stable solution. This is evident from figure 1 in which we solve equation 4 pictorially.

Even though the couplings between the different Fourier components of the weights in equation 3 are limited, a general *periodic* solution is not easily found. From substituting $s(k) = \delta(k) - \delta(k-k^*)$ in the equation it can be seen that in this case there is a coupling with only one higher harmonic $s(k) = \delta(k-2k^*)$. This suggests that a (numerical) iterative procedure to solve the integal equation could be fruitful. We will attempt such a solution in future work.

3 Discussion

We have shown that the weight dynamics of a neural field with a diffusing messenger can be described by a non-linear Fredholm integral equation and that non-zero honogeneous solutions for the weights are stable for stimuli wider than a critical width. We expect that in real tissue some mechanism would be needed to prevent this tendency to homogenise the weights: either the production of NO or its diffusion through the tissue has to be controlled. We expect such a mechanism to be found when the chemical process by which NO is synthesized is more fully understood.

The current model assumes that *all* learning is NO dependent and ignores any influence of the activity of the post-synaptic neurons. In reality, the NO effects we

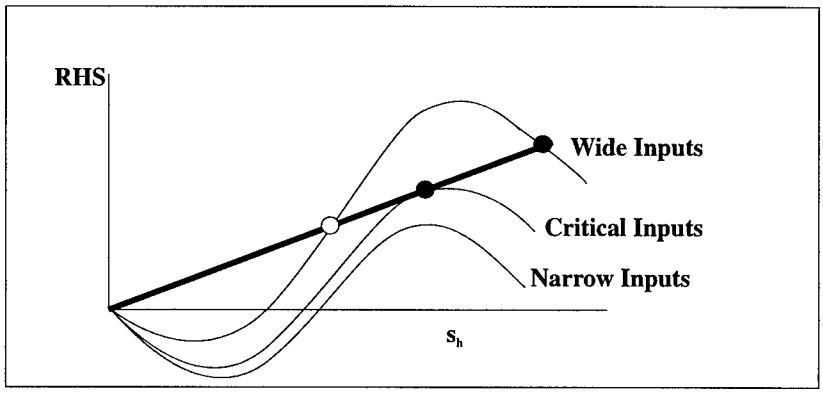

Figure 1 Solving for the homogeneous solutions of equation 3. **RHS** indicates the Right Hand Side of this equation and the solid line is the Left Hand Side. The closed bullets show stable fixed points whereas the open bullets are unstable fixed points. The critical size of the inputs is given by equation 5.

model and the more standard Hebbian learning rules could operate concurrently. In that case the interaction between the two learning rules needs to be investigated. Furthermore, we assumed that all NO is produced in the dendrites. There is evidence, however, that the production can take place in the soma and even the axons [1]. Our previous analyses [5, 6] considered production of NO in the soma, and showed different behaviour than that described here. A full model would include all the sources of NO and the interaction between them.

Lastly, we have modelled all time-dependent effects of the diffusion with the single parameter ρ. Interesting dynamics could result from including the time dependence explicitly, especially if the inputs are temporally correlated. We will address this issue in future work.

4 Appendix

Starting from equation 1 we substitute the Gaussian Green's function with spread ρ and the inputs to derive the fixed point equation. First we derive the NO concentration at position x when a stimulus is presented at x_0. The weights are written as an integral of Fourier components $s(k)$:

$$n(x, x_0) = \int dk' s(k') \int dx' \, \mathrm{e}^{ik'x'} a_0 \mathrm{e}^{-\sigma(x'-x_0)^2} \mathrm{e}^{-\rho(x-x')^2}.$$

This Fourier integral over a shifted gaussian can be evaluated explicitly:

$$n(x, x_0) = a_0 \sqrt{\frac{\pi}{\rho+\sigma}} \int dk' s(k') \mathrm{e}^{-\frac{k'^2}{4(\rho+\sigma)}} \mathrm{e}^{-ik'(\frac{\rho}{\rho+\sigma})x} \mathrm{e}^{-ik'(\frac{\rho}{\rho+\sigma})x_0} \mathrm{e}^{-(\frac{\sigma\rho}{\sigma+\rho})(x-x_0)^2}.$$

For the averaged weights' fixed point equation we have to average over all the patterns:

$$s(x) = \int dx_0 \, a_0 \mathrm{e}^{-\sigma(x-x_0)^2} f\left[n(x, x_0)\right].$$

For each of the terms in f, the integral over the distribution of patterns has to be done seperately. Here we do the linear case; the quadratic and cubic terms follow

by analogy but will include interactions betweeen the different fourier components. Substituting the non-linearity f from equation 2, the integral over the pattern positions x_0 in the linear term ($s^{(1)}$) is another Fourier integral and gives:

$$\begin{aligned} s^{(1)}(x) &= -a_0^2 DP \sqrt{\frac{\pi}{\rho+\sigma}} \sqrt{\frac{\pi}{\sigma+\frac{\rho\sigma}{\rho+\sigma}}} \\ &* \int dk'\, s(k') \mathrm{e}^{-ik'x} \mathrm{e}^{-k'^2/4(\rho+\sigma)} \mathrm{e}^{-\sigma^2 k'^2/((\rho+\sigma)(\sigma^2+2\rho\sigma))}. \end{aligned}$$

In Fourier space this integral equation can be written as:

$$s^{(1)}(k) = -DPN_1 s^{(1)}(k) \mathrm{e}^{-\beta_1 k^2}.$$

The quadratic and cubic terms can be determined analogously which results in equation 3.

REFERENCES

[1] C. Aoki, S. Fenstemaker, M. Lubin, C.-G. Go, *Nitric oxide synthase in the visual cortex of monocular monkeys as revealed by light and electron microscopic immunocytochemistry*, Brain Research, Vol. 620 (1993), pp97–113.

[2] Joseph A. Gally, P. Read Montague, George N., Reeke Jr., Gerald M. Edelman, *The NO hypothesis: Possible effects of a short-lived, rapidly diffusing signal in the development and function of the nervous system*, Proceedings of the National Academy of Sciences, USA (1990), pp3547–3551.

[3] J. Garthwaite, C.L. Boulton, *Nitric oxide signalling in the central nervous system*, Annual Review of Physiology, Vol. 57 (1995), pp683–706.

[4] Teuvo Kohonen, *Physiological interpretation of the self-organizing map*, Neural Networks, Vol. 6 (1993), pp895–905.

[5] Bart Krekelberg, John G. Taylor, *Modelling a diffusing messenger*, in: Proceedings of the WCNN, Washington DC., Vol. I (July 1995), pp557–560, New Jersey, Lawrence Erlbaum Associates, Inc.

[6] Bart Krekelberg, John G. Taylor, *Nitric oxide: A diffusing messenger in a topographic map*, in: Proceedings of ICANN (October 1995), pp525–530.

[7] P. Read Montague, Joseph A. Gally, Gerald M. Edelman, *Spatial signalling in the development of neural connections*, Cerebral Cortex, Vol. 1 (1991), pp199–220.

[8] Erin M. Schuman, Daniel V. Madison, *Nitric oxide and synaptic function*, Annual Review of Neuroscience., Vol. 17 (1994), pp153–183.

Acknowledgements

B. Krekelberg was supported by a grant from the European Human Capital and Mobility Programme.

A VARIATIONAL APPROACH TO ASSOCIATIVE MEMORY

Abderrahim Labbi

Dept. of Computer Science, University of Geneva,
24 Rue General Dufour, 1121 Geneva 4, Switzerland. Email: labbi@cui.unige.ch

The purpose of this paper is to show how fundamental results from variational approximation theory can be exploited to design recurrent associative memory networks. We begin by stating the problem of learning a set of given patterns with an associative memory network as a hypersurface construction problem, then we show that the associated approximation problem is well-posed. Characterizing and determining such a solution will lead us to introduce the desired associative memory network which can be viewed as a recurrent radial basis function (RBF) network which has as many attractor states as there are fundamental patterns (no spurious memories).
Subject classification: AMS(MOS) 65F10, 65B05.
Keywords: Associative Memory, Variational Approximation, RBF Networks.

1 Introduction

Learning from a set of input-output patterns, and sometimes from additional *a priori* knowledge, in neural networks usually amounts to determining a set of parameters relative to a given network. In the case of feedforward networks, the problem may be equivalent to determining a continuous mapping. Such a problem can be stated in the framework of multivariate approximation theory which, in some cases, is closely linked to regularization [11]. Concerning learning in recurrent associative memory networks, one usually has to determine a set of parameters connected with the dynamics of a given network so that the patterns (memories) to be stored are stable states of such a network [1, 3, 7]. Complete characterization of the network dynamics may be achieved by defining a global Lyapunov function (energy) which decreases during the network evolution (the recalling process) and whose local minima are the network's stable states [3, 6, 7].

The procedure followed here for the design of an associative memory network is the reverse of the general approach: using methods from variational approximation, we determine a function (or a hypersurface) which has as many local maxima as the number of patterns to be memorized, and then define a dynamics on such a hypersurface (actually, the gradient dynamics) which has its stable states *close* to the patterns to be memorized.

We begin by proving that the problem is well posed from the approximation point of view, and that the desired function can be explicitly computed when choosing convenient constraints and parameters in the variational formulation of the problem. We finally show that the derived gradient dynamics can be implemented by an associative memory network. Such a network can be viewed as a recurrent radial basis function network which has as many stable states as there are fundamental patterns to be stored. We also discuss how basins of attraction can be shaped so that no spurious stable states can be encountered during the recalling process.

2 Statement of the Problem

Let us consider a set of patterns, $\mathcal{A} = \{S_1, S_2, ..., S_m\} \subset \Omega \subset \mathbb{R}^n$. The first stage of the proposed approach is to construct a hypersurface defined by a bounded smooth function, $F : \mathbb{R}^n \rightarrow \mathbb{R}$ whose unique local maxima are *close* to the patterns $S_i, i = 1, ..., m$. Therefore, we will reduce the problem to a functionnal minimization

under constraints which aim to translate the following assumptions: i) F should interpolate the data $(S_i, y_i), i = 1, ..., m$, where $y_i = F(S_i)$ are large positive real values, and F should tend to zero outside of the data. This constraint is reduced here to the minimization of the L_2 norm of F. ii) F should not oscillate between the data. This constraint is reduced to *surface tension* minimization, which usually amounts to minimize the L_2 norm of the gradient of F. iii) F should be smooth *enough*. This constraint is usually imposed by minimizing the L_2 norm of smoothing differential operators (D^p) to be introduced in the following.

Let us define $C_Y = \{f \in \mathbb{R}^n \mapsto \mathbb{R}, f \in \mathcal{C}(\mathbb{R}^n), r > 0, \text{and } f(S_i) = y_i\}$. Determining an approximation of F regarding the given three constraints can be reduced to the minimization of a cost functional J over C_Y,

$$J(f) = \lambda_0 \|D^0 f\|^2 + \lambda_1 \|D^1 f\|^2 + ... + \lambda_p \|D^p f\|^2 \qquad f \in C_Y \qquad (1)$$

The operators D^k are defined by, $D^k f(X) = \sum_{i_1+...+i_n=k} \frac{\partial^k}{\partial x_1^{i_1} ... \partial x_n^{i_n}} f(X), k \geq 0$.

To solve the minimization problem, we can either use standard methods from the calculus of variations by means of the Euler-Lagrange equation [4, 11], or use direct methods based on functional analysis. Herein, we use the latter method which is closely related to the reproducing kernels method [5, 15].

First, let us consider the Hilbert space, $H^p(\mathbb{R}^n) = \{f \in L_2(\mathbb{R}^n); \sum_{k=0}^p \|D^k f\|^2 < \infty\}$endowed with the inner product, $< f, g >_{H^p} = \sum_{k=0}^p < f, g >_k$, where $< f, g >_k = < D^k f, D^k g >$. When p and n satisfy the condition, $p > \frac{n}{2} + r, r \geq 0$,then $H^p(\mathbb{R}^n)$ is a subset of $C^r(\mathbb{R}^n)$ [12]. We assume this condition is satisfied in the following.

To show that the problem is well-posed (i.e. it has a unique solution in C_Y), we consider the following vector space, $H^p_\Lambda(\mathbb{R}^n) = \{f \in L_2(R^n), \sum_{k=0}^p \lambda_k \|D^k f\|^2 < \infty, \text{and } \lambda_k > 0\}$. It can easily be shown [8, 12] that $H^p_\Lambda(\mathbb{R}^n)$ endowed with the inner product, $< f, g >_{H^p_\Lambda} = \sum_{k=0}^p \lambda_k < f, g >_k$, is a Hilbert space whose norm is, $\|f\|_{H^p_\Lambda} = (< f, f >_{H^p_\Lambda})^{\frac{1}{2}}$. Moreover, H^p and H^p_Λ are topologically equivalent since their norms are equivalent.

Now, observe that the norm of $H^p_\Lambda(\mathbb{R}^n)$ is identical to the functional J to be minimized, so the minimization problem can be rewritten as,

$$(\mathcal{P}) \quad Minimize \;\; J(f) = \| f \|^2_{H^p_\Lambda}, f \in C_Y$$

$(\mathcal{P})$ is then reduced to a special class of approximation problems in normed linear spaces [14, 9]. We will use convenient methods of such theory to prove the existence and give a characterization of a solution to the problem.

Theorem 1 *Given strictly positive real parameters, $\lambda_k, k = 1, ..., p$, the problem $(\mathcal{P})$ has a unique solution $F \in H^p_\Lambda(\mathbb{R}^n)$, which is characterized by,*
$< F, u >_{H^p_\Lambda} = \sum_{i=1}^m \beta_i . < \delta_i, u >, \;\; \forall u \in H^p_\Lambda$, *where β_i are real parameters and $< \delta_i, . >$ are Dirac operators supported by $S_i, i = 1, ..., m$.*

Proof The proof[1] is based on the projection theorem for the existence and the charactrization of the best approximation in a linear manifold of a Hilbert space [8, 9, 14]. In order to use such results, we first show that C_Y is a linear manifold of H^p_Λ. This is achieved by considering the set C_0 defined as,

[1] the details of the proof can be found in [8]

$\mathcal{C}_0 = \{v \in H^p_\Lambda, < \delta_i, v > = \ v(S_i) = 0,\ i = 1, ..., m\}$, which is a vector subspace of H^p_Λ, and observing that $\mathcal{C}_Y$ is a translation of $\mathcal{C}_0$. Therefore, the projection theorem asserts that there is a unique function $F \in \mathcal{C}_Y$ which solves $(\mathcal{P})$, and since $\mathcal{C}_Y$ is linear manifold associated to $\mathcal{C}_0$, F can be characterized by the relation, $< F, u >_{H^p_\Lambda} = \sum_{i=1}^m \beta_i . < \delta_i, u >, \quad \forall u \in H^p_\Lambda$ where β_i are real parameters. □
The previous theorem provides only a characterization of the solution, but we are interested in determining explicitly such a solution. Therefore, we consider the differential operator P defined as a combination of iterated Laplacians,
$Pf = \lambda_0 f - \lambda_1 \Delta f + ... + (-1)^p \lambda_p \Delta^{2p} f, \quad \forall f \in H^p_\Lambda(\mathbb{R}^n)$, which leads us to the following theorem.

Theorem 2 *Consider the functions (kernels) $G(., S_1), G(., S_2), ..., G(., S_m)$ as respective solutions of the partial differential equations (in the distributions sense), $PG(X, S_i) = \delta(X - S_i), i = 1, ..., m, \forall X \in \mathbb{R}^n$. Then, there exist unique parameters $\beta_1, \beta_2, ..., \beta_m$ such that the solution F of the problem $(\mathcal{P})$ is,*
$F(X) = \sum_{i=1}^m \beta_i . G(X, S_i)$, where $(\beta_1, ..., \beta_m)$ is the solution of the linear system,
$F(S_j) = \sum_{i=1}^m \beta_i . G(S_j, S_i) = y_j, \ j = 1, ..., m.$

Proof First, let us show that any function $f(X) = \sum_{i=1}^m \beta_i . G(X, S_i)$, with arbitrary β_i's, satisfies the characterization of theorem (1). If we consider any pair of functions ϕ and ψ in H^p_Λ, an integration by parts in the sense of distributions gives [13], $< \phi, \psi >_k = (-1)^k < \Delta^{2k}\phi, \psi >$ .This relation allows us to write, for any $u \in H^p_\Lambda$,

$$\begin{aligned} < F, u >_{H^p_\Lambda} &= \sum_{i=1}^m \beta_i < G(X, S_i), u >_{H^p_\Lambda} = \sum_{i=1}^m \beta_i < \sum_{k=0}^p (-1)^k \lambda_k \Delta^{2k} G(X, S_i), u > \\ &= \sum_{i=1}^m \beta_i < \delta_i, u > \end{aligned}$$

So the function F given in the theorem satisfies the characterization stated in theorem (1). Finally, to show that F is the solution of the problem $(\mathcal{P})$, we have to show that $F \in C_Y$, which amounts to show that there is a unique solution (in β_i's) to the following linear system, $F(S_i) = \sum_{j=1}^m \beta_i G(S_j, S_i) = y_i, i = 1, ..., m$. Since P is a linear combination of iterated Laplacians, it is rotation and translation invariant [5, 13], and the kernels $G(., S_i)$ are radial, centered respectively on S_i, and can be written as, $G(X, S_i) = G(\|X - X_i\|)$.
To show that the linear system has a unique solution, it suffices to show that the function $G(t)$ is positive definite [10]. Since G verifies the equations,
$\lambda_0 G(\|X - S_i\|) - \lambda_1 \Delta G(\|X - S_i\|) + ... + (-1)^p \lambda_p \Delta^p G(\|X - S_i\|) = \delta(\|X - S_i\|)$
it can be shown that $G(t)$ can be written as [11], $G(t) = \int_{\mathbb{R}} \frac{\exp(it\omega)}{\lambda_0 + \lambda_1 \omega^2 + ... + \lambda_p \omega^{2p}} d\omega = \int_{\mathbb{R}} \exp(it\omega) dV(\omega)$, where V is a bounded nondecreasing function. G is then written in the form required by the Bochner theorem [2] which characterizes positive definite functions. Therefore, $F(X) = \sum_{i=1}^m \beta_i . G(X, S_i)$ is the solution of $(\mathcal{P})$. □
Poggio & Girosi [11] considered a similar variational problem for learning continuous mappings under *a priori* assumptions. They derived similar kernels $G(t)$ using the Euler-Lagrange equation. Setting λ_k to some particular values gives some illustrations of the solution F in figure 1. If we let p tend to infinity in the problem $(\mathcal{P})$ as in [11] (considering only functions with infinite smoothness degree), and

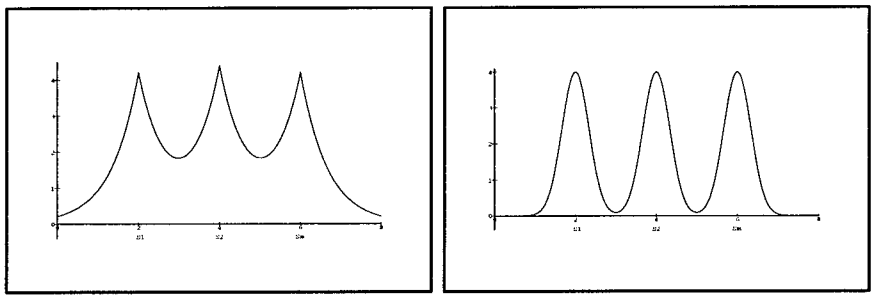

Figure 1 The solution F: (*left*) for $\lambda_0 = \sigma > 0, \lambda_1 = 1$, and $\lambda_k = 0$, $k \geq 2$, we have $G_1(t) = \frac{1}{2\sigma}.\exp(-\sigma.|t|)$ which is not differentiable at the origin; (*right*) for $\lambda_0 = \sigma^4, \lambda_1 = 2\sigma^2, \lambda_2 = 1$, and $\lambda_k = 0$, $k \geq 3$, we have $G_2(t) = G_1(t) * G_1(t)$ (the convolution product) which is differentiable.

choose $\lambda_k = \frac{1}{k!2^k\sigma^{2k}}$, then following the same reasoning as the previous sections, we obtain, $G(\omega) = \exp(-\frac{\omega^2}{2\sigma^2})$, and hence F is a linear combination of Gaussians centered on S_i's with positive coefficients β_i since, in the linear system, $Y = G.\mathcal{B}$ where $(\mathcal{B})_i = \beta_i, (G)_{ij} = \exp(-\frac{\|S_i - S_j\|^2}{2\sigma^2})$, and $(Y)_i = y_i >> 0$, if we take a small σ, and decompose the matrix G as $G = I + \mathcal{G}$, where I is the identity matrix, and $(\mathcal{G})_{ij} = \exp(-\frac{\|S_i - S_j\|^2}{2\sigma^2})$ for $i \neq j$, we can make the approximation, $G^{-1} = I - \mathcal{G}$. Therefore, we get, $\mathcal{B} = G^{-1}.Y \simeq (I - \mathcal{G}).Y$. Since the elements of $\mathcal{G}$ can be reduced as desired by choosing a small σ, we get positive $\beta_i's$, and so the computed function preserves the *a priori* constraints imposed on the desired function (see figure 1).

3 Building an Associative Memory Network

Let us consider the solution $F(X) = \sum_{j=1}^{m} \beta_j \exp(-\frac{\|X - S_j\|^2}{2\sigma^2})$ obtained by setting $\lambda_k = \frac{1}{k!2^k\sigma^{2k}}$. The last stage of our approach is to build an associative memory network whose unique attractor states are *close* to the patterns S_i. If we consider the gradient dynamics applied to F, then from any initial state X_0, we stabilize on a local maximum of F which is *close* to a pattern S_i. The closeness of the actual maxima of F to the patterns S_i depends on the size of σ. For a large σ, the deviation is more important because of the overlap between Gaussians, while it is less important for a small σ. This is a natural consequence, since large *penalty* parameters λ_k would result from a small σ, and hence the constraints would be better preserved. A discretization of the gradient dynamics applied to F gives,

$x_i(t+1) = x_i(t) + \alpha.\sum_{j=1}^{m}(x_i - S_j^i)\frac{\beta_j}{\sigma^2}\exp(-\frac{\|X - S_i\|^2}{2\sigma^2}),\ i = 1, ..., n$

This dynamics can be implemented by a two-layer recurrent RBF network (see figure 2). The first layer consists of n units encoding the input/output pattern, and the second -hidden- layer consists of m units computing radial functions centered on the patterns S_j, $G_j(X) = \frac{\beta_j}{\sigma^2}\exp(-\frac{\|X - S_j\|^2}{2\sigma^2})$. The connection weight between an input/output unit i and a hidden unit j is S_i^j (j^{th} component of S_i). The network has been used as a part of a system for handwritten character recognition and reconstruction [8].

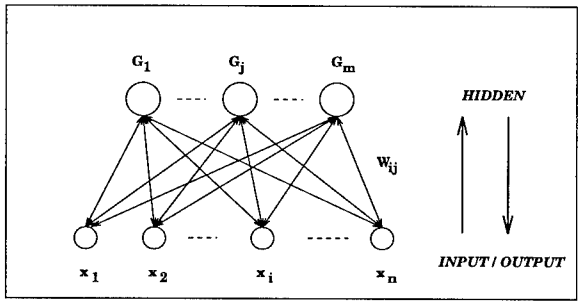

Figure 2 The associative memory network architecture.

REFERENCES

[1] Amari S., *Statistical Neurodynamics of Associative Memory* Neural Net, Vol. 1 (1988).
[2] Bochner S., *Lectures on Fourier Integrals*, Annals of Mathematical Studies, No. 42 (1959), Princeton Univ. Press.
[3] Cohen M.A., Grossberg S., *Absolute Stability of Global Pattern Formation and Parallel Memory Storage by Competitive Neural Networks*, IEEE Trans. on SMC, Vol. SMC-13 (1983).
[4] Courant R., Hilbert D., *Methods of Mathematical Physics*, Interscience, London (1962).
[5] Duchon J., *Spline Minimizing Rotation-Invariant Semi-norms in Sobolev Spaces*, Constructive Theory of Several Variables, in W. Schempp & K. Zeeller (Eds), Lecture Notes in Mathematics, No. 571 (1977), Springer-Verlag, Berlin.
[6] Goles E. *Lyapunov Functions Associated to Automata Networks*, in: Automata Networks in Computer Science, F. Fogelman et al. (eds), Manchester Univ. Press (1987).
[7] Hopfield J.J., *Neural Networks and Physical Systems with Emergent Collective Computational Abilities*, Proc. of the Nat. Acad. of Science, USA, Vol. 79 (1982).
[8] Labbi A., *On Approximation Theory and Dynamical Systems in Neural Networks*, Ph.D. Dissertation in Applied Mathematics, INPG, Grenoble (1993).
[9] Laurent P.J. *Approximation et Optimisation*, Hermann, Paris (1973).
[10] Micchelli C.A. *Interpolation of Scattered Data: Distance Matrices and Condionally Definite Functions*, Constr. Approx., Vol. 2 (1986).
[11] Poggio T., Girosi F. *Networks for Approximation and Learning*, Proc. IEEE, Vol. 78 (1990).
[12] Rudin W. *Functional Analysis.* McGraw-Hill, New York, St Louis, San Fransisco (1991).
[13] Schwartz L. *Théorie des Distributions.* Hermann, Paris (1966).
[14] Singer I. *Best Approximation in Normed Linear Spaces by Elements of Linear Subspaces.* Springer-Verlag, New York, Heidelberg, Berlin (1970).
[15] Wahba G. *Splines Models for Observational Data. Series in Applied Mathematics*, Vol. 59 (1990), SIAM, Philadelphia.

TRANSFORMATION OF NONLINEAR PROGRAMMING PROBLEMS INTO SEPARABLE ONES USING MULTILAYER NEURAL NETWORKS

Bao-Liang Lu and Koji Ito*

The Institute of Physical and Chemical Research (RIKEN), 3-8-31 Rokuban, Atsuta-ku, Nagoya 456, Japan. Email: lbl@nagoya.bmc.riken.go.jp

** Interdisciplinary Graduate School of Science and Engineering, Tokyo Institute of Technology, 4259, Nagatsuda, Midori-ku, Yokohama 226, Japan. Email: ito@ssie.titech.ac.jp*

In this paper we present a novel method for transforming nonseparable nonlinear programming (NLP) problems into separable ones using multilayer neural networks. This method is based on a useful feature of multilayer neural networks, i.e., any nonseparable function can be approximately expressed as a separable one by a multilayer neural network. By use of this method, the nonseparable objective and (or) constraint functions in NLP problems can be approximated by multilayer neural networks, and therefore, any nonseparable NLP problem can be transformed into a separable one. The importance of this method lies in the fact that it provides us with a promising approach to using modified simplex methods to solve general NLP problems.

Keywords: separable nonlinear programming, linear programming, multilayer neural network.

1 Introduction

Consider the following NLP problem:

$$\begin{array}{lll} \text{Minimize} & p(\boldsymbol{x}) & \text{for } \boldsymbol{x} \in \mathbb{R}^n \\ \text{subject to} & g_i(\boldsymbol{x}) \geq 0 & \text{for } i = 1,\ 2,\ \cdots,\ m, \\ & h_j(\boldsymbol{x}) = 0 & \text{for } j = 1,\ 2,\ \cdots,\ r. \end{array} \tag{1}$$

where $p(\boldsymbol{x})$ is called the objective function, $g_i(\boldsymbol{x})$ is called an inequality constraint and $h_j(\boldsymbol{x})$ is called an equality constraint.

NLP problems are widespread in the mathematical modeling of engineering design problems such as VLSI chip design, mechanical design, and chemical design. Unfortunately, for the general NLP problems, computer programs are not available for problems of very large size. For a class of NLP problems known as separable [4, 1], some variation of the simplex method, a well-developed and efficient method for solving linear programming (LP) problems, can be used as a solution procedure. Separable nonlinear programming (SNLP) problem refers to a NLP problem where the objective function and the constraint functions can be expressed as the sum of functions of a single variable. A SNLP problem can be expressed as follows:

$$\begin{array}{lll} \text{Minimize} & \displaystyle\sum_{k=1}^{n} p_k(x_k) & \\ \text{subject to} & \displaystyle\sum_{k=1}^{n} g_{ik}(x_k) \geq 0 & \text{for } i = 1,\ 2,\ \cdots,\ m, \\ & \displaystyle\sum_{k=1}^{n} h_{jk}(x_k) = 0 & \text{for } j = 1,\ 2,\ \cdots,\ r. \end{array} \tag{2}$$

An important problem in mathematical programming is to generalize the simplex method to solve NLP problems. In this paper we discuss how to use multilayer neural networks to transform nonseparable NLP problems into SNLP problems.

2 Transformation of Nonseparable Functions

Let $q(\boldsymbol{x})$ be a multivariable function. Given a set of training data sampled over $q(\boldsymbol{x})$, we can train a three-layer network[1] to approximate $q(\boldsymbol{x})$ [2]. After training the mapping $\hat{q}(\boldsymbol{x})$ formed by the network can be regarded as an approximation of $q(\boldsymbol{x})$ and expressed as follows:

$$\hat{q}(\boldsymbol{x}) = \alpha + \beta(f\left(\sum_{j=1}^{N_2} w_{31j} f\left(\sum_{i=1}^{N_1} w_{2ji}x_i + bias_{2j}\right) + bias_{31}\right) - \gamma), \tag{3}$$

where x_j is the input of the jth unit in the input layer, w_{kji} is the weight connecting the ith unit in the layer $(k-1)$ to the jth unit in the layer k, $bias_{kj}$ is the bias of the jth unit in the layer k, f is the sigmoidal activation function, N_k is the number of units in the layer k, α, β, and γ are three constants which are determined by the formula used for normalizing training data.

Introducing auxiliary variables b_{31}, b_{21}, b_{22}, $\cdots$, and b_{2N_2} into Eq. (3), we can obtain the following simultaneous equation

$$\begin{cases} \hat{q}(b_{31}) = \alpha + \beta(f(b_{31}) - \gamma) \\ b_{31} - \sum_{j=1}^{N_2} w_{31j} f(b_{2j}) = bias_{31} \\ \\ b_{21} - \sum_{i=1}^{N_1} w_{21i}x_i = bias_{21} \\ \vdots \\ b_{2N_2} - \sum_{i=1}^{N_1} w_{2N_2i}x_i = bias_{2N_2}, \end{cases} \tag{4}$$

where b_{kj} for $k = 2, 3$, $j = 1, 2, \cdots, N_K$, and x_i for $i = 1, 2, \cdots, N_1$, are variables. We see that all of the functions in Eq. (4) are separable. The importance of Eq. (4) lies in the fact that it provides us with an approach to approximately expressing nonseparable functions as separable ones by multilayer neural networks.

In comparison with conventional function approximation problems the training task mentioned above is easier to be dealt with. The reasons for this are that (a) an arbitrary large number of sample data for training and test can be obtained from $q(\boldsymbol{x})$, and (b) the goal of training is to approximate a given function $q(\boldsymbol{x})$, so the performance of the trained network can be easily checked.

3 Transformation of Nonseparable NLP problems

According to the locations of nonseparable functions in NLP problems, nonseparable NLP problems can be classified into three types: (I) only the objective function is nonseparable function; (II) only the constraint functions are nonseparable

[1] For simplicity of description, we consider only three-layer networks throughout the paper. The results can be extended to M-layer ($M > 3$) networks easily.

functions; and (III) both the objective and constraint functions are nonseparable functions.

For Type I nonseparable NLP problems, we only need to transform the objective function into separable one. Replacing the objective function with its approximation in Eq. (4), we can transform a Type I nonseparable NLP problem into a SNLP problem as follows:

$$\begin{aligned}
\text{Minimize} \quad & \alpha + \beta(f(b_{31}^O) - \gamma) \qquad (5)\\
\text{subject to} \quad & b_{31}^O - \sum_{j=1}^{N_2^O} w_{31j}^O f(b_{2j}^O) = bias_{31}^O \\
& b_{21}^O - \sum_{i=1}^{N_1} w_{21i}^O x_i = bias_{21}^O \\
& \vdots \\
& b_{2N_2^O}^O - \sum_{i=1}^{N_1} w_{2N_2^O i} x_i = bias_{2N_2^O}^O \\
& \sum_{k=1}^{n} g_{ik}(x_k) \geq 0 \quad \text{for } i = 1, \cdots, m, \\
& \sum_{k=1}^{n} h_{jk}(x_k) = 0 \quad \text{for } j = 1, \cdots, r,
\end{aligned}$$

where the "O" superscript refers to quantities on the *objective function.*

Using the similar approach mentioned above, we can transform the Type II and III nonseparable NLP problems into SNLP problems, and deal with unconstrained nonlinear programming problems.

Suppose that the accuracy of approximating nonseparable functions is good enough for a given problem. The transformed SNLP problems are equivalent to their original nonseparable NLP problems, since the transformations only change the expression forms of the objective function and (or) the constraint functions. The accuracy of approximation may be effected by many factors such as the network size, the learning algorithms and the number of training data. There are several methods for dealing with this problem, for example see [3, 8, 7]. We can use these results to guide our training and get a good accuracy.

4 Analysis of Complexity

Now let us analyze complexity of the original and transformed problems. Suppose that each nonseparable function is approximated by the network with same number of hidden units (N). Also suppose that there are s ($s \leq m$) nonseparable inequality and t ($t \leq r$) nonseparable equality constraint functions in Type II and III problems. The numbers of variables and constraints in original and transforming problems are shown in Table 1.

From Table 1 we see that as the number of hidden units grows both the number of variables and the number of constraints in the transformed problems increase. Therefore, it is desirable that each nonseparable function is approximated by a network with as few number of hidden units as possible. But on the other hand

Problem	No. of variables	No. of constraints
Original	n	$m+r$
I	$n+N+1$	$m+r+N+1$
II	$n+sN+tN+(s+t)$	$(m-s)+(r-t)$ $+sN+tN+s+t$
III	$n+N+sN+tN+(1+s+t)$	$(m-s)+(r-t)+N$ $+sN+tN+(1+s+t)$

Table 1 The numbers of variables and constraints in the original and transformed problems.

it may become more difficult for a smaller network (e.g., fewer number of hidden units) to approximate a nonseparable function. There exists a trade-off between the complexity of the transformed SNLP problems and the approximating capability of neural networks.

5 Simulation Results

Consider the following simple NLP problem:

$$\begin{aligned} \text{Minimize} \quad & 2-\sin^2 x_1 \sin^2 x_2 \\ \text{subject to} \quad & 0.5 \le x_1 \le 2.5 \\ & 0.5 \le x_2 \le 2.5 \end{aligned} \tag{6}$$

Clearly, this is a Type I nonseparable NLP problem. A three-layer perceptron with two input, ten hidden, and one output units is used to approximate the objective function. The training data set consists of 524 input-output data which are gathered by sampling the input space $[0.5, 2.5] \times [0.5, 2.5]$ in a uniform grid. The network is trained by the back-propagation algorithm [6]. In this simulation, the learning is considered complete when the sum of squared error between the target and actual outputs gets less than 0.05. Replacing the objective function with its approximation formed by the network, we obtain a SNLP problem.

Approximating the sigmoidal activation function in the SNLP problem over the interval $[-16, 16]$ via 14 grid points, we obtain an approximate SNLP problem. Solving this problem with the simplex method with the *restricted basis entry rule* [4], we obtain the solution: $x_1^* = 1.531488$ and $x_2^* = 1.595567$. If the sigmoidal activation function is approximated over the interval $[-16, 16]$ via 40 grid points, we can obtain a better solution: $x_1^* = 1.564015$ and $x_2^* = 1.569683$. Solving this problem directly with the Powell method [5], we obtain a more accurate solution: $x_1^* = 1.57079$ and $x_2^* = 1.57079$. It should be noted that there exits a trade-off between the accuracy of the approximation of SNLP problems and the number of grid points for each variable.

In general, several local solutions may exist in a SNLP problem. But only one solution can be obtained by solving the approximate SNLP problem using the simplex method with the restricted basis entry rule. It has been shown that if the objective function is strictly convex and all the constraint functions are convex, the solution obtained by the modified simplex method is sufficiently close to the global optimal

solution of the original problem by choosing a small grid. Unfortunately, the SNLP problems transformed by our method are non-convex since the sigmoidal activation function is non-convex. In such case, even though optimality of the solution can not be claimed with the restricted basis entry rule, good solutions can be obtained [1].

6 Conclusion and Future Work

We have demonstrated how multilayer neural networks can be used to transform nonseparable functions into separable ones. Applying this useful feature to nonlinear programming, we have proposed a novel method for transforming nonseparable NLP problems into separable ones. This result opens up a way for solving general NLP problems by some variation of the simplex method, and makes connection between multilayer neural networks and mathematical programming techniques. As future work we will perform simulations on large-scale nonseparable NLP problems.

REFERENCES

[1] M. S. Bazaraa, H. D. Sherali, and C. M. Shetty, *Nonlinear Programming: Theory and Algorithms*, 2nd Edition, John Wiley & Sons, Inc. (1993).

[2] K. Hornik, M. Stinchcombe and H. White, *Multilayer feedforward networks are universal approximators*, Neural Networks, Vol.2 (1989), pp359-366.

[3] J. Lee, *A novel design method for multilayer feedforward neural networks*, Neural Computation, Vol.6 (1994), pp885-901.

[4] C. E. Miller, *The Simplex Method for Local Separable Programming*, in: Recent Advances in Mathematical Programming, R. L. Graves and P. Wolfe eds., McGraw-Hill (1963), pp89-100.

[5] M. J. D. Powell, *A fast algorithm for nonlinearly constrained optimization calculations*, in: Lecture Notes in Mathematics No. 630 (1978), G. A. Waston ed., Springer-Verlag, Berlin.

[6] D. E. Rumelhart, G. E. Hinton and R. J. Williams, *Learning representations by backpropagating errors*, Nature, Vol. 323 (1986), pp533-536.

[7] X. H. Yu, G. A. Chen and S. X. Cheng, *Dynamic learning rate optimization of the backpropagation algorithm*, IEEE Transactions on Neural Networks, Vol.6 (1995), pp669-677.

[8] Z. Wang, C. D. Massimo, M. T. Tham, and A. J. Morris, *A procedure for determining the topology of multilayer feedforwar neural networks*, Neural Networks, Vol. 7 (1994), pp291-300.

Acknowledgements

We would like to thank Steve W. Ellacott and the reviewer for valuable comments and suggestions on the manuscript.

A THEORY OF SELF-ORGANISING NEURAL NETWORKS

S P Luttrell

Defence Research Agency, Malvern, Worcs, WR14 3PS, UK.
Email: luttrell@signal.dra.hmg.gb

The purpose of this paper is to present a probabilistic theory of self-organising networks based on the results published in [1]. This approach allows vector quantisers and topographic mappings to be treated as different limiting cases of the same theoretical framework. The full theoretical machinery allows a visual cortex-like network to be built.

1 Introduction

The purpose of this paper is to present a generalisation of the probabilistic approach to the static analysis of self-organising neural networks that appeared in [1]. In the simplest case the network has two layers: an input and an output layer. An input vector is used to clamp the pattern of activity of the nodes in the input layer, and the resulting pattern of individual "firing" events of the nodes in the output layer is described probabilistically. Finally, an attempt is made to reconstruct the pattern of activity in the input layer from knowledge of the location of the firing events in the output layer. This inversion from output to input is achieved by using Bayes' theorem to invert the probabilistic feed-forward mapping from input to output. A network objective function is then introduced in order to optimise the overall network performance. If the average Euclidean error between an input vector and its corresponding reconstruction is used as the objective function, then many standard self-organising networks emerge as special cases [1, 2].

In section 2 the network objective function is introduced, in section 3 a simpler form is derived which is an upper bound to the true objective function, and in section 4 the derivatives with respect to various parameters of this upper bound are derived. Finally, in section 5 various standard neural networks are analysed within this framework.

2 Objective Function

The basic mathematical object is the objective function D, which is defined as

$$\sum_{\mathbf{y}_1,\mathbf{y}_2,\cdots,\mathbf{y}_n=1}^{\mathbf{m}} \int d\mathbf{x}\, d\mathbf{x}'\, \Pr(\mathbf{x}) \Pr(\mathbf{y}_1,\mathbf{y}_2,\cdots,\mathbf{y}_n|\mathbf{x}) \Pr(\mathbf{x}'|\mathbf{y}_1,\mathbf{y}_2,\cdots,\mathbf{y}_n) \left\|\mathbf{x}-\mathbf{x}'\right\|^2 \tag{1}$$

where $\mathbf{x}$ is the input vector and $\mathbf{x}'$ is its reconstruction, $(\mathbf{y}_1,\mathbf{y}_2,\cdots,\mathbf{y}_n)$ are the locations in the output layer of n firing events, and $\left\|\mathbf{x}-\mathbf{x}'\right\|^2$ is the Euclidean distance between the input vector and its reconstruction. The various probabilities arise as follows: $\int d\mathbf{x} \Pr(\mathbf{x})(\cdots)$ integrates over the training set of input vectors, $\Pr(\mathbf{y}_1,\mathbf{y}_2,\cdots,\mathbf{y}_n|\mathbf{x})$ is the joint probability of n firing events at locations $(\mathbf{y}_1,\mathbf{y}_2,\cdots,\mathbf{y}_n)$, $\Pr(\mathbf{x}'|\mathbf{y}_1,\mathbf{y}_2,\cdots,\mathbf{y}_n)$ is the Bayes' inverse probability that input vector $\mathbf{x}'$ is inferred as the cause of the n firing events, $\sum_{\mathbf{y}_1,\mathbf{y}_2,\cdots,\mathbf{y}_n=1}^{\mathbf{m}}(\cdots)$ sums over all possible locations (on an assumed rectangular lattice of size $\mathbf{m}$) of the n firing events. The order in which the n firing events occurs will be assumed not to be observed, so that $\Pr(\mathbf{y}_1,\mathbf{y}_2,\cdots,\mathbf{y}_n|\mathbf{x})$ is a symmetric function of $(\mathbf{y}_1,\mathbf{y}_2,\cdots,\mathbf{y}_n)$.

A simplifying assumption will be made where the observed firing events are assumed to be statistically independent, so that

$$\Pr(\mathbf{y}_1, \mathbf{y}_2, \cdots, \mathbf{y}_n|\mathbf{x}) = \Pr(\mathbf{y}_1|\mathbf{x}) \Pr(\mathbf{y}_2|\mathbf{x}) \cdots \Pr(\mathbf{y}_n|\mathbf{x}) \tag{2}$$

Normally, a simple form for $\Pr(\mathbf{y}|\mathbf{x})$ is used such as

$$\Pr(\mathbf{y}|\mathbf{x}) = Q(\mathbf{x}|\mathbf{y}) / \sum_{\mathbf{y}'=\mathbf{1}}^{\mathbf{m}} Q(\mathbf{x}|\mathbf{y}')$$

where $Q(\mathbf{x}|\mathbf{y}) \geq 0$, which guarantees that the normalisation condition $\sum_{\mathbf{y}=\mathbf{1}}^{\mathbf{m}} \Pr(\mathbf{y}|\mathbf{x}) = 1$ holds. However, a more general expression will be used here based on the definition

$$\Pr(\mathbf{y}|\mathbf{x};\mathbf{y}') \equiv \frac{Q(\mathbf{x}|\mathbf{y})\, \delta_{\mathbf{y} \in \mathcal{N}(\mathbf{y}')}}{\sum_{\mathbf{y}'' \in \mathcal{N}(\mathbf{y}')} Q(\mathbf{x}|\mathbf{y}'')} \tag{3}$$

which implies that $\sum_{\mathbf{y} \in \mathcal{N}(\mathbf{y}')} \Pr(\mathbf{y}|\mathbf{x};\mathbf{y}') = 1$, where $\mathcal{N}(\mathbf{y}')$ is the set of node locations that lie in a predefined "neighbourhood" of $\mathbf{y}'$. This neighbourhood can be used to introduce "lateral inhibition" between the firing neurons if the expression for $\Pr(\mathbf{y}|\mathbf{x})$ is written as a sum over $\Pr(\mathbf{y}|\mathbf{x};\mathbf{y}')$ as follows

$$\Pr(\mathbf{y}|\mathbf{x}) = \frac{1}{M} \sum_{\mathbf{y}' \in \mathcal{N}^{-1}(\mathbf{y})} \Pr(\mathbf{y}|\mathbf{x};\mathbf{y}') = \frac{1}{M} Q(\mathbf{x}|\mathbf{y}) \sum_{\mathbf{y}' \in \mathcal{N}^{-1}(\mathbf{y})} \frac{1}{\sum_{\mathbf{y}'' \in \mathcal{N}(\mathbf{y}')} Q(\mathbf{x}|\mathbf{y}'')} \tag{4}$$

where $\mathcal{N}^{-1}(\mathbf{y})$ is the "inverse neighbourhood" of $\mathbf{y}$ defined as $\mathcal{N}^{-1}(\mathbf{y}) \equiv \{\mathbf{y}' : \mathbf{y} \in \mathcal{N}(\mathbf{y}')\}$, and M is the total number of locations in the output layer that have a non-zero neighbourhood size ($M \equiv \sum_{\mathbf{y}:\mathcal{N}(\mathbf{y}) \neq \emptyset} 1$). This expression for $\Pr(\mathbf{y}|\mathbf{x})$ is identical to one that arises in the context of optimising a special class of mixture distributions [3], and it satisfies $\sum_{\mathbf{y}=\mathbf{1}}^{\mathbf{m}} \Pr(\mathbf{y}|\mathbf{x}) = 1$. The expresson for $\Pr(\mathbf{y}|\mathbf{x})$ in (4) may readily be generalised to the case where the neighbourhood is non-uniformly weighted. The expression for D in (1) and the expression for $\Pr(\mathbf{y}|\mathbf{x})$ in (4) are the two basic ingredients in the theory of self-organising neural networks presented in this paper.

There is one further ingredient that proves to be very useful. $\Pr(\mathbf{y}|\mathbf{x})$ will be allowed to "leak" as follows [1, 3]

$$\Pr(\mathbf{y}|\mathbf{x}) \rightarrow \sum_{\mathbf{y}' \in \mathcal{L}^{-1}(\mathbf{y})} \Pr(\mathbf{y}|\mathbf{y}') \Pr(\mathbf{y}'|\mathbf{x}) \tag{5}$$

where $\Pr(\mathbf{y}|\mathbf{y}')$ is the amount of probability that leaks from location $\mathbf{y}'$ to location $\mathbf{y}$, and $\mathcal{L}^{-1}(\mathbf{y})$ is the "inverse leakage neighbourhood" of $\mathbf{y}$ defined as $\mathcal{L}^{-1}(\mathbf{y}) \equiv \{\mathbf{y}' : \mathbf{y} \in \mathcal{L}(\mathbf{y}')\}$, where $\mathcal{L}(\mathbf{y}')$ is the "leakage neighbourhood" of $\mathbf{y}'$. The purpose of leakage is to allow the network output to be "damaged" in a controlled way, so that when the network is optimised it automatically becomes robust with respect to such damage. For instance, if each node is allowed to leak probability onto its neighbours in the output layer, then when the network is optimised the node properties become topographically ordered.

3 Simplify the Objective Function

The network objective function can be simplified to yield [1]

$$D = 2 \int d\mathbf{x} \Pr(\mathbf{x}) \sum_{\mathbf{y}_1, \mathbf{y}_2, \cdots, \mathbf{y}_n = \mathbf{1}}^{\mathbf{m}} \Pr(\mathbf{y}_1, \mathbf{y}_2, \cdots, \mathbf{y}_n|\mathbf{x}) \left\| \mathbf{x} - \mathbf{x}'(\mathbf{y}_1, \mathbf{y}_2, \cdots, \mathbf{y}_n) \right\|^2 \tag{6}$$

where $\mathbf{x}'(\mathbf{y}_1, \mathbf{y}_2, \cdots, \mathbf{y}_n)$ is a "reference vector" defined as $\mathbf{x}'(\mathbf{y}_1, \mathbf{y}_2, \cdots, \mathbf{y}_n) \equiv \int d\mathbf{x} \Pr(\mathbf{x}|\mathbf{y}_1, \mathbf{y}_2, \cdots, \mathbf{y}_n)\, \mathbf{x}$. If $\mathbf{x}'(\mathbf{y}_1, \mathbf{y}_2, \cdots, \mathbf{y}_n)$ is treated as an independent variable (i.e. its definition is ignored) then minimisation of D with respect to it yields the result $\mathbf{x}'(\mathbf{y}_1, \mathbf{y}_2, \cdots, \mathbf{y}_n) = \int d\mathbf{x} \Pr(\mathbf{x}|\mathbf{y}_1, \mathbf{y}_2, \cdots, \mathbf{y}_n)\, \mathbf{x}$, which is consistent with how it should have been defined anyway. This convenient trick allows the inverse probability $\Pr(\mathbf{x}|\mathbf{y}_1, \mathbf{y}_2, \cdots, \mathbf{y}_n)$ to be eliminated henceforth, provided that D in (6) is tacitly assumed to be minimised with respect to $\mathbf{x}'(\mathbf{y}_1, \mathbf{y}_2, \cdots, \mathbf{y}_n)$.
D can be further simplified to the form $D = D_1 + D_2 - D_3$ [2], where

$$D_1 \equiv \frac{2}{n} \int d\mathbf{x} \Pr(\mathbf{x}) \sum_{\mathbf{y}=1}^{\mathbf{m}} \Pr(\mathbf{y}|\mathbf{x}) \left\|\mathbf{x} - \mathbf{x}'(\mathbf{y})\right\|^2 \tag{7}$$

$$D_2 \equiv \frac{2(n-1)}{n} \int d\mathbf{x} \Pr(\mathbf{x}) \sum_{\mathbf{y}_1, \mathbf{y}_2 = 1}^{\mathbf{m}} \Pr(\mathbf{y}_1, \mathbf{y}_2|\mathbf{x}) (\mathbf{x} - \mathbf{x}'(\mathbf{y}_1)) \cdot (\mathbf{x} - \mathbf{x}'(\mathbf{y}_2))$$

$$D_3 \equiv 2 \sum_{\mathbf{y}_1, \mathbf{y}_2, \cdots \mathbf{y}_n = 1}^{\mathbf{m}} \Pr(\mathbf{y}_1, \mathbf{y}_2, \cdots \mathbf{y}_n) \left\| \mathbf{x}'(\mathbf{y}_1, \mathbf{y}_2, \cdots \mathbf{y}_n) - \frac{1}{n} \sum_{i=1}^{n} \mathbf{x}'(\mathbf{y}_i) \right\|^2$$

To obtain this result $\Pr(\mathbf{y}_1, \mathbf{y}_2, \cdots, \mathbf{y}_n|\mathbf{x})$ has been assumed to be symmetric under permutation of the locations $\mathbf{y}_1, \mathbf{y}_2, \cdots, \mathbf{y}_n$ (e.g. the locations, but not the order of occurrence of the n firing events is known). If the independence assumption in (2) is now invoked, then D_2 may be simplified to

$$D_2 = \frac{2(n-1)}{n} \int d\mathbf{x} \Pr(\mathbf{x}) \left\| \mathbf{x} - \sum_{\mathbf{y}=1}^{\mathbf{m}} \Pr(\mathbf{y}|\mathbf{x})\, \mathbf{x}'(\mathbf{y}) \right\|^2 \tag{8}$$

The dependence of D_3 on the n-argument reference vectors $\mathbf{x}'(\mathbf{y}_1, \mathbf{y}_2, \cdots \mathbf{y}_n)$ is inconvenient, because the total number of such reference vectors is $\mathcal{O}(|\mathbf{m}|^n)$, where $|\mathbf{m}|$ is the total number of output nodes ($|\mathbf{m}| = m_1 m_2 \cdots m_d$ for a d-dimensional rectangular lattice of size $\mathbf{m}$). However, the positivity of D_3, together with $D = D_1 + D_2 - D_3$, will be used to obtain an upper bound to D as $D \leq D_1 + D_2$, which depends only on 1-argument reference vectors $\mathbf{x}'(\mathbf{y})$. The total number of 1-argument reference vectors is equal to $|\mathbf{m}|$.

4 Differentiate the Objective Function

In order to implement an optimisation algorithm the derivatives of D_1 and D_2 with respect to the various parameters must be obtained. The expressions that are encountered when differentiating are rather cumbersome, but they have a simple structure which can be made clear by the introduction of the following notation

$$\begin{array}{ll}
L_{\mathbf{y},\mathbf{y}'} \equiv \Pr(\mathbf{y}'|\mathbf{y}) & P_{\mathbf{y},\mathbf{y}'} \equiv \Pr(\mathbf{y}'|\mathbf{x};\mathbf{y}) \\
p_{\mathbf{y}} \equiv \sum_{\mathbf{y}' \in \mathcal{N}^{-1}(\mathbf{y})} P_{\mathbf{y}',\mathbf{y}} & \left(L^T p\right)_{\mathbf{y}} \equiv \sum_{\mathbf{y}' \in \mathcal{L}^{-1}(\mathbf{y})} L_{\mathbf{y}',\mathbf{y}} p_{\mathbf{y}'} \\
\mathbf{d}_{\mathbf{y}} \equiv \mathbf{x} - \mathbf{x}'(\mathbf{y}) & (L\mathbf{d})_{\mathbf{y}} \equiv \sum_{\mathbf{y}' \in \mathcal{L}(\mathbf{y})} L_{\mathbf{y},\mathbf{y}'} \mathbf{d}_{\mathbf{y}'} \\
(PL\mathbf{d})_{\mathbf{y}} \equiv \sum_{\mathbf{y}' \in \mathcal{N}(\mathbf{y})} P_{\mathbf{y},\mathbf{y}'} (L\mathbf{d})_{\mathbf{y}'} & \left(P^T PL\mathbf{d}\right)_{\mathbf{y}} \equiv \sum_{\mathbf{y}' \in \mathcal{N}^{-1}(\mathbf{y})} P_{\mathbf{y}',\mathbf{y}} (PL\mathbf{d})_{\mathbf{y}'} \\
e_{\mathbf{y}} \equiv \left\|\mathbf{x} - \mathbf{x}'(\mathbf{y})\right\|^2 & (Le)_{\mathbf{y}} \equiv \sum_{\mathbf{y}' \in \mathcal{L}(\mathbf{y})} L_{\mathbf{y},\mathbf{y}'} e_{\mathbf{y}'} \\
(PLe)_{\mathbf{y}} \equiv \sum_{\mathbf{y}' \in \mathcal{N}(\mathbf{y})} P_{\mathbf{y},\mathbf{y}'} (Le)_{\mathbf{y}'} & \left(P^T PLe\right)_{\mathbf{y}} \equiv \sum_{\mathbf{y}' \in \mathcal{N}^{-1}(\mathbf{y})} P_{\mathbf{y}',\mathbf{y}} (PLe)_{\mathbf{y}'} \\
\bar{\mathbf{d}} \equiv \sum_{\mathbf{y}=1}^{\mathbf{m}} \left(L^T p\right)_{\mathbf{y}} \mathbf{d}_{\mathbf{y}} & \text{or } \bar{\mathbf{d}} \equiv \sum_{\mathbf{y}=1}^{\mathbf{m}} (PL\mathbf{d})_{\mathbf{y}}
\end{array} \tag{9}$$

which allows (5) to be written as $\Pr(\mathbf{y}|\mathbf{x}) \rightarrow \frac{1}{M}\left(L^T p\right)_{\mathbf{y}}$. D_1 and D_2 may be differentiated with respect to $\mathbf{x}'(\mathbf{y})$ to obtain

$$\begin{aligned}\frac{\partial D_1}{\partial \mathbf{x}'(\mathbf{y})} &= -\frac{4}{nM}\int d\mathbf{x}\Pr(\mathbf{x})\left(L^T p\right)_{\mathbf{y}}\mathbf{d}_{\mathbf{y}} \\ \frac{\partial D_2}{\partial \mathbf{x}'(\mathbf{y})} &= -\frac{4(n-1)}{nM^2}\int d\mathbf{x}\Pr(\mathbf{x})\left(L^T p\right)_{\mathbf{y}}\bar{\mathbf{d}}\end{aligned} \tag{10}$$

D_1 and D_2 may be functionally varied with respect to $\log Q(\mathbf{x}|\mathbf{y})$ to obtain

$$\delta D_1 = \frac{2}{nM}\int d\mathbf{x}\Pr(\mathbf{x})\sum_{\mathbf{y}=1}^{\mathbf{m}}\delta\log Q(\mathbf{x}|\mathbf{y})\left(p_{\mathbf{y}}(Le)_{\mathbf{y}} - (P^T PLe)_{\mathbf{y}}\right) \tag{11}$$

$$\delta D_2 = \frac{4(n-1)}{nM^2}\int d\mathbf{x}\Pr(\mathbf{x})\sum_{\mathbf{y}=1}^{\mathbf{m}}\delta\log Q(\mathbf{x}|\mathbf{y})\left(p_{\mathbf{y}}(L\mathbf{d})_{\mathbf{y}} - (P^T PL\mathbf{d})_{\mathbf{y}}\right)\cdot\bar{\mathbf{d}}$$

If $Q(\mathbf{x}|\mathbf{y})$ is assumed to be a sigmoid function

$$Q(\mathbf{x}|\mathbf{y}) = 1/(1+\exp(-\mathbf{w}(\mathbf{y})\cdot\mathbf{x} - b(\mathbf{y})))$$

then the derivatives of D_1 and D_2 with respect to the "weight" vector $\mathbf{w}(\mathbf{y})$ and "bias" $b(\mathbf{y})$ may be written as

$$\begin{aligned}\frac{\partial D_1}{\partial\begin{pmatrix} b(\mathbf{y}) \\ \mathbf{w}(\mathbf{y})\end{pmatrix}} &= \frac{2}{nM}\int d\mathbf{x}\Pr(\mathbf{x})\begin{bmatrix}\left(p_{\mathbf{y}}(Le)_{\mathbf{y}} - (P^T PLe)_{\mathbf{y}}\right) \\ \times(1-Q(\mathbf{x}|\mathbf{y}))\begin{pmatrix}1\\ \mathbf{x}\end{pmatrix}\end{bmatrix} \\ \frac{\partial D_2}{\partial\begin{pmatrix} b(\mathbf{y}) \\ \mathbf{w}(\mathbf{y})\end{pmatrix}} &= \frac{4(n-1)}{nM^2}\int d\mathbf{x}\Pr(\mathbf{x})\begin{bmatrix}\left(p_{\mathbf{y}}(L\mathbf{d})_{\mathbf{y}} - (P^T PL\mathbf{d})_{\mathbf{y}}\right)\cdot\bar{\mathbf{d}} \\ \times(1-Q(\mathbf{x}|\mathbf{y}))\begin{pmatrix}1\\ \mathbf{x}\end{pmatrix}\end{bmatrix}\end{aligned} \tag{12}$$

The gradients in (10) and (12) may be used to implement a gradient descent algorithm for optimising $D_1 + D_2$, which then leads to a least upper bound on the full objective function D $(= D_1 + D_2 - D_3)$.

5 Special Cases

Various standard results that are special cases of the model presented above are discussed in the following subsections.

5.1 Vector Quantiser and Topographic Mapping

Assume $n = 1$ so that only 1 firing event is observed so that $D_2 = D_3 = 0$, $\mathbf{y} \in \mathcal{N}(\mathbf{y}')\,\forall \mathbf{y}, \mathbf{y}'$ so that the neighbourhood embraces all of the output nodes, and probability leakage of the type given in (5) is allowed. Then D reduces to $D = 2\int d\mathbf{x}\Pr(\mathbf{x})\sum_{\mathbf{y}=1}^{\mathbf{m}}\Pr(\mathbf{y}|\mathbf{y}(\mathbf{x}))\left\|\mathbf{x}-\mathbf{x}'(\mathbf{y})\right\|^2$ [1], which leads to a behaviour that is very similar to the topographic mappings described in [5], where $\Pr(\mathbf{y}|\mathbf{y}')$ now corresponds to the topographic neighbourhood function. In the limit where $\Pr(\mathbf{y}|\mathbf{y}(\mathbf{x})) = \delta_{\mathbf{y},\mathbf{y}(\mathbf{x})}$ this reduces to the criterion for optimising a vector quantiser [4].

5.2 Visual Cortex Network

A "visual cortex"-like network can be built if the full theoretical machinery presented earlier is used. This network has many of the emergent properties of the mammalian visual cortex, such as orientation maps, centre-on/surround-off detectors, dominance stripes, etc (see e.g. [7] for a review of these phenomena). There is

an input layer with a pattern of activity representing the input vector, an output layer with nodes firing in response to feed-forward connections (i.e. a "recognition" model), and a mechanism for reconstructing the input from the firing events via feed-back connections (i.e. a "generative" model). The output layer has lateral inhibition implemented as in (4); the neighbourhood of node $\mathbf{y}'$ has an associated inhibition factor $1/\sum_{\mathbf{y}''\in\mathcal{N}(\mathbf{y}')} Q\left(\mathbf{x}|\mathbf{y}''\right)$, and the overall inhibition factor for node $\mathbf{y}$ is $\sum_{\mathbf{y}'\in\mathcal{N}^{-1}(\mathbf{y})}\left(1/\sum_{\mathbf{y}''\in\mathcal{N}(\mathbf{y}')} Q\left(\mathbf{x}|\mathbf{y}''\right)\right)$, which is the sum of the inhibition factors over all nodes $\mathbf{y}'$ that have node $\mathbf{y}$ in their neighbourhood. This scheme for introducing lateral inhibition is discussed in greater detail in [3]. The leakage introduced by $\Pr\left(\mathbf{y}|\mathbf{y}'\right)$ induces topographical ordering as usual.

In the limit $n \to 1$ where D_1 is dominant, this network behaves like a topographic mapping network, except that the output layer splits up into a number of "domains" each of which is typically a lateral inhibition length in size, and each of which forms a separate topographic mapping. These domains are seamlessly joined together, so no domain boundaries are actually visible. In the limit $n \to \infty$ where D_2 is dominant, this network approximates its input as a superposition of reference vectors $\sum_{\mathbf{y}=1}^{\mathbf{m}} \Pr\left(\mathbf{y}|\mathbf{x}\right)\mathbf{x}'\left(\mathbf{y}\right)$ (see (8)). Thus the network is capable of explaining the input in terms of multiple causes.

6 Conclusions

A single theoretical framework has been shown to describe a number of standard self-organising neural networks. This makes it easy to understand the relationship between these neural networks, and it provides a useful framework for analysing their properties.

REFERENCES

[1] Luttrell S P, *A Bayesian analysis of self-organising maps*, Neural Computation, Vol. 6(5) (1994), pp767-794.

[2] Luttrell S P, *Designing analysable networks*, Handbook of Neural Computation, OUP (1996).

[3] Luttrell S P, *Partitioned mixture distribution: an adaptive Bayesian network for low-level image processing*, IEE Proc. Vision Image Signal Processing, Vol. 141(4) (1994), pp251-260.

[4] Linde Y, Buzo A and Gray R M, *An algorithm for vector quantiser design*, IEEE Trans. COM, Vol. 28(1) (1980), pp84-95.

[5] Kohonen T, *Self organisation and associative memory*, Springer-Verlag (1984).

[6] Luttrell S P, *Derivation of a class of training algorithms*, IEEE Trans. NN, Vol. 1(2) (1990), pp229-232.

[7] Goodhill G J, *Correlations, competition, and optimality: modelling the development of topography and ocular dominance*, CSRP 226 (1992), Sussex University.

Acknowledgements

© British Crown Copyright 1995/DRA. Published with the permission of the Controller of Her Britannic Majesty's Stationery Office.

NEURAL NETWORK SUPERVISED TRAINING BASED ON A DIMENSION REDUCING METHOD

G.D. Magoulas, M.N. Vrahatis*, T.N. Grapsa* and G.S. Androulakis*

Department of Electrical and Computer Engineering, University of Patras, GR-261.10, Patras, Greece. Email: magoulas@ee-gw.ee.upatras.gr

** Department of Mathematics, University of Patras, GR-261.10 Patras, Greece. Email: vrahatis—grapsa—gsa@math.upatras.gr*

In this contribution a new method for supervised training is presented. This method is based on a recently proposed root finding procedure for the numerical solution of systems of non–linear algebraic and/or transcendental equations in $\mathbb{R}^n$. This new method reduces the dimensionality of the problem in such a way that it can lead to an iterative approximate formula for the computation of $n-1$ connection weights. The remaining connection weight is evaluated separately using the final approximations of the others. This reduced iterative formula generates a sequence of points in $\mathbb{R}^{n-1}$ which converges quadratically to the proper $n-1$ connection weights. Moreover, it requires neither a good initial guess for one connection weight nor accurate error function evaluations. The new method is applied on some test cases in order to evaluate its performance.

Subject classification: AMS(MOS) 65K10, 49D10, 68T05, 68G05.

Keywords: Numerical optimization methods, feed forward neural networks, supervised training, back–propagation of error, dimension–reducing method.

1 Introduction

Consider a feed forward neural network (FNN) with l layers, $l \in [1, L]$. The error is defined as $e_k(t) = d_k(t) - y_k^L(t)$, for $k = 1, 2, ..., K$, where $d_k(t)$ is the desired response at the kth neuron of the output layer at the input pattern t, $y_k^L(t)$ is the output at the kth neuron of the output layer L. If there is a fixed, finite set of input–output cases, the square error over the training set which contains T representative cases is:

$$E = \sum_{t=1}^{T} E(t) = \sum_{t=1}^{T} \sum_{k=1}^{K} e_k^2(t). \tag{1}$$

The most common supervised training algorithm for FNNs with sigmoidal non–linear neurons is the Back–Propagation (BP), [4]. The BP minimizes the error function E using the Steepest Descent (SD) with fixed step size and computes the gradient using the chain rule on the layers of the network. BP converges too slow and often yields suboptimal solutions. The quasi–Newton method (BFGS) [2], converges much faster than the BP but the storage and computational requirements of the Hessian for very large FNNs make its use impractical for most current machines.
In this paper, we derive and apply a new training method for FNNs named Dimension Reducing Training Method (DRTM). DRTM is based on the methods studied in [3] and it incorporates the advantages of Newton and SOR algorithms (see [4]).

2 Description of the DRTM

Throughout this paper $\mathbb{R}^n$ is the n–dimensional real space of column weight vectors w with components $w_1, w_2, \ldots, w_n$; $(y; z)$ represents the column vector with components $y_1, y_2, \ldots, y_m, z_1, z_2, \ldots, z_k$; $\partial_i E(w)$ denotes the partial derivative of $E(w)$ with respect to the ith variable w_i; $g(w) = (g_1(w), \ldots, g_n(w))$ defines the gradient $\nabla E(w)$ of the objective function E at w while $H = [H_{ij}]$ defines the Hessian

$\nabla^2 E(w)$ of E at w; $\bar{A}$ denotes the closure of the set A and $E(w_1, \ldots, w_{i-1}, \cdot, w_{i+1}, \ldots, w_n)$ defines the error function obtained by holding $w_1, \ldots, w_{i-1}, w_{i+1}, \ldots, w_n$ fixed.

The problem of training is treated as an optimization problem in the FNN's weight space (i.e., n–dimensional Euclidean space). In other words, we want to find the proper weights that satisfy the following system of equations :

$$g_i(w) = 0, \quad i = 1, \ldots, n\,. \tag{2}$$

In order to solve this system iteratively we want a sequence of weight vectors $\{w^p\}, p = 0, 1, \ldots$ which converges to the point $w^* = (w_1^*, \ldots, w_n^*) \in \mathcal{D} \subset \mathbb{R}^n$ of the function E. First, we consider the sets $\mathcal{B}_i$, to be those connected components of $g_i^{-1}(0)$ containing w^* on which $\partial_n g_i \neq 0$, for $i = 1, \ldots, n$ respectively. Next, applying the Implicit Function Theorem (see [4, 3]) for each one of the components g_i we can find open neighborhoods $\mathcal{A}_1^* \subset \mathbb{R}^{n-1}$ and $\mathcal{A}_{2,i}^* \subset \mathbb{R}$ of the points $y^* = (w_1^*, \ldots, w_{n-1}^*)$ and w_n^* respectively, such that for any $y = (w_1, \ldots, w_{n-1}) \in \bar{\mathcal{A}}_1^*$ there exist unique mappings φ_i defined and continuous in $\mathcal{A}_1^*$ such that : $w_n = \varphi_i(y) \in \bar{\mathcal{A}}_{2,i}^*$, and $g_i\big(y; \varphi_i(y)\big) = 0, \quad i = 1, \ldots, n$. Moreover, the partial derivatives $\partial_j \varphi_i, j = 1, \ldots, n-1$ exist in $\mathcal{A}_1^*$ for each φ_i, they are continuous in $\bar{\mathcal{A}}_1^*$ and they are given by :

$$\partial_j \varphi_i(y) = -\frac{\partial_j g_i\big(y; \varphi_i(y)\big)}{\partial_n g_i\big(y; \varphi_i(y)\big)}, \quad i = 1, \ldots, n, \quad j = 1, \ldots, n-1\,. \tag{3}$$

Working exactly as in [3], we utilize Taylor's formula to expand $\varphi_i(y)$, about y^p. By straightforward calculations, utilizing approximate values for $g_i(\cdot)$ and $\partial_j g_i(\cdot) \equiv \partial_{ij}^2 E$ (see [5], where error estimates for these approximations can also be found) we obtain the following iterative scheme for the computation of the $n-1$ components of w^* :

$$y^{p+1} = y^p + A_p^{-1} V_p, \quad p = 0, 1, \ldots, \tag{4}$$

where $y^p = [w_i^p], V_p = [v_i] = [w_n^{p,i} - w_n^{p,n}]$ and the elements of the matrix A_p are :

$$[a_{ij}] = \left[\frac{g_i(y^p + he_j; w_n^{p,i}) - g_i(y^p; w_n^{p,i})}{g_i(y^p; w_n^{p,i} + he_n) - g_i(y^p; w_n^{p,i})} - \frac{g_n(y^p + he_j; w_n^{p,n}) - g_n(y^p; w_n^{p,n})}{g_n(y^p; w_n^{p,n} + he_n) - g_n(y^p; w_n^{p,n})} \right], \tag{5}$$

with $w_n^{p,i} = \varphi_i(y^p)$, h a small quantity and e_j the j–th unit vector. After a desired number of iterations of (4), say $p = m$, the nth component of w^* can be approximated by means of the following relation :

$$w_n^{m+1} = w_n^{m,n} - \sum_{j=1}^{n-1} \left\{ (w_j^{m+1} - w_j^m) \cdot \frac{g_n(y^m + he_j; w_n^{m,n}) - g_n(y^m; w_n^{m,n})}{g_n(y^m; w_n^{m,n} + he_n) - g_n(y^m; w_n^{m,n})} \right\}. \tag{6}$$

Note that the iterative formula (4) uses the matrices A_p and V_p. The matrix A_p constitutes the reduced–Hessian of our network and its components incorporate components of the Hessian but are evaluated at different points. The matrix V_p uses only the points $w_n^{p,i}$ $(i = 1, \ldots, n-1)$ and $w_n^{p,n}$ instead of the gradient values employed in Newton's method. A proof for the convergence of (4) and (6) can be found in [6].

Relative procedures for obtaining w^* can be constructed by replacing w_n with any one of the components $w_1, \ldots, w_{n-1}$, for example w_{int}. The above described method

	FR		*PR*		*BFGS*		*DRTM*		
w^0	*IT*	*FE*	*IT*	*FE*	*IT*	*FE*	*IT*	*FE*	*ASG*
$(0.3, 0.4)$	F	F	F	F	F	F	5	20	100
$(-1, -2)$	F	F	F	F	14	274	7	28	140
$(-1, 10)$	F	F	F	F	14	285	7	28	140
$(0.2, 0.2)$	F	F	F	F	F	F	5	20	100
$(2, 1)$	F	F	F	F	13	298	5	20	100
$(0.3, 0.3)$	F	F	F	F	F	F	5	20	100
$(-1.2, 1.2)$	F	F	F	F	F	F	7	28	140

Table 1 Comparative results for Example 1.

does not require the expressions φ_i but only the values $w_n^{p,i}$ which are given by the solution of the one–dimensional equations $g_i(w_1^p, \ldots, w_{n-1}^p, \cdot) = 0$. So, by holding $y^p = (w_1^p, \ldots, w_{n-1}^p)$ fixed, we can solve the equations : $g_i(y^p; r_i^p) = 0$, $i = 1, \ldots, n$, for an approximate solution r_i^p in the interval (a, b) with an accuracy D. In order to solve the one–dimensional equations, we employ a modified bisection method described in [3, 12] and given by the following formula :

$$w^{p+1} = w^p + \mathrm{sgn}\psi(w^p)\, q \,/\, 2^{p+1}, \qquad p = 0, 1, \ldots, \tag{7}$$

with $w^0 = a$, $q = \mathrm{sgn}\psi(a)\,(b-a)$ and where sgn defines the well known sign function. This method computes with certainty a root when $\mathrm{sgn}\psi(w^0)\,\mathrm{sgn}\psi(w^p) = -1$ (see [12]). It is evident from (7) that the only computable information required by this method is the algebraic signs of the function ψ.
A high–level description of the new algorithm can be found in [8].

3 Simulation Results

Here we present and compare the behavior of the DRTM with other popular methods on some artificially created but characteristic situations. For example, it is common in FNN training to take minimization steps that increase some weights by large amounts pushing the output of the neuron into saturation. Moreover, in various small and large scale neural network applications the error surface has flat and steep regions. It is well known that the BP is highly inefficient in locating minima in such surfaces. In the following examples, the gradient is evaluated using finite differences for the DRTM and analytically for all the other methods.

Example 1 *The objective function's surface has flat and steep regions*

$$E(w) = \sum_{i=1}^{10} g_i^2, \qquad g_i(w_1, w_2) = 2 + 2i - \left(e^{iw_1} + e^{iw_2}\right). \tag{8}$$

System (8), which is a well–known test case, *(Jennrich and Sampson Function)* (see [9]), has a global minimum at $w_1 = w_2 = 0.2578\ldots$. In Table 1 we present results obtained by applying the nonlinear conjugate gradient methods Fletcher–Reeves (FR) and Polak–Ribiere (PR) and the quasi–Newton Broyden–Fletcher–Goldfarb–Shanno (BFGS) method with the corresponding numerical results of DRTM. In this Table *IT* indicates the total number of iterations required to obtain w^* (iterations

BP			*DRTM*			
MN	*STD*	*SUC*	*MN*	*STD*	*SUC*	*MAS*
100.4	77.3	38.5	2.3	1.2	72.5	67.8

Table 2 Comparison of Back-propagation with DRTM for Example 2.

limit= 500); *FE* the total number of function evaluations (and derivatives) and *ASG* the total number of algebraic signs of the components of the gradient that are required for applying the iterative scheme (7). Because of the difficulty of the problem FR and PR failed to converge in all the cases (marked with an *F* in the table). The results are mixed with the BFGS method. Especially, when we are close to the minimum BFGS leaves the appropriate region moving to wrong direction in order to minimize the objective function.

Example 2 *The objective function's surface is oval shaped and bent.*

We can artificially create such a surface by training a single neuron with sigmoid non–linearity using the patterns $\{-6,1\}$, $\{-6.1,1\}$, $\{-4.1,1\}$, $\{-4,1\}$, $\{4,1\}$, $\{4.1,1\}$, $\{6,1\}$, $\{6.1,1\}$ for input and $\{0\}$, $\{0\}$, $\{0.97\}$, $\{0.99\}$, $\{0.01\}$, $\{0.03\}$, $\{1\}$, $\{1\}$ for output. The weights w_1, w_2 take values in the interval $[-3,3] \times [-7.5,7.5]$. The global minimum is located at the center of the surface and there are two valleys that lead to local minima. The step size for the BP was 0.05. The initial weights were formed by spanning the interval $[-3,3]$ in steps of 0.05 and the interval $[-7.5,7.5]$ in steps of 0.125.

The behavior of the methods is exhibited in Table 2, where *MN* indicates the mean number of iterations for simulations that reached the global minimum; *STD* the standard deviation of iterations; *SUC* the percentage of success in locating the global minimum and *MAS* the mean number of algebraic signs that are required for applying the iterative scheme (7). Note that for DRTM, since finite differences are used, two error function evaluations are required in each iteration. BP succeeds to locate the global minimum when initial weights take values in the intervals $w_1 \in [-0.8,1.5]$ and $w_2 \in [-2.5,2.5]$. On the other hand, DRTM is less affected by the initial weights. In this case we exploit the fact that we are able to isolate the weight vector component most responsible for unstable behavior by reducing the dimension of the problem. Therefore, DRTM is very fast and possesses high percentage of success.

4 Conclusion and Further Improvements

This paper describes a new training method for FNNs. Although the proposed method uses reduction to simpler one–dimensional equations, it converges quadratically to $n-1$ components of an optimal weight vector, while the remaining weight is evaluated separately using the final approximations of the others. Thus, it does not require a good initial estimate for one component of an optimal weight vector. Moreover, it is at the user's disposal to choose which will be the remaining weight, according to the problem. Since it uses the modified one–dimensional bisection method, it requires only that the algebraic signs of the function and gradient values be correct. It is also possible to use this method in training with block of

weights using different remaining weights. In this case, the method can lead to a network training and construction algorithm. This issue is currently under development and we hope to address it in a future communication.

Note that in general the matrix of our reduced system is not symmetric. It is possible to transform it to a symmetric one by using proper perturbations [6]. If the matrix is symmetric and positive definite the optimal weight vector minimizes the objective function. Furthermore, DRTM appears particularly useful when it is difficult to evaluate the gradient values accurately, as well as when the Hessian at the optimum is singular or ill–conditioned [8].

REFERENCES

[1] D. E. Rumelhart and J. L. McClelland eds., *Parallel Distributed Processing : Explorations in the Microstructure of Cognition*, Vol. 1, MIT Press, 1986, pp318–362.

[2] R. L. Watrous, *Learning algorithms for connectionist networks: applied gradient methods of non-linear optimization*, in Proc. IEEE Int. Conf. Neural Networks, San Diego, CA, Vol.2 (1987), pp619–627.

[3] T. N. Grapsa, M. N. Vrahatis, *A dimension–reducing method for solving systems of non–linear equations in* $\mathbb{R}^n$, Int. J. Computer Math., Vol.32 (1990), pp205–216.

[4] J. M. Ortega, W. C. Rheinboldt, *Iterative Solution of Non–linear Equations in Several Variables*, Academic Press, New York, (1970).

[5] J. E. Dennis, R. B. Schnabel, *Numerical methods for unconstrained optimization and non–linear equations*, Prentice–Hall, Englewood Cliffs, NJ, (1983).

[6] T. N. Grapsa, M. N. Vrahatis, *A dimension–reducing method for unconstrained optimization*, J. Comp. Appl. Math. Vol. 66 (1996), pp239–253.

[7] M. N. Vrahatis, *Solving systems of non–linear equations using the non zero value of the topological degree*, ACM Trans. Math. Software, Vol. 14 (1988), pp312–329.

[8] G. D. Magoulas, M. N. Vrahatis, T. N. Grapsa, G. S. Androulakis, *A dimension–reducing training method for feed–forward neural networks*, Tech. Rep. CSL–1095, Department of Electrical & Computer Engineering, University of Patras, (1995).

[9] B. J. Moré , B. S. Garbow, K. E. Hillstrom, *Testing unconstrained optimization*, ACM Trans. Math. Software, Vol. 7 (1981), pp17–41.

A TRAINING METHOD FOR DISCRETE MULTILAYER NEURAL NETWORKS

G.D. Magoulas, M.N. Vrahatis*,
T.N. Grapsa* and G.S. Androulakis*

Department of Electrical and Computer Engineering, University of Patras, GR-261.10, Patras, Greece. Email: magoulas@ee-gw.ee.upatras.gr
** Department of Mathematics, University of Patras, GR-261.10 Patras, Greece. Email: vrahatis—grapsa—gsa@math.upatras.gr*

In this contribution a new training method is proposed for neural networks that are based on neurons whose output can be in a particular state. This method minimises the well known least square criterion by using information concerning only the signs of the error function and inaccurate gradient values. The algorithm is based on a modified one–dimensional bisection method and it treats supervised training in networks of neurons with discrete output states as a problem of minimisation based on imprecise values.
Subject classification: AMS(MOS) 65K10, 49D10, 68T05, 68G05.

Keywords: Numerical analysis, imprecise function and gradient values, hard–limiting threshold units, feed forward neural networks, supervised training, back–propagation of error.

1 Introduction

Consider a Discrete Multilayer Neural Network (DMNN) consisting of L layers, in which the first layer denotes the input, the last one, L, is the output, and the intermediate layers are the hidden layers. It is assumed that the (l-1)–th layer has N_{l-1} units. These units operate according to the following equations :

$$net_j^l = \sum_{i=1}^{N_{l-1}} w_{ij}^{l-1,l} y_i^{l-1} + \theta_j^l, \qquad y_j^l = \sigma^l\left(net_j^l\right), \tag{1}$$

where net_j^l is the net input to the jth unit at the lth layer, $w_{ij}^{l-1,l}$ is the connection weight from the ith unit at the $(l-1)$–th layer to the jth unit at the lth layer, y_i^l denotes the output of the ith unit belonging to the lth layer, θ_j^l denotes the threshold of the jth unit at the lth layer, and σ is the activation function. In this paper we consider units where $\sigma(net_i^l)$ is a discrete activation function. We especially focus on units with two output states, usually called binary or hard–limiting units [1], i.e. $\sigma^l(net_j^l)$ = "*true*", if $net_j^l \geq 0$, and "*false*" otherwise.

Although units with discrete activation function have been superseded to a large extent by the computationally more powerful units with analog activation function, still DMNNs are important in that they can handle many of the inherently binary tasks that neural networks are used for. Their internal representations are clearly interpretable, they are computationally simpler to understand than networks with sigmoid units and provide a starting point for the study of the neural network properties. Furthermore, when using hard–limiting units we can understand better the relationship between the size of the network and the complexity of the training [2]. In [3] it has been demonstrated that DMNNs with only one hidden layer, can create any decision region that can be expressed as a finite union of polyhedral sets when there is one unit in the input layer. Moreover, artificially created examples were given where these networks create non convex and disjoint decision regions.

Finally, discrete activation functions facilitate neural network implementations in digital hardware and are much less costly to fabricate.

The most common feed forward neural network (FNN) training algorithm, the back–propagation (BP) [4] that makes use of the gradient descent, cannot be applied directly to networks of units with discrete output states, since discrete activation functions (such as hardlimiters) are non–differentiable. However, various modifications of the gradient descent have been presented [5, 6, 7]. In [8] an approximation to gradient descent, the so–called pseudo–gradient training method, was proposed. This method uses the gradient of a sigmoid as a heuristic hint instead of the true gradient. Experimental results validated the effectiveness of this approach.

In this paper, we derive and apply a new training method for DMNNs that makes use of the gradient approximation introduced in [8]. Our method exploits the imprecise information regarding the error function and the approximated gradient, like the pseudo–gradient method does, but it has an improved convergence speed and has potential to train DMNNs in situations where, according to our experiments, the pseudo–gradient method fails to converge.

2 Problem Formulation and Proposed Solution

We consider units with two discrete output states and we shall use the convention f (or $-f$) for "false" and t (or $+t$) for "true", where f, t are real positive numbers and $f < t$, instead of the classical 0 and 1 (or -1, and $+1$). Real positive values prevent units from saturating, give to the logic "false" some power of influence over the next layer of the DMNN, and help the justification of the approximated gradient value which we shall employ.

First, let us define the error for a discrete unit as follows: $e_j(t) = d_j(t) - y_j^L(t)$, for $j = 1, 2, ..., N_L$, where $d_j(t)$ is the desired response at the jth neuron of the output layer at the input pattern t, $y_j^L(t)$ is the output at the kth neuron of the output layer L. For a fixed, finite set of input–output cases, the square error over the training set which contains T representative cases is:

$$E = \sum_{t=1}^{T} E(t) = \sum_{t=1}^{T} \sum_{j=1}^{N_L} e_j^2(t). \tag{2}$$

The idea of the pseudo–gradient was first introduced in training discrete recurrent neural networks [9, 10] and extended to DMNNs [8]. The method approximates the true gradient of the error function with respect to the weights, i.e. $\nabla E(w)$, by introducing an analog set of values for the outputs of the hidden layer units and the output layer units.

Thus, it is assumed that y_j^l in (1) can be written as $y_j^l = \tilde{\sigma}^l\Big(s(net_j^l)\Big)$, where $\tilde{\sigma}$(x)= "*true*" if x$\geq$ 0.5, and "*false*" otherwise, if $s(\cdot)$ is defined in $[0, 1]$. If $s(\cdot)$ is defined in $[-1, 1]$ then $\tilde{\sigma}$(x)= "*true*" if x$\geq$ 0, and "*false*" otherwise.

Using the chain rule, the pseudo–gradient is computed :

$$\frac{\widetilde{\partial E}}{\partial w_{ij}^{l-1,l}} = \widetilde{\delta}_j^l y_i^{l-1}, \tag{3}$$

where the back–propagating error signal $\tilde{\delta}$ for the output layer is $\widetilde{\delta_j^L} = \Big(d_j - s(net_j^L)\Big) \cdot s'(net_j^L)$ and for the hidden layers ($l \in [2, L-1]$) is $\widetilde{\delta_j^l} = s'(net_j^l)$

$\sum_n w_{jn}^{l,l+1} \widetilde{\delta_n^{l+1}}$. In these relations $s'(net_j^l)$ is the derivative of the analog activation function.

By using real positive values for "true" and "false" we ensure that the pseudo–gradient will not reduce to zero when the output is "false". Note also that we do not use σ' which is zero everywhere and non–existent at zero. Instead, we use s' which is always positive, so $\tilde{\delta}_j^l$ gives an indication of the direction and magnitude of a step up or down as a function of net_j^l in the error surface E.

However, as pointed out in [8], the value of the pseudo–gradient is not accurate enough, so gradient descent based training in DMNNs is considerably slow when compared with BP training in FNNs.

In order to alleviate this problem we propose an alternative to the pseudo-gradient training method procedure. To be more specific, we propose to solve the one–dimensional equation :

$$E(w_1, \ldots, w_{i-1}^0, w_i^0, w_{i+1}^0, \ldots, w_n^0) - E(w_1^0, \ldots, w_{i-1}^0, w_i^0, w_{i+1}^0, \ldots, w_n^0) = 0,$$

for w_1 keeping all other components of the weight vector in their constant values. Now, if $\hat{w}_1$ is the solution of the above equation, then the point defined by the vector $(\hat{w}_1, w_2^0, \ldots, w_n^0)$ possesses the same error function value with the point w^0, so it belongs to the same contour line of w^0. Assuming that the error function curves up from w^* in all directions, we can claim that any point which belongs to the line with endpoints w^0 and $(\hat{w}_1, w_2^0, \ldots, w_n^0)$ possesses smaller error function value than these endpoints. With this fact in mind we can now choose such a point, say, for example $w_1^1 = w_1^0 + \gamma\,(\hat{w}_1 - w_1^0)$, $\gamma \in (0,1)$, and solve the one–dimensional equation :

$$E(w_1^1, w_2, \ldots, w_{i-1}^0, w_i^0, w_{i+1}^0, \ldots, w_n^0) - E(w_1^1, w_2^0, \ldots, w_{i-1}^0, w_i^0, w_{i+1}^0, \ldots, w_n^0) = 0,$$

for w_2 keeping all other components in their constant values. If $\hat{w}_2$ is the solution of this equation then we can obtain a better approximation for this component by taking $w_2^1 = w_2^0 + \gamma\,(\hat{w}_2 - w_2^0)$, $\gamma \in (0,1)$.

Continuing in a similar way with the remaining components of the weight vector we obtain the new vector $w^1 = (w_1^1, \ldots, w_n^1)$ and replace the initial vector w^0 by w^1. The procedure can then be repeated to compute w^2 and so on until the final estimated point is computed according to a predetermined accuracy. So, in general we want to find the parameter $\hat{x}$ (a weight or threshold) that satisfies :

$$E(x_1^{k+1}, \ldots, x_{i-1}^{k+1}, x, x_{i+1}^k, \ldots, x_n^k) - E(x_1^{k+1}, \ldots, x_{i-1}^{k+1}, x_i^k, x_{i+1}^k, \ldots, x_n^k) = 0,$$

by applying the modified bisection (see [12, 13]) in the interval (a_i, b_i) within accuracy d :

$$x_i^{p+1} = x_i^p + C\,\mathrm{sgn}\left(E(z^p) - E(z^0)\right)/2^{p+1}, \quad p = 0, 1, \ldots, \lceil \log_2((b_i - a_i)\,d^{-1}) \rceil,$$

where the notation $\lceil \cdot \rceil$ refers to the smallest integer not less than the real number quoted and $z^0 = (x_1^{k+1}, \ldots, x_{i-1}^{k+1}, a_i, x_{i+1}^k, \ldots, x_n^k)$, $z^p = (x_1^{k+1}, \ldots, x_{i-1}^{k+1}, x_i^p, x_{i+1}^k, \ldots, x_n^k)$, $C = \mathrm{sgn}E(z^0)(b_i - a_i)$, $a_i = \bar{x}_i^k - \frac{1}{2}\{1 + \mathrm{sgn}\partial_i \widetilde{E(\bar{x}^k)}\}h_i$, $b_i = a_i + h_i$. If an iteration of the algorithm fails we switch to the pseudo–gradient training method. So, the justification of the new procedure is based on the heuristic justification of the pseudo–gradient which can be found in any one of [8, 9, 10]. A formal justification of the proposed procedure in case of differentiable objective functions can be found in [11].

	BP			New method				
	MN	*STD*	*MNE*	*MN*	*STD*	*MNE*	*MAS*	*SAS*
a)	561	550.4	0.0396	40.6	4.2	0.0000008	239.6	54.12
b)	18121	3048.7	0.49	28.5	13.43	0.45	20673	9310.9

Table 1 Experimental results a) XOR, b) $\sin x \cos 2x$.

3 Experimental Results

Here we present and compare the behaviour of the new training method with the BP [4] and the pseudo–gradient training method [8] for the XOR problem and training an 1–10–1 network to approximate the function $\sin x \cos 2x$ (Table 1). In all problems $\gamma = 0.5$, $d = 10^{-10}$, $\bar{h} = 10$ and no pseudo–gradient subprocedure has been applied with the proposed method in order to get more fair evaluation. *MN* indicates the mean number of iterations; *STD* the standard deviation of iterations; *MNE* the mean value of the error; *MAS* the mean number of algebraic signs required for the bisection scheme and *SAS* the standard deviation of the required algebraic signs. The results are for 10 simulation runs, for the same initial weights; the maximum number of iterations was set to 2000, the weights were initialised in the interval $[-10, 10]$ and the step size for BP was set to the standard value 0.75. For the XOR the thresholds were set as follows: "*true*" = 0.8 and "*false*" = 0.2. Under the same conditions the pseudo–gradient training needed more than 2000 iterations to converge. The frequency with which the algorithm became trapped in local minima seems to be about the same as for BP for binary tasks. We also used the new method in training DMNN to learn smooth functions. One hidden layer of hard–limiting units and one output unit with linear activation function was used in all our experiments. We did not manage to train DMNNs using the pseudo–gradient training method due to oscillations, although various step sizes and different discrete activation functions have been tried. With the new algorithm and discrete activation functions such as 0.5 for "*true*" and −0.5 for "*false*" DMNNs were trained as fast as, and often faster than, BP trained FNNs until $E \leq 0.5$ (over 21 input/output cases). After this error bound, the convergence speed was reduced due to saturation problems.

However, it is worth noticing the difference in the behaviour between BP and the new method. Back–propagation trained FNNs exhibit a greater tendency to fit closely data with higher variation than data with low variation. On the other hand, although DMNNs do not produce smooth functions, they learn the general trend of the data values and therefore might be more useful than FNNs when there is noise in the data and the error goal can be set so high that the network does not have to fit all the target values perfectly. Situations like this usually occur in system identification and control (see [14]).

4 Conclusion and Further Improvements

This paper describes a new training method for DMNNs. The method does not directly perform gradient evaluations. Since it uses the modified one–dimensional bisection method it requires only that the algebraic signs of the function and gra-

dient values be correct; so it can be applied to problems with imprecise function and gradient values. The method can also be used in training with block of network parameters, for example train the entire network, then the weights to the output layer and the thresholds of the hidden units, etc. We have tested such configurations and the results were very promising, providing faster training.

REFERENCES

[1] W. McCullough, W. H. Pitts, *A logical calculus of the ideas imminent in nervous activity*, Bulletin Mathematical Biophysics, Vol. 5 (1943), pp115–133.

[2] S. E. Hampson, D. J. Volper, *Representing and learning boolean functions of multivalued features*, IEEE Trans. Systems, Man & Cybernetics, Vol. 20 (1990), pp67–80.

[3] G. J. Gibson, F. N. Cowan, *On the decision regions of multi–layer perceptrons*, Proc. IEEE, Vol. 78 (1990), pp1590–1594.

[4] D. E. Rumelhart and J. L. McClelland eds., *Parallel Distributed Processing : Explorations in the Microstructure of Cognition*, Vol. 1, MIT Press (1986), pp318–362.

[5] B. Widrow, R. Winter, *Neural nets for adaptive filtering and adaptive pattern recognition*, IEEE Computer (March 1988), pp25–39.

[6] D. J. Tom, *Training binary node feed forward neural networks by back–propagation of error*, Electronics Letters, Vol. 26 (1990), pp1745–1746.

[7] E. M. Gorwin, A. M. Logar, W. J. B. Oldham, *An iterative method for training multilayer networks with threshold functions*, IEEE Trans. Neural Networks, Vol. 5 (1994), pp507–508.

[8] R. Goodman, Z. Zeng, *A learning algorithm for multi–layer perceptrons with hard–limiting threshold units*, in: Proc. IEEE Neural Networks for Signal Processing (1994), pp219–228.

[9] Z. Zeng, R. Goodman, P. Smyth, *Learning finite state machines with self–clustering recurrent networks*, Neural Computation, Vol. 5 (1993), pp976–990.

[10] Z. Zeng, R. Goodman, P. Smyth, *Discrete recurrent neural networks for grammatical inference*, IEEE Trans. Neural Networks, Vol. 5 (1994), pp320–330.

[11] M. N. Vrahatis, G. S. Androulakis, G. E. Manoussakis, *A new unconstrained optimization method for imprecise function and gradient values*, J. Mathematical Analysis & Applications, Vol. 197 (1996), pp586–607.

[12] M. N. Vrahatis, *Solving systems of non–linear equations using the non zero value of the topological degree*, ACM Trans. Math. Software, Vol. 14 (1988), pp312–329.

[13] M. N. Vrahatis, *CHABIS: A mathematical software package for locating and evaluating roots of systems of non–linear equations*, ACM Trans. Math. Software, Vol. 14 (1988), pp330–336.

[14] H. J. Sira–Ramirez, S. H. Zak, *The adaptation of perceptrons with applications to inverse dynamics identification of unknown dynamic systems*, IEEE Trans. Systems, Man & Cybernetics, Vol. 21 (1991), pp634–643.

LOCAL MINIMAL REALISATIONS OF TRAINED HOPFIELD NETWORKS

S. Manchanda and G.G.R. Green*

Dept. of Chemical and Process Engineering,
University of Newcastle upon Tyne, Newcastle upon Tyne, NE1 7RU, UK.
** Dept. of Physiological Sciences, Email: gary.green@ncl.ac.uk*

A methodology for investigating the invariant structural characteristics of the different approximations produced by Hopfield networks is presented. The technique exploits the description of the dynamics of a network as a Generating series which relates the output of a network to the past history of inputs. Truncations of a Hopfield Generating series are approximations to unknown dynamics to a specified order. As a truncated series has finite Lie rank, a local minimal realisation can be formulated. This realisation has a dimension whose lower bound is determined by the relative order of the network and whose upper bound is determined by the order of truncation. The maximal dimension of the minimal realisation is *independent* of the number of nodes in the network.

Keywords: Hopfield networks, nonlinear dynamics, realisations, minimality.

1 Introduction

Trained recurrent networks are commonly used to provide models of an unknown nonlinear dynamic system. The representations are in the form of state-space models which are usually characterised as sets of nonlinear differential equations. However, different combinations of network weight parameters often produce comparable approximation capabilities. Thus a fundamental problem is the interpretation of these representations. One approach to this problem is to attempt to reduce the state-space model to a minimal form as this is the description to which all other representations are related by diffeo-morphisms.

In practice, network model building is concerned with producing a suitable approximation of the unknown dynamic system, thus what is required is a method for specifying the order of the approximation and for producing the corresponding minimal realisation which has the same approximation capability. The input-output behaviour of a trained network can be formulated as a formal power series in non-commutative variables. This formal power series, the Generating series [2], has a minimal realisation if its Lie rank is finite [1]. If the infinite Hopfield Generating series which, in general, is not of finite Lie rank can be truncated, it can be used to produce minimal realisations whose input-output behaviour match that of the network up to a specified arbitrary order. This is equivalent to producing the minimal realisation of the unknown dynamics to a specified order of approximation.

In this article the tools for constructing minimal realisations of truncated Generating series are applied to Hopfield recurrent networks. These tools were originally described by Fliess [1]. The approach was further developed by Jacob & Oussous [3].

2 Hopfield Networks and their Local Solutions

The Lie derivatives, A_0 and A_1, that define the state-space of the single-input ($m = 1$) single-output (SISO) Hopfield RNN are

$$A_0 = \sum_i^N (-\kappa_i x_i + \sum_j^N w_{ij}\sigma(x_j))\frac{\partial}{\partial x_i} \quad A_1 = \sum_i^N \gamma_i \frac{\partial}{\partial x_i}$$

where $\sigma(x_i)$ is the output of the ith node in a single layer of N hidden nodes, κ_i acts as a time constant of the ith node, w_{ij} is the weight between node i and j, and $\gamma_i u$ is the weighted input u into node i. It is assumed that the σ nonlinearity is the tanh function and that the output of the network is $y = h(x) = \sigma(x_1)$.
The Generating series solution of this specific linear analytic system is formed by the Peano-Baker iteration of the state-space differential equations. It can be shown to be [2]

$$y(t) = S = h_{|X_0} + \sum_{\nu \geq 0} \sum_{j_1,..,j_\nu=0}^{m} A_{j_1} A_{j_2} ... A_{j_\nu}(h)_{|X_0} z_{j_\nu} \cdots z_{j_2} z_{j_1}$$

where S is a mapping between the free monoid Z^*, constructed from the alphabet set z_0, z_1, into $\mathbb{R}$ and the subscript $_{|X_0}$ means evaluated at the initial conditions of the state vector. Each word, $z_{j_1} z_{j_2} .. z_{j_k}$ corresponds to the iterated integral

$$\int_0^t u_{j_1}(\tau_1) \int_0^{\tau_1} u_{j_2}(\tau_2) \cdots \int_0^{\tau_{k-1}} u_{j_k}(\tau_k) d\tau_k \cdots d\tau_2 d\tau_1$$

defined recursively on its length,(u_0 is defined to be unity). The coefficient of the word $z_{j_1} z_{j_2} .. z_{j_k}$ is the iterated Lie derivative $A_{j_k} .. A_{j_2} A_{j_1}$ operating on the output h and evaluated at the initial conditions. The Generating series is a causal functional expansion about a point and is valid local to this position in state space, for a short time and for small input u.
Two systems are locally equivalent *if and only if* their Generating series match. In this framework *any training algorithm* for a recurrent network can be viewed as a method for adjusting the coefficients of words to produce this matching by altering the contribution of the weights, to each term, in the Generating series.

3 Network Minimal Realisations

The Generating series form of the Hopfield network is an infinite series. Truncation of this series produces an approximation of the local input-output behaviour of the network and therefore of the unknown system.
To produce the minimal realisation of this approximation depends upon identifying the structural characteristics of a *truncated* Generating series which does not include a constant term. This latter constraint can always be satisfied by considering the dynamics from a specific position in state space. The truncated Generating series of arbitrary order k can be expressed in terms of a Lie-Hankel matrix [3]. A Lie-Hankel matrix, LH_S, of a Generating series S is an (infinite) array whose rows are indexed by a totally ordered basis of the Lie algebra of Z, $L\langle Z \rangle$, and the columns are indexed by Z^*. The finiteness of the rank of this matrix determines whether a corresponding minimal state-space realisation exists, while the magnitude of the rank governs the dimension of the realisation [1].
As the basis of $L\langle Z \rangle$, the Lyndon basis (the specific Lie polynomials, P_i) can be chosen [3, 4].
For example, if the Generating series of a n state Hopfield network is truncated so that the length of the words ≤ 2, then the Lyndon words are the set $\{z_0, z_1, z_0 z_1\}$ and the corresponding Lie polynomials P_i are $\{z_0, z_1, [z_0, z_1]\}$ where $[z_0, z_1]$ is the Lie bracket of the words z_0, z_1 and is defined as $z_0 z_1 - z_1 z_0$. The Lie-Hankel matrix is shown in Table 1 whose elements are evaluated at a point in the state space of the Hopfield network. Similar analyses can be made for truncated Generating series

	ϵ	z_0	z_1
z_0	$A_0(h)$	$A_0^2(h)$	$A_1A_0(h)$
z_1	$A_1(h)$	$A_0A_1(h)$	$A_1^2(h)$
$[z_0, z_1]$	$A_1A_0(h) - A_0A_1(h)$	0	0

Table 1

order	rank
1	1
2	3
3	5
4	8

Table 2

of higher order. The maximum rank, as a function of truncation order is shown in Table 2.

The rank, and therefore the dimension of the minimal realisation, is not determined by the number of hidden nodes in the network as the elements of the Lie-Hankel matrix are defined for an arbitrary number of hidden nodes. The rank reduces if certain network weights result in either linear row interdependence or rows having zero entries. This latter condition can occur if the networks have relative order greater then unity as then particular terms in the Generating series are zero. The lower bound on the rank of the Lie-Hankel matrix is determined by the relative order of the network.

3.1 Construction of the Minimal Realisation

Lyndon words can be used to construct a basis set of polynomials Q_j. The basis set Q represents the local coordinates of the minimal state-space realisation. The set Q is used to reconstruct the truncated Generating series S. The series is expressed in terms of linear combinations and shuffle products of the elements Q_j of the basis set Q. Thus, for the truncated Hopfield network of relative order unity, the set Q consists of the elements $Q_1 = z_0$, $Q_2 = z_1$ and $Q_3 = z_0z_1$.

The truncated series is reconstructed from the basis set Q by using a modification of the algorithm proposed by Jacob & Oussous [3] to deal with Generating series with arbitrary coefficients of words. The algorithm iteratively searches for and identifies proper left factors of the truncated series.

The vector fields are reconstructed in terms of linear combinations and shuffle products of the elements of Q and translated into the state space coordinates q. Thus, in the length two example, the vector fields of the minimal realisation are

$$A_0 = \frac{\partial}{\partial q_1}, A_1 = \frac{\partial}{\partial q_2} + q_1\frac{\partial}{\partial q_3}$$

The output function is given by

$$y = (A_0A_1(h) - A_1A_0(h))q_3 + \frac{1}{2}A_1^2(h)q_2^2 + A_1(h)q_2$$

$$+A_1A_0(h)q_1q_2 + \frac{1}{2}A_0^2(h)q_1^2 + A_0(h)q_1$$

4 Discussion

This article is concerned with local approximations to unknown nonlinear dynamics up to a specified order. The approximation order is in terms of the length of the Generating series that represents the input-output behaviour of a trained network. A trained recurrent network can closely approximate, in a local sense, an unknown dynamic when the network Generating series is similar to that of the unknown system. It should be noted that the unknown dynamic system may not necessarily be represented by a suitable global model and therefore one should seek local models in the first instance. The Generating series, like the Taylor series, is a *local* functional expansion.

In this article only an upper and lower bound on the rank of the Lie-Hankel matrix is described. The upper bound is determined by the length of the truncated Generating series and is directly related to the order of approximation of the unknown dynamics by the Hopfield network.

The rank determines the dimension of the minimal realisation. The dimension of the minimal realisation is *independent of the number of hidden nodes* in the Hopfield network. The network trajectory evolves locally on a submanifold of the Hopfield state-space.

The local minimal realisation of a truncated Generating series of a Hopfield network is a set of polynomial differential equations and an output which is polynomial in the states. The state-space dynamics are fixed and do not depend upon the position in the original Hopfield state space. The minimal state space dynamics are input driven, with zero initial conditions. The state space dynamics reflect the local influence of the system input. However, the output map is dependent upon the position in the Hopfield state space. These observations on the form of the local minimal realisations imply that any two networks which are used to approximate an unknown system have the same minimal state-space dynamics and differ only in the form of the output function.

Acknowledgements

We gratefully acknowledge support from the UK EPSRC and the Research Committee of the University of Newcastle upon Tyne, UK.

REFERENCES

[1] M. Fliess, *Realisation locale des systemes non lineaires, algebres de lie filtrees transitives et series generatrices non commutatives*, Invent. Math., Vol. 71 (1983), pp521–537.

[2] M. Fliess, M. Lamnabhi, and F. Lamnabhi-Lagarrigue, *An algebraic approach to nonlinear functional expansions*, IEEE Transactions on Circuits and Systems, Vol. 30 (1983) pp554–570.

[3] G. Jacob and N. Oussous, *Local and minimal realisation of nonlinear dynamical systems and lyndon words*, in: A. Isidori, editor, IFAC symposium: Nonlinear Control Systems Design (1989), pp155–160.

[4] G. Viennot. *Algebre de Lie libres et monoides libres. Lecture Notes in Mathematics*, Vol. 691 (1978), Springer-Verlag.

DATA DEPENDENT HYPERPARAMETER ASSIGNMENT

Glenn Marion and David Saad*

Department of Statistics and Modelling Science, Livingstone Tower, 26 Richmond Street, Glasgow G1 1XH, UK. Email: glenn@stams.strath.ac.uk

** Department of Computer Science and Mathematics, Aston University, The Aston Triangle, Birmingham B4 7ET, UK. Email: D.Saad@uk.ac.ed*

We show that in supervised learning from a particular data set Bayesian model selection, based on the evidence, does not optimise generalization performance even for a learnable linear problem. This is achieved by examining the finite size effects in hyperparameter assignment from the evidence procedure and its effect on generalisation. Using simulations we corroborate our analytic results and examine an alternative model selection criterion, namely cross-validation. This numerical study shows that in the learnable linear case for finite sized systems leave one out cross-validation estimates correlate more strongly with optimal performance than do those of the evidence.

1 Introduction

The problem of supervised learning, or learning from examples, has been much studied using the techniques of statistical physics (see *e.g.* [7]). A major advantage of such studies over the usual approach in the statistics community is that one can examine the situation where the fraction (α) of the number of examples (p) to the number of free parameters (N) is finite. This contrasts with the asymptotic (in α) treatments found in the statistics literature (see *e.g.* [6]). However, one draw back of the statistical physics approach is that it is based on the, so called, thermodynamic limit where one allows N and p to approach infinity whilst keeping α constant. A quantity is said to be *self averaging* if its variance over data sets of examples tends to zero in the thermodynamic limit. We show that in Bayesian model selection based on the evidence, conclusions drawn from the thermodynamic results are qualitatively at odds with the finite size behaviour.

In the supervised learning scenario one is presented with a set of data

$$\mathcal{D} = \{(y_t(\mathbf{x}^\mu), \mathbf{x}^\mu) : \mu = 1..p\}$$

consisting of p examples of an otherwise unknown *teacher* mapping denoted by the distribution $P(y_t \mid \mathbf{x})$. Furthermore, we assume that the N dimensional input space is sampled with probability $P(\mathbf{x})$. The learning task is to use this data $\mathcal{D}$ to set the N_s parameters $\mathbf{w}$ of some model (or student) such that it's output, $y_s(\mathbf{x})$, *generalizes* to examples not contained in the training data, $\mathcal{D}$. Often this is achieved by minimising a weighted sum, $\beta E_{\mathbf{w}}(\mathcal{D}) + \gamma C(\mathbf{w})$ of the quadratic error of the student on the training examples, $E_{\mathbf{w}}(\mathcal{D})$, and some *cost function*, $C(\mathbf{w})$, which penalises over complex models. Provided γ is non-zero this serves to alleviate the problem of *overfitting*. It is the setting of the, so-called, *hyperparameters* β and γ which we will examine in this presentation.

In terms of practical methods for hyperparameter assignment there are essentially two choices. Firstly one can attempt to estimate the generalisation error (*e.g.* by cross-validation [6]) and then optimise this measure with respect to the hyperparameters. However, such an approach can be computationally expensive. Secondly,

one can optimise some other measure and hope that the resulting assignments produce low generalisation error. In particular, MacKay [6] advocates the *evidence* as such a measure. Model selection based on the evidence, in the case of a linear student and teacher, has been studied by Bruce and Saad [1] in the thermodynamic limit. Their results show that optimising the average, over all possible data sets $\mathcal{D}$, of the log evidence with respect to the hyperparameters optimises the average generalization error. An average case analysis of an unlearnable scenario can be found in [3] and shows that in general the evidence need not be optimal on average. In this paper we examine hyperparameter assignment from the evidence *based on an individual data set*, in the learnable linear case. In the next section we review the evidence framework and introduce the generalization error. In section 3, we show that the evidence procedure is unbiased and that the evidence and generalization error are self averaging. In section 4 we examine hyperparameter assignment from the evidence based on a particular data set. First order corrections to the performance measures show that in general the evidence procedure does not lead to optimal performance. Finally, we corroborate these conclusions using a numerical study which, furthermore, reveals that even leave one out cross-validation is a superior model selection criterion to the evidence in the learnable linear case for small systems.

2 Objective Functions

2.1 The Evidence

Since $E_{\mathbf{w}}(\mathcal{D})$ is the sum squared error then, if we assume that our data is corrupted by Gaussian noise with variance $1/2\beta$, the probability, or *likelihood* of the data($\mathcal{D}$) being produced given the model $\mathbf{w}$ and β is $P(\mathcal{D} \mid \beta, \mathbf{w}) \propto e^{-\beta E_{\mathbf{w}}(\mathcal{D})}$. The complexity cost can also be incorporated into this Bayesian scheme by assuming the *a priori* probability of a rule is weighted against 'complex' rules, $P(\mathbf{w} \mid \gamma) \propto e^{-\gamma C(\mathbf{w})}$. Multiplying the likelihood and the prior together we obtain the post training or student distribution, $P(\mathbf{w} \mid \mathcal{D}, \gamma, \beta) \propto e^{-\beta E_{\mathbf{w}}(\mathcal{D}) - \gamma C(\mathbf{w})}$. It is clear that the most probable model $\mathbf{w}^*$ is given by minimizing the composite cost function $\beta E_{\mathbf{w}}(\mathcal{D}) + \gamma C(\mathbf{w})$ with respect to $\mathbf{w}$.

The evidence, $P(\mathcal{D} \mid \gamma, \beta)$, is the normalisation constant for the post training distribution. That is, the probability of (or evidence for) the data set ($\mathcal{D}$) given the hyperparameters β and γ. Throughout this paper we refer to the *evidence procedure* as the process of fixing the hyperparameters to the values that simultaneously maximize the evidence for a given data set.

2.2 The Generalization Error

We will use the notation $\langle f(z) \rangle_P$ to denote the average of the quantity $f(z)$ over the distribution $P(z)$. However, we will use the short hand $\langle . \rangle_{\mathbf{w}}$ to mean the average over the post training distribution $P(\mathbf{w} \mid \mathcal{D}, \gamma, \beta)$. As our performance measure we choose the expected difference over the input dimension $P(\mathbf{x})$ between the average student and the average teacher. That is, the data dependent generalisation error, $\epsilon_g(\mathcal{D}) = \langle (\langle y_t(\mathbf{x}) \rangle_{P(y_t|\mathbf{x})} - \langle y_s(x) \rangle_{\mathbf{w}})^2 \rangle_{P(\mathbf{x})}$. If we were to *average over all possible data sets* of fixed size then this would correspond to the generalization error studied in [1].

3 Finite System Size

Since the student is linear with output $y(\mathbf{x}) = \mathbf{w}.\mathbf{x}/\sqrt{N}$, $N_s = N$. We also assume that the teacher mapping is linear, with weights $\mathbf{w}^o$, and corrupted by zero mean Gaussian noise of variance σ^2. Thus, $P(y_t \mid \mathbf{x}_\mu) \propto e^{-(y_t^\mu - \mathbf{w}^o.\mathbf{x}_\mu/\sqrt{N})^2/2\sigma^2}$. Further, we assume $P(\mathbf{x})$ is $\mathcal{N}(0, \sigma_x)$[1] and adopt weight decay as our regularization procedure, that is $C(\mathbf{w}) = \mathbf{w}^T\mathbf{w}$. In this case we can explicitly calculate the evidence, or rather the normalised log of the evidence $f(\mathcal{D}) = -1/N \ln(P(\mathcal{D} \mid \lambda, \beta)$, where we have introduced the weight decay parameter $\lambda = \gamma/\beta$. The generalisation error and the consistency can be calculated from $f(\mathcal{D})$ by averaging appropriate expressions over the input distribution $P(\mathbf{x})$. Details of these calculations will appear in a subsequent paper [4].

3.1 Consistency, Unbiasedness and Self Averaging

Firstly, we examine the *free energy*, $f(\mathcal{D})$, and the generalisation error in the limit of large amounts of data (*i.e.* as $p \to \infty$ with N fixed). Using the central limit theorem we can show that, in this limit, to first order the generalisation error is independent of the weight decay whilst f is optimised by $\lambda_{ev} = \lambda_0 \equiv \sigma^2/(\sigma_x^2\sigma_w^2)$ and $\beta_{ev} = \beta_0 \equiv 1/(2\sigma^2)$. As we shall see later in the context of large N this insensitivity of the generalisation error to the value of the weight decay is associated with a divergence in the variance of the optimal weight decay as the number of examples grows large. This asymptotic insensitivity to the weight decay is a reflection of the fact that our linear student is *mean square consistent*. We will thus focus on the following quantity when assessing the evidence procedure's performance,

$$\kappa_{\epsilon_g}(\lambda_{ev}) = \frac{\epsilon_g(\lambda_{ev}(\mathcal{D})) - \epsilon_g(\lambda_{opt}(\mathcal{D}))}{\epsilon_g(\lambda_{opt}(\mathcal{D}))} \quad . \tag{1}$$

Secondly, it can be shown that $\langle g_{ij} \rangle_{P(\{\mathbf{x}^\mu : \mu = 1..p\})} \propto \delta_{ij}$, then the resulting average free energy, $f = \langle f(\mathcal{D}) \rangle_{P(\mathcal{D})}$ is extremised by $\lambda = \lambda_0$ and $\beta = \beta_0$. Similarly, the average generalisation error is optimised by λ_0. This corresponds to the average case result obtained for the thermodynamic limit in [1] but is valid for all N and p. Thus, the particular conclusion, of the thermodynamic average case analysis, for the learnable linear scenario, that the evidence procedure optimises average performance is valid for all N and in this sense the procedure is unbiased.

Finally using results of [9] [2] one can show that the variance, over possible realisations of the data set, of the free energy, $f(\mathcal{D})$ is order $\mathcal{O}(1/N)$ as we approach the thermodynamic limit; it is a self averaging quantity. Similarly, it can also be shown that the generalization error is self averaging. This means that in the thermodynamic limit the behaviour exhibited by the system for any particular data set will correspond to the average case behaviour, that is the fluctuations around the average vanish. Thus, the average case analysis of [1] corresponds to the case for a *particular data set* because their results were obtained in the thermodynamic limit.

4 Data Dependent Hyperparameter Assignment

Having now established that the evidence procedure is unbiased and that the free energy and performance measures are self averaging we now wish to examine the system behaviour for particular data sets of finite size. This is clearly the regime

[1] Where $\mathrm{N}(\bar{\mathbf{x}}, \sigma)$ denotes a normal distribution with mean $\bar{\mathbf{x}}$ and variance σ^2.

[2] Alternatively one can show this result using diagrammatic methods.

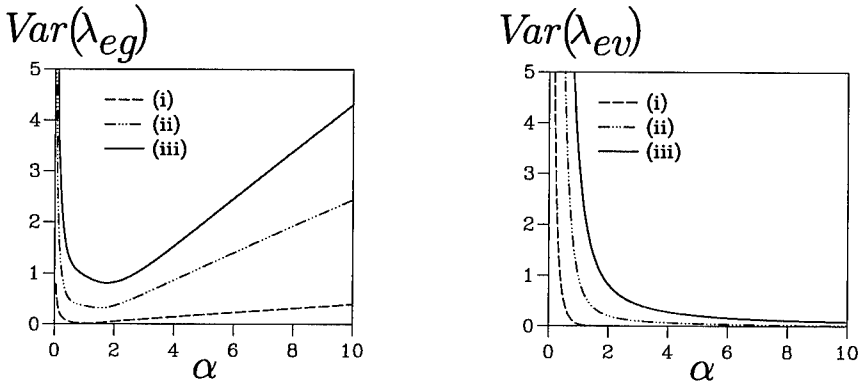

Figure 1 The variance in the optimal weight decay ($Var(\lambda_{eg})$) for various noise levels, (i) $\lambda_0 = 0.04$, (ii) $\lambda_0 = 0.25$ and (iii) $\lambda_0 = 4/9$ is shown in the left-hand graph. Notice the linear divergence in α which corresponds to our result in section 3.1 that, for sufficiently large p, the generalization error is independent of λ. The variance in the evidence optimal weight decay ($Var(\lambda_{ev})$) is shown, in the right-hand graph, for the same noise levels. The $\mathcal{O}(1/\alpha)$ decay of this quantity is a reflection of the fact that for large p $\lambda_{ev}(\mathcal{D}) = \lambda_0$.

of interest to *real world* applications since one is then in the business of optimising performance based on a particular data set. To obtain the hyperparameter assignments made by the evidence procedure we must simultaneously solve $\partial_\lambda f(\mathcal{D}) = 0$ and $\partial_\beta f(\mathcal{D}) = 0$, where $\partial_\theta f \equiv \partial f/\partial\theta$. We can linearize these equations, close to the thermodynamic limit, by expanding around $\lambda = \lambda_0$ and $\beta = \beta_0$. Similarly, we can also expand the true optimal weight decay about the thermodynamic limit value, λ_0.

We find that (co)-variances of these quantities are $\mathcal{O}(1/N)$. Figure 1 shows, to first order, the scaled variances [3] in the evidence optimal weight decay, $Var(\lambda_{ev})$ and that in the true optimal weight decay, $Var(\lambda_{opt})$. The asymptotic $\mathcal{O}(1/\alpha)$ decay of the former reflects the fact that, as discussed in section 3.1, $\lim_{\alpha\to\infty} \lambda_{ev}(\mathcal{D}) = \lambda_0$. Similarly, the divergence of the latter is indicative of the insensitivity of the generalization error to the weight decay for large α. The divergence of both curves for small α is order $\mathcal{O}(1/N\alpha)$ and reflects the break down of the thermodynamic limit when the number of examples p does not scale with the system size N,

Similarly we find that the average squared distance between the evidence assignment and the optimal, $< (\lambda_0(\mathcal{D}) - \lambda_{ev}(\mathcal{D}))^2 >_{P(\mathcal{D})}$, is order $\mathcal{O}(1/N)$. This distance is *non zero*, except for $\alpha > 1$ in the noiseless limit. Further, in the large α limit this distance diverges, revealing the inconsistency of the evidence weight decay assignment.

4.1 Effects on Performance

We now examine the effects on performance of this sub-optimal hyperparameter assignment. Firstly, to order $\mathcal{O}(1/\sqrt{N})$ the optimal performance, $\epsilon_g(\lambda_{opt}, \mathcal{D})$, and that resulting from use of the evidence procedure, $\epsilon_g(\lambda_{ev}, \mathcal{D})$ are the same. However,

[3] *i.e.* N times the true variances

to order $\mathcal{O}(1/N)$ they differ thus we can write the correlation between them, somewhat suggestively, as $1 - \mathcal{O}(1/N)$. Unfortunately, we are unable to calculate this correlation to $\mathcal{O}(1/N)$. Therefore, we examine $< \kappa_{\epsilon_g} >_{P(\mathcal{D})}$ which tends to $1/N$ in the limit of large α reflecting the inconsistency of the evidence weight decay assignments. In the limit of no noise for $\alpha > 1$ we find that $< \kappa_{\epsilon_g} >_{P(\mathcal{D})} = (\alpha+1)/N(\alpha-1)$ revealing that even for small noise levels the evidence procedure is sub-optimal.

4.2 Comparison with Cross-validation

Given, that the evidence procedure is sub-optimal it is natural to ask if another model selection criteria could do better. Here we compare the evidence procedure with leave-one-out cross-validation using simulations of a 1-dimensional system. That is we set the weight decay using the cross-validatory estimate and the evidence estimate and compare the resulting generalisation error to the optimal. The results, averaged over 1000 realisations of the data set for each value of p, are plotted in figure 2. These show that the evidence weight decay assignment results in sub-optimal performance with $\epsilon_g(\lambda_{ev}, \mathcal{D})$ not fully correlated with $\epsilon_g(\lambda_0, \mathcal{D})$. Moreover, the left-hand graph shows that the resulting error from the cross-validatory estimate correlates more strongly with the optimal generalisation error than does that resulting from the evidence estimate. In addition, the right-hand graph shows that the fractional increase in the generalisation error is considerably larger for the evidence procedure than for cross-validation.

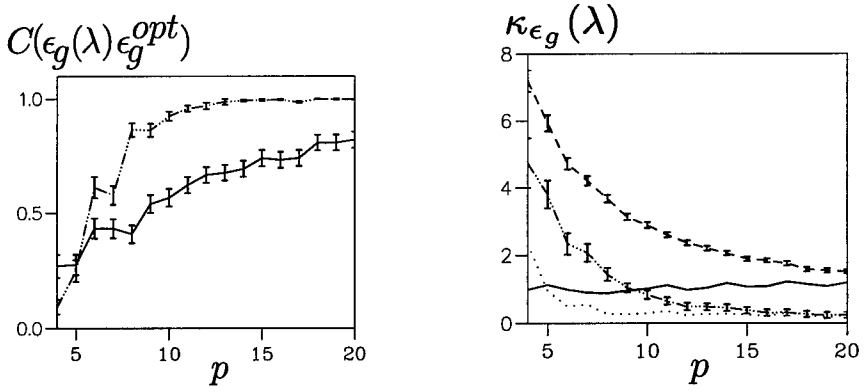

Figure 2 1-D simulation results: The left-hand graph shows the correlation between the optimal generalization error and those obtained using the evidence (solid) and cross-validation (chain) with $\lambda_0 = 1.0$. The right-hand graph shows the fractional increase in generalization error $\kappa_{\epsilon_g}(\lambda) = (\epsilon_g(\lambda) - \epsilon_g(\lambda_{opt}))/\epsilon_g(\lambda_{opt})$. λ is set by the evidence (dashed) and by cross-validation (chain) for $\lambda_0 = 1.0$. For $\lambda_0 = 0.01$ the evidence case is the solid curve cross-validation the dotted curve. In the latter case the error bars are not shown for the sake of clarity.

5 Conclusion

We have shown that, despite thermodynamic and average case results to the contrary, model selection based on the evidence does not optimise performance even in the learnable linear case. In addition, numerical studies indicate that for small systems cross-validation is closer, than the evidence procedure, to optimal perfor-

mance. However, for large systems the evidence might still be a reasonable alternative to the computationally expensive cross-validation.

REFERENCES

[1] Bruce A D and Saad D, *Statistical mechanics of hypothesis evaluation.* J. of Phys. A: Math. Gen. Vol. 27 (1994), pp3355–3363.

[2] MacKay D J C, *Bayesian interpolation*, Neural Comp. Vol. 4 (1992), pp415–447.

[3] Marion G and Saad D, *A statistical mechanical analysis of a Bayesian inference scheme for an unrealizable rule.* J. of Phys. A: Math. Gen. Vol. 28 (1995), pp2159–2171.

[4] Marion G and Saad D, *Finite size effects in Bayesian model selection and generalization.* J. of Phys. A: Math. Gen. Vol. 29 (1996), pp5387–5404.

[5] Sollich P, *Finite-size effects in learning and generalization in linear perceptrons.* J. of Phys. A: Math. Gen. Vol. 27 (1994), pp7771–7784.

[6] Stone M, *An asymptotic equivalence of choice of model by cross-validation and Akaikes criterion*, J. Roy. Statist. Soc. Ser. B Vol. 39 (1977), pp44–47.

[7] Watkin T L H, Rau A, Biehl M, *The statistical mechanics of learning a rule.* Reviews of Modern Physics Vol. 65 (1993), pp499–556.

Acknowledgements

The authors wish to thank the Physics Department, University of Edinburgh where this work was conducted.

TRAINING RADIAL BASIS FUNCTION NETWORKS BY USING SEPARABLE AND ORTHOGONALIZED GAUSSIANS

J. C. Mason, I. J. Anderson, G. Rodriguez* and S. Seatzu*

School of Computing and Mathematics, University of Huddersfield, Queensgate, Huddersfield HD1 3DH, UK.

** Department of Mathematics, University of Cagliari, viale Merello 92, 09123 Cagliari, Italy.*

Radial basis function (RBF) networks have the great advantage that they may be determined rapidly by solving a linear least squares problem, assuming that good positions for the radial centres may be selected in advance. Here it is shown that, if there is some structure in the data, for example if the data lie on lines, then variables in Gaussian RBFs may be separated and a near-optimal least squares solution may be obtained rather efficiently. Second, it is shown that a system of Gaussian RBFs with structured or scattered centres may be orthogonalized over a continuum or discrete data set and thereafter the least squares solution is immediate. Keywords: Gaussians, orthogonalization, RBF, separability.

1 Introduction

Suppose that there are m input data $\mathbf{x}^{(1)}, \ldots, \mathbf{x}^{(m)}$, and that each datum $\mathbf{x}$ has d components $x_1, \ldots, x_d$. Suppose that we adopt a radial basis function network with the centres $\mathbf{w}^{(1)}, \ldots, \mathbf{w}^{(n)}$, given by $\mathbf{w}^{(i)} = \left(w_1^{(i)}, w_2^{(i)}, \ldots, w_d^{(i)}\right)'$, for $i = 1, \ldots, n$. The components, $w_j^{(i)}$ of the centres are "weights" in the network, between the input and hidden layer. Frequently good choices of centres may be made by clustering techniques [3], and so we assume $w_j^{(i)}$ to be fixed. Suppose that coefficients c_i, for $i = 1, \ldots, n$, are associated with radial basis (transfer) functions $\phi_i(r)$ applied to the argument r_i, where

$$r_i = \left[\sum_j \left(x_j - w_j^{(i)}\right)^2\right]^{1/2} = \left\|\mathbf{x} - \mathbf{w}^{(i)}\right\|_2 .$$

The coefficients $\{c_i\}$ are weights between the hidden and output layers, and the output function $f(\mathbf{x})$ is approximated by an RBF, $F(\mathbf{x})$, as follows,

$$f(\mathbf{x}) \approx F(\mathbf{x}) = \sum_{i=1}^{n} c_i \phi\left(\left\|\mathbf{x} - \mathbf{w}^{(i)}\right\|_2\right).$$

Frequently the RBFs $\{\phi_i(r)\}$ are taken to be the same function $\phi(r)$ for each i. In this paper we consider the basis function $\phi(r) = \exp(-r^2)$.

2 Separability of Gaussians

The Gaussian has some particular advantages in terms of (i) its separability and (ii) the simplicity of its inner product. In this section, we consider separability and in Section 3 we exploit the inner product in discussing orthogonalization.

If $\phi(r) = \exp(-r^2)$, then

$$\phi(\|\mathbf{x}\|) = \phi(x_1)\phi(x_2)\ldots\phi(x_d).$$

Thus the RBF is a product of d one-dimensional Gaussians.

2.1 Fast Approximation on a Mesh

Suppose that the 2-dimensional data $\mathbf{x} = (x_1, x_2)'$ and the corresponding centres $\mathbf{w} = (w_1, w_2)'$ are each placed on meshes

$$\begin{aligned} \mathbf{x}_{k,\ell} &= \left(x_1^{(k)}, x_2^{(\ell)}\right) \quad \text{for } k = 1, \ldots, m_x \text{ and } \ell = 1, \ldots, m_y, \\ \mathbf{w}_{i,j} &= \left(w_1^{(i)}, w_2^{(j)}\right) \quad \text{for } i = 1, \ldots, n_x \text{ and } j = 1, \ldots, n_y, \end{aligned}$$

where $n_x \leq m_x$ and $n_y \leq m_y$.

Here n_x and n_y are the numbers of different values for the two respective components of the centres, and m_x and m_y are the corresponding numbers of different values for the two components of the data. Then our RBF approximation on the data is

$$f(\mathbf{x}_{k,\ell}) = \sum_{i=1}^{n_x} \left(\sum_{j=1}^{n_y} c_{i,j} \phi(x_2^{(\ell)} - w_2^{(j)}) \right) \phi(x_1^{(k)} - w_1^{(i)}). \tag{1}$$

For each $\ell = 1, \ldots, m_y$, we obtain the (overdetermined) linear system,

$$f(\mathbf{x}_{k,\ell}) = \sum_{i=1}^{n_x} b_i^{(\ell)} \phi(x_1^{(k)} - w_1^{(i)}) \tag{2}$$

for $k = 1, \ldots, m_x$, where, for each $i = 1, \ldots, n_x$, we have the (overdetermined) system

$$b_i^{(\ell)} = \sum_{j=1}^{n_y} c_{i,j} \phi(x_2^{(\ell)} - w_2^{(j)}) \tag{3}$$

for $\ell = 1, \ldots, m_y$.

Using matrix notation, we may express the system of equations (2) as

$$A_x \mathbf{b}^{(\ell)} = \mathbf{f}^{(\ell)}$$

for $\ell = 1, 2, \ldots, m_y$, where A_x is a matrix whose (k, i)th element is $\phi(x_1^{(k)} - w_1^{(i)})$, $\mathbf{b}^{(\ell)}$ is a vector of the elements $b_i^{(\ell)}$ for $i = 1, 2, \ldots, n_x$, and $\mathbf{f}^{(\ell)}$ is a vector of the elements $f(\mathbf{x}_{k,\ell})$ for $k = 1, 2, \ldots, m_x$. We note that the matrix A_x is independent of ℓ and so it is only necessary to factorize it once.

Similarly, we may express the system (3) as

$$A_y \mathbf{c}^{(i)} = \mathbf{b}_i$$

for $i = 1, 2, \ldots, n_x$, Here, the matrix A_y is independent of i and so, again, it is only necessary to factorize this matrix once. Thus, the solution of (2) and (3) by QR factorization can be achieved in $\mathcal{O}(m_y n_x (m_x + n_y))$ operations. This is a great saving over the $\mathcal{O}\left(m_x m_y n_x^2 n_y^2\right)$ operations that would be required if the system (1) of $m_x m_y$ equations were solved by least squares without exploiting any structure.

2.2 Data on Lines

If the data are less structured than a mesh, but do form lines, then fast methods may be adopted. Consider lines of data, where the x_2 values are fixed but the x_1 values are scattered (in different positions on each line). The data abscissae may be written as $(x_1^{(k,\ell)}, x_2^{(\ell)})$, for $k = 1, \ldots, m_\ell$ and $\ell = 1, \ldots, m_y$, so the x_1 values now vary with both k and ℓ. Equations (2) and (3) are still valid, but with $x_1^{(k)}$ and m_x replaced by $x_1^{(k,\ell)}$ and m_ℓ. We may therefore still solve (2) and (3) in the least

squares sense. However, the solution is no longer the true least squares solution of (1). Indeed the solution of (2) now involves a different matrix for each value of ℓ, and this also means that the solution is less efficient — $\mathcal{O}\left(m_x m_y n_x^2\right)$ operations are needed to solve (2), although only $\mathcal{O}\left(m_y n_y n_x\right)$ operations are still required for (3). The method we describe here is the Gaussian RBF analogue of the methods of Clenshaw and Hayes [2] for polynomial approximation and of Anderson, Cox and Mason [1] for spline approximation of data on lines.

3 Orthogonalized Gaussians

Gaussians can be orthogonalized in a number of ways. Suppose that for data $\{\mathbf{x}\} = \left\{(x_1, \ldots, x_d)'\right\}$, we have centres $\mathbf{w}^{(i)}$ for $i = 1, \ldots, n$, and Gaussian RBFs $\phi_i(\|\mathbf{x}\|) = \exp(-\|\mathbf{x} - \mathbf{w}^{(i)}\|^2)$ for $i = 1, \ldots, n$.

Then a general orthogonalization technique, based on the Gram-Schmidt procedure, is to form a new basis $\psi_1, \ldots, \psi_n$ as,

$$\psi_i = \sum_{k=1}^{i} d_k^{(i)} \phi_k \tag{4}$$

$$= \sum_{k=1}^{i} e_k^{(i)} \psi_k \tag{5}$$

for $i = 1, 2, \ldots, n$, where $e_k^{(i)}$ and $d_k^{(i)}$ are appropriate coefficients such that $d_i^{(i)} = 1$ and $e_i^{(i)} = 1$. The values of the remaining coefficients are determined by requiring the new basis functions, $\psi_1, \ldots, \psi_n$, to be orthogonal with respect to some specified inner product. Thus we have

$$< \psi_i, \psi_j >= 0 \qquad \text{for } i \neq j.$$

Let us define

$$t_{i,j} =< \phi_i, \phi_j >, \tag{6}$$

and

$$n_k =< \psi_k, \psi_k >,$$

the values of $t_{i,j}$ being constants that may be calculated once and for all, and the values of n_k being normalization constants. Then, by setting $< \psi_i, \psi_j >= 0$ where (without loss of generality) $i < j$ we deduce, using equations (4) and (5), that

$$e_i^{(j)} = \frac{-1}{n_i} \sum_{k=1}^{i} d_k^{(i)} t_{k,j}. \tag{7}$$

By taking inner products of both sides of equation (5) with themselves, we deduce that

$$n_1 = t_{1,1}, \qquad \text{and} \qquad n_i = t_{i,i} - \sum_{k=1}^{i-1} (e_k^{(i)})^2 n_k. \tag{8}$$

Expanding equation (5) using (4) and equating similar terms, we derive

$$d_i^{(j)} = \sum_{k=i}^{j-1} e_k^{(j)} d_i^{(k)}. \tag{9}$$

Equations (7)–(9) suffice to determine n_k, $e_i^{(j)}$ and $d_i^{(j)}$ for all $i < j$ given values of $t_{i,j}$.

3.1 Continuum

Let us adopt an inner product over $\mathbb{R}^d = (-\infty, \infty)^d$ and define

$$V = \int_{\mathbb{R}^d} \exp(-\|\mathbf{x}\|^2)\,\mathbf{dS} = \int_{\mathbb{R}^d} \exp(-\|\mathbf{x}-\mathbf{w}\|^2)\,\mathbf{dS},$$

for any fixed $\mathbf{w}$. Now $t_{i,j}$ is readily calculated by using the following formula (whose derivation follows from the cosine rule),

$$\|\mathbf{x}-\mathbf{w}^{(i)}\|^2 + \|\mathbf{x}-\mathbf{w}^{(j)}\|^2 = 2\|\mathbf{x}-\mathbf{w}_{ij}\|^2 + \frac{1}{2}\|\mathbf{w}^{(i)}-\mathbf{w}^{(j)}\|^2, \qquad (10)$$

where $\mathbf{w}_{ij} = \frac{1}{2}(\mathbf{w}^{(i)} + \mathbf{w}^{(j)})$.
Now equation (6) becomes,

$$\begin{aligned} t_{i,j} &= <\phi_i, \phi_j> \\ &= \int \exp(-\|\mathbf{x}-\mathbf{w}^{(i)}\|^2 - \|\mathbf{x}-\mathbf{w}^{(j)}\|^2)\,\mathbf{dS} \\ &= \exp(-\frac{1}{2}\|\mathbf{w}^{(i)}-\mathbf{w}^{(j)}\|^2) \int \exp(-2\|\mathbf{x}-\mathbf{w}_{ij}\|^2)\,\mathbf{dS} \\ &= (\sqrt{2})^{-d} V \left(\phi_i(\mathbf{w}^{(j)})\right)^{1/2}. \end{aligned}$$

Thus $t_{i,j}$ is immediately determined from $\{\mathbf{w}^{(i)}\}$ without sums or integrals (V being a scalar multiplier), and the orthogonalization procedure is particularly straightforward.
This inner product is the natural one to use for a continuum of data. Indeed the best least squares approximation to f of the form

$$F(\mathbf{x}) = \sum_{i=1}^{n} c_i \psi_i(\mathbf{x})$$

is defined by setting

$$c_i = < F, \psi_i > / n_i.$$

3.2 Scattered Discrete Data

We might also adopt this inner product for a discrete data set, since it has the advantage of being data independent. The snag is that we do not then obtain a diagonal system for determining a least squares approximation on the data set and must solve

$$[F, \psi_j] = \sum_{i=1}^{n} c_i [\psi_i, \psi_j]$$

for $i = 1, \ldots, n$, where $[F, \phi]$ denotes the inner product over the discrete data set. However, we would expect the matrix with entries $[\psi_i, \psi_j]$ to be "close to diagonal". Alternatively, if we define a discrete inner product over the data $\{\mathbf{x}^{(k)}\}$

$$< f, g >= \sum_{\mathbf{x}^{(k)}} f(\mathbf{x}^{(k)}) g(\mathbf{x}^{(k)})$$

and write

$$S_{k,i} = \exp(-\|\mathbf{x}^{(k)} - \mathbf{w}^{(i)}\|^2) = \phi_i(\mathbf{x}^{(k)})$$

then

$$t_{i,j} =< \phi_i, \phi_j >= (S^{\mathrm{T}} S)_{i,j}$$

where S is the matrix of $S_{k,i}$. Thus we are effectively forming the components of the normal matrix. The calculation is similar to that of Section 3.1, except that $S^{\mathrm{T}}S$ is now used rather than S (hence requiring a more complicated calculation).

4 Results

The validity of the procedure of Section 3.2 has been successfully tested by using orthogonalized RBFs to recognize the ten digits 0,. . .,9 from their pixel patterns — we do not have sufficient space here to give details, but note that the procedure is very fast compared with using back propagation procedures and sigmodal approximations. We have also calculated condition numbers for a variety of RBF matrices which occur in data fitting, and there are apparent advantages for conditioning in using orthogonality on a continuum rather than on a discrete data set. However further work is needed to develop an orthogonalization algorithm which consistently improves conditioning compared with the use of a conventional Gaussian basis.

REFERENCES

[1] I. J. Anderson, M. G. Cox and J. C. Mason, *Tensor-product spline interpolation to data on or near a family of lines.* Numerical Algorithms, Vol. 5 (1993), pp193–204.

[2] C. W. Clenshaw and J. G. Hayes, *Curve and surface fitting.* J. Inst. Math. Appl., Vol. 1 (1965), pp164–183.

[3] J. D. Mason, R. J. Craddock, J. C. Mason, P. C. Parks and K. Warwick, *Towards a stability and approximation theory for neuro-controllers.* Control 94. IEE Pub. 389 (1994), pp100–103.

ERROR BOUNDS FOR DENSITY ESTIMATION BY MIXTURES

Ronny Meir and Assaf J. Zeevi

Electrical Engineering Department, Technion, Haifa 32000, Israel.

We consider the problem of estimating a density function from a sequence of N independent and identically distributed observations $\mathbf{x}_i$ taking values in $\mathbb{R}^d$. The estimation procedure constructs a convex mixture of 'basis' densities and estimates the parameters using the maximum likelihood method. Viewing the error as a combination of two terms, the approximation error measuring the adequacy of the architecture, and the estimation error resulting from the finiteness of the sample size, we derive upper bounds to the total error, thus obtaining bounds for the rate of convergence. These results then allow us to derive explicit expressions relating the sample complexity and model complexity needed for learning.

1 Introduction

There have traditionally been two principal approaches to density estimation, namely the parametric approach which makes stringent assumptions about the density, and the nonparametric approach which is essentially distribution free. In recent years, a new approach to density estimation, often referred to as the method of sieves [2] has emerged. In this latter approach, one considers a family of parametric models, where each member of the family is assigned a 'complexity' index in addition to the parameters. In the process of estimating the density one usually sets out with a simple model (low complexity index) slowly increasing the complexity of the model as the need may be. This general strategy seems to exploit the benefits of both the parametric as well as the nonparametric approaches, namely fast convergence rates and universal approximation ability, while not suffering from the drawbacks of the other methods. In this paper we consider the representation of densities as convex combinations of 'basis' densities, thus permitting an interpretation as a mixture model. We split the problem into two separate issues, namely approximation and estimation, which are discussed at more length in section 2.

2 Statement of the Problem

The problem of density approximation by convex combinations of densities can be phrased as follows: we wish to approximate a class of density functions, by a convex combination of 'basis' densities. In this work we consider the class, $\mathcal{F}$, of compactly supported and continuous a.e density functions. We thus seek linear combinations of densities of the form

$$f_n^\theta(\mathbf{x}) = \sum_{i=1}^{n} \alpha_i \phi(\mathbf{x}; \boldsymbol{\theta}_i) \qquad (\alpha_i > 0 \quad \& \quad \sum_{i=1}^{n} \alpha_i = 1), \tag{1}$$

where $\phi(\mathbf{x}; \boldsymbol{\theta}_i)$ represent a family of densities, the members of which are parameterized by the parameter vectors $\{\boldsymbol{\theta}_i\}$. We denote the full set of parameters by $\boldsymbol{\theta}$, namely $\boldsymbol{\theta} = \{\{\alpha_i\}, \{\boldsymbol{\theta}_i\}\}$. In particular, we wish to find values n^* and $\boldsymbol{\theta}^*$ such that for any $\epsilon > 0$, $d(f, f^*) \leq \epsilon$, where f^* is the value of f_n^θ evaluated at $\boldsymbol{\theta} = \boldsymbol{\theta}^*$ and $n = n^*$. This objective can be attained by a specific choice of the basis densities ϕ, so that $\cup_{n=1}^{\infty} f_n^\theta$ is dense in $\mathcal{F}$ (see [2] for exact conditions). Here $d(f, g)$ represents some generic distance function between densities f and g, whose exact form will be specified in the next section. We note that in the usual formulation of mixture

estimation, one usually considers a fixed value of n, assuming that the true density is a member of the class. In our formulation n is a parameter, whose magnitude will be bounded.

Another line of recent work is that of function approximation through linear combinations of non-linearly parameterized 'basis' functions (for example neural networks). The novel feature concerning the representation given in eq. (1), as compared with the function approximation literature, is that we demand the coefficients α_i to be nonnegative and sum to one, and moreover require the functions $\phi(\mathbf{x};\boldsymbol{\theta})$ to be densities, i.e. $\phi(\mathbf{x};\boldsymbol{\theta}) > 0$ and $\int \phi(\mathbf{x};\boldsymbol{\theta})d\mathbf{x} = 1$.

As discussed above, the establishment of the existence of a good approximating density f^* is only the first step in the estimation procedure. One still needs to consider an effective procedure, whereby the optimal function can be obtained, at least in the limit of an infinite amount of data. Assuming the estimation is based on the finite data set $\{\mathbf{x}_i\}_{i=1}^N$, and denoting the estimated density by $\hat{f}_{n,N}$,the minimal requirement (referred to as consistency) is that $\hat{f}_{n,N} \to f^*$ as $N \to \infty$, where the convergence takes place in some well defined probabilistic sense. Since we are interested in this paper in convergence rates, we will in fact make use of stronger results [4] which actually characterize the rates at which the above convergence takes place (see section 4).

In summary then, the basic issue we address in this work is related to the relationship between the approximation and estimation errors and (i) the dimension of the data, d, (ii) the sample size, N, and (iii) the complexity of the model class parameterized by n.

3 Preliminaries

In order to discuss approximation of densities we must define an appropriate distance measure, $d(f,g)$, between densities f and g. A commonly used measure of discrepancy between densities is the so-called Kullback-Leibler (KL) divergence, given by $d_{\mathrm{K}}(f||g) = \int f \log \frac{f}{g}$. As is obvious from the definition, the KL divergence is not a true distance function since it is not symmetric. To circumvent this problem one often resorts to an alternative definition of distance, namely the squared Hellinger distance $d_{\mathrm{H}}^2(f,g) = \int \left(\sqrt{f} - \sqrt{g}\right)^2$, which can be shown to be a true metric and is particularly useful for problems of density estimation.

Using the results of [2] concerning the method of sieves we conclude that under appropriate conditions on ϕ, the target density f belongs to the closure of the convex hull of the set of basis densities $\Phi = \{\phi(\cdot,\boldsymbol{\theta})\}$. The question arises, however, as to how many terms are needed in the convex combination in order to achieve an approximation error smaller than some arbitrary $\epsilon > 0$. The answer to this question can be obtained using a remarkable lemma of Maurey which is proved for example in [1].

4 Main Results

Using the results of Maurey referred to above, it can be shown that given any $\epsilon > 0$ one can construct a convex combination of densities, $\phi_\sigma \in \Phi$, in such a way that the total error between an arbitrary density and the model is smaller than ϵ. We consider now the problem of estimating a density function from a sequence of d-dimensional samples, $\{\mathbf{x}_i\}$, $i = 1,2,\ldots,N$, which will be assumed throughout to be independent and identically distributed according to $f(\mathbf{x})$. As in eq. (1) we let

n denote the number of components in the convex combination. The total number of parameters will be denoted by m, which in the problem studied here is $O(nd)$.
In the remainder of this section we consider the problem of estimating the parameters of the density through a specific estimation scheme, namely maximum likelihood, corresponding to the optimization problem, $\hat{\boldsymbol{\theta}}_{n,N} = \text{argmax}_{\theta} L(\mathbf{x}^N; \boldsymbol{\theta})$ where $L(\mathbf{x}^N; \boldsymbol{\theta})$ is the likelihood function, $L(\mathbf{x}^N; \boldsymbol{\theta}) = \prod_k f_n^{\theta}(\mathbf{x}_k)$, $\mathbf{x}^N = \{\mathbf{x}_i\}_{i=1}^N$ and $f_n^{\theta}(\mathbf{x}) = \sum_{i=1}^n \alpha_i \phi(\mathbf{x}; \boldsymbol{\theta}_i)$. We denote the value of $f_{n,N}^{\theta}$ evaluated at the maximum likelihood estimate by $\hat{f}_{n,N}$. Now, for a fixed value of n, the finite mixture model, f_n^{θ}, may not be sufficient to approximate the density f, to the required accuracy. Thus, the model for finite n falls into the so called class of misspecified models [4] and the procedure of maximizing L should more properly be referred to as quasi maximum likelihood estimation. Thus, $\hat{\boldsymbol{\theta}}_{n,N}$ should be referred to as the quasi maximum likelihood estimator. Since the data are assumed to be i.i.d, it is clear from the strong law of large numbers that $\frac{1}{N} L(\mathbf{x}^N; \boldsymbol{\theta}) \rightarrow E \log f_n^{\theta}(\mathbf{x})$ almost surely as $N \rightarrow \infty$, where the expectation is taken with respect to the true (but unkown) density, $f(\mathbf{x})$, generating the examples. From the trivial equality $E \log f_n^{\theta}(\mathbf{x}) = -d_{\text{K}}(f \| f_n^{\theta}) + E \log f(\mathbf{x})$ we see that the maximum likelihood estimator $\hat{\boldsymbol{\theta}}_{n,N}$ is asymptotically given by $\boldsymbol{\theta}_n^*$, where $\boldsymbol{\theta}_n^* = \arg\min_{\theta} d_{\text{K}}(f \| f_n^{\theta})$. For further discussion see [4].
Now, the quantity of interest in density estimation is the distance between the true density, f, and the density obtained from a finite sample of size N. Using the previous notation and the triangle inequalitiy for metric $d(\cdot, \cdot)$ we have $d(f, \hat{f}_{n,N}) \leq d(f, f_n^*) + d(f_n^*, \hat{f}_{n,N})$. This inequality stands at the heart of the derivation which follows. We will show that the first term, namely the *approximation error*, is small. This demonstration utilizes Maurey's lemma as well as several inequalities. In order to evaluate the second term, the *estimation error*, we make use of the results of White [4] concerning the asymptotic distribution of the quasi maximum likelihood estimator $\hat{\boldsymbol{\theta}}_{n,N}$. The splitting of the error into two terms in the triangle inequality, is closely related to the expression of the mean squared error in regression as the sum of the bias (related to the approximation error) and the variance (akin to the estimation error).
As mentioned above, Maurey's lemma provides us with an existence proof, in the sense that there exists a parameter value $\boldsymbol{\theta}^0$ such that the error of the combination (1) is smaller than c/n. Since we are dealing here with a specific estimation scheme, namely maximum likelihood, which asymptotically approaches a particular parameter value $\boldsymbol{\theta}_n^*$, the question we ask, however, is whether the parameter $\boldsymbol{\theta}_n^*$ obtained through the maximum likelihood procedure also gives rise to an approximation error of the same order as that of $\boldsymbol{\theta}^0$. The answer to this question is affirmative, as we demonstrate in the next theorem, which is the first main result of this section.

Theorem 1 *(Approximation error) Given appropriate assumptions, the Hellinger distance between the true density f and the density f_n^* minimizing the Kullback-Leibler divergence, is bounded as follows: $d_{\text{H}}^2(f, f_n^*) \leq \epsilon + \frac{C_{\mathcal{F},\Phi}}{n}$ where $C_{\mathcal{F},\Phi}$ is a constant depending on the class of target densities $\mathcal{F}$ and the family of basis densities Φ and ϵ is an arbitrary precision constant.*

Proof (sketch) The proof follows by a series of inequalities relating the Kullback-Leibler divergence and the Hellinger distance. By bounding the KL divergence from above and below by the Hellinger distance and utilizing the fact that the maximum likelihood estimator minimizes the KL divergence we conclude the proof. □

We note that the arbitrary precision constant ϵ appearing in the theorem can be eliminated by restricting attention to densities belonging to the *information closure*, defined as $\bar{\mathcal{G}} = \{f \in \mathcal{F} \mid \inf_{g\in\mathcal{G}} d_{\mathrm{K}}(f\|g) = 0\}$, where $\mathcal{G} = \cup\mathcal{G}_n$ and $\mathcal{G}_n$ comprises all convex combinations of n terms as in (1). We will restrict ourselves in the sequel to this subspace. We stress that the main point of theorem 1 is the following. While Maurey's lemma guarantees the existence of a parameter value $\boldsymbol{\theta}^0$ and a corresponding function f_n^0 which lies within a distance of $O(1/n)$ from f, it is not clear apriori that f_n^*, evaluated at the quasi maximum likelihood estimate, $\boldsymbol{\theta}_n^*$, is also within the same distance from f. Theorem 1 establishes this fact.

Up to now we have been concerned with the first part of the triangle inequality. In order to bound the *estimation error* resulting from the maximum likelihood method, we need to consider now the second term in the same equation. To do so we will need to make use of a lemma of White [4], which characterizes the asymptotic distribution of the estimator $\hat{\boldsymbol{\theta}}_{n,N}$ obtained through the quasi maximum likelihood procedure. A quantity of interest, which will be used is $C(\boldsymbol{\theta}) = A(\boldsymbol{\theta})^{-1}B(\boldsymbol{\theta})A(\boldsymbol{\theta})^{-1}$ where $A(\boldsymbol{\theta}) = E\left[\nabla\nabla^T \log f_n^\theta(\mathbf{x})\right]$ and $B(\boldsymbol{\theta}) = E\left[\left(\nabla \log f_n^\theta(\mathbf{x})\right)\left(\nabla \log f_n^\theta(\mathbf{x})\right)^T\right]$ with the expectations taken with respect to the true density f, and the gradient operator ∇ represents differentiation with respect to $\boldsymbol{\theta}$. White's lemma then proceeds to give sufficient conditions so that the distribution of the quasi maximum likelihood estimator is asymptotically normal.

Finally, we will make use of the Fisher information matrix defined with respect to the density f_n^*, which we shall refer to as the pseudo-information matrix, given by $I^* = E^*[\nabla \log f_n^*(\mathbf{x})\nabla \log f_n^*(\mathbf{x})^T]$. The expectation E^* is taken with respect to f^*, the density f_n^θ evaluated at $\boldsymbol{\theta} = \boldsymbol{\theta}^*$. Denoting expectations over the data (according to the true density f) by $E_{\mathcal{D}}[\cdot]$, we have:

Theorem 2 *(Error bound) For sample size N sufficiently large, and given appropriate smoothness assumptions (see [4]), the expected estimation error,*

$$E_{\mathcal{D}} d_{\mathrm{H}}^2(f, \hat{f}_{n,N}),$$

obtained from the quasi maximum likelihood estimator, $\hat{f}_{n,N}$, is bounded as follows: $E_{\mathcal{D}}\left[d_{\mathrm{H}}^2(f, \hat{f}_{n,N})\right] \leq O\left(C_{\mathcal{F},\Phi}/n\right) + O\left(m^*/N\right)$, where d denotes the data dimension, and $m^* = \mathrm{Tr}(C^*I^*)$ with C^* and I^* given above.

Proof (sketch) The initial step in the proof is to expand $d_H^2(f_n^*, \hat{f}_{n,N})$ to a first order Taylor series with remainder. Some simple algebraic manipulations yield an approximation in terms of the quasi maximum likelihood estimator and the pseudo information matrix. Taking expectation with respect to the data we obtain the bound $O\left(\frac{m^*}{N}\right)$ utilizing the asymptotic results of White (1982). The final derivation follows by the triangle inequality and the approximation bound. □

If we take $n, N \to \infty$ so that $(n/N) \to 0$ the matrix C^* converges to the inverse of the 'true' density Fisher information matrix, which we shall denote by $I^{-1}(\boldsymbol{\theta})$, and

the pseudo-information matrix, I^*, converges to the Fisher information $I(\theta)$. This argument follows immediately from Theorem 2, which ensures the convergence of the misspecified model to the 'true', underlying density. Therefore their product converges to the identity matrix, with a dimension of the parameter vector $m = n(d+2)$. The bound on the estimation error will therefore be given asymptotically by $E_{\mathcal{D}}\left[d_{\mathrm{H}}^2(f, \hat{f}_{n,N})\right] \leq O\left(\frac{C_{\mathcal{F},\Phi}}{n}\right) + O\left(\frac{nd}{N}\right)$ which is valid in the limit ($N \to \infty$, $n \to \infty$, $\frac{n}{N} \to 0$). The optimal complexity index n may be obtained from the asymptotic convergence rate bound, and is given by $n_{\mathrm{opt}} = (C_{\mathcal{F},\Phi} N/d)^{1/2}$ where d is the dimension of the data in the sample space.

We remark that the parameter m^* may be interpreted as the *effective number* of parameters of the model, under the misspecification of finite n. This parameter correlates the misspecified model's generalized information matrix C^*, with the pseudo-information matrix related to the density f_n^*, so that the effect of misspecification results in a modification in the number of *effective* parameteres.

5 Discussion

We have considered in this paper the problem of estimating a density function over a compact domain X. Specifically, the problem is phrased in the language of mixture models, for which a great deal of theoretical and practical results are available. Moreover, one can immediately utilize the powerful EM algorithm for estimating the parameters. Finally, we comment that the method we used, namely combining approximation error bounds with White's framework for misspecified models, gave rise to lower estimation bounds than those obtained so far for function estimation. We believe that this result is not restricted to density estimation, and can be directly applied to function estimation using, for example, least-squares estimation.

REFERENCES

[1] A. R. Barron, *Universal Approximation Bounds for Superpositions of a Sigmoidal Function*, IEEE Trans. Inf. Theory, Vol. 39(3) (1993), pp930-945.

[2] S. Geman and C. Hwang, *Nonparametric density estimation by the method of sieves*, Ann. Statist., Vol. 13(2) (1982) pp435-475.

[3] M. I. Jordan and R. A. Jacobs, *Hierarchical mixtures of experts and the EM algorithm*, Neural Computation, Vol. 6 (1994), pp181-214.

[4] H. White, *Maximum Likelihood Estimation of Misspecified Models*, Econometrica, Vol. 50(1) (1982), pp1-25.

Acknowledgements

The authors thank Robert Adler, Paul Feigin and Allan Pinkus for helpful discussions.

ON SMOOTH ACTIVATION FUNCTIONS

H. N. Mhaskar

Department of Mathematics, California State University
Los Angeles, California, 90032, USA.

We had earlier constructed neural networks which are capable of providing optimal approximation rates for smooth target functions. The activation functions evaluated by the principal elements of these networks were infinitely many times differentiable. In this paper, we prove that the parameters of any network with these two properties must satisfy certain lower bounds. Our results can also be thought of as providing a rudimentary test for the hypothesis that the unknown target function belongs to a Sobolev class.

1 Introduction

The notion of a *generalized translation network* was introduced by Girosi, Jones and Poggio [4] (*generalized regularization networks* in their terminology). Let $1 \le d \le s$ be integers, and $\phi : \mathbb{R}^d \to \mathbb{R}$ be a fixed function. A generalized translation network with n *neurons* evaluates a function of the form

$$\sum_{k=1}^{n} a_k \phi(A_k \mathbf{x} + \mathbf{b}_k), \tag{1}$$

where $\mathbf{x} \in \mathbb{R}^s$, a_k's are real numbers, $\mathbf{b}_k$'s are vectors in $\mathbb{R}^d$, and A_k's are $d \times s$ real matrices. This mathematical model includes the traditional neural networks, where $d = 1$, as well as the radial basis function networks, where $d = s$, A_k's are all equal to the $s \times s$ identity matrix, and ϕ is a radial function. Girosi, Jones, and Poggio have discussed the importance of the more general networks for applications in computer graphics, robotics, control, image processing, etc., as well as emphasized the need for a theoretical investigation of the capabilities of these networks for function approximation.

One important reason for using generalized translation networks for function approximation is to obtain a concrete, trainable model for the typically unknown target function. Some of the features required of the model are the following. Of course, the model should approximate the target function within a given margin of error, utilizing as few neurons as possible. It is also desirable that the function evaluated by the model be smoother than the target function. Moreover, it is also expected that the parameters $a_k, A_k, \mathbf{b}_k$ of the model remain bounded as the margin of error approaches zero. In this paper, we prove that these goals are incompatible with each other: the parameters of a model that evaluates a good approximation, with ϕ smoother than the target function, must tend to infinity as the margin of error tends to zero. In order to motivate this result further, we first review certain known "positive" results.

It is well known [1], [2], [5], [6] that an arbitrary continuous function of s variables can be approximated arbitrarily closely on an arbitrary compact subset of $\mathbb{R}^s$ by neural networks. A similar result was established in [8] for the case of generalized translation networks. A deeper problem in this context is to determine the number of neurons required to approximate all functions in a given function class within a given margin of error. Equivalently, one seeks to estimate the *degree of approximation* of the target function in terms of the number of neurons, n. Since the target function is typically not known in advance, it is customary to assume that

it belongs to some known function class. A simple assumption is that the function possesses continuous derivatives up to order r, where $r \geq 1$ is some integer. It is well known [12] that for any function satisfying this condition, there is an algebraic polynomial of degree not exceeding m, which gives a uniform approximation to this function on $[-1,1]^s$ with an order of accuracy $\mathcal{O}(m^{-r})$. In terms of the number n of parameters involved, this order is $\mathcal{O}(n^{-r/s})$. According to a result of DeVore, Howard, and Micchelli [3], this is asymptotically the best order of approximation that can possibly be achieved for the entire class of target functions, using any "reasonable" approximation process involving n parameters. It is an open problem to determine whether the same degree of approximation can be achieved with generalized translation networks. One expects that the actual degree of approximation should depend upon certain growth and smoothness characteristics of the *activation function* ϕ.

This author and Micchelli investigated this problem in detail in [10], starting with the case when both the target function and the activation function are 2π-periodic. When ϕ is a 2π- periodic function, we were able to approximate the trigonometric monomials by generalized translation networks, with a bound on the accuracy of approximation in terms of the trigonometric degree of approximation of ϕ. This turned out to be a very fruitful idea, enabling us to establish a connection between the degree of approximation provided by generalized translation networks on one hand, and the degree of trigonometric polynomial approximation to the target function and to the activation function ϕ on the other hand. The general theorem was applied to the case when ϕ is not periodic, establishing degree of approximation theorems for a very wide class of activation functions. As far as we are aware, our estimates on the degree of approximation by radial basis functions were the first of their kind, in that the estimates were in terms of the number of function evaluations, rather than a scaling factor. These results were announced in [11]. In [10], we constructed networks to provide to an optimal recovery of functions, as well as networks to provide simultaneous approximation of a function and its derivatives. The idea was also applied in [9] to obtain certain *dimension-independent bounds.* Both in [9] and [10], we give explicit constructions of the networks. The results indicated that both the growth and smoothness of the activation function play a role in the complexity problem.

In [7], we concentrated on activation functions that are infinitely often differentiable in an open set, and for which there is at least one point in this open set at which none of the partial derivatives is zero. Using the ideas in the paper [6] of Leshno, Lin, Pinkus, and Schocken, we proved that generalized translation networks with such activation functions provide the optimal degree of approximation for all smooth functions. We also obtained estimates for the approximation of analytic functions. The activation functions to which our results are applicable include the squashing function, $(1+e^{-x})^{-1}$ when $d=1$, and the Gaussian function, the thin plate splines, and multiquadrics, when $1 \leq d \leq s$. We give explicit constructions, and the matrices A_k and "thresholds" $\mathbf{b}_k$ in the networks thus obtained are uniformly bounded, independently of the degree of approximation desired. Unfortunately, the coefficients a_k in the networks may grow exponentially fast as the desired degree of approximation tends to zero.

In this paper, we demonstrate that this phenomenon cannot be avoided if the activation function is a bounded analytic function in a poly-strip; the coefficients and the matrices cannot all be bounded independently of the desired degree of approximation. This fact persists even if ϕ satisfies less stringent conditions. In particular, all the special functions ϕ mentioned above necessarily have this drawback. For the sake of simplicity, we have presented our results in the context of uniform approximation. They are equally valid when the approximation is considered in an L^p space.

2 Main Results

Let $k, m \geq 1$ be integers, and B be a closed subcube of $\mathbb{R}^m$ (not necessarily compact). The class of all functions $f : \mathbb{R}^m \to \mathbb{R}$ having continuous and bounded partial derivatives of order up to (and including) k on B will be denoted by C_B^k. In this section, we prove that if the activation function $\phi \in C^\ell_{\mathbb{R}^d}$ for some integer $\ell \geq 1$, and the target function f is not infinitely often differentiable on $[-1,1]^s$, then the coefficients a_k in any generalized translation network of the form (1) that provides a uniform approximation of f on $[-1,1]^s$ must satisfy certain lower bounds. These lower bounds will be obtained in terms of the norms of the matrices A_k. If $\mathbf{x} = (x_1, \ldots, x_m) \in \mathbb{R}^m$, we define

$$|\mathbf{x}|_m := \max_{1 \leq j \leq m} |x_j|. \tag{2}$$

If $d, s \geq 1$ are integers, and A is a $d \times s$ matrix, we define its norm by

$$||A|| := \max_{|\mathbf{x}|_s \leq 1} |A\mathbf{x}|_d. \tag{3}$$

In the sequel, $c, c_1, \cdots$ will denote positive constants, which may depend upon fixed quantities, such as ϕ, d, and s, and other indicated parameters only.
We prove the following theorem.

Theorem 1 *Let $1 \leq d \leq s$, $\ell, r \geq 1$ be integers, and α, ϵ be positive real numbers. Suppose that $\phi \in C^\ell_{\mathbb{R}^d}$, $f : [-1,1]^s \to \mathbb{R}$, and $f \notin C^r_{[a,b]^s}$ for some $[a,b] \subset (-1,1)$. Suppose that for every integer $n \geq 1$, there exists a generalized translation network*

$$\mathcal{N}_n(\mathbf{x}) := \sum_{k=1}^{n} a_{k,n} \phi(A_{k,n}\mathbf{x} + \mathbf{b}_{k,n}), \tag{4}$$

such that

$$|f(\mathbf{x}) - \mathcal{N}_n(\mathbf{x})| \leq c n^{-\alpha}, \qquad \mathbf{x} \in [-1,1]^s, \tag{5}$$

where c is a positive constant that may depend upon f, ϕ, d, s, and α but is independent of n. Then there exists a subsequence Λ of integers and a positive constant c_1 depending on f, ϕ, d, s, α, and ϵ such that

$$\sum_{k=1}^{n} |a_{k,n}| \geq c_1 \left(\frac{n^{\alpha(1/(r+\epsilon)-1/\ell)}}{M_n} \right)^\ell, \qquad n \in \Lambda, \tag{6}$$

where

$$M_n := \max_{1 \leq k \leq n} ||A_{k,n}||. \tag{7}$$

We recall that one of the objectives of approximation is to obtain approximants which are smoother than the original function. The theorem is therefore most interesting if ϕ has more derivatives than f. In this case, if the matrices $A_{k,n}$ in the

approximating networks are $o(n^{\alpha(1/(r+\epsilon)-1/\ell)})$, then the sum of the absolute values of the coefficients must tend to infinity. The smoother the activation function ϕ, the faster is this growth. Thus, the goals of smoothing and having bounded parameters are not compatible.

Another way to interpret this theorem is that if, for a function f, a sequence of approximating networks of the form (4) can be found to yield the order of approximation as in (5), but with the growth of the matrices $A_{k,n}$ and the coefficients $a_{k,n}$ controlled so that (6) is not satisfied, then f must have continuous partial derivatives of order at least r. Thus, for an infinitely many times differentiable activation function ϕ, we have a "converse theorem" : the existence of networks with properly controlled growth for the matrices and coefficients implies a smoothness of the target function, which is unknown to start with. We observe that in the case of the neural networks ($d = 1$) constructed in [10], the "weights" $A_{k,n}$ are $\mathcal{O}(n)$ and an upper estimate on the sum of the absolute values of the coefficients is also known. The networks of [10] can therefore be used to verify the accuracy of the starting hypothesis about the smoothness class to which the target function belongs.

The ideas behind the proof of Theorem 1 lead us to the following corollary, which gives sharper lower bounds than in (6) in the case when the activation function is analytic.

Corollary 2 *Let $\delta > 0$ be a real number, $\phi : \mathbb{R}^d \to \mathbb{R}$ have an extension to the poly-strip*

$$\{(z_1, \ldots, z_d) \ : \ |\Im m z_k| \le \delta, \quad k = 1, \ldots, d\}$$

as a bounded, analytic function. Then the estimate (6) can be replaced by

$$\sum_{k=1}^{n} |a_{k,n}| \ge c_1 m^{-r-\epsilon} \left(1 + \frac{\pi}{2M_n}\right)^{m/2}, \qquad n \in \Lambda, \tag{8}$$

where $m := c_2 n^{\alpha/(r+\epsilon)}$.

Proof of Theorem 1. Let $n, m \ge 1$ be integers. We observe that the function ϕ has continuous and bounded partial derivatives of order ℓ on $\mathbb{R}^d$. Therefore, the Jackson theorem for algebraic polynomial approximation [12], §5.3.11, shows that there exist polynomials $P_{k,n}$, each of coordinatewise degree at most m, such that

$$|\phi(A_{k,n}\mathbf{x} + \mathbf{b}_k) - P_{k,n}(\mathbf{x})| \le cM_n^{\ell} m^{-\ell}, \qquad \mathbf{x} \in [-1,1]^s, k = 1, \ldots, n \tag{9}$$

Writing $Q_m := \sum_{k=1}^{n} a_{k,n} P_{k,n}$, we see that Q_m is a polynomial of coordinatewise degree at most m. Moreover, from (5) and (9), we obtain

$$|f(\mathbf{x}) - Q_m(\mathbf{x})| \le c\left\{n^{-\alpha} + M_n^{\ell} m^{-\ell} \sum_{k=1}^{n} |a_{k,n}|\right\}, \qquad \mathbf{x} \in [-1,1]^s, \ m, n = 1, 2, \cdots. \tag{10}$$

If possible, let (6) be not true. Then, choosing n to be the smallest integer exceeding $m^{(r+\epsilon)/\alpha}$, we see that

$$|f(\mathbf{x}) - Q_m(\mathbf{x})| \le cm^{-(r+\epsilon)}, \qquad \mathbf{x} \in [-1,1]^s$$

for all sufficiently large integer m. In view of the converse theorems for algebraic polynomial approximation, [12] §6.3.4, this implies that $f \in C^r_{[a,b]^s}$ for every $[a, b] \subset (-1, 1)$. This contradiction completes the proof of the theorem. □

The proof of Corollary 2.2 is similar, except that one uses Bernstein's estimates similar to [12] §5.4.1, instead of the Jackson-type estimates.

3 Conclusions

We have discussed our previous work on the degree of approximation by generalized translation networks. It is shown here that the goals of having a smooth approximation, and bounded coefficients and weights are incompatible when the target function to be approximated fails to have at least as many continuous partial derivatives as the activation function. Our theorem can also be thought of as providing a rudimentary test for the hypothesis that the unknown target function belongs to a Sobolev class.

REFERENCES

[1] C. K. Chui and X. Li, *Approximation by ridge functions and neural networks with one hidden layer*, J. Approx. Theory, Vol. 70 (1992), pp.131-141.

[2] G. Cybenko, *Approximation by superposition of sigmoidal functions*, Mathematics of Control, Signal and Systems, Vol. 2 (1989), pp.303-314.

[3] R. DeVore, R. Howard, and C. A. Micchelli, *Optimal nonlinear approximation*, Manuscripta Mathematica, Vol. 63 (1989), pp.469-478.

[4] F. Girosi, M. Jones, and T. Poggio, *Regularization theory and neural networks architectures*, Neural Computation, Vol. 7 (1995), pp.219-269.

[5] K. Hornik, M. Stinchcombe, and H. White, *Multilayer feedforward networks are universal approximators*, Neural Networks, Vol. 2 (1989), pp.359-366.

[6] M. Leshno, V. Lin, A. Pinkus, and S. Schocken, *Multilayer feedforward networks with a nonpolynomial activation function can approximate any function*, Neural Networks, Vol. 6 (1993), pp.861-867.

[7] H. N. Mhaskar, *Neural networks for optimal approximation of smooth and analytic functions*, Neural Computation, Vol.8 (1996), pp164–177.

[8] H. N. Mhaskar and C. A. Micchelli, *Approximation by superposition of a sigmoidal function and radial basis functions, Advances in Applied Mathematics*, Vol. 13 (1992), pp.350-373.

[9] H. N. Mhaskar and C. A. Micchelli, *Dimension independent bounds on the degree of approximation by neural networks*, IBM Journal of Research and Development, Vol. 38 (1994), pp.277-284.

[10] H. N. Mhaskar and C. A. Micchelli, *Degree of approximation by neural and translation networks with a single hidden layer, Advances in Applied Mathematics*, Vol. 16 (1995), pp.151-183.

[11] H. N. Mhaskar and C. A. Micchelli, *How to choose an activation function*, in NIPS*6 (J. D. Cowan, G. Tesauro, J. Alspector Eds.), Morgan Kaufmann, 1994, pp.319-326.

[12] A. F. Timan, *Theory of Approximation of Functions of a Real Variable*, Macmillan Co., New York, 1963.

Acknowledgements

This research was supported, in part, by National Science Foundation Grant DMS 9404513 and Air Force Office of Scientific Research Grant F49620-93-1-0150.

GENERALISATION AND REGULARISATION BY GAUSSIAN FILTER CONVOLUTION OF RADIAL BASIS FUNCTION NETWORKS

Christophe Molina and Mahesan Niranjan

Cambridge University Engineering Department, Trumpington Street
Cambridge CB2 1PZ, UK. Email: cm3/niranjan@eng.cam.ac.uk

This paper proposes a new technique called *Regularisation by Convolution* to improve the generalisation of GaRBF networks. The technique is based on the convolution after training of GaRBF networks with gaussian filters and, consequently, is independent of the learning stage and algorithm. Moreover, it alleviates the need for retraining. The performance of *Regularisation by Convolution* in improving regression is illustrated for Wahba's problem.
Keywords: convolution product, neural networks, Gaussian filter, Gaussian radial basis functions, regularisation.

1 Introduction

Nowadays *generalisation* and *regularisation* are two of the most challenging topics in neural computation. By generalisation it is generally understood that, from a given training set consisting of input-output observations $\{\mathbf{x}_i, y_i\}$, $i = 1, \ldots, n$, of an underlying event F_*, such that $F_*(\mathbf{x}_i) = y_i$, it is desired to construct an estimated map F which, for a new test set of input observations $\{\mathbf{x}_j\}$ will provide a good prediction for the unobserved output observations $\{y_j\}$.

One way of achieving generalisation, known as *regularisation* or *smoothing*, is to find the mapping F by means of a neural network, subject to some constraints on the solution. One possible constraint is to limit the number of units in the neural network, or to employ pruning techniques during learning in order to limit the degree of freedom of F and thus avoid overfitting of the observations (see [1] for a survey). A second class of regularisation techniques involves the determination of a mapping F in the d-dimensional Hilbert space $\mathcal{H}$ of functions with continuous first derivatives and square integrable second derivatives which minimise,

$$MSE = \frac{1}{n} \cdot \sum_{i=1}^{n} (y_i - F(\mathbf{x}_i))^2 \tag{1}$$

subject to the regularisation condition

$$\int (F^{(2)}(\mathbf{x}))^2 d\mathbf{x} \leq \kappa \tag{2}$$

for different values of a regularisation parameter κ (see [2] and references contained therein). Equation (1) is known as the Mean Squared Error (MSE) of the training set and (2) as the regularisation constraint, which is equal to the energy of the second derivative of the mapping F. If κ is made large the F will just interpolate the training data and, conversely, if it is chosen very small then the mapping, although smooth, will not represent the underlying event F_*. A good regularisation is achieved by adapting κ to reach the convenient tradeoff between the fitting and the smoothness of the solution. Normally this is achieved by choosing different values for κ, training under these κ constraints, and testing the generalisation error results

on a test set by cross-validation. Although this solution may generalise well, it is computationally expensive and needs retraining for each of the possible values of κ. Moreover, the final results may be biased by the capacity of the neural network or the training rule to escape from local minima. In this paper, we propose a new regularisation technique based on convolution after training a Gaussian Radial Basis Function (GaRBF) network with gaussian filters. This technique, which does not need retraining, consists in essence of the following steps:

- Training a GaRBF network with a large number of units.
- Convolve the network with gaussian filters of different widths and normalise the network so that the final L_1-norm of the convolved $F(\mathbf{x})$ remains the same (this implicitly leads to a reduction of the energy of the second derivative of $F(\mathbf{x})$).
- Verify the generalisation performance of the convolved GaRBF networks by cross-validation, and retain the best solution.

The paper is organised as follows: Section 2 presents the mathematical principles of this technique. Section 3 describes the main algorithm for regularisation and a binary technique for searching for the best gaussian filter. Section 4 gives an experimental evaluation of the regularisation technique on the regression of a synthetic problem.

2 GaRBF Network Convolution with Gaussian Filters

GaRBF networks are defined as a linear combination of Gaussian units. Let this be denoted by,

$$F(\mathbf{x}) = \sum_{i=1}^{N} \alpha_i f_i(\mathbf{x}) \tag{3}$$

where N is the number of GaRBF units of general expression, $f_i(\mathbf{x}) = e^{-\frac{(\mathbf{x}-\mu_i)^2}{\sigma_i^2}}$, and with amplitude $\alpha_i \in \Re$, centre $\mu_i \in \Re^d$ and width $\sigma_i \in \Re^+$.

Let $g(\mathbf{x}, \sigma)$ be a Gaussian filter given by, $g(\mathbf{x}, \sigma) = e^{-\frac{\mathbf{x}^2}{\sigma_j^2}}$, with σ_j as width. We first define the integral convolution in the Hilbert space $\mathcal{H}$ of these two functions, $f_i(\mathbf{x})$ and $g(\mathbf{x}, \sigma)$ as

$$h(\tau) = \int_{-\infty}^{\infty} f_i(\mathbf{x}) g(\tau - \mathbf{x}, \sigma) d\mathbf{x} \tag{4}$$

Since GaRBFs are bounded and absolutely integrable on $\mathcal{H}$, the computation of their convolution may more easily be done by means of the convolution property, $\mathcal{F}\{h\}(\omega) = \sqrt{2\pi}\mathcal{F}\{f_i\}\mathcal{F}\{g\}$, where $\mathcal{F}\{\cdot\}$ is the Fourier transform. Fourier transforms of f_i and g respectively are

$$\mathcal{F}\{f\}(\omega) = \sigma_i^d \sqrt{\pi^d}\, e^{-\left(\frac{\sigma_i^2\omega^2}{4} + \sqrt{-1}\frac{4\mu_i\omega}{\sigma_i^2}\right)} \tag{5}$$

and,

$$\mathcal{F}\{g\}(\omega) = \sigma_j^d \sqrt{\pi^d}\, e^{-\frac{{\sigma_j}^2 w^2}{4}} \tag{6}$$

Finally, from the inverse Fourier transform of their product, a new GaRBF of same location but different amplitude and width is obtained,

$$h(\tau) = \left(\frac{\sigma_i^2 \sigma_j^2}{\sigma_i^2 + \sigma_j^2}\pi\right)^{\frac{d}{2}} e^{-\frac{(\tau-\mu_j)^2}{\sigma_i^2+\sigma_j^2}} \tag{7}$$

The integral convolution of a GaRBF network $F(\mathbf{x})$ as defined in (3) and a gaussian filter $g(\mathbf{x}, \sigma)$ is a straightforward consequence of equation (7), since,

$$\int_{-\infty}^{\infty} F(\mathbf{x}) \cdot g(\tau - \mathbf{x}, \sigma) d\mathbf{x} = \sum_{i=1}^{N} \alpha_i \int_{-\infty}^{\infty} f_i(\mathbf{x}) \cdot g(\tau - \mathbf{x}, \sigma) d\mathbf{x} \tag{8}$$

and is equal to a new GaRBF network with same number of units, located at the same positions but with different amplitude and width. In the particular context of *regularisation by convolution*, it is of great importance to keep the convolved function $h(\tau)$ as close as possible to the original $F(\mathbf{x})$ except at those points where high frequencies have been filtered. This may be achieved by requiring the L_1-norm of the GaRBF network to remain constant. A good alternative is to calculate the L_1-norm of the gaussian filter, as follows,

$$\int_{-\infty}^{\infty} e^{-\frac{x^2}{\sigma_j^2}} dx = \sigma_j^d (\pi)^{\frac{d}{2}} \tag{9}$$

and then convolve the network with a normalised filter which leads to the same results as the normalisation of the GaRBF network. Thus, the L_1-normalised convolution $F(\mathbf{x}) \otimes g(\mathbf{x}, \sigma)$ of a GaRBF network $F(\mathbf{x})$ and a gaussian filter $g(\mathbf{x}, \sigma)$ which retains the same norm of the original network may then be stated as,

$$F(\mathbf{x}) \otimes g(\mathbf{x}, \sigma) \doteq \frac{\int_{-\infty}^{\infty} F(\mathbf{x}) g(\tau - \mathbf{x}, \sigma) d\mathbf{x}}{\sigma_j^d (\pi)^{\frac{d}{2}}} \tag{10}$$

3 The Regularising Technique

This section describes the regularising technique based on the convolution of GaRBF units with gaussian filters, developed in previous section. The technique is to be applied to a pre-trained GaRBF network as defined in equation (3), and uses the Root Mean Squared (RMS) error obtained on a cross-validation set after regularisation as a performance criterion. The best regularising gaussian filter is found by binary search under the assumption that the RMS error has no local minima in the search space. Reasonable bounds for the binary searching are easily obtained from the bounded space on which the underlying function F_* lies. Thus the minimal bound for the width filter is equal to zero and the maximal bound is equal to the maximal distance between two points of the bounded space $\mathcal{H}$.

The structure of the related regularisation algorithm and its initialisation is shown below as pseudo-code,

- **Initial parameters and data**
  - Neural Network : $F(\mathbf{x}) = \sum_{i=1}^{N} \alpha_i f_i(\mathbf{x})$
  - Cross Validation set : $CV = \{\mathbf{x}_j, y_j\}\ j = 1, \ldots, n$
  - Gaussian Filter : $g(\mathbf{x}, \sigma) = e^{-\mathbf{x}^2/\sigma^2}$
  - Bounds of Gaussian filter widths and their average:

    $\sigma_{min} = 0$

    $\sigma_{max} = \left(\max\left(\sum_{k=1}^{d} \left(x_i^k - x_j^k\right)^2\right)\right)^{1/2} \ \forall \mathbf{x} \in CV$

    $\sigma_{avg} = (\sigma_{max} + \sigma_{min})/2$
  - RMS errors obtained on the CV data set after convolving $F(\mathbf{x})$ with $g(\mathbf{x}, \sigma_{min})$, $g(\mathbf{x}, \sigma_{avg})$ and $g(\mathbf{x}, \sigma_{max})$:

    RMS_{min}, RMS_{avg} and RMS_{max}
  - Stop threshold for the binary search : ϵ
- **Regularising Algorithm**

  Loop until $\mid RMS_{max}$ - $RMS_{min} \mid < \epsilon$

  1. Calculate the RMS_1 and RMS_2 errors obtained after convolution of $F(\mathbf{x})$ with $g(\mathbf{x}, \sigma)$, for widths σ_1 and σ_2, where,

     $\sigma_1 = (\sigma_{min} + \sigma_{avg})/2$

     $\sigma_2 = (\sigma_{avg} + \sigma_{max})/2$
  2. If $RMS_1 < RMS_2$ then,

     $\sigma_{max} = \sigma_{avg}$ & $\sigma_{avg} = \sigma_1$

     $RMS_{max} = RMS_{avg}$ & $RMS_{avg} = RMS_1$

     else

     $\sigma_{min} = \sigma_{avg}$ & $\sigma_{avg} = \sigma_2$

     $RMS_{min} = RMS_{avg}$ & $RMS_{avg} = RMS_2$

  end loop

4 Numerical Results

In order to illustrate the performance of *Regularisation by Convolution*, we have applied the algorithm to *Wahba's synthetic problem* [2]. This problem consists of the regression of a noisy function generated synthetically according to the model, $F_*(x) = 4.26\left(e^{-2x} - 4e^{-x} + 3e^{-3x}\right) + \nu$, where ν is normally distributed random noise with zero mean and standard deviation 0.2. In the original problem, 100 noisy observations were generated and used as learning set for the training of a sigmoid feed-forward neural network. Wahba performed regularisation during training using equation (2). The κ value which provided the lowest RMS error was obtained

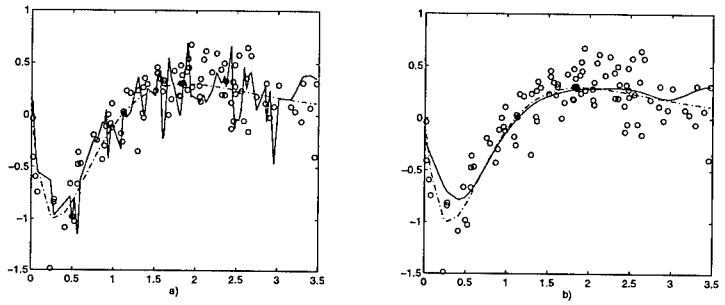

Figure 1 Original Wahba's function (dash-dot). Neural Network regression (solid). CV observations (circles). a) LRAN regression with RMS error equal to 0.3011 on the CV data set. b) The same LRAN after regularisation by convolution with the best Gaussian filter obtained by binary search ($\sigma_{avg} = 0.1709$) with RMS error equal to 0.2116.

by *leaving-one-out* cross-validation. Thus retraining was needed for each different choice of κ.

In our case we applied *Regularisation by Convolution* to the same problem after training a Limited Resource Allocating network (LRAN) by the *F-Projections* learning rule [3]. Training was only performed once, after which the network had learnt the underlying problem F_* with over-fitting of the noisy data as shown in Figure (1.a). The original training data was interpolated by a factor of ten to provide a sufficiently representative training set for the noisy problem, and a LRAN with 200 units (twice the number of training samples) was used to ensure learning with overfitting. We used an extra set of 100 samples as Cross-Validation set CV to calculate the best regularising filter. The stop threshold ϵ was fixed at 10^{-4}. Figure (1.b) illustrates the final result.

5 Summary

This paper has shown how a technique based on a convolution operator can be succesfully applied for regularising and then improving the performances on generalisation of Gaussian RBF networks. The advantage of this technique over other approaches is that it is independent of training processes and algorithms.

REFERENCES

[1] R. Reed, *Pruning algorithms-a survey*, IEEE Transactions on Neural Networks, Vol. 4 (September 1993), pp740–747.

[2] G. Wahba, *Generalisation and regularisation in nonlinear systems*, Tech. Rep. 921, Department of Statistics, University of Wisconsin, 1210 West Dayton ST. Madison, WI 53706, (1994).

[3] C. Molina and M. Niranjan, *Pruning with replacement on limited resource allocating networks by f-projections*, Neural Computation, Vol. 8 (1996), No. 4, pp855–868.

DYNAMICAL SYSTEM PREDICTION: A LIE ALGEBRAIC APPROACH FOR A NOVEL NEURAL ARCHITECTURE

Yves Moreau and Joos Vandewalle

Katholieke Universiteit Leuven, Dept. of Electrical Engineering, ESAT-SISTA
Kardinaal Mercierlaan 94, B-3001 Leuven (Heverlee), Belgium.
Email: moreau@esat.kuleuven.ac.be

In this paper we study the problem of the prediction of autonomous continuous-time dynamical systems from discrete-time measurements of the state variables. We show that the predictor of such a system needs to be an invertible map from the state-space into itself. The problem then becomes one of how to approximate invertible maps. We show that standard approximation schemes do not guarantee the property of invertibility. We therefore propose a new approximation scheme based on the composition of invertible basis functions which preserves invertibility. This approach can be cast in a Lie algebraic framework where the approximation is based on the use of the Baker-Campbell-Hausdorff formula. The method is implemented in a neural-like form. We also present a more general implementation which we call "MLP in dynamics space".

Keywords: System prediction, Lie algebras, Baker-Campbell-Hausdorff formula.

1 Introduction

We will study here the problem of the prediction of nonlinear dynamical systems from a set of sampled measurements of the state of the system. The nonlinear systems which we will consider are governed by a multidimensional ordinary differential equation. Although the dynamics of the system is continuous in time, the samples that we will use for prediction are the state variables measured at discrete time-intervals only. We are therefore led to postulate a discrete-time form for our prediction: $\hat{x}(k+1) = F(x(k))$. In the first section, we will show - using the fact that the underlying dynamics of the system is time-continuous - that the function F used for prediction should be invertible. The problem then becomes that of building an approximation scheme specifically designed for invertible maps. The main drawback of standard approximation schemes is that they are based on summing basis functions to build an approximation. However, this operation does not preserve invertibility. Using the operation of composition instead of addition, we are able to guarantee invertibility. We will thus build approximation schemes based on composition of invertible basis functions. In the second section, we will analyze those compositions within the framework of Lie algebra theory. Starting from a method from numerical analysis we will be able to derive a new approach to the prediction of nonlinear systems. In section three, this new method will be presented in a neural-like form and illustrated by an example. We will also present a general model for approximation which we call "MLP in dynamics space". Finally, we will conclude.

1.1 Invertibility of Dynamical Systems

The systems considered here are defined by an ordinary differential equation (ODE) on some n-dimensional manifold $\mathcal{M}$. We follow the differential geometric description of dynamical systems [2] and assume the standard smoothness assumptions. For each initial condition x_0, we can solve the initial value problem. We then collect all those solutions in one function $\Phi(x_0, t)$ which gives the solution of the ODE as a

function of the initial condition:

$$\begin{cases} \dot{x} = f(x(t)) \\ \\ x(0) = x_0 \end{cases} \Rightarrow x(t) = \Phi(x_0, t) \tag{1}$$

Φ is called the flow of the dynamical system. The flow is a remarkable object which possesses the group property. We refer the reader to [4] for a general presentation of the group theoretic approach to dynamical systems. If we assume, for simplicity, that the flow is defined for all times, the group property writes as follows:

$$\begin{gathered} \Phi \ : \ \mathcal{M} \times \mathbb{R} \rightarrow \mathcal{M} \\ \\ \Phi(x, t+s) = \Phi(\Phi(x,t), s), \quad \forall\, t, s \in \mathbb{R} \end{gathered} \tag{2}$$

As we will see, this gives the flow the structure of a group. We define the time-t map as

$$\varphi^t(x_0) \equiv \Phi(x_0, t) \tag{3}$$

This map φ^t associates to any initial condition its image under the flow of the differential equation after a given time t. The map φ^t is a map from the manifold $\mathcal{M}$ into itself. Using the group property of the flow, we can deduce the properties of φ:

$$\begin{array}{ll} \varphi^t \circ \varphi^s(x_0) = \Phi(\Phi(x_0, s), t) = \Phi(x_0, t+s) = \varphi^{t+s}(x_0) & \textit{composition} \\ \varphi^0 = I \Leftarrow \varphi^0(x_0) = \Phi(x_0, 0) = x_0 = I(x_0) & \textit{identity} \\ \varphi^t \circ \varphi^{-t}(x0) = \Phi(x_0, 0) = x_0 = I(x_0) \Rightarrow \varphi^{-t} = (\varphi^t)^{-1} & \textit{inverse} \end{array} \tag{4}$$

Moreover, if f is C^r then φ is C^r. Hence, since φ is a smooth invertible map with a smooth inverse, φ is a diffeomorphism. Furthermore, the properties of φ show that $\{\varphi^t\}$ is a group. We therefore say that a flow $\Phi(x,t)$ is a one-parameter group of diffeomorphisms φ^t.

1.2 Dynamical System Prediction

Even if we assume that the underlying dynamics of the system is governed by an ODE, the system is generally observed only at discrete time-intervals. So, if we choose a sampling period Δt, we can assume a functional relationship between the current state and the next sample. The system becomes of the form:

$$x((k+1).\Delta t) = F(x(k.\Delta t)), \qquad x(k) \in \mathcal{M} \tag{5}$$

And, from what we have shown before, we see that F is a diffeomorphism as

$$F(.) = \varphi^{\Delta t}(.) \tag{6}$$

The following figure (Fig. 1) summarizes those observations. On the left we consider a square grid of initial conditions. We let each point of that grid follow its trajectory for a time-interval Δt. After this time, all the points of the grid have moved and the shape of the grid has changed. The diffeomorphism $\varphi^{\Delta t}$ is that transformation from the manifold (here, $\mathbb{R}^2$) into itself which maps the square grid on the left into the deformed grid on the right. One can see that this transformation is smooth and invertible, hence a diffeomorphism. So, the question of predicting a continuous-time system observed at discrete time-intervals becomes one of how we can approximate those diffeomorphisms which arise from the sampling of an ODE. The basic idea is that the set of all C^r diffeomorphisms is also a group. In a group, the natural operation is the composition of the elements of the group. While most

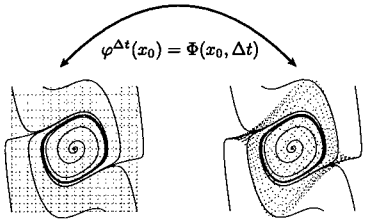

Figure 1 Diffeomorphic transformation of a square grid after one time-step.

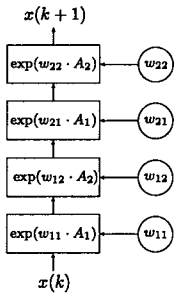

Figure 2 Implementation of the composition network.

standard approximation schemes are based on the summation of some basis functions, this operation does not preserve the property of being a diffeomorphism. On the other hand, composition does preserve this property, so we propose to build an approximation scheme based on composing basis functions instead of adding them.

2 Lie Algebra Theory

Lie algebra theory has a long history in physics, mostly in the areas of classical mechanics [1] and partial differential equations [8]. It is also an essential part of nonlinear system theory [5]. Our approach to system prediction can be best cast in this framework. A Lie algebra is a vector space where we define a supplementary operation: the bracket $[.,.]$ of two elements of the algebra. The bracket is an operation which is bilinear, antisymmetric and satisfies the Jacobi identity [8]. In the case where the Lie algebra is the vector space of all C^r vector fields, the time-t map φ^t plays a very important role. If the vector field is A, we define the *exponential map* as follows: $\exp(t.A) \equiv \varphi^t$. This notation is an extension of the case where the vector field is linear in space and where the solution is given by exponentiation of the matrix. The exponential is thus a mapping from the manifold into itself. And this map depends on the underlying vector field A and changes over time. From here on, the product of exponentials will denote the composition of the maps. One can then define the Lie bracket by

$$[A, B] = \left.\frac{\partial^2}{\partial s.\partial t}\right|_{t=s=0} \exp(-s.B).\exp(-t.A).\exp(s.B).\exp(t.A) \tag{7}$$

In the case where the manifold is $\mathbb{R}^n$, the bracket can be further particularized to

$$[A, B]_i = \sum_{i=1}^{n} \left(B_i.\frac{\partial A_j}{\partial x_i} - A_i.\frac{\partial B_j}{\partial x_i} \right) \tag{8}$$

2.1 The Baker-Campbell-Hausdorff Formula

The Baker-Campbell-Hausdorff (BCH) formula gives an expansion for the product of the exponentials of two elements of the Lie algebra, see [6]:

$$\exp(A).\exp(B) = \exp(A + B + \frac{1}{2}[A, B] + \frac{1}{12}([A, [A, B]] - [B, [B, A]]) + \ldots) \tag{9}$$

The problem of predicting a dynamical system with vector field X then becomes that of building an approximation for $\exp(\Delta t.X)$ as we have that $x(k+1) =$

$\exp(\Delta t.X)[x(k)]$. This problem has recently been the focus of much attention in the field of numerical analysis for the integration of Hamiltonian differential equations [6] [7]. Suppose that the vector field X is of the form $X = A + B$ where we can integrate A and B directly. We can use the BCH formula to produce a first-order approximation to the exponential map:

$$\text{BCH}: \exp(\Delta t.X) = \exp(\Delta t.A).\exp(\Delta t.B) + o(\Delta t^2) \tag{10}$$

This is the essence of the method as it shows that one can approximate an exponential map (that is the map arising from the solution of an ODE) by composing simpler maps. By repeated use of the BCH formula, we can show that the following leapfrog scheme is second-order.

$$\text{Leapfrog}: \exp(\Delta t.X) = \exp(\frac{\Delta t}{2}.A).\exp(\Delta t.B).\exp(\frac{\Delta t}{2}.A) + o(\Delta t^3) \tag{11}$$

Using this leapfrog scheme as a basis element for further leapfrog schemes, Yoshida [9] showed that it was possible to produce an approximation to $\exp(\Delta t.X)$ up to any order. Forest and Ruth [3] showed that approximations could be built for more than two vector fields. Combining the two we can state that it is possible to build an approximation to the solution of a linear combination of vector fields as a product of exponential maps:

$$\begin{array}{l} X = \sum_{i=1}^{m} a_i.A_i \\ \Rightarrow \exists w_{ij} : \exp(\Delta t.X) = \prod_{j=1}^{k} \prod_{i=1}^{m} \exp(w_{ij}.\Delta t.A_i) + o(\Delta t^{p+1}) \end{array} \tag{12}$$

3 Network Implementation

Such an approximation scheme can be easily implemented as a multilayer network as can be seen in the following figure (Fig. 2). The problem of predicting the system can now simply be solved by minimizing the prediction error of the model by tuning the weights w_{ij} using some gradient-based optimization technique.

3.1 Example

We will now present an example to illustrate how this method can be applied. We will do this by looking at the Van den Pol oscillator. This system can be written as a first-order system in state-space form which can be seen as a linear combination of two vector fields A_1, A_2 which can be solved analytically:

$$\begin{pmatrix} \dot{x} \\ \dot{y} \end{pmatrix} = \begin{pmatrix} y \\ -x \end{pmatrix} + \alpha.\begin{pmatrix} 0 \\ (1-x^2).y \end{pmatrix} = A_1 + \alpha.A_2 \tag{13}$$

One can then build a predictor according to the architecture just presented (Fig. 2), simply choosing an appropriate number of layers. One then finds the appropriate weights w_{ij} by minimizing the error on the training set. One interesting property of this method is that we are able to use the a priori knowledge we have about the system. Such a feature is uncommon in the field of system prediction using neural networks. This method allowed us to build a predictor for the Van der Pol oscillator in the case where the parameter α was unknown. We also produced a similar result for the Lorenz attractor.

3.2 MLP in Dynamics Space

If we decide to approximate the vector field of our system by a multi-layer perceptron, one can derive a composition network to implement this. The form of the

vector field is

$$X(x) = \sum_{j=1}^{n} \vec{c}_j . \sigma(\vec{b}_j . x + b_{j_0}) = \sum_{j=1} A_j^{\vec{c}_j, \vec{b}_j}(x) \tag{14}$$

where $\sigma(x) = \tanh(x)$ and $\vec{c}_j, \vec{b}_j \in \mathbb{R}^{d+1}, j = 1, ..., n$.
But the differential equation $\dot{x} = \sigma(x)$ can be solved explicitly in the one-dimensional case. We can use this to explicitly integrate the multidimensional system $\dot{x} = A^{\vec{c},\vec{b}}(x)$ for any value of the parameters $\vec{c}_j, \vec{b}_j$. So, we can design a network of the following form:

$$\hat{x}(k+1) = F(x(k)) = \exp(w_k . A^{\vec{c}_k, \vec{b}_k}) \circ \ldots \circ \exp(w_1 . A^{\vec{c}_1, \vec{b}_1})(x(k)) \tag{15}$$

We call this an "MLP in dynamics space" as the MLP is implicitly used to parametrize the vector field. Further work will be devoted to finding computationally efficient methods for the training of such a network.

4 Conclusions

We have studied the problem of predicting an autonomous continuous-time nonlinear dynamical system from discrete-time measurements of its state. We showed that because the predictor must have the form of an invertible map, it is interesting to have an approximation scheme which has this property. This can be achieved by using compositions instead of additions in the approximation. The theory of Lie algebras provided the framework to develop such a method. We showed that this resulted in a multi-layer architecture and we illustrated it by a simple example. Further, the method was extended to some form of "MLP in dynamics space".

REFERENCES

[1] V.I. Arnold, *Mathematical methods of classical mechanics*, Springer-Verlag, New York (1989).
[2] D.R.J. Chillingworth, *Differential topology with a view to applications*, Pitman Publishing, London (1977).
[3] E. Forest, R. Ruth, *Fourth-order symplectic integration*, Physica D, Vol. 43 (1990) pp105–117.
[4] M.C. Irwin, *Smooth Dynamical Systems*, Academic Press, New York (1980).
[5] A. Isidori, *Nonlinear control theory*, Springer-Verlag, New York (1989).
[6] P.-V. Koseleff, *Calcul formel pour les méthodes de Lie en mécanique hamiltonienne*, Ph.D. thesis, Ecole Polytechnique, Paris (1993).
[7] R.I. McLachlan, *On the numerical integration of ordinary differential equations by symmetric composition methods*, SIAM J. Sci. Comput., Vol. 16(1) (1995), pp151–168.
[8] P.J Olver, *Applications of Lie groups to differential equations*, Springer-Verlag, New York (1985).
[9] H. Yoshida, *Construction of higher order symplectic integrators*, Phys. Lett. A, Vol. 150 (1990), pp262–269.

Acknowledgements

This research work was carried out at the ESAT laboratory of the Katholieke Universiteit Leuven, in the framework of the Concerted Action Project of the Flemish Community GOA-MIPS, and within the framework of the Belgian program on inter-university attraction poles (IUAP-17) initiated by the Belgian State, Prime Minister's Office for Science. The scientific responsibility rests with its authors. Yves Moreau is a research assistant of the N.F.W.O. (Belgian National Fund for Scientific Research).

STOCHASTIC NEURODYNAMICS AND THE SYSTEM SIZE EXPANSION

Toru Ohira and Jack D. Cowan*

Sony Computer Science Laboratory 3-14-13 Higashi-gotanda, Shinagawa, Tokyo 141, Japan. Email: ohira@csl.sony.co.jp

** Departments of Mathematics and Neurology, The University of Chicago, Chicago, IL 60637, USA. Email: cowan@synapse.uchicago.edu*

We present here a method for the study of stochastic neurodynamics in the master equation framework. Our aim is to obtain a statistical description of the dynamics of fluctuations and correlations of neural activity in large neural networks. We focus on a macroscopic description of the network via a master equation for the number of active neurons in the network. We present a systematic expansion of this equation using the "system size expansion". We obtain coupled dynamical equations for the average activity and of fluctuations around this average. These equations exhibit non–monotonic approaches to equilibrium, as seen in Monte Carlo simulations.

Keywords: stochastic neurodynamics, master equation, system size expansion.

1 Introduction

The correlated firing of neurons is considered to be an integral part of information processing in the brain[12, 2]. Experimentally, cross–correlations are used to study synaptic interactions between neurons and to probe for synchronous network activity. In theoretical studies of stochastic neural networks, understanding the dynamics of correlated neural activity requires one to go beyond the mean field approximation that neglects correlations in non– equilibrium states[8, 6]. In other words, we need to go beyond the simple mean–field approximation to study the effects of fluctuations about average firing activities.

Recently, we have analyzed stochastic neurodynamics using a master equation[5, 8]. A network comprising binary neurons with asynchronous stochastic dynamics is considered, and a master equation is written in "second quantized form" to take advantage of the theoretical tools that then become available for its analysis. A hierarchy of moment equations is obtained and a heuristic closure at the level of second moment equations is introduced. Another approach based on the master equation via path integrals, and the extension to neurons with a refractory state are discussed in [9, 10].

In this paper, we introduce another master equation based approach to go beyond the mean field approximation. We concentrate on the macroscopic behavior of a network of two–state neurons, and introduce a master equation for the number of active neurons in the network at time t. We use a more systematic expansion of the master equation than hitherto, the "system size expansion"[11]. The expansion parameter is the inverse of the total number of the neurons in the network. We truncate the expansion at second order and obtain an equation for fluctuations about the mean number of active neurons, which is itself coupled to the equation for the average number of active neurons at time t. These equations show non–monotonic approaches to equilibrium values near critical points, a feature which is not seen in the mean field approximation. Monte Carlo simulations of the master equation itself show qualitatively similar non–monotonic behavior.

2 Master Equation and the System Size Expansion

We first construct a master equation for a network comprising N binary elements with two states, "active" or firing and "quiescent" or non–firing. The transitions between these states are probabilistic and we assume that the transition rate from active to quiescent is a constant α for every neuron in the network. We do not make any special assumption about network connectivity, but assume that it is "homogeneous", i.e., all neurons are statistically equivalent with respect to their activities, which depend only on the proportion of active neurons in the network. More specifically, the transition rate from quiescent to active is given as a function ϕ of the number of active neurons in the network. Taking the firing time to be about $2ms$, we have $\alpha \approx 500s^{-1}$. For the transition rate from quiescent to active, the range of the function is $\approx 30 - 100s^{-1}$ reflecting empirically observed firing–rates of cortical neurons. With these assumptions, one can write a master equation as follows.

$$-\frac{\partial}{\partial t}P_N[n,\ t] = \alpha(nP_N[n,\ t] - (n+1)P_N[(n+1),\ t])$$
$$+\quad N(1-\frac{n}{N})\phi(\frac{n}{N})P_N[n,\ t] - N(1-\frac{(n-1)}{N})\phi(\frac{n-1}{N})P_N[(n-1),\ t], \quad (1)$$

where $P_N[n,\ t]$ is the probability that the number of active neurons is n at time t. (We absorbed the parameter representing total synaptic weight into the function ϕ.) This master equation can be deduced from the second quantized form cited earlier, which will be discussed elsewhere. The standard form of this equation can be rewritten by introducing the "step operator", defined by the following action on an arbitrary function of n:

$$\mathcal{E}f(n) = f(n+1), \quad \mathcal{E}^{-1}f(n) = f(n-1) \quad (2)$$

In effect, $\mathcal{E}$ and $\mathcal{E}^{-1}$ shift n by one. Using such step operators, Eq. (1) becomes

$$\frac{\partial}{\partial t}P_N[n,\ t] = (\mathcal{E}-1)r_nP_N[n,\ t] + (\mathcal{E}^{-1}-1)g_nP_N[n,\ t], \quad (3)$$

where $r_n = \alpha n$, and $g_n = (N-n)\phi(\frac{n}{N})$. This master equation is non–linear since g_n is a nonlinear function of n. Linear master equations, in which both r_n and g_n are linear functions of n, can be solved exactly. However, in general, non–linear master equations cannot be solved exactly, so in our case, we seek an approximate solution.

We now expand the master equation to obtain approximate equations for the stochastic dynamics of the network. We use the system size expansion, which is closely related to the Kramers–Moyal expansion, to obtain the "macroscopic equation" and time–dependent approximations to fluctuations about the solutions of such equation. In essence, this method is a way to expand master equations in powers of a small parameter, which is usually identified as the inverse size of the system. Here, we identify the system size with the total number of neurons in a network.

We make a change of variables in the master equation given in (3). We assume that fluctuations about the macroscopic value of n are of order $N^{(1/2)}$. In other words, we expect that $P_N(n,t)$ will have a maximum around the macroscopic value of n

with a width of order $N^{(1/2)}$. Hence, we set

$$n(t) = N\mu(t) + N^{\frac{1}{2}}\xi(t) \tag{4}$$

where μ satisfies the macroscopic equation and ξ is a new variable, whose distribution is equivalent to $P_N(n,t)$, i.e., $P_N(n,\ t) = \Pi(\xi,t)$. We expand the step operators as:

$$\mathcal{E} = 1 + N^{-\frac{1}{2}}\frac{\partial}{\partial\xi} + N^{-1}\frac{\partial^2}{\partial\xi^2}\ldots, \quad \mathcal{E}^{-1} = 1 - N^{-\frac{1}{2}}\frac{\partial}{\partial\xi} + N^{-1}\frac{\partial^2}{\partial\xi^2}\ldots \tag{5}$$

as $\mathcal{E}$ shifts ξ by $\xi + N^{(-1/2)}$. With this change of variables, the master equation is given as follows:

$$\frac{\partial}{\partial t}\Pi(\xi,t) - N^{\frac{1}{2}}\frac{\partial}{\partial t}\mu(t)\frac{\partial}{\partial\xi}\Pi(\xi,t) = N(N^{-\frac{1}{2}}\frac{\partial}{\partial\xi} + \frac{1}{2}N^{-1}\frac{\partial^2}{\partial\xi^2}\ldots)[\alpha(\mu + N^{-\frac{1}{2}}\xi)\Pi]$$
$$+N(-N^{-\frac{1}{2}}\tfrac{\partial}{\partial\xi} + \tfrac{1}{2}N^{-1}\tfrac{\partial^2}{\partial\xi^2}\ldots)[1 - (\mu + N^{-\frac{1}{2}}\xi)][\phi(\mu + N^{-\frac{1}{2}}\xi)]\Pi(\xi,t) \tag{6}$$

Collecting terms, we obtain, to order $N^{(1/2)}$,

$$-\frac{\partial\mu}{\partial t} = \alpha\mu - (1-\mu)\phi(\mu) \tag{7}$$

This is the macroscopic equation, which can be obtained also by using a mean–filed approximation to the master equation. We make μ satisfy this equation so that terms of order $N^{(1/2)}$ vanish.

The next order is $N^{(0)}$, which gives a Fokker–Planck equation for the fluctuation ($\phi'(\mu) \equiv \frac{\partial}{\partial x}\phi(x)|_{x=\mu}$):

$$\frac{\partial}{\partial t}\Pi = -\frac{\partial}{\partial\xi}[-\alpha\xi - \xi\phi(\mu) + (1-\mu)\xi\phi'(\mu)]\Pi + \frac{1}{2}\frac{\partial^2}{\partial\xi^2}[\alpha\mu + (1-\mu)\phi(\mu)]\Pi \tag{8}$$

We note that this equation does not depend on the variable N justifying our assumption that fluctuations are of order $N^{(1/2)}$.

We now study the behavior of the equations obtained through the system size expansion to the second order. ¿From Eqs. (7) and (8), we obtain

$$\frac{d\chi}{dt} = -\alpha\chi + (1-\chi)\phi(\chi-\eta) + \eta(1-\chi+\eta)\phi'(\chi-\eta) \tag{9}$$

$$\frac{d\eta}{dt} = -\alpha\eta - \eta\phi(\chi-\eta) + \eta(1-\chi+\eta)\phi'(\chi-\eta) \tag{10}$$

where $\chi \equiv \frac{n}{N} = \mu + \eta$, and $\eta = N^{-\frac{1}{2}}\xi$. Equations (9) and (10) can be numerically integrated. Some examples are shown in Figure 1(B). For comparison, we plot solutions of the macroscopic equations with the same parameter sets in Figure 1(A). We observe a physically expected bifurcation into an active network state with decreasing α, for either approximation. However, different dynamics are seen as one approaches bifurcation points. In particular, the coupled–equations exhibit a non–monotonic approach to the limiting value. The validity of the system size expansion is limited to the region not close to the bifurcation point, as discussed in the last section. The point is that by incorporating higher order terms into the approximation, we can extend its validity to a domain closer to the bifurcation point and thereby better capture stochastic dynamical behavior of such networks.

Monte Carlo simulations [3] of the two dimensional network based on (1) with 2500 neurons with periodic boundary conditions were performed. The connectivity is

set up as follows: a neuron is connected to a specified number k of other neurons chosen randomly from the network. The strength of connection is given by the Poisson form:

$$w_{ij} = w_0 \frac{r_{ij}{}^s}{s!} e^{-r_{ij}} \tag{11}$$

where r_{ij} is the distance between two neurons, and w_0 and s are constants. We show in Figure 2 the average behavior of χ for (A) $k = 200$ ($k/N = 0.08$) and (B) $k = 15$m ($k/N = 0.006$). The non–monotonic dynamics is more noticeable in the low connectivity network. More quantitative comparisons between simulations and theory will be carried out in the future. The qualitative comparison shown here, however, indicate the need to model fluctuations of total activity near critical points in order to capture the dynamics of sparsely connected networks. This is consistent with our earlier investigations of a one–dimensional ring of neurons via a master equation.

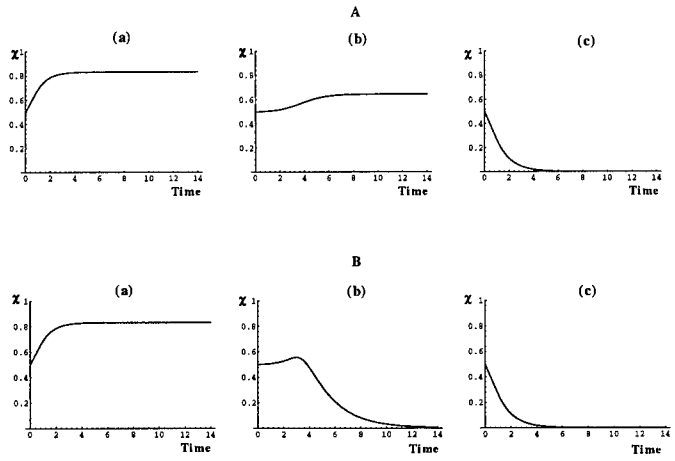

Figure 1 Comparison of solutions of (A) the macroscopic equation, and (B) (23) and (24). The parameters are set at $\beta = 15$, $\theta = 0.5$ and $\alpha =$ (a) 0.2, (b) 0.493, and (c) 0.9. The initial conditions are $\chi = 0.5$, and $\eta =$(A)0.01, and (B) 0.

3 Discussion

We have here outlined an application of the system size expansion to a master equation for stochastic neural network activity. It produced a dynamical equation for the fluctuations about mean activity levels, the solutions of which showed a non–monotonic approach to such levels near a critical point. This has been seen in model networks with low connectivity. Two issues raised by this approach require further comment: (1) In this work we have used the number of neurons in the network as a expansion parameter. Given the observation that the overall connectedness affects the stochastic dynamics, a parameter representing the average connectivity per neuron may be better suited as an expansion parameter. We note that this parameter is typically small for biological neural networks. (2) There are many studies of Hebbian learning in neural networks[1, 4, 7]. In such studies attempts

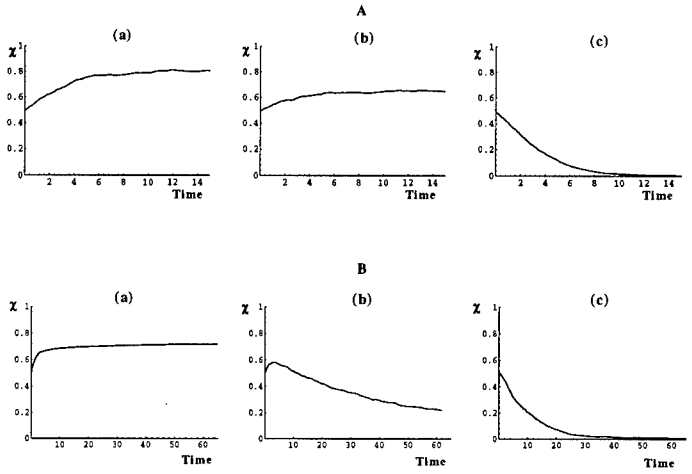

Figure 2 Comparisons of Monte Carlo simulations of the master equation with high ($k = 200$) and low ($k = 15$) connectivities per neuron. The parameters are set at $\beta = 15$, $\theta = 0.5$, $w_0 = 100.0$, $s = 3.0$, and for (A) $\alpha =$ (a) 0.05, (b) 0.1, and (c) 0.4, and for (B) $\alpha =$ (a) 0.001, (b) 0.05, and (c) 0.2. The initial condition is a random configuration.

have also been made to incorporate correlations of neural activities. It is of interest to see if we can formulate such attempts within the framework presented here.

REFERENCES

[1] S. Amari, K. Magiu, *Statistical neurodynamics of associative memory*, Neural Networks, Vol. 1 (1988), pp63–73.

[2] D. J. Amit, N. Brunel, M. V. Tsodyks, *Correlations of cortical Hebbian reverberations: theory versus experiment*, J. of Neuroscience, Vol. 14 (1994), pp6435–6445.

[3] K. Binder, *Introduction: Theory and "technical" aspects of Monte Carlo simulations*, Monte Carlo Methods in Statistical Physics, 2nd Ed., Springer-Verlag, Berlin (1986).

[4] A. C. C. Coolen, D. Sherrington, *Dynamics of fully connected attractor neural networks near saturation*, Phys. Rev. Lett., Vol. 71 (1994), pp3886–3889.

[5] J. D. Cowan, *Stochastic neurodynamics*, in: Advances in Neural Information Processing Systems 3, R. P. Lippman, J. E. Moody, and D. S. Toretzky, eds., Morgan Kaufmann Publishers, San Mateo (1991).

[6] I. Ginzburg, H. Sompolinsky, *Theory of correlation in stochastic neural networks*, Phys. Rev. E, Vol. 50 (1995), pp3171–3191.

[7] H. Nishimori, T. Ozeki, *Retrieval dynamics of associative memory of the Hopfield type*, J. Phys. A: Math. Gen., Vol. 26 (1993), pp859–871.

[8] T. Ohira, J. D. Cowan, *Master equation approach to stochastic neurodynamics*, Phys. Rev. E, Vol.48 (1993), pp2259–2266.

[9] T. Ohira, J. D. Cowan, *Feynman diagrams for stochastic neurodynamics* in: Proceedings of Fifth Australian Conference of Neural Networks, Brisbane (1994).

[10] Ohira, T., and Cowan, J. D., *Stochastic dynamics of three-state neural networks* in: Advances in Neural Information Processing Systems 7, G. Tesauro, D. S. Toretzky, T. K. Leen, eds., MIT Press, Cambridge (1995).

[11] N. G. van Kampen, *Stochastic Processes in Physics and Chemistry*. North-Holland, Amsterdam (1992).

[12] D. Wang, J. Buhmann, C. von der Malsburg, *Pattern segmentation in associative memory*, Neural Computation, Vol.2 (1990), pp94–106.

AN UPPER BOUND ON THE BAYESIAN ERROR BARS FOR GENERALIZED LINEAR REGRESSION

Cazhaow S. Qazaz, Christopher K. I. Williams and Christopher M. Bishop

Neural Computing Research Group, Dept. of Computer Science and Applied Mathematics, Aston University, Birmingham, UK. Email: ncrg@aston.ac.uk

In the Bayesian framework, predictions for a regression problem are expressed in terms of a distribution of output values. The mode of this distribution corresponds to the most probable output, while the uncertainty associated with the predictions can conveniently be expressed in terms of error bars given by the standard deviation of the output distribution. In this paper we consider the evaluation of error bars in the context of the class of generalized linear regression models. We provide insights into the dependence of the error bars on the location of the data points and we derive an upper bound on the true error bars in terms of the contributions from individual data points which are themselves easily evaluated.

1 Introduction

Many applications of neural networks are concerned with the prediction of one or more continuous output variables, given the values of a number of input variables. As well as predictions for the outputs, it is also important to provide some measure of uncertainty associated with those predictions.

The Bayesian view of regression leads naturally to two contributions to the error bars. The first arises from the intrinsic noise on the target data, while the second comes from the uncertainty in the values of the model parameters as a consequence of having a finite training data set [1, 2]. There may also be a third contribution which arises if the true function is not contained within the space of models under consideration, although we shall not discuss this possibility further.

In this paper we focus attention on a class of universal non-linear approximators constructed from linear combinations of fixed non-linear basis functions, which we shall refer to as *generalized linear regression* models. We first review the Bayesian treatment of learning in such models, as well as the calculation of error bars [3]. Then, by considering the contributions arising from individual data points, we provide insight into the nature of the error bars and their dependence on the location of the data in input space. This in turn leads to the key result of the paper which is an upper bound on the true error bars expressed in terms of the single-data-point contributions. Our analysis is very general and is independent of the particular form of the basis functions.

2 Bayesian Error Bars

We are interested in the problem of predicting the value of a noisy output variable t given the value of an input vector $\boldsymbol{x}$. Throughout this paper we shall restrict attention to regression for a single variable t since all of the results can be extended in a straightforward way to multiple outputs. To set up the Bayesian formalism we begin by defining a model for the distribution of t conditional on $\boldsymbol{x}$. This is most commonly chosen to be a Gaussian function in which the mean is governed by the output $y(\boldsymbol{x}; \boldsymbol{w})$ of a network model, where $\boldsymbol{w}$ is a vector of adaptive parameters

(weights and biases). Thus we have

$$p(t|\boldsymbol{x}, \boldsymbol{w}) = \frac{1}{(2\pi\sigma_\nu^2)^{1/2}} \exp\left\{-\frac{(y(\boldsymbol{x}; \boldsymbol{w}) - t)^2}{2\sigma_\nu^2}\right\} \tag{1}$$

where σ_ν^2 is the variance of the distribution.

In the Bayesian framework, our state of knowledge of the weight values is expressed in terms of a distribution function over $\boldsymbol{w}$. This is initially set to some *prior* distribution, from which a corresponding *posterior* distribution can be computed using Bayes' theorem once we have observed the training data. A common choice of prior is a Gaussian distribution of the form

$$p(\boldsymbol{w}) = \frac{1}{(2\pi)^{M/2}} |\boldsymbol{S}|^{1/2} \exp\left\{-\frac{1}{2}\boldsymbol{w}^{\mathrm{T}} \boldsymbol{S} \boldsymbol{w}\right\} \tag{2}$$

where M is the total number of weight parameters, $\boldsymbol{S}$ is the inverse covariance matrix of the distribution, and $|\boldsymbol{S}|$ denotes the determinant of $\boldsymbol{S}$. Since the parameters in $\boldsymbol{S}$ control the distribution of other parameters they are often referred to as *hyperparameters*. The noise variance σ_ν^2 is commonly also called a hyperparameter since, in a Bayesian framework, it can be treated using similar techniques to $\boldsymbol{S}$. Here we shall assume that the values of σ_ν^2 and $\boldsymbol{S}$ are fixed and known.

The training data set D consists of N pairs of input vectors $\boldsymbol{x}^n$ and corresponding target values t^n where $n = 1, \ldots, N$. From this data set, together with the noise model (1), we can construct the *likelihood* function given by

$$p(D|\boldsymbol{w}) = \prod_{n=1}^{N} p(t^n|\boldsymbol{x}^n, \boldsymbol{w}) = \frac{1}{(2\pi\sigma_\nu^2)^{N/2}} \exp\left\{-\frac{1}{2\sigma_\nu^2}\sum_{n=1}^{N}\{y(\boldsymbol{x}^n; \boldsymbol{w}) - t^n\}^2\right\} \tag{3}$$

We can then combine the likelihood function and the prior using Bayes' theorem to obtain the posterior distribution of weights given by $p(\boldsymbol{w}|D) = p(D|\boldsymbol{w})p(\boldsymbol{w})/p(D)$. The predictive distribution of t given a new input $\boldsymbol{x}$ can then be written in terms of the posterior distribution in the form

$$p(t|\boldsymbol{x}, D) = \int p(t|\boldsymbol{x}, \boldsymbol{w}) p(\boldsymbol{w}|D)\, d\boldsymbol{w} \tag{4}$$

where $p(t|\boldsymbol{x}, \boldsymbol{w})$ is given by (1).

Throughout this paper we consider a particular class of non-linear models of the form

$$y(\boldsymbol{x}; \boldsymbol{w}) = \sum_{j=1}^{M} w_j \phi_j(\boldsymbol{x}) = \boldsymbol{\phi}^{\mathrm{T}}(\boldsymbol{x})\boldsymbol{w} \tag{5}$$

which we shall call generalized linear regression models. Here the $\phi_j(\boldsymbol{x})$ are a set of fixed non-linear basis functions, with generally one of the basis functions $\phi_1 = 1$ so that w_1 plays the role of a bias parameter. Such models possess universal approximation capabilities for reasonable choices of the $\phi_j(\boldsymbol{x})$, while having the advantage of being linear in the adaptive parameters $\boldsymbol{w}$.

Since (5) is linear in $\boldsymbol{w}$, both the noise model $p(t|\boldsymbol{x}, \boldsymbol{w})$ and the posterior distribution $p(\boldsymbol{w}|D)$ will be Gaussian functions of $\boldsymbol{w}$. It therefore follows that, for a Gaussian prior of the form (2), the integral in (4) will be Gaussian and can be evaluated analytically to give a predictive distribution $p(t|\boldsymbol{x}, D)$ which will be a Gaussian function of t. The mean of this distribution is given by $y(\boldsymbol{x}; \boldsymbol{w}_{\mathrm{MP}})$ where $\boldsymbol{w}_{\mathrm{MP}}$ is

found by minimizing the regularized error function

$$\frac{1}{2\sigma_\nu^2}\sum_{n=1}^{N}\{\boldsymbol{\phi}^{\mathrm{T}}(\boldsymbol{x}^n)\boldsymbol{w}-t^n\}^2+\frac{1}{2}\boldsymbol{w}^{\mathrm{T}}\boldsymbol{S}\boldsymbol{w} \tag{6}$$

and is therefore given by the solution of the following linear equations

$$\boldsymbol{A}\boldsymbol{w}_{\mathrm{MP}}=\sigma_\nu^{-2}\boldsymbol{\Phi}^{\mathrm{T}}\boldsymbol{t} \tag{7}$$

where $\boldsymbol{t}$ is a column vector with elements t^n, $\boldsymbol{A}$ is the Hessian matrix given by

$$\boldsymbol{A}=\frac{1}{\sigma_\nu^2}\sum_{n=1}^{N}\boldsymbol{\phi}(\boldsymbol{x}^n)\boldsymbol{\phi}(\boldsymbol{x}^n)^{\mathrm{T}}+\boldsymbol{S}=\frac{1}{\sigma_\nu^2}\boldsymbol{\Phi}^{\mathrm{T}}\boldsymbol{\Phi}+\boldsymbol{S} \tag{8}$$

and $\boldsymbol{\Phi}$ is the $N\times M$ *design matrix* with elements $\Phi_{nj}=\phi_j(\boldsymbol{x}^n)$. Solving for $\boldsymbol{w}_{\mathrm{MP}}$ and substituting into (5) we obtain the following expression for the corresponding network output

$$y_{\mathrm{MP}}(\boldsymbol{x})=\boldsymbol{\phi}^{\mathrm{T}}(\boldsymbol{x})\boldsymbol{w}=\sigma_\nu^{-2}\boldsymbol{\phi}^{\mathrm{T}}(\boldsymbol{x})\boldsymbol{A}^{-1}\boldsymbol{\Phi}^{\mathrm{T}}\boldsymbol{t} \tag{9}$$

The covariance matrix for the posterior distribution $p(\boldsymbol{w}|D)$ is given by the inverse of the Hessian matrix. Together with (4) this implies that the total variance of the output predictions is given by

$$\sigma^2(\boldsymbol{x})=\sigma_\nu^2+\sigma_w^2(\boldsymbol{x})=\sigma_\nu^2+\boldsymbol{\phi}^{\mathrm{T}}(\boldsymbol{x})\boldsymbol{A}^{-1}\boldsymbol{\phi}(\boldsymbol{x}) \tag{10}$$

Here the first term represents the intrinsic noise on the target data, while the second term arises from the uncertainty in the weight values as a consequence of having a finite data set.

3 An Upper Bound on the Error Bars

We first consider the behaviour of the error bars when the data set consists of a single data point. As well as providing important insights into the nature of the error bars, it also leads directly to an upper bound on the true error bars.

In the absence of data, the variance is given from (8) and (10) by

$$\sigma^2(\boldsymbol{x})=\sigma_\nu^2+\boldsymbol{\phi}^{\mathrm{T}}(\boldsymbol{x})\boldsymbol{S}^{-1}\boldsymbol{\phi}(\boldsymbol{x}) \tag{11}$$

where the second term, due to the prior, is typically much larger than the noise term σ_ν^2. If we now add a single data point located at $\boldsymbol{x}^0$ then the Hessian becomes $\boldsymbol{S}+\sigma_\nu^{-2}\boldsymbol{\phi}(\boldsymbol{x}^0)\boldsymbol{\phi}^{\mathrm{T}}(\boldsymbol{x}^0)$. To find the inverse of the Hessian we make use of the identity

$$\left(\boldsymbol{M}+\boldsymbol{v}\boldsymbol{v}^{\mathrm{T}}\right)^{-1}=\boldsymbol{M}^{-1}-\frac{\left(\boldsymbol{M}^{-1}\boldsymbol{v}\right)\left(\boldsymbol{v}^{\mathrm{T}}\boldsymbol{M}^{-1}\right)}{1+\boldsymbol{v}^T\boldsymbol{M}^{-1}\boldsymbol{v}} \tag{12}$$

which is easily verified by multiplying both sides by $(\boldsymbol{M}+\boldsymbol{v}\boldsymbol{v}^{\mathrm{T}})$. The variance at an arbitrary point $\boldsymbol{x}$ for a single data point at $\boldsymbol{x}^0$ is then given by

$$\sigma^2(\boldsymbol{x})=\sigma_\nu^2+C(\boldsymbol{x},\boldsymbol{x})-\frac{C(\boldsymbol{x},\boldsymbol{x}^0)^2}{\sigma_\nu^2+C(\boldsymbol{x}^0,\boldsymbol{x}^0)} \tag{13}$$

where we have defined the *prior covariance function*

$$C(\boldsymbol{x},\boldsymbol{x}')=\boldsymbol{\phi}^{\mathrm{T}}(\boldsymbol{x})\boldsymbol{S}^{-1}\boldsymbol{\phi}(\boldsymbol{x}') \tag{14}$$

The first two terms on the right hand side of (13) represent the variance due to the prior alone, and we see that the effect of the additional data point is to reduce the variance from its prior value, as illustrated for a toy problem in Figure 1. From (13) we see that the length scale of this reduction is related to the prior covariance function $C(\boldsymbol{x},\boldsymbol{x}')$.

If we evaluate $\sigma^2(\boldsymbol{x})$ in (13) at the point $\boldsymbol{x}^0$ then we can show that the error bars satisfy the upper bound $\sigma^2(\boldsymbol{x}^0) \leq 2\sigma_\nu^2$. Since the noise level is typically much less than the prior variance level, we see that the error bars are pulled down very substantially in the neighbourhood of the data point. Again, this is illustrated in Figure 1.

We now extend this analysis to provide an upper bound on the error bars. Suppose we have a data set consisting of N data points (at arbitrary locations) and we add an extra data point at $\boldsymbol{x}^{N+1}$. Using (8) the Hessian $\boldsymbol{A}_{N+1}$ for the $N+1$ data points can be written in terms of the corresponding Hessian $\boldsymbol{A}_N$ for the original N data points in the form

$$\boldsymbol{A}_{N+1} = \boldsymbol{A}_N + \sigma_\nu^{-2}\boldsymbol{\phi}(\boldsymbol{x}^{N+1})\boldsymbol{\phi}^{\mathrm{T}}(\boldsymbol{x}^{N+1}) \tag{15}$$

Using the identity (12) we can now write the inverse of $\boldsymbol{A}_{N+1}$ in the form

$$\boldsymbol{A}_{N+1}^{-1} = \boldsymbol{A}_N^{-1} - \frac{\boldsymbol{A}_N^{-1}\boldsymbol{\phi}(\boldsymbol{x}^{N+1})\boldsymbol{\phi}^{\mathrm{T}}(\boldsymbol{x}^{N+1})\boldsymbol{A}_N^{-1}}{\sigma_\nu^2 + \boldsymbol{\phi}^{\mathrm{T}}(\boldsymbol{x}^{N+1})\boldsymbol{A}_N^{-1}\boldsymbol{\phi}(\boldsymbol{x}^{N+1})} \tag{16}$$

Substituting this result into (10) we obtain

$$\sigma_{N+1}^2(\boldsymbol{x}) = \sigma_N^2(\boldsymbol{x}) - \frac{\left[\boldsymbol{\phi}^{\mathrm{T}}(\boldsymbol{x}^{N+1})\boldsymbol{A}_N^{-1}\boldsymbol{\phi}(\boldsymbol{x})\right]^2}{\sigma_\nu^2 + \boldsymbol{\phi}^{\mathrm{T}}(\boldsymbol{x}^{N+1})\boldsymbol{A}_N^{-1}\boldsymbol{\phi}(\boldsymbol{x}^{N+1})} \tag{17}$$

From (8) we see that the Hessian $\boldsymbol{A}_N$ is positive definite, and hence its inverse will be positive definite. It therefore follows that the second term on the right hand side of (17) is negative, and so we obtain

$$\sigma_{N+1}^2(\boldsymbol{x}) \leq \sigma_N^2(\boldsymbol{x}) \tag{18}$$

This represents the intuitive result that the addition of an extra data point cannot lead to an increase in the magnitude of the error bars. Repeated application of this result shows that the error bars due to a set of data points will never be larger than the error bars due to any subset of those data points.

It can also be shown that the average change in the error bars resulting from the addition of an extra data point satisfies the bounds

$$\langle \Delta\sigma^2(\boldsymbol{x}) \rangle \equiv \frac{1}{N}\sum_{n=1}^{N}\left[\sigma_{N+1}^2(\boldsymbol{x}^n) - \sigma_N^2(\boldsymbol{x}^n)\right] \geq -\frac{\sigma_\nu^2}{N} \tag{19}$$

A further corollary of the result (18) is that, if we consider the error bars due to each of a set of N data points individually, then the *envelope* of those error bars constitutes an *upper bound* on the true error bars. This is illustrated with a toy problem in Figure 1. The contributions from the individual data points are easily evaluated using (13) and (14) since they depend only on the prior covariance function and do not require evaluation or inversion of the Hessian matrix.

4 Summary

In this paper we have explored the relationship between the magnitude of the Bayesian error bars and the distribution of data in input space. For the case of a single isolated data point we have shown that the error bar is pulled down close to the noise level, and that the length scale over which this effect occurs is characterized by the prior covariance function. From this result we have derived an upper bound on the error bars, expressed in terms of the contributions from individual data points.

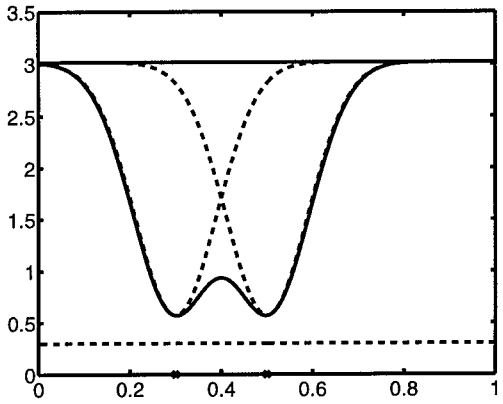

Figure 1 A simple example of error bars for a one-dimensional input space and a set of 30 equally spaced Gaussian basis functions with standard deviation 0.07. There are two data points at $x = 0.3$ and $x = 0.5$ as shown by the crosses. The solid curve at the top shows the variance $\sigma^2(x)$ due to the prior, the dashed curves show the variance resulting from taking one data point at a time, and the lower solid curve shows the variance due to the complete data set. The envelope of the dashed curves constitutes an upper bound on the true error bars, while the noise level (shown by the lower dashed curve) constitutes a lower bound.

REFERENCES

[1] C. M. Bishop. *Neural Networks for Pattern Recognition.* Oxford University Press, (1995).

[2] D. J. C. MacKay. Bayesian interpolation. *Neural Computing*, Vol. 4(3) (1992), pp415–447.

[3] C. K. I. Williams, C. Qazaz, C. M. Bishop, and H. Zhu. *On the relationship between Bayesian error bars and the input data density*, In Proceedings Fourth IEE International Conference on Artificial Neural Networks (1995), pp160–165, Cambridge, UK, IEE.

Acknowledgements

This work was supported by EPSRC grant GR/K51792 *Validation and verification of neural network systems.*

CAPACITY BOUNDS FOR STRUCTURED NEURAL NETWORK ARCHITECTURES

Peter Rieper, Sabine Kröner* and Reinhard Moratz**

FB Mathematik, Universität Hamburg, Bundesstr. 55, D-20146 Hamburg, Germany.

** Technische Informatik I, TU Hamburg-Harburg, Harburger Schloßstr. 20, D-21071 Hamburg, Germany. Email: Kroener@tu-harburg.d400.de*

*** AG Angewandte Informatik, Universität Bielefeld, Postfach 100131, D-33501 Bielefeld, Germany.*

In this paper an upper bound of the capacity or Vapnik-Chervonenkis dimension of structured multi-layer feedforward neural networks with shared weight vectors is derived. It mainly depends on the number of free network parameters analogous to the case of feedforward networks with independent weights. This means that weight sharing in a fixed neural architecture leads to a significant reduction of the upper bound of the capacity.

1 Introduction

Structured multi-layer feedforward neural networks gain more and more importance in speech- and image processing applications. Their characteristic is that a-priori knowledge about the task to be performed is already built into their architecture by use of nodes with shared weight vectors. Examples are time delay neural networks [10] and networks for invariant pattern recognition [4, 5]. One problem in the training of neural networks is the estimation of the number of training samples needed to achieve good generalization. In [1] is shown that for feedforward architectures this number is correlated with the capacity or Vapnik-Chervonenkis dimension of the architecture. So far an upper bound for the capacity has been derived for two-layer feedforward architectures with independent weights: it depends with $\mathcal{O}(\frac{w}{a} \cdot \ln \frac{q}{a})$ on the number w of connections in the architecture with q nodes and a output elements. In this paper we focus on the calculation of upper bounds for the capacity of structured multi-layer feedforward neural architectures. First we give some definitions and introduce a new general terminology for the description of structured neural networks. In section 3 we apply this terminology on structured feedforward architectures first with one layer then with multiple layers. We show that they can be transformed into equivalent conventional multi-layer feedforward architectures. By extending known estimations for the capacity we achieve upper bounds for the capacity of structured neural architectures which increase with the number of independent network parameters. This means that weight sharing in a fixed neural architecture leads to a significant reduction of the upper bound of the capacity. The capacity mainly depends on the number of free parameters analogous to the case with independent weights. At the end we comment the results.

2 Definitions

A *layered feedforward network architecture* $\mathcal{N}_{e,a}^{r}$ is a directed acyclic graph with a sequence of e input nodes, $r-1$ ($r \in \mathbb{N}$) intermediate (*hidden*) layers of nodes, and a final output layer with a nodes. Every node is connected only to nodes in the next layer. To every node k with indegree $n \in \mathbb{N}$ a triplet $(\boldsymbol{w}_k, s_k, f_k)$ is assigned, consisting of a weight vector $\boldsymbol{w}_k \in \mathbb{R}^n$, a threshold value $s_k \in \mathbb{R}$, and an activation

function $f_k : \mathbb{R} \to \{0,1\}$. The activation function for all but the input nodes is the hard limiter function, and without loss of generality we choose $s = 0$ for the threshold values of all nodes. We define an architecture $\mathcal{N}^r_{e,a}$ with given triplets $(\boldsymbol{w}, s, f)$ for all nodes as a *net* $N^r_{e,a}$. With the net itself a function $F : \mathbb{R}^e \mapsto \{0,1\}^a$ is associated.

Let S be a fixed $(m \times e)$-input-matrix for $\mathcal{N}^r_{e,a}$. All nets $N^r_{e,a}$ that map S on the same $(m \times a)$-output-matrix T are grouped in a *net class* of $\mathcal{N}^r_{e,a}$ related to S. $\Delta(S)$ is the number of net classes of $\mathcal{N}^r_{e,a}$ related to S. The *growth function* $g(m)$ of an architecture $\mathcal{N}^r_{e,a}$ with m input vectors is the maximum number of net classes over all $(m \times e)$-input matrices S. Now we consider the nodes of the architecture $\mathcal{N}^r_{e,a}$ within one layer (except the input layer) with the same indegree $d \in \mathbb{N}$. All nodes k whose components of their weight vectors $\boldsymbol{w}_k \in \mathbb{R}^d$ can be permuted through a permutation $\pi_k : \mathbb{R}^d \to \mathbb{R}^d$ so that $\pi_k(\boldsymbol{w}_k) = \boldsymbol{w}\ \forall k$ for some vector $\boldsymbol{w} \in \mathbb{R}^d$ are elements of the same *node class* $K_{\boldsymbol{w}}$. We call an architecture $\mathcal{N}^r_{e,a}$ *structured* if at least one node class has more than one element. Then the architecture with b node classes $K_{\boldsymbol{w}_i} (i = 1, \ldots, b)$ is denoted $\mathcal{N}^r_{e,a}(K_{\boldsymbol{w}_1}, \ldots, K_{\boldsymbol{w}_b})$.

The *Vapnik-Chervonenkis dimension* d_{VC} [9] of a feedforward architecture is defined by $d_{VC} := \sup\{m \in \mathbb{N} \mid g(m) = 2^{ma}\}$. Let $Q := \left\{ m \in \mathbb{N} \;\middle|\; \frac{g(m)}{2^{ma}} \geq \frac{1}{2} \right\}$. Then $c := \sup Q$ for $Q \neq \emptyset$, or $c := 0$ for $Q = \emptyset$, is an upper bound for the Vapnik-Chervonenkis dimension and is also defined as capacity in [2, 7].

3 Upper Bounds for the Capacity

In this section is shown how structured architectures can be transformed into conventional architectures with independent weights. The upper bounds for the capacity of these conventional architectures then are applied to the structured architectures. A basic transformation needed in the following derivations is the transformation of structured one-layer architectures $\mathcal{N}(K_{\boldsymbol{w}_1}, \ldots, K_{\boldsymbol{w}_b})$ with input nodes of outdegree ≥ 1 and input vectors $\boldsymbol{x}_l$ into structured one-layer architectures $\mathcal{N}'(K_{\boldsymbol{w}_1}, \ldots, K_{\boldsymbol{w}_b})$ with input nodes of outdegree 1 only and dependent input vectors $\boldsymbol{x}_l{}'$ $(l = 1, \ldots, m)$: Every input node with outdegree $z > 1$ is replaced by z copies of that input node. The outgoing edges of the input node are assigned to the copies in such a way that every copy has outdegree 1. The elements of the input vectors are duplicated in the same way. By permuting the input nodes and the corresponding components of the input vectors we get the architecture $\mathcal{N}''(K_{\boldsymbol{w}_1}, \ldots, K_{\boldsymbol{w}_b})$ without any intersecting edges.

3.1 Structured One-layer Architectures

I) First we focus on structured one-layer architectures $\mathcal{N}^1_{e,a}(K_{\boldsymbol{w}})$ with a set $I := \{u_1, \ldots, u_e\}$ of e input nodes and the output layer $K := \{k_1, \ldots, k_a\}$. Let $K_{\boldsymbol{w}} := K$ be the only node class. All nodes in $K_{\boldsymbol{w}} = K$ have the same indegree $d \in \mathbb{N}$.

Theorem 1 *Let a structured one-layer architecture $\mathcal{N}^1_{e,a}(K_{\boldsymbol{w}})$ with only one node class $K_{\boldsymbol{w}} = K$ be given. Suppose $d \in \mathbb{N}$ as the indegree of all nodes in $K_{\boldsymbol{w}}$. The number of input nodes is $e \leq a \cdot d$. For m input vectors of length e an upper bound for the growth function $g(m)$ of the structured one-layer architecture $\mathcal{N}^1_{e,a}(K_{\boldsymbol{w}})$ is*

given by

$$C(m{\cdot}a,d) := 2 \cdot \sum_{i=0}^{d-1} \binom{m{\cdot}a-1}{i} .$$

Proof At first we examine structured one-layer architectures with outdegree 1 for every input node, equivalent to architectures $\mathcal{N}^1_{e,a}(K_{\boldsymbol{w}})$ with $e = a \cdot d$ input nodes. By permuting the input nodes and the corresponding components of the input vectors we get the architecture $\mathcal{N}''(K_{\boldsymbol{w}})$. Without loss of generality we consider the permutation π of the node class $K_{\boldsymbol{w}}$ as the identity function. Thus we have $\boldsymbol{w} = \boldsymbol{w}(k_1) = \ldots = \boldsymbol{w}(k_a) \in \mathbb{R}^d$ for the a weight vectors (cf. Figure 1 a)). For m fixed input vectors $\boldsymbol{x}_l := (\boldsymbol{x}_l^1, \ldots, \boldsymbol{x}_l^a) \in \mathbb{R}^{ad}$ $(\boldsymbol{x}_l^i \in \mathbb{R}^d,\ l = 1, \ldots, m,\ i = 1, \ldots, a)$ let S be an $(m \times a{\cdot}d)$-input matrix for $\mathcal{N}^1_{e,a}(K_{\boldsymbol{w}})$:

$$S := \begin{pmatrix} \boldsymbol{x}_1 \\ \vdots \\ \boldsymbol{x}_m \end{pmatrix} = \begin{pmatrix} \boldsymbol{x}_1^1 & \ldots & \boldsymbol{x}_1^a \\ \vdots & \ddots & \vdots \\ \boldsymbol{x}_m^1 & \ldots & \boldsymbol{x}_m^a \end{pmatrix} .$$

A given weight vector $\boldsymbol{w}_1 \in \mathbb{R}^d$ defines a function $F_1 : \mathbb{R}^{ad} \to \{0,1\}^a$ or a net

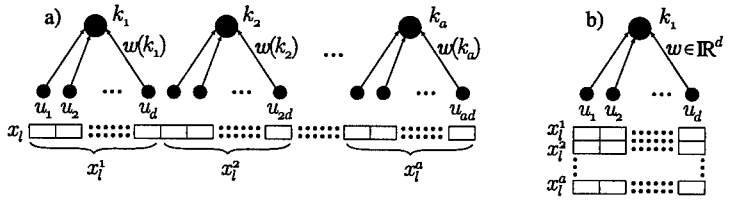

Figure 1 a) Structured architecture $\mathcal{N}(K_w)''$ with an input vector x_l $(l \in \{1, \ldots, m\})$. b) Architecture $\mathcal{N}^1_{d,1}$ with the corresponding a input vectors $x_l^1, \ldots, x_l^a$.

N_1, respectively. Let $\boldsymbol{w}_2$ be a weight vector that defines a function F_2 (a net N_2) different to F_1 on the input matrix S. Thus these two nets are elements of different net classes of $\mathcal{N}^1_{e,a}(K_{\boldsymbol{w}})$ related to the input matrix S. Now we consider the one-layer architecture $\mathcal{N}^1_{d,1}$, consisting of a single node with indegree d. By rearranging the m rows of the input matrix S for $\mathcal{N}''(K_{\boldsymbol{w}})$ to one column of the $m{\cdot}a$ input vectors $\boldsymbol{x}_l^i \in \mathbb{R}^d$ $(l = 1, \ldots, m,\ i = 1, \ldots, a)$ we derive the $(m{\cdot}a \times d)$-input matrix $\widetilde{S}$ for $\mathcal{N}^1_{d,1}$ (cf. Figure 1 b)):

$$\widetilde{S} := \begin{pmatrix} \boldsymbol{x}_1^1 \\ \boldsymbol{x}_1^2 \\ \vdots \\ \boldsymbol{x}_m^a \end{pmatrix} . \tag{1}$$

On $\mathcal{N}^1_{d,1}$ the weight vector $\boldsymbol{w}_1$ $(\boldsymbol{w}_2)$ defines a function $\widetilde{F_1} : \mathbb{R}^d \to \{0,1\}$ $(\widetilde{F_2} : \mathbb{R}^d \to \{0,1\})$ or a net $\widetilde{N_1}$ $(\widetilde{N_2})$, respectively. Because of $F_1(\boldsymbol{x}_s) \neq F_2(\boldsymbol{x}_s)$ for at least one input vector $\boldsymbol{x}_s$ $(s \in \{1, \ldots, m\})$ and definition (1) the nets $\widetilde{N_1}$ and $\widetilde{N_2}$ are elements of different net classes of $\mathcal{N}^1_{d,1}$ related to the input matrix $\widetilde{S}$. Summarizing we get: if two nets of the architecture $\mathcal{N}^1_{e,a}(K_{\boldsymbol{w}})$ are different related to any input matrix

S we can define an input matrix $\widetilde{S}$ for $\mathcal{N}^1_{d,1}$ by (1), so that the corresponding nets are different, too. For the number of net classes this yields

$$\Delta(S) \leq \Delta(\widetilde{S}) \,. \tag{2}$$

With the results of [7] the growth function of the architecture $\mathcal{N}^1_{d,1}$ is given by $C(m{\cdot}a, d)$. From (2) also follows that this is an upper bound for the growth function of the structured one-layer architecture $\mathcal{N}''(K_{\boldsymbol{w}})$ or $\mathcal{N}^1_{ad,a}(K_{\boldsymbol{w}})$ respectively: $g(m) \leq C(m{\cdot}a, d)$. The inequation $g(m) \geq C(m{\cdot}a, d)$ can easily be verified in a similar way, so it yields $g(m) = C(m{\cdot}a, d)$ for the growth function of structured one-layer architectures $\mathcal{N}^1_{e,a}(K_{\boldsymbol{w}})$ with outdegree 1 for every input node.
Now we consider structured one-layer architectures $\mathcal{N}^1_{e,a}(K_{\boldsymbol{w}})$ with outdegree $z > 1$ for some input nodes. These architectures can be transformed into structured one-layer architectures $\mathcal{N}''(K_{\boldsymbol{w}})$ with $e = a \cdot d$ input nodes all with outdegree 1. But the input vectors of the input matrix for the transformed architecture $\mathcal{N}''(K_{\boldsymbol{w}})$ cannot be chosen totally independent. Thus, $C(m{\cdot}a, d)$ is an upper bound for the growth function of structured one-layer architectures $\mathcal{N}^1_{e,a}(K_{\boldsymbol{w}})$ with exactly one node class $K_{\boldsymbol{w}} = K$. □

Remark 1 *With [7] we find $\frac{2{\cdot}d}{a}$ as an upper bound for the capacity of structured one-layer architectures $\mathcal{N}^1_{e,a}(K_{\boldsymbol{w}})$ with exactly one node class $K_{\boldsymbol{w}}$.*

II) Second we focus on structured one-layer architectures $\mathcal{N}^1_{e,a}(K_{\boldsymbol{w}_1}, \ldots, K_{\boldsymbol{w}_b})$ with b $(2 \leq b < a)$ node classes $K_{\boldsymbol{w}_1}, \ldots, K_{\boldsymbol{w}_b}$. These classes form the set K of the a output nodes: $K = K_{\boldsymbol{w}_1} \dot{\cup} \ldots \dot{\cup} K_{\boldsymbol{w}_b}$.

Theorem 2 *Assume a structured one-layer architecture $\mathcal{N}^1_{e,a}(K_{\boldsymbol{w}_1}, \ldots, K_{\boldsymbol{w}_b})$ with $e \leq \sum_{i=1}^{b} \alpha_i{\cdot}d_i$ input nodes, $a = \sum_{i=1}^{b} \alpha_i$ output nodes, and $b \in \mathbb{N}$ $(2 \leq b \leq a)$ node classes $K_{\boldsymbol{w}_i}$ $(i = 1, \ldots, b)$. Let $\alpha_i := |K_{\boldsymbol{w}_i}|$ be the sizes of the node classes $K_{\boldsymbol{w}_i}$, and d_i the indegrees of the nodes in $K_{\boldsymbol{w}_i}$ $(i = 1, \ldots, b)$. For m input vectors the product*

$$\prod_{i=1}^{b} C(m{\cdot}\alpha_i, d_i)$$

is an upper bound for the growth function of $\mathcal{N}^1_{e,a}(K_{\boldsymbol{w}_1}, \ldots, K_{\boldsymbol{w}_b})$.

Proof At first we examine structured one-layer architectures $\mathcal{N}^1_{e,a}(K_{\boldsymbol{w}_1}, \ldots, K_{\boldsymbol{w}_b})$ with $e = \sum_{i=1}^{b} \alpha_i{\cdot}d_i$ input nodes (all with outdegree 1) and an $(m \times e)$-input matrix S. The a nodes in the output layer K are permuted so that we get the ordered sequence $K = \{K_{\boldsymbol{w}_1}, \ldots, K_{\boldsymbol{w}_b}\}$ with $K_{\boldsymbol{w}_i} := \{k^i_1, \ldots, k^i_{\alpha_i}\}$ $(i = 1, \ldots, b)$. These permutations generate b structured one-layer sub architectures $\mathcal{N}^1_{e_i,\alpha_i}(K_{\boldsymbol{w}_i})$ with $e_i := \alpha_i{\cdot}d_i$ input nodes, α_i output nodes and $(m \times e_i)$-sub input matrices S^i $(i = 1, \ldots, b)$. With Theorem 1 we get $g_i(m) \leq C(m{\cdot}\alpha_i, d_i)$ for the growth functions $g_i(m)$ of these sub architectures. For the determination of the growth function $g(m)$ of $\mathcal{N}^1_{e,a}(K_{\boldsymbol{w}_1}, \ldots, K_{\boldsymbol{w}_b})$ the b input matrices S^i for the sub architectures can be chosen independently. Thus we get $g(m) = \prod_{i=1}^{b} g_i(m) \leq \prod_{i=1}^{b} C(m{\cdot}\alpha_i, d_i)$. The result for structured one-layer architectures $\mathcal{N}^1_{e,a}(K_{\boldsymbol{w}_1}, ..., K_{\boldsymbol{w}_b})$ with outdegree ≥ 1 for some input nodes, equivalent to $e < \sum_{i=1}^{b} \alpha_i{\cdot}d_i$ input nodes, follows in a similar way to Theorem 1. □

Theorem 3 *For the capacity of a structured one-layer architecture* $\mathcal{N}^1_{e,a}(K_{\boldsymbol{w}_1},\ldots,K_{\boldsymbol{w}_b})$ *with* $b \in \mathbb{N}$ $(2 \le b \le a)$ *node classes* $K_{\boldsymbol{w}_i}$ $(i=1,\ldots,b)$, *maximum indegree* $\widehat{d} \ge 2$ *for all nodes, maximum size* $\widehat{\alpha} := |K_{\boldsymbol{w}_i}|$ *of the node classes, and* $t := \frac{\widehat{\alpha}\cdot b}{a} \ge 2$ *we get*

$$c = \mathcal{O}\left(\frac{b\cdot\widehat{d}}{a}\cdot\ln t\right) .$$

Proof For the growth function $g(m)$ of the architecture $\mathcal{N}^1_{e,a}(K_{\boldsymbol{w}_1},\ldots,K_{\boldsymbol{w}_b})$ we get with the above definitions and Theorem 2:

$$g(m) \le \prod_{i=1}^{b} C(m\cdot\alpha_i, d_i) \le \prod_{i=1}^{b} C(m\cdot\widehat{\alpha},\widehat{d}) = C(m\cdot\widehat{\alpha},\widehat{d})^b .$$

This yields an upper bound for the capacity: $c \le \sup\left\{m\in\mathbb{N} \;\middle|\; \frac{C(m\cdot\widehat{\alpha},\widehat{d})^b}{2^{ma}} \ge \frac{1}{2}\right\}$.

With some estimations and $const := \frac{2+2\cdot\ln(2)}{(\ln(2))^2}$ it follows:

$$m \le const\cdot\frac{t\cdot\widehat{d}}{\widehat{\alpha}}\cdot\ln(t) .$$

For details and further information see [8]. □

3.2 Structured Multi-layer Architectures

Consider a structured r-layer architecture with e input nodes, a_j nodes in the hidden layers H^j $(j=1,\ldots,r-1)$ and a nodes in the output layer K. Let the layers H^j be the disjoint union of the $b_j \le a_j$ node classes $H_{\boldsymbol{w}^j_1},\ldots,H_{\boldsymbol{w}^j_{b_j}}$ and the output layer the disjoint union of the node classes $K_{\boldsymbol{w}_i}$ $(i=1,\ldots,b)$. The number of node classes is $\sum_{j=1}^{r-1} b_j + b =: \beta$. The structured architecture is denoted by $\mathcal{N}^r_{e,a}(H_{\boldsymbol{w}^1_1},\ldots,K_{\boldsymbol{w}_b})$. A structured r-layer feedforward architecture $\mathcal{N}^r_{e,a}(H_{\boldsymbol{w}^1_1},\ldots,K_{\boldsymbol{w}_b})$ can be regarded as a combination of r structured one-layer feedforward architectures since the output matrices of each layer are the input matrices for the following layer. Thus, we get an upper bound for the growth function $g(m)$ of $\mathcal{N}^r_{e,a}(H_{\boldsymbol{w}^1_1},\ldots,K_{\boldsymbol{w}_b})$ by multiplying the growth functions of the r structured one-layer architectures (refer to Theorem 2):

$$g(m) \le \prod_{j=1}^{r-1}\left(\prod_{i=1}^{b_j} C(m\cdot\alpha^j_i, d^j_i)\right)\cdot\prod_{i=1}^{b} C(m\cdot\alpha_i, d_i) . \tag{3}$$

With the maximum size $\widehat{\alpha} := \max\left\{\alpha_1,\ldots,\alpha_b,\alpha^1_1,\ldots,\alpha^{r-1}_{b_{r-1}}\right\}$ of the β node classes, and the maximum indegree $\widehat{d}$ of all nodes of the architecture $\mathcal{N}^r_{e,a}(H_{\boldsymbol{w}^1_1},\ldots,K_{\boldsymbol{w}_b})$, $C(m\cdot\widehat{\alpha},\widehat{d})^\beta$ is an upper bound for (3).

Theorem 4 *Let* $\mathcal{N}^r_{e,a}(H_{\boldsymbol{w}^1_1},\ldots,K_{\boldsymbol{w}_b})$ *be a structured* r*-layer feedforward architecture with* $\beta \ge 2$ *node classes* $H_{\boldsymbol{w}^1_1},\ldots,K_{\boldsymbol{w}_b}$, $\widehat{d} \ge 2$ *the maximum indegree of all nodes,* $\widehat{\alpha}$ *the maximum size of all* β *node classes, and* $\widehat{t} := \frac{\widehat{\alpha}\cdot\beta}{a} \ge 2$. *For the capacity of* $\mathcal{N}^r_{e,a}(H_{\boldsymbol{w}^1_1},\ldots,K_{\boldsymbol{w}_b})$ *we get*

$$c = \mathcal{O}\left(\frac{\beta\cdot\widehat{d}}{a}\cdot\ln\widehat{t}\right) .$$

Proof Analogous to the proof of Theorem 3. □

An architecture $\mathcal{N}^r_{e,a}(H_{\boldsymbol{w}^1_1}, \ldots, K_{\boldsymbol{w}_b})$ with $\sum_{j=1}^{r-1} b_j + b = \sum_{j=1}^{r-1} a_j + a$ node classes is equivalent to an architecture $\mathcal{N}^r_{e,a}$ in which every node class has size 1. So the above upper bounds for the capacity hold good for conventional r-layer feedforward architectures, too.

4 Conclusion

By transforming architectures with shared weight vectors into equivalent conventional feedforward architectures and the extension of the definitions of the growth function and the capacity to multi-layer feedforward architectures we obtain estimations for the upper bounds of the capacity of structured multi-layer architectures. These upper bounds depend with $\mathcal{O}(\frac{p}{a} \cdot \ln \widehat{t})$ on the number p of free parameters in the structured neural architecture with maximum size $\widehat{\alpha}$ of the β node classes, $\widehat{t} := \frac{\widehat{\alpha} \cdot \beta}{a} \geq 2$, and a nodes in the output layer. So weight sharing in a fixed neural architecture leads to a reduction of the upper bound of the capacity. The amount of the reduction increases with the extent of the weight sharing. With $\widehat{\alpha} = 1$ the upper bounds hold good for conventional feedforward networks with independent weights, too. It is known that the generalization ability of a feedforward neural architecture improves within certain limits with a reduction of the capacity for a fixed number of training samples. As a consequence of our results a better generalization ability can be derived for structured neural architectures compared to the same unstructured ones. This is a theoretic justification for the generalization ability of structured neural architectures observed in experiments [5]. Further investigations focus on an improvement of the upper bounds, on the determination of capacity bounds for special structured architectures, and on the derivation of capacity bounds for structured architectures of nodes with continuous transfer functions [3, 6].

REFERENCES

[1] E. B. Baum, D. Haussler, *What Size Net gives Valid Generalization?*, Advances in Neural Information Processing Systems, D. Touretzky, (Ed.), Morgan Kaufmann, (1989).

[2] T. M. Cover, *Geometrical and Statistical Properties of Systems of Linear Inequalities with Applications in Pattern Recognition*, IEEE Trans. on Electronic Computers, Vol. 14 (1965), pp326-334.

[3] P. Koiran, E.D. Sontag, *Neural Networks with Quadratic VC Dimension*, NeuroCOLT Technical Report Series, NC-TR-95-044, London (1995).

[4] S. Kröner, R. Moratz, H. Burkhardt: *An adaptive invariant transform using neural network techniques*, Proc. of 7th Europ. Sig. Proc. Conf., Holt et al. (Eds.), Vol. III (1994), pp1489-1491, Edinburgh.

[5] Y. le Cun, *Generalization and Network Design Strategies*, Connectionism in Perspective, R. Pfeiffer et al. (Eds.), Elsevier Science Publishers B.V. North-Holland (1989), pp143-155.

[6] W. Maass, *Vapnik-Chervonenkis Dimension of Neural Nets*, Preprint, Techn. Univ. Graz, (1994).

[7] G. J. Mitchison, R. M. Durbin, *Bounds on the Learning Capacity of Some Multi-Layer Networks*, Biological Cybernetics, Vol. 60 No. 5 (1989), pp345-356.

[8] P. Rieper, *Zur Speicherfähigkeit vorwärtsgerichteter Architekturen künstlicher neuronaler Netze mit gekoppelten Knoten*, Diplomarbeit, Universität Hamburg, (1994).

[9] V. Vapnik, *Estimation of Dependences Based on Empirical Data*, Springer-Verlag, Berlin (1982).

[10] A. Waibel, *Modular Construction of Time-Delay Neural Networks for Speech Recognition*, Neural Computation, Vol.1 (1989), pp39-46.

ON-LINE LEARNING IN MULTILAYER NEURAL NETWORKS

David Saad and Sara A. Solla*

Dept. of Computer Science and Applied Mathematics,
University of Aston, Birmingham B4 7ET, UK.
** CONNECT, The Niels Bohr Institute, Blegdamsvej 17,*
Copenhagen 2100, Denmark.

We present an analytic solution to the problem of on-line gradient-descent learning for two-layer neural networks with an arbitrary number of hidden units in both teacher and student networks. The technique, demonstrated here for the case of adaptive input-to-hidden weights, becomes exact as the dimensionality of the input space increases.

Layered neural networks are of interest for their ability to implement input-output maps [1]. Classification and regression tasks formulated as a map from an N-dimensional input space $\boldsymbol{\xi}$ onto a scalar ζ are realized through a map $\zeta = f_{\mathbf{J}}(\boldsymbol{\xi})$, which can be modified through changes in the internal parameters $\{\mathbf{J}\}$ specifying the strength of the interneuron couplings. Learning refers to the modification of these couplings so as to bring the map $f_{\mathbf{J}}$ implemented by the network as close as possible to a desired map $\tilde{f}$. Information about the desired map is provided through independent examples $(\boldsymbol{\xi}^{\mu}, \zeta^{\mu})$, with $\zeta^{\mu} = \tilde{f}(\boldsymbol{\xi}^{\mu})$ for all μ. A recently introduced approach investigates *on-line learning* [2]. In this scenario the couplings are adjusted to minimize the error after the presentation of each example. The resulting changes in $\{\mathbf{J}\}$ are described as a dynamical evolution, with the number of examples playing the role of time. The average that accounts for the disorder introduced by the independent random selection of an example at each time step can be performed directly. The result is expressed in the form of dynamical equations for *order parameters* which describe correlations among the various nodes in the trained network as well as their degree of specialization towards the implementation of the desired task. Here we obtain *analytic* equations of motion for the order parameters in a general two-layer scenario: a student network composed of N input units, K hidden units, and a single linear output unit is trained to perform a task defined through a teacher network of similar architecture except that its number M of hidden units is not necessarily equal to K. Two-layer networks with an arbitrary number of hidden units have been shown to be universal approximators [1] for N-to-one dimensional maps. Our results thus describe the learning of tasks of arbitrary complexity (general M). The complexity of the student network is also arbitrary (general K, independent of M), providing a tool to investigate realizable ($K = M$), over-realizable ($K > M$), and unrealizable ($K < M$) learning scenarios. In this paper we limit our discussion to the case of the soft-committee machine [2], in which all the hidden units are connected to the output unit with positive couplings of unit strength, and only the input-to-hidden couplings are adaptive. Consider the student network: hidden unit i receives information from input unit r through the weight J_{ir}, and its activation under presentation of an input pattern $\boldsymbol{\xi} = (\xi_1, \ldots, \xi_N)$ is $x_i = \mathbf{J}_i \cdot \boldsymbol{\xi}$, with $\mathbf{J}_i = (J_{i1}, \ldots, J_{iN})$ defined as the vector of incoming weights onto the i-th hidden unit. The output of the student network is $\sigma(\mathbf{J}, \boldsymbol{\xi}) = \sum_{i=1}^{K} g\,(\mathbf{J}_i \cdot \boldsymbol{\xi})$, where g is the activation function of the hidden units,

taken here to be the error function $g(x) \equiv \mathrm{erf}(x/\sqrt{2})$, and $\mathbf{J} \equiv \{\mathbf{J}_i\}_{1\leq i\leq K}$ is the set of input-to-hidden adaptive weights. Training examples are of the form $(\boldsymbol{\xi}^\mu, \zeta^\mu)$. The components of the independently drawn input vectors $\boldsymbol{\xi}^\mu$ are uncorrelated random variables with zero mean and unit variance. The corresponding output ζ^μ is given by a deterministic teacher whose internal structure is that of a network similar to the student except for a possible difference in the number M of hidden units. Hidden unit n in the teacher network receives input information through the weight vector $\mathbf{B}_n = (B_{n1}, \ldots, B_{nN})$, and its activation under presentation of the input pattern $\boldsymbol{\xi}^\mu$ is $y_n^\mu = \mathbf{B}_n \cdot \boldsymbol{\xi}^\mu$. The corresponding output is $\zeta^\mu = \sum_{n=1}^{M} g\,(\mathbf{B}_n \cdot \boldsymbol{\xi}^\mu)$. We will use indices $i, j, k, l \ldots$ to refer to units in the student network, and $n, m, \ldots$ for units in the teacher network. The error made by a student with weights $\mathbf{J}$ on a given input $\boldsymbol{\xi}$ is given by the quadratic deviation

$$\epsilon(\mathbf{J}, \boldsymbol{\xi}) \equiv \frac{1}{2}\left[\, \sigma(\mathbf{J}, \boldsymbol{\xi}) - \zeta \,\right]^2 = \frac{1}{2}\left[\sum_{i=1}^{K} g(x_i) - \sum_{n=1}^{M} g(y_n) \right]^2 . \tag{1}$$

Performance on a typical input defines the *generalization error* $\epsilon_g(\mathbf{J}) \equiv < \epsilon(\mathbf{J}, \boldsymbol{\xi}) >_{\{\xi\}}$ through an average over all possible input vectors $\boldsymbol{\xi}$, to be performed implicitly through averages over the activations $\mathbf{x} = (x_1, \ldots, x_K)$ and $\mathbf{y} = (y_1, \ldots, y_M)$. Note that both $< x_i >=< y_n >= 0$, while the components of the covariance matrix $\mathcal{C}$ are given by overlaps among the weight vectors associated with the various hidden units: $< x_i\, x_k > = \mathbf{J}_i \cdot \mathbf{J}_k \equiv Q_{ik}$, $< x_i\, y_n > = \mathbf{J}_i \cdot \mathbf{B}_n \equiv R_{in}$, and $< y_n\, y_m > = \mathbf{B}_n \cdot \mathbf{B}_m \equiv T_{nm}$. The averages over $\mathbf{x}$ and $\mathbf{y}$ are performed using a joint probability distribution given by the multivariate Gaussian:

$$\mathcal{P}(\mathbf{x}, \mathbf{y}) = \frac{1}{\sqrt{(2\pi)^{K+M}|\mathcal{C}|}} \exp\left\{ -\frac{1}{2}(\mathbf{x}, \mathbf{y})^T \mathcal{C}^{-1} (\mathbf{x}, \mathbf{y}) \right\} \text{ , with } \mathcal{C} = \begin{bmatrix} Q & R \\ R^T & T \end{bmatrix} . \tag{2}$$

The averaging yields an expression for the generalization error in terms of the order parameters Q_{ik}, R_{in}, and T_{nm}. For $g(x) \equiv \mathrm{erf}(x/\sqrt{2})$ the result is:

$$\epsilon_g(\mathbf{J}) = \frac{1}{\pi}\left\{ \sum_{ik} \arcsin \frac{Q_{ik}}{\sqrt{1+Q_{ii}}\,\sqrt{1+Q_{kk}}} + \sum_{nm} \arcsin \frac{T_{nm}}{\sqrt{1+T_{nn}}\,\sqrt{1+T_{mm}}} - 2 \sum_{in} \arcsin \frac{R_{in}}{\sqrt{1+Q_{ii}}\,\sqrt{1+T_{nn}}} \right\} . \tag{3}$$

The parameters T_{nm} are characteristic of the task to be learned and remain fixed, while the overlaps Q_{ik} and R_{in} are determined by the student weights $\mathbf{J}$ and evolve during training. A gradient descent rule for the update of the student weights results in $\mathbf{J}_i^{\mu+1} = \mathbf{J}_i^\mu + \frac{\eta}{N}\, \delta_i^\mu\, \boldsymbol{\xi}^\mu$, where the learning rate η has been scaled with the input size N, and $\delta_i^\mu \equiv g'(x_i^\mu)\left[\sum_{n=1}^{M} g(y_n^\mu) - \sum_{j=1}^{K} g(x_j^\mu)\right]$ is defined in terms of both the activation function g and its derivative g'. The time evolution of the overlaps R_{in} and Q_{ik} can be explicitly written in terms of similar difference equations. The dependence on the current input $\boldsymbol{\xi}^\mu$ is only through the activations $\mathbf{x}$ and $\mathbf{y}$, and the corresponding averages can be performed using the joint probability distribution (2). In the thermodynamic limit $N \to \infty$ the normalized example number $\alpha = \mu/N$

can be interpreted as a continuous time variable, leading to the equations of motion:

$$\frac{dR_{in}}{d\alpha} = \eta \left\{ \sum_m I_3(i,n,m) - \sum_j I_3(i,n,j) \right\} ,$$

$$\frac{dQ_{ik}}{d\alpha} = \eta \left\{ \sum_m I_3(i,k,m) - \sum_j I_3(i,k,j) \right\} + \eta \left\{ \sum_m I_3(k,i,m) - \sum_j I_3(k,i,j) \right\} + \eta^2 \left\{ \sum_{n,m} I_4(i,k,n,m) - 2 \sum_{j,n} I_4(i,k,j,n) + \sum_{j,l} I_4(i,k,j,l) \right\} . \quad (4)$$

The two multivariate Gaussian integrals: $I_3 \equiv < g'(u)\ v\ g(w) >$ and $I_4 \equiv < g'(u)\ g'(v)\ g(w)\ g(z) >$ represent averages over the probability distribution (2). The averages can be performed analytically for the choice $g(x) = \mathrm{erf}(x/\sqrt{2})$. Arguments assigned to I_3 and I_4 are to be interpreted following our convention to distinguish student from teacher activations. For example, $I_3(i,n,j) \equiv < g'(x_i)\ y_n\ g(x_j) >$, and the average is performed using the three-dimensional covariance matrix C_3 which results from projecting the full covariance matrix $\mathcal{C}$ of Eq. (2) onto the relevant subspace. For $I_3(i,n,j)$ the corresponding matrix is:

$$C_3 = \begin{pmatrix} Q_{ii} & R_{in} & Q_{ij} \\ R_{in} & T_{nn} & R_{jn} \\ Q_{ij} & R_{jn} & Q_{jj} \end{pmatrix} .$$

I_3 is given in terms of the components of the C_3 covariance matrix by

$$I_3 = \frac{2}{\pi} \frac{1}{\sqrt{\Lambda_3}} \frac{C_{23}(1+C_{11}) - C_{12}C_{13}}{1+C_{11}} , \quad (5)$$

with $\Lambda_3 = (1+C_{11})(1+C_{33}) - C_{13}^2$. The expression for I_4 in terms of the components of the corresponding C_4 covariance matrix is

$$I_4 = \frac{4}{\pi^2} \frac{1}{\sqrt{\Lambda_4}} \arcsin\left(\frac{\Lambda_0}{\sqrt{\Lambda_1}\sqrt{\Lambda_2}} \right) , \quad (6)$$

where $\Lambda_4 = (1+C_{11})(1+C_{22}) - C_{12}^2$, and

$$\Lambda_0 = \Lambda_4 C_{34} - C_{23}C_{24}(1+C_{11}) - C_{13}C_{14}(1+C_{22}) + C_{12}C_{13}C_{24} + C_{12}C_{14}C_{23} ,$$

$$\Lambda_1 = \Lambda_4(1+C_{33}) - C_{23}^2(1+C_{11}) - C_{13}^2(1+C_{22}) + 2C_{12}C_{13}C_{23} ,$$

$$\Lambda_2 = \Lambda_4(1+C_{44}) - C_{24}^2(1+C_{11}) - C_{14}^2(1+C_{22}) + 2C_{12}C_{14}C_{24} .$$

These dynamical equations provide a novel tool for analyzing the learning process for a general soft-committee machine with an arbitrary number K of hidden units, trained to perform a task defined by a soft-committee teacher with M hidden units. This set of coupled first-order differential equations can be easily solved numerically, even for large values of K and M, providing valuable insight into the process of learning in multilayer networks, and allowing for the calculation of the time evolution of the generalization error [3]. In what follows we focus on learning a realizable task ($K = M$) defined through uncorrelated teacher vectors of unit length

($T_{nm} = \delta_{nm}$). The time evolution of the overlaps R_{in} and Q_{ik} follows from integrating the equations of motion (3) from initial conditions determined by a random initialization of the student vectors $\{\mathbf{J}_i\}_{1 \leq i \leq K}$. Random initial norms Q_{ii} for the student vectors are taken here from a uniform distribution in the $[0, 0.5]$ interval. Overlaps Q_{ik} between independently chosen student vectors $\mathbf{J}_i$ and $\mathbf{J}_k$, or R_{in} between $\mathbf{J}_i$ and an unknown teacher vector $\mathbf{B}_n$ are small numbers, of order $1/\sqrt{N}$ for $N \gg K$, and taken here from a uniform distribution in the $[0, 10^{-12}]$ interval. We show in Fig. 1a-c the resulting evolution of the overlaps and generalization error for $K = 3$ and $\eta = 0.1$. This example illustrates the successive regimes of the learning process. The system quickly evolves into a symmetric subspace controlled by an unstable suboptimal solution which exhibits no differentiation among the various student hidden units. Trapping in the symmetric subspace prevents the specialization needed to achieve the optimal solution, and the generalization error remains finite, as shown by the plateau in Fig. 1c. The symmetric solution is unstable, and the perturbation introduced through the random initialization of the overlaps R_{in} eventually takes over: the student units become specialized and the matrix R of student-teacher overlaps tends towards the matrix T, except for a permutational symmetry associated with the arbitrary labeling of the student hidden units. The generalization error plateau is followed by a monotonic decrease towards zero once the specialization begins and the system evolves towards the optimal solution. Curves for the time evolution of the generalization error for different values of η shown in Fig. 1d for $K = 3$ identify trapping in the symmetric subspace as a small η phenomenon. We therefore consider the equations of motion (3) in the small η regime. The term proportional to η^2 is neglected and the resulting truncated equations of motion are used to investigate a phase characterized by students of similar norms: $Q_{ii} = Q$ for all $1 \leq i \leq K$, similar correlations among themselves: $Q_{ik} = C$ for all $i \neq k$, and similar correlations with the teacher vectors: $R_{in} = R$ for all $1 \leq i, n \leq K$. The resulting dynamical equations exhibit a fixed point solution at $Q^* = C^* = 1/(2K-1)$ and $R^* = \sqrt{Q^*/K} = 1/\sqrt{K(2K-1)}$. The corresponding generalization error is given by $\epsilon_g^* = (K/\pi)\left\{\pi/6 - K \arcsin\left((2K)^{-1}\right)\right\}$. A simple geometrical picture explains the relation $Q^* = C^* = K(R^*)^2$ at the symmetric fixed point. The learning process confines the student vectors $\{\mathbf{J}_i\}$ to the subspace $\mathcal{S}_B$ spanned by the set of teacher vectors $\{\mathbf{B}_n\}$. For $T_{nm} = \delta_{nm}$ the teacher vectors form an orthonormal set: $\mathbf{B}_n = \mathbf{e}_n$, with $\mathbf{e}_n \cdot \mathbf{e}_m = \delta_{nm}$ for $1 \leq n, m \leq K$, and provide an expansion for the weight vectors of the trained student: $\mathbf{J}_i^* = \sum_n R_{in}\mathbf{e}_n$. The student-teacher overlaps R_{in} are independent of i in the symmetric phase and independent of n for an isotropic teacher: $R_{in} = R^*$ for all $1 \leq i, n \leq K$. The expansion $\mathbf{J}_i^* = R^* \sum_n \mathbf{e}_n$ results in $Q^* = C^* = K(R^*)^2$. The length of the symmetric plateau is controlled by the degree of asymmetry in the initial conditions [2] and by the learning rate η. The small η analysis predicts trapping times inversely proportional to η, in quantitative agreement with the shrinking plateau of Fig. 1d. The increase in the height of the plateau with decreasing η is a second order effect [3], as the truncated equations of motion predict a unique value of $\epsilon_g^* = 0.0203$ at $K = 3$. Escape from the symmetric subspace signals the onset of hidden unit specialization. As shown in Fig. 1b, the process is driven by a breaking of the uniformity of the student-teacher correlations [3]: each student node becomes increasingly specialized to a specific teacher node, while its overlap with the remaining

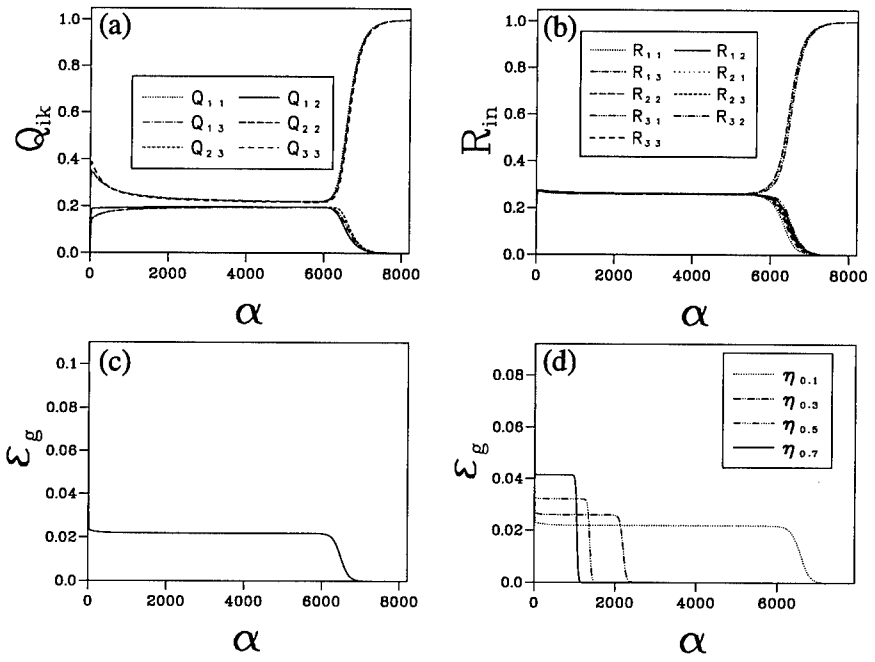

Figure 1 The overlaps and the generalization error as a function of α for a three-node student learning an isotropic teacher ($T_{nm} = \delta_{nm}$). Results for $\eta = 0.1$ are shown for (a) student-student overlaps Q_{ik}, (b) student-teacher overlaps R_{in}, and (c) the generalization error. The generalization error for different values of the learning rate η is shown in (d).

teacher nodes decreases and eventually decays to zero. We thus distinguish between a growing overlap R between a given student node and the teacher node it begins to imitate, and decaying secondary overlaps S between the same student node and the remaining teacher nodes. Further specialization involves the decay to zero of the student-student correlations C and the growth of the norms Q of the student vectors. The student nodes can be relabeled so as to bring the matrix of student-teacher overlaps to the form $R_{in} = R\delta_{in} + S(1-\delta_{in})$; the matrix of student-student overlaps is of the form $Q_{ik} = Q\delta_{ik} + C(1-\delta_{ik})$. The subsequent evolution of the system converges to an optimal solution with perfect generalization, characterized by a fixed point at $(R^*)^2 = Q^* = 1$ and $S^* = C^* = 0$, with $\epsilon_g^* = 0$. Linearization of the full equations of motion around the asymptotic fixed point results in four eigenvalues, of which only two control convergence. An initially slow mode is characterized by a negative eigenvalue that decreases monotonically with η, while an initially faster mode is characterized by an eigenvalue that eventually increases and becomes positive at $\eta_{max} = \pi/(\sqrt{3}K)$, to first order in $1/K$. Exponential convergence of R, S, C, and Q to their optimal values is guaranteed for all learning rates in the range $(0, \eta_{max})$; in this regime the generalization error decays exponentially to $\epsilon_g^* = 0$, with a rate controlled by the slowest decay mode.

REFERENCES

[1] G. Cybenko, *Approximation by superposition of sigmoidal functions*, Math. Control Signals and Systems Vol. 2 (1989), pp303–314.

[2] M. Biehl and H. Schwarze, *Learning by online gradient descent*, J. Phys. A Vol. 28 (1995), pp643–656.

[3] D. Saad and S. A. Solla, *Exact solution for on-line learning in multilayer neural networks*, Phys. Rev. Lett. Vol. 74 (1995), pp4337–4340.

[4] D. Saad and S. A. Solla, *On-line learning in soft committee machines*, Phys. Rev. E Vol 52 (1995), pp4225–4243.

Acknowledgements

Work supported by EU grant ERB CHRX-CT92-0063.

SPONTANEOUS DYNAMICS AND ASSOCIATIVE LEARNING IN AN ASSYMETRIC RECURRENT RANDOM NEURAL NETWORK

M. Samuelides, B. Doyon*, B. Cessac and M. Quoy*****

Centre d'Etudes et de Recherches de Toulouse, 2 avenue Edouard Belin, BP 4025, 31055 Toulouse Cedex, France. Email: samuelid@cert.fr.

** Unité INSERM 230, Service de Neurologie, CHU Purpan, 31059 Toulouse Cédex, France.*

*** University of New-Mexico, Department of Electrical and Computer Engineering, Albuquerque, NM 87131, USA.*

**** Universität Bielefeld, BiBos, Postfach 100131, 33501 Bielefeld, Germany.*

Freeman's investigations on the olfactory bulb of the rabbit showed that its dynamics was chaotic, and that recognition of a learned pattern is linked to a dimension reduction of the dynamics on a much simpler attractor (near limit cycle). We adress here the question wether this behaviour is specific of this particular architecture or if this kind of behaviour observed is an important property of chaotic neural network using a Hebb- like learning rule. In this paper, we use a mean-field theoretical statement to determine the spontaneous dynamics of an assymetric recurrent neural network. In particular we determine the range of random weight matrix for which the network is chaotic. We are able to explain the various changes observed in the dynamical regime when sending static random patterns. We propose a Hebb-like learning rule to store a pattern as a limit cycle or strange attractor. We numerically show the dynamics reduction of a finite-size chaotic network during learning and recognition of a pattern. Though associative learning is actually performed the low storage capacity of the system leads to the consideration of more realistic architecture.

1 Introduction

Most part of studies on recurrent neural networks assume sufficient conditions of convergence. Relaxation to a stable network state is simply interpreted as a stored pattern. Models with symmetric synaptic connections have relaxation dynamics. Networks with asymmetric synaptic connections lose this convergence property and can have more complex dynamics. However, as pointed out by Hirsch, [8], it might be very interesting, from an engineering point of view, to investigate non convergent networks because their dynamical possibilities are much richer for a given number of units.

Moreover, the real brain is a highly dynamic system. Recent neurophysiological findings have focused attention on the rich temporal structures (oscillations) of neuronal processes [7, 6] which might play an important role in information processing. Chaotic behavior has been found out in the nervous system [2] and might be implicated in cognitive processes [9]. Freeman's paradigm [9] is that the basic dynamics of a neural system is chaotic and that a particular pattern is stored as an attractor of lower dimension than the initial chaotic one. The learning procedure thus leads to the creation of such an attractor. During the recognition process, first, the network explores a large region of its phase space through a chaotic dynamics.

When the stimulus is presented then the dynamics is reduced and the systems follows the lower dimensional attractor which has been created during the learning process. The question arises wether this paradigm which has been simulated in [11] using an artifical neural network is due to a very specific architecture or if it is a general phenomenum for recurrent network.
The first step to adress this problem was to determine the conditions for the existence of chaotic dynamics among the various architecture of recurrent neural networks. A theoretical major advance in that direction was achieved by Sompolinsky [10]. They established strong theoretical results concernig the occurence of chaos for fully connected assymetric random recurrent networks in the thermodynamic limit by using dynamical mean field theory. In their model, neurons are formal neurons with activation state in [-1,1] with a symmetric transfer function and no threshold. The authors show that the system exhibits chaotic dynamics. These results were extended by us in [5] to the case of diluted networks with discrete time dynamics. One can ask whether such results remain valid in a more general class of neural networks with no reversal symmetry i.e. with activation state in [0,1] and thresholds. The presence of thresholds is biologically interesting. Moreover, it allows to study the behaviour of the network when submitted to an external input. In this paper, we describe this model and report the main results about spontaneous dynamics in section 2. In section 3, we define a hebbian learning rule. We study the reduction of the dynamics during the learning process and the recognition of a learned stimuli. We then discuss the results and conclude (4).

2 Spontaneous Dynamics of Random Recurrent Networks with Thresholds

The neurons states are continuous variables x_i, $i = 1 \dots N$. The network dynamics is given by:

$$i = 1 \dots N : \quad x_i(t+1) = f\left[\sum_{j=1} N J_{ij} x_j(t) - \theta_i\right] \tag{1}$$

where J_{ij} is the synaptic weight between the neuron j and the neuron i . The J_{ij}'s are independant identically distributed random variables with expectation $E(J_{ij}) = \frac{\overline{J}}{N}$ and a variance $Var(J_{ij}) = \frac{J^2}{N}$. The thresholds (θ_i) are independant identically distributed gaussian random variables of expectation $E(\theta_i) = \overline{\theta}$ and variance $Var(\theta_i) = \sigma_\theta^2$. Our numerical studies are made with the sigmoidal function: $f(x) = \frac{1}{1+e^{2gx}}$ so that the neurons states $x_i(t)$ belong to [0,1]. Thus $x_i(t)$ may be seen as the mean firing rate of a neuron.
This kind of system is known to present the "propagation of chaos" property in the thermodynamic limit. This approach was initiated for neural networks by Amari, [1]. Though the denomination of "chaos" for this basic properties of vanishing finite-size correlations is quite confusing and has nothing to do with determinsitic chaos which will be considered afterwards, we shall keep it. Namely the intra-correlations between finite sets of neuron activation state and between neurons and weights vanish and each neuronal activation state process converges in law in the thermodynamic limit towards independant gaussian processes. This statement allow us to

derive mean field equations

$$\text{governing the limits for } N \to \infty \text{ of } \begin{cases} m_N(t) &= \frac{1}{N}\sum_{i=1}^{N} x_i(t) \\ q_N(t) &= \frac{1}{N}\sum_{i=1}^{N} x_i(t)^2 \end{cases} \tag{2}$$

These mean field equations are

$$\begin{cases} m(t+1) &= \int_{-\infty}^{\infty} \frac{dh}{\sqrt{2\pi}} e^{\frac{-h^2}{2}} f[h\sqrt{J^2 q(t) + \sigma\theta^2} + m(t)\overline{J} - \overline{\theta} \\ q(t+1) &= \int_{-\infty}^{\infty} \frac{dh}{\sqrt{2\pi}} e^{\frac{-h^2}{2}} f^2[h\sqrt{J^2 q(t) + \sigma\theta^2} + m(t)\overline{J} - \overline{\theta} \end{cases} \tag{3}$$

We shall now restrict ourselves for numerical studies to the case where $\overline{J} = 0$. The second mean-field equation is self-consistent and we are able to determine the critical surface in the space $\left(\frac{\overline{\theta}}{J}, gJ, \frac{\sigma_\theta}{J}\right)$ between a single stable fixed point and two stable fixed points (saddle-node bifurcation) . Consider a fixed point x^* of the system (1). Its components (x_i^*) are i.i.d. gaussian random variables, their moments are given by the previous mean-field equations. To determine the stability of x^* in (1), we compute the Jacobi matrix of the evolution operator

$$D(x^*) = 2gL(x^*)J \tag{4}$$

where $L(x^*)$ is the diagonal matrix of components $(x_i^* - x_i^{*2})$ and where J is the connection weight matrix . The spectral radius of this random matrix can be computed and this computation determines a stability boundary surface as shown below in figure 1. At the thermodynamic limit, it is possible to use the "propagation of chaos" property to compute the evolution of the quadratic distance between two trajectories of the system coming for arbitrary close initial conditions [3]. 0 is a fixed point for this recurrence and the critical condition for its destabilization is exactly the same than the previous condition for the first destabilization of the fixed point of the network. This proves, that at the thermodynamic limit, one observes a sharp transition between a fixed point regime and a chaotic regime. So in the bifurcation map of figure 1 there are four different regions: - region 1 : there is only one stable fixed point - region 2 : there are two stable fixed points (actually region 2 is a very small cusp) - region 3 : one stable fixed point and one strange attractor coexist. One may converge towards one or the other depending on the intial conditions. - region 4 : there is only one strange attractor Regions 2 and 3 shrink when $\sigma\theta$ increases. When $\sigma\theta = 0.2$, only regions 1 and 4 remain. For finite size systems, the destabilization and apparition of chaos boundaries are different. There exists an intermediate zone where the system is periodic or quasiperiodic. This corresponds to the quasiperiodicity route to chaos we observe in the system when gJ is increased [5, 4]. The simulations confirm with accuracy all these theoretical predictions for medium-sized networks (from 128 units up to 512 units), showing the progressive stretching of the transition zone where periodic and almost-periodic attractors take place.

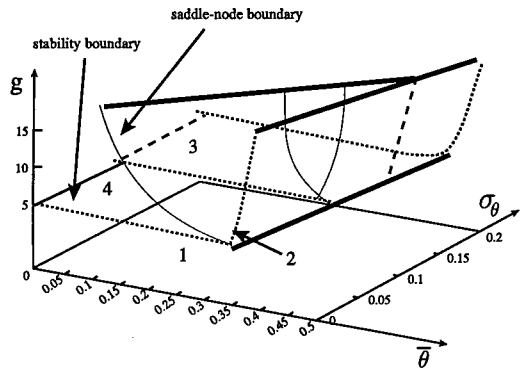

Figure 1 Saddle-node bifurcation surface and destabilization boundary in the $\left(\frac{\overline{\theta}}{J}, gJ, \frac{\sigma_\theta}{J}\right)$ space.

3 Learning and Retrieving Random Patterns.

3.1 Network Submitted to a Static Random Input

We study now the reaction of our network when submitted to an external input. The input is a vector of random gaussian variables I_i independent of θ_i's with a mean value $\overline{I}$ and a variance σ_I^2. We get

$$x_i(t+1) = f\left[\sum_{j=1}^{N} J_{ij}x_j(t) - \theta_i + I_i\right] \tag{5}$$

Hence the input is equivalent to a threshold. The global resulting threshold has a mean value $\overline{\theta} - \overline{I}$ and a variance. We can then interpret the presentation of an input as a change of the parameters of the system. Its effect can therefore be predicted from the bifurcation map.

If the configuration of the network stands in the chaotic region near the boundary of this region, then the presentation of an input will tend to reduce the dynamics of the system on a limit cycle by crossing the boundary, falling into the limit cycles and $T2$ torus area. The same input may lead to different answers by different networks with the same statistical parameters. This modification of the parameters by a pattern presentation creates a new system (with a different attractor).

3.2 Auto-associative Learning.

The learning procedure we define will enable us to associate a limit cycle or a strange attractor to a presented pattern. We modify the connection strength by a biologically motivated Hebb-like rule:

$$\text{if } x_j(t) > 0.5 \text{ then } J_{ij}(t+1) = J_{ij}(t) + \frac{\alpha}{N}\left[x_j(t) - 0.5\right]\left[x_i(t+1) - 0.5\right]$$
$$\text{else } J_{ij}(t+1) = J_{ij}(t)$$

We add the constraint that a weight cannot modify its sign. α is the learning rate. The learning procedure is implemented at each step when the network has reached the stationary regime.

In all our simulations the learning procedure reduces the fractal dimension of the chaotic attractors of the dynamics. Eventually the system follows an inverse quasi-periodicity route towards a fixed point. We have chosen to stop the procedure on a limit cycle, thus associating this cycle with the pattern learned.
In fact, one can speak of learning if the network has a selective response for the learned pattern, and if the learning procedure does not affect the dynamical behaviour when an other pattern is presented. On order to study this selectivity property, we make the following simulation. We learn one prototype pattern (ie. we iterate the learning dynamics upon reaching a limit cycle). Then we present 30 other random patterns (drawn randomly with the same statistics than the learned pattern), and we compare the attractors before, and after learning. For all patterns but one, the dynamics before learning were chaotic. For all these patterns, the dynamics were still chaotic after learning (the pattern whose response was periodic, had still a periodic attractor). Hence the network reduces its dynamics only for the learned prototype pattern.

3.3 Retrieval Property

In order to study the retrieval property of this associative learning process, we add noise to a pattern previously learned, and show how it affects the recognition. A pattern is a vector of gaussian random variables (for the simulations, each component has a mean zero and standard deviation 0.1). We add to each component a gaussian noise of mean zero and standard deviation 0.01, and 0.02, which thus corresponds to a level of noise of 10% and 20% on the pattern. We recall that the presentation of a noisy pattern changes the parameters of the system. So recognition has to be defined by some similarities between the attractors. In order to quantify the similarity between cycles, we compute their gravity center, their mean radius and winding (rotation) number and we define a crtierion of similarity based on these numerical indexes.
To estimate the recognition rate, we learn one prototype pattern. Then we present 30 noisy patterns (derived from the prototype one), and compute the similarity values. With a 10% level of noise recognition rate after 7 learning steps is 83%, with 20% noise it falls down to 27%.

4 Discussion and Conclusion

Our model reproduces the observations by Freeman concerning the dimension reduction of the system attractor by recognition of a learned pattern, in a model of the olfactory bulb [11]. The system does not need to wait until a fixed point is reached to perform recognition: relying on our experiments, convergence on an attractor is very fast. This gives an insight into the mechanism leading to such a phenomenon by the extraction of the few relevant parameters related to it.
However this model suffers severe drawbacks concerning the control of the learning process and the storage capacity. Moreover, the modifications supported by the weights during the learning process are difficult to interpret theoretically. These limitations suggest to introduce at the next step architectural and functional differentiation into the network (inhibitory and excitatory neurons, multiple layers, random geometric-dependant connectivity and time delays, modular architecture of chaotic oscillators).

Coding by dynamical attractors is also particularly suited for learning of temporal signals. For the moment, we only focused on the learning of static patterns. However, we performed with interesting results some preliminary simulations on presentation of temporals sequences. This could lead to connect different chaotic networks in order to perform recognition tasks using the synchronization processes highlighted by Gray [7].

REFERENCES

[1] Amari S.I., *Characteristics of random nets of analog neuron-like elements*, IEEE Trans.Syst.Man.Cyb, Vol. 2.5(1972), pp643–657.

[2] Babloyantz A., Nicolis C., Salazar J.M., *Evidence of chaotic dynamics of brain activity during the sleep cycle*, Phys. Lett. Vol. 111A (1985), pp152–156.

[3] Cessac B., *Increase in complexity in random neural networks*, J.PhysI, Vol. 5 (1995), pp409–432.

[4] Cessac B., Doyon B., Quoy M., Samuelides M., *Mean-field equations, bifurcation map and route to chaos* in: discrete time neural networks, Physica D, Vol. 74 (1994), pp24–44.

[5] Doyon B., Cessac B., Quoy M., Samuelides M., *Chaos in Neural Networks With Random Connectivity*, International Journal Of Bifurcation and Chaos, Vol. 3 (1993), No. 2, pp279–291.

[6] Eckhorn R., Bauer R., Jordan W., Brosch M., Kruse W., Munk M., Reitboeck H.J., *Coherent oscillations: A mechanism of feature linking in the visual cortex? Multiple electrode and correlation analysis in the cat*, Biol. Cybernet. Vol. 60 (1988), pp121–130.

[7] Gray C.M., Koenig P., Engel A.K., Singer W. *Oscillatory responses in cat visual cortex exhibit intercolumnar synchronisation which reflects global stimulus properties*, Nature Vol. 338 (1989), pp334–337.

[8] Hirsch .M.W., *Convergent Activation Dynamics in Continuous Time Networks*, Neural Networks Vol. 2 (1989), pp331–349.

[9] Skarda C.A., Freeman W.J., *How brains make chaos in order to make sense of the world*, Behav. Brain Sci. Vol. 10 (1987), pp161-195.

[10] Sompolinsky H., Crisanti A., Sommers H.J., *Chaos in random neural networks*, Phys. Rev. Lett. Vol. 61 (1988), pp259–262.

[11] Yao Y., Freeman W.J., *Model of biological pattern recognition with spatially chaotic dynamics*, Neural Networks Vol. 3 (1990), pp153–170.

Acknowledgements

This research has been supported by a grant from DRET (the National French Defense Agency) and by the COGNISCIENCE research program of the C.N.R.S.. M Quoy is supported by a Lavoisier grant of the French Foreign Office and B. Cessac by a Cognisciences grant of the C.N.R.S..

A STATISTICAL MECHANICS ANALYSIS OF GENETIC ALGORITHMS FOR SEARCH AND LEARNING

Jonathan L. Shapiro, Adam Prügel-Bennett* and Magnus Rattray

Department of Computer Science, University of Manchester, Manchester, M13 9PL, UK.

** NORDITA Blegdamsvej 17, DK-2100 Copenhagen O, Denmark.*

Statistical mechanics can be used to derive a set of equations describing the evolution of a genetic algorithm involving crossover, mutation and selection. This paper gives an introduction to this work. It is shown how the method can be applied to to very simple problems, for which the dynamics of the genetic algorithm can be reduced to a set of nonlinear coupled difference equations. Good results are obtained when the equations are truncated to four variables.

Keywords: Genetic Algorithms, Statistical Mechanics, Fitness Distributions.

1 Introduction

Genetic Algorithms (GA) are a class of search techniques which can be used to find solutions to hard problems. They have been applied in a range of domains: optimisation problems, machine learning, training neural networks or evolving neural network architectures, and many others. (For an introduction, see Goldberg [1].) They can be naturally applied to discrete problems for which other techniques are more difficult to use, and they parallelise well. Most importantly, they have been found to work in many applications.

Although GAs have been widely studied empirically, they are not well understood theoretically. Unlike gradient descent search and simulated annealing, genetic algorithms are not based on a well-understood process. The goal of the research described here is to develop a formalism which allows the study of genetic algorithm dynamics for problems of realistic size and finite population sizes. The problems we have studied are clearly toy problems; however, they contain some realistic aspects, and we hope their consideration will be a stepping stone to the study of more realistic problems.

2 The Statistical Mechanics Approach

Ideally, one would like to solve the dynamics of genetic algorithms exactly. This could be done, in principle, either by studying the stochastic equation directly, or by using a Markov Chain formulation to analyse the deterministic equation for the probability of being in a given population (see [2, 3]). However, it is very difficult to make progress in this way, because one must solve a high-dimensional, strongly interacting, nonlinear system which is extremely difficult to analyse.

In these exact approaches, the precise details of which individuals are in the population is considered. In our approach much less information is assumed to be known. We consider only statistical properties of the distribution of fitnesses in the population; from the distribution of fitnesses at one time, we predict the distribution of fitnesses at the next time step. Iterating this from the initial distribution, we propose to predict the fitness distribution for all times.

This distribution tells you want you want to know – for example the evolution of the best member of the population can be inferred. But is it possible, in principle, to predict the fitness at later times based on the fitness at earlier times?

The answer is no. Although it is possible to predict the effect of selection based solely on the fitness distribution, mutation and crossover depend upon the configurations of the strings in the population which cannot be inferred from their fitnesses. We use a statistical mechanics assumption to bridge this gap.

We characterise the distribution by its cumulants. Cumulants are statistical properties of a distribution which are like moments, but are more stable and robust. The first two cumulants are the mean and variance respectively. The third cumulant is related to the skewness; it measure asymmetry of the distribution about the mean. The fourth cumulant is related to the kurtosis; it measure whether the distribution falls off faster or more slowly than Gaussian.

3 Test Problems

The method has been applied to four problems. The simplest task, and one which will be used throughout this paper to illustrate the method, is the optimisation of a linear, spatially inhomogeneous function, *counting random numbers*. In this problem, each bit of the string contributes individually an arbitrary amount. The fitness is,

$$F[\tau] = \sum_{i=1}^{N} J_i \tau_i.$$

Here τ is a string of ± 1 of length N which the GA searches over. The J_i's are fixed random numbers.

Other problems to which the method has been applied include: the task of maximising the energy of a *spin-glass chain* [4, 5, 6], the *subset sum* problem [7] (an NP hard problem in the weak sense), and learning in an Ising perceptron [8]. For the first two problems, the dynamics can be solved, and the formalism predicts accurately the evolution of the genetic algorithm. The latter problem has been much more difficult to solve, however.

4 The Genetic Operators

We now discuss how our approach is applied to the study of three specific GA operators: selection, mutation, and crossover. We will use the *counting random numbers* task to illustrate how the calculations are done.

4.1 Selection

Selection is the operation whereby better members of the population are replicated and less good members are removed. The most frequently used method is to chose the members of the next population probabilistically using a weighting function $R(F^\alpha)$. We have studied Boltzmann selection

$$R(F) \propto \exp(\beta F)$$

where β is a parameter controlling the selection rate. Fitness proportional selection ($R(F) = F$), culling selection (choose the n best), and other forms can also be handled by the approach.

In an infinite population, the new distribution of fitness in terms of the old $\rho(F)$ would simply be $R(F)\rho(F)$ up to a normalisation factor. In a finite population, there will be fluctuations around this. The way to treat this is to draw P levels

from ρ. The generating function for cumulants is

$$G(\gamma) = \left[\prod_{\alpha=1}^{P} \int_{-\infty}^{\infty} \rho(F^\alpha) dF^\alpha\right] \log\left[\sum_{\alpha=1}^{P} R(F^\alpha)\exp(-\gamma F^\alpha)\right].$$

This problem is analogous to the Random Energy Model proposed and studied by Derrida [9], and can be computed by using the same methods developed for that problem.

For Boltzmann selection, the cumulant expansion for the distribution after selection in terms of selection before can be found as an expansion in the selection parameter β,

$$\begin{aligned}
\kappa_1^s &= \kappa_1 + \beta\left(1-\frac{1}{P}\right)\kappa_2 + \frac{\beta^2}{2}\left(1-\frac{3}{P}\right)\kappa_3 + \frac{\beta^3}{3!}\left[\left(1-\frac{7}{P}\right)\kappa_4 - \frac{6}{P}\kappa_2^2\right] + \cdots, \\
\kappa_2^s &= \left(1-\frac{1}{P}\right)\kappa_2 + \beta\left(1-\frac{3}{P}\right)\kappa_3 + \frac{\beta^2}{2}\left[\left(1-\frac{7}{P}\right)\kappa_4 - \frac{6}{P}\kappa_2^2\right] + \cdots, \qquad (1) \\
\kappa_3^s &= \left(1-\frac{3}{P}\right)\kappa_3 + \beta\left[\left(1-\frac{7}{P}\right)\kappa_4 - \frac{6}{P}\kappa_2^2\right] + \cdots.
\end{aligned}$$

Or the cumulants can be found for arbitrary β numerically.

For many problems, the initial distribution will be nearly Gaussian. Selection introduces a negative third cumulant – the low-fitness tail is more occupied than the high-fitness one. An optimal amount of selection is indicated. The improvement of the mean increases with β initially, but saturates for large β. Selection also decreases the variance; this effect is small for small β but becomes important for increasing values. The trade-off between these two effects of selection — increase in mean but decrease in genetic diversity — are balanced for intermediate values of β. This has been discussed in earlier work [5, 6].

4.2 Mutation

Mutation causes small random changes to the individual bits of the string. Thus, it causes a local exploration, in common with many other search algorithms. It acts on each member of the population independently.

To study the effect of mutation, we introduce a set of mutation variables, m_i^α, one for each site of each string, which take the value 1 if the site is mutated, 0 otherwise. Let m be the mutation probability. In terms of these variables, the fitness after mutation is (for *counting random numbers*)

$$F = \sum_i J_i\ (1 - 2m_i^\alpha)\ \tau_i^\alpha. \qquad (2)$$

Averaging over all variables gives the cumulants after mutation. This yields,

$$\begin{aligned}
\kappa_1^m &= (1-2m)\kappa_1 \\
\kappa_2^m &= \kappa_2 + \left(1-(1-2m)^2\right)(N-\kappa_2) \qquad (3) \\
\kappa_3^m &= \kappa_3(1-2m)^3 - 2(1-2m)\left(1-(1-2m)^2\right)\frac{1}{P_3}\sum_i J_i^3\ \langle\tau_i\rangle
\end{aligned}$$

where $< \tau >$ denotes population average. (The fourth cumulant can be calculated in a similar fashion).

The first two equations express obvious effects. Mutation brings the mean and variance back towards values of a random population — mean decreases to zero and the variance increases toward N. The equation for the third cumulant is more interesting. The first term decreases the third cumulant, but the second increases its magnitude if it is negative (which it typically is). This is the part which depends upon the configuration average.

4.3 Crossover

Crossover can be treated in a similar manner to mutation. Introduce a set of crossover variables, $\chi_i^{\alpha\beta}$ which are 1 if α crossed with β at site i and 0 otherwise, write equations for the cumulants in terms of these variables and average. One finds that both the mean and the variance remain unchanged. The third and higher cumulants are reduced and brought to natural values which depend upon configurational averages.

4.4 Using the Statistical Mechanics Ansatz to Infer Configurational Averages from Fitness Distribution Averages

In the previous section we showed that the effect of mutation on the cumulants depends upon the fitness distribution (i.e. on the cumulants) *and* upon properties of the configuration of the strings. As we have argued, one cannot, in principle, determine the configuration from the fitness distribution. We invoke a statistical mechanics ansatz. We assume that the string variables are free to fluctuate subject to the constraint that the cumulants are given. In other words, our assumption is that of all the configurations which have the same distribution of fitnesses, the more numerous ones are more likely to describe the actual one. This can be seen as a maximum entropy assumption. We use a simple statistical mechanics model to implement the proposed relationship between fitness statistics and configuration statistics. Details are presented in [6].

5 Discussion and Future Work

The equations for each of the genetic operators can be put together to predict the whole dynamics. Typical curves are shown in figure 1. The theoretical curves were produced by calculation of the initial distribution theoretically, and iterating the equations repeatedly. No experimental input was used. Although, the agreement between experiment and theory is not perfect, these results are as accurate as any approach of which we are aware.

This gives a picture of the role of crossover, for this simple problem. Selection improves the average fitness, but decreases variance and introduces a negative skewness. Mutation increases the variance, introducing genetic diversity; however, it also decreases the mean. Crossover has no effect on the first two cumulants. It reduces the magnitude of the skewness, however. This replaces some of the low-fitness tail with some high-fitness tail, which improves the best member of the population. Since, for this problem, crossover has no effect on the mean, there is no cost in doing this and crossover is helpful. For a realistic problem, however, crossover will introduce a deleterious effect to the mean; whether this effect dominates over the improvement due to the decrease of the third cumulant may determine whether the crossover operator is a useful one for the problem in question.

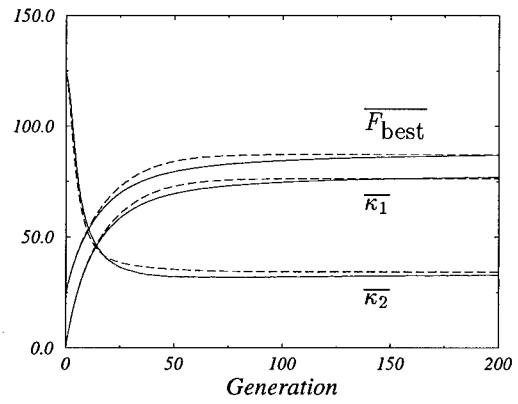

Figure 1 The solid curves show the evolution of the first two cumulants and the fitness of the best member of the population for $N = 127$, $P = 50$, $\beta = 0.1$ and $m = 1/2N$. The ground state is at $F_{\text{best}} \approx 101$. The dashed curve shows the theoretical prediction. The overscore indicates averaging over 10 000 runs. From reference [6].

REFERENCES

[1] David E. Goldberg, *Genetic Algorithms in Search, Optimization & Machine Learning*, Addison-Wesley, Reading, Mass. (1989).

[2] A Nix and Michael D. Vose, *Modelling genetic algorithms with Markov chains*, Annals of Mathematics and Artificial Intelligence, Vol. 5 (1991), pp79–88.

[3] Darrell Whitley. *An executable model of a simple genetic algorithm*, in: L. Darrel Whitley, ed., Foundations of Genetic Algorithms 2. Morgan Kaufmann, San Mateo (1993).

[4] A. Prügel-Bennett and J. L. Shapiro, *An analysis of genetic algorithms using statistical mechanics*, Phys. Rev. Letts., Vol. 72(9) (1994), pp1305–1309.

[5] J. L. Shapiro, A. Prügel-Bennett, and M. Rattray, *A statistical mechanical formulation of the dynamics of genetic algorithms*, Lecture Notes in Computer Science, No. 864 (1994), pp17–27.

[6] A. Prügel-Bennett and J. L. Shapiro, *Dynamics of genetic algorithms for simple random Ising systems*, Physica D, in press (1997).

[7] L. M. Rattray, *An analysis of a genetic algorithm with stabilizing selection*, Complex Systems Vol.9 (1995), pp213–234.

[8] L. M. Rattray and J. L. Shapiro, *The dynamics of a genetic algorithm for a simple learning problem*, Journal of Physics A, Vol.29(23) (1996), pp7451–7473.

[9] B. Derrida. *Random-energy model: An exactly solvable model of disordered systems*, Phys. Rev., Vol. B24 (1984), pp2613–2626.

VOLUMES OF ATTRACTION BASINS IN RANDOMLY CONNECTED BOOLEAN NETWORKS

Sergey A. Shumsky

P.N.Lebedev Physics Institute, Leninsky pr.53, Moscow, Russia.

The paper presents the distribution function of the volumes of attraction basins in phase portraits of Boolean networks with random interconnections for a special class of *uniform* nets, built from unbiased elements. The distribution density at large volumes tends to universal power law $\mathcal{F} \propto V^{-3/2}$.

1 Introduction

Randomly Connected Boolean Networks (RCBN) represent a wide class of connectionist models, which attempt to understand the behavior of systems, built from a large number of richly interconnected elements [1].

Since the early studies of Kauffman [2] RCBN became a classical model for studying the dynamical properties of random networks. The most intriguing feature of RCBN is the phase transition from the stochastic regime to the ordered behavior, first observed in simulations [2], and later explained analytically [3]-[5].

In the *chaotic phase* the phase trajectories are attracted by very long cycles, which lengths grow exponentially with the size of the system N [4]. Thus, even for not so large systems it is practically impossible to indicate these cycles, and their phase trajectories resemble random walks in the phase space.

On the contrary, in the *ordered phase* the short cycles dominate [4]. In fact, this paper will present a numerical evidence, that almost the whole system's phase space belongs to the attraction basins of the fixed points. The distribution of the volumes of these attraction basins is an important characteristic, since it gives the probabilities of different kinds of asymptotic behavior of the system.

So far, the distribution of attraction basins is known only for fully connected Boolean networks, namely the Random Map Model (RMM) [6], which represents the *chaotic* RCBN. The onset of the *ordered phase* implies, that the mean number of inputs per one element, K, does not exceed some critical value, which depends only on the type of the Boolean elements [5]. Thus, this phase takes place only in the case of extremely sparse interconnections: $K/N \to 0$ for $N \to \infty$.

In the present paper we calculate the distribution of attraction basins in the *ordered phase*, using the fact, that in sparsely connected networks there exists a correlation between the number of logical switchings at the consequent time steps, which is absent in the RMM. In Sec. 2 we formulate our model as the straightforward extention of the RMM, which takes into account the above correlation. Sec. 3 presents the solution for our problem found by means of the theory of branching processes. Sec. 4 presents the comparison of the theoretical predictions with the simulations results for the Izing neural networks. Sec. 5 gives some concluding remarks.

2 Model Description

The networks under consideration consist of N two-state automata receiving their inputs from the outputs (states) of other automata, connected with the given one. These connections are attached at random when the network is assembled and then

fixed. The parallel dynamics is governed by the map:

$$\mathbf{x} \Rightarrow \phi(\mathbf{x}), \qquad (\mathbf{x}, \phi \in \{\pm 1\}^N). \tag{1}$$

Function $\phi(\mathbf{x})$ depends vacuously on some of its arguments.

In a phase portrait of a network there is a unique phase vector, begining at each phase state. However, there are no restrictions on the number of vectors coming to that state. Thus, any phase portrait represents a forest of the trees with their roots belonging to the attractor set. For the *ordered phase* this attractor set is represented mainly by fixed points.

We shall be interested in the statistical properties of this forest, namely by the distribution of volumes of the trees. These statistical properties, of course, should characterize not an individual map, but some ensemble of maps. The ensemble of RCBN contains all possible variants of interconnections among N automata, chosen at random from some infinite basic set of automata. We assume, that this set of automata is *unbiased*, that is, the statistical properties of phase vectors do not depend on the state point. Such ensembles will be further referred to as *uniform* ones.

Such is, for example, the RMM, where phase vector starting in any state may come to each state with equal probability. Since there are Ω such possibilities for each state point (where $\Omega = 2^N$ is the phase volume of a system), this ensemble consists of Ω^Ω maps, corresponding to all possible variants of fully connected Boolean networks.

In the absence of correlations between consequent vectors, one can characterize the uniform ensemble by only one statistical characteristic - the distribution of vectors lengths (in the Hamming sense), W_m, which is binomial:

$$W_m = \left(\begin{array}{c} N \\ m \end{array} \right) (1 - w_0)^m (w_0)^{N-m}, \tag{2}$$

with $w_0 = (1 + \nu_0)/2$ being the mean fraction of fixed points in the phase portraits of automata from the basic set [5]. For the RMM, for example, $\nu_0 = 0$ and $w_0 = 1/2$. But in the absence of *selfexcitable* automata in the basic automata set (i.e. those, that oscillate for the fixed values of their inputs), $\nu_0 \geq 0$. This leads to exponentially large number of fixed points:

$$\Omega_0 = \Omega W_0 = (1 + \nu_0)^N. \tag{3}$$

In general case there exists a correlation between the lengths of consequent vectors. This correlation is more pronounced in diluted networks. Indeed, recall, that the vector's length is the number of automata, which change state at the corresponding time step. In diluted networks the probability, that a given automaton will change state is proportional to the probability, that at least one of its inputs has changed its value. As a consequence, the mean number of automata switchings at the next step is proportional to that at the previous step.

To take this fact into account we introduce the conditional probability P_{ml} that in phase trajectories from a given ensemble vector with length m will be followed by vector of length l. This is a straightforward generalization of the RMM, for which $P_{ml} = W_l$.

Summarizing, we will deal with an ensemble of phase portraits (1) with the statistical characteristics of phase trajectories given by W_m and P_{ml}. We are interested, however, not in the characteristics of trajectories, but rather in that of random trees

in phase portraits from our ensemble. Such is the mean number Π_{lm} of vectors with the length m, which precede the vector with the length l:

$$\Pi_{lm} = W_m P_{ml}/W_l, \quad (m = 1, \ldots, N; \quad l = 0, \ldots, N). \tag{4}$$

Zero-length vectors do not precede any state, and are thus excluded: $\Pi_{l0} \equiv 0$. The normalization condition $\sum_{l=0}^{N} P_{ml} = 1$ may be rewritten as:

$$\sum_{l=0}^{N} W_l \Pi_{lm} = W_m, \qquad (m = 1, \ldots, N). \tag{5}$$

To complete the description of random forest one needs not only the average number Π_{lm}, but the whole distribution function for the number of different vectors, preceding the given vector of length l. In the limit $\Omega \to \infty$ this distribution tends to a Poisson one with the generating function:

$$\boldsymbol{f}(\boldsymbol{s}) = \exp[\hat{\Pi}(\boldsymbol{s} - \mathbf{1})]. \tag{6}$$

The latter is a function of formal parameter $\boldsymbol{s}$:

$$f_l(\boldsymbol{s}) = \sum_{m_1, \ldots, m_N} f_{l;m_1,\ldots,m_N} s_1^{m_1}, \ldots, s_N^{m_N},$$

with $f_{l;m_1,\ldots,m_N}$ being the probability, that a vector of length l is preceded by m_1 vectors of length 1, ..., m_N vectors of length N. In the following of this paper all running indexes range from 1 to N.

3 Distribution of the Basins Volumes

Now, when all the characteristics of random trees are determined, one can use the well known results of the theory of brunching processes. For the sake of clarity we will not supply the details here, relegating the involved calculations to a more extensive publication.

3.1 General Solution

The theory of brunching processes allows one to find the distribution of the volumes of random trees, provided the generating function $\boldsymbol{f}(\boldsymbol{s})$ is known [7]. For the one given by (6) the fraction of trees of volume V is:

$$\mathcal{F}(V) = \frac{\exp\left(-\sum_i k_i \delta_i^2/2\right)}{\sqrt{2\pi \sum_i k_i p_i^2}}, \tag{7}$$

where $\mathbf{k}$, $\mathbf{p}$ and $\boldsymbol{\delta}$ satisfy the saddle point equations:

$$\sum_j \pi_{ij} \delta_j = -\beta, \tag{8}$$

$$\sum_i (\overline{k}_i - k_i)\pi_{ij} = k_j \delta_j, \qquad \sum_j \pi_{ij}(\overline{p}_j - p_j) = p_i \delta_i. \tag{9}$$

Here $\overline{p}_i = -\delta_i/\beta = \sum_j \pi^{-1}{}_{ij}$, and matrix $\pi_{ij} \equiv \delta_{ij} - \Pi_{ij}$ has the eigenvalues $\gamma_i = 1 - \kappa_i$, being the relaxation decrements for the initial Markov process (κ_i are eigenvalues of matrixes $\hat{P}$ and $\hat{\Pi}$).

The solution of this system of equations reads:

$$k_i = \sum_a \frac{l_i^a k^a}{\lambda_a - \beta}, \qquad p_i = \sum_a \frac{r_i^a p^a}{\lambda_a - \beta}, \tag{10}$$

with λ_a, l_i^a and r_i^a being the eigenvalues, the left and the right eigenvectors of the generalized eigenvalue problem:

$$\sum_i l_i^a \pi_{ij} = \lambda_a \overline{p}_j l_j^a, \qquad \sum_j \pi_{ij} r_j^a = \lambda_a \overline{p}_i r_i^a. \tag{11}$$

Coefficients k^a and p^a in (10) represent the spectral expansion of the known vectors $\overline{k}_i = \sum_a l_i^a k^a/\lambda_a$, $\overline{p}_i = \sum_a r_i^a p^a/\lambda_a$. The Lagrange parameter β is found from the equation:

$$V = \sum_i k_i = \sum_a \frac{p^a k^a}{\lambda_a - \beta}. \tag{12}$$

Multiplication of the first equation of (9) on δ_j with subsequent summation over j gives: $\sum_j k_j \delta_j^2 = \beta(V - \overline{V})$, and one finally obtains:

$$\mathcal{F}(V) = \frac{\exp[-\beta(V - \overline{V})/2]}{\sqrt{2\pi \sum_i k_i p_i^2}} \tag{13}$$

3.2 Distribution of Basins Volumes

Distribution (13) is valid for a general branching process with different types of branches. Now we will make use of the specific feature of our branching process in random phase portraits. Namely, in this particular case the first eigenvalue λ_1 of the above generalized eigenvalue problem is much less than the others, and is so small, that the exponential factor in (13) is negligible: $\lambda_a = O\left(N^a(1-\nu_0)^N/\Omega\right)$ The exponential cut-off of the distribution (13) occurs at $\beta \to \lambda_1$, that is at $V \sim 1/\lambda_1$. Since $1/\lambda_1 \gg \Omega$, the exponential factor is negligible, and distribution (13) is represented by a power law.

For $\beta < \lambda_1$ one can leave β only in the term with $m = 1$ in (10), obtaining:

$$\mathcal{F}(V) \propto P_3(V)^{-1/2}, \tag{14}$$

with $P_3(V)$ being the polynomial of the third degree. For $V \gg \overline{V}$ the asymptotic scaling is: $\mathcal{F}(V) \propto V^{-3/2}$, the same as for the RMM.

4 Simulations

The above theoretical predictions were checked in the computer simulations of neural networks with random diluted asymmetric Izing interconnections. The networks consisted of N two state elements $x_i \in \{\pm 1\}$, connected with K randomly chosen other elements. The states of the elements were updated in parallel according to the rule:

$$x_i \to \text{sign}(h_i), \quad h_i = \textstyle\sum_j J_{ij} C_{ij} x_j \tag{15}$$

where $\hat{C}$ is the random interconnection matrix with K units and $N - K$ zeros in each row ($C_{ii} = 0$), and matrix $\hat{J}$ has the Izing components $J_{ij} = \pm 1$ with equal probabilities. For a given network these matrixes are fixed during the simulations. If h_i appears to be zero, the state of the i-th neuron is unchanged. The latter case may occur only for the even number of interconnections K. The *ordered* phase for such model takes place only for $K \leq 2$. Since the case $K = 1$ is degenerate, we considered networks with $K = 2$.

The first thing we examined was the fraction of phase space in the basins of fixed points. This quantity was estimated by tracing 10^3 random trajectories till they

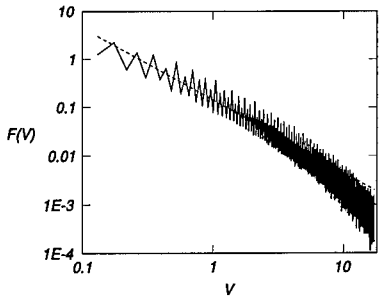

Figure 1 Distribution density of basins volumes in the ensemble of 25000 networks with $N = 11$ and $K = 2$.

reached their attractors. The results showed that for sufficiently large $N > 25$ all phase trajectories converge to some fixed point.

To obtain the distribution of the basins we examined the whole phase space. Since the computational time grows exponentially with the size of the network, we chose the networks of relatively small size, $N = 11$ (the measured probability of convergence was 0.97). For $K = 2$, 25000 random networks were generated, and each phase portrait was examined point by point. Fig. 4 shows the obtained distribution of the volumes of the basins of fixed points. The dotted line on this plot represents the asymptotic power law $\mathcal{F} \propto V^{-3/2}$. The correspondence is good in a wide range of volumes, except the very tail of the distribution. The observed cutt-off of the power law is due to the finiteness of the state space, ignored by the branching process approach.

5 Conclusions

The paper presented the distribution of the attraction basins of randomly connected Boolean networks, which generalize the Kauffman NK-model. The obtained results may be useful, for example, for studying the relaxation processes in nonergodic systems. At finite temperature the volumes of basins play a similar role as the energy levels of the valleys in spin glasses.

REFERENCES

[1] J. Doyne Farmer, *A Rosetta stone for connectionism*, Physica D, Vol. 42 (1990), pp153–187.

[2] S. A. Kauffman, *Metabolic stability and epigenesis in randomly connected nets*, J. Theor. Biol., Vol. 22 (1969), pp437–467.

[3] B. Derrida and Y. Pomeau, *Random networks of automata: a simple annealed approximation* Europhys. Lett., Vol. 1 (1986), pp45–49.

[4] K. E. Kűrten, *Critical phenomena in model neural networks* Phys. Lett. A, Vol. 129 (1988), pp157–160.

[5] S. A. Shumsky, *Phase portrait characteristics of random logical networks* J. Moscow Phys. Soc., Vol. 2 (1992), pp263–281.

[6] B. Derrida and H. Flyvbjery, *The random map model: a disordered model with deterministic dynamics*, J. Phys. France, Vol. 48 (1987), pp971–978.

[7] T. E. Harris, *The Theory of Branching Processes.* Springer-Verlag, Berlin (1963).

EVIDENTIAL REJECTION STRATEGY FOR NEURAL NETWORK CLASSIFIERS

A. Shustorovich

Business Imaging Systems, Eastman Kodak Company, Rochester, USA.

In this paper we present an approach to estimation of the confidences of competing classification decisions based on the Dempster-Shafer Theory of Evidence. It allows us to utilize information contained in the activations of all output nodes of a neural network, as opposed to just one or two highest, as it is usually done in current literature. On a test set of 8,000 ambiguous patterns, a rejection strategy based on this confidence measure achieves up to 30% reduction in error rates as compared to traditional schemes.

1 Introduction

Neural network classifiers usually have as many output nodes as there are competing classes. A trained network produces a high output activation of the node corresponding to the desired class and low activations of all the other nodes. In this type of encoding, the best guess corresponds to the output node with the highest activation. Our confidence in the chosen decision depends on the numeric value of the highest activation as well as on the difference between it and the others, especially the second highest. Depending on the desired level of reliability, a certain percentage of classification patterns can be rejected, and the obvious strategy is to reject patterns with lower confidence first. The rejection schemes most commonly used in literature are built around two common-sense ideas: the confidence increases with the value of the highest activation and with the gap between the two highest activations.

In some systems, only one of these values is used as the measure of confidence; in others, some ad-hoc combination of both. For example, Battiti and Colla [1] reject patterns with the highest activation (HA) below a fixed threshold, and also those with the difference between the highest and the second highest activation (DA) below a second fixed threshold. Martin et al. [5] use only DA in their Saccade System, whereas Gaborski [4] uses the ratio of the highest and the second highest activation (RA) as the preferred measure of confidence. Fogelman-Soulié et al. [3] propose a distance-based (DI) rejection criterion in addition to HA and DA schemes; namely they compare the Euclidean distance between the activation vector and the target activation vectors of all classes and reject the pattern if the smallest of these distances is greater than a fixed threshold. Bromley and Denker [2] mention experiments conducted by Yann Le Cun in support of their choice of the DA strategy.

Logically, one expects the two highest activations to provide almost all the information for the rejection decision, because usually ambiguities involve a choice between the right classification and, at most, one predominant alternative. Still, ideally, we would prefer a formula combining all the output activations into a single measure of confidence. Such formula can be derived if we view this problem as one of integration of information from different sources in the framework of the Dempster-Shafer Theory of Evidence [6]. We can treat the activation of each output node as the evidence in favor of the corresponding classification hypothesis and combine them into the measure of confidence of the final decision.

2 The Dempster-Shafer Theory of Evidence

The Dempster-Shafer Theory of Evidence is a tool for representing and combining measures of evidences. This theory is a generalization of Bayesian reasoning, but it is more flexible than Bayesian when our knowledge is incomplete, and, therefore, we have to deal with uncertainty. It allows us to represent only actual knowledge, without forcing us to make a conclusion when we are ignorant.

Let Θ be a set of mutually exhaustive and exclusive atomic hypotheses $\Theta = \{\theta_1, \ldots, \theta_N\}$. Θ is called the *frame of discernment.* Let 2^Θ denote the set of all subsets of Θ. A function $\mathbf{m}$ is called a *basic probability assignment* if

$$\mathbf{m} : 2^\Theta \rightarrow [0,1], \quad \mathbf{m}(\emptyset) = 0, \quad \text{and} \quad \sum_{A \subseteq \Theta} \mathbf{m}(A) = 1. \tag{1}$$

In the probability theory, a measure of *probability* analogous to the basic probability assignment is associated *only* with the atomic hypotheses θ_n. The probabilities of all other subsets are derived as sums of probabilities of its atomic components, and there is nothing left to express our measure of ignorance. In the Dempster-Shafer theory, $\mathbf{m}(A)$ represents the *belief* that is committed exactly to every (not necessarily atomic) subset A. It is useful to "...think of these portions of belief as semi-mobile 'probability masses', which can sometimes move from point to point but are restricted in that various of them are [...] confined to various subsets of Θ. In other words, $\mathbf{m}(A)$ measures the probability mass that is confined to A, but can move freely to every point of A" [6]. Now it is easier to understand why $\mathbf{m}(\Theta)$ represents our measure of ignorance: this portion of our total belief is not committed to any proper subset of Θ.

The simplest possible type of the basic probability assignment is a *simple evidence function*, that corresponds to the case in which all our belief is concentrated in only one subset $F \subseteq \Theta$, its *focal element.* If $F \neq \Theta$, then we can define $\mathbf{m}(F) = \mathbf{s}$, $\mathbf{m}(\Theta) = 1 - \mathbf{s}$, and $\mathbf{m}$ is 0 elsewhere. The *degree of support* $\mathbf{s}$ represents our belief in F, while $1 - \mathbf{s}$ represents our ignorance.

The Dempster-Shafer theory provides us with the rule for the combination of evidences from two sources. This combination $\mathbf{m} = \mathbf{m}_1 \oplus \mathbf{m}_2$ is called their *orthogonal sum:*

$$\mathbf{m}(A) = K \cdot \sum_{X \cap Y = A} \mathbf{m}_1(X) \cdot \mathbf{m}_2(Y) \text{ where } K^{-1} = \sum_{X \cap Y \neq \emptyset} \mathbf{m}_1(X) \cdot \mathbf{m}_2(Y). \tag{2}$$

The main idea expressed in this nonintuitive formula is actually rather simple: the portion of belief committed to the intersection of two subsets X and Y should be proportional to the product of $\mathbf{m}(X)$ and $\mathbf{m}(Y)$ (Figure 1). Only if this intersection is empty, do we have to exclude it from the sum and renormalize it. Obviously, this rule can be generalized to accommodate for more than two sources of information. Please refer to [6] for more detailed explanations.

3 Combination of Evidences as the Measure of Confidence

Consider a frame of discernment $\Theta = \{\theta_1, \ldots, \theta_N\}$, where θ_n is the hypothesis that a pattern belongs to class n. The activation of the n-th output node of a neural network, o_n, provides information in favor of the corresponding hypothesis θ_n. Our partial belief based on this information can be expressed as a simple evidence function

$$\mathbf{m}_n(\theta_n) = \phi_n, \qquad \mathbf{m}_n(\Theta) = 1 - \phi_n, \tag{3}$$

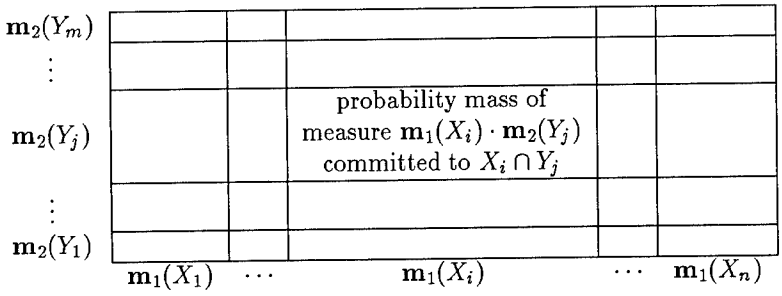

Figure 1 The Dempster combination rule.

where ϕ_n is a monotonic function of o_n. We shall discuss a specific form of this function later.

Now we have to combine these evidences into their orthogonal sum according to eqn. (2). Let us start with the case in which $N = 2$. The first simple evidence function $\mathbf{m}_1$, with its focal element θ_1, has the degree of support ϕ_1. Its only other nonzero value is $\mathbf{m}_1(\Theta) = 1 - \phi_1$. Similarly, θ_2 is the focal element of $\mathbf{m}_2$, with a degree of support of ϕ_2, and $\mathbf{m}_2(\Theta) = 1 - \phi_2$. When we produce the orthogonal sum $\mathbf{m} = \mathbf{m}_1 \oplus \mathbf{m}_2$, we have to compute beliefs for the total of four subsets of Θ: $\emptyset$, θ_1, θ_2, and Θ (Figure 2). The value $\mathbf{m}(\Theta)$ should be proportional to $\mathbf{m}_1(\Theta) \cdot \mathbf{m}_2(\Theta)$

$\mathbf{m}_2(\Theta) = 1 - \phi_2$	$\theta_1 : \phi_1 \cdot (1 - \phi_2)$	$\Theta : (1 - \phi_1) \cdot (1 - \phi_2)$
$\mathbf{m}_2(\theta_2) = \phi_2$	$\emptyset : \phi_1 \cdot \phi_2$	$\theta_2 : (1 - \phi_1) \cdot \phi_2$
	$\mathbf{m}_1(\theta_1) = \phi_1$	$\mathbf{m}_1(\Theta) = 1 - \phi_1$

Figure 2 Orthogonal sum of two simple evidence functions with atomic foci.

because this is the only way to obtain Θ as the intersection. Similarly, $\mathbf{m}(\theta_1)$ should be proportional to $\mathbf{m}_1(\theta_1) \cdot \mathbf{m}_2(\Theta)$, while $\mathbf{m}(\theta_2)$ should be proportional to $\mathbf{m}_2(\theta_2) \cdot \mathbf{m}_1(\Theta)$. The only way we can produce $\emptyset$ as an intersection of a subset with nonzero $\mathbf{m}_1$-evidence and another subset with nonzero $\mathbf{m}_2$-evidence is $\emptyset = \theta_1 \cap \theta_2$. The corresponding product, $\phi_1 \cdot \phi_2$, should be excluded from the normalization constant K. Finally,

$$\mathbf{m}(\theta_1) = K \cdot \phi_1 \cdot (1 - \phi_2) \quad , \qquad \mathbf{m}(\theta_2) = K \cdot \phi_2 \cdot (1 - \phi_1),$$
$$\mathbf{m}(\Theta) = K \cdot (1 - \phi_1) \cdot (1 - \phi_2) \quad , \qquad K = \frac{1}{1 - \phi_1 \cdot \phi_2} \tag{4}$$

It is obvious that if both $\phi_1 = 1$ and $\phi_2 = 1$, our formula cannot work because it involves division of $\frac{0}{0}$. However, this is quite appropriate, because it indicates that both $\mathbf{m}_1$ and $\mathbf{m}_2$ are absolutely confident and flatly contradict each other. In such a case, there is no hope of reconciling the differences. If only one of the two degrees of support equals 1, for example, $\phi_1 = 1$, then $\mathbf{m}(\theta_1) = 1$, $\mathbf{m}(\theta_2) = 0$, and $\mathbf{m}(\Theta) = 0$. In this case, $\mathbf{m}_2$ cannot influence the absolutely confident $\mathbf{m}_1$.

If neither of the degrees of support equals 1, we can denote $\alpha_n = \frac{\phi_n}{1 - \phi_n}$ and transform eqn. (4) into a more convenient form:

$$\mathbf{m}(\theta_1) = \frac{\alpha_1}{1 + \alpha_1 + \alpha_2}, \quad \mathbf{m}(\theta_2) = \frac{\alpha_2}{1 + \alpha_1 + \alpha_2}, \quad \mathbf{m}(\Theta) = \frac{1}{1 + \alpha_1 + \alpha_2}. \tag{5}$$

Using mathemaical induction, one can prove that when we have to combine N simple evidence functions with atomic focal elements, their orthogonal sum becomes

$$\mathbf{m}(\theta_n) = \frac{\alpha_n}{1+\sum_i \alpha_i}, \qquad \mathbf{m}(\Theta) = \frac{1}{1+\sum_i \alpha_i}. \tag{6}$$

The combined evidence $\mathbf{m}(\theta_n)$ represents our share of belief (or confidence) associated with each of N competing classification decisions. Our formula has a number of intuitively attractive properties:

- the highest confidence corresponds to the highest activation,
- the confidence increases with the growth of the corresponding activation,
- the confidence decreases with the growth of any other activation.

Now we can rate all patterns according to the confidence of the best-guess classification and reject them in order of increasing confidence. We will call this rejection strategy "evidential".

4 The Experiment

We tested the proposed method on the handprint digits classification problem. A trained neural network classifier was used to generate sets of activations for two test files, both of approximately 25,000 characters. To accentuate the comparisons, unambiguous patterns (those with the highest activation above 0.9 and all other activations below 0.1) were excluded from the experiment. Indeed, one can argue that any responsible rejection strategy should accept such patterns, especially because many neural networks are trained with target activations of 0.9 and 0.1 (sometimes even 0.8 and 0.2) instead of 1 and 0. In addition, the error vs reject curves differ for different test sets depending on the quality of the data. The exclusion of unambiguous patterns allows us to normalize the curves to some extent.

We found approximately 6,500 ambiguous patterns in the first set, and approximately 8,000 in the second set. The first subset was used to select the best monotonic transformation of the activations into the support functions. Comparison of a large number of possible functions led to the choice of the $\lambda(x) = \log_2(1+x)$ as the seed of a whole family of transformations λ^k, and finally we chose $\phi = \lambda^{15}$.

The evidential (EV) rejection strategy was then used on the second subset, and its results were compared to those achieved with the rejection scheme based on the highest activation (HA), the difference between the highest and the second highest activation (DA), the ratio of the highest and the second highest activation (RA), and the distance-based rejection criterion (DI) described above. Figure 3 presents the comparison of error vs reject graphs for all the five schemes studied. To compute data for each of the curves, all patterns are sorted according to the corresponding confidence measure. Then the patterns are rejected one by one, and the number of remaining misclassifications is counted. Their percent of the total number of the remaining patterns constitutes the error rate which is plotted against the percent reject. Obviously, there is no difference among the strategies at zero and hundred percent reject.

5 Conclusions

In this paper we demonstrated how the Dempster-Shafer Theory of Evidence can provide the framework for estimation of the confidences of competing classification

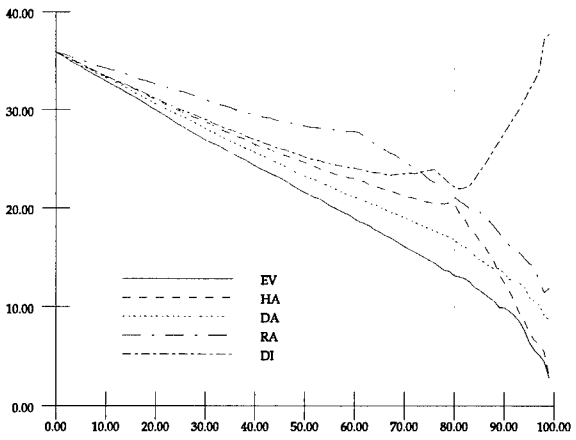

Figure 3 Percent error vs percent rejected for different strategies.

decisions. Although we worked with activations generated by a neural network, this approach can be applied if it is necessary to combine the outputs of any collection of single-class recognizers.

Our formula consistently utilizes all the output activations of a neural network classifier. Extensive experimentation allowed us to select a simple monotonic transformation of output activations as the basic probability assignment. The testing we conducted on the 8,000 strong set of ambiguous patterns confirmed that the evidential rejection strategy reduces the classification error up to 30%. It is necessary to mention here that the best choice of the monotonic transformation for the basic probability assignment depends on the concrete application.

Further work is needed, for we have not analyzed any information we can obtain from the distribution of output activation values for different classes. Another possible line of action is the analysis of the confusion matrix or, broader still, the joint distribution of activation pairs.

REFERENCES

[1] Battiti, R. and Colla, A.M., *Democracy in neural nets: voting schemes for classification,* Neural Networks Vol. 7 (4) (1994), pp691–707.

[2] Bromley, J. and Denker, J., *Improving rejection performance on handwritten digits by training with "rubbish",* Neural Computation Vol. 5 (3) (1993), pp367–370.

[3] Fogelman-Soulié, F., Viennet, E., and Lamy, B., *Multi-modular neural network architectures: applications in optical character and human face recognition,* International Journal of Pattern Recognition and Artificial Intelligence Vol. 7 (4) (1993), pp721–755.

[4] Gaborski, R.S., *Neural network with back propagation controlled through an output confidence measure.* United States Patent 5,052,043 (1991).

[5] Martin, G., Mosfeq, R., Chapman, D., and Pittman, J., *Learning to see where and what: training a net to make saccades and recognize handwritten characters,* in: S.J. Hanson, J.D. Cowan, and C.L. Giles (Eds.), Advances in Neural Information Processing Systems, Vol. 5 (1993), pp441–447. San Mateo: Morgan Kaufmann.

[6] Shafer, G., *A Mathematical Theory of Evidence,* Princeton: MIT Press (1976).

DYNAMICS APPROXIMATION AND CHANGE POINT RETRIEVAL FROM A NEURAL NETWORK MODEL

J. Smid and P. Volf*

Department of Mathematics Morgan State University, Baltimore, MD 21239 USA.
Email: smid@ltpsun.gsfc.nasa.gov
** UTIA The Czech Academy of Sciences, Prague 8,*
CZ 180 00, Czech Republic. Email: volf@utia.cas.cz

Discrete dynamical systems and nonlinear response models contaminated with random noise are considered. The objective of the paper is to propose a method of extraction of change–points of a mapping (system) from a neural network approximation. The method is based on the comparison of normalized Taylor series coefficients of the estimator and on the consistency of the estimator and its derivatives. The proposed algorithm is illustrated on a simple piecewise polynomial mapping.

1 Introduction

Consider real-valued variables y as output and x as input of a system. Their relation is modeled by a general piecewise smooth function $f : [0, d] \to \mathbb{R}$ in a model

$$y = f(x) + e, \tag{1}$$

where e stands for random noise. The analysis of the function $f(x)$ will be based on a sequence of observation data, x_i, y_i, generated by random variables $X_i, Y_i, i = 1, .., n$. We assume that random variables $e_i = Y_i - f(X_i)$, representing random noise entering the system, are mutually independent and identically distributed, with mean zero and finite variance σ^2. A discrete dynamical system

$$y_t = g(y_{t-h}) + e_t, \tag{2}$$

can be viewed as a system of the type (1) where we set $x_t = y_{t-h}$ and $y_t = g(x_t)+e_t$. Thus the estimation of the generator g of the equation (2) is transformed into a regression problem of the type (1).

Throughout the paper we will be mainly concerned with models (1) and (2). However, the proposed solution can be extended to the multivariable nonlinear function $y_i = f(x_{i1}, x_{i2}, ..., x_{ik}) + e_i$ and to autoregressive systems, dynamic regression and recursive response cases, e.g. $y_t = g(y_t, y_{t-h}, ..., y_{t-mh}) + e_t$.The present paper considers the use of a feedforward neural network approach. That is the spline network (as a representative of feedforward neural nets) will be used as the tool for estimation of the model functions.

2 Polynomial Splines and Feedforward Neural Networks

A neural network is a system of interconnected nonlinear units. The topology of connections between units can be complicated. In the simplest scenario a neural network model is no more than the sum of units. The nonlinear units are either localized (e.g. splines and radial basis functions) or their sums form localized functions (e.g. perceptrons). The local nature of the units has been exploited for classification/pattern recognition problems, e.g. in [4]. We will show usefulness of local processing units for the function change–point estimation problems.

2.1 Polynomial Spline Functions

A polynomial spline function $f(x)$ is a function that consists of polynomial pieces $f(x) = f_i(x) on [\lambda_i, \lambda_{i+1}], \quad (i = 0, ..., M)$ where f_i is a polynomial of degree k. The

points $\lambda_0, \lambda_1, ..., \lambda_M$ at which the function $f(x)$ changes its character are termed break points or knots in the theory splines (other authors prefer "joints" or "nodes") The polynomial pieces are joined together with certain smoothness conditions. The smoothness conditions are $\lim_{x\to\lambda_i-} f^{(j)}(x) = \lim_{x\to\lambda_i+} f^{(j)}(x), \quad (j = 1, ..., k-1)$. In other words, a spline function of degree $k \geq 0$, having as break points the strictly increasing sequence $\lambda_j, (j = 0, 1, ..M+1;\ \lambda_0 = 0, \lambda_{M+1} = d)$, is a piecewice polynomial on intervals $[\lambda_j, \lambda_{j+1}]$ of degree k at most, with continuous derivatives up to order $k-1$ on $[0, d]$. It is known that a uniformly continuous function can be approximated by polynomial splines to arbitrary accuracy, see for instance de Boor [2]. This concept can be naturally extended to higher dimensions. The set of spline functions is endowed with the natural structure of a finite vector space. The dimension of the vector space of spline functions of degree k with M interior break points is $m = M + k + 1$. A neural network–like basis of the space of spline functions is the basis of B-splines. Each spline function can be written as a unique linear combination of basis functions.In this paper we shall use the basis of B-splines, which may be defined, for example, in a recursive way (cf. de Boor [2]). Let us define $\{\lambda_{-k} = \lambda_{-k+1} = ... = \lambda_0 = 0 < \lambda_1 < \lambda_2 < ... < \lambda_M < d = \lambda_{M+1} = ... = \lambda_m\}$ an extended set of $M + 2k + 2$ knots associated with the interval $[0, d]$. Each B-spline basis function (a unit in neural network terminology) $B_j^k(x)$ is completely described by a set of $k + 2$ knots $\{\lambda_{j-k-1}, \lambda_{j-k}, ..., \lambda_j\}$. There are two important properties of these units [2], namely they are nonnegative, vanish everywhere except on a few contiguous subintervals $B_j^k(x) > 0$ if $\lambda_{j-k-1} \leq x \leq \lambda_j$, $B_j^k(x) = 0$ otherwise, and they define a partition of unity on $[0, d]$, $\sum_{j=1}^m B_j^k(x) = 1$ for all $x\epsilon[0, d]$. We shall mainly deal with cubic ($k = 3$) and quadratic ($k = 2$) B–splines because of their simplicity and importance in applications. Higher–degree splines are used whenever more smoothness is needed in the approximating function. For a chosen number m of units, the resulting polynomial spline is a function f_m from the set $\mathcal{S}_m^k = \{f_m : [0, d] \to \mathbb{R} \mid f_m(x) = \sum_{j=1}^m w_j B_j^k(x)\}$.By $\mathcal{S}^k = \bigcup_m \mathcal{S}_m^k$ we denote the set of all univariate splines of degree k (order $k+1$). All these properties allow us to think of spline functions as neural networks. The numbers w_j are called weights (in statistics and neural network theory) or control points (in computer aided geometric design).

2.2 Feedforward Neural Networks

The virtue of neural networks in our approach is their capability to capture more information about the true system structure then, e.g. by polynomials. There is a number of methods for estimation of the network parameters. For example, incremental learning algorithms are described in Fahlman and Lebier [4] or Jones's approach in [5]. We will assume that neural network parameters have been estimated by one of the available learning algorithms. In the case of B–spline networks, the simplest approach computes the weights by the least squares method and, eventually, iterates the placement of knots in order to optimize it. Neural networks do not provide immediate insight into how the modeled mechanism works. This insight can be gained by solving an extraction problem. What we mean by an extraction problem for a neural net is how to extract the underlying structure of dependence in terms of a local polynomial regression model. This framework is useful when a simple explicit description (e.g. in terms of the low-degree polynomial regression) is

required. Also this technique is more feasible than a 'direct' nonlinear polynomial regression for systems where the generator g is changing in time.

3 Extraction of a Piecewise Polynomial Model

Why we should use nets instead of polynomials? It is well known that the set of all polynomials is dense in the space of all continuous functions (Stone-Weierstrass theorem). However, for practical purposes approximation by a single polynomial may create polynomials of prohibitively high degree. These high degree polynomials most likely do not reflect the nature of underlying response function. A neural network may perform approximation tasks more efficiently. Important questions include how to extract the structure of the function f. When speaking about extraction of the underlying polynomial structure we envision a target function to be a polynomial or a piecewise polynomial. These functions admit a local approximation by a lower degree polynomial. This local approximation can be arbitrarily accurate provided that the interval over which we approximate is sufficiently small. This is true even across the break points of a piecewise polynomial. Polynomial extraction and diagnosis of the point of change is based on the consistency of the approximation and its derivatives, i.e. on their convergence to the target function and its derivatives.

It is well known that a smooth function f and its derivatives can be approximated to arbitrary accuracy by splines. This stems for example from the error bounds for polynomial splines and their derivatives established by Hall and Meyer [3], Marsden [6]. For cubic spline interpolants the error bound is

$$\|(f - f_m)^{(r)}\|_\infty \leq C_r \|f^{(4)}\| h^{4-r}, (r = 0, 1, 2, 3) \tag{3}$$

where h is the mesh gauge and C_r are constants. For noisy data the consistency of the functional need to be extended for the statistical estimators as well.

If we assume that the response function f is smooth and has bounded derivatives then it can be locally approximated to arbitrary accuracy by the Taylor polynomial of degree k. The Lagrange's remainder term of the Taylor expansion at the point a has the form

$$R_k = \frac{(x-a)^{k+1}}{(k+1)!} f^{(k+1)}((x-a)\theta + a),\ 0 \leq \theta \leq 1 \tag{4}$$

This is particularly true for $k = 2, 3$ when the mesh gauge $h = max_i|\lambda_{i+1} - \lambda_i|, i = 0, \ldots n-1$ is sufficiently small. It follows from the equations (3), (4) that good approximation of the smooth response function f implies good approximation of the coefficients of the local Taylor expansion of f. It means that one polynomial piece will be approximated by a spline having polynomial pieces with the same coefficients at a common point. If f is not smooth, i.e. it has a finite set of active break points, then good approximation by splines is still possible except for arbitrarily small neighborhoods around break points. In the neighborhood of a break point of f the polynomial piece of the spline approximation will reflect abrupt change of the function f. This approach can be generalized for noisy data. We will utilize the results of Stone [8] showing that a sequence of the optimal estimates $\hat{f}_{mn} \in \mathcal{S}_m$ of f from a noisy data set $(x_1, y_1), (x_2, y_2), .., (x_n, y_n)$ converges to f as m and n go to infinity, and that ,the same holds for derivatives $\hat{f}^{(k)}_{mn}$, $f^{(k)}$, for k not greater than the degree of estimating splines, provided $f^{(k)}$ is Lipschitz continuous.

4 Tests for Functional Change

A gradually changing response function will produce gradually changing normalized polynomial coefficients. By normalized coefficients we mean coefficients of polynomial pieces expanded about a common point. An abrupt change in response function will be reflected by an abrupt change in the normalized coefficients. To test for the points of change in the behavior of the neural network approximation $\hat{f}_{mn}$ the polynomial pieces, with coefficients $p_{ij}(\lambda_j)$ were recalculated about a common point $x = 0$. A set of new coefficients $p_{ij}(0, \lambda_j)$ was obtained and we call those coefficients normalized Taylor coefficients. The index i refers to the degree of the piece p_{ij} and j to the jth interval. The points with the same normalized coefficients indicate no change of the functional dependence.

For stationary functions/systems all normalized coefficients will be constant or almost constant (due to noise and approximation errors).

5 Large Sample Properties

To establish the consistency of the estimator $\hat{f}_{mn}$ and its derivatives we recall the results of Stone [8] who deals with optimal rates of convergence of response function estimator based on the spline functions $\hat{f}_{mn}(x) = \sum_{j=1}^{m} \hat{w}_j B_j^k(x)$. This representation is a very useful one because it casts the spline into a multiple linear regression context. If the set of knots is fixed, the estimator may be found as the least squares solution in parameters $w_j, j = 1, .., m$. Then the vector of weights $\hat{w} = (Z^T Z)^{-1} Z^T Y$, where $Y = (y_1, ..., y_n)^T$ and Z is a (n, m) matrix such that $z_{ij} = B_j^k(x_i)$. Let us denote $\mathcal{C}_p$ a set of all functions $f : [0, d] \rightarrow \mathbb{R}$ having continuous the pth derivatives, $\|.\|$ the L_2 norm on [0,d], and $E(.)$ the mean operator. For given sequences of numbers a_n, b_n, $b_n > 0$, by $a_n = O(b_n)$ we mean that sequence a_n/b_n is bounded. When A_n are random variables, $P\lim_{n\rightarrow\infty} A_n = 0$ means that for each $\varepsilon > 0$ $lim_{n\rightarrow\infty} P(|A_n| < \varepsilon) = 1$. For simplicity we assume that data points $x_1, ..., x_n$ and interior knots (break points) are uniformly distributed in the interval $[0, d]$. To assure good approximation of the response function we assume that we sampled more data points than the number of B-spline units, i.e. $m = O(n^\gamma)$, $\gamma\epsilon(0, 1)$.

Proposition 1 *Suppose f is from $\mathcal{C}_1$. Then $E\|\hat{f}_{mn} - f\|^2 = O(n^{\gamma-1}) + O(n^{-2\gamma})$. (This follows from the Lipschitz continuity of f). Suppose f is from $\mathcal{C}_p, p > 0$ and k is the degree of estimating spline. Let $\gamma = \frac{1}{2p+1}$. Then, for $l = 0, 1, .., min(k, p-1)$ it holds that $E\|\hat{f}_{mn}^{(l)} - f^{(l)}\|^2 = O(n^{-2r_l})$, where $r_l = \frac{p-l}{2p+1}$.*

The consistency of the derivatives gives supports diagnostics based on the Taylor expansion, especially for an analysis of the low-order derivatives. The procedure of the model retrieval is an iterative process combining techniques of estimation with methods of testing, i.e. of comparing the model with the actual behavior of the system.

6 Numerical Example of Estimation of 1-D Discrete Piecewise Quadratic Dynamical System

The algorithm has been applied on a time series of satellite data set, see reference [7]. Here, for the numerical illustration, let us consider a following simple example: A discrete dynamical system is defined by two quadratic maps: $f_n = 4f_{n-1} - 4f_{n-1}^2, f_{n-1} \leq 0.5$ and $f_n = 1.2 + 0.4f_{n-1} - 1.6f_{n-1}^2, f_{n-1} \geq 0.5$. This map

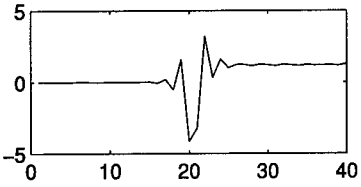

Figure 1 Constants at $x = 0$; $c_1 = 0$, $c_2 = 1.2$.

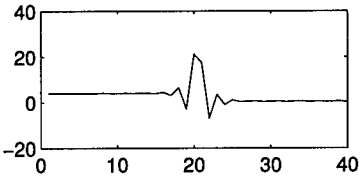

Figure 2 Lin. Coeff. at $x = 0$; $b_1 = 4$, $b_2 = 0.4$.

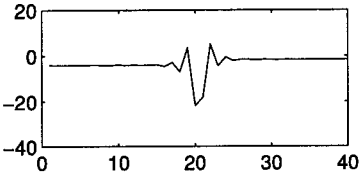

Figure 3 Qdr. Coeff. at $x = 0$; $a_1 = -4$, $a_2 = -1.6$.

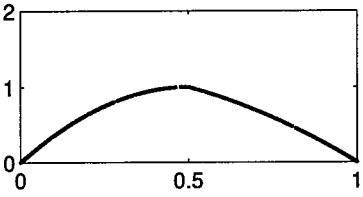

Figure 4 $y(n)$ vs. $y(n-1)$ for $n = 1$ to 800.

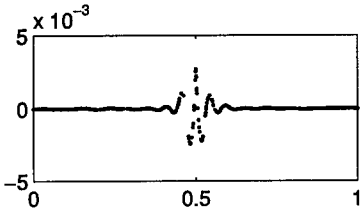

Figure 5 Spline fit error.

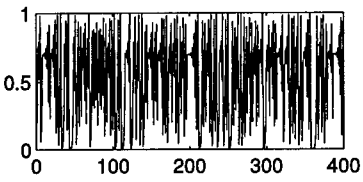

Figure 6 Quadratic Map time series.

is from the family of quadratic maps that is known to be chaotic and ergodic. The time series generated by this map cannot be predicted for many steps ahead but the generator of this series can be identified from the time series. We used a quadratic spline $\hat{f}_{mn}$ with 40 interior break points to identify sets of polynomial coefficients. Pieces of the spline $\hat{f}_{mn}$ are represented by local polynomials $a_j(x - \lambda_j)^2 + b_j(x - \lambda_j) + c_j, (j = 0, 1, \cdots, 39)$. Figures 1, 2 and 3 show polynomial coefficients $a_j(0), b_j(0), c_j(0)$. These coeffiecient were recalculated from the local coefficients at the common break point $\lambda_0 = 0$. Figure 4 shows the piecewise quadratic map. Figure 5 shows the error of the spline fit. Figure 6 shows 400 points of the chaotic time series generated by the piecewise quadratic map and additive gaussian noise $N(0, \sigma^2 = 0.0001)$. The dynamical problem then becomes the following approximation test: a domain is randomly partitioned into a finite number of subintervals. On each subinterval are generated data by a noisy polynomial. The aim of the analysis is to find those polynomials and/or to find all break points.

7 Concluding Remarks

We have proposed a method employing the B–splines network for estimation of an unknown response function from noisy data, and for extraction a potential piecewise polynomial submodel. It has been shown how the first terms of the Taylor expansion of the estimator, when expanded at different points of its domain, can be utilized for revealing the degree of the underlying polynomial model, and for the detection of changes in the model. This approach can be adapted for multidimensional and discrete dynamical systems (3) or (4). In these cases, we have to work with the partial derivatives. However, the multivariate case leads to the use of multivariate approximating functions. In such a situation, the estimation becomes less effective (a much greater amount of data is needed), even the theoretical rate of convergence is slower. Many authors (cf. Breiman[1], Stone[8]) recommend the use of additive approximations with low–dimensional components.

REFERENCES

[1] Breiman L., *Fitting additive models to regression data: diagnostics and alternative views*, Comp.Statistics and Data Analysis Vol. 15 (1993), pp13–46.

[2] de Boor C., *A Practical Guide to Splines*, Springer Verlag (1978).

[3] Hall C.A. and Meyer W.W., *Optimal error bounds for cubic spline interpolation*, Journal of Approximation Theory Vol. 16, No.2 (February 1976).

[4] Fahlman S.E. and Lebiere C., *The cascade correlation learning architecture*, Research Report CMU-CS-90-100 (1990).

[5] Kurkova V. and Smid J., *An incremental architecture algorithm for feedforward neural nets*, in: Computer Intensive Methods in Control and Signal Processing, Preprints of the European IEEE Workshop, Prague (1994).

[6] Marsden, M.J.(1974), *Quadratic Spline Interpolation*, Bulletin of the American Mathematical Society, Vol. 80, No.5 (September 1974).

[7] Smid J. and Volf P., *Dynamics retrieval and characterization from nonlinear time series*, Neural Network World, to appear (1995).

[8] Stone C.J., *Additive regression and other nonparametric models*, The Annals of Statistics Vol. 13 (1985), pp689–705.

Acknowledgements

This research is supported by NASA/GSFC under Grants NAG 5-2686, NCC 5-127 and by the Czech Academy of Science Grant No 275 408

QUERY LEARNING FOR MAXIMUM INFORMATION GAIN IN A MULTI-LAYER NEURAL NETWORK

Peter Sollich

Department of Physics, University of Edinburgh
Edinburgh EH9 3JZ, UK. Email: P.Sollich@ed.ac.uk

In supervised learning, the redundancy contained in random examples can be avoided by learning from queries, where training examples are chosen to be maximally informative. Using the tools of statistical mechanics, we analyse query learning in a simple multi-layer network, namely, a large tree-committee machine. The generalization error is found to decrease exponentially with the number of training examples, providing a significant improvement over the slow algebraic decay for random examples. Implications for the connection between information gain and generalization error in multi-layer networks are discussed, and a computationally cheap algorithm for constructing approximate maximum information gain queries is suggested and analysed.

1 Introduction

In supervised learning of input-output mappings, the traditional approach has been to study generalization from random examples. However, random examples contain redundant information, and generalization performance can thus be improved by *query learning*, where each new training input is selected on the basis of the existing training data to be most 'useful' in some specified sense. Query learning corresponds closely to the well-founded statistical technique of (sequential) *optimal experimental design*. In particular, we consider in this paper queries which maximize the expected information gain, which are related to the criterion of (Bayes) D-optimality in optimal experimental design. The generalization performance achieved by maximum information gain queries is by now well understood for single-layer neural networks such as linear and binary perceptrons [1, 2, 3]. For multi-layer networks, which are much more widely used in practical applications, several heuristic algorithms for query learning have been proposed (see e.g., [4, 5]). While such heuristic approaches can demonstrate the power of query learning, they are hard to generalize to situations other than the ones for which they have been designed, and they cannot easily be compared with more traditional optimal experimental design methods. Furthermore, the existing analyses of such algorithms have been carried out within the framework of 'probably approximately correct' (PAC) learning, yielding worst case results which are not necessarily close to the potentially more relevant average case results. In this paper we therefore analyse the average generalization performance achieved by query learning in a multi-layer network, using the powerful tools of statistical mechanics. This is the first quantitative analysis of its kind that we are aware of.

2 The Model

We focus our analysis on one of the simplest multi-layer networks, namely, the tree-committee machine (TCM). A TCM is a two-layer neural network with N input units, K hidden units and one output unit. The 'receptive fields' of the individual hidden units do not overlap, and each hidden units calculates the sign of a linear combination (with real coefficients) of the N/K input components to which it is connected. The output unit then calculates the sign of the sum of all the hidden

unit outputs. A TCM therefore effectively has all the weights from the hidden to the output layer fixed to one. Formally, the output y for a given input vector $\mathbf{x}$ is

$$y = \mathrm{sgn}\left(\sum_{i=1}^{K} \sigma_i\right) \qquad \sigma_i = \mathrm{sgn}\left(\mathbf{x}_i^{\mathrm{T}} \mathbf{w}_i\right) \tag{1}$$

where the σ_i are the outputs of the hidden units, $\mathbf{w}_i$ their weight vectors, and $\mathbf{x}^{\mathrm{T}} = (\mathbf{x}_1^{\mathrm{T}}, \ldots, \mathbf{x}_K^{\mathrm{T}})$ with $\mathbf{x}_i$ containing the N/K (real-valued) inputs to which hidden unit i is connected. The N (real) components of the K (N/K)-dimensional hidden unit weight vectors $\mathbf{w}_i$, which we denote collectively by $\mathbf{w}$, form the adjustable parameters of a TCM. Without loss of generality, we assume the weight vectors to be normalized to $\mathbf{w}_i^2 = N/K$. We shall restrict our analysis to the case where both the input space dimension and the number of hidden units are large $(N \to \infty, K \to \infty)$, assuming that each hidden unit is connected to a large number of inputs, i.e., $N/K \gg 1$. As our training algorithm we take (zero temperature) Gibbs learning, which generates at random any TCM (in the following referred to as a 'student') which predicts all the training outputs in a given set of p training examples $\Theta^{(p)} = \{(\mathbf{x}^\mu, y^\mu), \mu = 1 \ldots p\}$ correctly. We take the problem to be perfectly learnable, which means that the outputs y^μ corresponding to the inputs $\mathbf{x}^\mu$ are generated by a 'teacher' TCM with the same architecture as the student but with different, unknown weights $\mathbf{w}^0$. It is further assumed that there is no noise on the training examples. For learning from random examples, the training inputs $\mathbf{x}^\mu$ are sampled randomly from a distribution $P_0(\mathbf{x})$. Since the output (1) of a TCM is independent of the length of the hidden unit input vectors $\mathbf{x}_i$, we assume this distribution $P_0(\mathbf{x})$ to be uniform over all vectors $\mathbf{x}^{\mathrm{T}} = (\mathbf{x}_1^{\mathrm{T}}, \ldots, \mathbf{x}_K^{\mathrm{T}})$ which obey the spherical constraints $\mathbf{x}_i^2 = N/K$. For query learning, the training inputs $\mathbf{x}^\mu$ are chosen to maximize the expected information gain of the student, as follows. The information gain is defined as the decrease in the entropy S in the parameter space of the student. The entropy for a training set $\Theta^{(p)}$ is given by

$$S(\Theta^{(p)}) = -\int d\mathbf{w} P(\mathbf{w}|\Theta^{(p)}) \ln P(\mathbf{w}|\Theta^{(p)}). \tag{2}$$

For the Gibbs learning algorithm considered here, $P(\mathbf{w}|\Theta^{(p)})$ is uniform on the 'version space', the space of all students which predict all training outputs correctly (and which satisfy the assumed spherical constraints on the weight vectors, $\mathbf{w}_i^2 = N/K$), and zero otherwise. Denoting the version space volume by $V(\Theta^{(p)})$, the entropy can thus simply be written as $S(\Theta^{(p)}) = \ln V(\Theta^{(p)})$. When a new training example $(\mathbf{x}^{p+1}, y^{p+1})$ is added to the existing training set, the information gain is $I = S(\Theta^{(p)}) - S(\Theta^{(N+1)})$. Since the new training output y^{p+1} is unknown, only the *expected* information gain, obtained by averaging over y^{p+1}, is available for selecting a maximally informative query $\mathbf{x}^{p+1}$. As derived in Ref. [2], the probability distribution of y^{p+1} given the input $\mathbf{x}^{p+1}$ and the existing training set $\Theta^{(p)}$ is $P(y^{p+1} = \pm 1 | \mathbf{x}^{p+1}, \Theta^{(p)}) = v^{\pm}$, where $v^{\pm} = V(\Theta^{(N+1)})|_{y^{p+1}=\pm 1} / V(\Theta^{(p)})$. The expected information gain is therefore

$$\langle I \rangle_{P(y^{p+1}|\mathbf{x}^{p+1}, \Theta^{(p)})} = -v^+ \ln v^+ - v^- \ln v^- \tag{3}$$

and attains its maximum value $\ln 2$ ($\equiv 1$ bit) when $v^{\pm} = \frac{1}{2}$, i.e., when the new input $\mathbf{x}^{p+1}$ *bisects* the existing version space. This is intuitively reasonable, since $v^{\pm} = \frac{1}{2}$ corresponds to maximum uncertainty about the new output and hence to maximum information gain once this output is known.

Due to the complex geometry of the version space, the generation of queries which achieve exact bisection is in general computationally infeasible. The 'query by committee' algorithm proposed in Ref. [2] provides a solution to this problem by first sampling a 'committee' of $2k$ students from the Gibbs distribution $P(\mathbf{w}|\Theta^{(p)})$ and then using the fraction of committee members which predict +1 or -1 for the output y corresponding to an input $\mathbf{x}$ as an approximation to the true probability $P(y = \pm 1|\mathbf{x}, \Theta^{(p)}) = v^{\pm}$. The condition $v^{\pm} = \frac{1}{2}$ is then approximated by the requirement that exactly k of the committee members predict $+1$ and -1, respectively. An approximate maximum information gain query can thus be found by sampling (or *filtering*) inputs from a stream of random inputs until this condition is met. The procedure is then repeated for each new query. As $k \to \infty$, this algorithm approaches the exact bisection algorithm, and it is on this limit that we focus in the following.

3 Exact Maximum Information Gain Queries

The main quantity of interest in our analysis is the generalization error ϵ_g, defined as the probability that a given student TCM will predict the output of the teacher incorrectly for a random test input sampled from $P_0(\mathbf{x})$. It can be expressed in terms of the overlaps $R_i = \frac{K}{N}\mathbf{w}_i^{\mathrm{T}}\mathbf{w}_i^0$ of the student and teacher hidden unit weight vectors $\mathbf{w}_i$ and $\mathbf{w}_i^0$ [6]. In the thermodynamic limit, the R_i are self-averaging, and can be obtained from a replica calculation of the average entropy S as a function of the normalized number of training examples, $\alpha = p/N$; details will be reported in a forthcoming publication [7]. The resulting average generalization error is plotted in Figure 1; for large α, one can show analytically that $\epsilon_g \propto \exp(-\alpha \frac{1}{2}\ln 2)$. This exponential decay of the generalization error ϵ_g with α provides a marked

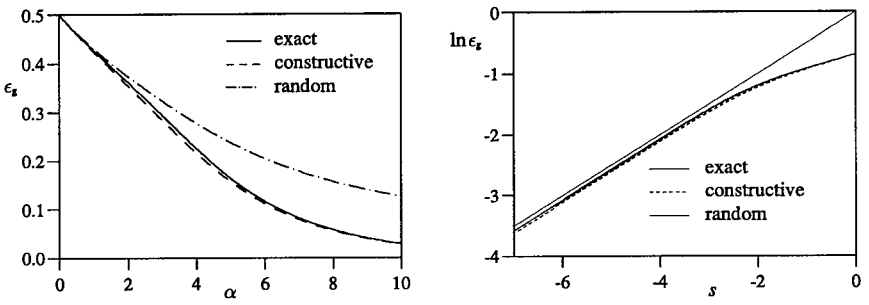

Figure 1 Left: Generalization error ϵ_g vs. (normalized) number of examples α, for *exact* maximum information gain queries (Section 3), queries selected by *constructive* algorithm (Section 4), and *random* examples. Right: $\ln\epsilon_g$ vs. (normalized) entropy s. For both queries and random examples, $\ln\epsilon_g \approx \frac{1}{2}s$ (thin full line) for large negative values of s (corresponding to large α).

improvement over the $\epsilon_g \propto 1/\alpha$ decay achieved by random examples [6]. The effect of maximum information gain queries is thus similar to what is observed for a binary perceptron learning from a binary perceptron teacher, but the decay constant c in $\epsilon_g \propto \exp(-c\alpha)$ is only half of that for the binary perceptron [2]. This means that asymptotically, twice as many examples are needed for a TCM as for a binary perceptron to achieve the same generalization performance, in agreement

with the results for random examples [6]. Since maximum information gain queries lead to an entropy $s = -\alpha \ln 2$ in both networks, we can also conclude that the relation $s \approx \ln \epsilon_g$ for the binary perceptron [2] has to be replaced by $s \approx \ln \epsilon_g^2$ for the tree committee machine. Figure 1 shows that, as expected, this relation holds independently of whether one is learning from queries or from random examples.

4 Constructive Query Selection Algorithm

We now consider the practical realization of maximum information gain queries in the TCM. The query by committee approach, which in the limit $k \to \infty$ is an exact algorithm for selecting maximum information queries, filters queries from a stream of random inputs. This leads to an exponential increase of the query filtering time with the number of training examples that have already been learned [3]. As a cheap alternative we propose a simple algorithm for *constructing* queries, which is based on the assumption of an approximate decoupling of the entropies of the different hidden units, as follows. Each individual hidden unit of a TCM can be viewed as a binary perceptron. The distribution $P(\mathbf{w}_i|\Theta^{(p)})$ of its weight vector $\mathbf{w}_i$ given a set of training examples $\Theta^{(p)}$ has an entropy S_i associated with it, in analogy to the entropy (2) of the full weight distribution $P(\mathbf{w}|\Theta^{(p)})$. Our 'constructive algorithm' for selecting queries then consists in choosing, for each new query $\mathbf{x}^{\mu+1}$, the inputs $\mathbf{x}_i^{\mu+1}$ to the individual hidden units in such a way as to maximize the decrease in their entropies S_i. This can be achieved simply by choosing each $\mathbf{x}_i^{\mu+1}$ to be orthogonal to $\bar{\mathbf{w}}_i^{\mu} = \langle \mathbf{w}_i \rangle_{P(\mathbf{w}|\Theta^{(\mu)})}$ (and otherwise random, i.e., according to $P_0(\mathbf{x})$) [7], thus avoiding the cumbersome and time-consuming filtering from a random input stream. In practice, one would of course approximate $\bar{\mathbf{w}}_i^{\mu}$ by an average of $2k$ (say) samples from the Gibbs distribution $P(\mathbf{w}|\Theta^{(\mu)})$; these samples would have been needed anyway in the query by committee approach.

The generalization performance achieved by this constructive algorithm can again be calculated by the replica method; as shown in Figure 1, it is actually slightly superior to that of exact maximum information gain queries. The α-dependence of the entropy, $s = -\alpha \ln 2$, turns out to be the same as for maximum information gain queries; this indicates that the correlations between the individual hidden units become sufficiently small for $K \to \infty$, so that queries selected to minimize the individual hidden units' entropies also minimize the overall entropy of the TCM.

5 Conclusions

We have analysed query learning for maximum information gain in a large tree-committee machine (TCM). Or main result is the exponential decay of the generalization error ϵ_g with the normalized number of training examples α, which demonstrates that query learning *can* yield significant improvements over learning from random examples (for which $\epsilon_g \propto 1/\alpha$ for large α) in multi-layer neural networks. The fact that the decay constant c in $\epsilon_g \propto \exp(-c\alpha)$ differs from that calculated for single-layer nets such as the binary perceptron raises the question of how large c would be in more complex multi-layer networks. Combining the worst-case bound in [3] in terms of the VC-dimension with existing storage capacity bounds, one would estimate that c could be as small as $O(1/\ln K)$ for networks with a large number of hidden units K. This contrasts with our result $c \to$ const. for $K \to \infty$, and further work is clearly needed to establish whether there are realistic networks which saturate the lower bound $c = O(1/\ln K)$.

We have also analysed a computationally cheap algorithm for constructing (rather than filtering) approximate maximum information gain queries, and found that it actually achieves slightly better generalization performance than exact maximum information gain queries. This result is particularly encouraging considering the practical application of query learning in more complex multi-layer networks. For example, the proposed constructive algorithm can be modified for query learning in a fully-connected committee machine (where each hidden unit is connected to all the inputs), by simply choosing each new query to be orthogonal to the subspace spanned by the average weight vectors of *all* K hidden units. As long as K is much smaller than the input dimension N, and assuming that for large enough K the approximate decoupling of the hidden unit entropies still holds for fully connected networks, one would expect this algorithm to yield a good approximation to maximum information gain queries. The same conclusion may also hold for a *general* two-layer network with threshold units (where, in contrast to the committee machine, the hidden-to-output weights are free parameters), which can approximate a large class of input-output mappings. In summary, our results therefore suggest that the drastic improvements in generalization performance achieved by maximum information gain queries can be made available, in a computationally cheap manner, for realistic neural network learning problems.

REFERENCES

[1] P. Sollich, *Query construction, entropy, and generalization in neural network models*, Phys. Rev. E, Vol. 49 (1994), pp4637–4651.

[2] H. S. Seung, M. Opper, and H. Sompolinsky, *Query by committee*, in: Proc. 5th Workshop on Computational Learning Theory (COLT '92), ACM, New York, (1992), pp287–294.

[3] Y. Freund, H. S. Seung, E. Shamir, and N. Tishby, *Information, prediction, and query by committee*, in: Advances in Neural Information Processing Systems 5, S. J. Hanson, J. D. Cowan, and C. Lee Giles eds., Morgan Kaufmann, San Mateo, CA (1993), pp483–490.

[4] E. Baum, *Neural network algorithms that learn in polynomial time from examples and queries*, IEEE Trans. Neural Netw., Vol. 2 (1991), pp5–19.

[5] J.-N. Hwang, J. J. Choi, S. Oh, and R.J. Marks II, *Query-based learning applied to partially trained multilayer perceptrons*, IEEE Trans. Neural Netw., Vol. 2 (1991), pp131–136.

[6] H. Schwarze and J. Hertz, *Generalization in a large committee machine*, Europhys. Lett., Vol. 20 (1992), pp375–380.

[7] P. Sollich, *Learning from minimum entropy queries in a large committee machine*, Phys. Rev. E, Vol.53 (1996), ppR2060–R2063.

Acknowledgements

This work was partially supported by European Union grant no. ERB CHRX-CT92-0063.

SHIFT, ROTATION AND SCALE INVARIANT SIGNATURES FOR TWO-DIMENSIONAL CONTOURS, IN A NEURAL NETWORK ARCHITECTURE

David McG. Squire and Terry M. Caelli

School of Computing, Curtin University of Technology Perth, Western Australia, Australia. Email: squizz@cs.curtin.edu.au, tmc@cs.curtin.edu.au

A technique for obtaining shift, rotation and scale invariant signatures for two dimensional contours is proposed and demonstrated. An *invariance factor* is calculated at each point by comparing the orientation of the tangent vector with vector fields corresponding to the generators of Lie transformation groups for shift, rotation and scaling. The statistics of these invariance factors over the contour are used to produce an *invariance signature*. This operation is implemented in a Model-Based Neural Network (MBNN), in which the architecture and weights are parameterised by the constraints of the problem domain. The end result after constructing and training this system is the same as a traditional neural network: a collection of layers of nodes with weighted connections. The design and modeling process can be thought of as *compiling* an invariant classifier into a neural network. We contend that these invariance signatures, whilst not unique, are sufficient to characterise contours for many pattern recognition tasks.

1 Introduction

1.1 The Model-Based Approach to Building Neural Networks

The MBNN approach aims to retain the advantages of Traditional Neural Networks (TNNs), i.e. parallel data-processing, but to constrain the process by which the architecture of the network and the values of the weights are determined, so that the designer can use expert knowledge of the problem domain. MBNNs were introduced in [1]. In that paper we proposed networks in which the weights were functions of the relative positions of nodes, and several, possibly shared, parameters. This reduced the dimensionality of the space searched during training, and the size of the training set required, since the network was guaranteed to respond only to certain features. The resultant network was just a collection of nodes and weighted connections, exactly as in a TNN. The key notion was that neural networks with highly desirable properties could be produced by using expert knowledge to constrain the weight determination process. The MBNN approach departs from the TNN view in that the operation is not determined entirely by the training set supplied.

1.2 Model-Based Neural Networks and Invariant Pattern Recognition

That the parameters of TNNs are entirely learnt can be a limitation. To achieve good performance, the training set must be sufficiently large and varied to span the input space. Collecting this data and training the network can be very time-consuming. The MBNN formulation allows the creation of networks guaranteed to respond to particular features in, and to be invariant under certain transformations of, the input image. A data set containing various shifted, distorted or otherwise transformed versions of the input patterns, such has long been a common approach to invariant pattern recognition using neural networks [2], is not required. The concept of MBNNs is here extended to include modular networks. Each module has a well-defined functionality. The weights in each module can be arrived at by

any technique at all: some may be set by the designer, others by training the module for a specific task. This approach allows the the network designer great flexibility. Separately trained modules can perform data processing tasks independent of the final classification of the input pattern.

2 Invariance Signatures

2.1 Functions Invariant With Respect To Lie Transformation Groups

We wish to determine the invariance of a function $F(x,y)$ with respect to a Lie transformation group.

$$\mathbf{G}(x,y) = \begin{bmatrix} g_x(x,y) & g_y(x,y) \end{bmatrix}^T \tag{1}$$

is the vector field corresponding to the generator of the group. F is constant with respect to the action of the generator if

$$\nabla F \cdot \mathbf{G}(x,y) = 0, \quad \text{i.e.} \quad \frac{\partial F}{\partial x} g_x + \frac{\partial F}{\partial y} g_y = 0. \tag{2}$$

Consider a contour parameterised by t on which F is constant:

$$F(x(t), y(t)) = C \ \forall \ t. \tag{3}$$

Since F is constant on the contour, we have:

$$\frac{dF}{dt} = \frac{\partial F}{\partial x}\frac{dx}{dt} + \frac{\partial F}{\partial y}\frac{dy}{dt} = 0, \quad \text{so that} \quad \frac{\frac{\partial F}{\partial x}}{\frac{\partial F}{\partial y}} = -\frac{dy}{dx}. \tag{4}$$

Thus the invariance condition given in equation 2, holds if

$$\frac{dy}{dx} = \frac{g_y}{g_x}. \tag{5}$$

2.2 Mapping Points from Image Space to Invariance Space

The tangent to the contour at each point is compared with the vector fields characterising given transformations. Both the tangent vector $\theta(x,y)$ and the vector fields $\mathbf{v_c}(x,y)$ are normalised everywhere. The measure of consistency with invariance class c at point (x,y) is:

$$\iota_c(x,y) = \left| \hat{\theta}(x,y) \cdot \mathbf{v_c}(x,y) \right|. \tag{6}$$

This operation maps points from the image to the interior of a unit hypercube in an n-dimensional *invariance space*:

$$\hat{\theta}(x,y) \longrightarrow \begin{bmatrix} \iota_{rot} & \iota_{dil} & \iota_{trans} \end{bmatrix}^T. \tag{7}$$

The origin of the image space is chosen to be the centroid of the contour, so that the *invariance signature* is shift invariant. The vector field for rotation invariance is:

$$\mathbf{v_{rot}}(x,y) = \frac{1}{\sqrt{x^2+y^2}} \begin{bmatrix} -y & x \end{bmatrix}^T. \tag{8}$$

The vector field for dilation invariance is similar. For the translation invariance case, the vector field $\mathbf{v_{trans}}(x,y)$ is constant for all (x,y). The direction is that of the dominant eigenvector of the coordinate covariance matrix of the contour. The invariance signature of an image consists of histograms of the invariance measures for all the "on" points. It is invariant under rotations, dilations, translations and reflections of the image. This encoding is not unique, unlike some previous integral transform representations [3].

3 A Neural Network System For Computing Invariance Signatures

A MBNN was constructed to compute invariance signatures and classify input patterns on this basis. This MBNN, consisting of a system of modules, some hand-coded and some trained, is shown in Figure 1. Whilst this system appears complex,

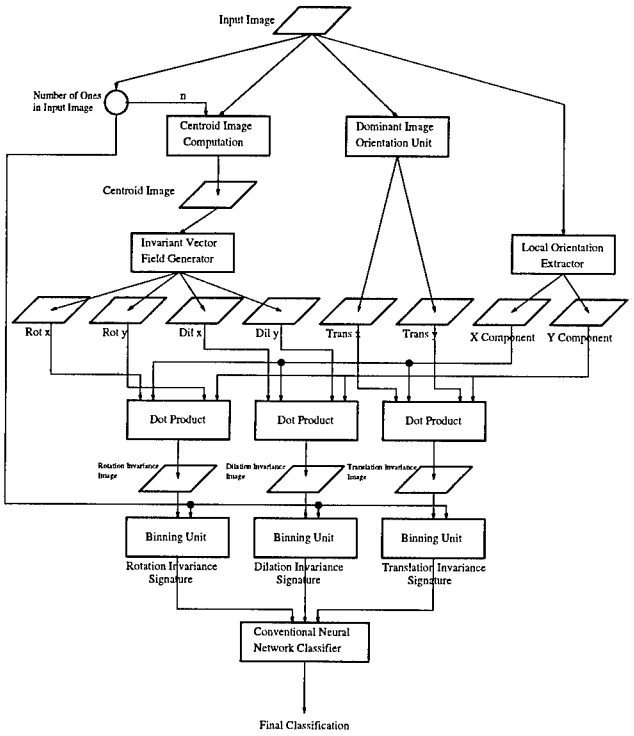

Figure 1 Invariance Signature-Based Contour Recognition System.

it retains the basic characteristics of a TNN[1]. Each node i computes the sum of its weighted inputs, $net_i = \sum_j w_{ij} x_j$. This is used as the input to the transfer function f, which is either linear, $f(net_j) = net_j$, or the standard sigmoid, $f(net_j) = \frac{1}{1+e^{-net_j}}$. The only departure from a TNN is that some of the weights are dynamic: the weight is calculated by a node higher up in the network. This allows the MBNN to compute dot products[2], and some nodes to act as gates. Since weights in any neural network implementation are just references to a stored value, this should not present any difficulty. There is insufficient space here to describe all the modules in the system. Descriptions of the *Local Orientation Extractor* and the *Binning Unit* are given as examples of the way the modules were constructed.

[1] with the exception of the *Dominant Image Orientation Unit*, for which a neural network solution is still being developed.

[2] The calculation of dot products is achieved by using the outputs of one layer as the *weights* on connections to another layer.

3.1 Local Orientation Extraction

A simple and robust estimate of the tangent vector at a point is the dominant eigenvector of the covariance matrix of a square window centred on that point. The vector magnitudes are weighted by the strength of the orientation. Let the eigenvalues be λ_1 and λ_2, $\lambda_1 \geq \lambda_2$. The corresponding unit eigenvectors are $\hat{\mathbf{e}}_1$ and $\hat{\mathbf{e}}_2$. The weighted tangent vector estimate $\mathbf{s}$ is:

$$\mathbf{s} = \begin{cases} \left(1 - \frac{\lambda_2}{\lambda_1}\right) \hat{\mathbf{e}}_1 & \lambda_1 \neq 0 \\ 0 & \lambda_1 = 0. \end{cases} \tag{9}$$

A TNN with a 3×3 input layer, 20 hidden nodes, and 2 output nodes was trained using backpropagation [4] to produce this output for all possible binary input images with a centre value of 1. Training was stopped after 6000000 iterations, when 96.89% of the training set variance was fitted. This problem is similar to edge extraction, except that edge extraction is usually performed on greyscale gradients rather than thin binary contours. Srinivasan *et al.* [5] have developed a neural network edge detector which produces a weighted vector output like that in equation 9. We intend to produce a more compact and accurate tangent estimator using a MBNN incorporating Gabor weighting functions, as used in [1].

3.2 The Binning Unit

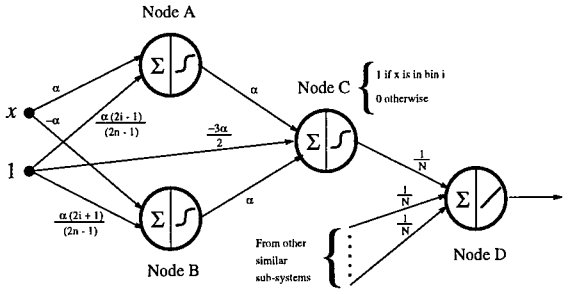

Figure 2 Neural Binning Subsystem.

The weights for the binning unit in figure 2 were determined by hand. There is a binning unit for each of the n bins in each invariance signature histogram. Each binning unit is connected to all nodes in the invariance image, and inputs to it are gated by the input image, so that only the N nodes corresponding to ones in the input image contribute. The bins have width $\frac{1}{n-1}$, since the first bin is centred on 0, and the last on 1 [3]. Nodes A and B only have an output of 1 when the input x is within bin i. This condition is met when:

$$\frac{2i-1}{2(n-1)} < x < \frac{2i+1}{2(n-1)}. \tag{10}$$

To detect this condition, the activations of nodes A and B are set to:

$$net_A = \alpha x - \frac{\alpha(2i-1)}{2(n-1)} \tag{11}$$

[3] A bin *ending* at 0 or 1 would miss contributions from the extrema since the edge of the neural bin is not vertical.

$$net_B = -\alpha x + \frac{\alpha(2i+1)}{2(n-1)} \quad (12)$$

where α is a large number, causing the sigmoid to approximate a step function. Here, $\alpha = 1000$ was used. Node C acts as an AND gate. Node D sums the contributions to bin i from all N nodes.

4 Simulation Results

To demonstrate the feasibility of such an invariance signature-based classifier, a small simulation was done. The task was to classify an input pattern as one of the ten first letters of the alphabet. The training set contained four examples of each letter[4], each differently rotated or reflected[5], within an 18 x 18 input image. The test set contained three differently transformed examples of each letter. The final classification stage of the MBNN used a 9 node hidden layer and was trained using backpropagation. A TNN with an 18 x 18 input layer, 9 node hidden layer and 10 node output layer was also trained. After 1000 iterations, both correctly classified 100% of the training data. The MBNN correctly classified 76.66% of the test data, whereas the TNN did not correctly classify *any* of it. It is clear that the MBNN massively outperformed the TNN. Had the *Local Orientation Extractor* been ideal, the optimal performance on the training data would have been 80%, since "b" and "d" are identical under reflection in the font used.

5 Conclusion

Using the MBNN approach, neural networks can be constructed which are guaranteed to classify input contours using invariance signatures which are rotation, dilation, translation and reflection invariant. The resultant MBNN retains the useful properties of being composed of similar simple nodes joined by weighted connections, with inherently parallel computation. The MBNN approach is thus a useful technique for *compiling* a neural network, incorporating the designer's expert knowledge.

REFERENCES

[1] Terry M. Caelli, David McG. Squire, and Tom P.J. Wild, *Model-based neural networks*, Neural Networks, Vol. 6 1993, pp613–625.

[2] K. Fukushima, S. Miyake, and T. Ito, *Neocognitron: A neural network model for a mechanism of visual pattern recognition*, IEEE Transactions on Systems, Man and Cybernetics, Vol. 13(5) (1983), pp826–834.

[3] Mario Ferraro and Terry M. Caelli, *Lie transform groups, integral transforms, and invariant pattern recognition*, Spatial Vision, Vol. 8(1) (1994), pp33–44.

[4] D.C. Plaut and G.E. Hinton, *Learning sets of filters using backpropagation*, Computer Speech and Language, Vol. 2 (1987), pp35–61.

[5] V. Srinivasan, P. Bhatia, and S. H. Ong, *Edge detection using a neural network*, Pattern Recognition, Vol. 27(12) (1994), pp1653–1662.

Acknowledgements

David Squire was funded by an Australian Postgraduate Award.

[4] More than one example of each letter was required since slightly different signatures were generated by different orientations, due to the residual error in the *Local Orientation Extractor*.

[5] all rotations were by multiples of $\frac{\pi}{2}$ radians.

FUNCTION APPROXIMATION BY THREE-LAYER ARTIFICIAL NEURAL NETWORKS

Shin Suzuki

Information Science Research Laboratory, NTT Basic Research Laboratories, 3-1 Morinosato-Wakamiya, Atsugi-Shi, Kanagawa Pref., 243-01 Japan. Tel: +81 462 40 3574, Fax: +81 462 40 4721, Email: shin@idea.brl.ntt.jp

This paper presents *constructive* approximations by three-layer artificial neural networks with (1) trigonometric, (2) piecewise linear, and (3) sigmoidal hidden-layer units. These approximations provide (a) approximating-network equations, (b) specifications for the numbers of hidden-layer units, (c) approximation error estimations, and (d) saturations of the approximations.
Keywords: Constructive Approximation, Saturation.

1 Introduction

Previous studies on function approximation by artificial neural networks show only the existence of approximating networks by *non-constructive* methods[1][2] and thus contribute almost nothing to developing the networks and to specifying the properties of the approximations. This paper presents *constructive* approximations by networks with (1) trigonometric, (2) piecewise linear, and (3) sigmoidal hidden-layer units. These approximations provide (a) approximating-network equations, (b) specifications for the numbers of hidden-layer units, (c) approximation error estimations, and (d) saturations of the approximations.

2 Preliminaries

Let $\mathbb{N}$ and $\mathbb{R}$ be the set of natural and real numbers, and $\mathbb{N}_0 = \mathbb{N} \cup \{0\}$. Let $|\mathbf{r}| = \sum_{i=1}^m |r_i|$ for $\mathbf{r} = (r_i)_{i=1}^m \in \mathbb{N}_0^m$ and $\|\mathbf{t}\| = \left(\sum_{i=1}^m t_i^2\right)^{1/2}$ for $\mathbf{t} = (t_i)_{i=1}^m \in \mathbb{R}^m$. For $p \geq 1$, we denote by $L_{2\pi}^p(\mathbb{R}^m)$ the space of 2π-periodic on each $\mathbb{R}$ of $\mathbb{R}^m$ pth-order Lebesgue-integrable functions defined on $\mathbb{R}^m$ to $\mathbb{R}$ with $L_{2\pi}^p$-norm $\|f\|_{L_{2\pi}^p} = \left\{(2\pi)^{-m} \int_{-\pi}^{\pi} \cdots \int_{-\pi}^{\pi} |f(\mathbf{x})|^p d\mathbf{x}\right\}^{1/p}$ and by $C_{2\pi}(\mathbb{R}^m)$ the space of 2π-periodic continuous functions defined on $\mathbb{R}^m$ to $\mathbb{R}$ with $C_{2\pi}$-norm $\|f\|_{C_{2\pi}} = \sup\{|f(\mathbf{x})| \ ; \ |x_i| \leq \pi, \ i = 1, \ldots, m\}$. Let $\Psi = L_{2\pi}^p(\mathbb{R}^m)$ or $C_{2\pi}(\mathbb{R}^m)$ throughout this paper. For $f, g \in \Psi$, $\langle f(\mathbf{t}), g(\mathbf{t})\rangle = (2\pi)^{-m} \int_{-\pi}^{\pi} \cdots \int_{-\pi}^{\pi} f(\mathbf{t}) g(\mathbf{t}) d\mathbf{t}$ and the convolution $f * g(\mathbf{x}) = (2\pi)^{-m} \int_{-\pi}^{\pi} \cdots \int_{-\pi}^{\pi} f(\mathbf{t}) g(\mathbf{x} - \mathbf{t}) d\mathbf{t}$. Let the sigmoidal function $\mathrm{sig}(x) = \{1 + \exp(-x)\}^{-1}$. Let $f \in \Psi$ and $\delta \geq 0$. We introduce the modulus of continuity of f in Ψ $\omega_\Psi(f, \delta) = \sup\{\|f(\cdot + \mathbf{t}) - f(\cdot)\|_\Psi \ ; \ \mathbf{t} \in \mathbb{R}^m, \ \|\mathbf{t}\| \leq \delta\}$, where $\|f(\cdot + \mathbf{t}) - f(\cdot)\|_{L_{2\pi}^p} = \left\{(2\pi)^{-m} \int_{-\pi}^{\pi} \cdots \int_{-\pi}^{\pi} |f(\mathbf{x} + \mathbf{t}) - f(\mathbf{x})|^p d\mathbf{x}\right\}^{1/p}$ and

$$\|f(\cdot + \mathbf{t}) - f(\cdot)\|_{C_{2\pi}} = \sup\{|f(\mathbf{x} + \mathbf{t}) - f(\mathbf{x})| \ ; \ |x_i| \leq \pi, \ i = 1, \ldots, m\}.$$

We say f satisfies a Lipschitz's condition with constant $M > 0$ and exponent $\nu > 0$ in Ψ, if

$$\|f(\cdot + \mathbf{t}) - f(\cdot)\|_\Psi \leq M \|\mathbf{t}\|^\nu$$

for $\mathbf{t} \in \mathbb{R}^m$. Let $\mathrm{Lip}_M(\Psi; \nu)$ be the set of functions satisfying this condition and Lipschitz's class of order ν $\mathrm{Lip}\,\nu = \cup\{\mathrm{Lip}_M(\Psi; \nu) \ ; \ M > 0\}$. We notice that if $f \in \Psi$ satisfies a Lipschitz's condition with constant M and exponent ν in Ψ, then $\omega_\Psi(f, \delta) \leq M\delta^\nu$.

3 Results

3.1 Constructive Approximations and approximation error estimations

Let $b_{\mathbf{r}}^{\lambda} = \prod_{i=1}^{m} \sin \frac{r_i+1}{\lambda+2}\pi$ for $\mathbf{r} = (r_i)_{i=1}^{m} \in \mathbb{N}_0^m$ and $B^{\lambda} = \left(\frac{2}{\lambda+2}\right)^m$ for $\lambda \in \mathbb{N}$ in this section.

Theorem 1 (trigonometric case) *Let $\mathbf{f} = (f_i)_{i=1}^{n}$ be a function defined on $\mathbb{R}^m$ to $\mathbb{R}^n$ such that $f_i \in \Psi$. For arbitrary parameter $\lambda \in \mathbb{N}$, a three-layer network with trigonometric hidden-layer units $\mathbf{TN}[\mathbf{f}]^{\lambda} = \left(TN[f_i]^{\lambda}\right)_{i=1}^{n}$ approximates to $\mathbf{f}$ with Ψ-norm, such that*

$$TN[f_i]^{\lambda}(\mathbf{x}) = \theta[f_i]^{\lambda} + \sum_{(\mathbf{p},\mathbf{q})}^{0\le p_i,\, q_i \le \lambda} \left\{ \alpha[f_i]^{\lambda}(\mathbf{p},\mathbf{q}) \cos(\mathbf{p}-\mathbf{q})\mathbf{x} + \beta[f_i]^{\lambda}(\mathbf{p},\mathbf{q}) \sin(\mathbf{p}-\mathbf{q})\mathbf{x} \right\}, \tag{1}$$

where $\theta[f_i]^{\lambda} = \langle f_i(\mathbf{t}), 1\rangle$, $\alpha[f_i]^{\lambda}(\mathbf{p},\mathbf{q}) = 2B^{\lambda} b_{\mathbf{p}}^{\lambda} b_{\mathbf{q}}^{\lambda} \langle f_i(\mathbf{t}), \cos(\mathbf{p}-\mathbf{q})\mathbf{t}\rangle$, and $\beta[f_i]^{\lambda}(\mathbf{p},\mathbf{q}) = 2B^{\lambda} b_{\mathbf{p}}^{\lambda} b_{\mathbf{q}}^{\lambda} \langle f_i(\mathbf{t}), \sin(\mathbf{p}-\mathbf{q})\mathbf{t}\rangle$. (The above summation is over combinations of $\mathbf{p} = (p_i)_{i=1}^{m}$, $\mathbf{q} = (q_i)_{i=1}^{m} \in \mathbb{N}_0^m$ such that $\mathbf{p} \neq \mathbf{q}$, $0 \le p_i, q_i \le \lambda$, i.e., if the summation is added in the case of $(\mathbf{p},\mathbf{q})$, it is not added in the case of $(\mathbf{q},\mathbf{p})$. This notation of the summation is used throughout this paper.) Then $\mathbf{TN}[\mathbf{f}]^{\lambda}$ has $(2\lambda+1)^m - 1$ hidden-layer units. Also the approximation error of each coordinate with Ψ-norm for $i = 1,\ldots,n$ is estimated by

$$\left\| f_i - TN[f_i]^{\lambda} \right\|_{\Psi} \le \left(1 + \frac{\pi^2}{2}\sqrt{m}\right) \omega_{\Psi}\left(f_i,\ (\lambda+2)^{-1}\right). \tag{2}$$

The next corollary means that $\mathbf{TN}[\mathbf{f}]^{\lambda}$ can approximate $\mathbf{f}$ with any degree of accuracy if λ increases i.e., the number of hidden-layer units increases.

Corollary 1 $\left\| f_i - TN[f_i]^{\lambda} \right\|_{\Psi} \to 0$ *as* $\lambda \to \infty$ $(i = 1,\ldots,n)$.

Theorem 2 (piecewise linear case) *Let $\mathbf{f} = (f_i)_{i=1}^{n}$ be a function defined on $\mathbb{R}^m$ to $\mathbb{R}^n$ such that $f_i \in L_{2\pi}^{p}(\mathbb{R}^m)$. For two arbitrary independent parameters $\lambda, \sigma \in \mathbb{N}$, a three-layer network with piecewise linear hidden-layer units $\mathbf{PN}[\mathbf{f}]^{\lambda,\sigma} = \left(PN[f_i]^{\lambda,\sigma}\right)_{i=1}^{n}$ approximates to $\mathbf{f}$ with $L_{2\pi}^{p}$-norm, such that*

$$PN[f_i]^{\lambda,\sigma}(\mathbf{x}) = \theta[f_i]^{\lambda,\sigma} + \sum_{(\mathbf{p},\mathbf{q})}^{0\le p_i,\, q_i \le \lambda} \sum_{k=0}^{4|\mathbf{p}-\mathbf{q}|\sigma-1} \alpha[f_i]^{\lambda,\sigma}(\mathbf{p},\mathbf{q},k)\, PL_k^{\sigma}((\mathbf{p}-\mathbf{q})\mathbf{x}), \tag{3}$$

where

$$PL_k^{\sigma}(\mathbf{rx}) = \begin{cases} 0 & \left(\mathbf{rx} \le -|\mathbf{r}|\pi + \frac{k\pi}{2\sigma}\right), \\ 1 & \left(\mathbf{rx} \ge -|\mathbf{r}|\pi + \frac{(k+1)\pi}{2\sigma}\right) \\ \frac{2\sigma}{\pi}\mathbf{rx} + 2|\mathbf{r}|\sigma - k & \left(-|\mathbf{r}|\pi + \frac{k\pi}{2\sigma} < \mathbf{rx} < -|\mathbf{r}|\pi + \frac{(k+1)\pi}{2\sigma}\right) \end{cases},$$

$$\theta[f_i]^{\lambda,\sigma} = \langle f_i(\mathbf{t}), 1\rangle + 2B^{\lambda} \sin\frac{\pi}{4\sigma} \sum_{(\mathbf{p},\mathbf{q})}^{0\le p_i,\, q_i \le \lambda} (-1)^{|\mathbf{p}-\mathbf{q}|} b_{\mathbf{p}}^{\lambda} b_{\mathbf{q}}^{\lambda} \langle f_i(\mathbf{t}), \cos(\mathbf{p}-\mathbf{q})\mathbf{t}\rangle,$$

$$\alpha[f_i]^{\lambda,\sigma}(\mathbf{p},\mathbf{q},k) = 4(-1)^{|\mathbf{p}-\mathbf{q}|} B^{\lambda} b_{\mathbf{p}}^{\lambda} b_{\mathbf{q}}^{\lambda} \sin\frac{\pi}{4\sigma} \times$$
$$\left\{ \langle f_i(\mathbf{t}), \sin(\mathbf{p}-\mathbf{q})\mathbf{t}\rangle \cos\frac{(2k+1)\pi}{4\sigma} - \langle f_i(\mathbf{t}), \cos(\mathbf{p}-\mathbf{q})\mathbf{t}\rangle \sin\frac{(2k+1)\pi}{4\sigma} \right\},$$

Then $\mathbf{PN}[\mathbf{f}]^{\lambda,\sigma}$ *has* $2m\sigma\lambda(\lambda+1)(2\lambda+1)^{m-1}$ *hidden-layer units. Also the approximation error of each coordinate with* $L_{2\pi}^p$*-norm is estimated by*

$$\left\| f_i - PN[f_i]^{\lambda,\sigma} \right\|_{L_{2\pi}^p} \leq \left(1+\frac{\pi^2}{2}\sqrt{m}\right)\omega_{L_{2\pi}^p}\left(f_i,\ (\lambda+2)^{-1}\right) +$$
$$2\|f_i\|_{L_{2\pi}^p}\left\{\left(\frac{8(\lambda+2)}{\pi^2}\right)^m - 1\right\}\left\{\frac{\pi\sqrt{m}}{(2\pi)^{m-1}\sigma}\left(\frac{4\sigma}{\pi} - \cot\frac{\pi}{4\sigma}\right)\right\}^{1/p}. \quad (4)$$

Theorem 3 (sigmoidal case) *Let* $\mathbf{f} = (f_i)_{i=1}^n$ *be a function defined on* $\mathbb{R}^m$ *to* $\mathbb{R}^n$ *such that* $f_i \in L_{2\pi}^p(\mathbb{R}^m)$*. For two arbitrary independent parameters* $\lambda, \sigma \in \mathbb{N}$*, a three-layer network with sigmoidal hidden-layer units* $\mathbf{SN}[\mathbf{f}]^{\lambda,\sigma} = \left(SN[f_i]^{\lambda,\sigma}\right)_{i=1}^n$ *approximates to* $\mathbf{f}$ *with* $L_{2\pi}^p$*-norm, such that*

$$SN[f_i]^{\lambda,\sigma}(\mathbf{x}) = \theta[f_i]^{\lambda,\sigma} +$$
$$\sum_{(\mathbf{p},\mathbf{q})}^{0\leq p_i,q_i\leq\lambda} \sum_{k=0}^{4|\mathbf{p}-\mathbf{q}|\sigma-1} \alpha[f_i]^{\lambda,\sigma}(\mathbf{p},\mathbf{q},k)\, SG_k^{\sigma}((\mathbf{p}-\mathbf{q})\mathbf{x}), \quad (5)$$

where $SG_k^{\sigma}(\mathbf{rx}) = \mathrm{sig}\left(\frac{8\sigma}{\pi}\mathbf{rx} + 8|\mathbf{r}|\sigma - 4k - 2\right)$*, and* $\theta[f_i]^{\lambda,\sigma}$ *and* $\alpha[f_i]^{\lambda,\sigma}(\mathbf{p},\mathbf{q},k)$ *are the same as in Theorem 2. Then* $\mathbf{SN}[\mathbf{f}]^{\lambda,\sigma}$ *has* $2m\sigma\lambda(\lambda+1)(2\lambda+1)^{m-1}$ *hidden-layer units. Also the approximation error of each coordinate with* $L_{2\pi}^p$*-norm is estimated by*

$$\left\| f_i - SN[f_i]^{\lambda,\sigma} \right\|_{L_{2\pi}^p} \leq \left(1+\frac{\pi^2}{2}\sqrt{m}\right)\omega_{L_{2\pi}^p}\left(f_i,\ (\lambda+2)^{-1}\right) +$$
$$2\|f_i\|_{L_{2\pi}^p}\left\{\left(\frac{8(\lambda+2)}{\pi^2}\right)^m - 1\right\}\left\{\frac{\pi\sqrt{m}}{(2\pi)^{m-1}\sigma}\left(\log 2 - \frac{1}{2} + \frac{4\sigma}{\pi} - \cot\frac{\pi}{4\sigma}\right)\right\}^{1/p} \quad (6)$$

Remark 1 $\mathbf{PN}[\mathbf{f}]^{\lambda,\sigma}$ *and* $\mathbf{SN}[\mathbf{f}]^{\lambda,\sigma}$ *in Theorems 2 and 3 are based on* $\mathbf{TN}[\mathbf{f}]^{\lambda}$ *in Theorem 1. In fact, for any* $\lambda \in \mathbb{N}$*,* $\mathbf{PN}[\mathbf{f}]^{\lambda,\sigma}$ *and* $\mathbf{SN}[\mathbf{f}]^{\lambda,\sigma}$ *approach* $\mathbf{TN}[\mathbf{f}]^{\lambda}$ *as* σ *increases. Therefore they are almost determined by* λ*, if* σ *is large enough for* λ*.*

For any $\lambda \in \mathbb{N}$, the second terms of the right-hand members of Inequalities (4) and (6) approach 0 as σ increases. Then, $\left\| f_i - PN[f_i]^{\lambda,\sigma} \right\|_{L_{2\pi}^p}$ and $\left\| f_i - SN[f_i]^{\lambda,\sigma} \right\|_{L_{2\pi}^p}$ are almost estimated by the first terms, which are the same as Inequality (2), when σ is large enough for λ. The following two corollaries give conditions on σ in terms of λ that the approximation errors approach 0, if λ increases. Under these conditions $\mathbf{PN}[\mathbf{f}]^{\lambda,\sigma}$ and $\mathbf{SN}[\mathbf{f}]^{\lambda,\sigma}$ can approximate $\mathbf{f}$ with any degree of accuracy, if the number of hidden-layer units increases.

Corollary 2 *If* σ *is a higher-order infinity than* $\lambda^{\frac{mp}{2}}$*, i.e.,* $\sigma = \sigma(\lambda) \to \infty$ *and* $\frac{\lambda^{\frac{mp}{2}}}{\sigma(\lambda)} \to 0$ *as* $\lambda \to \infty$*, then* $\left\| f_i - PN[f_i]^{\lambda,\sigma} \right\|_{L_{2\pi}^p} \to 0$ *as* $\lambda \to \infty \quad (i = 1, \ldots, n)$*.*

Corollary 3 *If σ is a higher-order infinity than λ^{mp}, i.e., $\sigma = \sigma(\lambda) \to \infty$ and $\frac{\lambda^{mp}}{\sigma(\lambda)} \to 0$ as $\lambda \to \infty$, then $\left\| f_i - SN[f_i]^{\lambda,\sigma} \right\|_{L^p_{2\pi}} \to 0$ as $\lambda \to \infty$ $(i = 1, \ldots, n)$.*

3.2 Saturation of Constructive Approximations

We denote $\theta_\lambda = o(\zeta_\lambda)$ $(\lambda \to \infty)$, if $\frac{\theta_\lambda}{\zeta_\lambda} \to 0$ as $\lambda \to \infty$ and $\theta_\lambda = O(\zeta_\lambda)$ $(\lambda \to \infty)$, if there exists a constant $M > 0$ such that $\left|\frac{\theta_\lambda}{\zeta_\lambda}\right| \leq M$ for large enough λ.

Definition 1 (Saturation of an approximation method) *A sequence of operators $\mathcal{U} = \{U_\lambda\}_{\lambda \in \mathbb{N}}$ in Ψ is called an approximation method in Ψ, if*

$$\lim_{\lambda \to \infty} \|U_\lambda(f) - f\|_\Psi = 0$$

for $f \in \Psi$. Let $\{\theta_\lambda\}_{\lambda \in \mathbb{N}}$ be a sequence of real numbers such that $\theta_\lambda \to 0$ as $\lambda \to \infty$. An approximation method $\mathcal{U}$ in Ψ is saturated with order θ_λ, if (S1) If $f \in \Psi$ and $\|U_\lambda(f) - f\|_\Psi = o(\theta_\lambda)$ $(\lambda \to \infty)$, then f is an identical element of $\mathcal{U}$, i.e., $U_\lambda(f) = f$ for $\lambda \in \mathbb{N}$ and (S2) The saturation class of $\mathcal{U}$ $S[\mathcal{U}] = \{ f \in \Psi \,;\, \|U_\lambda(f) - f\|_\Psi = O(\theta_\lambda) \ (\lambda \to \infty)\}$ contains at least one element which is not an identical element of $\mathcal{U}$.

Theorem 4 (trigonometric case) *Approximation by $\mathcal{TN} = \left\{\mathbf{TN}^\lambda\right\}_{\lambda \in \mathbb{N}}$ in Theorem 1 is an approximation method saturated with order λ^{-2} in Ψ and its identical elements are just constant functions almost everywhere on $\mathbb{R}^m$. When $\Psi = C_{2\pi}(\mathbb{R}^m)$, the saturation class $S[\mathcal{TN}]$ is characterized as*

$$S[\mathcal{TN}] \supset \left\{ f \in \Psi \,;\, \frac{\partial f}{\partial x_s} \in \text{Lip } 1,\ s = 1, \ldots, m \right\}$$

and, if $m = 1$, $S[\mathcal{TN}] = \left\{ f \in \Psi \,;\, \frac{df}{dx} \in \text{Lip } 1 \right\}$.

Remark 2 (piecewise linear and sigmoidal cases) *Approximations by $\mathbf{PN}[\mathbf{f}]^{\lambda,\sigma}$ and $\mathbf{SN}[\mathbf{f}]^{\lambda,\sigma}$ in Theorems 2 and 3 are also saturated with order λ^{-2} in $L^p_{2\pi}(\mathbb{R}^m)$, if σ is large enough for λ. This is because, for any $\lambda \in \mathbb{N}$, $\mathbf{PN}[\mathbf{f}]^{\lambda,\sigma}$ and $\mathbf{SN}[\mathbf{f}]^{\lambda,\sigma}$ approach $\mathbf{TN}[\mathbf{f}]^\lambda$ as σ increases stated in Remark 1.*

3.3 Outline of the Proof

Multidimensional extension of approximation by the convolution operator and the multidimensional Fejér-Korovkin kernel, which are introduced in this study, provide a construction of an approximating network with trigonometric hidden-layer units, the approximation error estimation, and sturation of the approximation. Then, from the network and constructive approximation to multidimensional trigonometric functions by networks with piecewise linear and sigmoidal hidden-layer units, a constructions of approximating networks with piecewise linear and sigmoidal hidden-layer units, the approximation error estimations, and sturation of the approximations are derived.

4 Example

This is an example of an approximation to the function $\exp\left(-\left(x^2 + y^2\right)\right)$. Approximating networks are calculated at $\lambda = 2, 4, 6, 8, 10$ and $\sigma = 60$. The numbers of hidden-layer units are respectively 24, 80, 168, 288, 440 in the trigonometric case

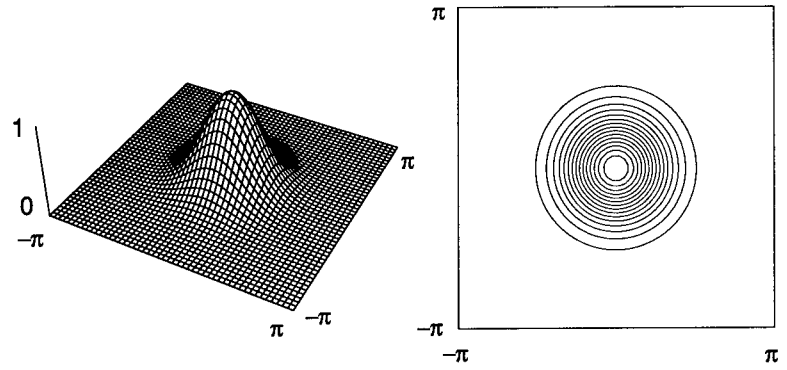

Figure 1 The approximated function.

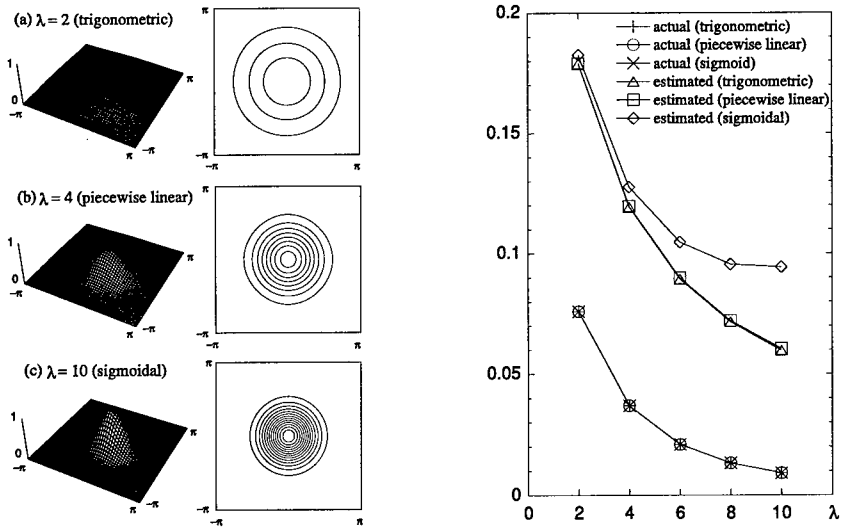

Figure 2 Approximating networks with three kinds of hidden layer units at $\sigma = 60$. (When λ is the same, the three kinds of networks have almost the same figures.)

and 7.2×10^3, 4.3×10^4, 1.3×10^5, 2.9×10^5, 5.5×10^5 in the piecewise linear and sigmoidal cases. The actual errors with $L^1_{2\pi}$-norm are numerically calculated from the left-hand members of Inequalities (2), (4), and (6), and the estimated errors are calculated from their left-hand members.

5 Conclusion

This paper presents constructive approximations by three-layer artificial neural networks with (1) trigonometric, (2) piecewise linear, and (3) sigmoidal hidden-layer units to 2π-periodic pth-order Lebesgue integrable functions defined on $\mathbb{R}^m$ to $\mathbb{R}^n$ for $p \geq 1$ with $L^p_{2\pi}$-norm. (In the case of (1), networks with trigonometric hidden-layer units can also approximate 2π-periodic continuous functions defined

on $\mathbb{R}^m$ to $\mathbb{R}^n$ with $C_{2\pi}$-norm in the same time.) The approximations provide (a) approximating-network equations, (b) specifications for the numbers of hidden-layer units, (c) approximation error estimations, and (d) saturations of the approximations. These results can easily be applied to non-periodic functions defined on a bounded subset of $\mathbb{R}^m$.

REFERENCES

[1] Cybenko, G., *Approximation by superpositions of sigmoidal function*, Mathematics of Control, Signals and System, Vol. 2(4) (1989), pp305–314.

[2] Hornik, K., *Approximation capabilities of multilayer feedforward networks*, Neural Networks, Vol. 4 (1991), pp251–257.

[3] Lorentz, George G., *Approximation of Functions*, Holt, Rinehart and Winston (1966).

[4] Davis, Philip J., *Interpolation and Approximation*, Dover (1975).

[5] Takenouchi, O. and Nishishiraho, T., *Kinji Riron (Approximation theory)*, in Japanese, Baifuukan (1986).

[6] DeVore, Roland A. and Lorentz, George G., *Constructive Approximation*, Springer-Verlag (1993).

[7] Suzuki, S., *Function Approximation by Three-Layer Artificial Neural Networks*, Proc. of 1993 Int. Symposium on Nonlinear Theory and its Applications, Vol. 4 (1993), pp1269–1272.

Acknowledgements

The author would like to thank Dr.Masaaki Honda, and other members of HONDA Research Group of Information Science Research Laboratory for many useful and helpful discussions.

NEURAL NETWORK VERSUS STATISTICAL CLUSTERING TECHNIQUES: A PILOT STUDY IN A PHONEME RECOGNITION TASK

G.Tambouratzis, T.Tambouratzis* and D.Tambouratzis

Dept. of Mathematics, Agricultural Univ.of Athens,
Iera Odos 75, Athens 118 55, Greece.
** Institute of Nuclear Technology - Radiation Protection,*
NRCPS "Demokritos", Aghia Paraskevi 153 10, Greece.

In this article, two neural network clustering techniques are compared to classical statistical techniques. This is achieved by examining the results obtained when applying each technique to a real-world phoneme recognition task. An analysis of the phoneme datasets exposes the clusters which exist in the pattern space. The study of the similarity of the patterns which are clustered together allows an objective evaluation of the clustering efficiency of these techniques. It also gives rise to a revealing comparison of the way each technique clusters the dataset.

1 Introduction

Clustering algorithms attempt to organise unclassified patterns into groups in such a way that patterns within each group are more similar than patterns belonging to different groups. In classical statistics, there exist a wide range of agglomerative and divisive clustering techniques [1], which use as distance measures either Euclidean-type distances or other metrics suitable for binary data. Recently, techniques based on neural networks have been developed and have been found well-suited to clustering large, high-dimensional pattern spaces. In this article, the clustering potential of two fundamentally different neural network models is studied and compared to that of statistical techniques. The network models are: (a) the Self-Organising Logic Neural Network (SOLNN) [2], which is based on the n-tuple sampling method and (b) the Harmony Theory Network (HTN) [3] which constitutes a derivative of the Hopfield network and a variant of the Boltzmann machine.

In an effort to evaluate the effectiveness of the two network models when discovering the clusters which exist in the pattern space, a comparison is made to a number of established statistical methods. This comparison is performed in a series of experiments which use real-world phoneme data. A number of phonemes is selected and used as prototypes. Various levels of noise are injected to the prototypes, resulting in different datasets, each consisting of well defined phoneme-classes. The varying levels of noise cause each dataset to have fundamentally different characteristics. The behaviour of the clustering techniques is then studied for each dataset.

2 Overview of the Clustering Techniques

The Self-Organising Logic Neural Network (SOLNN) shares the main structure of the discriminator network [4]. It is consequently based on the decomposition of the input pattern into tuples of n pixels and the comparison of these tuples to the corresponding tuples of training patterns. In the SOLNN model, the basic discriminator structure has been extended by allocating m bits to each tuple combination rather than a single one. This allows the network to store information concerning the frequency of occurrence of the corresponding tuple combination during learning and

is instrumental to the SOLNN's ability to learn in the absence of external supervision. The SOLNN has been shown to successfully perform clustering tasks in an unsupervised manner [2,5]. The SOLNN model is characterised by the distribution constraint mechanism [5] which enables the user to determine the desired radius of the SOLNN clusters. This mechanism is similar to the vigilance parameter of Adaptive Resonance Theory (ART) [6].

The Harmony Theory Network (HTN) [3] consists of binary nodes arranged in exactly two layers. For this task, the lower layer encodes the features of the unclassified patterns and the upper layer encodes the candidate patterns of the clustering task. Each connection between a feature and a classified pattern specifies the positive or negative relation between them, i.e. whether or not the pattern contains the feature. No training is required to adapt the weights, which depend on the local connectivity of the HTN [3]. During clustering, each candidate pattern is input to the lower layer of the HTN; the activated nodes of the upper layer constitute the patterns to which the candidate pattern is clustered (also see [7] for a more detailed description). Both the required degree of similarity between clustered patterns and the desired number of clusters are monitored by the parameter k of Harmony Theory, which resembles the vigilance parameter of ART [6] and the radius of RBF (Radial-Basis Function) networks [8]. Its value is changed, in a uniform manner for all candidate patterns, in the search for optimal clustering results.

Hierarchical statistical clustering techniques [1] of the agglomerative type are used for clustering in this article. The techniques employed are (i) the single linkage, (ii) the complete linkage, (iii) the median cluster, (iv) the centroid cluster and (v) the average cluster.

3 Description of the Clustering Experiments

The data employed in the experiments are real-world phonemes which have been obtained from the dataset of the LVQ-PAK simulation package [9]. The phonemes in this package have been pre-processed so that each phoneme consists of 20 real-valued features. The selected phonemes (called prototypes) correspond to the letters "A", "O", "N", "I", "M", "U" and "S". Since both the SOLNN and the HTN networks require binary input patterns, the phonemes have been digitised, by encoding each real-valued feature into four bits via the thermometer-coding technique [10]. Consequently, the resulting prototypes are 80-dimensional binary patterns.

Each of the prototypes has been used to generate a number of noisy patterns by adding random noise of a certain level, namely 2.5, 5, 7.5 and 10%. A different dataset (experiment-dataset) is created for each level of noise. Every experiment-dataset consists of groups of noisy patterns whose centroids coincide with, or are situated very near to, the prototypes. The different levels of noise cause the experiment-datasets to occupy varying portions of the input space and the groups of noisy patterns to overlap to a different extent. The prototype and the noisy patterns for each level of noise constitute a phoneme class. An analysis of the phoneme classes in each experiment-dataset indicates that the patterns of each phoneme class are closer to other patterns of the same class than to patterns of other phoneme classes. As the noise level increases, each phoneme class occupies a larger portion of the pattern space and the distance between phonemes from different classes is reduced, while the probability of an overlap occurring between different classes in-

Phoneme Class	Average Distance within class	Minimum Distance within class	Maximum Distance within class	Minimum Distance between classes
A	16.11%	10.00%	20.00%	22.50% (A & O)
O	16.67%	10.00%	20.00%	22.50% (O & A)
N	16.22%	7.50%	20.00%	23.75% (N & O)
I	16.33%	10.00%	20.00%	20.00% (I & M)
M	16.22%	10.00%	20.00%	20.00% (M & I)
U	16.06%	10.00%	20.00%	23.75% (U & O)
S	16.22%	10.00%	20.00%	26.25% (S & I)

Table 1 Characteristics of the pattern space used for 10% noise level. Distances are calculated as percentages of the total number of pixels.

creases. The 10%-noise dataset is probably the most interesting one since, in that case, the minimum distance between two phonemes from different classes (more specifically classes "I" and "M") becomes equal to the maximum distance between patterns within any phoneme class. Due to this fact, it is expected to be the most difficult experiment-dataset to cluster successfully. Its characteristics are summarised in Table 1 to allow for a detailed evaluation of the clustering results.

The task consists of grouping the patterns of each experiment-dataset so that the phoneme classes are uncovered. The results obtained by each of the three clustering techniques are evaluated by taking into account the characteristics and topology of each experiment-dataset, i.e. the pixel-wise similarity between the patterns and the clusters in which they have been organised by each technique. This enables (i) a comparison of the way in which each technique operates for various data distributions and (ii) an evaluation of the effect that the relation between the maximum distance of patterns of the same phoneme class and the minimum distance of patterns of different phoneme classes has on clustering.

Additionally, a statistical analysis of the pattern space created by each experiment-dataset has been performed to investigate how effective the clustering techniques actually are. This investigation is based on the similarity between classes in the pattern space. The comparison of the two neural network techniques and the statistical methods, together with an in-depth analysis of the pattern space, provides an accurate insight to the capabilities and limitations of each of the techniques studied.

4 Experimental Results

The different clustering techniques are applied to the clustering task described in the previous paragraph. The results obtained are summarised in Table 2, where the following information is contained:

(i) the proportion of dataset phonemes that are correctly classified, that is of patterns assigned to a cluster representing their phoneme class;

(ii) the number of multi-phoneme clusters, that is clusters containing patterns from more than one phoneme class;

Noise Level	Criterion	SOLNN	HTN	Statistical
2.5%, 5%, 7.5%	Correct classification	100%	100%	100%
	Multi-phoneme clusters formed	0	0	0
	Phonemes in multi-phoneme cluster	1	1	1
	Number of created clusters	7	7	7
	Number of clusters per phoneme	1	1	1
10%	Correct classification	86%/100%	97%	100%
	Multi-phoneme clusters formed	4 / 0	1	0
	Phonemes in multi-phoneme cluster	4 / 1	2	1
	Number of created clusters	7 / 10	21	7
	Number of clusters per phoneme	4 / 2	4	1

Table 2 Comparative results of the three methods for the different noise levels. In the case of the SOLNN, for 10% noise, two sets of results are noted, the first corresponding to a 7-discriminator network and the second to a 10-discriminator network. In the case of statistical methods, the results are obtained using the Hamming distance metric.

(iii) the maximum number of phoneme classes contained in any multi-phoneme cluster;

(iv) the number of clusters created by each method;

(v) the maximum number of clusters to which patterns of any phoneme class are assigned.

As can be easily seen, the value of criterion (i) should ideally be equal to 100%, the value of criterion (ii) should be equal to 0, the value of criterion (iv) should be equal to 7, while the values of criteria (iii) and (v) should be equal to 1.
In the application of the SOLNN to the experiment-dataset, several network sizes ranging from 7 to 70 discriminators are simulated in order to investigate the effect of the network size on the SOLNN clustering performance. As has been shown [5], the SOLNN requires several iterations before settling to a clustering result, gradually separating each class. As the clustering task becomes more difficult, that is as the pattern classes become less clearly separated, the number of required iterations increases. For noise levels up to 7.5%, the SOLNN succeeds in separating all phoneme classes for all network sizes by creating a single group for each class. In the case of the 10% noise level, when the distance between the phoneme classes is considerably reduced, the SOLNN requires a larger number of iterations to settle to a clustering result. More specifically, the number of required iterations is of the order of 20, 50, 150 and 500 for noise levels of 2.5, 5, 7.5 and 10%, respectively. For high noise levels (10%), more than one cluster is generated for some phoneme classes. Misclassifications are occasionally observed, as some nodes have patterns assigned to them from more than one phoneme class. Such multi-phoneme clusters occur in particular when the number of nodes in the SOLNN is reduced. Characteristically, for a 10% level of noise, multi-phoneme clusters occur for a 7-node but not for a 10-node network. The formation of multi-phoneme clusters for the 7-node SOLNN (see

Table 2) is due to the fact that the network uses two nodes for the "U"-phoneme class, and is thus unable to form a cluster dedicated exclusively to the "O"-phoneme class. It is worth noting that multi-phoneme clusters consist of phonemes which have a relatively high degree of similarity. It has been reported [5] that for the optimal clustering to be achieved there need to be more nodes in the network than there are classes in the dataset. Indeed, this is confirmed by the results obtained with the 10-node SOLNN. Still, even for the 7-node system, the SOLNN succeeds in consistently clustering the majority of patterns in single-phoneme clusters.

For the HTN, each test pattern is input into the lower layer of the HTN. In contrast to the SOLNN, a single pass of activation-flow from the lower to the upper layer, at a pre-specified k value, reveals the patterns to which the test pattern becomes clustered. Optimum clustering with a HTN requires finding one (or more) value of k for which each test pattern becomes clustered with all the nodes of the upper layer representing patterns of the same phoneme class but with no nodes representing patterns of different phoneme classes. This has been established for noise levels up to 7.5% for k values around 0.650. The range of k values which result in the optimum clustering becomes narrower as the noise level increases. This can be explained by the fact that as the noise level rises (i) lower k values are required for grouping patterns of the same phoneme class, while at the same time, (ii) higher k values are required for patterns of different phoneme classes not to be grouped together. When the noise level reaches 10%, no value of k generating the optimum clustering can be found; some dataset patterns fail to be clustered with all the nodes of the upper layer representing patterns the same phoneme class, while they are clustered with nodes representing patterns of other phoneme classes. It is possible, however, to achieve a sub-optimum clustering by raising the value of k, whereas the problem of multi-phoneme clusters is avoided at the expense of multiple clusters for each phoneme class. As shown in Table 2, the sub-optimum clustering performed by the HTN for the 10% noise level is due to the network grouping together an "I" with an "M", which are the two phoneme patterns from different classes with the minimum distance. Due to the fact that this distance is equal to the maximum distance within any class (see Table 1), the structure of the pattern space justifies the sub-optimal clustering produced by the HTN.

For the statistical analysis, the five agglomerative clustering techniques mentioned in Section 2 have been used to cluster all patterns in the minimum possible number of groups, while avoiding the creation of any multi-phoneme clusters. Both the Hamming distance and the Euclidean distance were considered as distance measures. In the case of the Hamming distance in the 80-dimensional space, which in the case of binary patterns is equal to the square of the Euclidean distance, the seven phoneme classes are consistently separated by all statistical methods. When using the Euclidean distance metric, the seven phoneme classes are separated by all statistical methods for all noise levels except for the hierarchical average cluster method for the 10%-noise level dataset. In this case, for seven clusters, the phonemes "A", "O", "M" and "U" are grouped together, "N" and "S" form an independent cluster each, whilst "I" is split into four clusters. The minimum number of clusters, in order to avoid multi-phoneme clusters, is fourteen.

5 Conclusions

Both the neural network (SOLNN and HTN) and the statistical techniques have been found to perform the selected clustering task satisfactorily. For low noise levels, all techniques cluster the dataset successfully, by forming exclusively single-phoneme clusters. For higher noise levels, the statistical methods always generate the optimum clustering according to the Hamming distance metric, as witnessed by the study of the dataset structure. The quality of the clustering generated by the two neural network models is slightly inferior to that of the statistical techniques. This is indicated by the creation of multiple clusters for a few phoneme classes. However, the vast majority of clusters consist of patterns from a single phoneme class (see Table 2), thus producing successful clustering.

It is worth noting that the study of the Hamming distances between the different phoneme patterns in the dataset indicates that the clustering behaviour of all three techniques is justified. In particular, for the noise level of 10% when the most differences between the clustering results of the three methods are detected, the minimum distance between the phoneme classes is equal to the maximum distance between phonemes of the same class. This allows for more than one possible clustering results of almost the same quality.

REFERENCES

[1] Kaufman, L., Rousseeuw, P.J., *Finding Groups in Data*, Wiley, New York (1990).

[2] Tambouratzis, G., Tambouratzis, D., *Self-Organisation in Complex Pattern Spaces Using a Logic Neural Network*, Network: Computation in Neural Systems, Vol. 5 (1994), pp599–617.

[3] Smolensky, P., *Information processing in dynamical systems: foundations of Harmony Theory*, in: Rumelhart, D.E., McClelland, J.L. (eds.) Parallel Distributed Processing, Vol.1: Foundations, MIT Press, Cambridge MA. (1986), pp194–281.

[4] Aleksander, I., Morton, H., *An Introduction to Neural Computing*, Chapman and Hall, London, England (1990).

[5] Tambouratzis, G., *Optimising the Topology-Preservation Characteristics of a Discriminator-Based Logic Neural Network*, Pattern Recognition Letters, Vol. 15 (1994), pp1019–1028.

[6] Carpenter, G.A., Grossberg, S., *The ART of Adaptive Pattern Recognition by a Self-Organising Neural Network*, IEEE Computer (March 1988), pp77–88.

[7] Tambouratzis, T., Tambouratzis, D., *Optimal Training Pattern Selection Using a Cluster-Generating Artificial Neural Network*, in: Proceedings of the 1995 International Conference on Artificial Neural Networks and Genetic Algorithms, Mines d' Ales, France (April 1995), Springer-Verlag, pp472–475.

[8] Chen, S., Cowan, C.F.N., Grant, P.M., *Orthogonal Least Squares Learning Algorithm for Radial Basis Function Networks*, IEEE Transactions on Neural Networks, Vol. 2 (1991), pp302–309.

[9] Kohonen, T., Kangas, J., Laaksonen, J., Torkkola, K., *LVQ_PAK: The Learning Vector Quantisation Program Package*, (1992).

[10] Aleksander, I., Stonham, T.J., *Guide to Pattern Recognition using Random-Access Memories*, Computers and Digital Techniques, Vol. 2 (1979), pp29–40.

MULTISPECTRAL IMAGE ANALYSIS USING PULSED COUPLED NEURAL NETWORKS

Gregory L. Tarr, Xavier Clastres*, Laurent Freyss*, Manuel Samuelides*, Christopher Dehainaut and William Burckel

Phillips Laboratory, Kirtland Air Force Base Albuquerque, New Mexico, USA.

** Centre d'Etudes and Recherche de Toulouse, Toulouse, France.*

Pulsed oscillatory neural networks are examined for application to analysis and segmentation of multispectral imagery from the Satelite Pour l'Observation de la Terre (SPOT). These networks demonstrate a capacity to segment images with better performance against many of the resolution uncertainty effects caused by local area adaptive filtering. To enhance synchronous behavior, a reset mechanism is added in the model. Previous work suggests that a reset activation pulse is generated by sacatic motor commands. Consequently, an algorithm is developed, which behaves similar to adaptive histogram techniques. These techniques appear both biologically plausible and more effective than conventional techniques. Using the pulse time-of-arrival as the information carrier, the image is reduced to a time signal which allows an intelligent filtering using feedback.

1 Introduction

Histogram image analysis may play an important role in biological vision image processing. Structures of artificial neurons can be used to create histogram like signals quickly. In this paper, we will examine how algorithms based on fast histogram processing may offer advantages for computer vision systems.

In a biological vision system, the signals detected at the retina are passed to the LGN then to the Visual Cortex, where neighborhood preserving maps of the retina are repeated at least 15 times over the surface of the cortex. For every path forward, there are several neurological pathways in the reverse direction. Reverse direction transmission of information suggest feedback signals. Using appropiate feedback, the image processing can be controlled using recurrence. Pulses generated by dynamic neuronal models suggest a method for building recurrance into vision models.

1.1 Dynamic Neural Networks

Dynamic neural networks, first examined by Stephen Grossberg, Maas and others [3] were an attempt to construct models closer to their biological counterpart. In this model, the basic computational unit is not the usual static matrix multiplier with a non-linear transfer function between layers, but a leaky integrator with a pulsed oscillatory output. This work is sometimes refereed to as *Integrate and Fire Networks.*

To understand the role of synchrony in the cat visual cortex, Eckhorn devised a model which would replicate some of this behavior. The Eckhorn [1] dynamic model represents a visual neuron as a multi-input element with a single output. The output is made up of oscillatory electrical pulses in time. Three types of connections make up the input section: the feeding, the linking and the direct inputs. The direct input provides pixel information. The feeding inputs provide local information in the region of the direct inputs. The combination of the direct and feeding input provide texture information in a local region around the direct input. The linking field provides a global connection for all sub-regions in the image. The linking

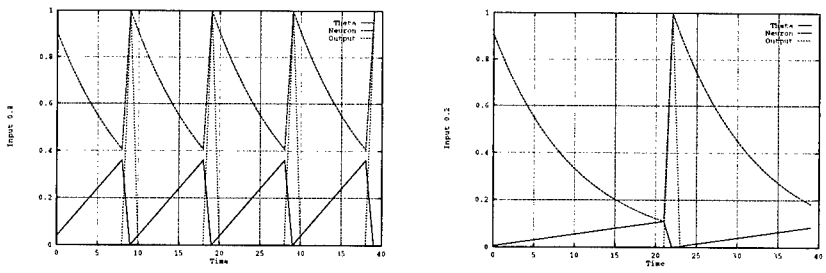

Figure 1 Behavior of a clean and noisy signal.

connections enforce synchrony between local regions. The information is extracted using correlation techniques.

Given these characteristics, several image processing functions are possible. In this paper we will explore only one, usually the most difficult: segmentation. If information in a particular part of the image is similar to information in another part of the image, they should have the same pulse repetition frequency as the feeding field, and the same phase after the linking fields. This information can easily be extracted using correlation filters.

For a single neuron, $U_j(t)$ is given by:

$$U_j(t) = (1 + \beta L_j(t))X_j(t) \tag{1}$$

$X_j(t)$, are the direct inputs to a neuron, $L_j(t)$ is the contribution from nearby neurons weighted by β the link coefficients. The spiking output, Y_j, is provided by a step function of a time dependent threshold $\theta_j(t)$ and the neuronal activity according to

$$Y_j = step[U_j(t) - \theta_j(t)] \tag{2}$$

$\theta_j(t)$ and $L_j(t)$ can have different decay constants α_θ and α_L. The dynamics of the linking field and threshold are given by

$$L_j(t) = \sum_k w_{k_j} e^{-t/\alpha_L} \cdot Y_k(t), \theta_j(t) = \theta_{max} e^{-(t-t_j)/\alpha_\theta} \tag{3}$$

where w_{k_j} is the connection weighting for the local field neurons. Sufficient neural activity combined with a decaying threshold lead to a spike output which resets the threshold to the maximum from which it decays again.

Built into this neuronal model are a number of characteristics common to biological vision: integrate and fire, latency and lateral interconnectivity. Figure 1 provides a means to visualize the firing behavior of a one dimensional signal in time. In the first graph, the input to the system is 0.8. The energy is integrated and plotted. The threshold, a decaying exponential relaxes from its initial maximum. This ensures a minimum pulse rate and a refractory period. When the two are equal, the neuron fires and both θ, the threshold, and $U_j(t)$ the neuron potential are reset. In the second graph, a lower energy input is used, which is characterized by a slower firing rate.

For large clusters of neurons, the group behavior can be characterized by the total firing rates over time. A signal based on the total number of neurons firing at a

specific time could be used as a control signal for modification of the structure and appearance of the image. This is the basis for using pulse coupled neural networks to segment images.

In the following graphs, only the firing patterns are shown. A one dimensional signal is used to demonstrate the temporal encoding nature of the output signal. The first image, without using coupling between neurons shows, how the pulse frequency rate is related to the input strength.

In the second figure, coupling is added between adjacent neurons. The effect is to cluster neurons into separate time bins. By evaluating the behavior of the temporal signal, processing is performed on the actual image.

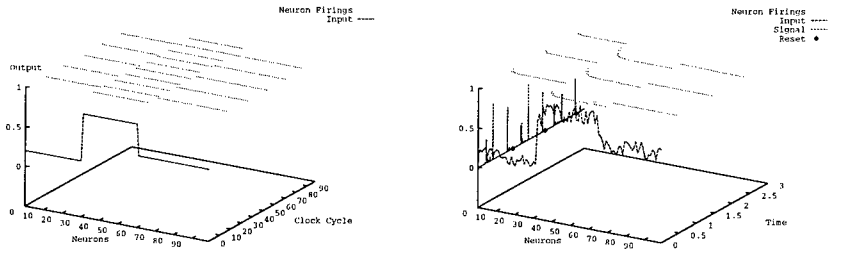

Figure 2

2 Pulse Coupled Neurons for Adaptive Histogram Analysis of Imagery

Most dynamic models of neural computation suggest that synchronization between regions is the primary information carrier. But if time of arrival is used as the information carrier, it demonstrates that mechanisms exist in the cellural architectures to perform histogram analysis and adaptive histogram analysis of images.

The following 32x32 image chips are taken for the SPOT satellite imagery and represent common problems in image segmentation.

Several variations of edge detection are currently used on these type of images, the most common being the Sobel and Canny operators. The difficulty lies in that the size of the window used for the operator affects the size of the detectable gradients, and the width of the edge. An improvement on the Sobel operator is the Canny edge detector, which effectively finds the center of the gradient and places an edge there. Its weakness, as with most convolution filter segmentation methods, is that overall resolution is usually reduced to the size of the filter window. This effect results in rounded and wide edges. In low resolution systems like SPOT, this loss of resolution is often unacceptable.

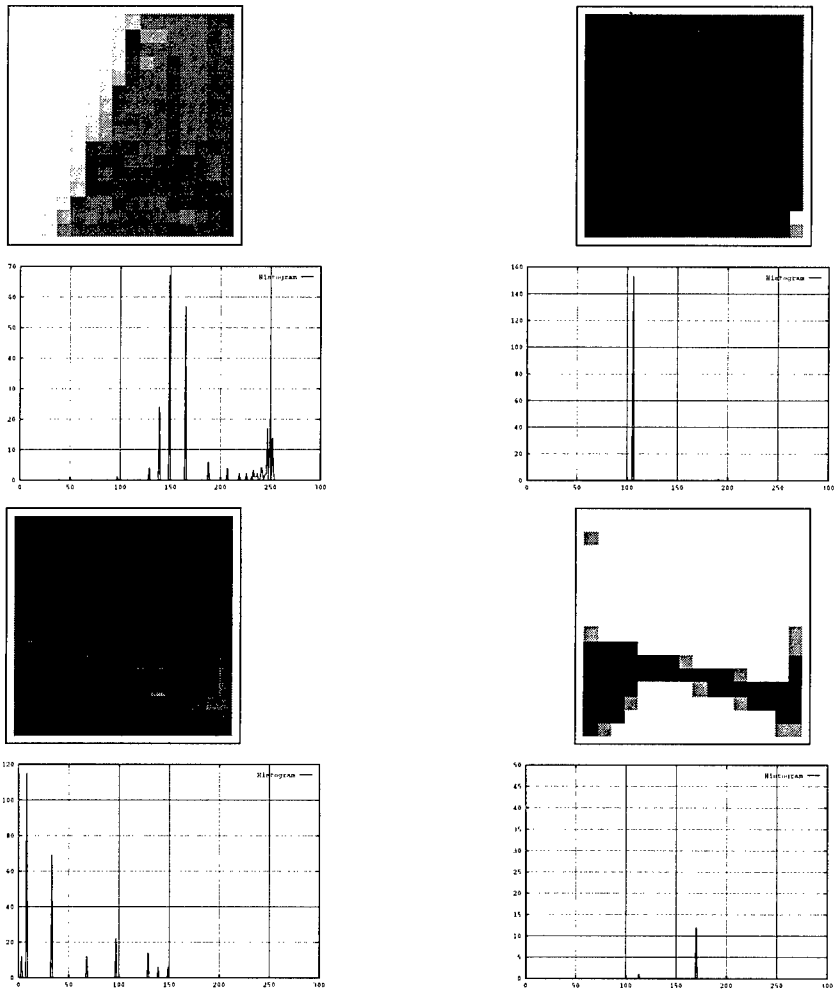

Figure 3

An important advantage of the pulsed coupled methods is that segmentation is possible for objects smaller than the window size. In the above image a road is detected having a width less than two pixels wide in some places. General threshold settings for the previous problem are not compatible with detection of features in the second image.

The adaptive nature of the algorithm allows pulses in the histogram to represent whole regions in the segmented image. The signal can be used to modify the image on the next cycle.

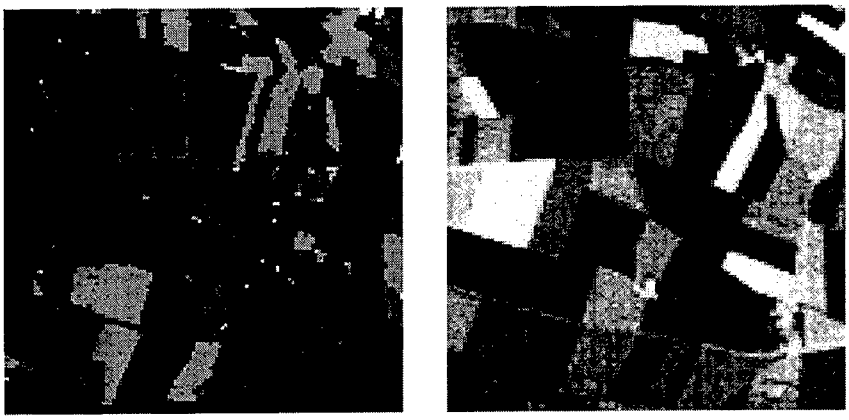

Figure 4

This image was segmented as part of a larger project to perform terrain categorization using a linear approximation to the Eckhorn model developed by Freyss. For a relatively complex image such as this, most of the common techniques perform relatively poorly. The advantage with this new technique is that there are almost no parameters to be set and no buried decisions being made by the operator.

3 Conclusions and Future Work

The model we developed demonstrates effective image segmentation over a wide variety of image class types. Although many of the results demonstrated here could be duplicated using standard techniques, these methods offer a simple modular approach to the image analysis, and are easily implemented in silicon devices.

Our work suggests that the group behavior of clusters of neurons provides a technique which encodes images into one dimensional signals in time. Using the temporal encoded group output as a control signal will add a large measure of robustness to a visual system.

An important aspect of this work is the new approach to image processing; that is expectation filtering for particular characteristics with feedback to enhance desired qualities in the signal. Donaho's [2] work on histogram equalization approximation for manufacturing processes could easily be implemented using this architecture.

REFERENCES

[1] R. Eckhorn H. Reitboeck M. Arndt P. Dicke, *Feature linking via synchronization among distributed assemblies simulations of results from cat visual cortex*, Neural Computation, Vol. 1(2) (1990), pp293-307.

[2] G.W. Donohoe and C. Jeong, *A combined analog-digital technique for normalizing video signals for the detection of moving objects*, in: Proceedings of the International Conference on Acoustics, Speech and Signal Processing (March 23-26).

[3] Stephen Grossberg, *Nonlinear neural networks: Principles, mechanisms, and architectures*, Neural Networks, Vol. 1 (1988), pp17–61.

REASONING NEURAL NETWORKS

Rua-Huan R. Tsaih

Department of Management Information Systems,
National Chengchi University, Taipei, Taiwan, ROC.

The Reasoning Neural Network (RN) has a learning algorithm belonging to the weight-and-structure-change category, because it puts only one hidden node in the initial network structure, and will recruit and prune hidden nodes during the learning process. Empirical results show that learning of the RN is guaranteed to be completed, the number of required hidden nodes is reasonable, that the speed of learning is much faster than back propagation networks, and that the RN is able to develop good internal representation.

1 Introduction

Intuitively, human learning consists of cramming and reasoning at a high level of abstraction [5]. This observation has suggested a learning algorithm as shown in Figure 1. This learning algorithm belongs to the weight-and-structure-change category, because it puts only one hidden node initially, and will recruit and prune hidden nodes during the learning process. Our learning algorithm guarantees to achieve perfectly the goal of learning. There are some similar learning algorithms; however, most of them have more complex pruning strategies. [7, 4, 1, 2].

2 The RN's Network Architecture

The RN adopts the layered feedforward network structure. Let's suppose that the network has three layers with m input nodes at the bottom, p hidden nodes, and q output nodes at the top. Let $\mathbf{B}_c \in \{-1,1\}^m$ be the cth given stimulus input, b_{cj} the stimulus value received in the jth input node when $\mathbf{B}_c$ is presented to the network, w_{ij} the weight of the connection between the jth input node and the ith hidden node, θ_i the negative of the threshold value of the ith hidden node, $\mathbf{w}_i \equiv (w_{i1}, w_{i2}, ..., w_{im})^t$ the vector of weights of the connections between all input nodes and the ith hidden node, where the superscript t indicates the transposition, $\mathbf{X}_i^t \equiv (\theta_i, \mathbf{w}_i^t)$, and $\mathbf{X}^t \equiv (\mathbf{X}_1^t, \mathbf{X}_2^t, ..., \mathbf{X}_p^t)$. Then, given the stimulus $\mathbf{B}_c$, the activation value of the ith hidden node is computed:

$$h(\mathbf{B}_c, \mathbf{X}_i) \equiv \tanh(\theta_i + \sum_{j=1}^{m} w_{ij} b_{cj}).$$

Let $\mathbf{h}(\mathbf{B}_c, \mathbf{X}) \equiv (h(\mathbf{B}_c, \mathbf{X}_1), h(\mathbf{B}_c, \mathbf{X}_2), \ldots, h(\mathbf{B}_c, \mathbf{X}_p)^t$ be the activation value vector of all hidden nodes when $\mathbf{B}_c$ is presented to the network, r_{li} the weight of the connection between the ith hidden node and the lth output node, $\mathbf{r}_l \equiv (r_{l1}, r_{l2}, ..., r_{lp})^t$ the vector of weights of the connections between all hidden nodes and the lth output node, s_l the negative of the threshold value of the lth output node, $\mathbf{Y}_l^t \equiv (s_l, \mathbf{r}_l^t)$, $\mathbf{Y}^t \equiv (\mathbf{Y}_1^t, \mathbf{Y}_2^t, ..., \mathbf{Y}_q^t)$, and $\mathbf{Z}^t \equiv (\mathbf{Y}^t, \mathbf{X}^t)$. The activation value of the lth output node is computed after $\mathbf{h}(\mathbf{B}_c, \mathbf{X})$:

$$O(\mathbf{B}_c, \mathbf{Y}_l, \mathbf{X}) \equiv \tanh(s_l + \sum_{i=1}^{p} r_{li} h(\mathbf{B}_c, \mathbf{X}_i)).$$

3 The Learning Algorithm

The block diagram of the learning algorithm is shown in Figure 1. There are four distinguished aspects of this learning algorithm: the linearly separating condition

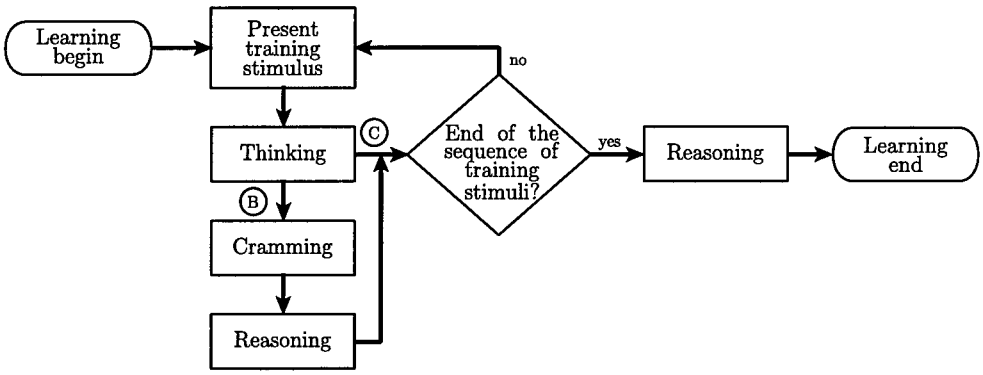

Figure 1 The block diagram of the learning algorithm. The details of the thinking box, the reasoning box and the cramming box are shown in Figure 2 and Figure 3.

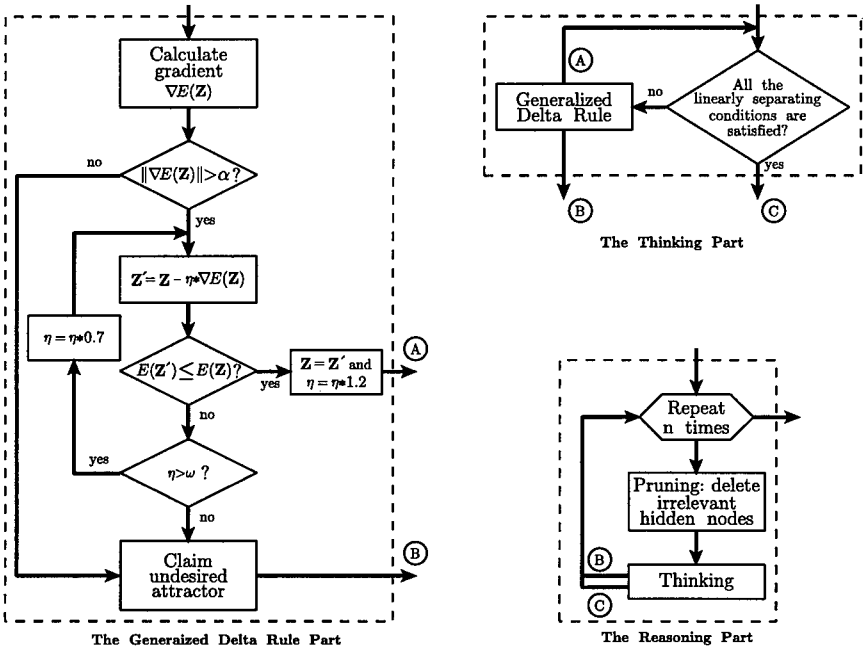

Figure 2 The Generalised Delta Rule part, the thinking part and the reasoning part. The values of given constants α and ω in the Generalised Delta Rule part are tiny.

(LSC), the thinking mechanism, the cramming mechanism; and the reasoning mechanism. These aspects are explained in the following.

With respect to each output node, the network is used as a classifier which learns to distinguish if the stimulus is a member of one class of stimuli, called class 1, or

$p+1 \rightarrow p$, then adds the new P^{th} hidden node with $\mathbf{w}_p = \mathbf{B}_k, \theta_p = 1 - m$, and $r_{lp} = 0$ for every $l \in L$, and, for every $l \notin L$

$$r_{lp} = \begin{cases} \max_{v \in K_{l2}(k-1)} \sum_{i=1}^{p-1} r_{li} h(\mathbf{B}_v, \mathbf{X}_i) - \sum_{i=1}^{p-1} r_{li} h(\mathbf{B}_k, \mathbf{X}_i) \text{ if } d_{kl} = 1.0 \\ \min_{u \in K_{l1}(k-1)} \sum_{i=1}^{p-1} r_{li} h(\mathbf{B}_u, \mathbf{X}_i) - \sum_{i=1}^{p-1} r_{li} h(\mathbf{B}_k, \mathbf{X}_i) \text{ if } d_{kl} = -1.0 \end{cases}$$

Figure 3 The Cramming part. Suppose that $l \in L$ if, before implementing the cramming mechanism, the LSC with respect to the lth output node is satisfied.

of a different class, called class 2, by being presented with exemplars of each class. With respect to the lth output node, let $K \equiv K_{l1} \cup K_{l2}$, where K_{l1} and K_{l2} are the sets of indices of all given training stimuli in classes 1 and 2, respectively; and let d_{cl} be the desired output value of the lth output node of the cth stimulus, with 1.0 and -1.0 being respectively the desired output values of classes 1 and 2. Learning seeks Z where, for all l,

$$d_{cl} O(\mathbf{B}_c, \mathbf{Y}_l, \mathbf{X}) \geq v \qquad \forall c \in K \tag{1}$$

and $0 < v < 1$. With respect to the lth output node, let the LSC be that

$$\min_{c \in K_{l1}} O(\mathbf{B}_c, \mathbf{Y}_l, \mathbf{X}) > \max_{c \in K_{l2}} O(\mathbf{B}_c, \mathbf{Y}_l, \mathbf{X}).$$

When the LSC with respect to the lth output node is satisfied, the requirement (1) with respect to the lth output node could be achieved by merely adjusting $\mathbf{Y}_l$ [5]. At the learning stage, the training stimuli are presented one by one. At the kth given stimulus, the objective function is defined as:

$$E(\mathbf{Z}) \equiv \sum_{c=1}^{k} \sum_{l=1}^{q} (O(\mathbf{B}_c, \mathbf{Y}_l, \mathbf{X}) - d_{cl})^2$$

and let $K(k) \equiv \{1, ..., k\}$ and $K(k) \equiv K_{l1}(k) \cup K_{l2}(k)$, where $K_{l1}(k)$ and $K_{l2}(k)$ are, respectively, the sets of indices of the first k training stimuli in classes 1 and 2, with respect to the lth output node. Then the thinking mechanism is implemented, in which the momentum version of the generalized delta rule (with automatic adjustment of learning rate) is adopted. Learning might converge to the bottom of a very shallow steep-sided valley [3], where the magnitude of the gradient will be tiny and the consecutive adaptive learning rates will also be tiny. Therefore, as shown in the generalized delta rule part of Figure 2, these two criteria are adopted to detect if the learning hits the neighborhood of an undesired attractor.

The desired solution is not required to render the requirement (1) satisfied or to be a stationary point in which $\nabla_z E(\mathbf{Z}) = 0$. Thus, the magnitude of $\|\nabla_z E(\mathbf{Z})\|$ before hitting the desired solution is not necessarily tiny and the learning time is rather less, compared with conventional stopping criteria (for example, small $E(\mathbf{Z})$ or $\|\nabla_z E(\mathbf{Z})\| = 0$).

The thinking mechanism does not guarantee that the LSC with respect to all output nodes will be satisfied. Two ideas could render the learning capable of escaping from the undesired attractor: add a hidden node and alter the objective function.

By adding a hidden node, the dimension of the weight space is increased; while altering the objective function will change its function surface on the weight space such that the trapped attractor could be no more an attractor. These two ideas are implemented in our learning algorithm via the cramming mechanism and that the objective function is altered by introducing a new training stimulus.

The cramming mechanism can be viewed as that, at first a new hidden node with the near threshold activation function is added, then the softening mechanism of [6] is used immediately to render the activation function of the new hidden node a tanh one. The Lemma in [6] shows that the mechanism of adding a new hidden node with the near threshold activation function and a finite value of the gain parameter can immediately render the LSC with respect to all output nodes satisfied, if the training set has no internal conflicts (different outputs for the same input).

However the number of required hidden nodes may be too many and the generalization ability of the network may be bad. Thus it is necessary to adopt the reasoning mechanism for the purpose of rendering the network more compact. The reasoning mechanism includes the thinking mechanism and the pruning mechanism of removing irrelevant hidden nodes. In a $\mathbf{Z}$, the ith hidden node is said to be irrelevant to the LSC with respect to the lth output node if the LSC is still satisfied with the same $\mathbf{Z}$ except $r_{li} = 0$; and a hidden node is irrelevant if it is irrelevant to the LSC with respect to all output nodes [5].

4 The Performance of the RN

We report three experiments. In each simulation, there are 100 testing cases, each with different input sequence of training stimuli. One experiment is the m-bits parity learning problem. In Figure 4a, the numbers of used hidden nodes during the 6-bits parity learning process are plotted. The variance of p is due to the different input sequence of training stimuli. Figure 4b shows the summary of the simulation results, and it shows that the average value p of the m-bits parity problems is merely a little bigger than m. However, it is surprising to see that the RN can solve the m-bits parity problems with less than m hidden nodes.

The output/hidden experiment is used to identify the relationship between the number of required hidden nodes and the number of used output nodes. The number of input nodes is fixed to be 8. The training stimuli and their input sequence are randomized; but the number of used output nodes is varied from 1 to 6. In Figure 4c, the simulation result of the "$m = 8$, $q = 3$, and $K = 100$" problem are plotted. Figure 4d shows the summary of the simulation results, and it shows that the relationship between the average value p of the RN and the value of q is rather a linear one.

One significant phenomenon of above simulations is that the value of q influences the value of p more significantly than the values of K and m do. Another interesting phenomenon is that if there is no correlation within current given training stimuli, the RN tends to cram them (in other words, memorize them individually) by using many more hidden nodes. But when there are correlation within the current given training stimuli, it seems that the RN will figure out a smart way to classify the given training stimuli by using less hidden nodes. In other words, the RN has the ability of developing a good internal representation for the given training stimuli.

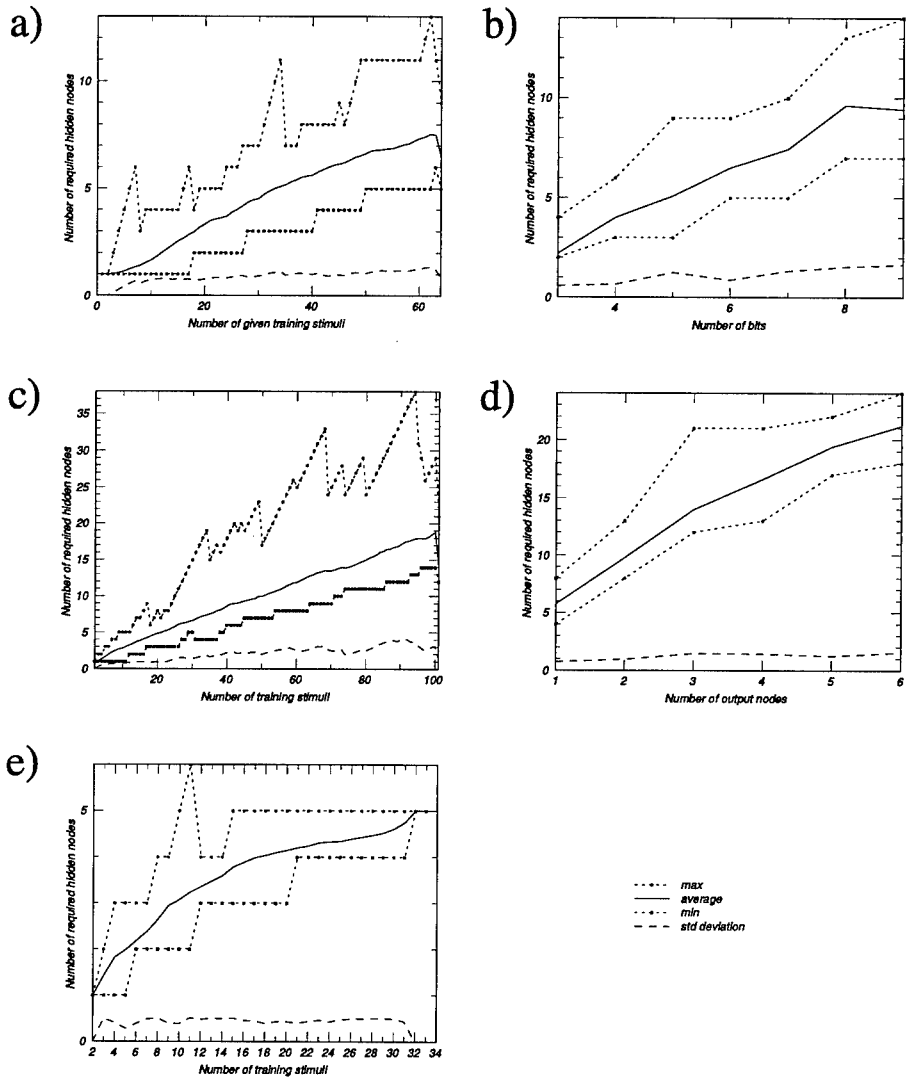

Figure 4 a) The simulation result of the 6-bits parity problem. b) The summary of simulation results of the m-bits parity problem. c) The simulation result of the "$m = 8$, $q = 3$, and $K = 100$" problem. d) The summary of simulation results of the output/hidden problems. e) The simulation result of the 5-p-5 problem.

The third experiment is the 5-p-5 problem (Figure 4e)), in which the training stimuli are the same as those of the 5-bits parity problem and the desired output vector is the same as the stimulus input vector. Somewhat surprisingly, as shown in Figure 5, each hidden node of one final RN has only one strong connection strength from input nodes, and each output node has only one strong connection strength from

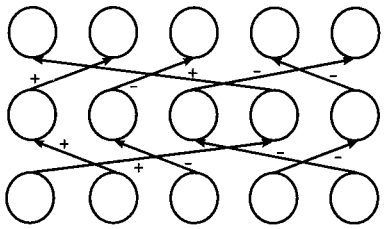

Figure 5 One final RNN of the 5-p-5 encoder problem, where we show only the connections with weights of large magnitude, and the signs of their weights. Note that the signs of two connected strongest connections are the same.

hidden nodes. In addition, different hidden nodes have strongest connections from different input nodes, different output nodes have strongest connections from a different hidden node, and the signs of connected strongest connections are the same. It seems that, after learning the full set of training stimuli, the RN had learned to use the hidden nodes to bypass the input stimulus, rather than to encode them.

5 Discussions and Future work

The empirical results show that the learning of the RN is much faster than the back propagation learning algorithm, and that the RN is able to develop good internal representation with good generalization. The RN has flexibility in its learning algorithm; different algorithms have been obtained by integrating the prime mechanisms in different way. These yield different simulation results: it seems that we should use different management in the RN for different application problems.

REFERENCES

[1] Fahlman, S. & C. Lebiere, *The Cascade-Correlation Learning Architecture*, in: Touretzky, D. (eds), Advances in Neural Information Processing Systems II, Denver (1989), San Mateo, Morgan Kaufmann.

[2] Frean, M., *The Upstart Algorithm: A Method for Constructing and Training Feedforward Neural Networks*, Neural Computation Vol. 2 (1990), pp198–209.

[3] McInerny, J., K. Hainer, S. Biafore, & R. Hecht-Nielsen,. *Back Propagation Error Surfaces Can Have Local Minima*, Proceedings of the International Joint Conference on Neural Networks (1989), Vol II, p627.

[4] Mézard, M & J. Nadal, *Learning in Feedforward Layered Networks: The Tiling Algorithm*, Journal of Physics Vol. A 22 (1989), pp2191–2204.

[5] Tsaih, R., *The Softening Learning Procedure*, Mathematical and Computer Modelling, Vol. 18 (1993), No. 8, pp61–64.

[6] Tsaih, R., *The Softening Learning Procedure for The Networks With Multiple Output Nodes*, MIS Review, Vol. 4 (1994), pp89–93, Taipei.

[7] Watanabe, E., & H. Shimizu, *Algorithm for Pruning Hidden nodes in Multi-Layered Neural Network for Binary Pattern Classification Problem*, Proceedings of the International Joint Conference on Neural Networks (1993), Vol I, pp327–330.

CAPACITY OF THE UPSTART ALGORITHM

Ansgar H. L. West* and David Saad

Neural Computing Research Group, Aston University,
Aston Triangle, Birmingham B4 7ET, UK.
Email: A.H.L.West@aston.ac.uk, D.Saad@aston.ac.uk
** Also affiliated to: Department of Physics, University of Edinburgh,*
Mayfield Road, Edinburgh, EH9 3JZ, UK.

The storage capacity of multilayer networks with overlapping receptive fields is investigated for a constructive algorithm within a one-step replica symmetry breaking (RSB) treatment. We find that the storage capacity increases logarithmically with the number of hidden units K without saturating the Mitchison-Durbin bound. The slope of the logarithmic increase decays exponentionally with the stability with which the patterns have been stored.

1 Introduction

Since the ground breaking work of Gardner [1] on the storage capacity of the perceptron, the replica technique of statistical mechanics has been successfully used to investigate many aspects of the performance of simple neural network models. However, progress for multilayer feedforward networks has been hampered by the inherent difficulties of the replica calculation. This is especially true for capacity calculations, where replica symmetric (RS) treatments [2] violate the upper Mitchison-Durbin bound [3] derived by information theory. Other efforts [4] break the symmetry of the hidden units explicitly prior to the actual calculation, but the resulting equations are approximations and difficult to solve for large networks. This paper avoids these problems by addressing the capacity of a class of networks with variable architecture produced by a constructive algorithm. In this case, results derived for simple binary perceptrons above their saturation limit [5] can be applied iteratively to yield the storage capacity of two-layer networks.

Constructive algorithms (e.g., [6, 8]) are based on the idea that in general it is *a priori* unknown how large a network must be to perform a certain classification task. It seems appealing therefore to start off with a simple network, e.g., a binary perceptron, and to increase its complexity only when needed. This procedure has the added advantage that the training time of the whole network is relatively short, since each training step consists of training the newly added hidden units only, whereas previously constructed weights are kept fixed. Although constructive algorithm seem therefore rather appealing, their properties are not well understood. The aim of this paper is to analyse the performance of one constructive algorithm, the upstart algorithm [8], in learning random dichotomies, usually referred to as the capacity problem.

The basic idea of the upstart algorithm is to start with a binary perceptron unit with possible outputs {1,0}. Further units are created only if the initial perceptron makes any errors on the training set. One unit may have to be created to correct WRONGLY ON errors (where the target was 0 but the actual output is 1) another to correct WRONGLY OFF errors (where the target was 1 but the output is 0). If these units still cause errors in the output of the network, more units are created in the next generation of the algorithm until all outputs are correct. Different versions of the upstart algorithm differ in the way new units are connected to the old units and

to the output unit. The original upstart algorithm produces a hierarchical network where the number of hidden units tends to increase exponentionally with each generation. Other versions of the upstart algorithm[8] build a two-layer architecture and show only a linear increase of the number of units with each generation, which is in general easier to implement.

We have therefore analysed a non-hierarchical version of the upstart algorithm. Within a one-step replica symmetry breaking (RSB) treatment [9], networks constructed by the upstart algorithm show a logarithmic increase of the capacity with the number of nodes in agreement with the Mitchison-Durbin bound

$$(\alpha_c \propto \ln K / \ln 2)$$

, whereas the simpler RS treatment violates this bound. Furthermore, the algorithm does not saturate the Mitchison-Durbin bound for zero stability. We further find that the slope of the logarithmic increase of the capacity against network size decreases exponentionally with the stability.

2 Model Description and Framework

2.1 Definition of the Upstart Algorithm

The upstart algorithm first creates a binary perceptron (or unit) $\mathcal{D}_0$ which learns a synaptic weight vector $\boldsymbol{W} \in \mathbb{R}^N$ and a threshold θ which minimize the error on a set of p input-output mappings $\boldsymbol{\xi}^\mu \in \{-1,1\}^N \rightarrow \zeta^\mu \in \{0,1\}$ $(\mu = 1,\ldots,p)$ from an N–dimensional binary input space to binary targets. The output of the binary perceptron is determined by

$$\sigma^\mu = \Theta\left(\frac{1}{\sqrt{N}}\boldsymbol{W}\cdot\boldsymbol{\xi}^\mu - \theta\right) = \Theta(h^\mu)$$

where $\Theta(x)$ is the Heavyside stepfunction, which is 1 for $x \geq 0$ and 0 otherwise, and h^μ is the activation of the perceptron. The error is defined as

$$E = \sum_\mu \Theta\left[\kappa - 2(\zeta^\mu - 1)h^\mu\right],$$

where κ is the stability with which we require the patterns to be stored. A suitable algorithm (e.g., [10]) will converge to a set of weights $\boldsymbol{W}$ which minimizes the above error. If the set of examples is not linearly separable with a minimum distance κ of all patterns to the hyperplane, the binary perceptron will not be able to classify all patterns correctly, i.e., $\sigma^\mu \neq \zeta^\mu$ for some μ's and the upstart algorithm has to create further daughter units an a hidden layer to realize the mapping. The upstart algorithm therefore creates a binary $\{0,1\}$ output unit $\mathcal{O}$ with threshold one and the initial perceptron $\mathcal{D}_0$ and all further daughter units to be built by the algorithm will form the hidden layer. The first perceptron is then connected to $\mathcal{O}$ with a $+1$ weight, i.e., $\mathcal{O}$ has initially the same outputs as $\mathcal{D}_0$.

The basic idea of the upstart algorithm is to create further daughter units $\mathcal{D}^+$ and $\mathcal{D}^-$ in the hidden layer to correct WRONGLY OFF and WRONGLY ON errors respectively. Consider, for example, the creation of the new hidden unit $\mathcal{D}^-$, which is connected with a large negative weight to $\mathcal{O}$, whose role is to inhibit $\mathcal{O}$. $\mathcal{D}^-$ should be active (1) for patterns for which $\mathcal{O}$ was WRONGLY ON and inactive (0) for patterns for which $\mathcal{O}$ was CORRECTLY ON. Similarly, $\mathcal{D}^-$ ought to be 0 if $\mathcal{O}$ was WRONGLY OFF, in order to avoid further inhibition of $\mathcal{O}$. However, we do not have to train $\mathcal{D}^-$ on patterns for which $\mathcal{O}$ was CORRECTLY OFF, since an active $\mathcal{D}^-$

would only reinforce $\mathcal{O}$'s already correct response. The resulting training sets and the targets of both daughter units are illustrated in Table 1. More formally we

	$\zeta = 1$	$\zeta = 0$
$\sigma = 1$	CORRECTLY ON $\mathcal{D}^+$ $*$ $\mathcal{D}^-$ 0	WRONGLY ON $\mathcal{D}^+$ 0 $\mathcal{D}^-$ 1
$\sigma = 0$	WRONGLY OFF $\mathcal{D}^+$ 1 $\mathcal{D}^-$ 0	CORRECTLY OFF $\mathcal{D}^+$ 0 $\mathcal{D}^-$ $*$

Table 1 The targets of the upstart II algorithm depending on the requested target ζ and the actual output σ of the output unit $\mathcal{O}$. The target "$*$" means that the pattern is not included in the training set of $\mathcal{D}^{\pm}$.

define the algorithm upstart II by the following steps which are applied recursively until the task is learned:

Step 0: Follow the above procedure for the original unit $\mathcal{D}_0$ and the creation of the output unit $\mathcal{O}$. Evaluate the number of WRONGLY OFF and WRONGLY ON errors.

Step 1: If the output unit $\mathcal{O}$ of the upstart network of i generations makes more WRONGLY OFF than WRONGLY ON errors, a new unit $\mathcal{D}^-_{i+1}$ is created and trained on the training set and targets given in Table 1. If there are more WRONGLY ON than WRONGLY OFF errors, a new unit $\mathcal{D}^+_{i+1}$ is created with training set and targets also given in Table 1. If both kind of errors occur equally, two units $\mathcal{D}^-_{i+1}$ and $\mathcal{D}^+_{i+1}$ are created with training sets and targets as above.

Step 2: The new units are trained on their training sets and their weights are frozen. The units $\mathcal{D}^+_{i+1}$, $\mathcal{D}^-_{i+1}$ are then connected with positive, negative weights to the output unit respectively. The modulus of the weights are adjusted so that $\mathcal{D}^{\pm}_{i+1}$ overrules any previous decisions if active. The total number of WRONGLY OFF and WRONGLY ON errors of the upstart network of generation $i+1$ is then reevaluated. If the network still makes errors the algorithm goes back to Step 1.

The algorithm will eventually converge as a daughter unit will always be able to correct at least one of the previously misclassified patterns without upsetting any already correctly classified examples.

2.2 Statistical Mechanics Framework for Calculating the Capacity Limit

Since the upstart algorithm trains only perceptrons, we can apply knowledge of the capacity limit and of the error rate of perceptrons above saturation derived in a statistical mechanics framework to calculate the capacity limit of the upstart II algorithm for an arbitrary number of generations. Below, we briefly review this

statistical mechanics calculation and refer the reader to [5] and to previous work [1] for a more detailed treatment.

In the capacity problem the aim is to find the maximum number p of random input-output mappings of binary N–dimensional input vectors $\boldsymbol{\xi}^\mu$ to targets $\zeta^\mu \in \{0, 1\}$, which can be realized by a network on average. We assume that each component of the input vectors $\boldsymbol{\xi}^\mu$ is drawn independently with equal probability from $\{-1, 1\}$. The distribution of targets is taken to be pattern independent with a possible bias b: $P(\zeta) = \frac{1}{2}(1+b)\delta(1-\zeta) + \frac{1}{2}(1-b)\delta(\zeta)$. We will here only consider an unbiased output distribution for the intial perceptron. The target distributions for daughter units however will in general be biased.

Each binary perceptron is trained stochastically and we only allow weight vector solutions with the minimal achievable error. The error rate, i.e., the number of errors divided by the total number of examples, is assumed to be self-averaging with respect to the randomness in the training set in the thermodynamic limit $N \to \infty$. In this limit the natural measure for the number of examples p is $\alpha = p/N$. With increasing α the weight space of possible solutions shrinks, leaving a unique solution at the capacity limit of the binary perceptron. Above the capacity limit many different weight space solutions with the same error are possible. In general the solution space will be disconnected as two solutions can possibly missclassify different patterns. As α diverges, the solution space becomes increasingly fragmented.

The replica trick is used to calculate the solution space and the minimal error rate averaged over the randomness of the training set. This involves the replication of the perceptron weight vector, each replica representing a different possible solution to the same storage problem. In order to make significant progress, one has further to assume some kind of structure in the replica space. Below the capacity limit, the connectedness of the solution space is reflected by the correctness of a replica symmetric (RS) ansatz. Above the capacity, the disconnectedness of the solution space breaks the RS to some degree. We have restricted ourselves to a one-step replica symmetry breaking (RSB) calculation, which is expected to be at least sufficient for small error rates. The form of the equations for the error rate resulting from the RS and one-step RSB calculations are quite cumbersome and will be reported elsewhere [5, 11]. For the perceptron, the error rate is a function of the output bias b and the load α only.

3 Results of the Upstart Algorithm

The capacity of an upstart network with K hidden units can now be calculated. The initial perceptron is trained with an example load of α and an unbiased output distribution $b = 0$. The saddlepoint equations and the WRONGLY ON and WRONGLY OFF error rates are calculated numerically. These error rates determine the load and bias for the unit(s) to be created in the next generation. Now its (their) error rates and the errors of the output unit can in turn be calculated by solving the saddlepoint equations. This is iterated until K units have been built. If the output unit still makes error, we are above the capacity limit of the upstart net with K hidden units and α has to be decreased. On the other hand, if the output unit makes no errors, α can be increased. The maximal α for which the output unit makes no errors defines the saturation point of the network. The capacity limit, defined here

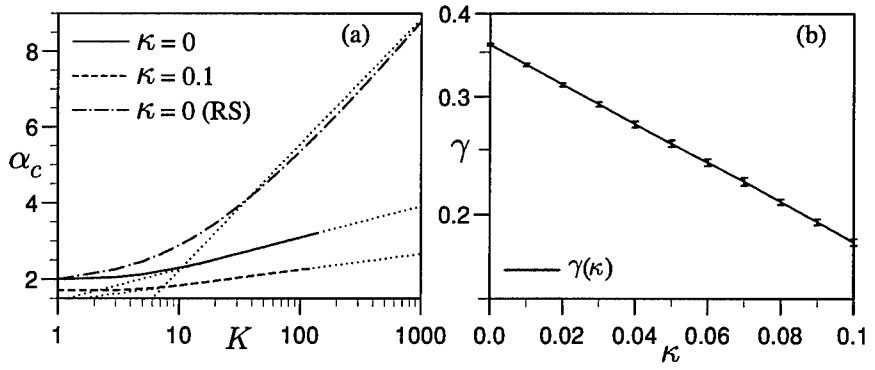

Figure 1 (a) Within the one-step RSB theory, the capacity α_c increases logarithmically with the number of hidden units K for large K for the stabilities $\kappa = 0$ (0.1), i.e., $\alpha_c \propto 0.3595$ (0.182) $\ln K$ (see superimposed asymptotics). The RS theory violates the Mitchison-Durbin bound (third asymptotic: $\alpha_c \propto \ln K / \ln 2$) for $K \geq 180$. (b) The slope γ of the logarithmic increase of the capacity decreases exponentionally with the stability κ.

as the maximal number of examples per adjustable weight of the network, then becomes simply $\alpha_c(K) = \alpha/K$.

In Fig. 1a we present the storage capacity as a function of the number of hidden units for both a one-step RSB and a RS treatment at zero stability of the patterns ($\kappa = 0$). Whereas one-step RSB predicts a logarithmic increase $\alpha_c(K) \propto \ln(K)$ for large networks, in agreement with the Mitchison-Durbin bound, the results for the RS-theory violate this upper bound[1], i.e., the RS theory fails to predict the qualitative behaviour correctly.

In Fig. 1a we also show that the storage capacity still increases logarithmically with the number of units K for non-zero stability, but with a smaller slope γ. Fig. 1b shows the dependence of the slope γ as a function of the stability κ for one-step RSB. The maximal slope for zero stability $\gamma = 0.3595 \pm 0.0015$ does not saturate the Mitchison-Durbin bound $\gamma = 1/\ln 2 \approx 1.4427$, but is about four times lower. With increasing stabilities κ this slope decreases exponentionally $\gamma \propto \exp(-6.77 \pm 0.02\,\kappa)$.

4 Summary and Discussion

The objective of this work has been to calculate the storage capacity of multilayer networks created by the constructive upstart algorithm in a statistical mechanics framework using the replica method. We found that the RS-theory fails to predict the correct results even qualitatively. The one-step RSB theory yields qualitatively and quantitatively correct results over a wide range of network sizes and stabilities. In the one-step RSB treatment, a logarithmic increase with slope γ of the capacity of the upstart algorithm with the number of units K was found for all stabilities. The slope decreases exponentionally [$\gamma \propto \exp(-6.77\kappa)$] with the stability κ. It would be interesting to investigate if this result carries over to other constructive algorithms or even to general two-layer networks.

[1] The violation occurs for $K \geq 180$ and the largest networks in the RS case were $K = 999$.

For zero stability the slope of this increase is around four times smaller than the upper bound $(1/\ln 2)$ predicted by information theory. We suggest that this indicates that the upstart algorithm uses its hidden units less effectively than a general two-layer network. We think this is due to the fact that the upstart algorithm uses the hidden units to overrule previous decisions, resulting in an exponential increase of the hidden layer to output unit weights. This is in contrast to general two-layer networks which usually have hidden-output weights of roughly the same order and can therefore explore a larger space of internal representations. For the upstart algorithm a large number of internal representations are equivalent and others cannot be implemented as they are related to erroneous outputs. However, it would be interesting to investigate how other constructive algorithms (e.g., [6]) perform in comparison. A systematic investigation of the storage capacity of constructive algorithms may ultimately lead to a better understanding, and thus possibly to novel, much improved algorithms.

REFERENCES

[1] E. Gardner, *The space of interactions in neural network models*, J. Phys. A Vol. 21 (1988), pp257–270.

[2] E. Barkai, D. Hansel and H. Sompolinsky, *Broken symmetries in multilayered perceptrons*, Phys. Rev. A Vol. 45 (1992), pp4146–4161.

[3] G. J. Mitchison and R. M. Durbin, *Bounds on the learning capacity of some multi-layer networks*, Biological Cybernetics Vol. 60 (1989), pp345–356.

[4] D. Saad, *Explicit symmetries and the capacity of multilayer neural networks*, J. Phys. A Vol. 27 (1994), pp2719–2734.

[5] A. H. L. West, and D. Saad, *Threshold induced phase transitions in perceptrons*, To appear in J. Phys. A (March 1997).

[6] M. Mézard and J.-P. Nadal, *Learning in feed-forward layered networks: the tiling algorithm*, J. Phys. A Vol. 22 (1989), pp2191–2203.

[7] J.-P. Nadal, *Study of a growth algorithm for a feed-forward network*, International Journal of Neural Systems, Vol.1 (1989), pp55–59.

[8] M. Frean, *The upstart algorithm: a method for constructing and training feed-forward neural networks*, Neural Computation Vol. 2 (1990), pp198–209.

[9] For an overview, see e.g., M. Mézard, G. Parisi and M. G. Virasoro, *Spin Glass Theory and Beyond*, World Scientific, Singapore (1987).

[10] M. Frean, *A thermal perceptron learning rule*, Neural Computation Vol. 4 (1992), pp946–957, and references therein.

[11] A. H. L. West and D. Saad, *Statistical mechanics of constructive algorithms*, in preparation (1997).

Acknowledgements

AHLW would like to acknowledge gratefully financial support by the EPSRC. This work has been supported by EU grant ERB CHRX-CT92-0063.

REGRESSION WITH GAUSSIAN PROCESSES

Christopher K. I. Williams

Neural Computing Research Group, Department of Computer Science and Applied Mathematics, Aston University, Birmingham B4 7ET, UK.

Email: c.k.i.williams@aston.ac.uk

The Bayesian analysis of neural networks is difficult because the prior over functions has a complex form, leading to implementations that either make approximations or use Monte Carlo integration techniques. In this paper I investigate the use of Gaussian process priors over functions, which permit the predictive Bayesian analysis to be carried out exactly using matrix operations. The method has been tested on two challenging problems and has produced excellent results.

1 Introduction

In the Bayesian approach to neural networks a prior distribution over the weights induces a prior distribution over functions. This prior is combined with a noise model, which specifies the probability of observing the targets $\boldsymbol{t}$ given function values $\boldsymbol{y}$, to yield a posterior over functions which can then be used for predictions. For neural networks the prior over functions has a complex form which means that implementations must either make approximations [4] or use Monte Carlo approaches to evaluating integrals [6].

As Neal [7] has argued, there is no reason to believe that, for real-world problems, neural network models should be limited to nets containing only a "small" number of hidden units. He has shown that it is sensible to consider a limit where the number of hidden units in a net tends to infinity, and that good predictions can be obtained from such models using the Bayesian machinery[1]. He has also shown that a large class of neural network models will converge to a Gaussian process prior over functions in the limit of an infinite number of hidden units.

Although infinite networks are one method of creating Gaussian processes, it is also possible (and computationally easier) to specify them directly using parametric forms for the mean and covariance functions. In this paper I investigate using Gaussian processes specified parametrically for regression problems[2], and demonstrate very good performance on the two test problems I have tried. The advantage of the Gaussian process formulation is that the integrations, which have to be approximated for neural nets, can be carried out exactly (using matrix operations) in this case. I also show that the parameters specifying the Gaussian process can be estimated from training data, and that this leads naturally to a form of "Automatic Relevance Determination" [4], [7].

2 Prediction with Gaussian Processes

A stochastic process is a collection of random variables $\{Y(\boldsymbol{x})|\boldsymbol{x} \in X\}$ indexed by a set X. Often X will be a space such as $\mathbb{R}^d$ for some dimension d, although it could be more general. The stochastic process is specified by giving the probability distribution for every finite subset of variables $Y(\boldsymbol{x}_1), \ldots, Y(\boldsymbol{x}_k)$ in a consistent manner. A Gaussian process is a stochastic process which can be fully specified by its mean function $\mu(\boldsymbol{x}) = E[Y(\boldsymbol{x})]$ and its covariance function $C(\boldsymbol{x}, \boldsymbol{x}') = E[(Y(\boldsymbol{x}) -$

[1] Large networks cannot be successfully used with maximum likelihood training because of the overfitting problem.

[2] By regression problems I mean those concerned with the prediction of one or more real-valued outputs, as compared to classification problems.

$\mu(\boldsymbol{x}))(Y(\boldsymbol{x}')-\mu(\boldsymbol{x}'))]$; any finite set of points will have a joint multivariate Gaussian distribution.

Below I consider Gaussian processes which have $\mu(\boldsymbol{x}) \equiv 0$. This is the case for many neural network priors [7], and otherwise assumes that any known offset or trend in the data has been removed. A non-zero $\mu(\boldsymbol{x})$ can be incorporated into the framework, but leads to extra notational complexity.

Given a prior covariance function $C_P(\boldsymbol{x}, \boldsymbol{x}')$, a noise process $C_N(\boldsymbol{x}, \boldsymbol{x}')$ (with $C_N(\boldsymbol{x}, \boldsymbol{x}') = 0$ for $\boldsymbol{x} \neq \boldsymbol{x}'$) and data $\mathcal{D} = ((\boldsymbol{x}_1, t_1), (\boldsymbol{x}_2, t_2), \ldots, (\boldsymbol{x}_n, t_n))$, the prediction for the distribution of Y corresponding to a test point $\boldsymbol{x}$ is obtained simply by marginalizing the $(n+1)$-dimensional joint distribution to obtain the mean and variance

$$\hat{y}(\boldsymbol{x}) = \boldsymbol{k}_P^T(\boldsymbol{x})(K_P + K_N)^{-1}\boldsymbol{t} \quad (1)$$

$$\sigma_{\hat{y}}^2(\boldsymbol{x}) = C_P(\boldsymbol{x}, \boldsymbol{x}) + C_N(\boldsymbol{x}, \boldsymbol{x}) - \boldsymbol{k}_P^T(\boldsymbol{x})(K_P + K_N)^{-1}\boldsymbol{k}_P(\boldsymbol{x}) \quad (2)$$

where $[K_\alpha]_{ij} = C_\alpha(\boldsymbol{x}_i, \boldsymbol{x}_j)$ for $\alpha = P, N$, $\boldsymbol{k}_P(\boldsymbol{x}) = (C_P(\boldsymbol{x}, \boldsymbol{x}_1), \ldots, C_P(\boldsymbol{x}, \boldsymbol{x}_n))^T$ and $\boldsymbol{t} = (t_1, \ldots, t_n)^T$. $\sigma_{\hat{y}}^2(\boldsymbol{x})$ gives the "error bars" of the prediction. In the work below the noise process is assumed to have a variance σ_ν^2 independent of $\boldsymbol{x}$ so that $K_N = \sigma_\nu^2 I$.

The Gaussian process view provides a unifying framework for many regression methods. ARMA models used in time series analysis and spline smoothing (e.g. [10]) correspond to Gaussian process prediction with a particular choice of covariance function[3], as do generalized linear regression models ($y(\boldsymbol{x}) = \sum_i w_i \phi_i(\boldsymbol{x})$, with $\{\phi_i\}$ a fixed set of basis functions) for a Gaussian prior on the weights $\{w_i\}$. Gaussian processes have also been used in the geostatistics field (e.g. [3], [1]), and are known there as "kriging", but this literature has concentrated on the case where $\boldsymbol{x} \in \mathbb{R}^2$ or $\mathbb{R}^3$, rather than considering more general input spaces. Regularization networks (e.g. [8], [2]) provide a complementary view of Gaussian process prediction in terms of a Fourier space view, which shows how high-frequency components are damped out to obtain a smooth approximator.

2.1 Adapting Covariance Functions and ARD

Given a covariance function $C = C_P + C_N$, the log probability l of the training data is given by

$$l = -\frac{1}{2}\log\det K - \frac{1}{2}\boldsymbol{t}^T K^{-1}\boldsymbol{t} - \frac{n}{2}\log 2\pi \quad (3)$$

where $K = K_P + K_N$. If C has some adjustable parameters $\boldsymbol{\theta}$, then we can carry out a search in $\boldsymbol{\theta}$-space to maximize l; this is simply maximum likelihood estimation of $\boldsymbol{\theta}$ [4]. For example, in a d-dimensional input space we may choose

$$C(\boldsymbol{x}, \boldsymbol{x}') = v_0 \exp\left(-\sum_{i=1}^{d} \frac{w_i}{2}(x_i - x_i')^2\right) + v_1\delta(\boldsymbol{x}, \boldsymbol{x}') \quad (4)$$

where v_0, v_1 and the $\{w_i\}$ are adjustable. In MacKay's terms [4] l is the log "evidence", with the parameter vector $\boldsymbol{\theta}$ roughly corresponding to his hyperparameters $\boldsymbol{\alpha}$ and β; in effect the weights have been exactly integrated out.

One reason for constructing a model with variable w's is to express the prior belief that some input variables might be irrelevant to the prediction task at hand, and

[3] Technically splines require generalized covariance functions.

[4] See section 4 for a discussion of the hierarchical Bayesian approach.

Method	No. of inputs	sum squared test error
Gaussian process	2	1.126
Gaussian process	6	1.138
MacKay	2	1.146
Neal	2	1.094
Neal	6	1.098

Table 1 Results on the robot arm task.

we would expect that the w's corresponding to the irrelevant variables would tend to zero as the model is fitted to data. This is closely related to the Automatic Relevance Determination (ARD) idea of MacKay and Neal [5], [7].

3 Experiments with Gaussian Process prediction

Prediction with Gaussian processes and maximum likelihood training of the covariance function has been tested on two problems : (i) a modified version of MacKay's robot arm problem and (ii) the Boston housing data set.

For both datasets I used a covariance function of the form given in equation 4 and a gradient-based search algorithm for exploring $\boldsymbol{\theta}$-space; the derivative vector $\partial l/\partial \boldsymbol{\theta}$ was fed to a conjugate gradient routine with a line-search[5].

3.1 The Robot Arm Problem

I consider a version of MacKay's robot arm problem introduced by Neal (1995). The standard robot arm problem is concerned with the mappings

$$y_1 = r_1 \cos x_1 + r_2 \cos(x_1 + x_2) \qquad y_2 = r_1 \sin x_1 + r_2 \sin(x_1 + x_2) \qquad (5)$$

The data was generated by picking x_1 uniformly from [-1.932, -0.453] and [0.453, 1.932] and picking x_2 uniformly from [0.534, 3.142]. Neal added four further inputs, two of which were copies of x_1 and x_2 corrupted by additive Gaussian noise of standard deviation 0.02, and two further irrelevant Gaussian-noise inputs with zero mean and unit variance. Independent zero-mean Gaussian noise of variance 0.0025 was then added to the outputs y_1 and y_2. I used the same datasets as Neal and MacKay, with 200 examples in the training set and 200 in the test set.

The theory described in section 2 deals only with the prediction of a scalar quantity Y, so I constructed predictors for the two outputs separately, although a joint prediction is possible within the Gaussian process framework (see co-kriging, §3.2.3 in [1]). Two experiments were conducted, the first using only the two "true" inputs, and the second one using all six inputs. For each experiment ten random starting positions were tried. The $\log(v)$'s and $\log(w)$'s were all chosen uniformly from [-3.0, 0.0], and were adapted separately for the prediction of y_1 and y_2. The conjugate gradient search algorithm was allowed to run for 100 iterations, by which time the likelihood was changing very slowly. Results are reported for the run which gave the highest probability of the training data, although in fact all runs performed

[5] In fact the parameterization $\log\theta$ was used in the search to ensure that the v's and w's stayed positive.

Procedure used	ave. squared test error
Guessing overall mean	84.4
Best result in Quinlan (1993)	10.9
Gaussian process	8.6
Neal (Bayesian network with 2 hidden layers)	6.5

Table 2 Results on the Boston housing data task.

very similarly. The results are shown in Table 1 [6] and are encouraging, as they indicate that the Gaussian process approach is giving very similar performance to two well-respected techniques. All of the methods obtain a level of performance which is quite close to the theoretical minimum error level of 1.0. It is interesting to look at the values of the w's obtained after the optimization; for the y_2 task the values were 0.243, 0.237, 0.0650, 1.7×10^{-4}, 2.6×10^{-6}, 9.2×10^{-7}, and v_0 and v_1 were 7.920 and 0.0022 respectively. The w values show nicely that the first two inputs are the most important, followed by the corrupted inputs and then the irrelevant inputs.

3.2 Boston Housing Data

The Boston Housing data has been used by several authors as a real-world regression problem (the data is available from `ftp://lib.stat.cmu.edu/datasets`). For each of the 506 census tracts within the Boston metropolitan area (in 1970) the data gives 13 input variables, including per capita crime rate and nitric oxides concentration, and one output, the median housing price for that tract.

A ten-fold cross-validation method was used to evaluate the performance, as detailed in [9]). The dataset was divided into ten blocks of near-equal size and distribution of class values (I used the same partitions as in [9]). For each block in turn the parameters of the Gaussian process were trained on the remaining blocks and then used to make predictions for the hold-out block. For each of the ten experiments the input variables and targets were linearly transformed to have zero mean and unit variance, and five random start positions used, choosing the $\log(v)$'s and $\log(w)$'s uniformly from [-3.0,0.0]. In each case the search algorithm was run for 100 iterations. In each experiment the run with the highest evidence was used for prediction, and the test results were then averaged to give the entry in Table 2.

The fact that the Gaussian process result beats the best result obtained by Quinlan (who made a reasonably sophisticated application of existing techniques) is very encouraging. It was observed that different solutions were obtained from the random starting points, and this suggests that an hierarchical Bayesian approach, as used in Neal's neural net implementation and described in section 4, may be useful in further increasing performance.

[6] The bottom three lines of the table were obtained from [7]. The MacKay result is the test error for the net with highest "evidence".

4 Discussion

I have presented a Gaussian process framework for regression problems and have shown that it produces excellent results on the two test problems tried.

In section 2 I have described maximum likelihood training of the parameter vector $\boldsymbol{\theta}$. Obviously a hierarchical Bayesian analysis could be carried out for a model M using a prior $P(\boldsymbol{\theta}|M)$ to obtain a posterior $P(\boldsymbol{\theta}|\mathcal{D}, M)$. The predictive distribution for a test point and the "model evidence" $P(\mathcal{D}|M)$ are then obtained by averaging the conditional quantities over the posterior. Although these integrals would have to be performed numerically, there are typically far fewer parameters in $\boldsymbol{\theta}$ than weights and hyperparameters in a neural net, so that these integrations should be easier to carry out. Preliminary experiments in this direction with the Hybrid Monte Carlo method [7] are promising.

I have also conducted some experiments on the approximation of neural nets (with a finite number of hidden units) by Gaussian processes, although space limitations do not allow me to describe these here. Other directions currently under investigation include (i) the use of Gaussian processes for classification problems by softmaxing the outputs of k regression surfaces (for a k-class classification problem), and (ii) using non-stationary covariance functions, so that $C(\boldsymbol{x}, \boldsymbol{x}') \neq C(|\boldsymbol{x} - \boldsymbol{x}'|)$.

REFERENCES

[1] N. A. C. Cressie, *Statistics for Spatial Data*, Wiley (1993).

[2] F. Girosi, M. Jones, and T. Poggio, *Regularization Theory and Neural Networks Architectures*, Neural Computation, Vol. 7(2) (1995), pp219–269.

[3] A. G. Journel and Ch. J. Huijbregts, *Mining Geostatistics*, Academic Press (1978).

[4] D. J. C. MacKay, *A Practical Bayesian Framework for Backpropagation Networks*, Neural Computation, Vol. 4(3) (1992), pp448–472.

[5] D. J. C. MacKay, *Bayesian Methods for Backpropagation Networks*, In J. L. van Hemmen, E. Domany, and K. Schulten, editors, Models of Neural Networks II, Springer (1993).

[6] R. M. Neal, *Bayesian Learning via Stochastic Dynamics*, in: S. J. Hanson, J. D. Cowan, and C. L. Giles, eds., Neural Information Processing Systems, Vol. 5 (1993), pp475–482. Morgan Kaufmann, San Mateo, CA,.

[7] R. M. Neal, *Bayesian Learning for Neural Networks*, PhD thesis, Dept. of Computer Science, University of Toronto (1995).

[8] T. Poggio and F. Girosi, *Networks for approximation and learning*, Proceedings of IEEE, Vol. 78 (1990), pp1481–1497.

[9] J. R. Quinlan, *Combining Instance-Based and Model-Based Learning*, in: P. E. Utgoff, ed., Proc. ML'93, Morgan Kaufmann, San Mateo, CA (1993).

[10] G. Wahba, *Spline Models for Observational Data*, Society for Industrial and Applied Mathematics, CBMS-NSF Regional Conference series in applied mathematics (1990).

Acknowledgements

I thank Radford Neal and David MacKay for many useful discussions and for generously proving data used in this paper, Chris Bishop, Peter Dayan, Radford Neal and Huaiyu Zhu for comments on earlier drafts, George Lindfield for making his implementation of the scaled conjugate gradient search routine available and Carl Rasmussen for his C implementation which runs considerably faster than my MATLAB version. This work was supported by EPSRC grant GR/J75425.

STOCHASTIC FORWARD-PERTURBATION, ERROR SURFACE AND PROGRESSIVE LEARNING IN NEURAL NETWORKS

Li-Qun Xu

Intelligent Systems Research Group, BT Research Laboratories
Martlesham Heath, Ipswich, IP5 7RE, UK.

We address the issue of progressive learning of neural networks, focusing on the situation in which the environment or the training set for a learner is of fixed size.[1] We concentrate on the phenomenon of the change in *shape* of the error surface of a neural network (defined over the weight space) as a result of presenting it with a range of *intermediate* tasks during the course of learning, and a *goal-driven mechanism* is therefore proposed and analysed. The stochastic gradient smoothing algorithm (SGSA) [14, 16] is found to be effective in implementing this idea, experiments done demonstrate the usefulness of our approach towards progressive learning.

1 Active Learning: Non-fixed vs Fixed Data Set

The findings in cognitive science have shown that a learning process is normally a bidirectional process involving the interactive actions (information exchange) between a learner and its surrounding environment [3]. In active learning of neural networks, the *learner* is a neural network of specified configuration $\mathcal{A}$ parameterised by some connection weight vector $\mathbf{W} \in \mathbb{R}^N$, learning to perform a particular task such as function mapping [8], pattern classification [11] and robot control [13] among many others. The *environment* is characterised by a training data set of fixed or non-fixed size, or some exploratory space of certain underlying structures.

Current research on active learning of neural networks has been focusing on the design of various well-defined information and/or generalisation criteria [6, 8, 13, 9, 4] based on which the selection, can be made from among a set of available data examples, of a *new* data example, which, when added to the previous training set and learned, allow the trained network has the maximum accuracy of fit to the data and improved generalisation performance [10]. Notably, this strategy imposes no restrictions on the size of the data set.

However other approaches to active learning, given that the training data set is of fixed size, follow a slight different trend which essentially emphasises the principle of *progressive* learning [11]. This is usually achieved by letting the neural network learn a succession of varied subsets that represent, on one occasion, a different level of abstraction of the final complex task. Subsequently, the response of the learner to the changeable environment – the particular subsets engaged – is monitored, and the performance, in terms of model misspecification and network variance, thus far achieved will determine what aspects of the environment the learner is to face next time.

There are various ways whereby the whole environment can be decomposed : one can consider to divide the entire data set according to sample *size* from small to large [1], the *degree of difficulty* from low to high [5], [3], etc. This way of division of the entire data set is by and large based on the results of empirical studies and

[1] which is often the case in practical applications of neural networks, especially pattern recognition.

the understanding of individual experimenters to the tasks at hand. In this paper we propose an alternative way of performing progressive learning while freeing from the difficulties of artificially decomposing the environment. In the following section we introduce the view of progressive learning in terms of dealing with the change in shape of error surfaces. In section 3 we propose to use stochastic gradient smoothing algorithm (SGSA) to implement this idea. In section 4 experiments are conducted to demonstrate the usefulness of the approach for active learning of neural networks. The paper is concluded in section 5.

2 Progressive Learning – a Goal-driven Perspective

It would be instructive if we interpret the progressive way of learning an entire environment by a neural network based on the change in *shape* of its error surface vs connection weights : Given a neural network $\mathcal{A}$ specified by a connection weight vector $\mathbf{W} \in \mathbb{R}^N$, a training set $\Theta^{(S)}$ of $|S|$ pairs of labelled examples, $\Theta^{(S)} = \{x_j, y_j\}_{j=1}^{|S|}$ describing the whole environment, an error function can then be expressed as,

$$f_{\Theta^{(S)}}(\mathbf{W}) \ : \ \mathbb{R}^N \longrightarrow \mathbb{R}^1, \tag{1}$$

the notation $\Theta^{(S)}$ in the equation is meant to show the fact that the shape of the error surface in the weight space $\mathbf{W} \in \mathbb{R}^N$ is entirely determined by the training set. (Figure 1 (a) shows a two-dimensional profile of such an error surface when a final convergence has been reached.) Consequently, the strategy of using a varied

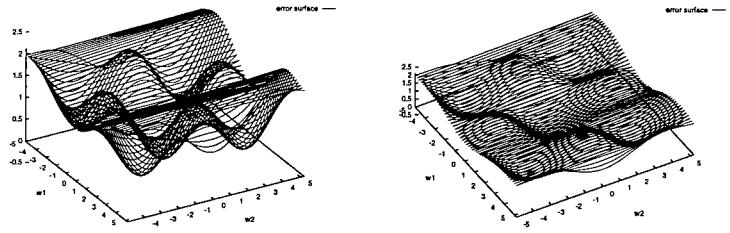

Figure 1 (a) A two-dimensional profile of an error surface with multiple valleys and ridges. (b) A smoothed version of case (a), retaining much of its main features while freeing from details – *steepness, roughness and ravine*. In between, there exist a range of *intermediate* error surfaces that may arise from either of the two mechanisms discussed below.

data subset in session k, $\Theta^{(s_k)}$, $s_k \subset S$, for the training of $\mathcal{A}$ will invariably lead to the change in shape of its error surface, or $f_{\Theta^{(s_k)}}(\mathbf{W})$, $s_k \subset S$. This is what we mean by the *data-driven mechanism* detailed in Figure 2 (a). With $\Theta^{(s_k)}$, $s_k \subset S$ being properly constructed, it is expected that the shape of the error surface will change from initially coarse and more or less smooth terrain to the final one bearing all the details but somehow with less regularities.

We are interested, however, in exploring the idea from an opposite perspective. In fact, we can manipulate the shape of the error surface by subjecting it to some mathematically smoothing operations to generate at our own disposal a sequence of *intermediate* error surfaces to achieve the same effects as that of previous strategy.

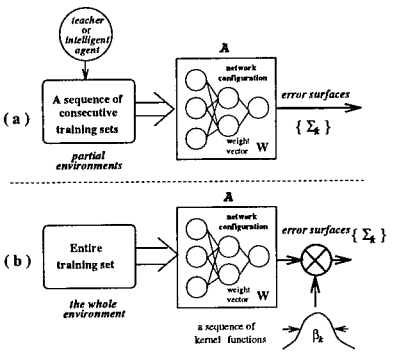

Figure 2 Two alternative mechanisms giving rise to a sequence of error surfaces $\{\mathbf{\Sigma}_k\}$ (*intermediate* tasks), given a neural network, $\mathcal{A}$, specified by its weight vector $\mathbf{W} \in \mathbb{R}^N$: see Note (i) below.

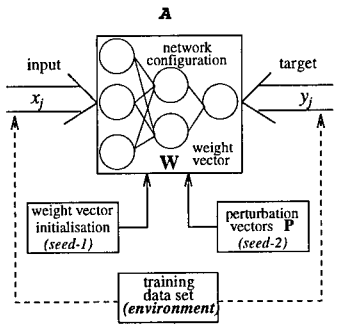

Figure 3 A model-free neural network learning paradigm for stochastic forward perturbation algorithms. See Note (ii) below.

Note (i): The *data-driven mechanism* (a) where $\{\mathbf{\Sigma}_k \equiv f_{\mathbf{\Theta}^{(s_k)}}(\mathbf{W}), s_k \subset S\}$. The learner is faced, each time, with a varied training set describing different details of the environment, and consequently has to learn a different error surface defined by the training (sub)set engaged By learning the preceding error surfaces, the weight vector $\mathbf{W} \in \mathbb{R}^N$ tends to be positioned in an advantageous location to facilitate the process of learning the following error surfaces; The *goal-driven mechanism* (b) where $\{\mathbf{\Sigma}_k \equiv \tilde{f}_{\mathbf{\Theta}^{(S)}}(\mathbf{W}, \beta_k), k = 1, 2, \cdots\}$. The learner in (b) is confronted with the entire training set $\mathbf{\Theta}^{(S)}$, or the whole environment, though the actual task for the learner at a time is a simplified version of the error surface obtainable by convolving it with an appropriate $N-$dimensional kernel function (p.d.f.) of the same family but a varied "width" β_k. Consequently, this strategy also results in a sequence of error surfaces of different shapes. Note that in (b), the convolution operation is implicitly carried out in the course of learning by the SGSA.

Note (ii): The environment is given by the training data set $\mathbf{\Theta}^{(S)} = \{x_j, y_j\}_{j=1}^{|S|}$. All the connection weights in $\mathcal{A}$ are arranged as a weight vector $\mathbf{W} \in \mathbb{R}^N$. In this paradigm an extra dimension of randomness characterised by the perturbation vectors $\mathbf{P}$ can be explored.

Figure 2 (b) illustrates this idea which we call *goal-driven mechanism*, where the *sequence of error surfaces* at the output end can be equally viewed as those ranging between Figure 1 (b), a smooth shallow surface with established prominent characteristics, and Figure 1 (a), a surface with all the details (and idiosyncrasies). It is from this viewpoint we argue that the stochastic forward-perturbation algorithms [15] – the category of learning algorithm that has its roots nurtured by the theory of stochastic approximation of nonlinear dynamical processes – can be employed to accomplish the task of progressive learning without caring about how to divide the training set.

3 Mathematical Analysis

As opposed to the back-propagation (BP) algorithm, the operations of updating the weight vector $\mathbf{W}$ by stochastic forward-perturbation algorithms generally follow an

F – P – F – G pattern (Figure 3) i.e. one *forward* propagation of the training set through $\mathcal{A}$ to measure as it currently stands error the function; one *perturbation* of the weight vector with some controllable noises $\mathbf{P} \in \mathbb{R}^N$; and another *forward* propagation to measure the response of $\mathcal{A}$ due to the perturbation just introduced; based on these measurements a gradient estimation can be taken by employing some intuitive *difference* approximation or more subtle *correlation* methods. The estimated gradient can then be incorporated into stochastic approximation algorithms to update the weight vector.

In the following, the advanced algorithm called *stochastic gradient smoothing algorithm* [16] is employed. According to Figure 2 (b), the following smoothing operation has been invoked (Note that the data-dependent notation $\Theta^{(S)}$ has been dropped.)

$$\begin{aligned} \tilde{f}(\mathbf{W}, \beta) &= f(\mathbf{W}) \otimes [\hat{G}(-\mathbf{W}, \beta) + \hat{G}(\mathbf{W}, \beta)] \\ &= \int_{\mathbb{R}^N} \hat{G}(\mathbf{\Lambda}, \beta)\, [f(\mathbf{W} + \mathbf{\Lambda}) + f(\mathbf{W} - \mathbf{\Lambda})] d\mathbf{\Lambda} \end{aligned} \tag{2}$$

where the symbol '$\otimes$' denotes the convolution operator. Following some mathematical manipulations, one stochastic gradient estimator ξ_k is shown as follows :

$$\xi_k \equiv \hat{\nabla}_w \tilde{f}(\hat{\mathbf{W}}_k, \beta_k) = \frac{1}{n_k} \frac{1}{2\beta_k} \sum_{i=1}^{n_k} \mathbf{\Lambda}_i\, \delta^{(i)} f(\hat{\mathbf{W}}_k) \tag{3}$$

where $\mathbf{\Lambda}_i$ is a random (perturbation) vector generated from an independent Gaussian p.d.f. $G(\mathbf{\Lambda})$. The scalar β_k, referred to as the *smoothing factor*, determines the *width* of the underlying p.d.f. or the *perturbation strength* of the generated random vectors. Finally, the difference in the cost function due to the ith perturbation of $\hat{\mathbf{W}}_k$ is $\delta^{(i)} f(\hat{\mathbf{W}}_k)$. Based on the estimated gradient ξ_k, the weight vector $\hat{\mathbf{W}}_k$ is updated according to,

$$\mathbf{d}_k = \rho_k \cdot \xi_k + (1 - \rho_k) \cdot \mathbf{d}_{k-1}, \tag{4}$$

$$\hat{\mathbf{W}}_{k+1} = \hat{\mathbf{W}}_k - \eta_k \cdot \mathbf{d}_k \tag{5}$$

where the *direction* vector $\mathbf{d}_k = (d_{k1}\ d_{k2}\ \cdots\ d_{kN})' \in \mathbb{R}^N$ represents a running average over the current gradient estimate ξ_k and the previous direction vector $\mathbf{d}_{k-1}$. The other two important parameters appeared in the above formulas include η_k – the learning rate (or adaptive step size) and ρ_k – the accumulating factor. It is desirable that with the iteration $k \to \infty$, $\eta_k \to 0$, $\rho_k \to 1$. The parameters η_k and ρ_k are locally adaptable.

4 Experimental Results

A simulated two-class pattern classification problem, of which the details can be found in [7], is used to demonstrate our approach for active learning of neural networks. The distributions of these two classes (C_1 and C_0) are overlapped, and a complete separation of their examples is impossible even for an optimal classifier. In the experiments, the training set consists of 200 examples with 100 drawn from each class, while the test set contains 1000 examples with 500 belonging to each class. The neural network used for this task has a fully-connected three-layer 2 – 4 – 1 structure, amounting to 17 weights including biases. The single output of the trained network should ideally be for examples in C_1 a "1" and in C_0 a "0" when being shown the unseen data in the testing phase.

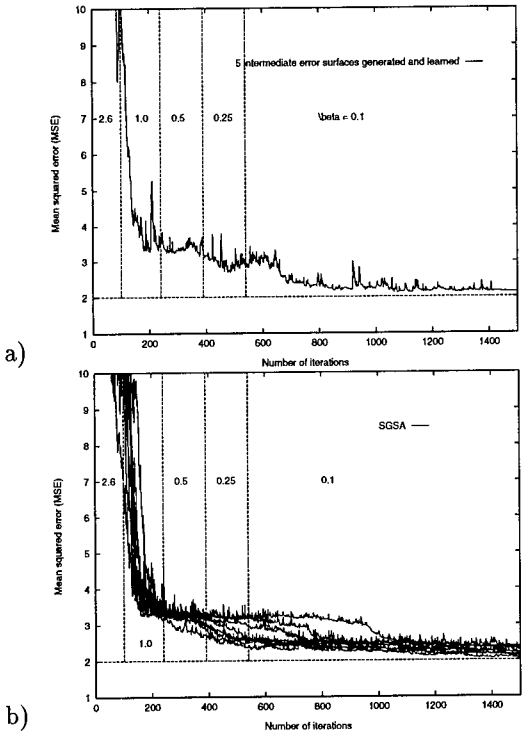

Figure 4 (a) A typical learning trajectory achieved by the SGSA. The vertical dashed lines mark the boundaries where a new *intermediate* error surface, characterised by a different value of β_k shown along the lines, is encountered by the learner. In this case, there are 4 intermediate error surfaces (where β_k assumes a value of 2.6, 1.0, 0.5 and 0.25 in order) to be learned before the learner faces the final task (where $\beta_k = 0.1$) which is approximate to the error surface imposed by the complete environment for which $\beta_k = 0$. (b) A set of 10 learning trajectories for the test problem by the SGSA with different initial weight vectors.

For the problem, 10 trials are performed, each starting with a different weight vector $\hat{\mathbf{W}}_0$ having random values ranging between ± 0.5. Figure 4 (a) shows a typical learning trajectory, the mean squared error vs number of iterations, achieved by the SGSA.

Table 1 summarises the average performance among ten trials for the SGSA, where E_{tr} denotes the mean squared error (MSE) for the training set; n_{tr} gives, up to the indicated iterations, the number of examples yet to be correctly learned in the training set (200 examples in total); n_{te} shows the generalisation performance measured by the number of examples that are still misclassified, up to the given training iterations, in the test set (1000 examples in total). An important result is that the generalisation performance given by the n_{te} tends to saturate rather than deteriorate with more iterations, as is not the case with the experiments using deterministic Quick-prop algorithm (an advanced version of the BP algorithm) [15].

ALGO.	Iter.	700	800	900	1000	1100	1200	1300	1400	1500
SGSA	E_{tr}	2.658	2.551	2.477	2.410	2.367	2.313	2.290	2.261	2.229
	n_{tr}	11.4	9.9	9.7	9.6	8.9	8.6	8.3	8.4	8.3
	n_{te}	66.9	66.0	64.6	62.2	62.1	62.5	63.2	61.9	61.9

Table 1 The average performance among 10 trials of the SGSA at selected iterations when applied to the simulated two-class pattern classification problem.

Thus the SGSA compares favourably with the Quick-prop in this regard. Figure 4 (b) describes the corresponding set of 10 learning trajectories obtained.

5 Summary

An alternative way has been explored for active learning of neural networks, focusing on the viewpoint of interpreting the error surface imposed by the whole training set (a certain task) in terms of a range of its intermediate versions, or a set of intermediate tasks. We analysed two different perspectives, called, respectively, *data-driven mechanism* and *goal-driven mechanism*, that give rise to such a range of error surfaces. We argued that the later approach could well be an effective way to control the amount of information about a complex environment at a time accessible to a learner, therefore fulfilling the same objective (of progressive learning) as the former without explicitly decomposing the environment in a hard fashion. The stochastic gradient smoothing algorithm (SGSA) was employed to implement this idea. Experiments have been conducted to support our claims. Further theoretical studies of this issue are needed.

REFERENCES

[1] C. Cachin, *Neural Networks*, Vol. 7(1) (1994).
[2] D.A. Cohn, Z. Ghahramani, Z., M.I. Jordan, in: [12].
[3] J.E. Elman, *Technical Report CRL-9101*, UCSD (1991).
[4] A. Krogh, J. Vedelsby, in [12].
[5] J. Ludik, I. Cloete, *Proc. of ESANN* (April 1994), Brussels.
[6] D.J.C. MacKay, *Neural Computation*, Vol. 4(4) (1992).
[7] L. Niles, H. Silverman et al., *Proc. of ICASSP'89*, Glasgow (1989).
[8] M. Plutowski, H. White, *Technical Report CS91-180*, UCSD (1991).
[9] P. Sollich, *Physical Review E*, Vol. 49 (1994).
[10] E.M. Strand, W.T. Jones, *Proc. of IJCNN* Vol. I, Baltimore (1992).
[11] N. Szilas, E. Ronco, *Proc. of ECCS'95*, Saint-Malo, France (1995).
[12] G. Tesauro, D.S. Touretzky, and T.K. Leen eds., *Advances in Neural Information Processing Systems 7*, MIT Press, Cambridge, MA (1995).
[13] S.B. Thrun, in D.A. White and D.A. Sofge (eds.), *Handbook of intelligent control: Neural, Fuzzy and Adaptive Approaches*, Van Nostrand Reinhold, Kentucky (1993).
[14] L.Q. Xu, T.J. Hall, *Proc. of ICANN'94*, Naples, Italy (1994).
[15] L.Q. Xu, *Proc. of EANN'95*, Helsinki, Finland (1995).
[16] L.Q. Xu, T.J. Hall, submitted to *Neural Networks*, (May 1995).

Acknowledgements

This research was conducted at the University of Abertay, Dundee, and was funded in part by a grant from the Nuffield Foundation.

DYNAMICAL STABILITY OF A HIGH-DIMENSIONAL SELF-ORGANIZING MAP

Howard Hua Yang

Lab for Information Representation, FRP, RIKEN, 2-1 Hirosawa, Wako-Shi, Saitama 351-01, Japan. Email: hhy@murasaki.riken.go.jp

The convergence and the convergence rate of one self-organization algorithm for the high-dimensional self-organizing map in the linearized Amari model are studied in the context of stochastic approximation. The conditions on the neighborhood function and the learning rate are given to guarantee the convergence. It is shown that the convergence of the algorithm can be accelerated by averaging.

Keywords: high-dimensional self-organizing map, neighborhood function, convergence, stochastic approximation, acceleration by averaging.

1 Introduction

The self-organizing neural networks were found in modeling some self-organized phenomena in nervous systems. The typical models are those given by Willshaw and von der Malsburg (1976)[14], Grossberg (1976)[8], Amari (1980)[1], and Kohonen (1982)[9]. These self-organization systems can alter their internal connections to represent the statistical features and topological relations in an input space.

The self-organizing maps (SOMs) are expressed by the weights of the self-organizing networks. They are very effective in modeling the topographic mapping among neural fields. Although the SOMs are widely used in neural modeling and applications, the theory of the SOMs is far from being complete. The question whether the self-organizing maps converge to the topological correct mappings is still open especially in the high dimensional case.

There are many models for the SOMs. Due to the space limit we only consider Amari's nerve field model[1, 2]. Another important SOM model is the feature map[9]. The stability of the feature map is discussed in [3, 6, 7, 10, 12].

The stability of the SOM in the nerve field model is analyzed in [1, 5, 13, 15]. The existing convergence results are most for the one-dimensional model. It is very difficult to analyze the stability of the SOM in any high dimension. The results in [5, 15] are only valid for some special cases of the linearized Amari model. We shall formulate the linearized Amari model in any high dimension and discuss not only the convergence but also the convergence rate of the self-organization algorithm for updating the weights. The approach used can also be used to analyze the stability of the feature map.

2 High-dimensional Self-organizing Maps

Let the K-dimensional grid $\mathcal{L}_K = \{0, 1, \cdots, N\}^K$ of $(N+1)^K$ neurons be the presynaptic field in the Amari model. A neuron in $\mathcal{L}_K$ is denoted by $J = (j_1, \cdots, j_K) \in \mathcal{L}_K$.

Let $\mathcal{W}_K$ be the space of all mappings $W = W(J) : \mathcal{L}_K \to \mathcal{C}_n \subseteq R^n$ where each $W(J)$ is a column vector in R^n. The weight vectors in $\mathcal{W}_K$ are labeled by the neurons in $\mathcal{L}_K$.

2.1 High Dimensional Topographic Map

Let us consider a system consisting of a presynaptic field $\mathcal{L}_K$ and a postsynaptic field $\mathcal{C}_n$. The neighborhood relation between each pair of neurons in $\mathcal{L}_K$ is determined by

their relative positions in $\mathcal{L}_K$. A high dimensional topographic map is an ordered mapping in $\mathcal{W}_K$ under which the neighborhood relation in $\mathcal{L}_K$ is preserved in $\mathcal{C}_n$. To achieve a topographic map, we choose a random mapping in $\mathcal{W}_K$, then use the following algorithm to update the mapping recursively:

$$W_{t+1}(J) = \begin{cases} (1-\lambda_t)W_t(J) + \frac{\lambda_t}{c_t}\sum_{J'\in N_c(t)} W_t(J'), & J \in N_c(t) \bigcap \mathcal{L}_K^0 \\ W_t(J), & J \in \mathcal{L}_K^0 - N_c(t) \\ B(J) \text{ (boundary condition)}, & J \in \delta\mathcal{L}_K \end{cases} \quad (1)$$

where

λ_t is a learning rate, $\mathcal{L}_K^0 = \{1, \cdots, N-1\}^K$ the inner lattice of $\mathcal{L}_K$,
$\delta\mathcal{L}_K = \mathcal{L}_K - \mathcal{L}_K^0$, $N_c(t) = \sigma_t(I_t)$ a neighborhood set,
$I_t = (i_1(t), \cdots, i_K(t))$ a random stimulus process on $\mathcal{L}_K$,
$\sigma_t(I)$ a neighborhood set around I such that $\sigma_t(I) \subseteq \mathcal{L}_K$ for each $I \in \mathcal{L}_K$ and t, and c_t the number of points in the set $N_c(t)$.

The equation (1) is a linearized version of the learning equation in [1]. It does not update the mapping on the boundary of $\mathcal{L}_K$. But the boundary condition will affect the map on $\mathcal{L}_K^0$ (the inner lattice) whenever the neighborhood set touches the boundary of the grid $\mathcal{L}_K$, and eventually shape the topographic map.
Let $h_t(I,J) = \mathbf{1}_{(J\in\sigma_t(I)\bigcap\mathcal{L}_K^0)}$ be the characteristic function of the set $\sigma_t(I)\bigcap\mathcal{L}_K^0$. The equation (1) can be rewritten as the following:

$$W_{t+1}(J) = W_t(J) - \lambda_t h_t(I_t,J)\{W_t(J) - \frac{1}{c_t}\sum_{J'\in\mathcal{L}_K^0} h_t(I_t,J')W_t(J')\}$$
$$+\frac{\lambda_t}{c_t}h_t(I_t,J)\sum_{J'\in\delta\mathcal{L}_K} h_t(I_t,J')B(J') \quad (2)$$

where $c_t = \sum_{J\in\mathcal{L}_K} h_t(I_t,J)$. Note from the definition of c_t, it is easy to show that $W_t(J)$ is bounded.
In the rest of this paper, we assume a general neighborhood function $h_t(I,J) \geq 0$ on $\mathcal{L}_K \times \mathcal{L}_K$ in (2). Let the neurons in $\mathcal{L}_K^0$ be arranged in the dictionary order $\{J_1, J_2, \cdots, J_m\}$ by their indexes in $\mathcal{L}_K^0$, where $J_1 = (1, \cdots, 1)$, $J_2 = (1, \cdots, 1, 2)$, $\cdots$, $J_m = (N-1, \cdots, N-1)$ and $m = (N-1)^K$. Each mapping

$$W_t = (W_t(J_1), \cdots W_t(J_m))$$

is a $n \times m$ matrix. Using w_t^i to denote the transpose of the i-th row of W_t, we find the following vector form for (2):

$$w_{t+1}^i = w_t^i - \lambda_t U_t w_t^i + \frac{\lambda_t}{c_t}u_t u_t^T w_t^i + \lambda_t b_t^i \quad (3)$$

where $(\cdot)^T$ denotes the transpose, $u_t = (h_t(I_t,J_1), h_t(I_t,J_2), \cdots, h_t(I_t,J_m))^T$, $U_t = diag(u_t)$, $b_t^i = \frac{1}{c_t}u_t\sum_{J'\in\delta\mathcal{L}_K} h_t(I_t,J')B^i(J')$.
To analyze the convergence of the algorithm (2), we rewrite the system (3) as:

$$w_{t+1}^i = w_t^i - \lambda_t(Q_t w_t^i - b_t^i) = w_t^i - \lambda_t(\bar{Q}_t w_t^i - \bar{b}_t^i + \xi_t^i) \quad (4)$$

where $Q_t = U_t - \frac{1}{c_t}u_t u_t^T$, $\bar{Q}_t = E[Q_t]$, $\bar{b}_t^i = E[b_t^i]$, $\xi_t^i = (Q_t - \bar{Q}_t)w_t^i - (b_t^i - \bar{b}_t^i)$, and ξ_t^i is a martingale-difference process, i.e., $E[\xi_t^i|\mathcal{F}_{t-1}] = 0$ for $\mathcal{F}_t = \sigma(I_0, \cdots, I_t)$.
We need the following assumptions:

A1 $h_t(I,J) \to h(I,J)$ and $c_t \to c$ (a positive constant) as $t \to \infty$.

A2 I_t is a independent random sequence in $\mathcal{L}_K^0$ with the probability distribution $\{P(J_k)\}$.

Denote

$$u(I) = (h(I,J_1),\cdots,h(I,J_m))^T,$$

$$Q(I) = diag(u(I)) - \frac{1}{c}u(I)u(I)^T, \quad Q = \sum_{k=1}^{m} Q(J_k)P(J_k),$$

$$b^i(I) = \frac{1}{c}u(I)\sum_{J'\in\delta\mathcal{L}_K} h(I,J')B^i(J'), \quad b^i = \sum_{k=1}^{m} b^i(J_k)P(J_k)$$

From (4), we have

$$w_{t+1}^i = w_t^i - \lambda_t(Qw_t^i - b^i + \xi_t^i + \eta_t^i) \tag{5}$$

where $\eta_t^i = (\bar{Q}_t - Q)w_t^i - (\bar{b}_t^i - b^i) \to 0$ as $t \to \infty$ because of **A1**.
Let $m^i = Q^{-1}b^i$ be the stationary state of the system (5). The next theorem shows that W_t^T almost surely converges to $M = (m^1,\cdots,m^n)$.

Theorem 1 *Under the assumptions* **A1** *and* **A2**, *if* $Q > 0$ *(positive definite) and the learning rate* $\lambda_t > 0$ *satisfies the following conditions:*

$$\sum_t \lambda_t = \infty, \quad \sum_t \lambda_t^2 < \infty, \tag{6}$$

then for $i = 1,\cdots,n$, $w_t^i \to m^i$ *a.s. (almost sure convergence).*

Proof Let x_t be generated by the following equation: $x_{t+1} = x_t - \lambda_t(Q(x_t - m^i) + \xi_t^i)$. Let $h(x) = Q(x - m^i)$, then $(x-m^i)^TQh(x) = (x-m^i)^TQ^TQ(x-m^i) > 0$, $\forall x \neq m^i$. Therefore, applying Gladyshev's Theorem (see Theorem 2.2 in [4]), we have $x_t \to m^i$, a.s.
Let $y_t = w_t^i - x_t$, then y_t satisfies $y_{t+1} = y_t - \lambda_t(Qy_t + \eta_t^i)$. Since $Q > 0$ and η_t^i tends to zero as t tends to infinity, y_t also tends to zero. Therefore, $w_t^i \to m^i$, a.s. □
Note an example is given in [15] where $Q > 0$. When the first condition in (6) is not satisfied, the map may still converge but not to the desired stationary state.
We shall use an approach in [11] to discuss the convergence of $\overline{W}_t = \frac{1}{t}\sum_{s=0}^{t-1} W_t$ assuming that the learning rate satisfies one of the following conditions:

$$\lambda_t \equiv \lambda, \quad 0 < \lambda < 2(\min_i \mu_i(Q))^{-1}. \tag{7}$$

$$\lambda_t \downarrow 0, \quad \frac{\lambda_t - \lambda_{t+1}}{\lambda_t} = o(\lambda_t) \tag{8}$$

where $\{\mu_i(Q)\}$ are eigenvalues of Q. Note the learning rate $\lambda_t \propto t^{-\alpha}$ with $0 < \alpha < 1$ satisfies the condition (8).
The next theorem gives the convergence rate of the averaged weight $\overline{W}_t$. It also shows that $\overline{W}_t^T$ converges to M in mean square.

Theorem 2 *Let* $Q > 0$, *the learning rate satisfy (7) or (8), and the following conditions hold:*

A3 $\gamma > \frac{1}{2}$, $\bar{Q}_t - Q = O(t^{-\gamma})$, *and* $\bar{b}_t^i - b^i = O(t^{-\gamma})$;

A4 *for each* J, $\sup_t \sum_{k=1}^m |h_t(J_k, J) - \bar{h}_t(J)|^\beta P(J_k) < \infty$, *where* $\beta > 2$ *and* $\bar{h}_t(J) = \sum_{k=1}^m h_t(J_k, J) P(J_k)$;

A5 *for each* J *and* J', $\sup_t \sum_{k=1}^m |h_t(J_k, J)h_t(J_k, J') - \bar{h}_t(J, J')|^\beta P(J_k) < \infty$, *where* $\bar{h}_t(J, J') = \sum_{k=1}^m h_t(J_k, J)h_t(J_k, J')P(J_k) < \infty$;

A6 $lim_{t\to\infty} E[\xi_t^i(\xi_t^i)^T] = S^i > 0$.

Denote $V = Q^{-1}S^iQ^{-1}$. *Then for* $\bar{w}_t^i = \frac{1}{t}\sum_{s=0}^{t-1} w_t^i$, *we have*

$$\sqrt{t}(\bar{w}_t^i - m^i) \xrightarrow{\mathcal{D}} N(0, V)$$
$$lim_{t\to\infty} E[t(\bar{w}_t^i - m^i)(\bar{w}_t^i - m^i)^T] = V. \tag{9}$$

Proof From **A4** and **A5**, we have $\sup_t E[|Q_t - \bar{Q}_t|^\beta] < \infty$ and $\sup_t E[|b_t^i - \bar{b}_t^i|^\beta] < \infty$. Therefore,

$$\sup_t E[|\xi_t^i|^\beta] < \infty. \tag{10}$$

Because w_t^i is bounded, we have $\sup_t E[|\xi_t^i|^2|\mathcal{F}_{t-1}] < \infty$. From (10), we have

$$\lim_{C\to\infty} \overline{\lim}_{t\to\infty} E[|\xi_t^i|^2 \mathbf{1}_{(|\xi_t^i|>C)}|\mathcal{F}_{t-1}] = 0, \quad a.s.$$

So Assumptions 2.1-2.5 in [11] are satisfied. However, we cannot apply the results there directly due to the term η_t^i in the system (5). We can use the same approach in [11] to get the following:

$$\sqrt{t}\bar{\Delta}_t = \frac{1}{\sqrt{t}}\alpha_t\bar{\Delta}_0 - \frac{1}{\sqrt{t}}\sum_{s=1}^{t-1} Q^{-1}(\xi_s^i + \eta_s^i) - \frac{1}{\sqrt{t}}\sum_{s=1}^{t-1} V_s^t(\xi_s^i + \eta_s^i), \tag{11}$$

where $\bar{\Delta}_t = \bar{w}_t^i - m^i$, and $\bar{\Delta}_0 = w_0^i - m^i$, $\alpha_t = \alpha_1^t$, $V_j^t = \alpha_j^t - Q^{-1}$, with $\alpha_j^t = \lambda_j \sum_{i=j}^{t-1}\prod_{k=j+1}^{i}(I - \lambda_k Q)$, α_t and V_j^t are bounded, and $\lim_{t\to\infty}\frac{1}{t}\sum_{j=1}^{t-1}\|V_j^t\| = 0$. Noticing the assumption **A3** implies $\eta_t^i = O(t^{-\gamma})$,

$$\frac{1}{t}\sum_{s=1}^{t-1}\eta_s^i(\eta_s^i)^T \to 0, \quad \text{and} \quad \frac{1}{\sqrt{t}}\sum_{s=1}^{t-1} Q^{-1}\eta_s^i \to 0, \quad \text{as} t \to \infty,$$

we can apply the proofs in [11] to (11) and conclude that $\sqrt{t}(\bar{w}_t^i - m^i)$ is asymptotically normal with zero mean and the covariance matrix V, and (9) holds. □

Theorem 2 allows us to use a small constant learning rate or even the learning rate $\lambda_t \propto t^{-\alpha}$ with $0 < \alpha < \frac{1}{2}$ which tends to zero slower than $\frac{1}{\sqrt{t}}$. The assumption $\beta > 2$ in **A4** and **A5** can be relaxed to $\beta = 2$ if we only want to obtain (9).

Note we showed the convergence of the SOM but we did not show that the stationary states are the topographic mappings which preserves the topology. Based on the simulation results in [5, 13] we believe that the SOM converges to a topographic map, or a micro-structure consisting of several topographic sub-maps.

3 Conclusion

The convergence of the learning algorithm for updating the SOM is studied. The conditions on the neighborhood function and the learning rate have been found to guarantee the convergence. The learning algorithm can be accelerated by averaging the weight vectors in the training history. For the learning algorithm with averaging, the convergence rate has been found.

REFERENCES

[1] S.-I. Amari, *Topographic organization of nerve fields*, Bulletin of Mathematical Biology, Vol. 42 (1980), pp339–364.

[2] S.-I. Amari, *Field theory of self-organizing neural nets*, IEEE Trans. on Systems, Man and Cybernetics, Vol. 13(5) (September/October 1983), pp741–748.

[3] M. Budinich and J. G. Taylor, *On the ordering conditions for self-organising maps*, Neural Computation, Vol. 7(2) (March 1995).

[4] Han-Fu Chen, *Recursive Estimation and Control for Stochastic Systems*, John Wiley & Sons, Inc. (1985).

[5] M. Cottrell and J. C. Fort, *A stochastic model of retinotopy: A self organizing process*, Biological Cybernetics, Vol. 53 (1986), pp405–411.

[6] M. Cottrell, J. C. Fort, and G. Pages, *Two or three things that we know about the kohonen algorithm*, in: Proc. ESANN94 Conf., De Facto Ed., Brussels (April 1994).

[7] E. Erwin, K. Obermayer, and K. Schulten, *Self-organizing maps: Ordering, convergence properties and energy functions*, Biological Cybernetics, Vol. 67 (1992), pp47–55.

[8] S. Grossberg, *Adaptive pattern classification and universal recording: I. Parallel development and coding of neural feature detectors*, Biological Cybernetics, Vol. 22 (1976), pp121–134.

[9] T. Kohonen, *Self-organized formation of topologically correct feature maps*, Biological Cybernetics, Vol. 43 (1982), pp59–69.

[10] Z.-P. Lo and B. Bavarian, *On the Rate of Convergence in Topology Preserving Neural Networks*, Biological Cybernetics, Vol. 65 (1991), pp55–63.

[11] T. Polyak and A. B. Juditsky, *Acceleration of stochastic approximation by averaging*, SIAM Journal of Control and Optimization, Vol. 30(4) (July 1992), pp838–855,.

[12] H. Ritter and K. Schulten, *Convergence properties of kohonen's topology conserving maps: Fluctuations, stability, and dimension selection*, Biological Cybernetics, Vol. 60 (1988), pp59–71.

[13] A. Takeuchi and S.-I Amari, *Formation of topographic maps and columnar microstructures*, Biological Cybernetics, Vol. 35 (1979), pp63–72.

[14] D.J. Willshaw and C. von der Malsburg, *How patterned neural connections can be set up by self-organization*, Proceedings of the Royal Society of Longdon, Vol. B 194 (1976), pp431–445.

[15] Hua Yang and T. S. Dillon, *Convergence of self-organizing neural algorithms*, Neural Networks, Vol. 5 (1992), pp485–493.

MEASUREMENTS OF GENERALISATION BASED ON INFORMATION GEOMETRY

Huaiyu Zhu* and Richard Rohwer**

Neural Computing Research Group, Department of Computer Science and Applied Mathematics, Aston University, Birmingham B4 7ET, UK

** Current address: Santa Fe Institute, 1399 Hyde Park Road, Santa Fe, NM87501, USA. Email: zhuh@santafe.edu*

*** Current address: Prediction Co., 320 Aztec Street, SuiteB, Santa Fe, NM87501, USA.*

Neural networks are statistical models and learning rules are estimators. In this paper a theory for measuring generalisation is developed by combining Bayesian decision theory with information geometry. The performance of an estimator is measured by the information divergence between the true distribution and the estimate, averaged over the Bayesian posterior. This unifies the majority of error measures currently in use. The optimal estimators also reveal some intricate interrelationships among information geometry, Banach spaces and sufficient statistics.

1 Introduction

A neural network (deterministic or stochastic) can be regarded as a parameterised statistical model $P(y|x,w)$, where $x \in X$ is the input, $y \in Y$ is the output and $w \in W$ is the weight. In an environment with an input distribution $P(x)$, it is also equivalent to $P(z|w)$, where $z := [x,y] \in Z := X \times Y$ denotes the combined input and output as data [11]. Learning is the task of inferring w from z. It is a typical statistical inference problem in which a neural network model acts as a "likelihood function", a learning rule as an "estimator", the trained network as an "estimate" and the data set as a "sample". The set of probability measures on sample space Z forms a (possibly infinite dimensional) differential manifold $\mathcal{P}$ [2, 16]. A statistical model forms a finite-dimensional submanifold $\mathcal{Q}$, composed of representable distributions, parameterised by weights w acting as coordinates.

To infer w from z requires additional information about w. In a Bayesian framework such auxiliary information is represented by a prior $P(p)$, where p is the true but unknown distribution from which z is drawn. This is then combined with the likelihood function $P(z|p)$ to yield the posterior distribution $P(p|z)$ via the Bayes formula $P(p|z) = P(z|p)P(p)/P(z)$.

An estimator $\tau : Z \to \mathcal{Q}$ must, for each z, fix one $q \in \mathcal{Q}$ which in a sense approximate p. [1] This requires a measure of "divergence" $D(p,q)$ between $p,q \in \mathcal{P}$ defined independent of parameterisation. General studies on divergences between probability distributions are provided by the theory of information geometry (See [2, 3, 7] and further references therein). The main thesis of this paper is that generalisation error should be measured by the posterior expectation of the information divergence between true distribution and estimate. We shall show that this retains most of the mathematical simplicity of mean squared error theory while being generally applicable to any statistical inference problems.

[1] Some Bayesian methods give the entire posterior $P(p|z)$ instead of a point estimate q as the answer. They will be shown later to be a special case of the current framework.

2 Measurements of Generalisation

The most natural "information divergence" between two distribution $p, q \in \mathcal{P}$ is the δ-divergence defined as [2] [2]

$$D_\delta(p,q) := \frac{1}{\delta(1-\delta)}\left(1 - \int p^\delta q^{1-\delta}\right), \qquad \forall \delta \in (0,1). \tag{1}$$

The limits as δ tends to 0 and 1 are taken as definitions of D_0 and D_1, respectively. Following are some salient properties of the δ-divergences [2]:

$$D_\delta(p,q) = D_{1-\delta}(q,p) \geq 0. \qquad D_\delta(p,q) = 0 \iff p = q. \tag{2}$$

$$D_0(q,p) = D_1(p,q) = K(p,q) := \int p \log \frac{p}{q}. \tag{3}$$

$$D_{1/2}(p,q) = D_{1/2}(q,p) = 2\int \left(\sqrt{p} - \sqrt{q}\right)^2. \tag{4}$$

$$D_\delta(p, p+\Delta p) \approx \frac{1}{2}\int \frac{(\Delta p)^2}{p} \approx \frac{1}{2}\langle(\Delta \log p)^2\rangle. \tag{5}$$

The quantity $K(p,q)$ is the Kullback-Leibler divergence (cross entropy). The quantity $D_{1/2}(p,q)$ is the Hellinger distance. The quantity $\int (\Delta p)^2/p$ is usually called the χ^2 distance between two nearby distributions.

Armed with the δ-divergence, we now define the generalisation error

$$E_\delta(\tau) := \int_p P(p) \int_z P(z|p) D_\delta(p, \tau(z)), \qquad E_\delta(q|z) := \int_p P(p|z) D_\delta(p,q), \tag{6}$$

where p is the true distribution, τ is the learning rule, z is the data, and $q = \tau(z)$ is the estimate. A learning rule τ is called δ-optimal if it minimises $E_\delta(\tau)$. A probability distribution q is called a δ-optimal estimate, or simply a δ-estimate, from data z, if it minimises $E_\delta(q|z)$. The following theorem is a special case of a standard result from Bayesian decision theory.

Theorem 1 (Coherence) *A learning rule τ is δ-optimal if and only if for any data z, excluding a set of zero probability, the result of training $q = \tau(z)$ is a δ-estimate.*

Definition 2 (δ-coordinate) *Let $\mu := 1/\delta$, $\nu := 1/(1-\delta)$. Let L_μ be the Banach space of μth power integrable functions. Then L_μ and L_ν are dual to each other as Banach spaces. Let $p \in \mathcal{P}$. Its δ-coordinate is defined as $l_\delta(p) := p^\delta/\delta \in L_\mu$ for $\delta > 0$, and $l_0(p) := \log p$ [2]. Denote by $l_{1/\delta}$ the inverse of l_δ.*

Theorem 3 (δ-estimator in $\mathcal{P}$) *The δ-estimate $\widehat{q} \in \mathcal{P}$ is uniquely given [14] by $\widehat{q} \sim l_{1/\delta}(\int P(p|z) l_\delta(p))$.*

3 Divergence between Finite Positive Measures

One of the most useful properties of the least mean square estimate is the so called $MSE = VAR + BIAS^2$ relation, which also implies that, for a given linear space W, the LMS estimate of w within W is given by the projection of the posterior mean $\widehat{w}$ onto W. This is generalised to the following theorem [16], applying the generalised Pythagorean Theorem for δ-divergences [2].

[2] This is essentially Amari's α-divergence, where $\alpha \in [-1,1]$, re-parameterised by $\delta = (1-\alpha)/2 \in [0,1]$ for technical convenience, following [6].

Theorem 4 (Error decomposition in $\mathcal{Q}$) *Let $\mathcal{Q}$ be a δ-flat manifold. Let $P(p)$ be a prior on $\mathcal{Q}$. Then $\forall q \in \mathcal{Q}$, $\forall z \in Z$,*

$$E_\delta(q|z) = E_\delta(\widehat{p}|z) + D_\delta(\widehat{p}, q), \tag{7}$$

where $\widehat{p}$ is the δ-estimate in $\mathcal{Q}$.

To apply this theorem it is necessary to extend the definition of δ-divergence to $\widetilde{\mathcal{P}}$, the space of finite positive measures, which is δ-flat for any δ for a finite sample space Z [2], following suggestions in [2].

Definition 5 (δ-divergence on $\widetilde{\mathcal{P}}$) *The δ-divergence on $\widetilde{\mathcal{P}}$ is defined by*

$$D_\delta(p, q) := \frac{1}{\delta(1-\delta)} \int \left(\delta p + (1-\delta)q - p^\delta q^{1-\delta}\right) \tag{8}$$

This definition retains most of the important properties of δ-divergence on $\mathcal{P}$, and reduces to the original definition when restricted to $\mathcal{P}$. It has the additional advantage of being the integral of a positive measure, making it possible to attribute the divergence between two measures to their divergence over various events [16]. In particular, the generalised cross entropy is [16]

$$K(p, q) := \int \left(q - p + p \log \frac{p}{q}\right). \tag{9}$$

The δ-divergence defines a differential structure on $\widetilde{\mathcal{P}}$. The Riemannian geometry and the δ-affine connections can be obtained by the Eguchi relations [2, 7] The most important advantage of this definition is that the following important theorem is true and can be proved by pure algebraic manipulation [16].

Theorem 6 (Error Decomposition on $\widetilde{\mathcal{P}}$) *Let $P(p)$ be a distribution over $\widetilde{\mathcal{P}}$. Let $q \in \widetilde{\mathcal{P}}$. Then*

$$\langle D_\delta(p, q)\rangle = \langle D_\delta(p, \widehat{p})\rangle + D_\delta(\widehat{p}, q), \tag{10}$$

where $\widehat{p}$ is the δ-average of p given by $\widehat{p}^\delta := \langle p^\delta \rangle$.

Theorem 7 (δ-estimator in $\widetilde{\mathcal{P}}$) *The δ-estimate $\widehat{p} = \tau_\delta(z)$ in $\widetilde{\mathcal{P}}$ is given by $\widehat{p}^\delta = \langle p^\delta \rangle_z$. In particular, the 1-estimate is the posterior marginal distribution $\widehat{p} = \langle p \rangle_z$.*

Theorem 8 (δ-estimator in $\mathcal{Q}$) *Let $\mathcal{Q}$ be an arbitrary submanifold of $\widetilde{\mathcal{P}}$. The δ-estimate $\widehat{q}$ in $\mathcal{Q}$ is given by the δ-projection of $\widehat{p}$ onto $\mathcal{Q}$, where $\widehat{p}$ is the δ-estimate in $\widetilde{\mathcal{P}}$.*

4 Examples and Applications to Neural Networks

Explicit formulas are derived for the optimal estimators for the multinomial [15] and normal distributions [14].

Example 1 *Let $m \in \mathbb{N}^n$, $p \in \mathcal{P} = \Delta^{n-1}$, $a \in \mathbb{R}^n_+$. Consider multinomial family of distributions $M(m|p)$ with a Dirichlet prior $D(p|a)$. The posterior is also a Dirichlet distribution $D(p|a+m)$. The δ-estimate $\widehat{p} \in \widetilde{\mathcal{P}}$ is given by $(\widehat{p}_i)^\delta = (a_i + m_i)_\delta / (|a+m|)_\delta$, where $|a| := \sum_i a_i$ and $(a)_b := \Gamma(a+b)/\Gamma(a)$. In particular, $\widehat{p}_i = (a_i + m_i)/|a+m|$ for $\delta = 1$, and $\widehat{p}_i = \exp\left(\Psi(a_i + m_i) - \Psi(|a+m|)\right)$ for $\delta = 0$, where Ψ is the the digamma function. The δ-estimate $\widehat{q} \in \mathcal{P}$ is given by normalising $\widehat{p}$.*

Example 2 *Let $z, \mu \in \mathbb{R}$, $h \in \mathbb{R}_+$, $a \in \mathbb{R}$, $n \in \mathbb{R}_+$. Consider the Gaussian family of distributions $f(z|\mu) = N(z - \mu|h)$, with fixed variance $\sigma^2 = 1/h$. Let the prior be another Gaussian $f(\mu) = N(\mu - a|nh)$, Then the posterior after seeing a sample z of size k, is also a Gaussian $f(\mu|z) = N(\mu - a_k|n_k h)$, where $n_k = n + k$, $a_k = (na + \sum z)/n_k$, which is also the posterior least squares estimate. The δ-estimate $\widehat{q} \in \mathcal{P}$ is given by the density $f(z'|\widehat{q}) = N\left(z' - a_k\middle|h/(1 + \delta/n_k)\right)$.*

The entities $|a|$ for the multinomial model and n for the Gaussian model are effective previous sample sizes, a fact known since Fisher's time. In a restricted model, the sample size might not be well reflected, and some ancillary statistics may be used for information recovery [2].

Example 3 *In some Bayesian methods, such as the Monte Carlo method [10], no estimator is explictly given. Instead, the posterior is directly used for sampling p. This produces a prediction distribution on test data which is the posterior marginal distribution. Therefore these methods are implicitly 1-estimators.*

Example 4 *Multilayer neural networks are usually not δ-convex for any δ, and there may exist local optima of $E_\delta(\cdot|z)$ on $\mathcal{Q}$. A practical learning rule is usually a gradient descent rule which moves w in the direction which reduces $E_\delta(q|z)$. The 1-divergence can be minimised by a supervised learning rule, the Boltzmann machine learning rule [1]. The 0-divergence can be minimised by a reinforcement learning rule, the simulated annealing reinforcement learning rule for stochastic networks[13].*

$$\mathrm{Min}_q K(p,q) \iff \Delta w \sim \langle \partial_w l_0(q) \rangle_p - angle \partial_w l_0(q) \rangle_q \tag{11}$$

$$\mathrm{Min}_q K(q,p) \iff \Delta w \sim \langle \partial_w l_0(q),\ l_0(p) - \lambda_0(q) \rangle_q \tag{12}$$

5 Conclusions

The problem of finding a measurement of generalisation is solved in the framework of Baysian decision theory, with machinery developed in the theory of information geometry.

By working in the Bayesian framework, this ensures that the measurement is internally coherent, in the sense that a learning rule is optimal if and only if it produces optimal estiamtes for almost all the data. By adopting an information geometric measurement of divergence between distributions, this ensures that the theory is independent of parameterisation. This resolves the controversy in [8, 12, 9].

To guarantee a unique and well-defined solution to the learning problem, it is necessary to generalise the concept of information divergence to the space of finite positive measures. This development reveals certain elegant relations between information geometry and the theory of Banach spaces, showing that the dually-affine geometries of statistical manifolds are in fact intricately related to the dual linear geometries of Banach spaces.

In a computational model, such as a classical statisitical model or a neural network, the optimal estimator is the projection of the ideal estimator to the model. This theory generalises the theory of linear Gaussian regression to general statistical estimation and function approximation problems. Further research may lead to Kalman filter type learning rules which are not restricted to linear and Gaussian models.

REFERENCES

[1] D. H. Ackley, G. E. Hinton, and T. J. Sejnowski, *A learning algorithm for Boltzmann machines*, Cog. Sci., Vol. 9 (1985), pp147–169.

[2] S. Amari, *Differential-Geometrical Methods in Statistics*, Vol. 28 of Springer Lecture Notes in Statistics. Springer-Verlag, New York 1985.

[3] S. Amari, *Differential geometrical theory of statistics*, In Amari et al. [4], Ch. 2, pp19–94.

[4] S. Amari, O. E. Barndoff-Nieldon, R. E. Kass, S. L. Lauritzen, and C. R. Rao, eds., *Differential Geometry in Statistical Inference*, Vol. 10 of IMS Lecture Notes Monograph. IMS, Hayward, CA (1987).

[5] S. J. Hanson, J. D. Cowan, and C. L. Giles, eds., *Advances in Neural Information Processing Systems*, Vol. 5 (1993), San Mateo, CA. Morgan Kaufmann.

[6] R. E. Kass, *Canonical parameterization and zero parameter effects curvature*, J. Roy. Stat. Soc., B, Vol. 46 (1984), pp86–92.

[7] S. L. Lauritzen, *Statistical manifolds*, in: Amari et al. [4], Ch. 4, pp163–216.

[8] D. J. C. MacKay, *Bayesian Methods for Adaptive Models*. PhD thesis, California Institute of Technology, Pasadena, CA (1992).

[9] D. J. C. MacKay, *Hyperparameters: Optimise, or integrate out?*, Technical report, Cambridge (1993).

[10] R. M. Neal, *Bayesian learning via stochastic dynamics*, in: Hanson et al. [5], pp475–482.

[11] H. White, *Learning in artificial neural networks: A statistical perspective*, Neural Computation, Vol. 1(4) (1989), pp425–464.

[12] D. H. Wolpert, *On the use of evidence in neural neworks*, In Hanson et al. [5], pp539–546.

[13] H. Zhu, *Neural Networks and Adaptive Computers: Theory and Methods of Stochastic Adaptive Computations*. PhD thesis, Dept. of Stat. & Comp. Math., Liverpool University (1993), `ftp://archive.cis.ohio-state.edu/pub/neuroprose/Thesis/zhu.thesis.ps.Z`.

[14] H. Zhu and R. Rohwer, *Bayesian invariant measurements of generalisation for continuous distributions*, Technical Report NCRG/4352, Dept. Comp. Sci. & Appl. Math., Aston University (August 1995), `ftp://cs.aston.ac.uk/neural/zhuh/continuous.ps.Z`.

[15] H. Zhu and R. Rohwer, *Bayesian invariant measurements of generalisation for discrete distributions*, Technical Report NCRG/4351, Dept. Comp. Sci. & Appl. Math., Aston University (August 1995), `ftp://cs.aston.ac.uk/neural/zhuh/discrete.ps.Z`.

[16] H. Zhu and R. Rohwer, *Information geometric measurements of generalisation*, Technical Report NCRG/4350, Dept. Comp. Sci. & Appl. Math., Aston University (August 1995), `ftp://cs.aston.ac.uk/neural/zhuh/generalisation.ps.Z`.

Acknowledgements

We are grateful to Prof. S. Amari for clarifying a point of information geometry. We would like to thank many people in the Neural Computing Research Group, especially C. Williams, for useful comments and practical help. This work was partially supported by EPSRC grant (GR/J17814).

TOWARDS AN ALGEBRAIC THEORY OF NEURAL NETWORKS: SEQUENTIAL COMPOSITION

R. Zimmer

Computer Science Department, Brunel University, Uxbridge, Middx. UB8 3PH, UK. Email: Robert.Zimmer@brunel.ac.uk

This paper marks a step towards an algebraic theory of neural networks. In it, a new notion of sequential composition for neural networks is defined, and some observations are made on the algebraic structure of the class of networks under this operation. The composition is shown to reflect a notion of composition of state spaces of the networks. The paper ends on a very brief exposition of the usefulness of similar composition theories for other models of computation.

1 What is an Algebraic Study?

The view of mathematics that underlies this work is one forged by Category Theory (see for example [1]). In Category Theory scrutiny is focused less on objects than on mappings between them. Thus the natural question is: "What are the mappings?". In this kind of study the answer tends to be: "Functions (or sometimes partial functions) that preserve the relevant operations." So before we can start looking at the category of neural networks we need to answer the question: "What are the relevant operations?"

For example, recall that a **group** is a set, G, with a binary operation (*), a constant (e), and a unary operation $()^{-1}$. To be a group, it is also necessary that these operations satisfy some equations to the effect that * is associative, e is a two-sided identity for * and $()^{-1}$ forms inverses, but these are the defining group operations. A **group homomorphism** is a function, ϕ, from one group to another satisfying

$$\phi(a * b) = \phi(a) * \phi(b), \qquad \phi(e) = e' \qquad \text{and} \qquad \phi(a)^{-1} = (\phi(a))^{-1}.$$

That is a group homomorphism is defined to be a function that preserves all of the defining operations of a group.

2 What are the Defining Operations of Neural Nets?

A synchronous neural net is a set of nodes each one of which computes a function; the input for the function at a node at a given time is the output of some nodes at the previous time step (the nodes that supply the input to the given node is fixed for all time and determined by the interconnection structure of the net). This structure is captured diagrammatically by drawing a circle for each node and an arrow from node N to node M if M acts as an input for N. For example, the following is a picture of a two-noded net each of whose nodes takes an input from node f, and g takes another input from itself:

Figure 1

The letters indicate that node on the left computes the function $f(n)$ and the node on the right computes function $g(n, m)$. So a neural net is a finite directed graph

each of whose nodes is labelled by a function. We will call the underlying unlabelled graph the **shape** of the net.
As well as the shape (the interconnection structure), there is a recursive computational structure generated by the network. In this example we get the two recursive functions:

$$f_{n+1} = f(f_n).$$
$$g_{n+1} = g(f_n, g_n).$$

where, for example, f_i denotes the state of the node labelled by f at time i. Once f and g are known, these equations entirely determine the dynamics of the system: that is, the sequence of values of the pair $< f_i, g_i >$.

3 The State Space of a Boolean Net

In this section we will restrict ourselves to nets whose nodes compute boolean functions. A **state** of such a net is a vector of 0's and 1's, representing the states of the nodes of the net. When we say that a net is in state vect, we mean that for all i, the i^{th} node of the net has most recently computed the i^{th} value of vect. Since the next state behaviour of a net is completely determined by the recursion equations, we can completely compute a graph of the possible states of the net. In the example above if f is *invert* and g is *and* then the state graph is given below:

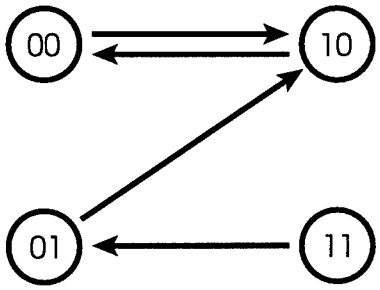

Figure 2

This exemplifies a mapping from boolean neural nets to state spaces and points to an algebraic relationship whose desirability can guide us in our setting out of our algebraic theory: we should ensure that the space of boolean neural networks is **fibred** over the space of boolean state spaces. For a detailed discussion of fibred categories see [2], for now it will suffice to give an informal definition.
Recall that a category is simply a collection of objects and maps between them. In essence, what it means for a category , **E**, to be a fibred over a category, **C**, is that there is a projection from **E** to **C** (the part of **E** that gets projected to a particular **C**-object C constitutes the **fibre** over C) such that: for every **C**-mapping $f : C \to C'$ and **E**-object, E, in the fibre over C, there is a unique lifting of f to a map starting at E and projecting onto f. The idea is that what happens in **E** gets reflected down to **C**, and, if we are lucky, what happens in **C** is liftable to **E**. This can hold for maps and operations. We want to ensure that the category of Neural Networks is in this relationship to the category of state spaces, and that the state space composition is liftable.

4 Composition in the State Space

We wish to define a notion of composition of nets that is a lifting of state space composition. The sequential composition of two graphs with the same nodes is quite well-known: an arc in the composite graph is an arc in the first graph followed by an arc in the second. Two nets with the same nodes automatically yield state graphs with the same nodes. Our first lifting of state-space composition will take advantage of this fact and only be defined for networks on the same (perhaps after renaming) nodes. We shall see that this lifting is all we need to explain the closure properties of state spaces under composition.

To continue with our example, consider the net given by the equations

$$\begin{aligned} f_{n+1} &= f_n * g_n \\ g_{n+1} &= \sim f_n. \end{aligned}$$

Notice that the shape of this net differs from the other. The shape is shown by:

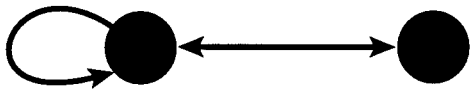

Figure 3

The state space and the result of composing it with the graph above are pictured below:

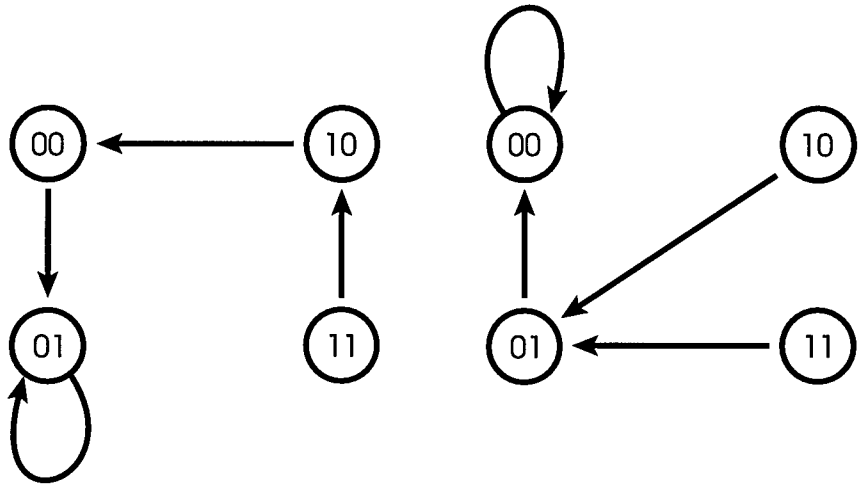

Figure 4

The observation that initiated this work is that the composite state space (and all others that can be similarly derived) is the state space of a neural network. That is, if SS denotes the function that sends a neural net to its state space, then for any two boolean nets, N and M, the composition $SS(N) * SS(M)$ turns out

to be $SS(something)$. We will now describe an operation on the nets such that $SS(N) * SS(M) = SS(N * M)$.

5 Simple Composition of Nets

The first form of neural network composition is direct functional composition on the recursion equations. The concept is most readily understood in terms of an example. Thus, to continue the example above:

$$\begin{array}{lllll} \text{First Net} & f_{n+1} =\sim f_n & \text{and} & g_{n+1} = f_n * g_n \\ \text{Second Net} & f_{n+1} = f_n * g_n & \text{and} & g_{n+1} =\sim f_n \end{array}$$

The composition consists of the second net using the results of the first net:

$$\begin{array}{ll} \text{Composite Net} & f_{n+2} = f_{n+1} * g_{n+1} =\sim f_n * f_n * g_n = 0 \\ & g_{n+2} =\sim f_{n+1} =\sim\sim f_n = f_n \end{array}$$

Note that the composite net works with $n + 2$ as one step, since its one step is a sequence of one step in each of two nets. With that rewriting in mind ($n + 1$ for $n + 2$), the equations for the composite net yield the composite state space above. And it is not hard to see that this will hold for any two boolean nets with the same set of nodes.

The set of nets with the same nodes is a monoid under this operation: the composition is associative and has an identity.

6 Two More Complex Notions of Sequential Composition

More interesting notions of composition allow us to compose nets with different nodes. The first of these compositions requires a function from the nodes of the second net to the nodes of the first. The composition is then very like the simple one except that instead of simply using the same names to say, for example,

$$f_{n+2} = f_{n+1} * g_{n+1} =\sim f_n * f_n * g_n$$

there is an extra dimension, say

$$f_{n+2} = f_{n+1} * g_{n+1}$$

in the second net and translate to

$$\phi(f)_{n+1} * \phi(g)_{n+1}$$

in the first net.

This is obviously more general (the simple version is just the special case in which f is the identity) and we believe it will lead to rich composition theories.

An even more general composition comes from taking the union of these compositions for all functions ϕ. This composition is related to the concept of **wreath product** for groups and automata (see [3]).

7 What use is a Composition Theory?

A proper composition theory can be used to explain how complex things can and do get built from simple ones. The theory can be used to break things down as well. For example, there could well be a set of primitive objects and a theorem that all objects can be built from them. A famous instance of such a theorem was given by Krohn and Rhodes:

Theorem [Krohn-Rhodes 4] *Given a finite monoid, M, M divides a wreath product of simple groups and switches each of which divides M.*

And an instance that we've been using is given by:

Theorem [5] *Given a finite concrete category, C, divides a wreath product of primitive minimal categories each of which divides C.*

This paper marks only the beginning of a composition theory of neural nets. The Krohn-Rhodes theorem has fostered a whole branch of algebra that has shed much light on automata and semigroups, while the other theorem has found application in various fields of computing. We would like our neural net composition to be useful in both of these fashions. The mathematics will consist of a study of the category of Networks as a fibred category and some projects that natural arise are: uncover a set of primitives, study the ordering determined by the decomposition, devise a homomorphism theorem, and extend the work to other operations, such as parallel composition. And to give some idea of the kinds of application we envisage, here are two applications of the categorical composition theory:

Designing Chips: We take an algebraic description of a chip design and use the decomposition to implement it using pre-defined primitive modules (see [6]).

Problem Solving: We turn difficult problems into sequences of problems that are more easily solved (see [7]).

We hope to find applications that are akin to these. The problem solving work automatically makes hierarchies of search spaces. Could we form similar neural network hierarchies? Moreover, if one wanted to design a net with a particular behaviour this might be a modular way to do it. And to finish with an interesting entirely open question: how can we apply a theory like this to nets as they are trained?

REFERENCES

[1] Saunders MacLane. *Categories for the Working Mathematician*, Graduate Texts in Mathematics 5, Springer-Verlag, Berlin (1971).

[2] John Gray, Fibred and Cofibred Categories, *Proceedings of The Conference on Categorical Algebra*, S. Eilenberg et al eds., Springer Verlag, Heidleberg (1965).

[3] Samuel Eilenberg, *Automata, Languages and Machines*, Vol. B (1976), Academic Press, New York.

[4] K. Krohn and J. Rhodes, *Algebraic Theory of Machines, I. Prime Decomposition Theorem for Finite Semigroups and Machines*, Trans. Amer. Soc. Vol. 116 (1965), pp450–464.

[5] Robert Zimmer, *Decomposing Categories*, to appear in Categorical Structures in Computer Science.

[6] R. Zimmer, A MacDonald and R Holte, *Automated Representation Changing for Problem Solving and Electronic CAD*, Applications of Artificial Intelligence 1993: Knowledge-Based Systems in Aerospace and Industry, Usama M. Fayad, Ramasmy Uthurusamy, eds., Proc. SPIE (1993), pp126–137.

[7] R. Holte, C. Druumond, R. Zimmer, Alan MacDonald, *Speeding Up Problem-Solving by Abstraction: A Graph-Oriented View*, to appear (1996).